



HAL
open science

Catalytic activity of sewage sludge-derived char composite catalysts towards the oxidation of organic contaminants in water

Yuting Tu

► **To cite this version:**

Yuting Tu. Catalytic activity of sewage sludge-derived char composite catalysts towards the oxidation of organic contaminants in water. Catalysis. Université Claude Bernard - Lyon I; Sun Yat-sen University, 2014. English. NNT : 2014LYO10260 . tel-01128280

HAL Id: tel-01128280

<https://theses.hal.science/tel-01128280>

Submitted on 9 Mar 2015

HAL is a multi-disciplinary open access archive for the deposit and dissemination of scientific research documents, whether they are published or not. The documents may come from teaching and research institutions in France or abroad, or from public or private research centers.

L'archive ouverte pluridisciplinaire **HAL**, est destinée au dépôt et à la diffusion de documents scientifiques de niveau recherche, publiés ou non, émanant des établissements d'enseignement et de recherche français ou étrangers, des laboratoires publics ou privés.

THESE
DE L'UNIVERSITE DE LYON
ET DE L'UNIVERSITE SUN YAT-SEN

Délivrée par
L'UNIVERSITE CLAUDE BERNARD LYON 1,
ECOLE DOCTORALE DE CHIMIE DE L'UNIVERSITE DE LYON
ET L'UNIVERSITE SUN YAT-SEN

DIPLOME DE DOCTORAT

(Arrêté du 7 août 2006)

Soutenue publiquement le 5 décembre 2014

Par

Madame Yuting TU

**Catalytic activity of sewage sludge-derived char composite catalysts
towards the oxidation of organic contaminants in water**

Directeur de thèse : M. Claude DESCORME, Université Claude Bernard Lyon 1

Directeur de thèse : M. Ya XIONG, Sun Yat-Sen University, Canton, Chine

JURY

Madame Florence EPRON, Chargée de recherche CNRS, Université de Poitiers, Rapporteur

Madame Shaoxia YANG, Professeur, North China Electrical Power University, Pékin, Chine, Rapporteur

Madame Anne GIROIR-FENDLER, Professeur des Universités, Université Claude Bernard Lyon 1

Madame Michèle BESSON, Directeur de Recherche CNRS, Université Claude Bernard Lyon 1, Invitée

Monsieur Ya XIONG, Professeur, Sun Yat-Sen University, Canton, Chine

Monsieur Claude DESCORME, Directeur de recherche CNRS, Université Claude Bernard Lyon 1

THESE
DE L'UNIVERSITE DE LYON
ET DE L'UNIVERSITE SUN YAT-SEN

Délivrée par
L'UNIVERSITE CLAUDE BERNARD LYON 1,
ECOLE DOCTORALE DE CHIMIE DE L'UNIVERSITE DE LYON
ET L'UNIVERSITE SUN YAT-SEN

DIPLOME DE DOCTORAT

(Arrêté du 7 août 2006)

Soutenue publiquement le 5 décembre 2014

Par

Madame Yuting TU

**Catalytic activity of sewage sludge-derived char composite catalysts
towards the oxidation of organic contaminants in water**

Directeur de thèse : M. Claude DESCORME, Université Claude Bernard Lyon 1

Directeur de thèse : M. Ya XIONG, Sun Yat-Sen University, Canton, Chine

JURY

Madame Florence EPRON, Chargée de recherche CNRS, Université de Poitiers, Rapporteur

Madame Shaoxia YANG, Professeur, North China Electrical Power University, Pékin, Chine, Rapporteur

Madame Anne GIROIR-FENDLER, Professeur des Universités, Université Claude Bernard Lyon 1

Madame Michèle BESSON, Directeur de Recherche CNRS, Université Claude Bernard Lyon 1, Invitée

Monsieur Ya XIONG, Professeur, Sun Yat-Sen University, Canton, Chine

Monsieur Claude DESCORME, Directeur de recherche CNRS, Université Claude Bernard Lyon 1

UNIVERSITE CLAUDE BERNARD - LYON 1

Président de l'Université

M. François-Noël GILLY

Vice-président du Conseil d'Administration

M. le Professeur Hamda BEN HADID

Vice-président du Conseil des Etudes et de la Vie Universitaire

M. le Professeur Philippe LALLE

Vice-président du Conseil Scientifique

M. le Professeur Germain GILLET

Directeur Général des Services

M. Alain HELLEU

COMPOSANTES SANTE

Faculté de Médecine Lyon Est – Claude Bernard

Directeur : M. le Professeur J. ETIENNE

Faculté de Médecine et de Maïeutique Lyon Sud – Charles Mérieux

Directeur : Mme la Professeure C. BURILLON

Faculté d'Odontologie

Directeur : M. le Professeur D. BOURGEOIS

Institut des Sciences Pharmaceutiques et Biologiques

Directeur : Mme la Professeure C. VINCIGUERRA

Institut des Sciences et Techniques de la Réadaptation

Directeur : M. le Professeur Y. MATILLON

Département de formation et Centre de Recherche en Biologie Humaine

Directeur : Mme. la Professeure A-M. SCHOTT

COMPOSANTES ET DEPARTEMENTS DE SCIENCES ET TECHNOLOGIE

Faculté des Sciences et Technologies

Directeur : M. F. DE MARCHI

Département Biologie

Directeur : M. le Professeur F. FLEURY

Département Chimie Biochimie

Directeur : Mme Caroline FELIX

Département GEP

Directeur : M. Hassan HAMMOURI

Département Informatique

Directeur : M. le Professeur S. AKKOUCHE

Département Mathématiques

Directeur : M. le Professeur Georges TOMANOV

Département Mécanique

Directeur : M. le Professeur H. BEN HADID

Département Physique

Directeur : M. Jean-Claude PLENET

UFR Sciences et Techniques des Activités Physiques et Sportives

Directeur : M. Y. VANPOULLE

Observatoire des Sciences de l'Univers de Lyon

Directeur : M. B. GUIDERDONI

Polytech Lyon

Directeur : M. P. FOURNIER

Ecole Supérieure de Chimie Physique Electronique

Directeur : M. G. PIGNAULT

Institut Universitaire de Technologie de Lyon 1

Directeur : M. le Professeur C. VITON

Ecole Supérieure du Professorat et de l'Education

Directeur : M. le Professeur A. MOUGNIOTTE

Institut de Science Financière et d'Assurances

Directeur : M. N. LEBOISNE

Résumé

L'élimination des boues de station d'épuration devient une source de préoccupation majeure du fait de l'augmentation constante des quantités produites à travers le monde. Par comparaison avec les méthodes traditionnelles d'élimination des boues de station d'épuration, tels que l'épandage, la mise en décharge et l'incinération, la pyrolyse peut être considérée comme une voie économiquement viable et respectueuse de l'environnement. Les charbons produits par pyrolyse de boues de station d'épuration (SC) ont été utilisés comme adsorbants pour les polluants organiques et les métaux lourds dans le domaine du traitement des eaux usées. Ceci n'est toutefois pas efficace pour une application à long terme, car les charbons actifs préparés à partir de boues de station d'épuration (SBAC) se saturent rapidement de molécules d'adsorbat. L'utilisation de SC pour préparer des matériaux composites et les utiliser comme catalyseurs dans les procédés d'oxydation avancée (POA) peut permettre de surmonter cette limitation à l'utilisation des SBAC pour le traitement en continu des eaux usées. En outre, étant donné que les SC sont un mélange organique-inorganique, ceux-ci pourraient avoir certains comportements spécifiques par rapport à d'autres supports de catalyseurs couramment utilisés. Cette situation nous a encouragés à employer les SC comme supports de catalyseurs composites et à étudier leur potentiel dans l'oxydation catalytique des contaminants organiques dans l'eau.

Les principaux travaux et réalisations dans cette thèse sont les suivants:

(1) Les charbons issus des boues de station d'épuration (SC) ont été utilisés en tant que support de catalyseur à base d'oxyde de fer (FESC). Dans cette étude, les

modifications chimiques intervenant au cours de la préparation de catalyseurs par pyrolyse ont été suivies par analyse thermique couplée à l'infrarouge (TGA-FTIR). Les catalyseurs ont été caractérisés en termes de composition élémentaire pour la fraction inorganique (cendres), DRX, MEB-EDX et XPS. Les résultats de caractérisation ont montré, après imprégnation du fer, l'existence d'une phase Fe_3O_4 presque uniformément répartie sur le support SC. L'activité catalytique du catalyseur FeSC a été évaluée dans la décoloration et la minéralisation de l'orange acide II (AOII) en présence de peroxyde d'hydrogène (H_2O_2). Il a été démontré que le catalyseur FeSC, obtenu par pyrolyse à 800°C pendant 2 h présente l'efficacité la plus élevée dans la décoloration de l'AOII. L'utilisation de $2,0 \text{ g L}^{-1}$ de catalyseur, $15,0 \text{ mM}$ de H_2O_2 et 100 mg L^{-1} de l'AOII permet d'atteindre une décoloration quasi complète et une minéralisation de l'ordre de 74 % après 1 h d'adsorption puis 2 h de réaction (Procédé d'oxydation Fenton hétérogène). Seulement $0,37 \text{ mg L}^{-1}$ de fer a été détecté dans le filtrat à la fin de la réaction. L'efficacité de ce type de catalyseur dans la décoloration de l'AOII peut être maintenue à 94% environ après 600 min d'essai en continu dans un réacteur membranaire intégré mettant en œuvre le procédé Fenton hétérogène. Ce résultat indique que le catalyseur FeSC présente à la fois une très bonne activité catalytique et une grande stabilité à long terme.

Le catalyseur FeSC présente de meilleures performances dans la décoloration de l'AOII que certains oxydes de fer commerciaux tels que $\alpha\text{-Fe}_2\text{O}_3$, Fe_3O_4 et $\gamma\text{-FeOOH}$, et que le catalyseur supporté sur charbon préparé à partir de sciure de bois (FeWC). Il a été conclu que la teneur élevée en composants inorganiques dans les boues de station d'épuration avait un impact majeur sur l'activité catalytique du catalyseur FeSC. Pour mieux analyser l'effet co-catalytique de ces composants inorganiques dans les boues de station d'épuration, les composés inorganiques ont été éliminés des boues de station d'épuration préalablement à l'introduction du fer. Une nouvelle série de catalyseurs a ensuite été préparée par addition de fer ou encore de silice et/ou d'alumine. Il a été observé que l'élimination de la fraction inorganique des boues de station d'épuration (cendres) s'accompagnait d'une diminution notable de l'activité catalytique des catalyseurs contenant du fer. L'ajout de SiO_2 favorise l'augmentation

de l'activité catalytique du fait de la possible formation de liaisons hydrogène entre H_2O_2 et les ponts siloxane du support de catalyseur et de l'existence d'un micro-environnement acide, favorable à la réaction, à proximité de la surface de la phase de silice. L'introduction d'alumine dans les boues de station d'épuration se traduit par la présence à la surface du catalyseur de sites basiques permettant de faciliter la dégradation de H_2O_2 , alors que l'acidité de Lewis de l'alumine permettra quant à elle d'accélérer la réduction de Fe^{3+} en Fe^{2+} par le peroxyde d'hydrogène.

(2) Les performances du catalyseur composite Fe_3O_4 supporté sur SC (Fe_3O_4/SC) dans l'Oxydation en Voie Humide Catalytique (OVHC) du 2-chlorophénol (2-CP) ont été évaluées. Lorsque la réaction est mise en œuvre en réacteur au toclave (discontinu) à $120^\circ C$ et sous 0,9 MPa de pression partielle d'oxygène (50 bars de pression totale), une décomposition presque complète du 2-CP est obtenue en 5 heures, alors qu'une conversion de 90% du Carbone Organique Total (COT) est atteinte après 24 heures de réaction. L'énergie d'activation de la réaction d'Oxydation en Voie Humide Catalytique du 2-chlorophénol est abaissée de 140 kJ mole^{-1} à 50 kJ mol^{-1} en présence du catalyseur Fe_3O_4/SC , confirmant tout l'intérêt du procédé d'OVHC par rapport au procédé thermique. Toutefois, une corrélation quasi linéaire a été observée entre le pH du mélange réactionnel, la quantité de fer lixivié dans la solution et la conversion du 2-CP à un temps de réaction donné. Sans contrôle du pH au cours de la réaction, 30 ppm de fer sont détectés dans la phase liquide à la fin de la réaction. Lorsqu'un tampon acétate ($pH = 4,5$) est ajouté dans le réacteur dès le démarrage de la réaction, la lixiviation du fer peut être maintenue à un niveau inférieur à 1 ppm, tout en préservant l'activité du catalyseur. Les intermédiaires de réaction générés lors de l'OVHC du 2-CP sur le catalyseur Fe_3O_4/SC sont principalement des composés aromatiques et des acides carboxyliques de faible poids moléculaire, tels que le 4-chlororesorcinol, 2-chlorohydroquinone, le catéchol, l'hydroquinone, l'acide maléique, l'acide succinique, l'acide formique, l'acide oxalique et l'acide chlorhydrique. Enfin, à partir de tous les produits identifiés, un schéma

réactionnel simplifié de la dégradation du 2-CP par OVHC sur FeSC a pu être proposé. Dans une première étape, la molécule de 2-CP est principalement déchlorée avec la production à la fois d'intermédiaires aromatiques et de HCl. La molécule de 2-CP peut également être partiellement oxydée avant déchloration avec production intermédiaire de composés aromatiques chlorés partiellement oxydés. Par la suite, l'oxydation des intermédiaires aromatiques procède par une ouverture de cycle avec la production d'acides carboxyliques à chaîne courte. Enfin, tous les intermédiaires oxydés sont progressivement convertis en CO₂ et H₂O.

(3) Un nouveau catalyseur (Mn-g-C₃N₄) à base de nanoparticules de Mn₂O₃ (NPs) supportées sur nitrure de carbone graphitique a été synthétisé par polycondensation à température élevée. Le charbon actif préparé à partir de boues de station d'épuration (SBAC), qui présente une grande surface spécifique, a ensuite été utilisé comme support pour ce nouveau catalyseur Mn-g-C₃N₄, permettant ainsi de préparer un catalyseur composite (Mn-g-C₃N₄ / SBAC). Les résultats de diffraction des rayons X, FTIR, SEM-EDX ainsi que la cartographie et la caractérisation par microscopie électronique en transmission (TEM) ont révélé que le catalyseur Mn-g-C₃N₄ présente une structure de type graphite constituée d'unité triazine comme brique de construction élémentaire. Le manganèse apparaît principalement sous la forme de nanoparticules de Mn₂O₃ à la surface du support g-C₃N₄, riche en électrons. L'ozonation catalytique d'une solution antibiotique de sulfaméthoxazole (SMZ) en présence du catalyseur Mn-g-C₃N₄ a été étudiée dans un réacteur discontinu à l'échelle du laboratoire. Les résultats ont montré que l'ajout du catalyseur Mn-g-C₃N₄ dans le réacteur d'ozonation permettait d'accélérer grandement la vitesse de dégradation de la SMZ. Lorsque la vitesse d'agitation est fixée à 750 tours par minute et que la dose d'ozone dans le gaz d'entrée est maintenue constante à 0,4 mg min⁻¹ pendant toute l'expérience, le rendement d'élimination de la SMZ (50 mg L⁻¹) après 30 minutes d'adsorption puis 1h d'oxydation, passe 62 à 95% en présence de 1 g L⁻¹ du catalyseur Mn-g-C₃N₄.

Cette étude a par ailleurs montré que la préparation du catalyseur composite Mn-g-C₃N₄/SBAC par la méthode de réaction à l'état solide permettait d'obtenir une dispersion uniforme de Mn-g-C₃N₄ dans la structure du charbon préparé à partir de boues de stations d'épuration (SBAC). La dégradation de SMZ en utilisant le catalyseur composite Mn-g-C₃N₄/SBAC peut être décrite de manière tout à fait satisfaisante par le modèle de Langmuir-Hinshelwood. Sur la base de la vitesse de réaction mesurée à faible taux de conversion, la charge optimale en Mn-g-C₃N₄ dans le catalyseur composite a été estimée à 30%. L'activité catalytique du catalyseur composite Mn-g-C₃N₄/SBAC est environ 1,6 fois supérieure à celle du catalyseur Mn-g-C₃N₄ non supporté, indiquant le rôle prépondérant du support SBAC dans la réaction d'ozonation de la sulfaméthoxazole. Le catalyseur composite présente également une très bonne résistance à l'oxydation, sans lixiviation significative du manganèse ainsi qu'une bonne stabilité puisque l'activité reste constante après quatre essais consécutifs.

Mots clé : Charbons issus de boues de station d'épuration, Catalyseurs composites, Oxydation avancée, Polluants organiques

Abstract

The disposal of sewage sludge becomes an issue of particular concern due to its continuous increase quantity. Compared with the traditional methods of sewage sludge disposal, such as ocean dumping, landfilling and incineration, pyrolysis could be considered as an economically feasible and eco-friendly route. Sludge derived carbons (SC) produced upon pyrolysis of sewage sludge have been used as adsorbents for organic pollutants and heavy metals in wastewater treatment area, however it is not efficient for long-term application since the sewage sludge-based activated carbon (SBAC) will be saturated with adsorbing molecules. Using SC to prepare some composite materials and use them as catalysts in advanced oxidation processes (AOPs) can offset the limitation of SBAC. Furthermore, since SC is an inorganic-carbon alloyed mixture, it should have some special behaviors compared with other commonly used supports. This situation encouraged us to employ the SC as the support of composite catalysts and investigate their potential to catalytic oxidation of organic contaminants in water. The main work and achievements in this thesis are as follows:

(1) Sewage sludge derived carbon (SC) was employed as the support of iron oxide containing catalyst (FeSC). The chemical changes during the preparation of catalysts by pyrolysis were monitored upon TGA-FTIR study. The catalysts were characterized in terms of inorganic elemental composition, XRD, SEM-EDX and XPS. The characterization results revealed the impregnated iron was existed as Fe_3O_4 in the FeSC catalyst and almost uniformly distributed on the SC support. The catalytic activity of FeSC was evaluated from the discoloration and mineralization of acid orange II (AOII) in the presence of H_2O_2 . It was found that the FeSC catalyst, which was pyrolyzed at 800°C for 2 h, displayed the highest discoloration efficiency. Using 2.0 g/L catalyst, 15.0 mM H_2O_2 , 100 mg/L AOII and an initial pH 4.0, almost complete discoloration and 74 % mineralization were achieved after 1 h adsorption and 2 h heterogeneous Fenton-like oxidation. And only 0.37 mg/L iron was detected in the filtrate at the end of the reaction. The discoloration efficiency could be kept around 94% after 600 min test in an integrated membrane-heterogeneous Fenton-like catalytic continuous reactor (MHFR). It indicates that FeSC presents both a high catalytic activity and a long-term stability.

FeSC exhibited better performance in discoloration of AOII than some commercial iron oxides such as $\alpha\text{-Fe}_2\text{O}_3$, Fe_3O_4 , $\gamma\text{-FeOOH}$, and wood sawdust-based carbon supported iron oxide catalyst (FeWC). The high inorganic components content of sewage sludge was concluded to have strong correlations with the high catalytic activity of FeSC. To further interpret the co-catalytic effect of inorganic components in sewage sludge, the inorganic components were removed from the sewage

sludge and then a series of catalysts were prepared by the addition of iron, as well as silica and/or alumina to the sewage sludge free of the inorganic components. It was found that the removal of inorganic fraction remarkably decreased the catalytic activity of iron-containing catalyst. The insertion of SiO₂ favors the increase in catalytic activity due to the formation of both hydrogen bonds between H₂O₂ and siloxane bridges and the acidic microenvironment near the surface of silica phase. While the addition of Al₂O₃ in sewage sludge as basic sites can facilitate the degradation of H₂O₂, and the characteristic of Lewis acidity of alumina can accelerate the reduction of Fe³⁺ to Fe²⁺ by H₂O₂.

(2) The performances of the Fe₃O₄ and SC composite catalyst (Fe₃O₄/SC) in the Catalytic Wet Air Oxidation (CWAO) of 2-chlorophenol (2-CP) was assessed. When a batch reaction operated at 120°C under 0.9 MPa oxygen partial pressure (50 bar total pressure), an almost complete decomposition of 2-CP was achieved within 5 hours, and 90% Total Organic Carbon (TOC) abatement was obtained after 24 hours of reaction. The activation energy for the CWAO of 2-CP was decreased from 140 kJ/mol to 50 kJ/mol by using Fe₃O₄/SC catalyst, indicating the advantage of the CWAO process compared with the thermal process. Quite a straight correlation was observed between the pH of the reaction mixture, the amount of iron leached in the solution and the 2-CP conversion at a given reaction time. Without controlling the pH during the reaction, 30 ppm iron could be detected in the liquid phase at the end of the reaction. When the acetate buffer (pH = 4.5) was added into the reactor, the iron leaching could be kept lower than 1 ppm while keeping some catalytic activity. The reaction intermediates generated upon CWAO of 2-CP over the Fe₃O₄/SC catalyst were mainly some aromatic compounds and low molecular weight acids, such as 4-chlororesorcinol, 2-chlorohydroquinone, catechol, hydroquinone, maleic acid, succinic acid, formic acid, oxalic acid and hydrochloric acid. Finally, from all the identified reaction products, the reaction pathway for the degradation of 2-CP upon CWAO over Fe₃O₄/SC was proposed: In the first step, the 2-CP molecule was predominantly dechlorinated and both dechlorinated aromatic intermediates and HCl were produced. The 2-CP molecule might also be partly oxidized before dechlorination occurs and partly-oxidized chlorinated aromatic intermediates were generated. Further oxidation of the aromatic intermediates led to ring opening and short chain carboxylic acids were formed. At last, all oxidized intermediates gradually converted into CO₂ and H₂O.

(3) A novel Mn₂O₃ nanoparticles (NPs) loaded graphitic carbon nitride catalyst (Mn-g-C₃N₄) was synthesized through a polycondensation process under elevated temperatures. And then the sewage sludge-based activated carbon (SBAC) with large surface area was used as the support for Mn-g-

C₃N₄ to prepare composite catalyst (Mn-g-C₃N₄/SBAC). The results of XRD, FTIR, SEM-EDX mapping and TEM characterization revealed that the synthesized Mg-g-C₃N₄ presented a graphitic-like structure with the triazine unit as the primary building block. The loaded Mn compound doped in the electron-rich g-C₃N₄ mainly as Mn₂O₃ nanoparticles. The catalytic ozonation of the antibiotic sulfamethoxazole (SMZ) solution in the presence of Mn-g-C₃N₄ catalyst was investigated in a laboratory scale batch reactor. The results indicated that adding Mn-g-C₃N₄ catalyst into the ozonation reactor could greatly accelerate the rate of SMZ degradation. When the agitation speed was fixed at 750 rpm, and the dose of ozone in the inlet gas was controlled constant at 0.4 mg/min throughout the experiment, after adsorption for 30 min and oxidation for 1 h, the removal efficiency of 50 mg/L SMZ could increase from 61.6% to 95.1% by using 1 g/L Mn-g-C₃N₄ catalyst.

The study showed that the Mn-g-C₃N₄/SBAC composite catalyst prepared by solid-state reaction method could result in the uniform dispersion of Mn-g-C₃N₄ on the framework of SBAC. The degradation of SMZ by using Mn-g-C₃N₄/SBAC composite catalyst fitted well with Langmuir-Hinshelwood model. Considering the reaction rate and the utilization of loaded Mn-g-C₃N₄, the optimal content of Mn-g-C₃N₄ was decided to be 30%. The catalytic activity of the composite catalyst was about 1.6 times compared with the non-supported Mn-g-C₃N₄ catalyst, indicating the positive trend by employing SBAC as support for ozonation catalyst. The composite catalyst also exhibited very good inoxidability, limited Mn leaching and good stability since the activity almost remained constant over four consecutive runs.

Keywords: Sewage sludge-derived carbon, Composite catalyst, Advance oxidation, Organic contaminants.

List of publications

1. **Y.T. Tu**, Y. Xiong, S.H. Tian, L.J. Kong, C. Descorme, Catalytic wet air oxidation of 2-chlorophenol by sewage sludge-derived carbon based catalysts. *J. Hazard. Mater.* 276 (2014) 88-96 (*IF*=4.331)
2. **Y.T. Tu**, Y. Xiong, C. Descorme, L.J. Kong, S.H. Tian, Heterogeneous photo-Fenton oxidation of acid orange II over iron-sewage sludge derived carbon under visible irradiation. *J. Chem. Technol. Biotechnol.* 89 (2014) 544-551 (*IF*=2.494)
3. **Y.T. Tu**, S.H. Tian, L.J. Kong, Y. Xiong, Co-catalytic effect of sewage sludge-derived char as the support of Fenton-like catalyst. *Chem. Eng. J.* 185-186 (2012) 44-51 (*IF*=3.461)
4. L.J. Kong, S.H. Tian, C.He, C.M. Du, **Y.T. Tu**, Y. Xiong, Effect of waste wrapping paper fiber as a “solid bridge” on physical characteristics of biomass pellets made from wood sawdust. *Appl. Energ.* 98 (2012) 33-39 (*IF*=5.261)
5. S.H. Tian, **Y.T. Tu**, D.S. Chen, X. Chen, Y. Xiong, Degradation of Acid Orange II at neutral pH using $\text{Fe}_2(\text{MoO}_4)_3$ as a heterogeneous Fenton-like catalyst. *Chem. Eng. J.* 169 (2011) 31-37 (*IF*=3.074)
6. Y.Y. Zhang, C. He, J.H. Deng, **Y.T. Tu**, J.K. Liu, Y. Xiong, Photo-Fenton-like catalytic activity of nano-lamellar $\text{Fe}_2\text{V}_4\text{O}_{13}$ in the degradation of organic pollutants. *Res. Chem. Intermediat.*, 35 (2009) 727-737 (*IF*=1.54)

List of communications

1. **Y.T. Tu**, S.H. Tian, Y.Y. Zhang, Y. Xiong, Fe-sewage sludge carbon as novel heterogeneous photo-Fenton-like catalyst for degradation of Orange II. 17th National Conference on Solar Energy Photochemistry and Photocatalysis in China, Kungming, 2010, 5-6 August

Table of content

Introduction	1
Chapitre 1 - A review of the preparation and utilization of sewage sludge derived materials	5
Chapitre 2 - Heterogeneous Fenton-like oxidation of Acid Orange II over sewage sludge-derived carbon-based catalysts	23
Chapitre 3 - Catalytic wet air oxidation of 2-chlorophenol over iron–sewage sludge derived carbon	59
Chapitre 4 - Catalytic ozonation of antibiotic sulfamethoxazole in aqueous solution over a Mn-g-C ₃ N ₄ modified Sewage sludge-based activated carbon	85
General conclusions	109
Acknowledgements	111

Introduction

Municipal sewage sludge are produced in huge quantity in conventional wastewater treatment plants. In 2010 for instance, the total production of dry sewage sludge in the United States, the European Union and China were ca. 8.2, 10.0 and 8.0 million tons, respectively. Furthermore, it is predicted that the production of sludge all over the world will continue to rise with an annual increase of about 2 vol.% [1-3]. Several traditional methods of sewage sludge disposal, such as landfilling, farmland application and incineration, remain the major disposal outlets for sewage sludge. However, landfilling has been limited by diminishing the supply of suitable landfilling sites. Farmland application has to deal with the low societal acceptance and the prevention of the accumulation of toxic compounds in soils and vegetation, such as heavy metals. And the widespread use of incineration has been constrained by its high cost and poor public image. The limitations applied to the traditional sludge disposal methods make the treatment of sewage sludge an issue of serious environmental concern, and has raised a high demand for more cost effective and environmental friendly routes to deal with residual sewage sludge [4,5].

It is known that sewage sludge is mainly a mixture of exhausted biomass generated in the aerobic or anaerobic digestion of the organic contaminants in municipal sewage. In recent years, the resource utilization of sewage sludge has attracted more and more attention and some new processes are being developed, such as sewage sludge composting, pyrolysis and gasification [6-8]. Among them, pyrolysis is considered as an interesting route since it is effective in reducing the volume of sludge and producing useful end products [9].

Sludge derived carbons (SC) produced upon pyrolysis of sewage sludge have been used as adsorbents for organic pollutants and heavy metals [10], however it is not efficient for long-term application since the sewage sludge-based activated carbon (SBAC) will be saturated with adsorbing molecules. On the other hand, using SC to prepare some composite materials to be implemented as catalysts in advanced oxidation processes (AOPs) can offset the limitation of SBAC by combining adsorption-oxidation processes. Furthermore, since SC is an inorganic-carbon alloyed mixture, it should have some special behaviors compared with other commonly used supports. This situation encouraged us to employ the SC as the support of composite catalysts and investigate their potential in the catalytic oxidation of organic contaminants in water.

In this Ph.D. thesis, the catalytic behavior of the prepared SC based catalysts was investigated in three kinds of typical oxidation reactions, including heterogeneous Fenton-like oxidation, catalytic wet air oxidation and catalytic ozonation, which have been proved to be very effective for the treatment of bio-recalcitrant organic compounds in wastewater. Acid orange II (AOII), 2-chlorophenol (2-CP) and sulfamethoxazole (SMZ) were chosen as representative model target pollutants in our study.

The manuscript is subsequently organized as follows:

Chapter 1: the background of the research work and literatures survey.

Chapter 2: Sewage sludge-derived char (SC) was employed as the catalyst support for iron oxides. The catalytic activity of the prepared catalysts in heterogeneous Fenton-like reaction was evaluated from the discoloration and mineralization of acid orange II (AOII). The influence of different reaction conditions was investigated. And the catalytic mechanism for using this kind of Fenton-like composite catalyst was discussed.

Chapter 3: A sewage sludge derived carbon supported iron oxide catalyst (FeSC) was prepared and used in catalytic wet air oxidation of 2-chlorophenol. The effects of heterogeneous and homogeneous reactions on the 2-CP removal were investigated, and different attempts to prevent the iron leaching were also tested.

Chapter 4: The sewage sludge-based activated carbon (SBAC) was used as the support for Mn₂O₃ nanoparticles modified graphitic carbon nitride (Mn-g-C₃N₄) to prepare composite catalysts. The catalytic ozonation of the antibiotic sulfamethoxazole (SMZ) solution in the presence of these catalysts was carried out. The catalytic activity, antioxidant properties and catalytic stability were investigated in detail.

Chapter 5: General conclusions

References

- [1] R.R.N. Marques, F. Stüber, K.M. Smith, A. Fabregat, C. Bengoa, J. Font, A. Fortuny, S. Pullket, G.D. Fowler, N.J.D. Graham, Sewage sludge based catalysts for catalytic wet air oxidation of phenol: Preparation, characterisation and catalytic performance, *Appl. Catal. B: Environ.* 101 (2011) 306-316.

- [2] T.L. Jones-Lepp, R. Stevens, Pharmaceuticals and personal care products in biosolids/sewage sludge: the interface between analytical chemistry and regulation, *Anal. Bioanal. Chem.* 387 (2007) 1173-1183.
- [3] K.M. Smith, G.D. Fowler, S. Pullket, N.J.D. Graham, The production of a attrition resistant, sewage-sludge derived, granular activated carbon, *Sep. Purif. Technol.* 98 (2012) 240-248.
- [4] L. Yu, Q. Zhong, Preparation of adsorbents made from sewage sludges for adsorption of organic materials from wastewater, *J. Hazard. Mater.* 137 (2006) 359-366.
- [5] E. Fumoto, Y. Mizutani, T. Tago, T. Masuda, Production of ketones from sewage sludge over zirconia-supporting iron oxide catalysts in a steam atmosphere, *Appl. Catal. B: Environ.* 68 (2006) 154-159.
- [6] S. Werle, R.K. Wilk, A review of methods for the thermal utilization of sewage sludge: the Polish perspective, *Renew. Energ.* 35 (2010) 1914-1919.
- [7] B. Jin, B. Li, Comprehensive Utilization of Sewage Sludge in Municipal Wastewater Treatment Plant, *Environ. Sci. Manage.* 35 (2010) 106-109.
- [8] J. Villaseñor, L. Rodríguez, F.J. Fernández, Composting domestic sewage sludge with natural zeolites in a rotary drum reactor, *Bioresour. Technol.* 102 (2011) 1447-1454.
- [9] A. B agreeev, T.J. B andosz, D.C. Locke, Pore structure and surface chemistry of adsorbents obtained by pyrolysis of sewage sludge-derived fertilizer, *Carbon* 39 (2001) 1971-1979.
- [10] K.M. Smith, G.D. Fowler, S. Pullket, N.J.D. Graham, Sewage sludge-based adsorbents: A review of their production, properties and use in water treatment applications, *Water Res.* 43 (2009) 2569-2594.

Chapter 1

A review of the preparation and utilization of sewage sludge derived materials

1.1 The production and disposal situation of sewage sludge

In recent decades, sewage sludge is produced in ever increasing amounts due to the rapid urbanization and more stringent water quality standards. In 2010 for instance, the total production of dry sewage sludge in the United States, the European Union and China were ca. 8.2, 10.0 and 8.0 million tons, respectively. Furthermore, it is predicted that the production of sludge all over the world will continue to rise with an annual increase of about 2 vol.%. Therefore, the disposal of sewage sludge is an issue of serious environmental concern [1,2].

Sewage sludge is regarded as the residue produced from the wastewater treatment process. The main type of sewage sludge including primary sludge (physical and/or chemical), the secondary sludge (biological) and the tertiary sludge (additional to secondary, often nutrient removal) treatment. Among them, secondary sludge is the commonly occurring form of sludge. It is a mixture of exhausted biomass generated in the aerobic and anaerobic digestion, containing organic and inorganic materials, such as proteins, fats (soap, oil, grease), urea, cellulose, humic substances, nitrogen, phosphoric acid, silica, iron, calcium oxide, alumina, magnesium oxide and potash [3,4].

The organisms in the fresh biosolids will be decomposed under natural conditions, resulting in the production of harmful and smelly odor. Furthermore, because of the complexity of wastewater, the generated sludge usually containing plenty of heavy metals such as zinc (Zn), copper (Cu), nickel (Ni), cadmium (Cd), lead (Pb), mercury (Hg) and chromium (Cr). The bacteria, viruses, organic contaminants and heavy metals presented in the sewage sludge have some potential to lead to significant environmental impacts, including public health risks and the possibility of contamination of atmosphere, soil and water resources [5,6]. Therefore, the safe and economic disposal of sewage sludge has become the most concerning problem in the wastewater treatment process

1.2. Common disposal strategies for sewage sludge

1.2.1. Landfill

Landfilling is always the most frequently chosen disposal method for sewage sludge in EU and the US from the 1960s [7]. However, since the moisture content of dewatered sewage sludge is around 80%, which is much higher than the 30% dryness requirement given by the Environmental Protection Department (EPD). When the sewage sludge is co-disposed with other solid waste (including municipal solid waste and construction waste, instability of landfill slopes may occur. Furthermore, the generation of excessive leachate and its potential for the surface water contamination were also concerned. The increasing amount of sewage sludge and diminishing supply of suitable landfill sites indicate the sludge disposal by landfilling is not always a feasible option [8].

1.2.2. Agricultural reuse

Since the sewage sludge contains nitrogen and phosphorus, which give it the unique fertilizing benefits. It is truly that the agricultural use has become the principal disposal method for sewage sludge until last decade [9]. Roig et al. [10] found that use the sewage sludge as an agricultural fertilizer could increase the organic matter content, the soil nitrogen, and the microbial activity of the soil. However, except for the nutrient elements, sludge also contains various other elements, such as heavy metals, organic pesticides, polychlorinated biphenyls (PCBs), polycyclic aromatic hydrocarbons (PAHs), may cause soil pollution and accumulate in human tissues through the food-chain. Resulted from these obstacles, the reuse of sewage sludge for agricultural purposes has been limited by the imposition of legislation in many countries recent years.

1.2.3. Incineration

Incineration is the most attractive disposal method that involves the firing of sewage sludge at high temperatures (800-900°C) in an enclosed structure. This sludge disposal option can achieve large reduction of sludge volume (ca. 20%). Since many urban sewage plants produce large volumes of sludge every day, and have limited available space for sludge management. They are likely to choose incineration as the most viable option [11,12]. So far, there are approximately 170 sewage sludge incineration plants in the United States. However, some environmental and health problems may be eliminated from sludge incineration during destruction of pathogens and toxic organic chemicals. The air

emissions from incineration are un-desirable and restricted since it usually contain plenty of carbon dioxide (CO₂), sulfur dioxide (SO₂), nitrogen oxides (NO_x) and a certain amount of Polychlorinated dibenzo-p-dioxins (PCDDs). The significant quantities of ash are considered as highly toxic because of its heavy metal content [13]. Moreover, the operation fee is about 210-310 € per tonne of dry solids [14]. Because of these technical and social obstacles, the application of sewage sludge incineration is hampered.

1.3. Resource utilization of sewage sludge

From the point of economic and environmental evaluation, traditional disposal routes for sewage sludge have many disadvantages and shortages. Thus, the development of more cost effective and environmentally benign alternative methods is imperative. During the last decades, many resource utilization of sewage sludge have attracted significant scientific interest, including land application, use as a construction material, use as an alternative fuel source and resource recovery from sewage sludge using the other emerging technologies.

As mentioned in last section, the application of raw (untreated) sludge is banned, or in the process of being banned, in most countries. Sewage sludge is rich in organic matter, nitrogen and phosphorus, resulting in the large manurial and soil-forming value [15]. Nowadays, the most preferred method of neutralization of sewage sludge is composting [16]. The process of composting is very complicated. At the beginning, the sludge is mixed with sources of carbon contain cellulose (ie. wood chips, sawdust, leaf litter). After bacteria digest for enough time. the pathogenic organisms are destroyed, organic matter was stabilized and the moisture content decreased. After composting, the resulting digested solids are allowed to be safely applied to land used as soil amendment materials or fertilizers [17,18].

The most common industrial application of the dewatered sludge or its incineration ash is the utilization as an addition to construction or building material including brick [19-21], cement-like materials [22-24] and ceramics [25-27]. The prospective benefits of this technology include immobilizing heavy metals in the fired matrix, oxidizing organic matter, destroying any pathogens during the firing process and producing useful materials [28,29]. It is considered as a win-win solution for the disposal problem since it can reduce the volume of sludge in significant quantity and convert the wastes into valuable industrial materials.

It is estimated that there are about 80% organic matters in sewage sludge, which can be changed into the form of renewable energy such as solid fuel or biogas. The most popular practice of energy recovery from sewage sludge is produce biogas via anaerobic digestion [30]. The generated biogas

can be used for power and heating, thereby reducing the use of fossil fuels. In recent years, some new technologies with high efficiency such as pyrolysis and gasification of sewage sludge are in development. These processes can produce bio-fuels very fast and minimize the environmental impacts at the same time. These thermal technologies can offer some alternative trends to the sewage sludge disposal. Among these technologies, pyrolysis is considered as the most promising way for the beneficial utilization of sewage sludge in recent years [31,32].

1.4. Pyrolysis of sewage sludge

Pyrolysis is the process of thermal degradation of organic substances in an inert atmosphere, with the temperature range from 300°C to 900°C, and consequently results in the conversion of sewage sludge into water vapours, combustible gases, bio-oil and fixed carbon [33,34]. Pyrolysis is considered to be less pollutant and more environmental friendly, compared to conventional combustion and incineration, since the gas emissions are clean and the heavy metals can be concentrated in a solid carbonaceous residue to prevent from leaching [35,36].

The products after pyrolysis process of the sludge present as the following form: (i) the liquid fraction (tar or oil), which contains carbonyl compounds of high molecular weight phenols, methanol, acetone and organic acids; (ii) the gaseous fraction (non-condensable gases), which mainly consists hydrogen, carbon dioxide, carbon monoxide, methane and some other low molecular weight hydrocarbons; (iii) the solid fraction, which is a mixture with carbon and ash [37,38].

1.4.1. Liquid products

A majority of organic compounds can be transferred into oily matters by a series of reactions, such as decomposition, dehydrogenation and condensation. In general, the liquid products produced from pyrolysis treatment usually consists hydrocarbons, organic acids, carbonyl compounds, phenols, aromatic compounds, aliphatic alcohols and water [39].

Many researchers have focused on how to increase the yield of oil during pyrolysis.

Shen and Zhang et al. [40] investigated influence of temperature and gas residence time on the oil yield under inert conditions in a fluidised-bed. The results reveal that the oil yield increases with temperature and the residence time. The maximum oil yield (30%) can be achieved at the temperature of 525°C and gas residence time 1.5 s. Fonts et al [41] carried out the pyrolysis of sewage sludge in a fluidized bed, and found that the liquid (oil) yield was mainly influenced by the bed temperature and the nitrogen flow rate. The maximum liquid yield was achieved at around 540°C and 4.5 L(NTP)

min⁻¹ of nitrogen. And Inguanzo et al. [42] found that the heating rate was very important for the yield of liquid fraction at low final pyrolysis temperatures. When the pyrolysis temperature is under 650°C, the higher heating rate will generate larger amount of gases and liquids

Furthermore, it is found that the addition of catalysts during the pyrolysis could increase the yield and quality of liquid products. The usage of catalyst could reduce pyrolysis time and reaction temperature, and control the distribution range of pyrolysis products [43]. Shie and Lin [44] investigated the pyrolysis of sewage sludge with the sodium and potassium compounds catalysts from 650-710 K. It appears that the addition of catalysts could result in the improvement of the quality of pyrolysis oil in the order of KOH>KCl>K₂CO₃>NaOH>Na₂CO₃>NaCl>no additives. And the additives improve the oil yields in the order of KCl>Na₂CO₃>NaCl> no additives >NaOH>K₂CO₃>KOH.

However, the low temperature sludge pyrolysis technology merely requires the water ratio of dry basis is below 5% before thermal treatment, which may consume too much energy. On the other hand, the method of direct thermochemical liquefaction occurs in the liquid phase. Thus, the raw sludge can be used directly. Nowadays, many attentions have been paid on the technology of sludge direct thermochemical liquefaction [45]. Suzuki et al. [46] studied the bio-oil yield rate of various kinds of sewage sludge. The average oil yields of these sludges reached as high as 43%. Furthermore, they found that the inorganic components in sewage sludge could catalytic the oil production satisfactorily. Furthermore, some polycyclic aromatic hydrocarbons (PAHs), substituted aromatics containing N, S, Cl, and aromatic nitriles were detected in the oil produced from sludge pyrolysis [47]. Further separation and purification is necessary before practical application of the bio-oil. Compared with fossil fuel, the economic advantage of this bio-oil producing method is not obviously. But from the point of environmental protection and sustainable development, this technology has great developmental potential and broad application prospect.

1.4.2. Gasses products

The gas generated from pyrolysis has the potential to be used as fuel gases, since the gas presences high heating value (ranges between 12,000 and 200,000 kJ/m³) [48]. The yield and composition of the gas will be influenced by the pyrolysis process conditions. Conesa et al. [49] used the thermogravimetry/mass spectrometry (TG/MS) to monitor the mass loss and the evolution profiles of the thermal decomposition products generated during thermal treatment of sewage sludge digested anaerobically and aerobically. High quantities of gasses were produced, which consisted with hydrogen, water, saturated and unsaturated hydrocarbons (C₁-C₄), methanol, chloromethane, carbon dioxide and acetic acid. According to the published literatures, the main components of the gaseous

released during sewage sludge pyrolysis include Many studies [50,51] confirm that H₂, CO, CO₂, CH₄, and some light hydrocarbons (C₂H₂, C₂H₄, C₂H₆ and C₃H₈).

1.4.3. Solid products

The solid product generated from the pyrolysis of sewage sludge is a carbonaceous material known as pyrolytic char. The physical and chemical properties of the biochar are influenced by the character of raw sewage sludge, the operating conditions such as pyrolysis temperature, residence time and heating rate [52-54].

The quality of the obtained biochar can be changed during the pyrolysis procedure according to the end purpose. If the sewage sludge based biochar is used as a soil amendment, then the nutrients and heavy metals content in materials and leaching potential are important factors [55,56]. If the biochar is intended to be used as a adsorbent material to remove organic or inorganic contaminants in liquid or gas phase, then the surface area, pore size distribution, surface functional groups and hydraulic conductivity of the biochar will be important for adsorption performance [57-59].

1.5. Application of sewage sludge derived char

Since the pyrolytic char produced by pyrolysis of sewage sludge presents high ash content and relatively low heating value compared to that of the other biomass or fossil fuels. And high content of heavy metals residues was identified in the sewage sludge char. Therefore, there is not too much potential to exploit this kind of material as bio-fuels. On the other hand, the application of sludge-based materials has been successfully reported for use as soil amendments, adsorbents for metal ions and phenolic compounds.

1.5.1. Use as soil amendments

During pyrolysis most of the mineral nutrients are concentrated into the biochar fraction. The characterization of char obtained from sewage sludge reveals that this kind of materials is free of pathogens but rich in carbon and nutrient contents [60]. Hence soil application of sewage sludge derived biochar is a convenient means of recycling those nutrients to agricultural lands.

In recent years, the application of sewage sludge derived biochar as soil amendment has received increasing attention. It is found that use sludge derived char as soil amendment could increase long-term nutrient retention of the soil, thereby reduced nutrient leaching, improving fertiliser utilisation

efficiency, and enhancing crop production [61-63]. Hossain et al. [64] found that the using of sewage sludge derived biochar produced at 550°C as soil amendment could increase the grown of cherry tomato by 64%, and the soil properties were also improved. And the application of sludge derived char to agricultural soils also can improve soil physical, chemical and biological conditions. Furthermore, the accumulation of heavy metals in the soil and crops is another important problem correlated with the application of sewage sludge derived biochar. Méndez et al. [65] reported that compared to the directly agricultural reuse of raw sewage sludge, the use of its bio-char as soil amendment could lower the leaching of Cu, Ni and Zn, as well as reduce the plant availability of Ni, Zn, Cd and Pb. Recently Waqas et al. [66] reported that sewage sludge derived biochar produced at 550°C was effective in reducing the accumulation of As, Pb and Cu during the cultivation of grapes, but the content of Cd and Zn in the plants were exceptional. Song et al. [67] revealed that proper pyrolysis temperature choice could prevent the leaching of heavy metal and inhibited the heavy metal accumulation in plants.

1.5.2. Use as adsorbents

The conversion of sewage sludge into low cost adsorbents is considered as an interesting route to deal with sewage sludge for it is effective in reducing its volume and producing useful end products.

The producing adsorbents from dried sewage sludge via pyrolysis, named as sewage sludge-based adsorbents (SBAs), was first proposed by Kemmer et al. [68] at 1971. At the same year, Beeckmans and Ng [69] prepared the biochar based adsorbent with 14.1% carbon content from the pyrolysis of sludge, and the adsorbing capacity of pyrolysate was between fly ash and activated coconut charcoal. After these studies, a wealth of research on the production and application of SBAs has been carried out in the subsequent years.

The porosity and surface area were considered as two of the most important characteristics of adsorbents produced from sewage sludge. Generally, the studies indicated that the BET surface area and porosity of sewage sludge chars may be affected by many factors, such as carbonisation temperature, heating rates, dwell times, pyrolysis atmosphere [70,71]. Kojima et al. [71] investigated the effect of carbonization temperature (773, 823 and 873K), carbonization time (20, 30, 60 and 90 min), heating rate (4, 7 and 11 K/s) on specific surface area of SBAs. The results showed that the S_{BET} of the SBAs decreased with the increasing of pyrolysis temperature. The heating rate didn't presence significant influence on the S_{BET} of the SBAs. The SBAs formed after pyrolysed at 823 K for 1 h with the heating rate at 3 K/s had the largest surface area for the micro pores as well as total pores.

According to the literatures, the highest and second highest BET surface areas achieved from the carbonization of sewage sludge alone were 359 m²/g and 141 m²/g [72], which are relatively low compared to commercial activated carbon. Different approaches have been used in order to obtain SBAs with high surface area, including (i) acid washing to reduce the inorganic content of SBAs [73]; (ii) physical activation under the treatment of air, CO₂, H₂ or steam [74-76]; (iii) chemical activation with the addition of activation reagents, such as ZnCl₂ [77,78], KOH [79-81], H₂SO₄ [82,83] and H₃PO₄ [84].

In recent years, extensive research has been conducted on the use of SBAs to liquid phase organic pollutants capture. It was revealed that the higher mesopore volume and BET surface area of the SBAs are beneficial for the uptake of pollutants with large molecular size, such as dyes [86]. Investigations have been carried out on the uptake by SBAs of anionic and cationic dyes. Jindarom et al. [87] ascribed the adsorption capacity of SBAs for dyes was influenced by the chemical nature of the dye. They observed that basic (cationic) dye was adsorbed in greater quantities than acid dye and reactive dye on the SBAs produced by carbonization and CO₂ activation. Otero et al. [88] proposed that the high cationic dye uptake on SBAs was attributed to the negatively charged acidic functional groups on the surface of SBAs.

On the other hand, the uptake of phenol and phenolic compounds attained by SBAs were mainly connected with the high degree of microporosity [89], as well as its electronegativity and basic nature [90,91]. The high concentration of hydrophilic carboxyl and hydroxyl groups on the surface of SBAs is not beneficial for the uptake of phenol. Higher phenol uptakes could be achieved by increasing the alkalinity of SBAs via heating the adsorbents in ammonia [92].

Except for the uptake of organic contaminants, the SBAs were also used as adsorbents for the removal of heavy metals in aqueous solutions, such as Cd²⁺, Ni²⁺, Pb²⁺, Cu²⁺ and Zn²⁺ [93,94]. Rio et al. [95] investigated the Cu²⁺ ion uptake by commercial activated carbon (AC) and an SBA carbonized at 800°C. And 182 mg/g and 227 mg/g of Cu²⁺ uptake was achieved for AC and SBA respectively, even though the SBA presented lower BET surface area (only 63 m²/g). Rio et al. further indicated that the adsorption of Cu²⁺ on SBAs was mainly through an ion exchange mechanism with the Ca²⁺ ions in SBAs. Additionally, Seredych et al. [96] proposed that Cu²⁺ could also be uptake by the cation exchange with Mg and Zn. Martin et al. [97] found that the high content of functional groups, such as carboxyl group and hydroxyl, were beneficial for the increasing of cation exchange capacity of the SBAs.

As mentioned above, most of the carbonaceous residue was used as adsorbents in wastewater treatment for the effective removal of dyes, phenol, metals and chemical oxygen demand (COD), and adsorption properties of which can be improved by chemical or physical activation stages if

necessary. On the other hand, SBAs were also found to be very efficient media for removal of some contaminants generated in pyrolysis or gasification, such as hydrogen sulfide, sulfur dioxide or nitric oxides.

Bashkova et al. [98] investigated the adsorption of SO₂ on sewage sludge-derived materials. It was found that the capacity of the adsorbents increases with increasing temperature of carbonization, and the maxima adsorption capacity of SO₂ is 30 mg/g.

The development of adsorbent/catalyst from municipal wastewater sludge for H₂S removal was firstly proposed by Lu et al. [99,100]. They prepared SBAs from dewatered sewage sludge via chemical activation by ZnCl₂. The BET of surface area was 309 m²/g for the synthesized SBA. Although the adsorption capacity of H₂S on SBA is relatively low (about 25% as that of commercial activated carbon), considering sewage sludge is a waste material in abundant supply at virtually no cost, the application of SBAs still present the potential for odour control. Subsequent to these studies, Ros and Bandosz et al. made great efforts to investigate the influence of different factors on the performance of SBAs for H₂S adsorption. They found that the hydrogen sulfide reactive adsorption capacity increased with an increase in pyrolysis temperature and holding time [101]. Furthermore, high BET surface area [102], high hydrophilicity [103], strong basicity [104] and the presence of mineral phases [79] are considered to benefit for H₂S adsorption.

1.5.3. Use as catalysts

During the study on H₂S abatement, Bagreev et al. [105,106] found that the metallic oxides, such as iron, zinc, and copper, carbonates of calcium and magnesium and other alkaline earth metal oxides could favor the oxidation of hydrogen sulfide to elemental sulfur in moist air via the formation of HS⁻ ions. They proposed this to be an adsorption/oxidation process. Furthermore, the interactions between SBA and NO₂ in moist air were also investigated by Bandosz et al. The results revealed that the high pyrolysis temperature could favor the physical adsorption of water. In the formed water film, nitrous and nitric acid could react with inorganic and carbonaceous phases in SBAs and resulting the generation of nitrates and nitrite [107].

Compared with the large number of research on the application of sewage sludge derived char as adsorbents in wastewater treatment area, scarcely study was carried out about employing the sewage sludge derived char as catalyst or catalyst support. Zhang et al. [108] combined sewage sludge activated carbon with TiO₂ and recovery of ionic mercury [Hg(II)] in the solution by photoreduction. The optimum amount of SBA and TiO₂ for the photocatalytic reaction was 2.0 g/L and 0.4 g/L. This is the earliest study about the application of SBA in catalytic reaction in solution. In this reaction, the

role of SBA in this reaction is mainly played as support for TiO₂ particles attributed to the high surface area of SBA (555 m²/g). However, the potential of SBA as catalyst was not investigated.

1.6. Objectives of the thesis

Municipal sewage sludge are produced in huge quantity in conventional wastewater treatment plants. As a result, the disposal of sewage sludge becomes a matter of great concern. Compared with the traditional methods of sewage sludge disposal, such as ocean dumping, landfilling and incineration, pyrolysis could be considered as an economically feasible and eco-friendly route. Sludge derived carbons (SC) produced upon pyrolysis of sewage sludge have been used as adsorbents for organic pollutants and heavy metals abatement in liquid phase. However the sewage sludge-based activated carbon (SBAC) is not efficient for long-term application due to the saturation adsorption of targeted pollutant molecules. On the other hand, using SC to prepare some composite materials and employ them as catalysts in advanced oxidation processes (AOPs) can offset the limitation of SBAC. Furthermore, since SC is an inorganic-carbon alloyed mixture, it should have some special behaviors compared with other commonly used catalyst supports. Hence the main objectives of this thesis is to synthesis a series of sewage sludge derived carbon composite materials, and investigate their potential to be used as catalysts in AOPs.

References

- [1] R.R.N. Marques, F. Stüber, K.M. Smith, A. Fabregat, C. Bengoa,, J. Font, A. Fortuny, S. Pullket, G.D. Fowler, N.J.D. Graham, Sewage sludge based catalysts for catalytic wet air oxidation of phenol: Preparation, characterisation and catalytic performance. *Appl. Catal. B: Environ.*, 101 (2011) 306-316.
- [2] J.L. Jones-Lepp, R. Stevens, Pharmaceuticals and personal care products in biosolids/sewage sludge: the interface between analytical chemistry and regulation. *Anal. Bioanal. Chem.*, 387 (2007) 1173-1183.
- [3] S. Ren, Assessing wastewater toxicity to activated sludge: recent research and developments. *Environ. Int.* 30 (2004) 1151-1164.
- [4] I.S. Turovskiy, P.K. Mathai, Wastewater sludge processing. John Wiley & Sons, Inc., Hoboken, New Jersey. 2006.
- [5] P. Hsiau, S. Lo, Extractabilities of heavy metals in chemically-fixed sewage sludges. *J Hazard*

Mater, 58 (1998) 73–82.

- [6] U. Krogmann, L.S. Boyles, W.J. Bamka, S. Chaiprapat, C.J. Martel, Biosolids and sludge management. *Water Environ Res*, 71(1999) 692–714.
- [7] E. Pokorna, N. Postelmans, P. Jenicek, S. Schreurs, R. Carteer, J. Yperman, Study of Bio-Oils and Solids from Flash Pyrolysis of Sewage Sludges. *Fuel* 88(2009) 1344-1350.
- [8] D. Fytli, A. Zabaniotou, Utilization of sewage sludge in EU application of old and new methods - a review. *Renew. Sust. Energ. Rev.*, 12(1) (2007) 116-140.
- [9] A.T.J. Pigozzo, E. Lenzi, J.D. Luca, Transition metal rates in latosol twice treated with sewage sludge. *Braz. Arch. Biol. Techn.*, 49(3) (2006) 515-526.
- [10] N. Roig, J. Sierra, E. Marti, M Nadal, M. Schuhmacher, J.L. Domingo, Long-term amendment of Spanish soils with sewage sludge: Effects on soil functioning. *Agr. Ecosyst. Environ.*, 158(1) (2012) 41-48
- [11] T. Murakami, Y. Suzuki, H. Nagasawa, H. Nagasawa, T. Yamamoto, T. Koseki, H. Hirose, S. Okamoto, Combustion characteristics of sewage sludge in an incineration plant for energy recovery. *Fuel Process. Technol.* 90 (2009) 778-783
- [12] J. Werther, T. Ogada, Sewage sludge combustion. *Prog. Energ. Combust. Sci.*, 25(1): (1999) 55-116.
- [13] B. Fabrellas, P. Sanz, E. Abad, J. Rivera, D. Larrazábai, Analysis of dioxins and furans in environmental samples by GC-ion-trap MS/MS. *Chemosphere*, 55(11) (2004) 1469-1475.
- [14] S. Rio, L. Le Coq, C. Faur, P. Le Cloirec, Production of porous carbonaceous adsorbent from physical activation of sewage sludge: application to wastewater treatment. *Water Sci. Technol.*, 53 (3) (2006) 237-244
- [15] J. Doublet, C. Franco, M. Poitrenaud, S. Houot, Influence of bulking agents on organic matter evolution during sewage sludge composting; consequences on compost organic matter stability and N availability. *Bioresource Technol.*, 102 (2011) 1298-1307.
- [16] P. Oleszczuk, The evaluation of sewage sludge and compost toxicity to *Heterocypris incongruens* in relation to inorganic and organic contaminants content. *Environ Toxicol.*, 22 (6) (2007) 587-96.
- [17] E. Epstein, J.M. Taylor, R.L. Chancy, Effects of sewage sludge and sludge compost applied to soil on some soil physical and chemical properties. *J. Environ. Qual.*, 5 (1976) 422-426.
- [18] P. Kosobucki, A. Chmarzyński, B. Buszewski, Sewage Sludge Composting. *Polish J. Environ. Studies*, 9 (2000) 243-248.
- [19] C.H. Weng, D.F. Lin, P.C. Chiang, Utilization of sludge as brick materials. *Adv. Environ. Res.*, 7 (2003) 679-685.

- [20] D.F. Lin, C.H. Weng, Use of sewage sludge ash as brick material. *J Environ. Eng.* 127 (2001) 922-927.
- [21] J. Cusidó, L.V. Cremades, Environmental effects of using clay bricks produced with sewage sludge: Leachability and toxicity studies. *Waste Manage.* 32 (2012) 1202-1208
- [22] A. Zabaniotou, C. Theofilou, Green energy at cement kiln in Cyprus-Use of sewage sludge as a conventional fuel substitute. *Renew. Sust. Energ. Rev.*, 12 (2008) 53-541.
- [23] T. Onaka, Sewage can make Portland cement: a new technology for ultimate reuse of sewage sludge. *Water Sci. Technol.*, 41 (2000) 93-98.
- [24] N.H. Rodríguez, S. Martínez-Ramírez, M.T. Blanco-Varela, S. Donatello, M. Guillern, J. Pulg, C. Fos, E. Larrotcha, J. Flores, The effect of using thermally dried sewage sludge as an alternative fuel on Portland cement clinker production. *J. Clean. Prod.*, 52(1) (2013) 94-102
- [25] G.R. Xu, J.L. Zou, Y. Dai, Utilization of dried sludge for making ceramsite. *Water Sci. Technol.*, 54 (2006) 69-79.
- [26] G.R. Xu, J.L. Zou, G.B. Li, Stabilization of heavy metals in ceramsite made with sewage sludge. *J. Hazard. Mater.*, 152 (2008) 56-61.
- [27] S.N. Monteiro, J. Alexandre, J.L. Margem, R. Sánchez, C.M.F. Vieira, Incorporation of sludge waste from water treatment plant into red ceramic. *Constr. Build. Mater.*, 22 (2008) 1281-1287.
- [28] M. Cyr, M. Coutand, P. Clastres, Technological and environmental behavior of sewage sludge ash (SSA) in cement-based materials. *Cement Concrete Res.*, 37 (2007) 1278-1289.
- [29] M.M. Jordán, M.B. Almendro-Candel, M. Romero, Application of sewage sludge in the manufacturing of ceramic tile bodies. *Appl. Clay Sci.*, 30 (2005) 219-224.
- [30] Y. Han, S. Sung, R.R. Dague, Temperature-phased anaerobic digestion of wastewater sludges. *Water Sci. Technol.* 36 (1997) 367-374
- [31] B. Khiari, F. Marias, F. Zagrouba, J. Vaxelaire, Analytical study of the pyrolysis process in a wastewater treatment pilot station. *Desalination* 167 (2004) 39-47
- [32] J.S. Dennis, R.J. Lambert, A.J. Milne, S.A. Scott, A.N. Hayhurst, The kinetics of combustion of chars derived from sewage sludge. *Fuel* 84 (2005) 117-26.
- [33] W. Rulkens, Sewage sludge as a biomass resource for the production of energy: overview and assessment of the various options. *Energ. Fuel.*, 22 (2007) 9-15
- [34] S. Yaman, Pyrolysis of biomass to produce fuels and chemical feedstocks. *Energ. Convers. Manage.*, 45 (2004) 651-671.
- [35] J.A. Menéndez, M. Inguanzo, J.J. Pis, Microwave-induced pyrolysis of sewage sludge. *Water Res.*, 36 (2002) 3261-3264.
- [36] E.S. Park B.S. Kang J.S. Kim, Recovery of oils with high calorific value and low contaminant

content by pyrolysis of digested and dried sewage sludge containing polymer flocculants. *Energy Fuel* 22 (2008)1335-1340

- [37] L. Shen, D.K. Zhang, An experimental study of oil recovery from sewage sludge by low-temperature pyrolysis in a fluidized-bed. *Fuel* 82 (2003) 465-72.
- [38] P. Manara, A. Zabaniotou, Towards sewage sludge based biofuels via thermochemical conversion - A review. *Renew. Sust. Energ. Rev.*, 16 (2012) 2566-2582
- [39] E. Bayer, M. Kutubuddin, Low temperature conversion of sludge and waste to oil. *Proceeding of the International Recycling Congress*. Berlin: EF Verlag, (1987) 314-318
- [40] L. Shen, D.K. Zhang, An experimental study of oil recovery from sewage sludge by low-temperature pyrolysis in a fluidised-bed. *Fuel* 82 (2002) 465-72.
- [41] I. Fonts, A. Juan, G. Gea, M.B. Murillo, J.L. Sánchez, Sewage Sludge Pyrolysis in Fluidized Bed, 1: Influence of Operational Conditions on the Product Distribution. *Ind. Eng. Chem. Res.*, 47 (2008) 5376-5385
- [42] M. Inguanzo, A. Dominguez, J.A. Menéndez, C.G. Blanco, J.J. Pis, On the pyrolysis of sewage sludge: the influence of pyrolysis conditions on solid, liquid and gas fractions. *J. Anal. Appl. Pyrol.*, 69 (2002) 209-222
- [43] V.A. Doshi, H.B. Vuthaluru, T. Bastow, Investigations into the control of odour and viscosity of biomass oil derived from pyrolysis of sewage sludge, *Fuel Process. Technol.*, 86 (2005) 885-897.
- [44] J.L. Shie, J.P. Lin, C.Y. Chang, D.J. Lee, C.H. Wu, Pyrolysis of oil sludge with additives of sodium and potassium compounds. *Resour. Conserv. Recy.*, 2003, 39: 51-64
- [45] J. Liu, X. Zhang, G. Chen, Overview of bio-oil from sewage sludge by direct thermochemical liquefaction technology. *J. Sustain. Bioenerg. Syst.*, 2 (2012) 112-116
- [46] A. Suzuki, T. Nakamura, S.Y. Yokoyama, T. Ogi, K. Koguchi, An advanced treatment of sewage sludge by direct thermochemical liquefaction. *Res. Thermochem. Biomass Convers.*, (1988) 816-826
- [47] Y. Tian, W. Zuo, Z. Ren, D. Chen, Estimation of a novel method to produce biooil from sewage sludge by microwave pyrolysis with the consideration of efficiency and safety. *Bioresource Technol.*, 102 (2011) 2053-2061.
- [48] J. Piskorz, D.S. Scott, I.B. Westerberg, Flash pyrolysis of sewage sludge. *Ind. Eng. Chem. Process Des. Dev.* 25 (1986) 265-70
- [49] J.A. Conesa, A. Marcilla, R. Moral, J. Moreno-Caselles, A. Perez-Espinosa, Evolution of gases in the primary pyrolysis of different sewage sludge. *Thermochim Acta* 313 (1998) 63-73.
- [50] A. Dominguez, J.A. Menendez, J.J. Pis, Hydrogen rich fuel gas production from the pyrolysis

of wet sewage sludge at high temperature. *J. Anal. Appl. Pyrol.* 77 (2006) 127-132.

- [51] T. Kasakura, M. Hiraoka, Pilot plant study on sewage sludge pyrolysis-I. *Water Res.* 16 (1982) 1335-48.
- [52] N. Kojima, A. Mitomo, Y. Itaya, S. Mori, S. Yoshida, Adsorption removal of pollutants by active cokes produced from sludge in the energy recycle process of wastes. *Waste Manage.* 22 (2002) 399-404.
- [53] J. Ábrego, J. Arauzo, J.L. Sánchez, A. Gonzalo, T. Cordero, J. Rodríguez-Mirasol, Structural changes of sewage sludge char during fixed-bed pyrolysis. *Ind. Eng. Chem. Res.*, 48 (2009) 3211-3221.
- [54] X.D. Song, D.Z. Chen, Z.H. Wang, W. He, Analysis on the target product from sewage sludge pyrolysis and experiments on using the char for enhancing plant cultivation. *Huan Jing Ke Xue*. 32 (2011) 2604-2609
- [55] T. Liu, B. Liu, W. Zhang, Nutrients and heavy metals in biochar produced by sewage sludge pyrolysis: its application in soil amendment. *Pol. J. Environm. Stud.*, 23 (2014) 271-275
- [56] X.D. Song, X.Y. Xue, D.Z. Chen, P.J. He, X.H. Dai, Application of biochar from sewage sludge to plant cultivation: Influence of pyrolysis temperature and biochar-to-soil ratio on yield and heavy metal accumulation. *Chemosphere*, 109 (2014) 213-220
- [57] S. Brunauer, P.H. Emmett, E. Teller, Adsorption of gases in multimolecular layers. *J. Am. Chem. Soc.*, 60 (1938) 309-319
- [58] C. Wu, M. Song, B. Jin, Y. Wu, Y. Huang, Effect of biomass addition on the surface and adsorption characterization of carbon-based adsorbents from sewage sludge. *J. Environ. Sci.*, 25 (2013) 405-412
- [59] J. Zou, Y. Dai, X. Wang, Z. Ren, C. Tian, K. Pan, S. Li, M. Abuobeidah, H. Fu, Structure and adsorption properties of sewage sludge-derived carbon with removal of inorganic impurities and high porosity. *Bioresource Technol.* 142 (2013) 209-217
- [60] M.K. Hossain, V. Strezov, P.F. Nelson, Thermal characterisation of the products of wastewater sludge pyrolysis. *J. Anal. Appl. Pyrolysis.* 85 (2009) 442-446.
- [61] S.P. Sohi, E. Krull, E. Lopez-Cape, R. Bol, A review of biochar and its use and function in soil. *Adv. Agron.*, 105 (2010) 47-82.
- [62] J.H. Yuan, R.K. Xu, H. Zhang, The forms of alkalis in the biochar produced from crop residues at different temperatures. *Bioresource Technol.*, 102 (2011) 3488-3497.
- [63] J. Lehmann, J. Gaunt, M. Rondon, Bio-char sequestration in terrestrial ecosystems - a review. *Mitig. Adapt. Strat. Global Change*, 11 (2006) 403-427.
- [64] M.K. Hossain, V. Strezov, K.Y. Chan, Agronomic properties of wastewater sludge biochar and

- bioavailability of metals in production of cherry tomato (*Lycopersicon esculentum*). *Chemosphere* 78 (2010) 1167-1171.
- [65] A. Méndez, A. Gómez, J. Paz-Ferreiro, G. Gascó, Effects of sewage sludge biochar on plant metal availability after application to a Mediterranean soil. *Chemosphere* 89 (2012) 1354-1359.
- [66] M. Waqas, S. Khan, H. Qing, B.J. Brian, C. Chao, The effects of sewage sludge and sewage sludge biochar on PAH and potentially toxic element bioaccumulation in *Cucumis sativa* L. *Chemosphere* 105 (2014) 53-61
- [67] X.D. Song, X.Y. Xue, D.Z. Chen, P.J. He, X.H. Dai, Application of biochar from sewage sludge to plant cultivation: Influence of pyrolysis temperature and biochar-to-soil ratio on yield and heavy metal accumulation. *Chemosphere*, 109 (2014) 213-220.
- [68] F.N. Kemmer, R.S. Robertson, R.D. Mattox, Sewage treatment process. *General Chemical Company*. US Patent Office. 1971, Patent No. 3,619,420.
- [69] J.M. Beckmans, P.C. Ng, Pyrolyzed sewage sludge - its production and possible utility. *Environ. Sci. Technol.* 5 (1971) 69-71.
- [70] H.L. Chiang, C.G. Chao, C.Y. Chang, C.F. Wang, P.C. Chiang, Residue characteristics and pore development of petrochemical industry sludge pyrolysis. *Water Res.* 35 (2001) 4331-4338.
- [71] N. Kojima, A. Mitomo, Y. Itaya, S. Mori, S. Yoshida, Adsorption removal of pollutants by active cokes produced from sludge in the energy recycle process of wastes. *Waste Manage.* 22 (2002) 399-404.
- [72] K.M. Smith, G.D. Fowler, S. Pullket, N.J.D. Graham, Sewage sludge-based adsorbents: A review of their production, properties and use in water treatment applications. *Water Res.*, 43 (2009) 2569-2594.
- [73] M.A. Ros, E. Montes-Moran, D.M. Fuente, M.J. Nevskaja, Dried sludges and sludge-based chars for H₂S removal at low temperature: influence of sewage sludge characteristics. *Environ. Sci. Technol.* 40 (2006) 302-309.
- [74] S. Rio, C. Faur-Brasquet, L. Le Coq, P. Courcoux, P. Le Cloirec, Experimental design methodology for the preparation of carbonaceous sorbents from sewage sludge by chemical activation - application to air and water treatments. *Chemosphere*, 58 (2005) 423-437.
- [75] A. Méndez, G. Gascó, M.M.A. Freitas, G. Siebielec, T. Stuczynski, J.L. Figueiredo, Preparation of carbon-based adsorbents from pyrolysis and air activation of sewage sludges. *Chem. Eng. J.*, 108 (2005) 169-177.
- [76] C. Jindarom, V. Meeyoo, B. Kitiyanan, T. Rirksomboon, P. Rangsunvigit, Surface characterization and dye adsorptive capacities of char obtained from pyrolysis/gasification of sewage sludge. *Chem. Eng. J.*, 133 (2007) 239-246

- [77] P.C. Chiang, J.H. You, Use of sewage-sludge for manufacturing adsorbents. *Can. J. Chem. Eng.*, 65 (1978) 922-927
- [78] X. Chen, S. Jeyaseelan, N. Graham, Physical and chemical properties study of the activated carbon made from sewage sludge. *Waste Manage.*, 22 (2002): 755-760
- [79] A. Ros, M.A. Lillo-Rodenas, C. Canala-Battle, E. Fuente, M.A. Montes-Morán, M.J. Martin, A. Linares-Solano, A new generation of sludge-based adsorbents for H₂S abatement at room temperature. *Environ. Sci. Technol.*, 41 (2007) 4375-4381.
- [80] M.A. Lillo-Rodenas, A. Ros, E. Fuente, M.A. Montes-Morán, M.J. Martin, A. Linares-Solano, Further insights into the activation process of sewage sludge-based precursors by alkaline hydroxides. *Chem. Eng. J.*, 142 (2008) 168-174.
- [81] W. Shen, Q. J. Guo, H. Wang, X. P. Yang, Y.H. Liu, Y.L. Zhang, Product composition of pyrolyzed sewage sludge and adsorption of Methylene Blue by porous material derived from it. *Environ. Eng. Sci.*, 25 (2008) 99-105.
- [82] M.J. Martin, E. Serra, A. Ros, M. D. Balaguer, M. Rigola, Carbonaceous adsorbents from sewage sludge and their application in a combined activated sludge-powdered activated carbon (AS-PAC) treatment. *Carbon*, 42 (2004) 1383-1388.
- [83] F.S. Zhang, J.O. Nriagu, H. Itoh, Mercury removal from water using activated carbons derived from organic sewage sludge. *Water Res.*, 39 (2005) 389-395.
- [84] Y. Guo, D.A. Rockstraw, Physicochemical properties of carbons prepared from pecan shell by phosphoric acid activation. *Bioresource Technol.*, 98 (2007): 1513-1521.
- [86] F. Rozada, M. Otero, A. Mora, A.I. Garcia, Activated carbons from sewage sludge and discarded tyres: production and optimization. *J. Hazard. Mater.*, 124 (2005) 181-191.
- [87] C. Jindarom, V. Meeyoo, B. Kitiyanan, T. Rirksomboon, P. Rangsunvigit, Surface characterization and dye adsorptive capacities of char obtained from pyrolysis/ gasification of sewage sludge. *Chem. Eng. J.*, 133 (2007) 239-246
- [88] M. Otero, F. Rozada, L.F. Calvo, A.I. Garcia, A. Moran, Elimination of organic water pollutants using adsorbents obtained from sewage sludge. *Dyes Pigments*, 57 (2003) 55-65.
- [89] M.J. Martin, M. D. Balaguer, M. Rigola, Feasibility of activated carbon production from biological sludge by chemical activation with ZnCl₂ and H₂SO₄. *Environ. Technol.*, 17 (1996) 667-671.
- [90] J.H. Tay, X.G. Che, S. Jeyaseelan, N. Graham, A comparative study of anaerobically digested and undigested sewage sludges in preparation of activated carbons. *Chemosphere*, 44 (2001) 53-57.
- [91] C.O. Ani, J.B. Parra, J.J. Pis, Effect of texture and surface chemistry on adsorptive capacities

- of activated carbons for phenolic compounds removal. *Fuel Process. Technol.*, 77-78 (2002) 337-343.
- [92] J. Przepiorski, Enhanced adsorption of phenol from water by ammonia-treated activated carbon. *J. Hazard. Mater.*, 135 (2006) 453-456
- [93] Y.B. Zhai, X.X. Wei, G.M. Zeng, D.J. Zhang, K.F. Chu, Study of adsorbent derived from sewage sludge for the removal of Cd^{2+} , Ni^{2+} in aqueous solutions. *Sep. Purif. Technol.*, 38 (2004) 191-196.
- [94] M. Sprynskyy, Solid-liquid-solid extraction of heavy metals (Cr, Cu, Cd, Ni and Pb) in aqueous systems of zeolite-sewage sludge. *J. Hazard. Mater.*, 161 (2009) 1377-1383
- [95] S. Rio, L. Le Coq, C. Faur, D. Lecomte, P. Le Cloirec, Preparation of adsorbents from sewage sludge by steam activation for industrial emission treatment *Process. Saf. Environ. Protect.*, 84(B4) (2006) 258-264
- [96] M. Seredych, T.J. Bandosz, Removal of copper on composite sewage sludge/industrial sludge-based adsorbents: the role of surface chemistry. *J. Colloid Interf. Sci.*, 302 (2006) 379-388
- [97] M.J. Martin, A. Artola, M.D. Balaguer, M. Rigola, Towards waste minimisation in WWTP: activated carbon from biological sludge and its application in liquid phase adsorption. *J. Chem. Technol. Biot.*, 77(7) (2002) 825-833.
- [98] S. Bashkova, A. Bagreev, D.C. Locke, Adsorption of SO_2 on sewage sludge-derived materials. *Environ. Sci. Technol.*, 35(15) (2001) 3263-3269.
- [99] S. Jeyaseelan, G.Q. Lu, Development of adsorbent/catalyst from municipal wastewater sludge. *Water Sci. Technol.*, 34 (1996) 499-505.
- [100] G.Q. Lu, D.D. Lau, Characterization of sewage sludge derived adsorbents for H_2S removal. *Gas Sep. Purif.*, 10 (1996) 103-111.
- [101] T.J. Bandosz, K. Block, Effect of pyrolysis temperature and time on catalytic performance of sewage sludge/industrial sludge-based composite adsorbents. *Appl. Catal. B: Environ.* 67 (2006) 77-85.
- [102] K. Kante, J. Qiu, Z. Zhao, Y. Cheng, T.J. Bandosz, Development of surface porosity and catalytic activity in metal sludge/waste oil derived adsorbents: Effect of heat treatment. *Chem. Eng. J.*, 138 (2008) 155-165.
- [103] M. Seredych, T.J. Bandosz, Sewage sludge as a single precursor for development of composite adsorbents/catalysts. *Chem. Eng. J.*, 128 (2007) 59-67.
- [104] A. Bagreev, F. Adib, T.J. Bandosz, pH of activated carbon surface as an indication of its suitability for H_2S removal from moist air streams. *Carbon*, 2001, 39: 1897-1905
- [105] A. Bagreev, T.J. Bandosz, H_2S adsorption/oxidation on materials obtained using sulfuric acid

- activation of sewage sludge derived fertilizer. *J. Colloid Interface Sci.* 252 (2002) 188-194.
- [106] A. Bagreev, T.J. Bandosz, On the mechanism of hydrogen sulfide adsorption/oxidation on catalytic carbons. *Ind. Chem. Eng. Res.* 44 (2005) 530–538.
- [107] R. Pietrzak, T.J. Bandosz, Interactions of NO₂ with sewage sludge based composite adsorbents. *J. Hazard. Mater.*, 154 (2008) 946-953
- [108] F.S. Zhang, J.O. Nriagu, H. Itoh, Photocatalytic removal and recovery of mercury from water using TiO₂-modified sewage sludge carbon. *J. Photochem. Photobiol. A: Chem.*, 167 (2004) 223-228

Chapter 2

Heterogeneous Fenton-like oxidation of Acid Orange II over sewage sludge-derived carbon-based catalysts

2.1. Introduction

It is known that water-soluble organic dyes are biorecalcitrant compounds existing in a wide concentration range in effluents from the textile and photographic industries [1,2]. In the recent years, extensive research has been made to remove this kind of organic pollutants. Among those technologies, Fenton oxidation, in which hydrogen peroxide is used as oxidant and Fe(II) ions as catalyst [3], has been proved to be very effective for the treatment of industrial wastewater containing non-biodegradable organic dyes [4,5]. During recent decades, heterogeneous Fenton and Fenton-like catalysts have attracted a great deal of interest as they exhibit wider applicable pH range and can avoid the continuous loss of catalyst compared with the homogeneous Fenton process [6,7].

Iron oxides, such as hematite (α -Fe₂O₃), goethite (α -FeOOH), magnetite (Fe₃O₄), have been widely studied as heterogeneous Fenton-like catalysts [8-10]. This kind of Fe-containing solids have been studied in detail because of their physicochemical properties and relatively cheap production [11-12]. Compared with the other iron oxides, magnetite (Fe₃O₄) is the most commonly reported as a suitable Fenton-like catalyst because of its high catalytic activity due to the existence of Fe²⁺, and its stable octahedral structure to prevent the iron leaching during oxidation reaction [13,14]. In recent years, it is reported that the catalytic activity of magnetite could be improved by immobilizing them on solid supports. Hu et al. [15] decorated nano Fe₃O₄ particles on multiwalled carbon nanotubes, and used this kind of composite catalyst for the removal of trace artificial androgen 17 α -methyltestosterone (MT) via Fenton-like reaction. The results showed that 85.9% of MT, with initial concentration of 212 μ g/L, could be removed after 8 h reaction by using 2 g/L Fe₃O₄/MWCNTs catalyst. Furthermore, this removal efficiency is about 20% higher than the same amount of bare Fe₃O₄ nanoparticles.

Many organic and inorganic materials have been used as the support for the preparation of heterogeneous Fenton-like catalyst. Among those supports, Nanofiber membrane [16,17], activated carbon [18,19], silica [20,21], Al₂O₃ [22,23], zeolite [24], clay [25] are commonly used. And in recent years, some research has been carried out to explore the applications of solid waste as support of

heterogeneous Fenton-like catalysts, such as coffee used grounds [26], rice husk ash [27], fly ash [28], red mud [29] and so on.

The solid residue formed during pyrolysis of sewage sludge is known as ‘sludge-derived char (SC)’ in the literatures [30,31]. Most of them were used as adsorbents of dyes, phenol and metals in wastewater treatment [32,33]. Recently, SC was employed as an emerging catalyst support in aqueous and gaseous reactions. For example, Fu-Shen Zhang et al. [34] used sewage sludge carbon as the support of photocatalyst TiO_2 for the removal and recovery of ionic mercury [$\text{Hg}(\text{II})$] from water. Ansari and Badosz [35] prepared H_2S adsorbents/catalysts by incorporating calcium oxide into the dried sewage sludge and waste paper mixture-based carbonization material. However, there is no report about using SC as the support of Fenton-like catalysts. Furthermore, since SC is an inorganic-organic alloyed mixture, it should have some special behaviors compared with other commonly used supports. This situation encouraged us to investigate the potential of SC as the support of heterogeneous Fenton-like catalyst. And a representative azo dye, Acid Orange II (AOII), was used as a model target pollutant in our study.

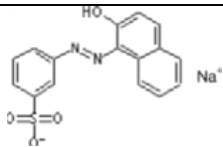
The objectives of this chapter were: (i) to synthesize and to characterize the sewage sludge-derived carbon supported iron oxide catalyst (named as FeSC); (ii) to investigate the effects of various operating parameters on the activity of the FeSC catalysts; (iii) to evaluate the mineralization of Acid Orange II (AOII), (iv) to compare the catalytic activity of FeSC with the other iron oxide catalysts and (v) considering the high ash content of SC obtained after pyrolyzed at 800°C (70wt.% [36]), to evaluate the co-catalytic effect of these inorganic components.

2.2. Experimental

2.2.1. Materials

Analytical grade of ferrous sulfate ($\text{FeSO}_4 \cdot 7\text{H}_2\text{O}$), tetraethyl orthosilicate (TEOS), anhydrous ethanol, hydrogen peroxide solution (30%, w/v), aluminum sulfate ($\text{Al}_2(\text{SO}_4)_3$), titanium(IV) oxysulfate ($\text{H}_2\text{O}_9\text{S}_2\text{Ti}$), ammonium ferrous sulfate ($(\text{NH}_4)_2\text{SO}_4 \cdot \text{FeSO}_4 \cdot 6\text{H}_2\text{O}$), silver sulfate (Ag_2SO_4), potassium dichromate ($\text{K}_2\text{Cr}_2\text{O}_7$), H_2SO_4 and NaOH were obtained from Guangzhou Chemical Reagent Company, China. Analytical grade of Fe_2O_3 , Fe_3O_4 , FeOOH , MnO_2 and commercial activated carbon prepared from coconut husk were obtained from Tianjin Kermel Chemical Reagent Co. Ltd., China. The AOII was a commercial dye (Hengrun Dyestuff Chemical Co., Ltd., Guangzhou) and used without further purification. Some properties of AOII are shown in Table 2-1 [37].

Table 2-1. Physicochemical properties of Acid Orange II

Molecular structure	Chemical Formula	Molecular weight (g/mol)	Width (Å)	Length (Å)	Depth (Å)	λ_{\max} (nm)	Solubility (g/L)	pKa
	C ₁₆ H ₁₁ N ₂ O ₄ SNa	350.32	7.3	13.6	2.3	484	100 (100°C)	11.4

Dewatered sewage sludge was obtained on June 2010, from Lie De municipal wastewater treatment plant in Guangzhou, China. Table 2-2 listed the chemical analysis results of the received sewage sludge. Pine wood sawdust was washed thoroughly with deionized water before use. Commercial activated carbon prepared from coconut husk was purchased from Tianjin Chemical Reagent Co. Ltd., China. These three kinds of precursors were dried at 105 °C to constant weight, subsequently ground and sifted through a 100-mesh sieve, and stored in a desiccator at room temperature.

Table 2-2. Analysis of sewage sludge sample

Proximate analysis			Elemental analysis				
Moisture (wt %)	Ash (wt %)	Volatiles (wt %)	C (%)	H (%)	N (%)	S (%)	
84.4	44.6	56.2	22.9	4.0	4.4	0.7	
Ash analysis (wt.%)							
Si	Al	Fe	P	Ca	K	Mg	Na
14.1	3.6	4.5	4.1	2.7	2.3	1.9	0.6
Ash analysis (mg/kg)							
Zn	Cu	Pb	Cr	Cd	Hg		
825	147	40.7	45.1	2.4	4.5		

2.2.2. Preparation of the catalysts

Two different methods were used to prepare the sewage sludge derived carbon supported iron oxide catalysts:

One method is to prepare the sewage sludge-derived carbon supported iron oxide catalyst (named as FeSC) by a “one-step method”, which combining the carbon synthesis with the Fe loading. At first, 20 g dried sludge were added into 150 mL of a ferrous sulfate solution (0.5 mol/L FeSO₄, pH = 2.5). After the suspension was stirred for 24 h, it was slowly evaporated in a rotary evaporator at 60°C under reduced pressure, and then dried at 105°C for 12 h. Subsequently, the received solid was

pyrolyzed under flowing nitrogen (40 mL/min) in a horizontal furnace at 800°C for 2 h (heating rate: 20°C/min). The pyrolyzed sample was washed several times with deionized water until the conductivity became constant in order to make sure there is no soluble iron salts anymore on the catalyst surface. Then, the sample was dried at 105°C overnight and grinded to less than 200-mesh size.

Another way was to synthesize the catalyst via a “two-step method”, where the carbonization of the sewage sludge and the iron addition were processed separately. Firstly, 20 g dried sludge were pyrolyzed at 800°C (20°C/min) for 2 h in flowing nitrogen (40 mL/min). The pyrolyzed char was named as SC. The Fe addition to SC was carried out through the classical impregnation method. 20.8 g $\text{FeSO}_4 \cdot 7\text{H}_2\text{O}$ was dissolved in the minimum amount of water and then added dropwise to the SC support. The sample was dried at 105°C overnight and finally treated in flowing N_2 at 800°C for another 2 h. It was then washed several times with deionized water, and dried overnight at 105°C and ground to less than 200-mesh.

Furthermore, the wood sawdust-based carbon supported iron oxide catalyst (labeled as FeWC) was also prepared via a “one step method” with the same procedure as Fe-SC, except that 20 g wood sawdust was mixed with 35 mL of FeSO_4 solution (0.5 mol/L, pH = 2.5).

To remove the inorganic components in sewage sludge, some activated sludge mixed liquor was obtained directly from the aeration tank of Lie De, and then was incubated for about two weeks in laboratory till the ratio of volatile suspended solids (VSS) and total suspended solids (TSS) was over 85 %. Then some suspension was filtrated and dried. The obtained bacteria powder was suspended in 0.5 mol/L HCl solution for 12 h, subsequently filtrated and washed with deionized water several times until the pH of the rinse water was about 6. The ash content of the resulted dry sludge (referred to as SS-A) was 4.31 wt%. Then the SS-A was used as precursor for catalysts preparation. Various amounts of SiO_2 and Al_2O_3 were added to the precursor. The name of the catalysts and their preparation conditions are listed in table 2-3. To synthesize SiO_2 -containing samples, fixed amounts of ethanol, TEOS and SS-A were stirred and heated at 80 °C for 2 h, then the mixture was dried at 105 °C for 12 h, and ground to fine powders (labeled as SiSS-A). After that, given amounts of FeSO_4 or/and $\text{Al}_2(\text{SO}_4)_3$ solution were mixed with SiSS-A for 24 h, then dried and pyrolyzed as described above.

To evaluate the role of carbon phase, which generated from the carbonization of sewage sludge, in the heterogeneous Fenton-like catalytic reaction, FeAlSi catalyst was also prepared without the addition of any sewage sludge.

Table 2-3. Preparation conditions for SC-A based catalysts.

Sample	SS-A (g)	TEOS (mmol)	Ethanol (mmol)	Fe (mmol)	Al (mmol)	Fe/Si/Al
FeSC-A	2.5	0	0	3.60	0	1/0/0
SiSC-A	2.5	3.60	3.60	0	0	0/1/0
AlSC-A	2.5	0	0	0	3.60	0/0/1
FeSiSC-A ₁	2.5	1.80	1.80	3.60	0	2/1/0
FeSiSC-A ₂	2.5	3.60	3.60	3.60	0	1/1/0
FeSiSC-A ₃	2.5	7.20	7.20	3.60	0	1/2/0
FeAlSC-A ₁	2.5	0	0	3.60	1.80	2/0/1
FeAlSC-A ₂	2.5	0	0	3.60	3.60	1/0/1
FeAlSiSC-A	2.5	3.60	3.60	3.60	3.60	1/1/1
FeAlSi	0	3.60	3.60	3.60	3.60	1/1/1

2.2.3. Characterization of catalysts

The average particle size was obtained on MasterSizer 2000 Particle Size Analyzer. The ash contents of catalysts were determined using a standard method according to ASTM D2866-94. The pH values of isoelectric point (pH_{IIEP}) were determined from electrophoretic mobility measurements using a zeta potential analyzer (Zetasizer Nano ZS, Malvern). The specific surface area (S_{BET}) was determined with a Nanosorb-iQ-MP gas sorption analyzer (Quantachrome Instruments, USA) by nitrogen adsorption at 77K. The chemical state of iron on catalysts were followed by X-ray diffraction (XRD) using D/max 2200 vpc Diffractometer (Rigaku Corporation, Japan) with a Cu K α radiation at 40 kV and 30 mA. Scanning electron microscopy (SEM) images were recorded using a JEOL JSM-6330F-mode Field Emission Scanning Electron Microscope equipped with an energy-dispersive X-ray (EDX) detector (JED-2300). X-ray photoelectron spectroscopy (XPS) measurements were performed using an ESCALAB 250, Thermo-VG Scientific (UK) system, with Advantage software for data acquisition and analysis. An Al K α monochromatized radiation operating at 15 kV (150 W) was used, and the spectrometer, calibrated with reference to Au 4f_{7/2} (84.0 eV), Ag 3d_{5/2} (368.3 eV) and Cu 2p_{3/2} (932.6 eV), was operated in CAE mode with 20.0 eV pass energy. Data acquisition was performed with a pressure lower than 10⁻⁷ Pa. Spectra analysis was performed using peak fitting with XPS peak 4.1 and Shirley type background subtraction. Bulk iron, alumina and silica content of the synthesized samples were measured by inductively coupled plasma optical emission spectrometry (ICP-OES, optima 5300DV, Perkin-Elmer).

2.2.4. Catalytic activity

All the batch experiments were carried out in a glass conical beaker (250ml) with a stopper shaken in a thermostatic bath at an equivalent stirring velocity around 200 rpm at 30 °C. In each run, a given amount of powder catalyst was added into 100 mL AOII solution. The solution pH was adjusted to 4.0 ± 0.1 with NaOH and H₂SO₄ during the experiments. The samples for determination of adsorption kinetics were taken at predetermined time intervals and were analyzed immediately after filtration through 0.22 μm Millipore membrane filters to remove suspended particles. After the adsorption/desorption equilibrium was established in 60 min, 60 mL suspension was used for Fenton-like reaction and initiated by adding 15mM H₂O₂ to the solution. Samples were withdrawn at a given time interval during the reaction and immediately analyzed after filtration. Each experiment was repeated thrice, the data points represent the average value and error bars indicate the standard deviation.

To investigate the lifetime of catalysts, a continuous catalytic oxidation was conducted in a novel integrated membrane-heterogeneous Fenton-like catalytic continuous reactor (MFR) designed by our laboratory. As shown in Fig. 2-1, the MFR consists of a reaction tank, a submerged membrane module, a liquid feed system, an effluent collecting system, and an air bubbling system. The reaction tank was made of polymethylmethacrylate (PMMA). An Al₂O₃ ceramic membrane with the bore diameter of 3μm was used in the submerged membrane module. Before reaction, 2.4 L AOII solution (100 mg/L), 4.8 g catalyst and 36 mmol H₂O₂ (30 % w/v) were added into the reaction tank. At the same time, two pumps start to supply AOII (100 mg/L) and H₂O₂ (1.02 % w/v) to the tank continuously. Their flow rate was controlled to be 20 mL/min and 1 mL/min respectively. And the third pump was used to control the flux speed of the effluent from the reactor. The hydraulic residence time was controlled to be 120 min. The air flow rate was kept at 5 L/min to hydraulically suspend the catalyst particles and to clean the membrane surface by the shear force of air bubble. All experiments were conducted at ambient temperature (23°C), and the pH was kept at 4.0 ± 0.1 during the reaction.

2.2.5. Analytical methods

The pH of AOII solution was measured with a PHS-3C pH meter (Rex Instrument Factory, Shanghai, China). The concentration of AOII was analyzed on UV-vis spectrophotometer (UV-3150, Shimadzu) with maximum absorbance at 484 nm. H₂O₂ was analyzed spectrophotometrically by the titanium sulfate method. The leaching concentration of Fe in the solution was measured by inductively coupled plasma optical emission spectrometry (ICP-OES, optima 5300DV, Perkin-

Elmer). The total organic carbon (TOC) of the reaction solution was measured by a TOC analyzer (Shimadzu, Japan).

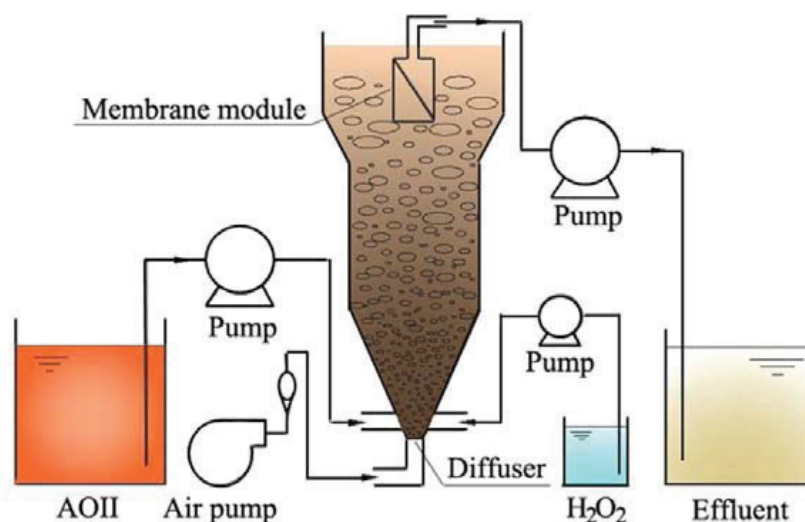


Fig. 2-1. Schematic diagram of the submerged MHFR reactor.

2.3. Results and discussion

2.3.1. Thermal analysis of sewage sludge upon pyrolysis

In order to characterize the chemical changes which take place during the pyrolysis process, a TGA-FTIR study was performed. The TG curves of SS and Fe-SS are shown in Fig. 2-2. A larger mass loss was observed on the TG curve of Fe-SS between 470 °C and 600 °C compared with that of SS. The mass loss of SS and Fe-SS ended at 550 and 600 °C, respectively. As shown on the three-dimensional (3D) diagrams obtained upon the pyrolysis of SS and Fe-SS (Fig.2-3A1 and B1), more visible peaks appeared in the 3D diagram of Fe-SS compared to SS, especially in the temperature range from 470°C to 600°C.

According to Fig. 2-3A1, Three main kind of volatile compounds were generated during the thermal treatment: H₂O (bending and stretching vibrations at 1350-1700 cm⁻¹ and 3500-3700 cm⁻¹), CO₂ (asymmetric stretching mode at 2250-2392 cm⁻¹) and C-H_n (asymmetric vibration of the methylene group at 2250-2392 cm⁻¹). While on Fig. 2-3B1, in addition to the three main products mentioned above, some extra SO₂ (asymmetric stretching vibration at 1300-1420 cm⁻¹) is observed in the 3D diagram corresponding to FeSS.

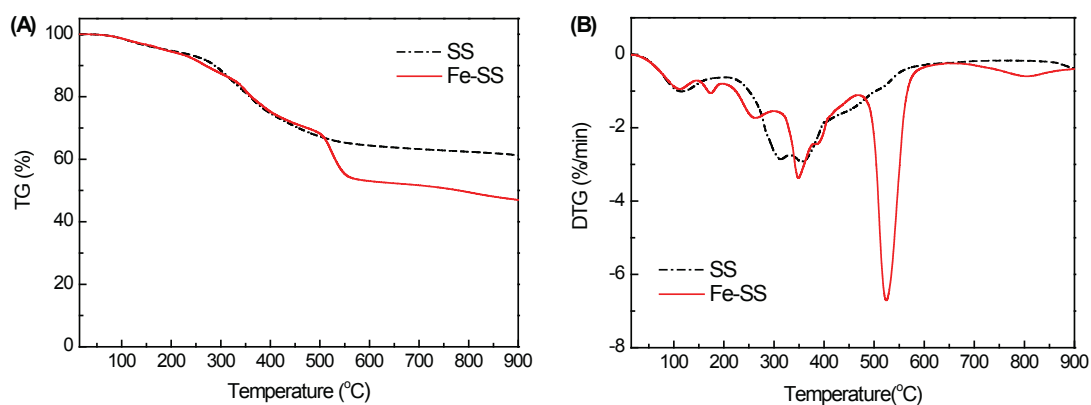


Fig. 2-2. TG and DTG curves of SS and Fe-SS (heating rate: 20°C/min, nitrogen flow rate: 40 mL/min).

To go further, the evolution versus temperature of the intensity of the bands associated to CO₂ (2359 cm⁻¹), SO₂ (1375 cm⁻¹), C-H_n (2933 cm⁻¹) and H₂O (1508 cm⁻¹) were plotted on Fig. 2-3A2 and B2. Differences in the evolution of these bands between the two samples can clearly be observed. The amount of CO₂ evolved from FeSS is much higher than that of SS. The evolution of SO₂ from FeSS is also much better defined and ends around 600°C on Fig. 2-3B2.

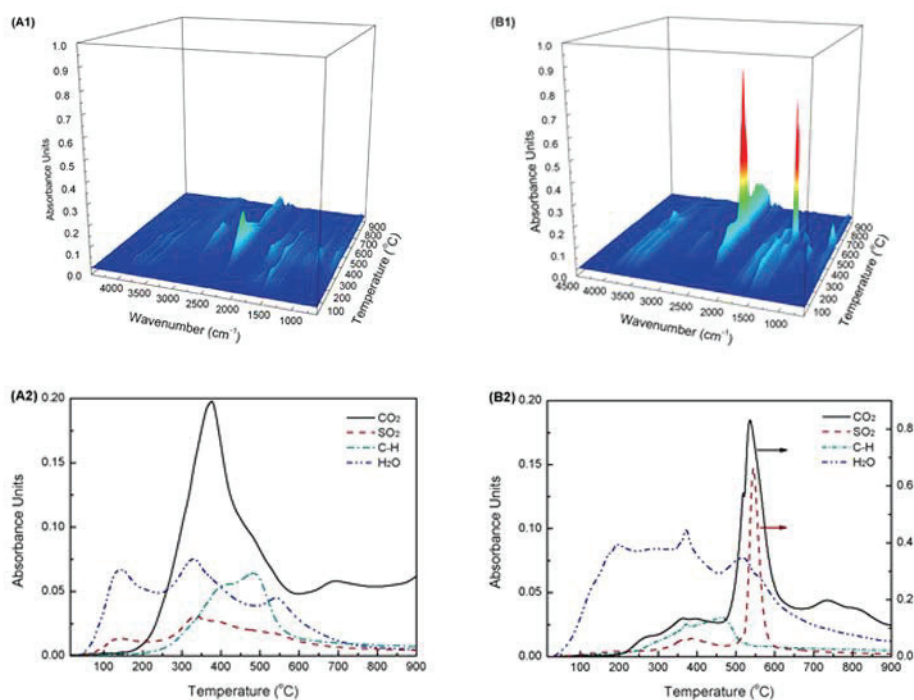


Fig. 2-3. 3D diagrams corresponding to the gases evolved from SS (A1) and Fe-SS (B1). Evolution versus temperature of the bands characteristic of H₂O (1508 cm⁻¹), SO₂ (1375 cm⁻¹), CO₂ (2359cm⁻¹), C-H_n (2933cm⁻¹) for SS (A2) and Fe-SS (B2).

It is worth mentioning that, in terms of intensities, CO₂ and SO₂ showed equivalent evolutions with temperature as shown in Fig. 2-3B2. This is because the thermal decomposition of ferrous sulfate produces SO₃, which decomposes to SO₂ and O₂ [38]. The produced O₂ reacts with the carbon support and results in the formation of CO₂. The iron sites trapped into the carbon before can then be exposed, which means that more reactive sites were accessible for the heterogeneous Fenton-like reaction.

2.3.2. Characterization of Fe-SC catalysts

The particle size distribution of SC and Fe-SC pyrolyzed at 800°C for 2h are shown in Fig. 2-4. The average particle size in volume of SC and Fe-SC are 23.0 and 27.1 μm, respectively, indicating that the amendment of iron on the SC support didn't change the particle size of the catalyst significantly.

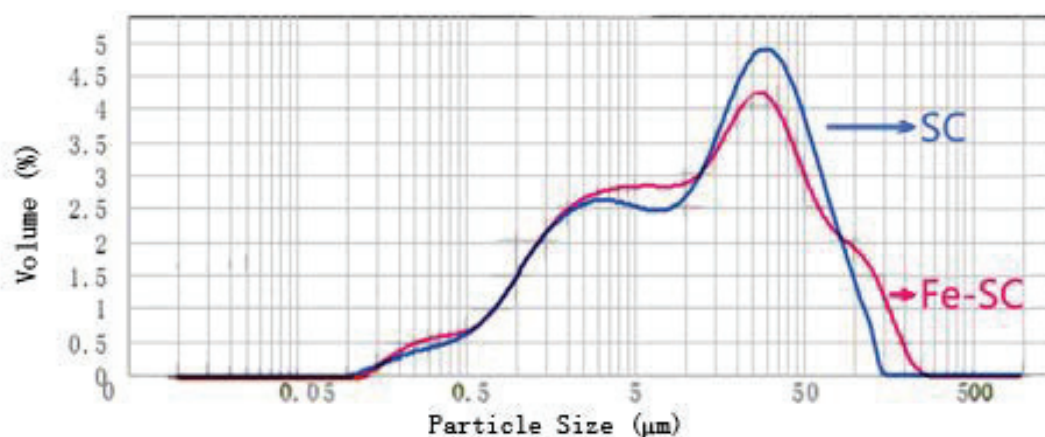


Fig. 2-4. Particle size distributions of SC and Fe-SC.

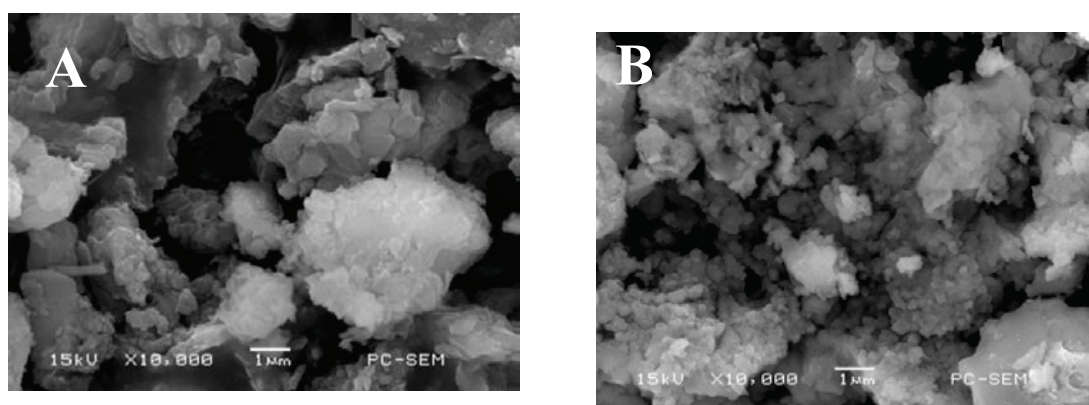


Fig. 2-5. SEM images of the SC (A) and Fe-SC (B) pyrolyzed at 800°C for 2 h

The SEM micrographs of SC and Fe-SC are shown in Fig. 2-5. Compared to SC, the surface of Fe-SC appears a little more rough. In addition, the element content (for the zone shown in Fig. 2-5)

measured by EDX was listed in table 2-4. The main elements on the surface of SC are C、O、Si and Al. Compared with SC, the Fe content on the surface of Fe-SC increased from 3.4% to 15.3% after iron impregnation.

Table 2-4. Results of EDX analysis

Element	(keV)	Mass content (wt.%)		Atom content (At.%)	
		SC	Fe-SC	SC	FeSC
C	0.277	22.1	11.9	37.1	22.9
O	0.525	27.0	21.1	34.1	30.0
P	2.013	3.2	5.4	2.1	4.0
S	2.307	1.9	2.6	1.2	1.9
Mg	1.253	0.9	1.5	0.8	1.4
Al	1.486	11.9	14.2	8.9	12.1
Si	1.739	17.8	20.1	12.8	16.5
K	3.312	1.8	3.7	0.9	2.4
Ca	3.690	2.1	4.2	0.9	2.7
Fe	6.398	3.4	15.3	1.2	6.3

Table 2-5. Physicochemical properties of SC and Fe-SC pyrolyzed at 800°C for 2h.

Sample	Fe (wt. %)	Si (wt.%)	Al (wt.%)	Ash (wt. %)	S _{BET} (m ² /g)	pH _{IEP}
SC	3.9	10.4	11.5	68.5	18.9	3.6
Fe-SC	12.9	8.4	7.5	89.6	14.3	3.4

The metal content in the SC and Fe-SC was also measured by ICP-OES (Table 2-5). Compared to the results obtained by EDX, some discrepancy was observed, this could be attributed to the inhomogeneity of sewage sludge material. However, the Fe content on the surface of Fe-SC measured by ICP-OES (12.9%), in agreement with the result obtained by EDX analysis (15.3%). Hence, it could be deduced that the iron particles are almost uniformly distributed on the SC support.

Furthermore, the Fe-SC sample was analyzed by ICP-OES. The results evidenced the presence of 0.9% Ca, 0.6% Mg, 1.5% P, 1.6% K, 0.2% Na as well as trace amounts of heavy metal such as 650 ppm Zn, 11.5 ppm Cd, 134 ppm Cu and 627 ppm Mn. As shown in Table 2-5, the ash content of SC is 74.63% and the Fe content is only 3.91%. That means the Fe in Fe-SC is mainly the added element during the preparation process of Fe-SC, while Si and Al are the native element in original sewage

sludge.

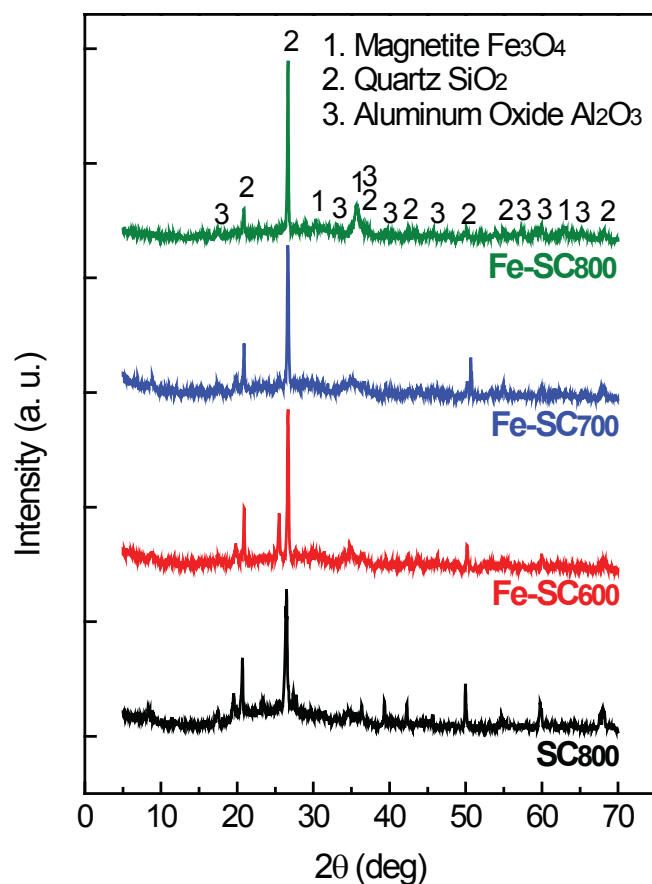


Fig. 2-6 XRD patterns of SC, Fe-SC₆₀₀, Fe-SC₇₀₀ and Fe-SC₈₀₀

The iron chemical state in Fe-SC was studied by XRD (Fig. 2-6). New broad bands at 2θ angles of 35.5° , 62.6° and 30.1° are distinctly observed by comparing the XRD pattern of Fe-SC catalyst with that of SC. These diffraction peaks are assigned to (3 1 1), (4 4 0) and (2 2 0) planes of Fe_3O_4 crystallite (JCPDS 8 8-0866), respectively [39, 40]. The oxidation state of Fe on the surface of catalysts was also characterized by XPS (Fig. 2-7). The binding energy of Fe 3p was determined to be 56.4 eV, which was ascribable to Fe_3O_4 [41]. According to the results of XRD, other elements, Si, Al, Ca and Na in the forms of SiO_2 , Al_2O_3 , CaSO_4 and NaPO_3 are also detected in FeSC. It is noteworthy that crystallographic structure of SiO_2 and Al_2O_3 are particularly more recognizable compared with other oxides due to their higher content in the bulk powder sample [42]. The average size of the crystalline particles for Fe_3O_4 is calculated to be 12.1 nm based on the Debye-Scherrer formula from XRD study.

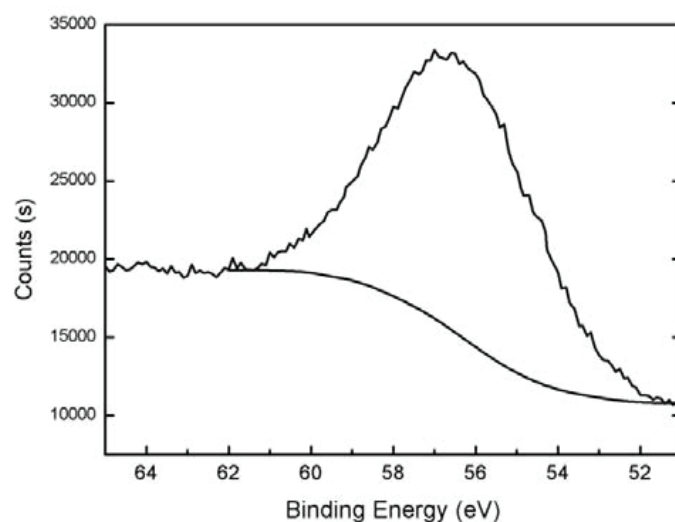


Fig. 2-7. XPS patterns of the Fe3p region for FeSC catalyst.

2.3.3. Effect of the pyrolysis temperature on the Fe-SC catalyst performances

According to the TGA-FTIR results, the pyrolysis process should finish at temperature higher than 600°C, hence 600, 700, 800 and 900°C were chosen as the maximum temperatures for the catalyst preparation. The corresponding catalysts are referred to as Fe-SC₆₀₀, Fe-SC₇₀₀, Fe-SC₈₀₀ and Fe-SC₉₀₀. As shown in Fig. 2-8A, the increase of mass loss during the pyrolysis at higher temperature, the yield of Fe-SC catalysts decreased a bit, while the ash content increased accordingly. The Fenton-like catalytic activity of Fe-SC catalysts were tested after 60 min in adsorption. When the adsorption/desorption equilibrium was established, the color removal efficiency for the four systems are 16.9%, 15.2%, 14.3% and 12.8%, respectively. While after 2 h Fenton-like oxidation, the discoloration efficiency of AOII were 90.7%, 93.5%, 97.5% and 95.6%. The results indicated that the Fe-SC₈₀₀ catalyst presented the highest catalytic activity.

As shown in Fig. 2-8B, the iron content in Fe-SC catalyst increased from 12.3% for Fe-SC₆₀₀ to 13.4% for Fe-SC₉₀₀. Hence there is more amount of iron oxide in the system for the catalyst that pyrolyzed under higher temperature, which means there are more active sites for accelerating the decomposition of H₂O₂ to generate hydroxyl radicals. Moreover, while the pyrolysis temperature increased to 900°C, the oxidation activity decreased a bit. Since the life-time for hydroxyl radical is extremely short (about 1 ns [43]), the decrease of adsorption ability and increase of iron content possibly resulted in the reactions between excess iron and hydroxyl radicals or the scavenging reaction between radicals. Hereafter the experiments will be performed on the sample pyrolyzed at 800 °C as the heterogeneous Fenton-like catalyst.

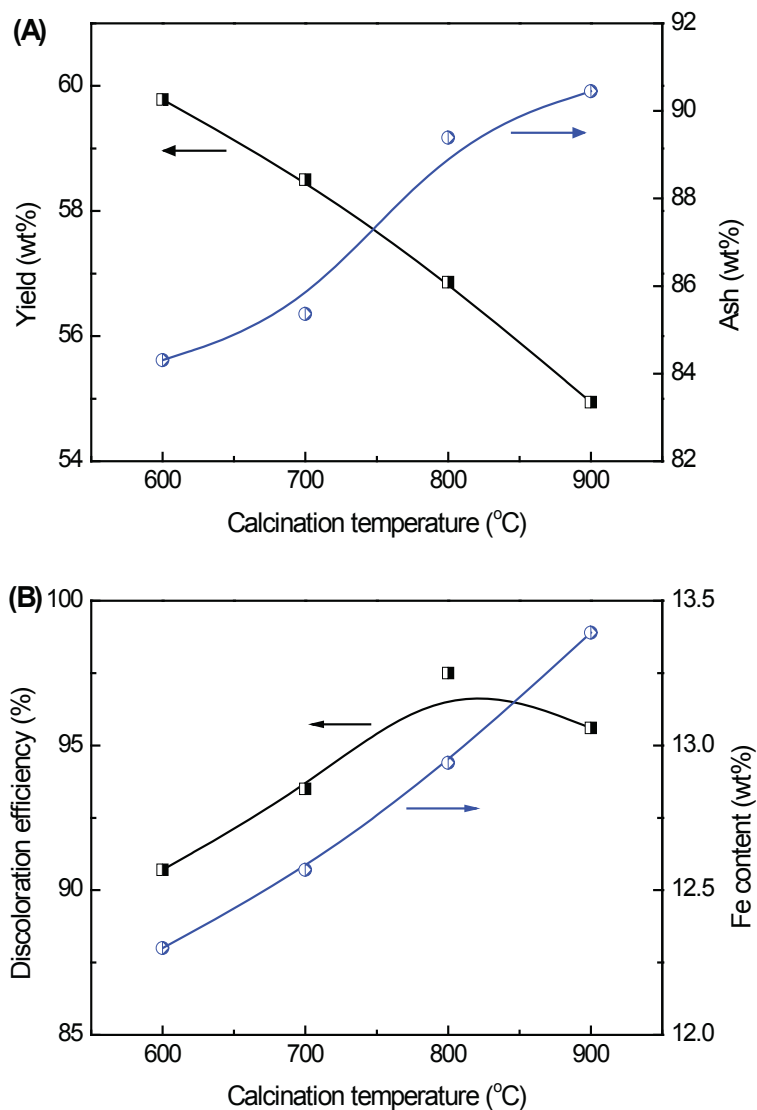


Fig. 2-8 Effect of calcination temperature on the Fe-SC production and ash content (A) and influence on the Fe content in the catalysts and the degradation efficiency of AOII (B) (Fe-SC: 2.0 g/L; H₂O₂: 15 mM; AOII: 100 mg/L; initial pH 4.0; reaction temperature: 30°C and reaction time: 120 min).

2.3.4. Effect of the preparation method on the activity of catalyst

The Fe content in Fe/SC prepared via “two-step” method was determined to be 14.2% by ICP-OES, the average particle size in volume of Fe/SC is 26.6 μm, pI_{IEP} is 3.8 and the BET surface area is 13.3 m²/g, which are quite similar to that of Fe-SC.

The heterogeneous Fenton-like catalytic activity of Fe-SC and Fe/SC was firstly compared by batch experiments. After 60 min in adsorption, the 14.3% and 19.7% of AOII were removed in Fe-SC and Fe/SC system, respectively. The degradation efficiency of AOII catalyzed by Fe-SC and Fe/SC

located at 97.5 % and 98.8% after oxidation for 2 h. Therefore, these two systems presented the similar catalytic activity. At the end of reaction, 0.373 and 1.223 mg/L leached iron were detected in Fe-SC and Fe/SC catalytic system, the later was about twice higher than the former.

The preliminary evaluation of the stability of these two kinds of catalysts was evaluated by AOII degradation in the integrated membrane-heterogeneous Fenton-like catalytic continuous reactor (MHFR). Fig. 2-9A shows the discoloration change of AOII with operation time in the continuous MHFR. For catalyst Fe/SC, the AOII concentration in the effluent decreased rapidly during the initial 210 min, reaching round 96.6% removal efficiency. But an increasing loss of activity was observed as the reaction went on. While, for Fe-SC system, the AOII removal rate could be kept around 97% at 600 min, indicating that FeSC presents both a high catalytic activity and a long-term stability.

To find out the reason for the observed activity decay of Fe/SC, the turbidity values of the effluent were measured. The results showed that the turbidity values of the permeate water were kept below 0.300 NTU, which means the continuous MHF reactor could intercept the catalysts and the running off particles in the effluent were negligible. So the most possible cause of deactivation of Fe/SC was the loss of Fe from the catalyst by leaching. As shown in Fig. 2-9B, the concentration of the leached Fe from Fe/SC decreased after 210 min which led to the both of homogeneous and heterogeneous Fenton reactions activity decay, this result was in agreement with the dye degradation performances of Fe/SC shown in Fig. 2-9A. On the other hand, the iron leaching of Fe/SC showed slightly higher than Fe-SC (Fig. 2-9B), about 1.74 times from the beginning to 210 min by integrating. The activity of the leached iron could, in part, explain the better performance of Fe/SC than Fe-SC at the initial 210 min. The Fe leaching could attribute to the coordination effect of organic acid generated during the degradation of Orange II, as observed for other solid Fenton-like catalysts [44]. For Fe/SC, the iron particles were anchored to the surface of the supporter, while for Fe-SC, most of the iron salts particles were immobilized within the supporter. So the coordination effect could happen more easily to Fe/SC than Fe-SC. These results confirm that the direct synthesis by incipient impregnation allows Fe particles to be incorporated into the sewage sludge-based carbon framework more strongly bonded than by the classical impregnation method. Therefore, it seems that Fe-SC can avoid iron lost from the support better than Fe/SC, and show a long-term stability for application in industry. Thus, the subsequent runs will consequently be carried out using the best sample: the Fe-SC catalyst.

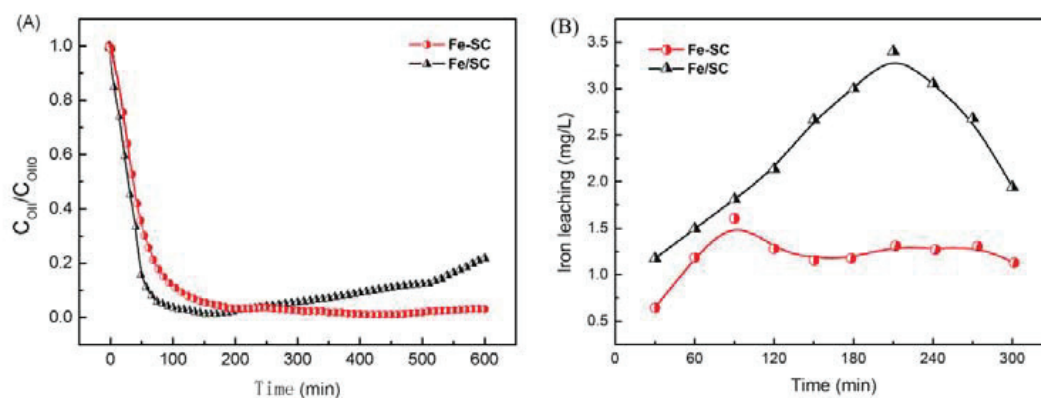


Fig. 2-9. Effect of consecutive experiments with the Fe-SC and Fe/SC catalysts on the degradation of AOII solution (A) and iron leaching (B) (Catalysts: 2.0 g/L; H₂O₂: 15 mM; Orange II: 100 mg/L; reaction temperature: 23°C; total volume of reaction solution: 2.4 L and residence time: 120 min).

2.3.5. Influence of the experimental conditions in the Fe-SC catalysts performance

2.3.5.1. Effect of hydrogen peroxide concentration

The reaction between AOII and H₂O₂ could be written as Equation (2-1):



According to this chemical formula, when the initial concentration of AOII was 100 ppm, the theoretically concentration of H₂O₂ should be 12 mM. Thus, in this study, the concentration of H₂O₂ was varied from 9 mM to 18 mM, and the removal efficiency of AOII in the oxidation process as a function of reaction time were displayed in Fig. 2-10. The reaction performance increased when the amount of H₂O₂ increased from 9 to 15 mM, because more radicals are formed. However, a bit decline was observed for a higher concentration at 18 mM, due to the well-known hydroxyl radicals scavenging effect as shown below [45,46]:



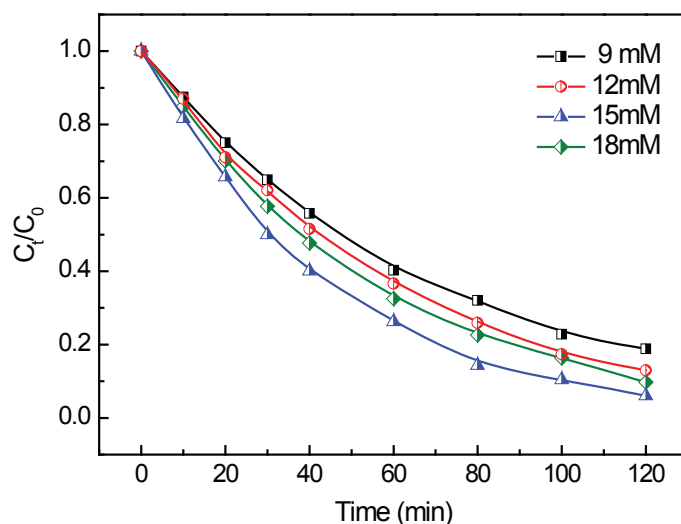


Fig. 2-10 Effect of hydrogen peroxide concentration on the discoloration of AOII (Fe-SC: 2.0 g/L; AOII: 100 mg/L; initial pH 4.0; reaction temperature: 30°C)

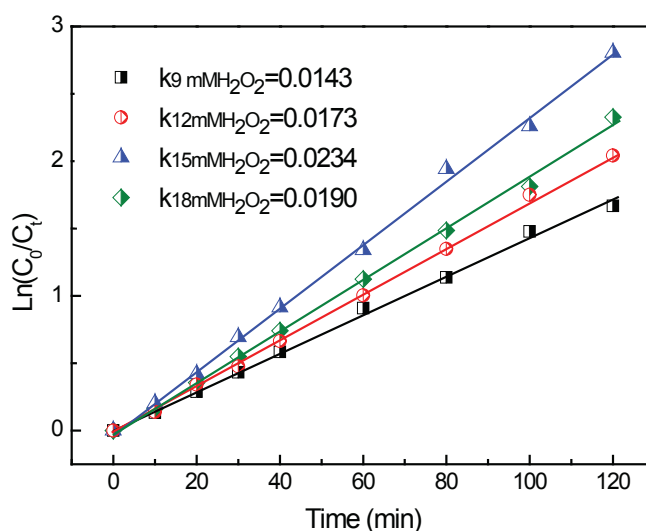


Fig.2-11. Effect of hydrogen peroxide concentration on Pseudo-first-order rate constants for OA II discoloration

The pseudo first-order kinetic model (Equation 2-5), which has been widely applied in the literature for the description of the heterogeneous Fenton oxidation of organic pollutants [47,48], was used to calculate the apparent rate constant (k_{app}) of the AOII degradation when using different amount of H_2O_2 .

$$\ln \frac{C_0}{C_t} = k_{app} t \quad \text{(Equation 2-5)}$$

As shown in Fig. 2-11, the highest AOII degradation efficiency for the Fenton-like reaction system was achieved when 15 mM H₂O₂ was used. Therefore, the concentration of H₂O₂ will be controlled at 15 mM in the subsequent runs.

2.3.5.2. Effect of initial concentration of AOII

The influence of the initial concentration of AOII in solution on the degradation of AOII upon Fenton-like reaction over Fe-SC was studied. From Fig. 2-12, it can be seen that the pseudo-first-order degradation rate constant of AOII decreased when the initial concentration of AOII increased from 25 to 200 mg/L.

This behavior could be plausibly explained as follows: more AOII molecules were adsorbed on the Fe-SC surface as the initial concentration of AOII increased, while the amount of H₂O₂ used in this study was constant. Consequently, the relative probability of an •OH attacking an AOII molecule decreased, inducing a decrease in the AOII degradation efficiency.

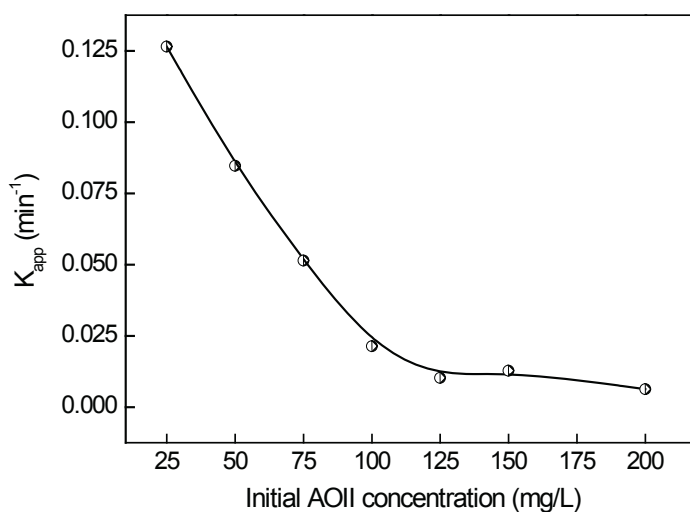


Fig. 2-12. Effect of initial concentration of AOII on the apparent rate constant (Fe-SC: 2.0 g/L; H₂O₂: 15 mM; initial pH 4.0; reaction temperature: 30°C).

2.3.5.3. Effect of reaction temperature

Reaction temperature has been found to be a critical parameter to influence the activity of Fenton-like catalyst. In this study, the changes in the degradation rate of AOII as a function of the applied temperature (range from 20 to 60°C) were monitored. And the apparent rate constant (k_{app}) of the

AOII degradation was obtained by fitting the results with pseudo first-order kinetic equation. As shown in Fig. 2-13, the increase in temperature had a beneficial effect for the AOII degradation.

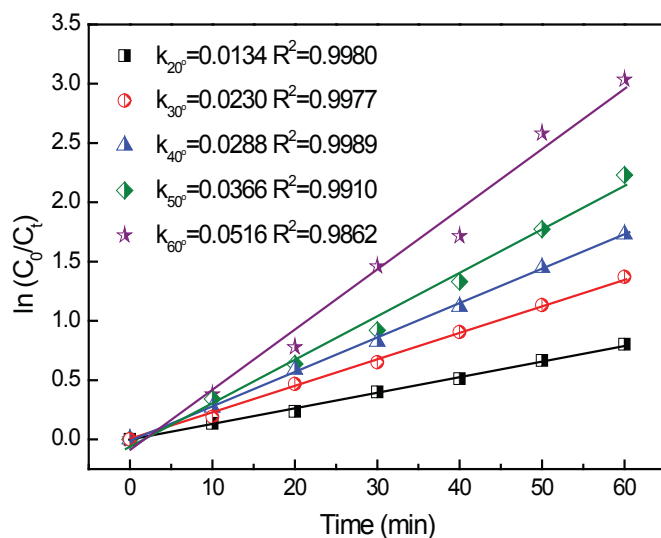


Fig. 2-13. Effect of the reaction temperature on the pseudo-first-order rate constants for AOII degradation (Fe-SC: 2.0 g/L; H₂O₂: 15 mM; AOII: 100 mg/L; initial pH 4.0; reaction temperature: 30°C).

The Arrhenius law was used to calculate the activation energy, Ea:

$$K_{abs} = A \exp\left(-\frac{Ea}{RT}\right) \quad (\text{Equation 2-6})$$

where K_{abs} is the kinetic rate, A is the preexponential factor, T is the absolute temperature (K), R is the gas constant.

The linear form of Arrhenius law could be expressed as:

$$\ln(K_{abs}) = \ln(A) - \frac{Ea}{RT} \quad (\text{Equation 2-7})$$

The logarithm of K_{abs} was plotted versus the reciprocal of temperature, and the slope of the curve was used to determine the activation energy. As shown in Fig. 2-14, the dependence of the kinetic constant on the reaction temperature evidences the Arrhenius behavior, with activation energy of 25.8 kJ/mol. The Ea values for usual chemical reaction varied from 40 to 400 kJ/mol [49]. The low value of the activation energy confirms the very high efficiency and suitability of FeSC as a heterogeneous Fenton-like catalyst.

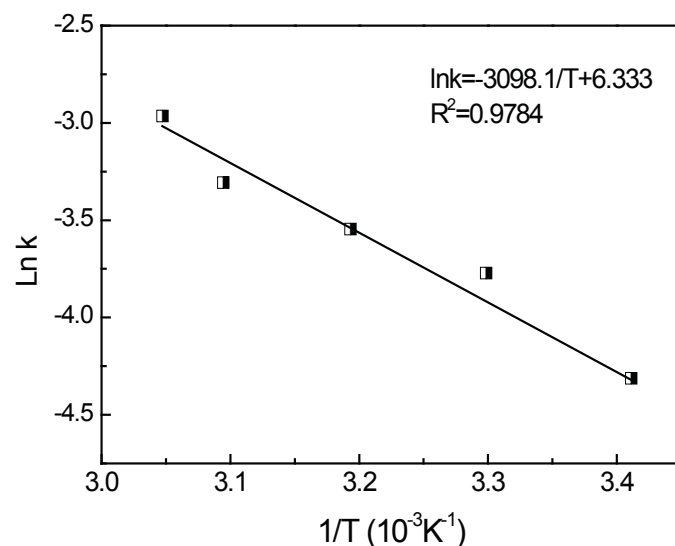


Fig. 2-14. Arrhenius plot of AOII degradation

2.3.5.4. Influence of initial solution pH

The removal of azo dye, catalyzed by Fe-catalysts, was a pH-dependent process [50,51], so the effect of the initial solution pH was studied. As shown in Fig. 2-15A, after 120 min reaction, over 97.5% AOII was transformed at pH 3.0, 94.0% at pH 4.0, 31.4% at pH 5.0 and 14.9% at pH 6.0. These results indicate that the higher the initial solution pH is, the slower the reaction rate is. The lower performances of the Fe-SC catalyst at high pH can be attributed to a decrease in the production of radical oxidants capable of reacting with AOII. Jing Guo et al. pointed out that at neutral pH the decomposition of H₂O₂ predominately leads to O₂ which is not able to oxidize the organics under the mild operating conditions of this study [51].

The iron leaching from the catalyst was also checked all along the experiments. As shown in Fig. 2-15B, the iron concentration in solution was 2.2 and 0.4 mg/L after 1 h adsorption and 2 h oxidation at pH 3.0 and 4.0, respectively. When the initial pH were 5.0 and 6.0, the leached iron were less than 1.0 mg/L during all the reaction. The leaching of Fe at pH 3.0 is not desirable since it is higher than the EU discharge limits (<2 ppm). In conclusion, the optimal initial solution pH was 4.0, since the AOII removal efficiency was as high as at pH 3.0 but the iron leaching was lower. It is worth mentioning that the amount of iron lost from the Fe-SC catalyst, even at pH 3.0 is only 1.1% of the total iron content initially incorporated in the catalyst, significantly lower than in the case of the Fe/active carbon prepared by classical incipient wetness impregnation (ca. 2.6 wt. %) [39].

Considering the complexity of sewage sludge, the concentrations of the other metals in the filtrate from FeSC system with initial pH 4.0 were detected by ICP-OES. Except for Fe, little amount of Ca,

Mg, Cu and Zn were also detected in the filtrate, their concentrations were 0.813 mg/L, 0.271 mg/L, 0.029 mg/L and 0.027 mg/L, respectively. And the concentrations of Cr, Mn, Ni and Pb were below the detection limit of ICP-OES. In these conditions some, although relatively low, contribution of aqueous catalytic reaction may take place. To determine the influence of homogeneous phase reaction, 2.0 g/L Fe-SC catalyst was added into deionized water with initial pH 4.0, and shaken for 3 h. After that the filtrate was used to prepare 100 mg/L AOII solution, and 15 mM H₂O₂ was added. When the homogeneous experiment was carried out for 120 min, the discoloration efficiency of AOII were only 7.3%. This result suggests that degradation of AOII for the Fe-SC based Fenton-like system could mainly be attributed to heterogeneous process, not homogeneous phase reaction.

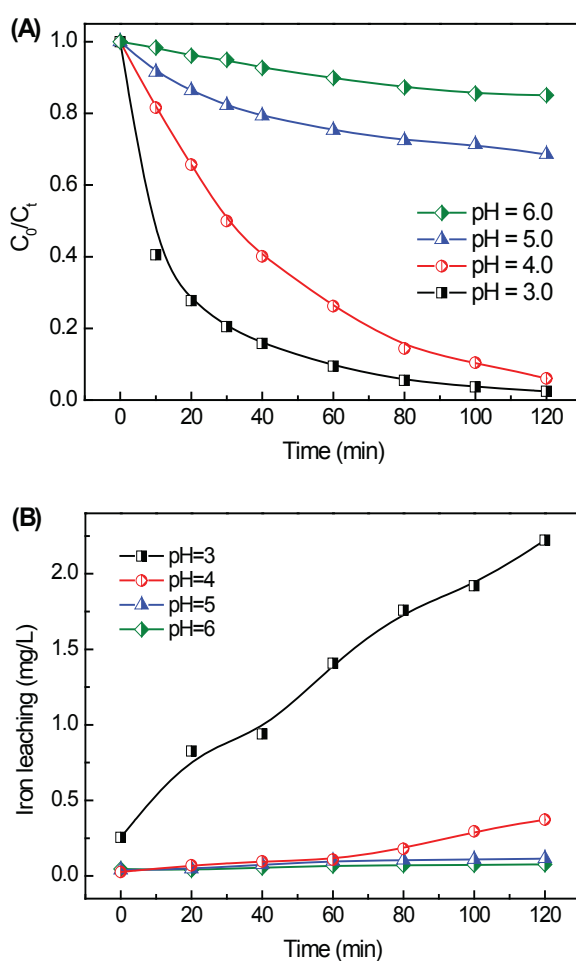


Fig. 2-15 Effect of initial solution pH on the degradation of AOII and on the iron leaching (Fe-SC: 2.0 g/L; H₂O₂: 15 mM; AOII: 100 mg/L; reaction temperature: 30°C)

2.3.6. Mineralization of AOII

Fig. 2-16 shows the UV–Vis spectral changes of AOII in the Fenton-like degradation process. The peaks at 310, 228, and 254 nm are assigned to the aromatic rings in AOII molecule, and the peaks at 484 and 430 nm are assigned to the conjugated structure formed by the azo bond [52]. As the reaction proceeded, the three characteristic absorption peaks decreased dramatically and almost disappeared after 120 min, indicating that the chromophore and conjugated π^* system were completely destroyed. On the other hand, it is known that complete discoloration of AOII does not mean that the dye is completely oxidized. Hence, the mineralization of AOII, in terms of COD removal, was investigated in parallel time. As shown on Fig. 2-16, the COD removal remarkably increases as the reaction time goes on, reaching 73.6% COD removal at the end of the reaction. Compared with the 96.7% AOII removal, it can be seen that the mineralization of AOII is slower than the discoloration. This is due to the fact that some partially-oxidized refractory intermediates are generated upon the AOII degradation [53]. The results shown in Fig. 2-16 also indicate that Fe-SC as a heterogeneous Fenton-like catalyst can lead to a fast discoloration of AOII as well as a remarkable mineralization degree of the solution.

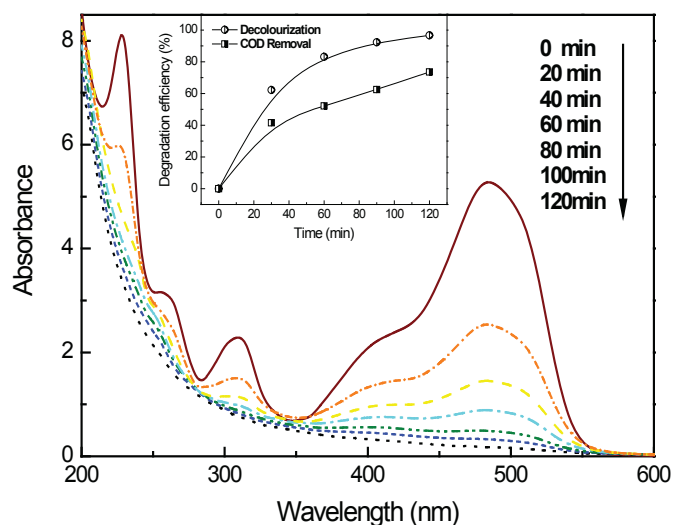


Fig. 2-16. The UV–vis spectral changes of AOII (Fe-SC: 2.0 g/L; H₂O₂: 15 mM; AOII: 100 mg/L; initial pH 4.0 and reaction temperature: 30°C), inset: corresponding decolorization and COD removal efficiency.

2.3.7 Comparison of the catalytic activity of Fe-SC with other catalysts

In order to more clearly understand the catalytic activity of Fe-SC, we carried out comparable experiments between FeSC catalyst and other three heterogeneous Fenton-like catalysts mentioned

frequently in references, α -Fe₂O₃, Fe₃O₄ and γ -FeOOH. This comparison was based on the identical amount of iron and carried out under identical conditions. As shown in Fig. 2-17, the degradation efficiency of the three iron–oxygen series of compounds were very low, only 3.4% for α -Fe₂O₃, 4.7% for Fe₃O₄ and 23.5% for γ -FeOOH were observed after adsorption for 60 min and oxidation for 120 min, respectively. It is obviously that Fe-SC system has the highest discoloration efficiency.

There are many reasons for the better catalytic performance of the Fe-SC system compared to the other iron oxides. Firstly, the porous carbon matrix in the SC can facilitate the adsorption of dyes. Secondly, some inorganic components in the SC support (SiO₂ and Al₂O₃) may also act as co-catalysts in the degradation of AOII upon the heterogeneous Fenton-like process. Therefore, it can be deduced that SC is a favorable Fenton-like catalyst support for the degradation of AOII.

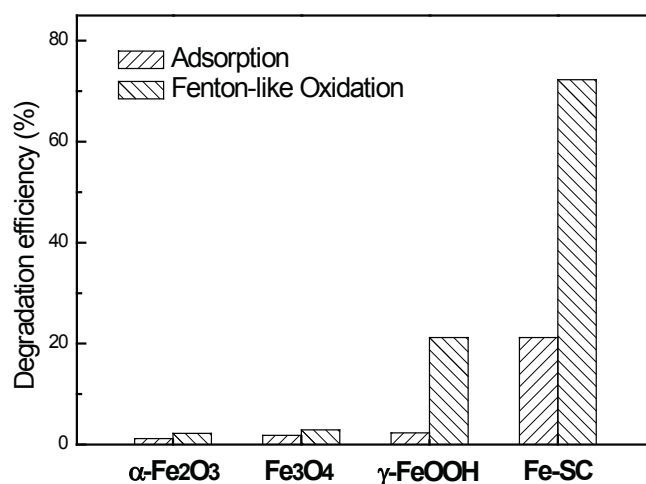


Fig. 2-17. Comparison of the adsorption and heterogeneous Fenton-like catalytic activity by using various compounds (the iron concentrations are all 0.258 g/L; H₂O₂: 15 mM; AOII: 100 mg/L; reaction temperature: 30°C, adsorption for 60 min and Fenton-like oxidation for 120 min).

2.3.8. Co-catalytic effect of inorganic components in SC

2.3.8.1. Characterization of FeWC catalyst

To further investigate the effect of inorganic components in FeSC on the catalytic performance in Fenton-like reaction, another kind of biomass material with low ash content, wood sawdust, was used as catalyst support for comparison. The main physicochemical parameters of FeWC and its corresponding support (WC) are listed in Table 2-6. The Fe content of FeWC is similar to that of FeSC, however, FeWC is almost free of Si and Al elements. The BET surface area of FeWC is a little

smaller than that of FeSC. As shown in Fig. 2-18, the surface morphology of FeWC presents in the form of plates which come from the carbonization of the cellulosic materials with small particle size iron oxide dispersed on them, while FeSC presents a more heterogeneous appearance.

Table 2-6. Physicochemical properties of WC and FeWC.

Sample	Fe (wt %)	Ash (wt %)	\bar{d}_v^a (μm)	S_{BET} (m^2/g)	pH _{IEP}
WC	0.5	4.6	29.6	10.4	3.1
FeWC	16.2	26.3	26.7	12.1	3.1

^a \bar{d}_v : volume average particle diameter

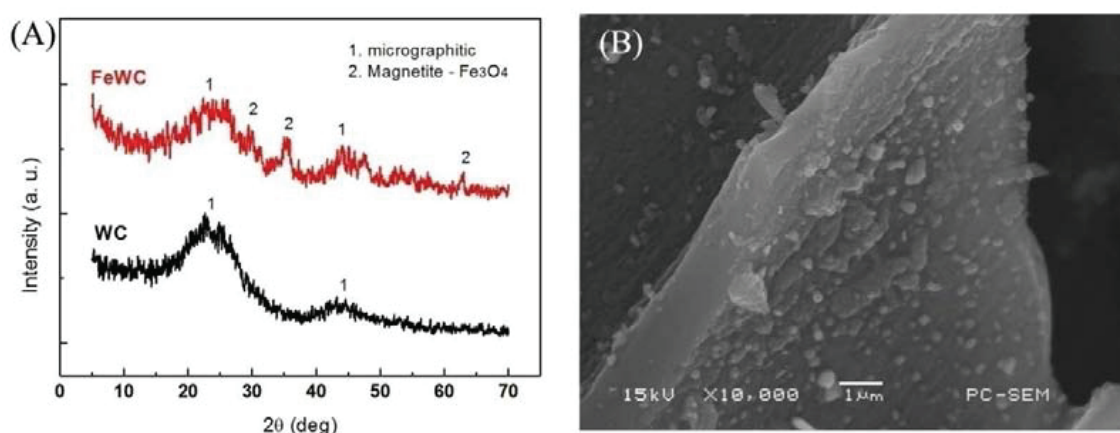


Fig. 2-18. XRD patterns of WC and FeWC (A) and SEM image of FeWC (B).

2.3.8.2. Comparison of the catalytic activity of FeSC and FeWC

In order to understand the catalytic potential of FeSC more clearly, a comparative Fenton-like experiment was performed with FeWC. As shown in Fig. 2-19, removal efficiency of AOII in adsorption phase is 21.9% and 17.8% for FeSC and FeWC system, respectively. This can be explained by the lower BET surface area of FeWC. And the degradation efficiency of AOII catalyzed by FeSC locates at 94.6% after oxidation for 2 h., which is only 66.2% for FeWC system. The apparent rate constants (k_{ap}) of AOII degradation were obtained by fitting the results from 60 min to 180 min showed in Fig. 2-19 with pseudo first-order kinetic equation. As shown in table 2-7, very high and good correlation coefficients (R^2) were gotten, meaning there is good linear correlation between $\ln(C_0/C_t)$ and time. The k_{ap} for FeSC system was calculated to be $22.45 \times 10^{-3} \text{ min}^{-1}$, while that for FeWC system was only $7.31 \times 10^{-3} \text{ min}^{-1}$, the former was about 2 times higher than the later. Since the contents and existence forms of Fe in FeSC and FeWC are similar, the difference of their

catalytic activities is possibly dependent on non-iron inorganic components co-existing in them.

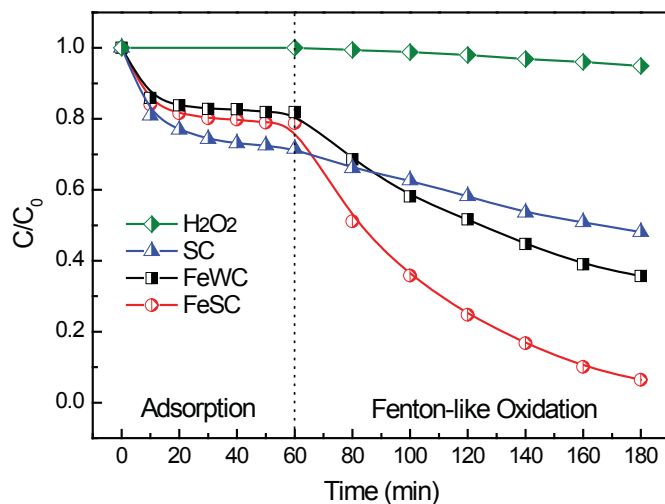


Fig. 2-19. Degradation of AOII through adsorption and oxidation by hydrogen peroxide and different catalysts (Catalysts: 2.0 g/L; H₂O₂: 15 mM; AOII: 100 mg/L; reaction pH: 4.0±0.1; reaction temperature: 30°C).

Table 2-7. Discoloration of AOII with H₂O₂ in the presence of different catalysts.

Sample	Discoloration efficiency of AOII (%)		Pseudo first-order model parameters	
	By adsorption, t = 60 min	By oxidation, t = 180 min	kap ($\times 10^{-3} \text{ min}^{-1}$)	R ²
H ₂ O ₂	0	5.1	0.44	0.9850
SC	26.9	48.8	2.98	0.9973
FeSC	22.8	94.6	22.45	0.9972
FeWC	17.8	66.2	7.31	0.9987
SC-A	5.0	11.2	0.57	0.9975
FeSC-A	19.8	51.3	4.21	0.9875
SiSC-A	2.8	8.6	0.63	0.9964
AlSC-A	6.6	14.8	0.81	0.9904
FeSiSC-A ₁	14.2	59.8	6.00	0.9804
FeSiSC-A ₂	13.8	68.8	8.44	0.9885
FeSiSC-A ₃	13.4	80.5	12.41	0.9765
FeAlSC-A ₁	22.1	65.7	6.71	0.9988
FeAlSC-A ₂	39.7	77.7	8.17	0.9870
FeAlSiSC-A	34.8	89.9	15.11	0.9917
FeAlSi	8.5	39.6	3.39	0.9977

2.3.8.3. Co-catalytic effect and mechanism of inorganic components in SC

To further investigate the effect of inorganic components in FeSC on the catalytic performance in Fenton-like reaction, the inorganic components of sewage sludge was firstly removed and then the remainder was used as precursor (SS-A) for SC-A and FeSC-A preparation. The physicochemical data of the prepared SC-A and FeSC-A are presented in Table 2-8. The ash content of SC-A and FeSC-A are only 10.02 % and 39.97 %, much lower than that of FeSC, and the Al and Si contents are at micro level. Then the catalytic behavior of SC-A and FeSC-A was also evaluated in the presence of H₂O₂ at pH 4.0 (See curve B and C in Fig. 2-20). After 1 h adsorption and 2 h oxidation, the discoloration efficiencies of AOII are 11.2 % and 51.3 % for SC-A and FeSC-A, much lower than the 94.6 % removal efficiency obtained with the FeSC catalyst. The pseudo first-order degradation kinetic constant for FeSC-A system is calculated to be $4.21 \times 10^{-3} \text{ min}^{-1}$ (As shown in Table 2-8), which is also less than that for FeSC. This experimental result further indicates that the inorganic components in the SC have co-catalytic effect on the degradation of AOII in heterogeneous Fenton-like process.

Table 2-9. Physicochemical properties of different catalysts.

Sample	Fe (wt %)	Al (wt %)	Si (wt %)	Ash (wt %)	S _{BET} (m ² /g)	Zeta potential at pH _{IEP} pH 4.0 (mV)	pH _{IEP}
SC-A	1.50	0.13	2.50	10.02	13.7	-17.16	3.13
FeSC-A	19.45	0.06	1.21	39.97	21.1	-16.84	3.21
SiSC-A	0.93	0.08	13.68	39.32	12.2	-26.44	2.64
AlSC-A	0.82	9.66	1.29	28.65	18.3	-11.81	3.51
FeSiSC-A ₁	20.38	0.07	6.31	48.89	19.2	-20.15	3.06
FeSiSC-A ₂	19.53	0.06	11.09	49.92	16.5	-21.46	2.94
FeSiSC-A ₃	18.43	0.06	16.28	55.42	13.1	-24.53	2.37
FeAlSC-A ₁	17.24	4.04	1.07	44.92	15.8	-8.16	3.56
FeAlSC-A ₂	16.83	7.88	1.04	45.99	21.9	-0.85	3.82
FeAlSiSC-A	15.92	7.45	8.70	55.03	17.3	-10.74	2.98
FeAlSi	29.81	14.40	15.01	90.35	6.1	4.12	5.24

As mentioned previously, except for Fe the other inorganic elements in SC are mainly Si and Al, which exist in the forms of SiO₂ and Al₂O₃ confirmed by XRD (Fig. 2-6). Their contents in SC are

calculated to be 22.14 % and 16.09 % , respectively, being 73.46 % of total non-iron inorganic components. In other words, the co-catalytic effect of SC compared with WC is possibly mainly originated from the SiO₂ and Al₂O₃. In order to understand the enhancement mechanism, a series of Fe-loaded sewage sludge carbon with various SiO₂ and Al₂O₃ content as Fenton-like catalysts were prepared by employing the SS-A as precursor, their physicochemical properties are listed in Table 2-9, and their catalytic activities were also determined, respectively. As shown in Table 2-9, all the modified SS-A based catalysts present low BET surface area (less than 25.0 m² / g), and the values are very close to each other.

Before comparing the activity of silica and/or alumina incorporated iron-containing catalysts, two blank runs were performed to evaluate the ability of SiSC-A and AlSC-A to oxidize AOII in aqueous solutions in the presence of H₂O₂. Only 8.6 % and 14.8 % AOII removal was observed by these two kinds of Fe free catalysts through adsorption and oxidation processes under the same conditions as mentioned above. That means neither SiSC-A nor AlSC-A exhibits any considerable catalytic activity towards the degradation of AOII by H₂O₂.

The change of the AOII discoloration rate with the various contents of SiO₂ in catalyst support is presented in Fig. 2-20A. The comparison was based on the identical amount of iron. It is found that increase of degradation rate is followed by the order of FeSiSC-A₃ > FeSiSC-A₂ > FeSiSC-A₁ > FeSC-A, which is consistent with that of SiO₂ content. The changes of H₂O₂ concentration in the liquid phase during the experiments (Fig. 2-20B) follow a parallel trend to the AOII oxidation: a better performance is reached when the content of SiO₂ in the FeAlSiSC-A catalysts increased. The results further confirm that co-catalytic effect of SC partly originates from SiO₂-like inorganic component in it. There are several possible explanations for the co-catalytic effect of SiO₂. Firstly, H₂O₂ can adsorb on SiO₂ by hydrogen bonds with the oxygen in siloxane bridges, Si-O-Si [54] (Fig. 2-21A), leading to a higher concentration of H₂O₂ on surface of FeSC than that in the bulk solution and hence facilitating Fenton-like reaction. Except for siloxane, there is another kind of functional group on the silica surface, silanol (Si-OH) [55], which undergoes protonation when the pH values are lower than the p_{HIEP} of SiO₂ and deprotonation at pH > p_{HIEP} [56,57]. The p_{HIEP} value of SiO₂ is widely reported at 2.0-3.5 [57,58], lower than the solution pH in our experiments. Therefore, H⁺ has an obvious tendency to release from Si-O-H, and result in the formation of negative charge SiO₂ particles and an acidic microenvironment near the catalyst surface [59], as shown in Fig. 2-21B. This explanation can be partly evidenced by the different zeta potential at pH 4.0 of SiO₂-containing catalysts that are presented in Table 2-8, the surface charge became more negative when the content of SiO₂ increases. It is known that low pH favors •OH generation and •OH has higher oxidation potential at pH around 3.0 than that in less acidic solution [60]. Hence it is possible that the insertion

of SiO₂ can facilitate the adsorption of H₂O₂ on the catalyst surface and increase the activity to generate •OH.

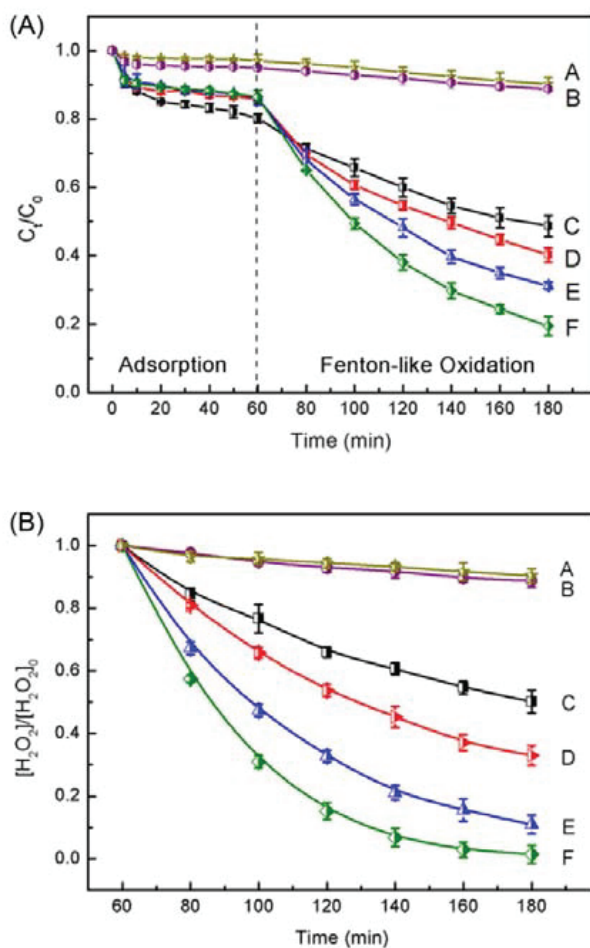


Fig. 2-20. Effect of SiO₂ content in FeSC on AOII removal (A) and H₂O₂ consumption (B) (the iron concentrations are all 0.2588 g/L: (A) SiSC-A: 1.6085 g/L, (B) SC-A: 1.2882 g/L, (C) FeSC-A: 1.3306 g/L, (D) FeSiSC-A₁: 1.2699 g/L, (E) FeSiSC-A₂: 1.3251 g/L, (F) FeSiSC-A₃: 1.4042 g/L; H₂O₂: 15 mM; AOII: 100 mg/L; reaction pH: 4.0±0.1; reaction temperature: 30°C).

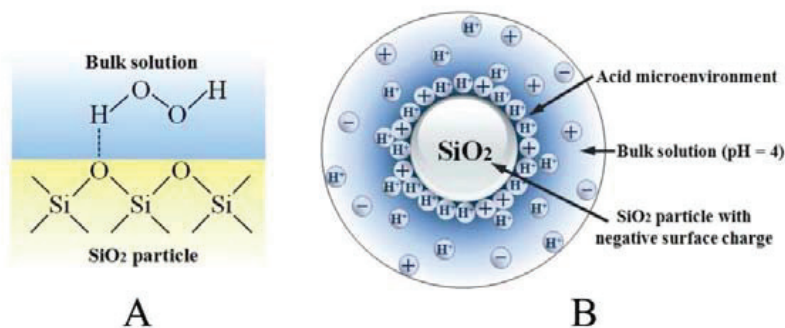


Fig. 2-21. H₂O₂ adsorb over siloxane by hydrogen bonds (A) and acidic microenvironment form near the surface of SiO₂ particle (B).

The role of alumina phase in iron-containing sample as heterogeneous Fenton-like catalyst was also investigated. As shown in Fig. 2-22, the removal efficiency of AOII after the preliminary adsorption process is 21.1 % for FeAlSC-A₁, 39.7 % for FeAlSC-A₂ and 18.2 % for FeSC-A. The different adsorption capacities can be correlated with the different BET surface area values and different zeta potential of these three catalysts as shown in Table 2-8. The p*H*_{IEP} values of Al₂O₃ and SC-A are located at 8.5-10.4 [57] and 3.13, thus the insertion of Al₂O₃ will lead to an increase in p*H*_{IEP} of the particle, and presents less negative charge, which can facilitate the adsorption of sulfonic dye numerator by electrostatic phenomena. In consideration of AOII discoloration, the increase in the content of Al₂O₃ also resulted in a higher AOII degradation efficiency. The pseudo first-order kinetic constant of AOII oxidation are determined to be $6.71 \times 10^{-3} \text{ min}^{-1}$ for FeAlSC-A₁ and $8.17 \times 10^{-3} \text{ min}^{-1}$ for FeAlSC-A₂, respectively. As mentioned before, the surfaces of FeAlSC-A catalysts are much less negatively charged than that of FeSiSC-A catalysts. Therefore, the p*H* in microenvironment around the Al₂O₃ particles is almost neutral and not as acidic as that of FeSiSC-A catalysts. It indicates that the co-catalytic mechanism of alumina phase is different from that of silica phase. For the enhancement mechanism of Al₂O₃ in the catalyst, Timofeeva et al. [61] demonstrated that insertion of alumina phase can increase the strength of basic sites of Fe-containing samples detected with CDCl₃ adsorption, leading to the acceleration of H₂O₂ degradation and the increase in activity of catalysts. This explanation is in agreement with the result of our work that insertion of Al₂O₃ can increase the p*H*_{IEP} of catalyst. Furthermore, alumina as a Lewis acid can attract electron density from ferric ion, and destabilizing the Fe³⁺ state, then facilitate the reduction of Fe³⁺ to Fe²⁺ by H₂O₂, which usually is the rate-limiting step in the Fenton's reagent chain reaction [62].

SiO₂ presents lower p*H*_{IEP} value compared with that of Al₂O₃, the surface charge of silica-containing catalyst FeAlSiSC-A at p*H* 4.0 is lower than that of FeAlSC-A₂ (Table 2-8), and resulting in a slightly decrease of AOII adsorption. While as can be seen from Fig. 2-22, FeAlSiSC-A shows higher catalytic activity than FeAlSC-A₂. The pseudo first-order degradation kinetic constant is calculated to be $1.511 \times 10^{-2} \text{ min}^{-1}$ for FeAlSiSC-A (Table 2-7), which is about 1.8 times as much as that of FeAlSC-A₂ and FeSiSC-A₂. This experimental result can further indicate the co-catalytic effect of SiO₂ and Al₂O₃ in SC. On the other hand, maybe there is a synergistically catalytic effect of silica and alumina in FeAlSiSC-A, further research will be carried out to confirm this hypothesis.

To evaluate the function of sewage sludge-based carbon as support in heterogeneous Fenton-like reaction, the degradation of AOII with bare FeAlSi was carried out. The catalyst concentration is 0.8682 g/L for FeAlSi and 1.6256 g/L for FeAlSiSC-A to get the similar amount of Fe, Al and Si in these two systems. It can be observed that both the adsorption and oxidation of AOII in FeAlSi system are less significant than that of FeAlSiSC-A system (Fig. 2-22). The rate constant is calculated to be

only $3.39 \times 10^{-3} \text{ min}^{-1}$ for FeAlSi using the pseudo-first-order equation, much lower than that of FeAlSiSC-A. This comparison suggests that the carbon in FeSC also plays a very important role in the Fenton-like process. As is known, carbon materials are good adsorbents for aromatic chemicals and the preconcentration of AOII to be oxidized in the vicinity of reactive centers is considered to be beneficial in many literatures [39,63]. Furthermore, the dispersion of the inorganic oxide within the carbon matrix could prevent them from aggregating into clusters during thermal treatment, and increase the number and properties of the reaction surface sites.

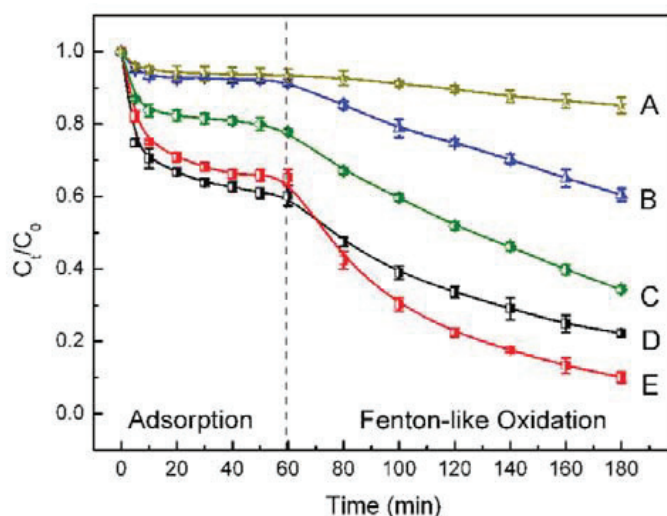


Fig. 2-22. Degradation of AOII through adsorption and oxidation in the presence of Al_2O_3 -containing catalysts (the iron concentrations are all 0.2588 g/L: (A) AlSC-A: 1.9540 g/L, (B) FeAlSi: 0.8682 g/L; (C) FeAlSC-A₁: 1.5012 g/L, (D) FeAlSC-A₂: 1.5377 g/L, (E) FeAlSiSC-A: 1.6256 g/L; H_2O_2 : 15 mM; AOII: 100 mg/L; reaction pH: 4.0 ± 0.1 ; reaction temperature: 30 °C).

2.4. Conclusions

A novel heterogeneous Fenton-like catalyst was first successfully prepared by employing the sewage sludge-derived char (SC) as the catalyst support. The characterization results revealed the impregnated iron was existed as Fe_3O_4 in the FeSC catalyst and almost uniformly distributed on the SC support. The catalytic activity of FeSC was evaluated from the discoloration and mineralization of acid orange II (AOII) in the presence of H_2O_2 . It was found that the FeSC catalyst that pyrolyzed at 800°C for 2 h displayed the highest catalytic activity. Almost complete discoloration and 73.6% mineralization of 100 mg/L AOII were achieved after 1 h adsorption and 2 h oxidation, by using 2.0

g/L catalyst, 15.0 mM H₂O₂ and initial pH 4.0. And only 0.37 mg/L iron was detected in the filtrate at the end of the reaction. The discoloration efficiency could be kept around 94% after 600 min test in a n integrated membrane-heterogeneous Fenton-like catalytic continuous reactor (MHFR). It indicates that FeSC presents both a high catalytic activity and a long-term stability. The catalytic activation energy was calculated to be 25.8 kJ/mol.

Compared to some commercial iron oxides such as α -Fe₂O₃, Fe₃O₄, γ -FeOOH, and wood sawdust-based carbon supported iron oxide catalyst (FeWC). the FeSC catalyst presented a higher catalytic efficiency. After compared the physicochemical properties of these iron-containing catalysts, the presence of inorganic components in sewage sludge, mainly SiO₂ and Al₂O₃, was speculated to be the main reason for the good catalytic performance of FeSC. To further confirm this interpretation, the inorganic components in sewage sludge were firstly removed, and various amounts of iron, silica and alumina were added into the treated precursor to prepare heterogeneous Fenton-like catalysts. It was found that the removal of inorganic fraction yielded significant deterioration of catalytic activity. While the impregnation of SiO₂ and Al₂O₃ resulted in substantial promoting effects on discoloration of AOII. The addition of SiO₂ will facilitate the adsorption of H₂O₂ due to the formation of hydrogen bonds between H₂O₂ and Si-O-Si, and increase the activity of \cdot OH for the formation of a acidic microenvironment near the silica phase. The insertion of Al₂O₃ as basic sites can facilitate the adsorption of AOII, activate H₂O₂ degradation and accelerate the reduction of Fe³⁺ to Fe²⁺ by H₂O₂ due to the Lewis property of alumina.

References

- [1] P. Bautista, A.F. Mohamedano, J.A. Casas, J.A. Zazo, J.J. Rodriguez, An overview of the application of Fenton oxidation to industrial wastewaters treatment. *J. Chem. Technol. Biotechnol.*, 83 (2008) 1323-1338.
- [2] D. Chebli, F. Fourcade, S. Brosillon, S. Nacef, A. Amrane, Supported photocatalysis as a pre-treatment prior to biological degradation for the removal of some dyes from aqueous solutions; Acid Red 183, Brilliant Scarlet, Methyl Red Sodium Salt, Orange II. *J. Chem. Technol. Biotechnol.*, 85 (2010) 555-563.
- [3] H.J.H. Fenton, Oxidation of tartaric acid in the presence of iron. *Chem. Soc. Trans.*, 65 (1984) 899-910.
- [4] J.A. Zazo, J.A. Casas, C.B. Molina, A. Quintanilla, J.J. Rodriguez, Evolution of ecotoxicity upon Fenton's oxidation of phenol in Water, *Environ. Sci. Technol.* 41 (2007) 7164-7170.

- [5] C.K. Duysterberg, S.E. Mylon, T.D. Waite, pH Effects on iron-catalyzed oxidation using Fenton's reagent. *Environ. Sci. Technol.*, 42 (2008) 8522-8527.
- [6] M.L. Luo, D. Bowden, P. Brimblecombe, Catalytic property of Fe-Al pillared clay for Fenton oxidation of phenol by H₂O₂. *Appl. Catal. B: Environ.* 85 (2009) 201-206.
- [7] H. Hassan, B.H. Hameed, Fe-clay as effective heterogeneous Fenton catalyst for the decolorization of Reactive Blue, *Chem. Eng. J.* 171 (2011) 912-918.
- [8] M.C. Lu, J.N. Chen, H.H. Huang, Role of goethite dissolution in the oxidation of 2-chlorophenol with hydrogen peroxide. *Chemosphere*, 46 (2002) 131-136.
- [9] J.C. Barreiro, M.D. Capelato, Oxidative decomposition of atrazine by a Fenton-like reaction in a H₂O₂/ferrihydrite system. *Water Res.*, 41 (2007) 55-62.
- [10] S.P. Sun, A.T. Lemley, p-Nitrophenol degradation by a heterogeneous Fenton-like reaction on nano-magnetite: Process optimization, kinetics, and degradation pathways. *J. Mol. Catal. A: Chem.*, 349 (2011) 71-79.
- [11] M.C. Pereira, L.C.A. Oliveira, E. Murad, Iron oxide catalysts: Fenton and Fenton-like reactions - a review. *Clay Miner.*, 47 (2012) 258-302.
- [12] M. Usman, P. Faure, C. Ruby, K. Hanna. Remediation of PAH-contaminated soils by magnetite catalyzed Fenton-like oxidation. *Appl. Catal. B: Environ.*, 117-118 (2012) 10-17.
- [13] R.C.C. Costa, M.F.F. Lelis, L.C.A. Oliveira, J.D. Fabris, J.D. Ardisson, R.R.V.A. Rios, C.N. Silva, R.M. Lago, Novel active heterogeneous Fenton system based on Fe_{3-x}M_xO₄ (Fe, Co, Mn, Ni): The role of M²⁺ species on the reactivity towards H₂O₂ reactions. *J. Hazard. Mater.*, 129 (2006) 171-178.
- [14] L. Xu, J. Wang, Fenton-like degradation of 2,4-dichlorophenol using Fe₃O₄ magnetic nanoparticles. *Appl. Catal. B: Environ.*, 123-124 (2012) 117-126.
- [15] X.B. Hu, B.Z. Liu, Y.H. Deng, H.Z. Chen, S. Luo, C. Sun, P. Yang, S.G. Yang, Adsorption and heterogeneous Fenton degradation of 17 alpha-methyltestosterone on nano Fe₃O₄/MWCNTs in aqueous solution. *Appl. Catal. B: Environ.*, 107 (2011) 274-283.
- [16] M.R. Dhananjayan, J. Kiwi, P. Albers, O. Enea, Photo-assisted immobilized Fenton degradation up to pH 8 of azo dye orange II mediated by Fe³⁺/Nafion/Glass Fibers, *Helv. Chim. Acta*, 84 (2001) 3433-3445.
- [17] S. Parra, V. Nadtochenko, P. Albers, J. Kiwi, Discoloration of Azo-Dyes at Biocompatible pH-Values through an Fe-Histidine Complex Immobilized on Nafion via Fenton-like Processes, *J. Phys. Chem. B*, 108 (2004) 4439-4448.

- [18] T.L.P. Dantas, V.P. Mendonça, H.J. José, A.E. Rodrigues, R.F.P.M. Moreira, Treatment of textile wastewater by heterogeneous Fenton process using a new composite Fe₂O₃/carbon, *Chem. Eng. J.*, 118 (2006) 77-82.
- [19] E. Kan, S.G. Huling, Effects of temperature and acidic pre-treatment on Fenton-driven oxidation of MTBE-spent granular activated carbon, *Environ. Sci. Technol.*, 43 (2009) 1493-1499.
- [20] A.L.T. Pham, C. Lee, F.M. Doyle, D.L. Sedlak, A Silica-Supported Iron Oxide Catalyst Capable of Activating Hydrogen Peroxide at Neutral pH Values, *Environ. Sci. Technol.*, 43 (2009) 8930-8935.
- [21] J.A. Botas, J.A. Melero, F. Martínez, M.I. Pariente, Assessment of Fe₂O₃/SiO₂ catalysts for the continuous treatment of phenol aqueous solutions in a fixed bed reactor, *Catal. Today*, 149 (2010) 334-340.
- [22] I. Muthuvel, M. S waminathan, Photoassisted Fenton mineralisation of Acid Violet 7 by heterogeneous Fe (III)-Al₂O₃ catalyst, *Catal. Commun.*, 8 (2007) 981-986.
- [23] Q. Zhang, W.F. Jiang, H.L. Wang, M.D. Chen, Oxidative degradation of dinitro butyl phenol (DNBP) utilizing hydrogen peroxide and solar light over a Al₂O₃-supported Fe(III)-5-sulfosalicylic acid (ssal) catalyst, *J. Hazard. Mater.* 176 (2010) 1058-1064.
- [24] M. Aleksić, H. Kušić, N. Koprivanac, D. Leszczynska, A.L. Božić, Heterogeneous Fenton type processes for the degradation of organic dye pollutant in water - The application of zeolite assisted AOPs, *Desalination* 257 (2010) 22-29.
- [25] E.G. Garrido-Ramirez, B.K.G. Theng, M.L. Mora, Clays and oxide minerals as catalysts and nanocatalysts in Fenton-like reactions - a review, *Appl. Clay Sci.* 47 (2010) 182-192.
- [26] C.S. Castro, M.C. Guerreiro, L.C.A. Oliveira, M. Gonçalves, A.S. Anastácio, M. Nazzarro, Iron oxide dispersed over activated carbon: Support influence on the oxidation of the model molecule methylene blue, *Appl. Catal. A: Gen.* 367 (2009) 53-58.
- [27] F. Adam, K. Kandasamy, S. Balakrishnan, Iron incorporated heterogeneous catalyst from rice husk ash, *J. Colloid Interface Sci.* 304 (2006) 137-143.
- [28] Y. Flores, R. Flores, A.A. Gallegos, Heterogeneous catalysis in the Fenton-type system reactive black 5/H₂O₂, *J. Mol. Catal. A: Chem.* 281 (2008) 184-191.
- [29] R.C.C. Costa, F.C.C. Moura, P.E.F. Oliveira, F. Magalhães, J.D. Ardissou, R.M. Lago, Controlled reduction of red mud waste to produce active systems for environmental applications: Heterogeneous Fenton reaction and reduction of Cr (VI), *Chemosphere* 78 (2010) 1116-1120.

- [30] C. J. Indarom, V. M. Eeyoo, B. K. Itiyanan, T. R. Irsomboon, P. R. Angsunvigit, Surface characterization and dye adsorptive capacities of char obtained from pyrolysis/gasification of sewage sludge, *Chem. Eng. J.* 133 (2007) 239-246.
- [31] J.S. Cha, J.C. Choi, J.H. Ko, Y.K. Park, S.H. Park, K.E. Jeong, S.S. Kim, J.K. Jeon, The low-temperature SCR of NO over rice straw and sewage sludge derived char, *Chem. Eng. J.* 156 (2010) 321-327.
- [32] M.J. Martin, E. Serra, A. Ros, M.D. Balaguer, M. Rigola, Carbonaceous adsorbents from sewage sludge and their application in a combined activated sludge-powdered activated carbon (AS-PAC) treatment, *Carbon* 42 (2004) 1389-1394.
- [33] C. Hsiu-Mei, C. Ting-Chien, P. San-De, C. Hung-Lung, Adsorption characteristics of Orange II and Chrysophenine on sludge adsorbent and activated carbon fibers, *J. Hazard. Mater.* 161 (2009) 1384-1390.
- [34] F.S. Zhang, J.O. Nriagu, H. Itoh, Photocatalytic removal and recovery of mercury from water using TiO₂-modified sewage sludge carbon, *J. Photochem. Photobiol. A: Chem.* 167 (2004) 223-228.
- [35] A. Ansari, T.J. Bandosz, Inorganic-organic phase arrangement as a factor affecting gas-phase desulfurization on catalytic carbonaceous adsorbents, *Environ. Sci. Technol.* 39 (2005) 6217-6224.
- [36] J. Ábrego, J. Arauzo, J.L. Sánchez, A. Gonzalo, T. Cordero, J. Rodríguez-Mirasol, Structural changes of sewage sludge char during fixed-bed pyrolysis, *Ind. Eng. Chem. Res.* 48 (2009) 3211-3221.
- [37] Oaks J, Gratton P. Kinetic investigations of azo dye oxidation in aqueous media. *J. Chem. Soc. Perkin Trans.*, 1998, 2: 2563-2568.
- [38] M.S.R. Swamy, T.P. Prasad, B.R. Sant, Thermal analysis of ferrous sulphate heptahydrate in air. *J. Therm. Anal. Calorim.*, 16 (1979) 471-478.
- [39] J.H. Ramirez, F.J. Maldonado-Hódar, A.F. Pérez-Cadenas, C. Moreno-Castilla, C.A. Costa, L.M. Madeira, Azo-dye Orange II degradation by heterogeneous Fenton-like reaction using carbon-Fe catalysts, *Appl. Catal. B: Environ.* 75 (2007) 312-323.
- [40] F. Duarte, F.J. Maldonado-Hódar, A.F. Pérez-Cadenas, L.M. Madeira, Fenton-like degradation of azo-dye Orange II catalyzed by transition metals on carbon aerogel, *Appl. Catal. B: Environ.* 85 (2009) 139-147.
- [41] P. Mills, J. L. Sullivan, A study of the core level electrons in iron and its three oxides by means of X-ray photoelectron spectroscopy, *J. Phys. D.* 16 (1983) 723.

- [42] M. Muruganandham, S.H. Chen, J.J. Wu, Evaluation of water treatment sludge as a catalyst for aqueous ozone decomposition, *Catal. Commun.* 8 (2007) 1609-1614.
- [43] Wu F, Deng N, Hua H. Degradation mechanism of azo dye C. I. reactive red 2 by iron powder reduction and photooxidation in aqueous solutions. *Chemosphere*, 2000, 41(8): 1233-1238
- [44] M. Neamtu, C. Catrinescu, A. Kettrup, Effect of dealumination of iron(III)-exchanged Y zeolites on oxidation of Reactive Yellow 84 azo dye in the presence of hydrogen peroxide. *Appl. Catal. B: Environ.* 51 (2004) 149-157.
- [45] G.V. Buxton, C. Greenstock, W.P. Hellman, A.B. Ross, Critical review of rate constants for reactions of hydrated electrons, hydrogen atoms, and hydroxyl radicals ($\cdot\text{OH}/\text{OH}^-$) in aqueous solution. *J. Phys. Chem.*, 17 (1988) 513-518.
- [46] C. Walling, Fenton's reagent. *Acc.Chem.Res.*, 8 (1975) 125-131.
- [47] X. Xue, K. Hanna, M. Abdelmoula, N. Deng, Adsorption and oxidation of PCP on the surface of magnetite: Kinetic experiments and spectroscopic investigations. *Appl. Catal. B: Environ.*, 89 (2009) 432-440.
- [48] G.E. Üstün, S.K.A. Solmaz, T. Morsünbül, H.S. Azak, Advanced oxidation and mineralization of 3-indole butyric acid (IBA) by Fenton and Fenton-like processes. *J. Hazard. Mater.*, 180 (2010) 508-513.
- [49] A. Bozzi, T. Yuranova, P. Lais, J. Kiwi, Degradation of industrial waste waters on Fe/C-fabrics. Optimization of the solution parameters during reactor operation. *Water Res.*, 39 (2005) 1441-1450.
- [50] N. Panda, H. Shahoo, S. Mohapatra, Decolourization of Methyl Orange using Fenton-like mesoporous $\text{Fe}_2\text{O}_3\text{-SiO}_2$ composite. *J. Hazard. Mater.*, 185 (2011) 359-365.
- [51] J. Guo, M. Al-Dahhan, Catalytic wet oxidation of phenol by hydrogen peroxide over pillared clay catalyst. *Ind. Eng. Chem. Res.*, 42 (2003) 2450-2460.
- [52] S.J. Zhang, H.Q. Yu, Y. Zhao, Kinetic modeling of the radiolytic degradation of Acid Orange 7 in aqueous solutions. *Water Res.*, 39 (2005) 839-846.
- [53] J. Chen, L. Zhu, UV-Fenton discolouration and mineralization of Orange II over hydroxyl-Fe-pillared bentonite. *J. Photochem. Photobiol. A: Chem.*, 188 (2007) 56-64
- [54] J. Żegliński, G.P. Piotrowski, R. Piękoś, A study of interaction between hydrogen peroxide and silica gel by FTIR spectroscopy and quantum chemistry, *J. Mol. Struct.* 794 (2006) 83-91.
- [55] J.H. Clark, Solid Acids for Green Chemistry, *Acc. Chem. Res.* 35 (2002) 791-797.
- [56] M.S. Kang, Y.J. Choi, S.H. Moon, Effects of inorganic substances on water splitting in ion-exchange membranes: I. Optimal contents of inorganic substances in preparing bipolar membranes, *J. Colloid Interface Sci.* 273 (2004) 533-539.

- [57] Y.H. Wang, W.K. Siu, Structure characteristics and mechanical properties of kaolinite soils. I. Surface charges and structural characterizations, *Can. Geotech. J.* 43 (2006) 587–600.
- [58] M. Mullet, P. Fievet, J.C. Reggiani, J. Pagetti, Comparison of two electrokinetic methods- electroosmosis and streaming potential- to determine the zeta-potential of plane ceramic membranes, *J. Membrane Sci.* 123 (1997) 255-265.
- [59] S.H. Tian, Y.T. Tu, D.S. Chen, X. Chen, Y. Xiong, Degradation of Acid Orange II at neutral pH using $\text{Fe}_2(\text{MoO}_4)_3$ as a heterogeneous Fenton-like catalyst, *Chem. Eng. J.* 169 (2011) 31-37.
- [60] A. Chen, X. Ma, H. Sun, Decolorization of KN-R catalyzed by Fe-containing Y and ZSM-5 zeolites, *J. Hazard. Mater.* 156 (2008) 568-575.
- [61] M.N. Timofeeva, M.E. Malyshev, V.N. Panchenko, A.N. Shmakov, A.G. Potapov, M.S. Mel'gunov, FeAl₁₂-Keggin type cation as an active site source for Fe,Al-silica mesoporous, *Appl. Catal. B: Environ.* 95 (2010) 110-119.
- [62] H. Lim, J. Lee, S. Jin, J. Kim, J. Yoon, T. Hyeon, Highly active heterogeneous Fenton catalyst using iron oxide nanoparticles immobilized in alumina coated mesoporous silica, *Chem. Commun.* 4 (2006) 463-465.
- [63] F. Rodríguez-Reinoso, The role of carbon materials in heterogeneous catalysis, *Carbon* 36 (1998) 159-175.

Chapter 3

Catalytic wet air oxidation of 2-chlorophenol over iron–sewage sludge derived carbon

3.1. Introduction

Wet air oxidation (WAO) uses oxygen or air to oxidize organic substances in an aqueous solution under elevated temperature (ca. 200-320°C) and pressure (ca. 2-20 MPa) [1]. The widespread use of this technology was limited by its severe reaction conditions. To solve this problem, some catalysts were added into the reactor to achieve faster destruction rates of organic pollutants under much lower temperature and pressures. This process is referred to as catalytic wet air oxidation (CWAO) [2]. In the past decades, several catalysts have been developed for the CWAO reaction. They could be divided into homogeneous catalysts and heterogeneous catalysts. Compared to homogeneous catalysts, the development of active heterogeneous catalysts has received much more attention because a separation step could be avoided. Various solid catalysts including noble metal and transition metal oxide catalysts have been evaluated.

Qin et al. [3] compared the activities of Pd, Pt and Ru loaded activated carbon, γ -Al₂O₃ and CeO₂ catalysts in the CWAO of 4-CP, and found that Pt loaded catalysts exhibited the highest catalytic activity. Li et al. [4] used Ru/ZrO₂ and Ru/Ce_xZr_{1-x}O₂ as the catalysts for the CWAO of 2-CP. The results showed that complete decomposition of 2-CP could be achieved within 5 h under mild reaction temperature (393 K) and moderate pressure (5 MPa). Furthermore, no Ru leaching could be detected during the reaction. However, although noble metal catalysts exhibited high activities [5,6], they are quite expensive.

Therefore, transition metal oxide based catalysts were used as an alternative in the CWAO process [7-9]. Quintanilla et al. [10] compared the performances of activated carbon (AC) and Fe/activated carbon (Fe/AC) in the CWAO of phenol. Higher activities were evidenced for the Fe/AC catalyst because of the presence of higher amounts of acidic oxygen functional groups at the surface of the catalysts after the introduction of iron. Posada et al. [11] have studied the catalytic wet air oxidation of 2-CP at 160°C under 1.0 MPa in the presence of 1.5 g L⁻¹ of a 4 wt.% Cu/CeO₂ catalyst. The results showed that 2-CP (50 mg/L) could be degraded with 130 min. However, 54.5 ppm Cu were detected

at the end of reaction, corresponding to ca. 91 wt.% of the total amount of copper in the catalyst. CuO-based catalysts were repeatedly proposed as effective catalysts for the CWAO of different pollutants, but copper leaching was critical. Therefore, leaching is a major issue when using transition metal oxide based catalysts in the CWAO process and it could be more interesting to use iron salts or ferric oxides as catalysts since they are less toxic and more economical [12].

In the wastewater treatment area, 2-chlorophenol (2-CP), which is widely used in the paper, the pulp, the pesticide and the herbicide industries, is unambiguously identified as a severe environmental pollutant of major concern due to its high toxicity and low biodegradability. The maximum allowable concentration of 2-CP in drinking water was fixed at $10 \mu\text{g L}^{-1}$ [13]. Among the different techniques applied to date for the treatment of 2-CP, the catalytic wet air oxidation (CWAO) has attracted some interest. Compared to the biological, electrochemical or photocatalytic treatments, CWAO is more efficient at treating high concentrations of organic pollutants [14]. Compared to the incineration and the supercritical water oxidation, CWAO might further be considered as an energy-saving catalytic method [15].

Since sewage sludge are rich in iron, and carbon materials are widely studied as catalysts in CWAO. In this chapter, the sewage sludge derived carbon (SC) was employed as catalyst in the CWAO of 2-CP. Furthermore, sewage sludge derived carbon supported iron oxide catalysts (named as FeSC) were also prepared, following an optimized method, in order to stabilize the iron. Compared with the costly noble-metal catalysts, the prepared FeSC catalysts are potentially low cost. Since the metal leaching remains the main drawback for an extensive application of transition-metal based catalysts in CWAO processes, the reasons and effects of the iron leaching upon the reaction were investigated in this study. And different attempts to prevent the iron leaching were also tested.

3.2. Experimental

3.2.1. Chemicals and solutions

All the following reagents were analytical-reagent grade and used without additional purification: ferrous sulfate heptahydrate ($\text{FeSO}_4 \cdot 7\text{H}_2\text{O}$), disodium phosphate dodecahydrate (Na_2HPO_4), sodium dihydrogen phosphate (NaH_2PO_4), acetic acid (CH_3COOH), sodium acetate ($\text{CH}_3\text{COONa} \cdot 3\text{H}_2\text{O}$), $\text{Ru}(\text{NO})(\text{NO}_3)_3$, purchased from Alfa Aesar, France. 2-Chlorophenol and Methanol (for chromatography) were obtained from Sigma-Aldrich, France. The water for the preparation of all the solutions was double distilled water.

The dewatered sewage sludge was obtained from the Lie De municipal wastewater treatment plant in Guangzhou, China. Its Physicochemical properties were the same as described in the Chapter 2, Section 2.2.1. The sludge was dried at 105°C to constant weight (ca. 78 wt.% water was evaporated), subsequently grinded, sieved (100-mesh), and the sewage sludge-derived carbon (SC) was finally stored in a desiccator at room temperature.

3.2.2. Preparation of the catalysts

The sewage sludge-derived char supported iron oxide catalyst (named as FeSC) was prepared following a one-step method combining the carbon synthesis with the Fe loading. At first, 20 g dried sludge were added into 150 mL of a ferrous sulfate solution (0.5 mol L⁻¹ FeSO₄, pH = 2.5). After the suspension was stirred for 24 h, it was slowly evaporated in a rotary evaporator at 60°C under reduced pressure, and then dried at 105°C for 12 h. Subsequently, the received solid was pyrolyzed under flowing nitrogen (40 mL min⁻¹) in a horizontal furnace at 800°C for 2 h (heating rate: 20°C·min⁻¹). The pyrolyzed sample was washed several times with deionized water until the conductivity became constant in order to make sure there is no soluble iron salts anymore on the catalyst surface. Then, the sample was dried at 105°C overnight and grinded to less than 200-mesh size.

Finally, in order to reduce the ash content, 5 g of the sludge-derived carbon (SC), formed after pyrolysis at 800°C for 2 h, was treated in a 80 mL acid solution (25 vol.% HCl + 25 vol.% HF) at 70°C for 2 h before, washing with distilled water and drying. The sample was named as SC-A.

3.2.2. Characterizations

The ash content of the catalysts was determined using the standard ASTM D2866-94 method. The metal content in the synthesized samples was measured by inductively coupled plasma optical emission spectroscopy (ICP-OES, Horiba Jobin-Yvon).

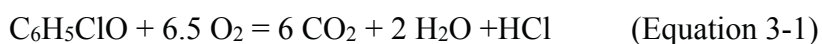
The specific surface area (S_{BET}) was determined using an Autosorb-iQ-MP gas sorption analyzer (Quantachrome Instruments, USA) via nitrogen adsorption at 77K.

The pH at the point of zero charge (pH_{PZC}) of the catalyst was measured according to the method developed by Brunelle [16]. Increasing amounts of solid were added sequentially to a 50 mL 0.0005M NaCl solution until the pH reached a plateau. The pH at the plateau corresponds to the pH_{PZC}.

The X-ray diffraction (XRD) measurement was carried out under the same conditions as described in the Chapter 2, Section 2.2.2.

3.2.3. Catalytic tests

The catalytic wet air oxidation of 2-chlorophenol over the SC-based catalysts was studied in a conventional batch reactor made of Hastelloy C 22 (Model 4836, Parr Instrument Inc). The experimental apparatus is described in Fig. 3-1. In each run, the 300 mL autoclave was loaded with 150 mL of a 2 g L⁻¹ 2-CP aqueous solution (ca. 2.3 mmoles 2-CP in the reactor) and a defined amount of catalyst. After the reactor was repeatedly outgassed with argon at ambient temperature, the reactor was heated up to the desired temperature (120°C). When the temperature was stabilized, synthetic air (20 vol.% O₂ + 80 vol.% N₂) was introduced into the reactor until the total pressure reached 5 MPa. This point was taken as “zero” time for the reaction. The oxygen partial pressure was ca. 0.9 MPa (ca. 42.8 mmoles O₂ in the reactor), corresponding globally to a large excess of oxygen according Equation 1. Noteworthy, the oxygen solubility in water under such conditions was only ca. 0.2 g O₂ L⁻¹.



Furthermore, to avoid any mass transfer limitation in the liquid phase, the stirrer speed was fixed at 1300 rpm [17]. Liquid samples were taken from the reactor at regular time intervals and analyzed after centrifugation.

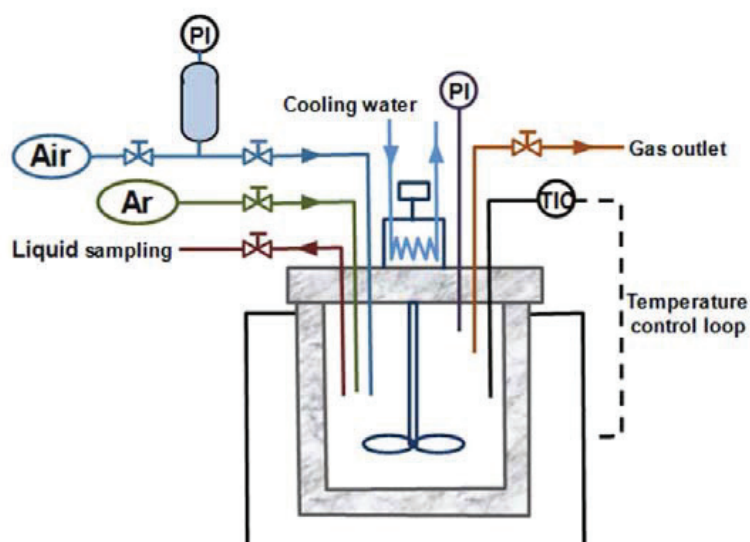


Fig. 3-1. Schematic of the experimental setup.

3.2.4. Analytical methods

The concentrations of 2-chlorophenol and the oxidation intermediates were measured by HPLC using a UV-detector set at 210 and 281 nm (Shimadzu). The HPLC system was equipped with a Kinetex

PFP 100A 2.6 μ m 100 \times 4.6 mm column (Phenomenex), operated at constant temperature (40°C). The mobile phase was a mixture of 4 vol.% methanol and 96 vol.% water, which pH was acidified down to 2.0 using a 85 wt.% H₃PO₄ solution. The flow rate was fixed at 0.6 mL·min⁻¹.

The Total Organic Carbon (TOC) in the liquid samples was determined by using a Shimadzu 5050 TOC analyzer. The pH of the solution was measured with a Radiometer Analytical PHM240 pH meter. The Fe concentration in the liquid samples was further analyzed by ICP-OES to check for lixiviation.

3.3. Results and discussion

3.3.1. Characterization of the catalysts

The basic physical and chemical characteristics of the SC, FeSC and SC-A samples are summarized in Table 3-1.

Table 3-1. Physicochemical properties of the SC, FeSC and SC-A samples.

Sample	Ash content (wt.%)	Fe (wt.%)	Si (wt.%)	Al (wt.%)	Ca (wt.%)	S _{BET} (m ² g ⁻¹)	pH _{PZC}
SC	74.6	4.5	23.4	10.6	1.7	19	7.5
FeSC	93.0	12.0	19.9	9.1	1.8	14	4.2
SC-A	56.1	0.4	28.6	1.8	<0.1	33	3.7

The ash content values and the results of the ICP-OES analysis indicated a high content in inorganic components, such as iron, silicon and aluminium. After the acidic washing, the ash fraction was partial removed. The iron content in SC, FeSC and SC-A, determined by ICP-OES, was 4.5, 12.0 and 0.4 wt.%, respectively. SC and FeSC exhibited quite a low specific surface area, while SC-A showed a higher surface as a result of the acidic washing and the efficient ash removal. As indicated in Table 3-1, the pH_{PZC} value decreased upon incorporation of iron in the SC support. This variation could be attributed to the higher amount of acidic oxygen surface functional groups induced by the presence of iron, which could be beneficial for the CWAO reaction [10].

The iron phase in the FeSC sample obtained by XRD measurement was the same as the result we got in the Chapter 2 (Fig. 3-2). Compared with the diffractogram of the pure SC and SC-A samples, the XRD pattern for FeSC exhibited several extra diffraction lines at 2 θ equal 35.5°, 62.6° and 30.1°.

These lines could respectively be assigned to the (311), (440) and (220) planes of Fe₃O₄ (magnetite, JCPDS n°88-0866).

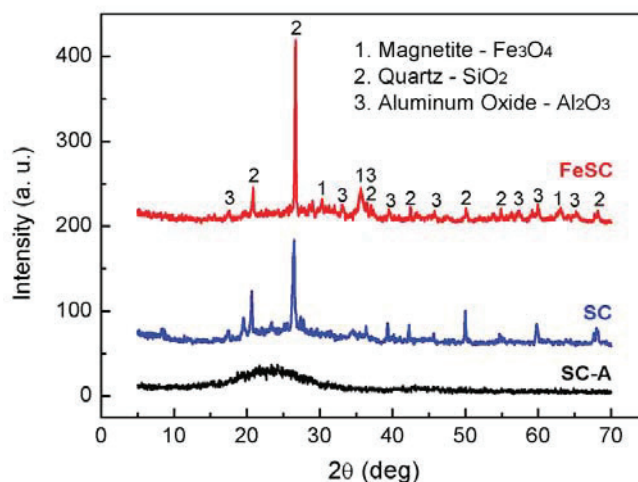


Fig. 3-2. XRD patterns of FeSC, SC and SC-A.

3.3.2. CWAO of 2-chlorophenol over the different catalysts

The wet air oxidation of 2-CP, in absence of any catalyst, was shown to be very slow. Upon reaction at 120°C under 0.9 M Pa oxygen partial pressure, 6% 2-CP conversion was achieved via thermal decomposition at the very beginning of the oxidation reaction ($t=0$). After 24 hours of reaction, the 2-CP and TOC removal were lower than 15% (Fig. 3-3), indicating that the 2-CP molecule was thermally stable under the applied reaction conditions.

The 2-CP molecule was observed to adsorb on the SC based catalysts. The initial adsorption, before the introduction of air ($t=0$), accounted for ca. 3% after subtraction of the 6% 2-CP conversion due to thermal decomposition. The untreated SC sample appeared to be only moderately active in the CWAO of 2-CP. After 24 hours of reaction, the 2-CP conversion was only 50% and TOC abatement reached 39%.

After acidic treatment (HCl + HF), the 2-CP adsorption increased up to 9%. This observation could be simply explained by the higher specific surface area of the SC-A sample compared to the initial SC (33 vs. 19 m² g⁻¹). On the contrary, the catalytic activity decreased upon removal of the ash fraction. The initial reaction rate decreased from 0.4 to 0.1 mmol_{2-CP} g_{catalyst}⁻¹ h⁻¹. The much smaller amount of iron in the treated sample (0.4 vs. 4.5 wt.%) could be responsible for this difference.

After incorporation of iron on the SC support, a substantial increase of the 2-CP conversion was observed. The complete removal of 2-CP could be reached within 5 hours of reaction. The initial reaction rate was calculated to be 3.0 mmol_{2-CP} g_{catalyst}⁻¹ h⁻¹, which was almost 7 times higher than the

rate measured on the untreated SC, while the iron concentration in the catalyst was only tripled. Compared with the classical Ru/ZrO₂ catalyst [18], which is known as a kind of high efficient noble metal catalyst, the FeSC catalyst displayed higher catalytic activity under identical reaction conditions. As shown in Fig. 3-3B, the TOC removal also remarkably increased upon addition of the FeSC catalyst, reaching 91% at the end of the reaction (24 hours). By comparison with the evolution of the 2-CP conversion, it could be deduced that the mineralization of the 2-CP molecule was not complete and occurred at a slower rate. Several partially-oxidized intermediates formed upon 2-CP degradation and appeared to be resistant towards further conversion to carbon dioxide.

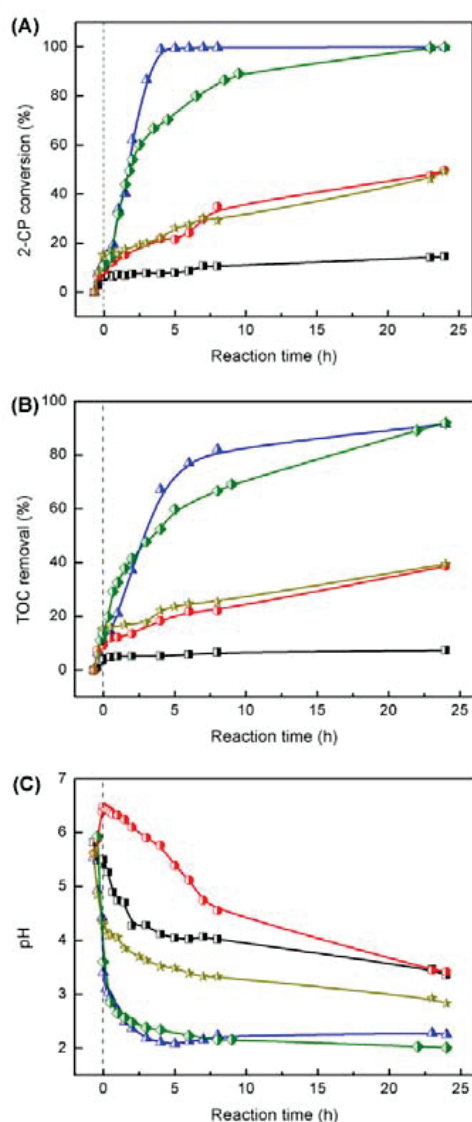


Fig. 3-3. Evolution of the 2-chlorophenol conversion (A), the TOC removal (B) and the pH (C) upon wet air oxidation (WAO) of 2-CP over FeSC (\blacktriangle), SC (\bullet), SC-A (\star) and Ru/ZrO₂ (\blacklozenge) or in the absence of catalyst (\blacksquare)

(0.5 g catalyst, 120°C, P_{O2}: 0.9 MPa, 1300 rpm, 150 mL [2-CP]₀=2g·L⁻¹).

Furthermore, as the decomposition of 2-CP occurred, the pH of the reaction mixture decreased from an initial value of 5.5 to very acidic values (Fig. 3-3C). This increase of the acidity of the reaction mixture could be attributed to (i) the production of HCl as a result of the initial dechlorination of the 2-CP molecule; and (ii) the formation of some small chain organic acids such as maleic acid, succinic acid, formic acid and oxalic acid, as detected by HPLC (Fig. 3-4). Some aromatic intermediates, such as 4-chlororesorcinol, chlorohydroquinone (ClHQ), catechol and hydroquinone (HQ), were also detected.

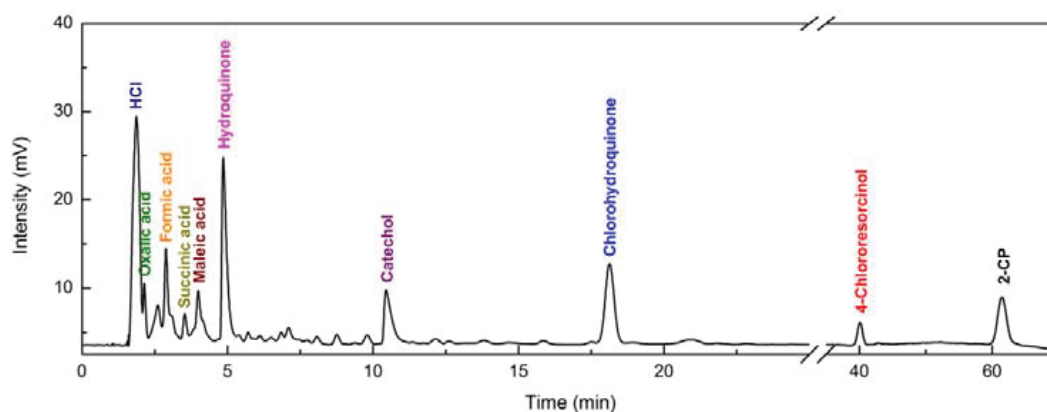


Fig. 3-4. Typical intermediates detected by HPLC (Column: 100 × 4.6 mm, Phenomenex, Kinetex 2.6 μm PFP 100A, Mobile phase: 4 vol. % MeOH & H₂O (pH = 2.0 justed by H₃PO₄), Flow rate: 0.6 mL·min⁻¹, Column temperature: 40°C) upon catalytic wet air oxidation of 2-chlorophenol.

3.3.3. Effect of the reaction temperature on the activity of FeSC

The reaction temperature is an important parameter affecting the CWAO of organic compounds. In our study, the effect of reaction temperature on the CWAO of 2-CP over FeSC catalyst was studied by running the reaction at 105, 120, 135 and 150°C.

As shown in Fig.3-5A, the increase of the reaction temperature accelerated the conversion of 2-CP. When the reaction was carried out at 105°C, 12 h were required to reach complete conversion of 2-CP. When the reaction temperature increased to 150°C, total 2-CP conversion could be achieved within 1.5 h.

The apparent activation energy could be deduced from the Arrhenius plot as shown on Fig. 3-6. The apparent activation energy for the CWAO of 2-CP over FeSC was calculated to be ca. 51 kJ/mol. Joglekar et al [21] reported that the activation energy for the non-catalytic WAO of 2-CP was about 145 kJ/mol. Obviously, the FeSC catalyst could efficiently decrease the reaction activation energy and significantly accelerate the elimination of 2-CP.

Fig. 3-5B also showed that the TOC removal efficiency increased as the reaction temperature increased, since more and more refractory intermediates could be completely oxidized as the temperature increased. For example, Gallezot et al. [22] reported that the activation energy for the CWAO of acetic acid over Ru/C was as high as 101 kJ/mol.

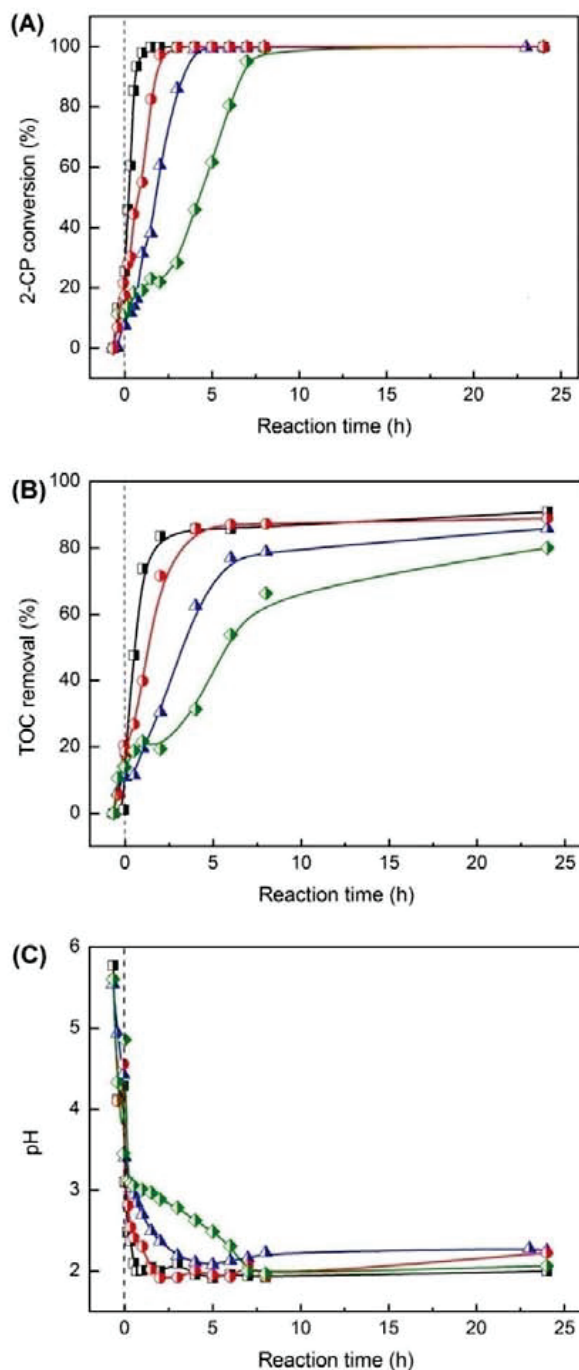


Fig. 3-5. Evolution of the 2-CP conversion (A), the TOC removal (B) and the pH (C) upon catalytic wet air oxidation (CWAO) of 2-CP at different reaction temperature: 105°C (◆), 120°C (▲), 135°C (●), 150°C (■) (0.5g catalyst, 5 MPa, 1300 rpm, 150 mL [2-CP]₀ =2g/L).

Table 3-2 Effect of temperature on the CWAO of 2-CP over FeSC

Temperature (K)	Reaction rate mol/(h·g _{catal})	Ea (kJ/mol)
423	4.7	51
408	1.9	
393	1.3	
378	0.8	

It is clear that higher temperatures favored the CWAO of 2-CP. However, the pH of the solution also decreased sharply when increasing the temperature (Fig. 3-5C). Such consequence would cause severe corrosion problems for the reactor. Additionally, higher temperatures usually mean higher operating costs. On the other hand, to be able to detect the reaction intermediates, slower reactions are preferred. Finally, to evaluate the effect of other operating parameters, it is required to operate the reaction under chemical control. Therefore, 120°C was chosen as the optimum temperature for the subsequent studies of the CWAO of 2-CP over the FeSC catalyst.

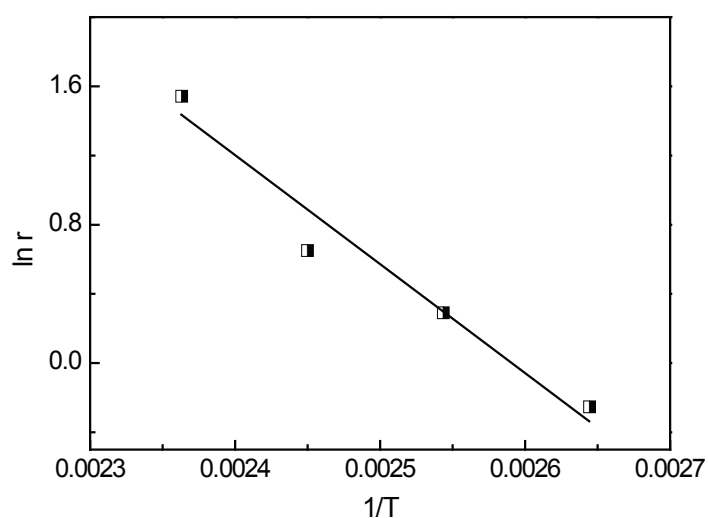


Fig. 3-6. Evolution of the initial 2-CP conversion rate as a function of temperature (105 - 150°C) upon CWAO of 2-CP over FeSC: Arrhenius plot

3.3.4. Heterogeneous vs. homogeneous reaction

Considering the very low pH achieved at the end of the reaction, the leaching of metal (Fe, Al and Ca et al.) was suspected. Therefore, the concentration of iron, as the most notably catalytically active metals [1], in the liquid phase at the end of the reaction (24 hours) was systematically measured. As

shown in Table 3-3, 27 mg L⁻¹ of iron was detected in the reaction mixture after reaction over the FeSC system, which corresponded to ca. 7 wt.% of the total amount of iron initially incorporated in the FeSC catalyst. Significant amounts of metallic ions were also detected in the liquid phase upon reaction over different catalysts based on transition metals such as Cu, Zn, Mn, Ni [2,24,25]. For example, Santos et al. [25] have studied the catalytic wet air oxidation of phenol with a commercial copper-based catalyst (Cu-0203T) in fixed bed reactors (FBRs), at 140 °C and at 16 bar of oxygen pressure. 100 ppm Cu was detected at the end of reaction when the initial pH was 3.5. Therefore, leaching is a major issue when using transition metal oxide based catalysts under acidic conditions.

Table 3-3. Iron leaching upon catalytic wet air oxidation (CWAO) of 2-chlorophenol over different catalysts (120 °C, P_{O₂}: 0.9 MPa, 1300 rpm, 150 mL [2-CP]₀ = 2g·L⁻¹, 0.5g catalyst).

Sample	Iron concentration in the reaction mixture after 24 h (mg·L ⁻¹)	Percentage of iron leached in the solution after 24 h (wt.%)
FeSC	27.0	7
SC	0.8	0.5
SC-A	3.8	29

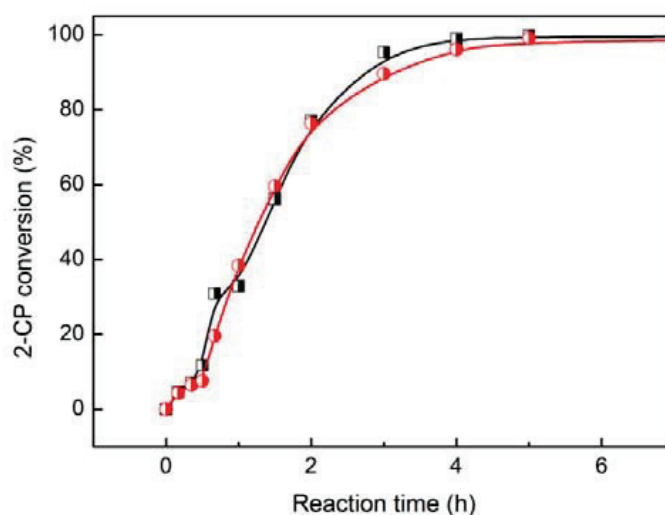


Fig. 3-7. 2-CP conversion attained by heterogeneous: 0.5g FeSC (■) and homogeneous reaction: hot filtrate from 0.5 g FeSC system after 10 min reaction (●) (120°C, P_{O₂}: 0.9 MPa, 1300 rpm, 150 mL [2-CP]₀ = 2g·L⁻¹).

To determine the contribution of the homogeneous phase reaction, 0.5 g FeSC catalyst was first introduced into the reaction mixture for 10 min, after that the hot reaction mixture was filtrated in order to remove any catalyst particle. The reaction was then continued in the absence of any solid catalyst. From Fig. 3-7, it is observed that the conversion of 2-CP continues, even after the hot filtration, indicating that part of the active phase which has been leached into the reaction mixture is active in the homogeneous phase reaction. Indeed, although after hot filtration, the reaction proceeded the same as that in the absence of hot filtration, that is when the catalyst is maintained in the mixture all along during the reaction. The 2-CP conversion profiles are similar in these two systems.

To further check the contribution of the homogeneous phase reaction, the evolution of the 2-CP conversion as a function of time was studied at different catalyst loading (Fig. 3-8A).

We observed first that the amount of 2-CP adsorbed on the FeSC catalyst surface increased while increasing the catalyst dosage. At a “zero” time, after subtraction of the thermal decomposition contribution, adsorption was accounted for 4.5, 6.5 and 8.1% of the 2-CP removal in the presence of 1.0, 1.5 and 2.0 g L⁻¹ catalyst, respectively. The average 2-CP adsorption capacity of the FeSC catalyst was calculated to be ca. 60 mg_{2-CP} g_{catalyst}⁻¹.

The iron concentration in the filtrate was systematically measured after 10, 30 and 60 minutes by ICP-OES. Fig. 3-8B shows the relation between the instantaneous reaction rate at 10, 30 and 60 minutes of reaction (expressed as per unit of time and per unit of volume), and the amount of iron detected in solution at the same time. The linear variation between those two parameters clearly indicated that (i) the reaction definitively occurred in the homogeneous phase since the initial reaction rate did not correlate with the amount of catalyst but with the volume of the reaction mixture and (ii) the reaction was strongly dependent on the iron concentration in the liquid phase.

To explain further the irreversible leaching of iron in the solution, the potential taken by the reaction mixture was systematically measured as a function of time and recalculated with respect to the standard hydrogen electrode (SHE). According to the pH and the potential of each liquid sample shown in the Pourbaix diagram (Fig. 3-8C) [26], we could find that the most stable form of iron in the aqueous phase all along the reaction would be Fe(II). This result could be explained by the low solubility of oxygen in water under the applied reaction conditions (ca. 0.2 g L⁻¹) and the rapid consumption of oxygen, resulting in anoxic conditions in the liquid phase. Noteworthy, the potential of the solution increased slightly as the reaction proceeded, indicating the Fe(II) could be progressively converted to Fe(III). Considering the excellent redox property of Fe(II), the formation of free radicals, such as alkyl peroxy radicals, oxygen radicals and hydroxyl radicals would be promoted [2,27,28] and the CWAO reaction could be initiated.

Since the leached iron existed as Fe²⁺ in the liquid phase, according to Equation 3-3:



The ion product data (IP) for Fe^{2+} and OH^- was calculated as follows:

$$\text{IP} = [\text{Fe}^{2+}] [\text{OH}^-]^2 \quad (\text{Equation 3-4})$$

The IP value got by curvilinear regression analysis was 1.39×10^{-26} , and good correlation coefficient ($R^2 = 0.9900$) was gotten. It should be noted that the solubility product constant (K_{sp}) for $\text{Fe}(\text{OH})_2$ was 3.16×10^{-14} [29]. Therefore, when under the same pH condition, the dissolved ferrous iron concentration in the FeSC system is much lower than the value got from theoretic solubility calculation, indicating the using of SC support could stabilize the iron and reduce the leaching problem. Furthermore, from the result of curve fitting, in order to meet the EU discharge standards for Fe (< 2 ppm) [30], the solution pH need to be kept higher than 3.29.

Conclusively, the 2-CP conversion in the homogeneous phase, the pH of the solution and the amount of iron leached in the reaction mixture were shown to be interconnected.

3.3.5. Minimization of the iron leaching

Based on the first results presented above, the minimization of the iron leaching from the FeSC catalysts upon CWAO of 2-chlorophenol clearly appeared as a key point. Since the iron leaching was shown to be mainly driven by the acidic conditions generated during the initial 2-CP degradation process, the pH of the reaction mixture was tentatively controlled following different approaches; i.e. adjusting the initial pH of the reaction mixture or using a buffer solution to keep the pH constant all along the reaction.

Alkaline agents, such as NaOH, are often used to neutralize the acids produced upon treatment of chlorinated organics via supercritical water oxidation [31] or wet air oxidation [32]. In our study, NaOH was used to adjust the initial pH value of the reaction mixture from 5.6 to 10.0. The results are shown in Fig. 3-9A. In the absence of any catalyst, the 2-CP conversion after 24 hours of reaction increased from ca. 14 to 68% and the TOC abatement increased from 7 to 40% when NaOH was initially added into the solution. These results are similar to what was reported by Pintar et al [33] in the WAO of substituted phenols (p-chlorophenol, p-nitrophenol) in the absence of any catalyst. It was concluded that, when the pH value is higher than the pK_a values of the substituted phenol, the phenolate anions (ArO^-) will yield phenoxy radicals (ArO^\cdot) which are considered to be much more reactive than the protonated form (ArOH) [32]. In our case, 2-CP would also yield phenoxy radicals

since the pKa of the 2-CP molecule is 8.6. However, almost no additional catalytic activity was observed under such reaction conditions in the presence of the FeSC catalyst (64% 2-CP conversion and 42% TOC removal after 24 h). While, the iron concentration in the liquid at the end of the reaction was only 0.7 mg L^{-1} , indicating that the contribution from the homogeneous reaction could be somehow neglected. This could be the main explanation for the much lower performances of the FeSC catalyst under alkaline conditions.

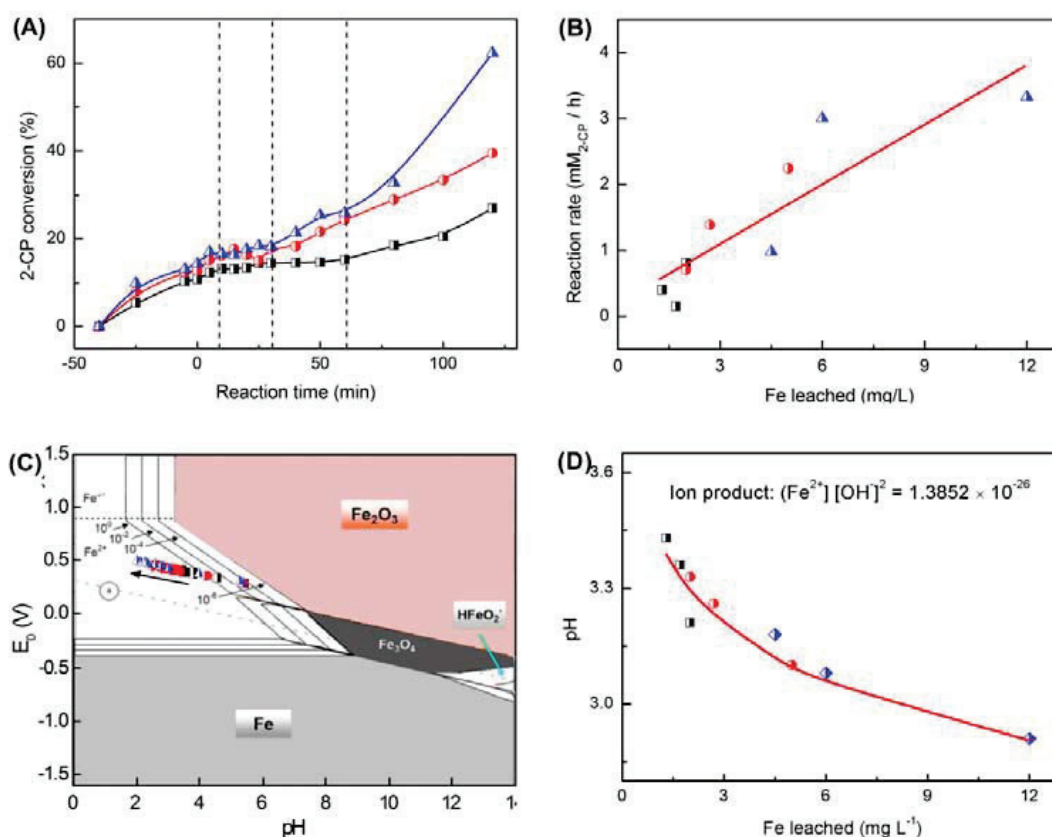


Fig. 3-8. Contribution of the homogeneous phase reaction. (A): 2-CP conversion during the first 2h of reaction in the presence of different concentration in FeSC; (B): Correlation between the 2-CP conversion rate and the amount of iron leached in the reaction mixture; (C): Pourbaix diagram for iron and evolution of the potential and pH of the reaction mixture as a function of time; (D): Correlation between the solution pH and the amount of iron leached in the reaction mixture; [120°C, P_{O₂}: 0.9 MPa, 1300 rpm, 150 mL [2-CP]₀ = 2g·L⁻¹, catalyst dosage: 1.0 g L⁻¹ (■), 1.5 g L⁻¹ (●) and 2.0 g L⁻¹ (▲)].

The addition of a buffer solution to the reaction mixture was tested as a second attempt to avoid the iron leaching. Firstly, the impact of a 40 mM phosphate buffer (pH = 6.8) was investigated. The amount of iron leached after 24 h reaction markedly decreased down to 0.4 ppm. However, compared

to the experiment performed in the absence of any catalyst, no extra 2-CP conversion or TOC removal could be observed over the FeSC catalyst (Fig. 3-9B). A posteriori, this inhibition of the catalytic activity in the presence of the phosphate buffer was tentatively related to the poisonous effect of phosphates on the iron oxide catalyst with the formation of iron phosphate chelates [34]. Conclusively, the phosphate buffer was not appropriate in this specific case.

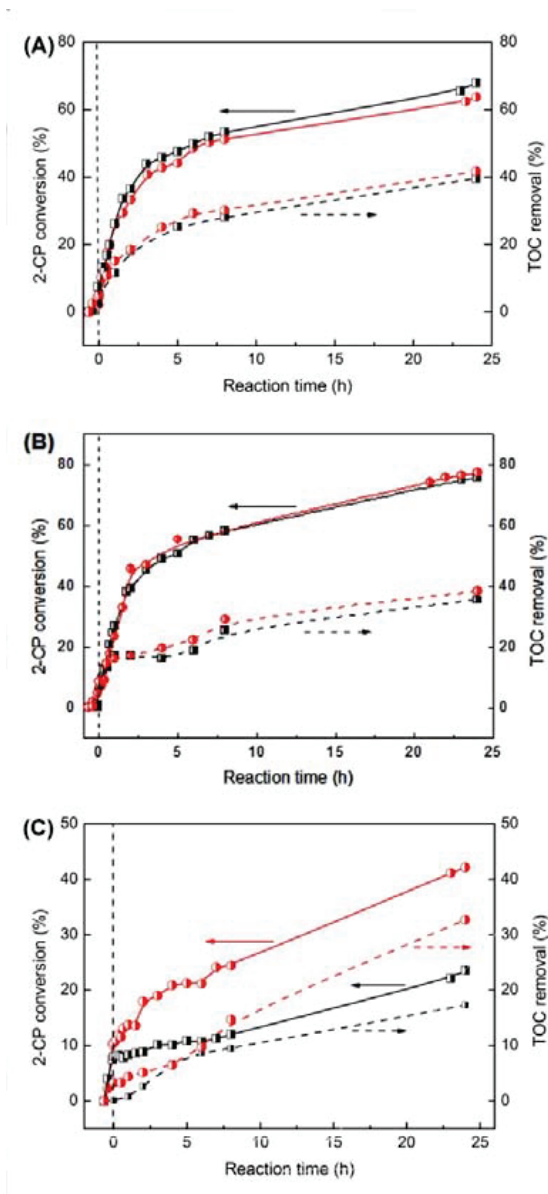


Fig. 3-9. Evolution of the 2-CP conversion upon wet air oxidation (WAO) in the absence of any catalyst (■) or in the presence of the FeSC catalyst (●) and with the initial addition of NaOH to pH=10.0 (A) or in the presence of a 40 mM phosphate buffer at pH=6.8 (B) or in the presence of a 50 mM acetate buffer at pH=4.5 (C) (120°C, P_{O₂}: 0.9 MPa, 1300 rpm, 150 mL [2-CP]₀ = 2g·L⁻¹, catalyst dosage: 2.0 g L⁻¹).

Alternatively, an acetate buffer (pH = 4.5) could be reliably used to control the pH since acetic acid was shown to be refractory towards wet air oxidation up to 200°C [35]. The results are presented on Fig. 3-9C.

In the absence of any catalyst, the 2-CP conversion and the TOC removal after 24 h reaction didn't change too much by the using of acetate buffer, ca. 17% 2-CP conversion and 8% TOC removal (the effective TOC removal was calculated after subtracting the TOC content due to the acetate buffer). When the FeSC catalyst was introduced, the 2-CP conversion was 42% and the TOC abatement reached 33% at the end of the reaction. In comparison with the results obtained when the same amount of FeSC catalyst was used but in the absence of any buffer (almost complete decomposition of 2-CP and 90% TOC abatement), a detrimental effect of the acetate buffer was observed. Nevertheless, the amount of iron leached in the filtrate at the end of reaction decreased from 30 to only 0.9 ppm in the presence of the acetate buffer. Furthermore, the contribution of homogeneous phase containing 0.9 ppm iron in the solution was also checked, and no further CWAO catalytic activity was observed. In conclusion, the use of the acetate buffer (pH = 4.5) could effectively help to prevent the iron leaching while preserving part of the catalytic activity of the catalyst. From a practical point of view, although the TOC content of the acetate buffer is high (ca. 4.5 g L⁻¹) and the acetic acid is refractory towards further oxidation the implementation of such a buffer for the treatment of 2-CP via CWAO might still be viable since acetic acid is non-toxic and would even be easily biodegraded in a conventional wastewater treatment plant.

3.3.6. Stability tests

It is known that dissolved iron in the effluent could generate an unwanted secondary pollution. To prevent such type of environmental damage, the iron leached upon CWAO was tentatively recovered at the end of the reaction via pH adjustment (precipitation) before filtration of the solid catalyst. At the end of each experiment, the reactor was cooled down to room temperature, opened to the air and NaOH was finally added to adjust the pH to neutral values. The catalyst was then recovered by filtration, washed with distilled water and dried at 105°C over night before being used again in a new run. Bernat et al. [36] revealed that the iron recovery efficiency strongly depends on the pH since it strongly impacts on the iron (III) retention. In our case, the iron concentration in the filtrate decreased to 0.24 ppm when the pH was increased to 5.2 and no iron leaching at all was ever detected (<0.1 ppm) at pH value higher than 6.0. Therefore, pH = 6.0 was chosen for the FeSC catalyst recovery before any subsequent re-utilizations.

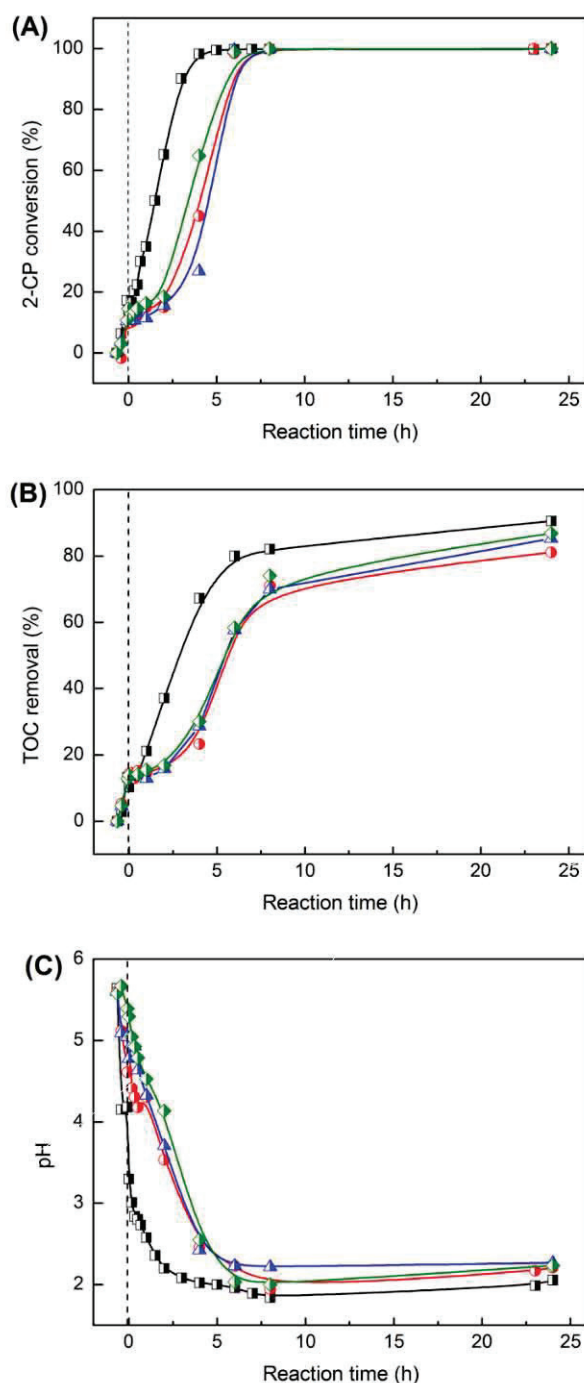


Fig. 3-10. Evolution of the 2-CP conversion (A), the TOC removal (B) and the pH (C) upon wet air oxidation (WAO) of 2-CP while recycling a 0.3g sample of the FeSC catalyst (120°C, P_{O_2} : 0.9 MPa, 1300 rpm, 150 mL $[2\text{-CP}]_0 = 2\text{g}\cdot\text{L}^{-1}$, 1st run (\blacksquare), 2nd run (\bullet), 3rd run (\blacktriangle), 4th run (\blacklozenge)].

Four successive runs were carried out using the same catalyst sample after recovery (recycling) but without implementing any buffer. As shown on Fig. 3-10, even after 4 runs, the 2-CP conversion and the TOC removal were still very high. Only a small decrease in activity was observed between the first run and the subsequent ones. Furthermore, an initial induction period appeared from the second

run. From the evolution of the pH during the reaction, we could deduce that in subsequent runs the pH decrease was not as sharp as in the first run. This observation is consistent with the differences observed in the amount of the iron which is leached after 1 or 24 hours of reaction (Table 3-4). It could be proposed that the induction period was somehow related to the formation of Fe(OH)₂ or Fe(OH)₃ precipitates on the catalyst surface upon pH adjustment, which would slow the iron transfer from the FeSC catalyst into the solution upon recycling. This observation would gain confirm that, in the absence of any control on the pH, the reaction would mainly proceed in the homogeneous phase and mostly depend on the iron concentration in the reaction mixture.

Table 3-4. Iron leaching upon successive batch experiments (120°C, P_{O2}: 0.9 MPa, 1300 rpm, 150 mL [2-CP]₀ = 2g·L⁻¹).

Run time	Catalyst dosage (g·L ⁻¹)	Reaction after 1 h			Reaction after 24 h		
		Fe leached (mg·L ⁻¹)	Fe leached (wt.%)	pH	Fe leached (mg·L ⁻¹)	Fe leached (wt.%)	pH
1	2.00	12	5.0	2.6	30	13	2.1
2	1.96	2.0	0.9	4.3	32	14	2.2
3	1.78	0.4	0.2	4.3	40	19	2.3
4	1.58	1.3	0.7	4.5	34	18	2.2

3.3.7. Reaction intermediates

Fig. 3-11 shows the evolutions of the concentrations of 2-chlorophenol and the different reaction intermediates we could identify upon CWAO of 2-CP over the FeSC catalyst. These intermediates have been classified in two different groups: the low molecular weight acids and the aromatic compounds, which ones were only detected in trace amounts.

As reported earlier, the dechlorination reaction also appeared in the present study as the first and essential step in the 2-CP decomposition route [37]. Chlorhydric acid was the only reaction product accumulating in the liquid phase all along the reaction. As shown in Fig. 3-11, 93% of the chlorine atoms in the 2-CP molecule are released in the reaction mixture as HCl by the end of the reaction. However, two different regimes might be differentiated. Up to t=1h, the accumulation of HCl in the reaction mixture was very rapid and the pH dropped drastically, indicating that in the first step of the

reaction the chlorine atom on the aromatic ring was removed and released in the solution as HCl. After one hour, the formation of HCl markedly slowed down. In this later period, HCl probably originated from partially oxidized chlorinated intermediates.

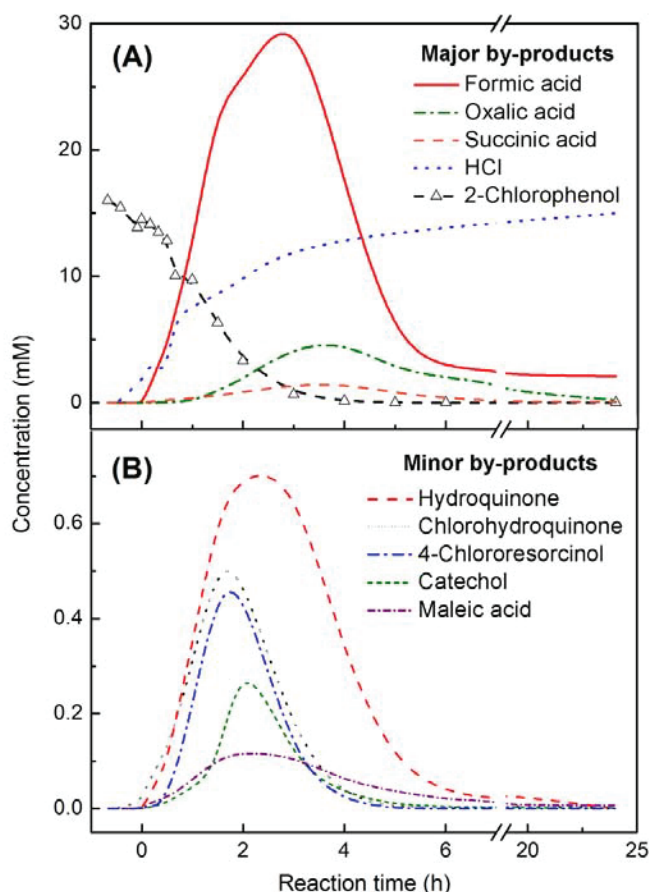


Fig. 3-11. Concentration profiles of 2-CP and the identified intermediates formed during the catalytic wet oxidation of 2-CP over FeSC (2 g L^{-1} FeSC, 120°C , P_{O_2} : 0.9 MPa , 1300 rpm , 150 mL $[2\text{-CP}]_0 = 2 \text{ g L}^{-1}$).

The concentrations of the different aromatic by-products reached a maximum at different reaction times before being totally oxidized by the end of the reaction (Table 3-5). The selectivity at the maximum was calculated based on the number of carbon atoms. The selectivity of all aromatic intermediates was very low, indicating that (i) under the applied reaction conditions, most of the 2-CP molecules are directly mineralized and (ii) the oxidation of these aromatic intermediates took place very rapidly.

Compared with the aromatic intermediates already reported in the literature upon CWAO of phenol and 2-CP [18,38], the major differences came from the absence of any 2-chloro-p-benzoquinone (2-CIBQ) and benzoquinone (BQ) detected in our studies. According to the literature, these

intermediates would form upon oxidation of chloro-hydroquinone (ClHQ) and hydroquinone (HQ) even at room temperature under atmospheric pressure [28]. However, it is also reported that these intermediates are very easily oxidized into smaller acids [39]. Therefore, we deduced from our observation that 2-ClBQ and BQ, if they would form, would decomposed too rapidly in our reaction conditions to be detected.

As shown in Fig. 3-11, some other short chain acids were also detected, such as formic acid, oxalic acid, succinic acid and small amounts of maleic acid. The time at the maximum concentration for these acids appeared to be delayed compared to the aromatic intermediates, offering an extra indication that they are produced in a second step only from the aromatic ring opening.

Table 3-5. The maximum selectivities in the different reaction intermediates calculated on a carbon basis.

Intermediate	Formula	Maximum time (h)	Max selectivity (%)
Chlorohydroquinone	C ₆ H ₃ (OH) ₂ Cl	1.70	5.4
4-Chloroesoreinol	C ₆ H ₅ O ₂ Cl	1.77	3.7
Catechol	C ₆ H ₆ O ₂	2.12	2.8
Hydroquinone	C ₆ H ₆ O ₂	2.33	5.6
Maleic acid	C ₄ H ₄ O ₄	2.37	0.6
Formic acid	CH ₂ O ₂	2.82	35.3
Oxalic acid	C ₂ H ₂ O ₄	3.60	10.2
Succinic acid	C ₄ H ₆ O ₄	3.63	6.3

Moreover, although many different intermediates have been considered, the carbon mass balance was not complete and some reaction intermediates remained unidentified. From the difference between the measured and the calculated TOC values, we obtained a maximum discrepancy in the carbon balance of 26% (Fig. 3-12). This discrepancy only appeared at the end of the reaction, indicating that some short chain carboxylic acids remained unidentified or that they were inappropriately quantified. Finally, from the identified reaction products, a simplified reaction pathway for the degradation of 2-CP upon C WAO over FeSC was proposed (Fig. 3-13). In the first step, the 2-CP molecule was predominantly dechlorinated and both dechlorinated aromatic intermediates and HCl were produced. The 2-CP molecule might also be partly oxidized before dechlorination occurs and partly-oxidized chlorinated aromatic intermediates were generated. Further oxidation of the aromatic intermediates led to ring opening and short chain carboxylic acids were formed. At last, all oxidized intermediates gradually converted into CO₂ and H₂O.

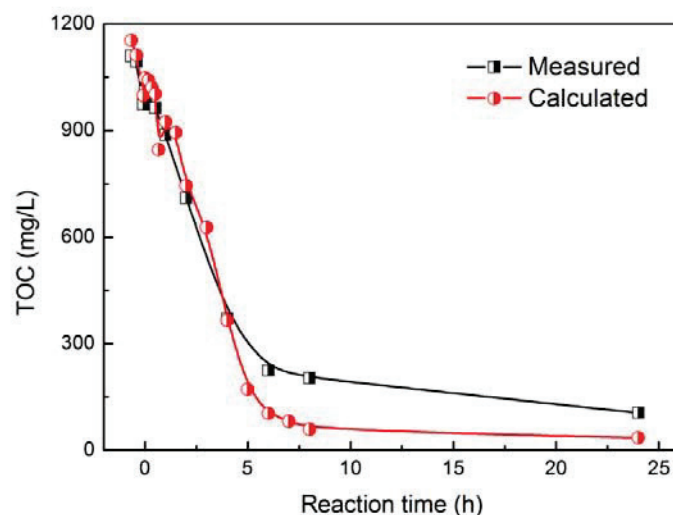


Fig. 3-12. Evolution of the measured (■) and calculated (●) TOC values as a function of time upon catalytic wet air oxidation of 2-CP over the FeSC catalyst (0.3g FeSC 120°C, P_{O₂}: 0.9 MPa, 1300 rpm, 150 mL [2-CP]₀ =2g/L).

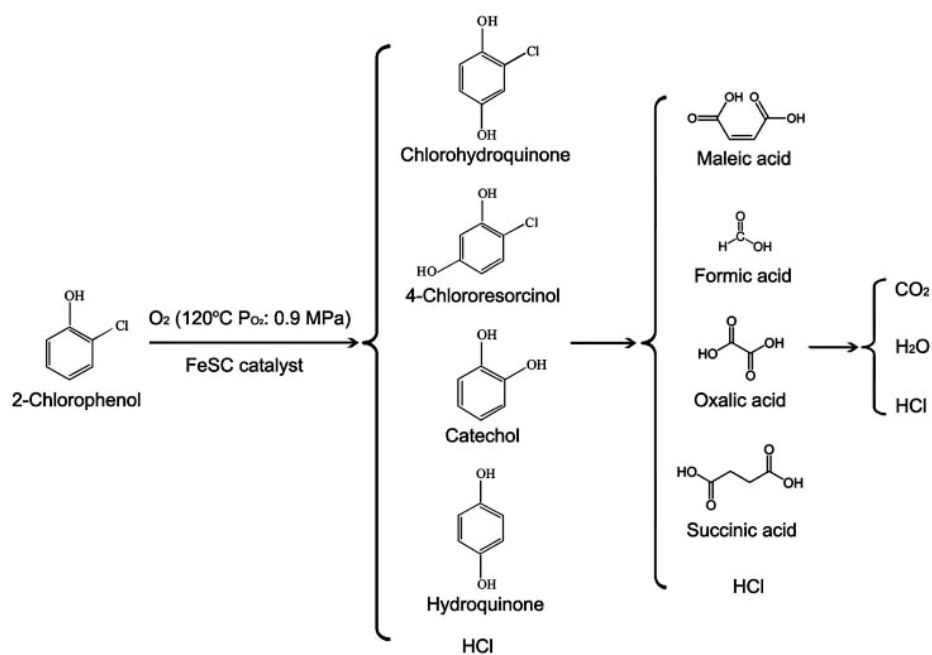


Fig. 3-13. Simplified reaction pathway upon catalytic wet air oxidation of 2-chlorophenol over FeSC catalysts.

3.4. Conclusions

Although the catalytic wet air oxidation of phenol using heterogeneous transition metal catalysts has been extensively studied in the literature, little attention has been paid to the use of this kind of catalysts for the treatment of 2-chlorophenol. In this work a sewage sludge derived carbon supported iron oxide catalyst (FeSC) was prepared and used in catalytic wet air oxidation of 2-chlorophenol. After 24 h reaction, high 2-CP conversion and TOC removal could be reached even at moderate reaction temperature (120°C) and low oxygen partial pressure (0.9 MPa). However, iron leaching rapidly occurred upon decrease of the pH, promoting the activity in the homogeneous phase. The pH evolution essentially resulted from the release of HCl after dechlorination of 2-CP and the formation of small chain carboxylic acids at the end of the reaction. Much attention was paid to the iron leaching and different attempts to prevent the iron leaching were tested, such as the use of alkaline reagents or buffer solutions. The iron leaching could be kept at a negligible level by controlling the pH, but a significant decrease of the catalytic activity was observed at the same time. Among the different approaches, the use of the acetate buffer was successful in minimizing the iron leaching while keeping some catalytic activity.

Therefore, the use of this type of catalyst in the CWAO of 2-CP has to be carefully considered. The iron leaching would indeed require an additional treatment before discharge. In our study, the iron could be recovered by adjusting the pH to neutral pH at the end of the reaction. Only a very slight catalyst deactivation was observed upon successive batch experiments.

References

- [1] F. Luck, A review of industrial catalytic wet air oxidation processes, *Catal. Today*, 27 (1996) 195-202.
- [2] K.H. Kim, S.K. Ihm, Heterogeneous catalytic wet air oxidation of refractory organic pollutants in industrial wastewaters: A review, *J. Hazard. Mater.* 186 (2011) 16-34.
- [3] J.Y. Qin, Q.L. Zhang, K.T. Chuang, Catalytic wet oxidation of p-chlorophenol over supported noble metal catalysts, *Appl. Catal. B: Environ.*, 29 (2011) 115-123.
- [4] N. Li, C. Descorme, M. Besson, Catalytic wet air oxidation of a aqueous solution of 2-chlorophenol over Ru/zirconia catalysts, *Appl. Catal. B: Environ.*, 71 (2007) 262-270.

- [5] N. Li, C. Descorme, M. Besson, Application of $\text{Ce}_{0.33}\text{Zr}_{0.63}\text{Pr}_{0.04}\text{O}_2$ -supported noble metal catalysts in the catalytic wet air oxidation of 2-chlorophenol: Influence of the reaction conditions, *Appl. Catal. B: Environ.* 80 (2008) 237-247.
- [6] J. Gaálová, J. Barbier Jr, S. Rossignol, Ruthenium versus platinum on cerium materials in wet air oxidation of acetic acid, *J. Hazard. Mater.* 181 (2010) 633-639.
- [7] K.H. Kim, J.R. Kim, S.K. Ihm, Wet oxidation of phenol over transition metal oxide catalysts supported on $\text{Ce}_{0.65}\text{Zr}_{0.35}\text{O}_2$ prepared by continuous hydrothermal synthesis in supercritical water, *J. Hazard. Mater.* 167 (2009) 1158-1162.
- [8] S. Yang, Z. Liu, X. Huang, B. Zhang, Wet air oxidation of epoxy acrylate monomer industrial wastewater, *J. Hazard. Mater.* 178 (2010) 786-791
- [9] A. Vallet, M. Besson, G. Ovejero, J. García, Treatment of a non-azo dye aqueous solution by CWAO in continuous reactor using a Ni catalyst derived from hydroxalcalite-like precursor, *J. Hazard. Mater.* 227-228 (2012) 410-417.
- [10] A. Quintanilla, J.A. Casas, J.J. Rodríguez, Catalytic wet air oxidation of phenol with modified activated carbons and Fe/activated carbon catalysts, *Appl. Catal. B: Environ.* 76 (2007) 135-145.
- [11] D. Posada, P. Betancourt, F. Liendo, J.L. Brito, Catalytic Wet Air Oxidation of Aqueous Solutions of Substituted Phenols, *Catal. Lett.* 106 (2006) 81-88.
- [12] X.H. Xu, P. He, J. Jin, Z.W. Hao, Fe salts as catalyst for the wet oxidation of o-chlorophenol. *J. Zhejiang Univ. SCI*, 6B (6) (2005) 569-573.
- [13] M. Pera-Titus, V. García-Molina, M.A. B años, J. Giménez, S. Esplugas, Degradation of chlorophenols by means of advanced oxidation processes: a general review, *Appl. Catal. B: Environ.* 47 (2004) 219-256.
- [14] B. Meunier, Catalytic degradation of chlorinated phenols, *Science*, 296 (2002) 270-271.
- [15] G. Lee, T. Nunoura, Y. Matsumura, K. Yamamoto, Effects of a sodium hydroxide addition on the decomposition of 2-Chlorophenol in supercritical water, *Ind. Eng. Chem. Res.* 41 (2002) 5427-5431.
- [16] J.P. Brunelle, Preparation of catalysts by metallic complex adsorption on mineral oxides, *Pure Appl. Chem.* 50 (1978) 1211-1229.
- [17] N. Li, C. Descorme, M. Besson, Catalytic wet air oxidation of a aqueous solution of 2-chlorophenol over Ru/zirconia catalysts, *Appl. Catal. B: Environ.* 71 (2007) 262-270.
- [18] N. Li, C. Descorme, M. Besson, Catalytic wet air oxidation of chlorophenols over supported ruthenium catalysts, *J. Hazard. Mater.* 146 (2007) 602-609.

- [19] J. Barbier Jr., F. Delanoë, F. Jabouille, D. Duprez, G. Blanchard, P. Isnard, Total oxidation of acetic acid in aqueous solutions over noble metal catalysts. *J. Catal.*, 77 (1999) 378-385.
- [20] J.C. Béziat, M. Besson, P. Gallezot, S. Durécu, Catalytic wet air oxidation of carboxylic acids on TiO₂-supported ruthenium catalysts, *J. Catal.*, 182 (1999) 129-135.
- [21] H.S. Joglekar, S.D. Samant, J.B. Joshi, Kinetics of wet air oxidation of phenol and substituted phenols, *Water Res.*, 25 (1991) 135-145.
- [22] P. Gallezot, S. Chaumet, A. Perrard, P. Isnard, Catalytic wet air oxidation of acetic acid on carbon-supported ruthenium catalysts, *J. Catal.*, 168 (1997) 104-109.
- [23] Y. Kojima, T. Fukuta, T. Yamada, M.S. Onyango, E.C. Bernardo, H. Matsuda, K. Yagishita, Catalytic wet oxidation of o-chlorophenol at mild temperatures under alkaline conditions, *Water Res.*, 39 (2005) 29-36.
- [24] A. Santos, P. Yustos, A. Quintanilla, G. Ruiz, F. Garcia-Ochoa, Study of the copper leaching in the wet oxidation of phenol with CuO-based catalysts: Causes and effects, *Appl. Catal. B: Environ.* 61 (2005) 323-333.
- [25] Santos A, Yustos P, Quintanilla A, Garcia-Ochoa F. Influence of pH on the wet oxidation of phenol with copper catalyst. *Top. Catal.*, 2005, 33: 181-192
- [26] L. Wei, M. Hervé, P. Edouard, Use of different rapid mixing devices for controlling the properties of magnetite nanoparticles produced by precipitation, *J. Cryst. Growth* 342 (2012) 21–27
- [27] R. Robert, S. Barbati, N. Ricq, M. Ambrosio, Intermediates in wet oxidation of cellulose: identification of hydroxyl radical and characterization of hydrogen peroxide, *Water Res.* 36 (2002) 4821-4829.
- [28] F. Arena, C. Italiano, A. Raneri, C. Saja, Mechanistic and kinetic insights into the wet air oxidation of phenol with oxygen (CWAO) by homogeneous and heterogeneous transition-metal catalysts, *Appl. Catal. B: Environ.* 99 (2010) 321-328.
- [29] K.M. Yin, J.H. Wei, J.R. Fu, Mass transport effects on the electrodeposition of iron-nickel alloys at the presence of additives, *J. Appl. Electrochem.*, 25 (1995) 543-555.
- [30] S. Sabhi, J. Kiwi, Degradation of 2,4-dichlorophenol by immobilized iron catalysts, *Water Res.* 35 (2001) 1994-2002.
- [31] G. Lee, T. Nunoura, Y. Matsumura, K. Yamamoto, Comparison of the effects of the addition of NaOH on the decomposition of 2-chlorophenol and phenol in supercritical water and under supercritical water oxidation conditions, *J. Supercrit. Fluids*, 24 (2002) 239-250.

- [32] Y. Kojima, T. Fukuta, T. Yamada, M.S. Onyango, E.C. Bernardo, H. Matsuda, K. Yagishita, Catalytic wet oxidation of o-chlorophenol at mild temperatures under alkaline conditions, *Water Res.* 39 (2005) 29-36.
- [33] A. Pintar, J. Levec, Catalytic oxidation of aqueous p-chlorophenol and p-nitrophenol solutions, *Chem. Eng. Sci.* 49 (1994) 4391-4407.
- [34] J. Guo, M. Al-Dahhan, Activity and stability of iron-containing pillared clay catalysts for wet air oxidation of phenol, *Appl. Catal. A: Gen.* 299 (2006) 175-184.
- [35] N.D. Tran, M. Besson, C. Descorme, K. Fajferweg, C. Louis, Influence of the pretreatment conditions on the performances of CeO₂-supported gold catalysts in the catalytic wet air oxidation of carboxylic acids, *Catal. Commun.* 16 (2011) 98-102.
- [36] X. Bernata, A. Fortuny, F. Stüber, C. Bengoa, A. Fabregat, J. Font, Recovery of iron (III) from aqueous streams by ultrafiltration, *Desalination* 221 (2008) 413-418.
- [37] S.G. Pouloupoulos, C.A. Korologos, A. Boulamanti, C.J. Philippopoulos, Treatment of 2-chlorophenol aqueous solutions by wet oxidation, *Water Res.* 41 (2007) 1263-1268.
- [38] M.E. Suarez-Ojeda, F. Stüber, A. Fortuny, A. Fabregat, J. Carrera, J. Font, Catalytic wet air oxidation of substituted phenols using activated carbon as catalyst, *Appl. Catal. B: Environ.* 58 (2005) 105-114.
- [39] A. Quintanilla, J.A. Casas, J.J. Rodriguez, Hydrogen peroxide-promoted-CWAO of phenol with activated carbon, *Appl. Catal. B: Environ.* 93 (2010) 339-345.

Chapter 4

Catalytic ozonation of antibiotic sulfamethoxazole in aqueous solution over a Mn-g-C₃N₄ modified Sewage sludge-based activated carbon

4.1. Introduction

In recent years, a huge amount of pharmaceutical compounds are produced and distributed annually [1]. After medication, approximately 50–90% of these administered drugs are excreted from animal body without undergoing metabolism. The disposed pharmaceutical compounds have been detected in different water environments in a range of ng/L to µg/L [2]. Among all the pharmaceutical pollutions, sulfonamides (SAs) have been identified most frequently, due to their widespread consumption, low biodegradability, and hydrophilicity. Toxicity induced by these antibiotics or their metabolites can have potential health impacts on aquatic animals and humans [3,4]. As a consequence, it is necessary to remove these sulfonamides compounds from water drastically. Among all the reported technologies, advanced oxidation processes (AOPs) have already been considered as the most appropriate ones for this task. Catalytic ozonation is a new AOPs technology, which employed a useful catalyst to decompose dissolve ozone or to oxidize the pollutant compound [5]. According to literatures, activated carbon and Mn containing oxides are classical catalysts in ozonation reactions [6-8].

Graphitic carbon nitride (g-C₃N₄) material, which presented graphite like sp²-bonded C-N structure (Fig. 4-1) [9], has recently received a great deal of attention. To date, g-C₃N₄ has been extensively applied in different fields, including photocatalytic [10,11], hydrogen production [12,13], base catalysis [14,15] and so on. The graphitic structure and the presence of so-called “nitrogen pots” with abundant melon moieties in g-C₃N₄ were considered as potential ideal sites for the heteroatomic doping of substituent atoms or metal oxides, such as Fe, Co, Fe₃O₄, CuO. The modified g-C₃N₄-based catalysts with enhanced activity mainly used as photocatalysts [16-18]. To the best of our knowledge, the chemical doped g-C₃N₄ materials have never been applied as effective ozonation catalysts so far.

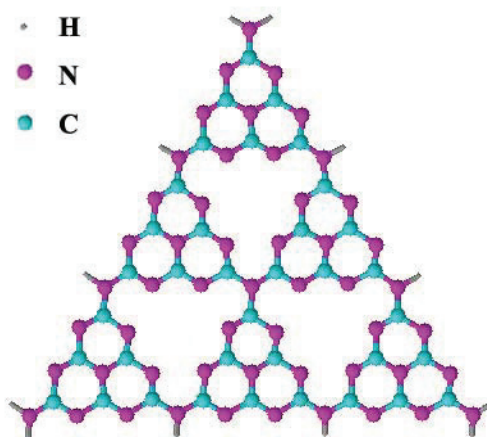


Fig. 4-1 An idealized g-C₃N₄ sheet.

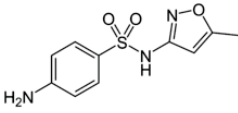
In this chapter, g-C₃N₄ was employed as the template and host to synthesize Mn oxide nanoparticles (NPs) via a one-pot in-situ method. The synthesized Mn oxide NPs modified g-C₃N₄ catalyst (Mn-g-C₃N₄) catalysts were structurally characterized by SEM, EDX mapping, XRD, FTIR and TEM. The catalytic ozonation activity of Mn-g-C₃N₄ was also investigated by using Sulfamethoxazole (SMZ) as target pollutant. It is known that the bulk g-C₃N₄ materials generally have very low surface areas (<10 m² g⁻¹ [19]), which may limit its adsorption capacity for the organic pollutant. Considering the sewage sludge-based activated carbon (SBAC) presents high surface area and large pore volume, in this study, the SBAC was used as support for the Mn-g-C₃N₄ to synergize the oxidation and adsorption properties. Degradation kinetics of SMZ by using Mn-g-C₃N₄/SBAC composite catalysts were determined. The antioxidant properties and catalytic stability of Mn-g-C₃N₄/SBAC catalyst was also checked.

4.2. Experimental

4.2.1 Chemicals

The dewatered sewage sludge was still obtained from the Lie De municipal wastewater treatment plant in Guangzhou, China. The melamine and sulfamethoxazole (SMZ) were purchased from Shanghai Aladdin Reagent Company. The Physicochemical properties of SMZ were listed in Table 4-1. All of the chemical reagents were of analytical grade purity and used without further purification. Deionized water was used for all experiments.

Table 4-1. Physicochemical properties of Sulfamethoxazole [20]

Structure	Formula	Molecular weight (g/mol)	Width (nm)	Length (nm)	Depth (nm)	Solubility at 25°C (g/L)	Acid pKa
	C ₁₀ H ₁₁ N ₃ O ₃ S	253.28	0.71	1.33	0.58	< 1.0	5.7

4.2.2. Synthesis of the catalysts

Manganese oxide nanoparticles modified g-C₃N₄ composite catalysts were prepared via a one-pot method. 2.0 g melamine and desired amount of manganese acetate tetrahydrate was grinded in a mortar. The resulting mixture was transferred into a crucible, and pyrolyzed under N₂ (40 mL min⁻¹) in a horizontal furnace at 550°C for 4 h (heating rate: 3 °C min⁻¹). Afterwards, the pyrolyzed sample was washed with deionized water for several times. Then the sample was dried at 105°C overnight and grinded to less than 200-mesh size.

g-C₃N₄ modified with different amounts of manganese oxide is denoted as X%Mn-g-C₃N₄ (shown in Table 4-2), where X, ranging from 0 to 40, is used to note the Mn content in the composite catalyst. Pure g-C₃N₄ was also synthesized through a polycondensation process under the same conditions by only using melamine.

Table 4-2. Preparation conditions for Mn-g-C₃N₄ catalysts

Sample	Melamine (g)	Manganese (II) acetate tetrahydrate (g)
g-C ₃ N ₄	2.000	0
10%Mn-g-C ₃ N ₄	2.000	0.583
20%Mn-g-C ₃ N ₄	2.000	1.402
30%Mn-g-C ₃ N ₄	2.000	2.633
40%Mn-g-C ₃ N ₄	2.000	4.697

The Sewage sludge-based activated carbon (SBAC) was prepared by means of ZnCl₂ chemical activation-pyrolysis-carbonization. 100 g dried sewage sludge was impregnated into 250 mL 5 mol/L ZnCl₂ solution under stirring overnight. Then the slurry was dried and heated in a programmable tube electric furnace under nitrogen flow at 650°C for 1 h (heating rate: 20 °C/min). After cooling down to room temperature, the sample washed with 3 mol/L hydrochloric acid solution to remove metal

ions and then rinsed with deionized water until the pH was constant. Then the product was dried at 105°C, and grinded to less than 200-mesh size.

Table 4-3. Preparation conditions for Mn-g-C₃N₄/SBAC catalysts

Sample	SBAC (g)	Melamine (g)	Manganese(II) acetate tetrahydrate
Mn-g-C ₃ N ₄ /SBAC ₁	1.000	0.142	0.049
Mn-g-C ₃ N ₄ /SBAC ₂	1.000	0.285	0.097
Mn-g-C ₃ N ₄ /SBAC ₃	1.000	0.569	0.194
Mn-g-C ₃ N ₄ /SBAC ₄	1.000	0.853	0.290

And then the prepared sewage sludge-based activated carbon (SBAC) with large surface area was used as the support for Mn-g-C₃N₄ to prepare composite catalyst (Mn-g-C₃N₄/SBAC). For the preparation procedure, the SBAC powder, melamine and manganese (II) acetate tetrahydrate were mixed homogeneously, and then synthesized through a polycondensation process under 550°C.

4.2.3. Characterization of the catalysts

The prepared catalysts were characterized with XRD, FTIR, SEM-EDX mapping and TEM. The instruments used and testing conditions were the same as described in the Section 2.2.2 in Chapter 2.

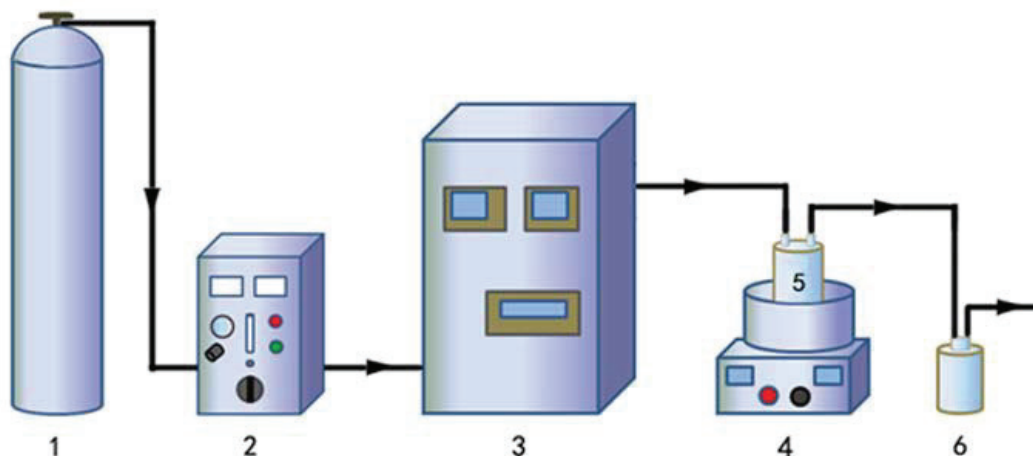
4.2.4. Catalytic ozonation experiments

Experiments were carried out in a batch ozone oxidation system as shown in Fig. 4-2. Ozone was generated from an ozone generator and delivered into glass reactor through a sand core aerator from its bottom. The ozone system was stably controlled at least 30 min before experiment.

4.2.5. Analytical methods

The concentration of SMZ was measured by high performance liquid chromatography (Shimadzu LC-15C), using a UV-detector (SPD-10AV) set at 265 nm. The HPLC system was equipped with a Wondasil C18 (4.6×150 mm, Shimadzu GL) column. The analysis was carried out with an aqueous solution containing 30 vol.% methanol and 70 vol.% water. 85 wt.% H₃PO₄ was used to acidified the mobile phase to 2.5. The flow rate was 1.2 mL·min⁻¹ at 30°C.

The pH of the solution was measured with a PHS-3C pH meter (Rex Instrument Factory, Shanghai, China). The chemical oxygen demand (COD) was measured with potassium dichromate method. The metal concentration in the liquid samples was further analyzed by ICP-OES to check for lixiviation.



1-High-pressure oxygen tank; 2-Ozone generator;
3-Online ozone concentration detector;
4-Stirring hot plate; 5-Reactor; 6-2% KI solution

Fig. 4-2 Diagram of ozone oxidation system

4.3. Results and discussion

4.3.1. Characterization of Mn-g-C₃N₄ catalyst

As shown in Fig. 4-3, the color of the catalyst will change from yellow to be a little green, when manganese (II) acetate tetrahydrate was added during the synthesis of catalyst, indicating the changes of physicochemical properties for the Mn containing catalysts.

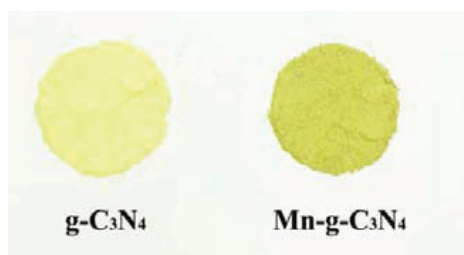


Fig. 4-3. Photos of g-C₃N₄ and 10%Mn-g-C₃N₄ catalysts

This speculate can be confirmed by the SEM micrographs of g-C₃N₄ and 10%Mn-g-C₃N₄ catalysts

(Fig. 4-4). After Mn species are impregnated in the g-C₃N₄ support, the shape of the catalyst layer changes significantly. Furthermore, EDX mapping were performed to check the distribution of loaded Mn on the surface of Mn-g-C₃N₄ catalyst. From Fig. 4-5, we could found that the Mn containing particles are almost uniformly distributed on the g-C₃N₄ support.

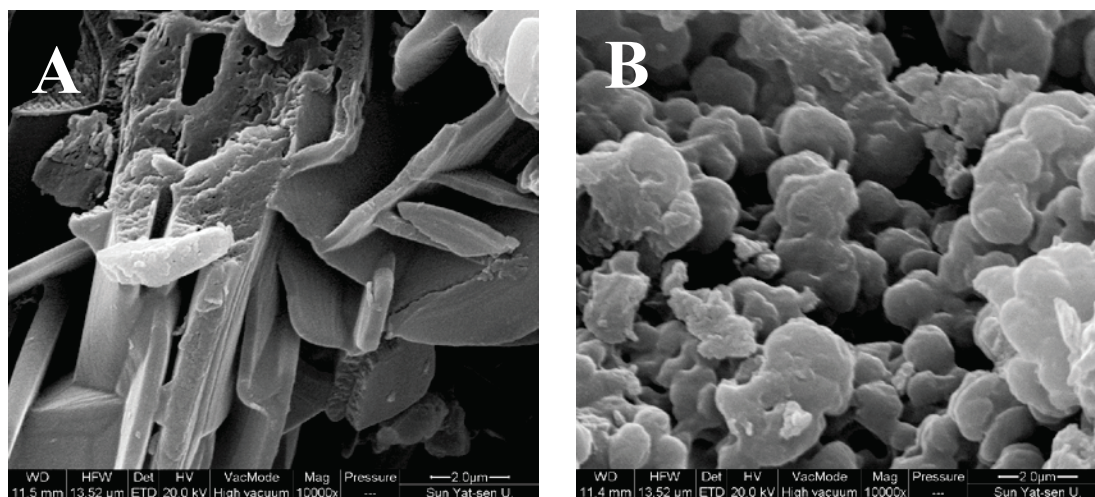


Fig. 4-4. SEM image of g-C₃N₄ (A) and 10%Mn-g-C₃N₄ (B) catalysts.

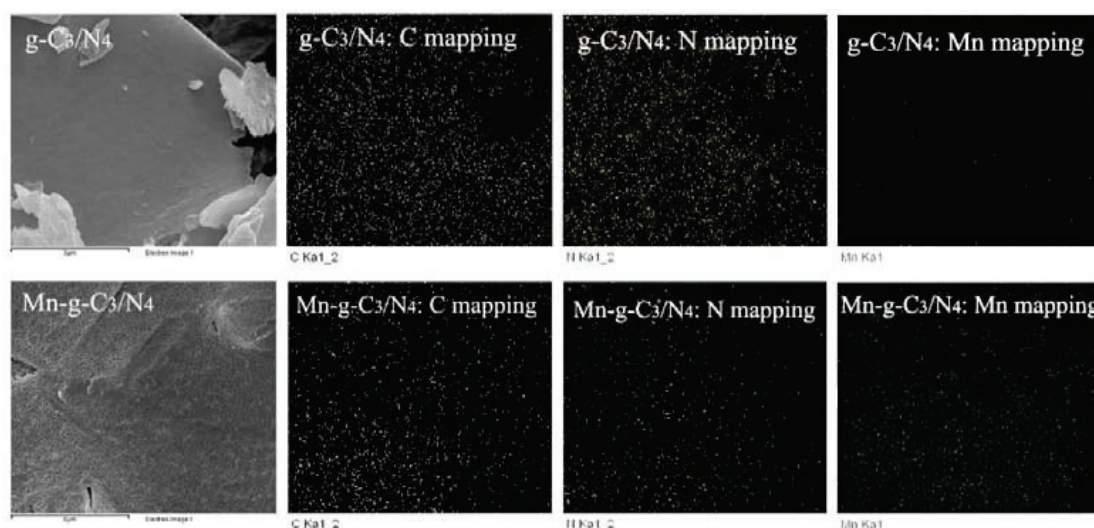


Fig. 4-5. EDX mapping of C, N and Mn elements for g-C₃N₄ and 10%Mn-g-C₃N₄ catalysts.

Elemental analysis results (listed in Table 4-4), revealed that the g-C₃N₄ and Mn-g-C₃N₄ catalyst present similar C, N and H elements containing, and the C/N molar ratio are 0.68 and 0.70 for g-C₃N₄ and Mn-g-C₃N₄ catalyst, which are very closed to the theoretical value of g-C₃N₄ (0.75).

The X-ray diffraction (XRD) patterns of the g-C₃N₄ catalysts with different Mn content are presented in Fig. 4-6. The (1 0 0) and (0 0 2) peaks located around $2\theta=12^\circ$ and 27° were observed for all the catalysts, which are corresponding to in-plane structural packing motif of tri-s-triazine units and the

interlayer stacking of aromatic segments, respectively [21]. Furthermore, the intensity of the (0 0 2) peak remarkably decreases with the increasing of Mn content in the catalysts, indicating a host-guest interaction and an inhibition of polymeric condensation by excessive Mn species.

Table 4-4. The content of C, N and H element in g-C₃N₄ and Mn-g-C₃N₄ catalysts

Sample	C (wt.%)	N (wt.%)	H (wt.%)	C/N ratio
g-C ₃ N ₄	34.3	59.3	1.8	0.68
Mn-g-C ₃ N ₄	33.15	55.6	1.5	0.70

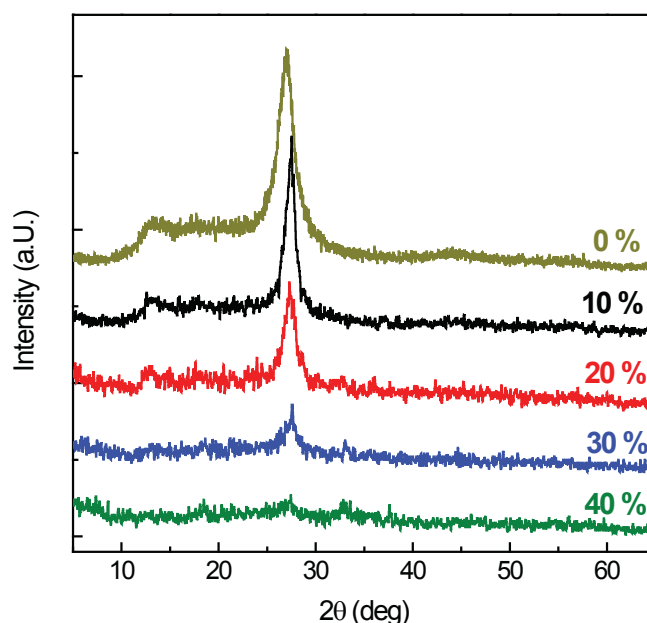


Fig. 4-6. XRD patterns of Mn-g-C₃N₄ with different Mn content.

When the Mn content increased to as high as 40 wt.%, peaks located at $2\theta=32.9^\circ, 45.2^\circ$ and 55.2° were observed, which could be assigned to the (2 2 2), (3 3 2) and (4 4 0) planes of Mn₂O₃ particles (JCPDS 41d-1442). The average size of the Mn₂O₃ crystallites was calculated to be 5.2 nm from the major diffraction peak (2 2 2) using Debye-Scherrer's formula.

The interlayer spacing of Mn-g-C₃N₄ attributes to (0 0 2) peak was calculated by Bragg equation [22]:

$$d = \frac{\lambda}{2 \sin \theta} \quad (\text{Equation 4-1})$$

As shown in Table 4-5, the calculated interplanar distance of the aromatic units decreased with increasing Mn content. This is attributed to the presence of a small tilt angularity in the structure [23]. Thus, we could deduce that the Mn species were coordinated to the g-C₃N₄ host successfully. In the subsequent experiments, 10% Mn-g-C₃N₄ was chosen for the other characterization and catalytic ozonation activity test.

Table 4-5. Bragg angle and interlayer spacing of the Mn-g-C₃N₄.

Sample	2θ for (0 0 2) plane (deg)	d spacing (Å)
g-C ₃ N ₄	26.983	3.30
10%Mn-g-C ₃ N ₄	27.374	3.26
20%Mn-g-C ₃ N ₄	27.443	3.25
30%Mn-g-C ₃ N ₄	27.569	3.23
40%Mn-g-C ₃ N ₄	27.580	3.23

Fig. 4-7 shows the FTIR spectra of the g-C₃N₄ and Mn-g-C₃N₄ catalysts. The sharp band at 807 cm⁻¹ gives strong evidence of the characteristic absorption peak of triazine units. Several strong bands located in the 1200-1600 cm⁻¹ range are found, which corresponds to the typical stretching modes of aromatic C-N heterocycles. Additionally, the broad band at 3100-3500 cm⁻¹ range may be related to the characteristic stretching vibration modes of -NH group [24-26].

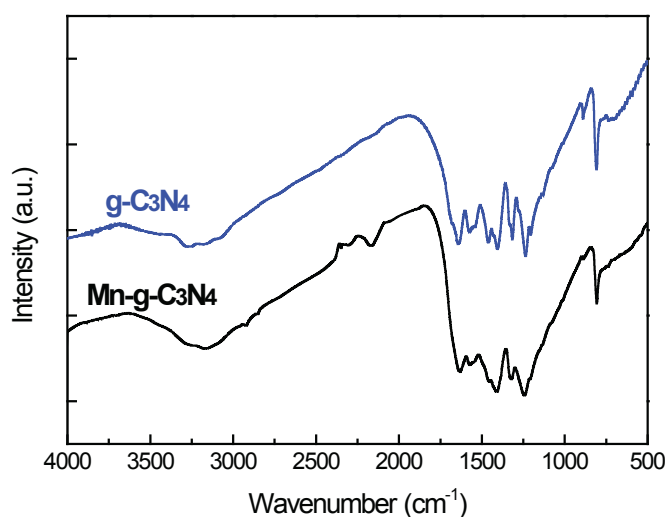


Fig. 4-7. FTIR spectra of g-C₃N₄ and Mn-g-C₃N₄.

The FTIR absorption bands and corresponding metal loaded compounds for g-C₃N₄ and Mn-g-C₃N₄ were listed in Table 4-6. Compared to g-C₃N₄, the adsorption assigned to C-N and C=N groups

stretching in the 1200-1600 cm^{-1} range became weaker for the FTIR spectra of Mn-g-C₃N₄. In addition, a luminescence peak at 2163 cm^{-1} may be related to the stretching mode of C≡N [27]. These phenomena indicate that some of the triazine units are destroyed partly after the Mn species was loaded.

Table 4-6. The FTIR absorption bands of g-C₃N₄ and corresponding Mn loaded compounds.

Wavenumber (cm^{-1})	Functional group
807	Out-of plane bending modes of C-N heterocycles
1247,1327,1407	Aromatic C-N stretching
1635	C-N stretching
3100-3500	Stretching modes of terminal NH₂ or NH groups at the defect sites of the aromatic ring
2163	C≡N stretching when coordinated nitrile in Metal-CN complexes
2925 and 2850	C-H stretching

In order to further confirm the chemical state of Mn species in the Mn-g-C₃N₄ catalysts, g-C₃N₄ and Mn-g-C₃N₄ catalysts were characterized by TEM. As shown in Fig. 4-8A, the TEM image of pure g-C₃N₄ shows a sheet-like morphology. The crystal lattice fringes with d-spacing of 0.329 nm can be assigned to the (002) crystallographic plane of g-C₃N₄. For the Mn modified sample, the Mn₂O₃ nanoparticles (NPs) are dispersed on the layered structure of g-C₃N₄ in the form of single particles or small particles aggregates (Fig. 7B). The fringes spacing was measured to be 0.271 nm, which is corresponded to (222) lattice plane of Mn₂O₃ (JCPDS 41-1442). The diameters of Mn₂O₃ NPs in Mn-g-C₃N₄ are about 4.5 nm, which is quite similar to the value predicted by XRD. Thus, it could deduce that the g-C₃N₄ can act as substrate for loading of Mn₂O₃ NPs.

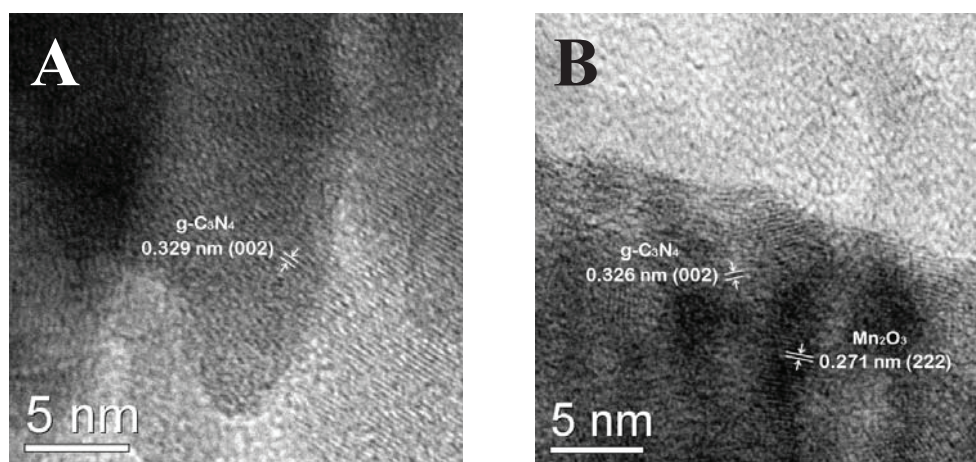


Fig. 4-8. TEM images of g-C₃N₄ (A) and Mn-g-C₃N₄ catalysts (B).

The Mn content, specific surface area and pH_{PZC} of $g-C_3N_4$ and $Mn-g-C_3N_4$ catalysts were also investigated (Table 4-7). Compared with the pure $g-C_3N_4$, the loaded of Mn_2O_3 NPs increased the S_{BET} and pH_{PZC} of the catalysts.

Table 4-7. Physicochemical properties of $g-C_3N_4$ and $Mn-g-C_3N_4$ catalysts

Sample	Metal content (wt.%)	S_{BET} ($m^2 g^{-1}$)	pH_{PZC}
$g-C_3N_4$	-	9.3	6.4
$Mn-g-C_3N_4$	10.7	24.0	7.5

4.3.2. Evaluation of the catalytic ozonation activity of $Mn-g-C_3N_4$ catalysts

The catalytic ozonation activity of $g-C_3N_4$, $Mn-g-C_3N_4$ and commercial Mn_2O_3 NPs were ascertained by monitoring the degradation of SMZ. The results were presented in Fig. 4-9. When $g-C_3N_4$ was used as ozonation catalyst, only 67.1% of SMZ was removed after 60 min oxidation, no significant enhancement of SMZ removal was observed. By comparison, 95.1% of SMZ was decomposed using $Mn-g-C_3N_4$. Furthermore, the removal efficiency of SMZ was improved by 15.2% by using $Mn-g-C_3N_4$ compared to that of single Mn_2O_3 NPs. Hence, Mn_2O_3 NPs loaded on $g-C_3N_4$ support, allowed the oxidative removal of pollutants from wastewater by ozonation to proceed more efficiently.

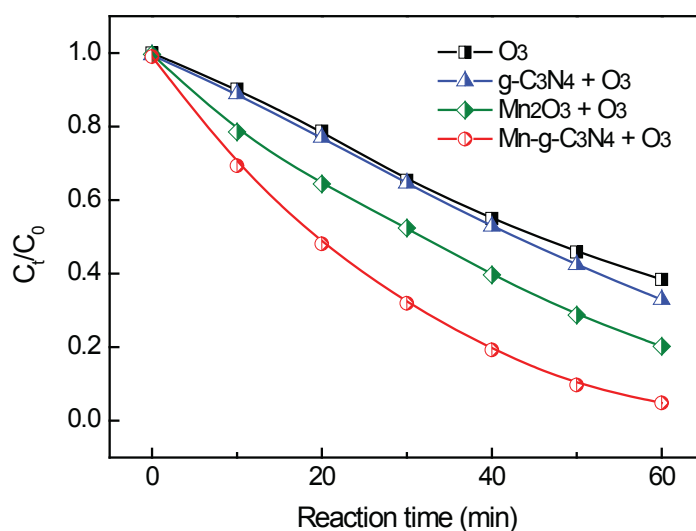


Fig. 4-9. Degradation of SMZ through adsorption and catalytic ozonation by using O_3 and different catalysts ($Mn-g-C_3N_4$: 1.0 g/L, $g-C_3N_4$: 1.0 g/L, Mn_2O_3 : 0.154 g/L; C_{O_3} : 2.0 mg/L; 200 mL 50mg/L SMZ; initial pH 5.3; reaction temperature: 18°C)

4.3.3. Influence of reaction conditions on the activity of Mn-g-C₃N₄ catalyst

4.3.3.1. Effect of agitation speed

Heterogeneous catalytic ozonation of SMZ solution is a gas-liquid-solid reaction, the agitation speed may have some influence on external mass transfer. As shown in Fig. 4-10, agitation speeds higher than 750 rpm didn't lead to any improvement of the SMZ removal rate, indicating the external mass transfer resistances are negligible when the agitation speed was kept higher than 750 rpm. As a result, remaining experimental runs were carried out with the agitation speed fixed at 750 rpm.

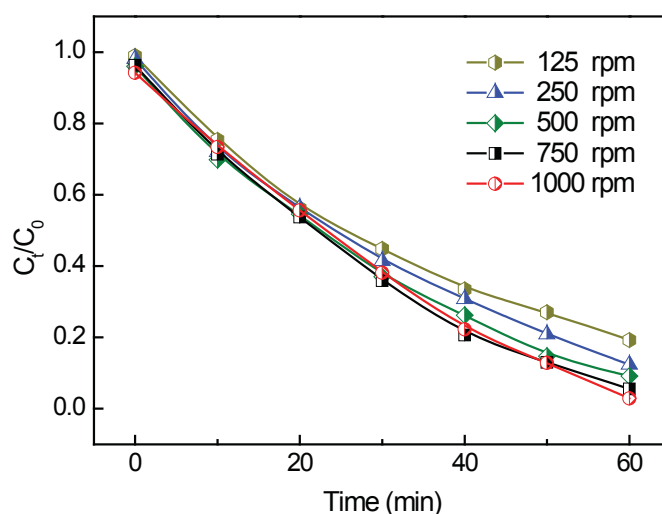


Fig. 4-10. Effect of agitation speed on the degradation efficiency of SMZ through adsorption and catalytic ozonation (C_{O_3} : 2.0 mg/L; Mn-g-C₃N₄: 1.0 g/L; 200 mL 50mg/L SMZ; initial pH 5.3; reaction temperature: 18°C)

4.3.3.2. Effect of Mn-g-C₃N₄ catalyst dosage

In order to avoid the use of excess catalyst, it is necessary to find out the optimum dosage for the efficient application. The effect of catalyst loading on the degradation of SMZ was carried out from 0 to 2 g/L. Fig. 4-11 shows the effect of various catalyst dosages on the removal rate as a function of the reaction time. It seems that the removal efficiency of SMZ increased when the catalyst loading increases from 0 to 1.0 g/L. However, when the catalyst dosage increased from 1.0 to 2.0 g/L, the degradation rate didn't increase significantly. As shown in Fig. 4-12, the initial rate of SMZ conversion was kept **constant when** the catalyst dosage increased from 1.0 g/L to 2.0 g/L. Hence, 1.0 g/L of Mn-g-C₃N₄ catalyst was found to be optimum dosage.

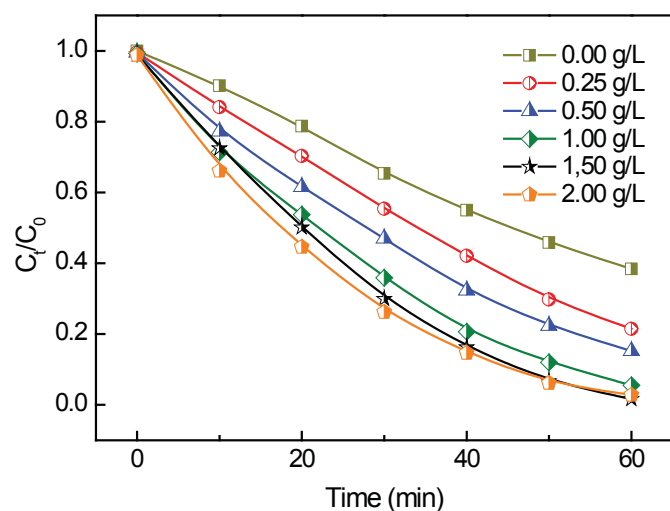


Fig. 4-11. Effect of catalyst dosage on the degradation efficiency of SMZ through adsorption and catalytic ozonation (C_{O_3} : 2.0 mg/L; 200 mL 50mg/L SMZ; initial pH 5.3; reaction temperature: 18°C)

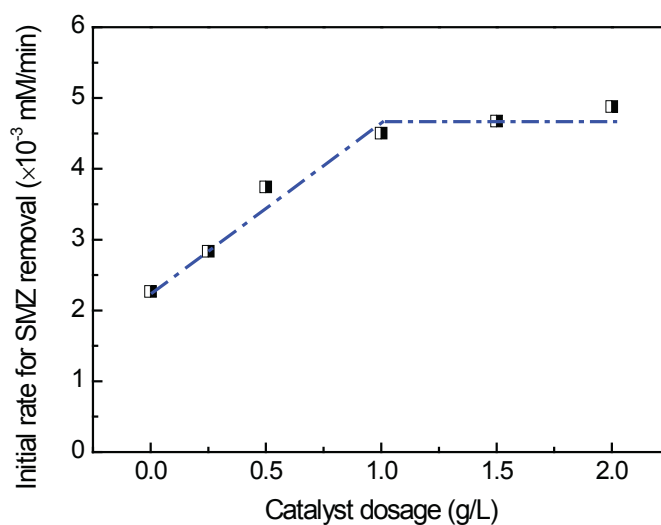


Fig. 4-12. Evolution of the initial rate of SMZ conversion as a function of the catalyst dosage (C_{O_3} : 2.0 mg/L; 200 mL 50mg/L SMZ; initial pH 5.3; reaction temperature: 18°C)

4.3.3.3. Effect of initial SMZ concentration

Fig. 4-13A presents the degradation of SMZ with different initial concentration (ranged from 25 to 200 ppm) as a function of reaction time. And the corresponding removal rate was shown in Fig 4-13B. The removal rate decreased with the increasing of initial SMZ concentration.

The apparent decomposition rate, r_{obs} of SMZ in the ozonation reaction can be written as below [28]:

$$r_{obs} = k_{obs} [O_3]^\alpha [C_{SMZ}]^\beta \quad (\text{Equation 4-2})$$

Where $[O_3]$ is the concentration of dissolved ozone in the liquid phase (mg/L), $[C_{SMZ}]$ is the SMZ concentration at the beginning of ozonation reaction (mmol/L), α and β are the reaction orders of ozone and SMZ.

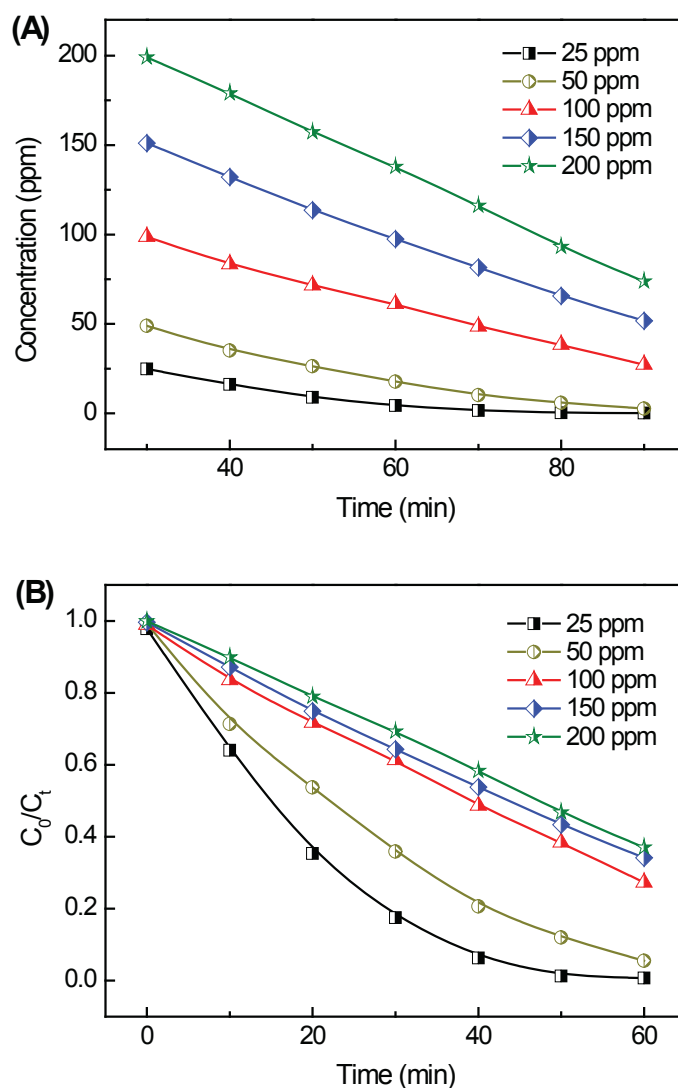


Fig. 4-13. The degradation of SMZ with different initial concentration (A) and corresponding removal efficiency (B) (Mn-g-C₃N₄: 1.0 g/L; O₃: 2.0 mg/L; 200 mL SMZ; initial pH 5.3; reaction temperature: 18°C)

The dependence of the decomposition rate on SMZ concentration was shown in Fig. 4-14. We could find that the SMZ removal rate was 0.46 order with respect to the initial SMZ concentration by nonlinear fitting. This means the reaction is somehow controlled by the adsorption of the SMZ molecule since the Mn-g-C₃N₄ catalyst surface is not fully saturated with the SMZ molecule.

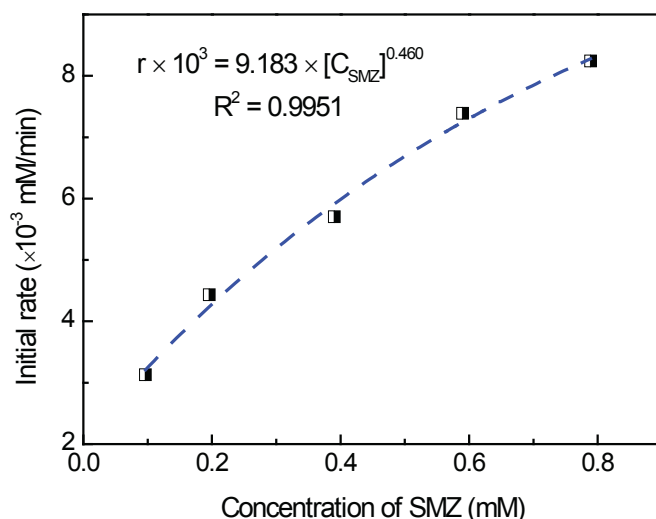


Fig. 4-14 Correlation between the SMZ concentration and initial reaction rate

4.3.4. Characterization of Mn-g-C₃N₄/SBAC composite catalysts

According to the results shown in the previous section, increase the concentration of SMZ on the surface of catalyst is beneficial to the ozonation of SMZ. Considering the low specific surface area of Mn-g-C₃N₄ catalyst ($S_{\text{BET}}=24.0 \text{ m}^2/\text{g}$), the sewage sludge-based activated carbon (SBAC) with large surface area was employed as the support for Mn-g-C₃N₄, the prepared composite catalyst was labeled as Mn-g-C₃N₄/SBAC. As presented in Fig. 4-15, the color of Mn-g-C₃N₄/SBAC composite catalyst is a little gray compared to the SBAC support.



Fig. 4-15. Photos of dry sewage sludge, sludge-based activated carbon and the Mn-g-C₃N₄ and SBAC composite catalysts.

The SEM images of the SBAC support and the Mn-g-C₃N₄/SBAC composite catalyst were shown in Fig. 4-16. The surface morphology of the synthesized Mn-g-C₃N₄/SBAC seemed to be smooth, which probably due to presence of the sheet-like morphology of the Mn-g-C₃N₄. Furthermore, the successful loading of Mn-g-C₃N₄ on the SBAC support was also confirmed by the results of EDX mapping.

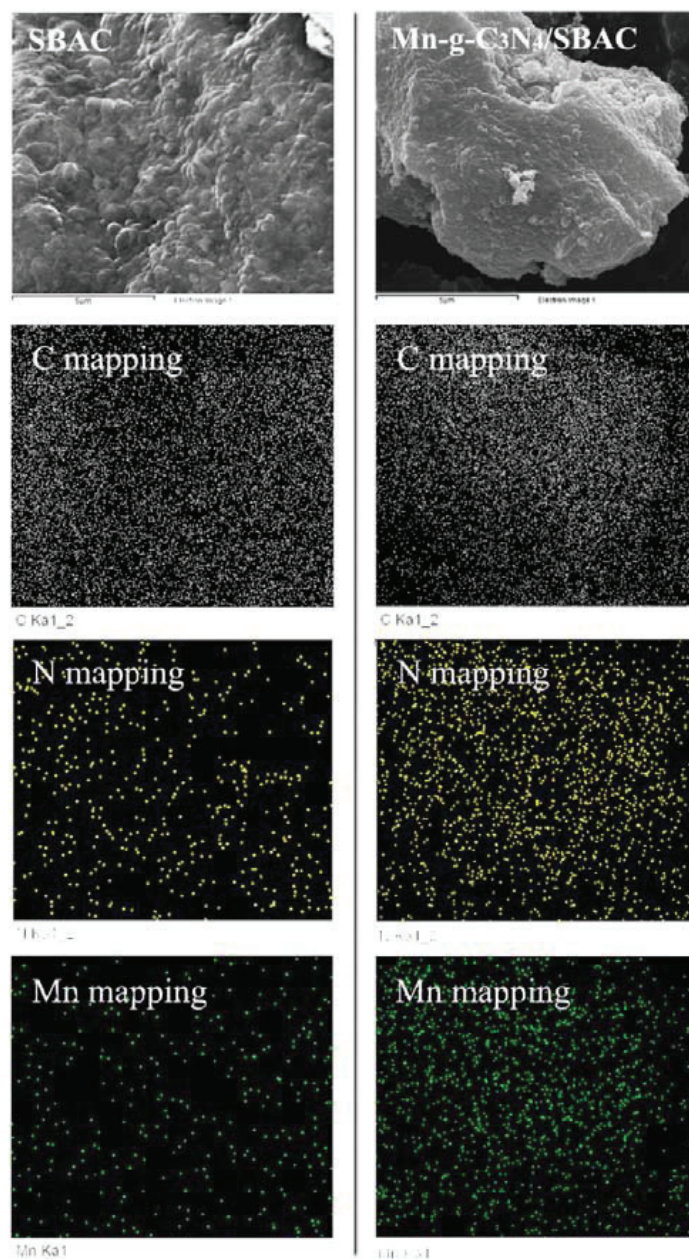


Fig. 4-16. SEM images and EDX mapping of C, N and Mn elements for SBAC and Mn-g-C₃N₄/SBAC composite catalysts.

The structure of as-prepared samples was further investigated by powder XRD. In Fig. 4-17, for the XRD pattern of Mn-g-C₃N₄/SBAC, a new peak at 27° is indicative of (0 0 2) interlayer stacking of g-C₃N₄ structure, indicating that Mn-g-C₃N₄ is well dispersed on the surface of SBAC.

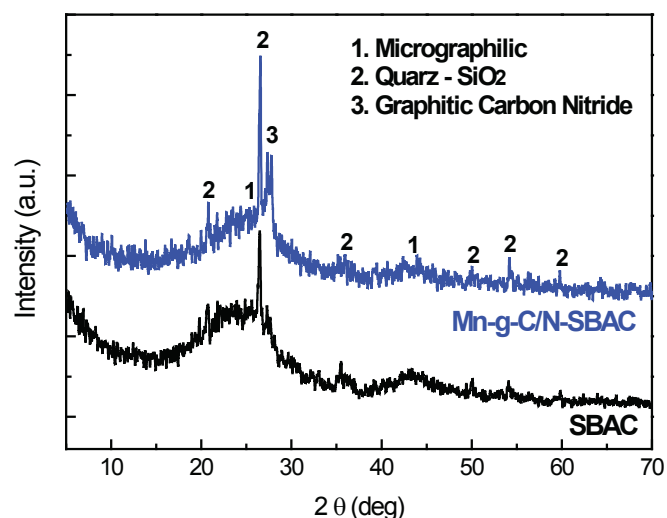


Fig. 4-17. XRD patterns of SBAC and Mn-g-C₃N₄/SBAC composite catalysts.

Fig. 4-18 shows the FTIR patterns of SC, SBAC and Mn-g-C₃N₄/SBAC composite catalysts. All the peaks and their corresponding functional groups were listed in Table 4-9. Compared to the pristine SBAC, the peaks at 1400 and 2930 cm⁻¹ disappeared, which attribute to the C-OH and C-H stretching. And new peaks located at 1566 cm⁻¹ was observed, which is ascribed to C-N functional group in g-C₃N₄. These results further confirmed that the Mn-g-C₃N₄ was successful anchored on t he SBAC surface.

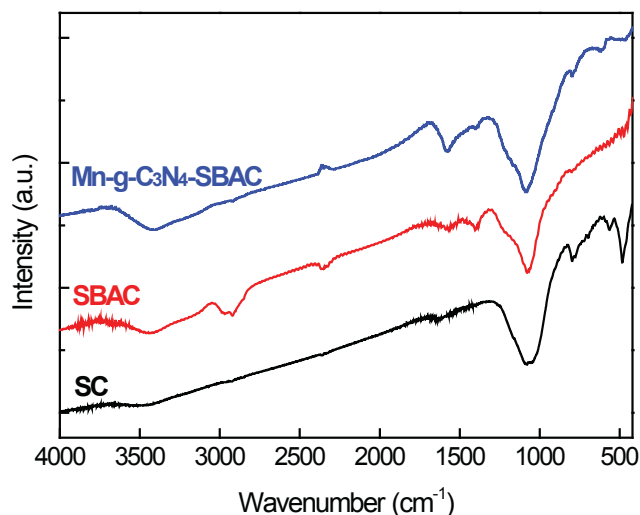


Fig. 4-18. FTIR patterns of SC, SBAC and Mn-g-C₃N₄/SBAC composite catalysts.

Table 4-9. The FTIR absorption bands of sewage sludge-based carbon derived catalysts

Wavenumber (cm ⁻¹)	Functional group
<800	Inorganic components
1045-1084	Si-O-Si and Si-O-C stretching
1350-1460	C-OH stretching
1240-1650	C-N stretching
1500-1900	C=O and C=C stretching
2830-2980	C-H stretching
3400-3450	O-H stretching
3100-3500	N-H stretching

4.3.5. Catalytic ozonation activity of Mn-g-C₃N₄/SBAC composite catalyst

In order to determine the optimal loading of Mn-g-C₃N₄ on the SBAC support, a series of Mn-g-C₃N₄/SBAC composite catalysts with different loading amount were prepared, and their physicochemical properties were presented in Table 4-10. We could find that the S_{BET} of the composite catalysts decreased significantly with the increasing of Mn-g-C₃N₄ loading, which may affect the SMZ adsorption ability of the catalyst in ozonation reactions.

Table 4-10. Physicochemical properties of SBAC and Mn-g-C₃N₄/SBAC composite catalysts.

Sample	Theoretical Mn-g-C ₃ N ₄ content (wt.%)	Yield (%)	Mn (wt.%)	S _{BET} (m ² /g)	pHPZC
SBAC	0	84.9	-	480.4	4.5
Mn-g-C ₃ N ₄ /SBAC ₁	10	76.1	1.3	450.6	6.4
Mn-g-C ₃ N ₄ /SBAC ₂	20	69.2	2.5	359.4	6.6
Mn-g-C ₃ N ₄ /SBAC ₃	30	65.6	3.7	283.7	6.8
Mn-g-C ₃ N ₄ /SBAC ₄	40	59.7	5.1	120.8	7.2

The Langmuir–Hinshelwood model was used for the comparison of catalytic ozonation activity of these composite catalysts [29.30]:

$$r = -\frac{dC}{dt} = -\frac{kK_{abs}C}{1 + K_{abs}C} \quad (\text{Equation 4-3})$$

where r is the rate of degradation for the SMZ molecules ($\text{mol L}^{-1} \text{min}^{-1}$), k is the rate constant ($\text{mol L}^{-1} \text{min}^{-1}$), C is the concentration of SMZ (mol L^{-1}), and K_{ads} is the dynamic Langmuir adsorption constant (L mol^{-1}).

The L-H model also can be expressed as Equation 4-4, which is an equivalent expression applied for the evaluation of k and K_{ads} values.

$$\frac{1}{r_0} = \frac{1}{k} + \frac{1}{kK_{\text{ads}}C_0} \quad (\text{Equation 4-4})$$

where r_0 is the initial rate, C_0 is the concentration of SMZ at the beginning of catalytic ozonation reaction.

In this study, 0.5 g/L composite catalyst was used in each reaction, the initial concentration of SMZ ranged from 50 to 200 mg/L. Fig. 4-19 shows the L-H fitted kinetic profiles of SBAC and Mn-g-C₃N₄/SBAC composite catalysts. Good linear relationship between $1/r_0$ and $1/C_0$ was observed for all the catalysts. As presented in Fig. 4-19F, the K_{ads} decreased with the increasing of loaded Mn-g-C₃N₄. These results could be explained by the decreasing of S_{BET} for the composite catalysts. The value of k increased when more amount of Mn-g-C₃N₄ was loaded on the SBAC support. However, when the content of Mn-g-C₃N₄ in the composite catalyst was higher than 30%, the k value didn't change significantly. In order to avoid the excess loading, the optimal content of Mn-g-C₃N₄ was determined to 30%.

In order to check whether the employed of SBAC support could improve the catalytic activity, the k value for Mn-g-C₃N₄ catalyst was also evaluated by L-H model. As shown in Fig. 4-20, the rate constant k was calculated to be 5.74×10^{-3} mM/min for Mn-g-C₃N₄ catalyst. After the Mn-g-C₃N₄ was incorporated with SBAC, the k increased to 9.05×10^{-3} mM/min, which was 1.6 times compared to the no supported Mn-g-C₃N₄ catalyst. These results show the positive trend by employing SBAC as support for ozonation catalyst.

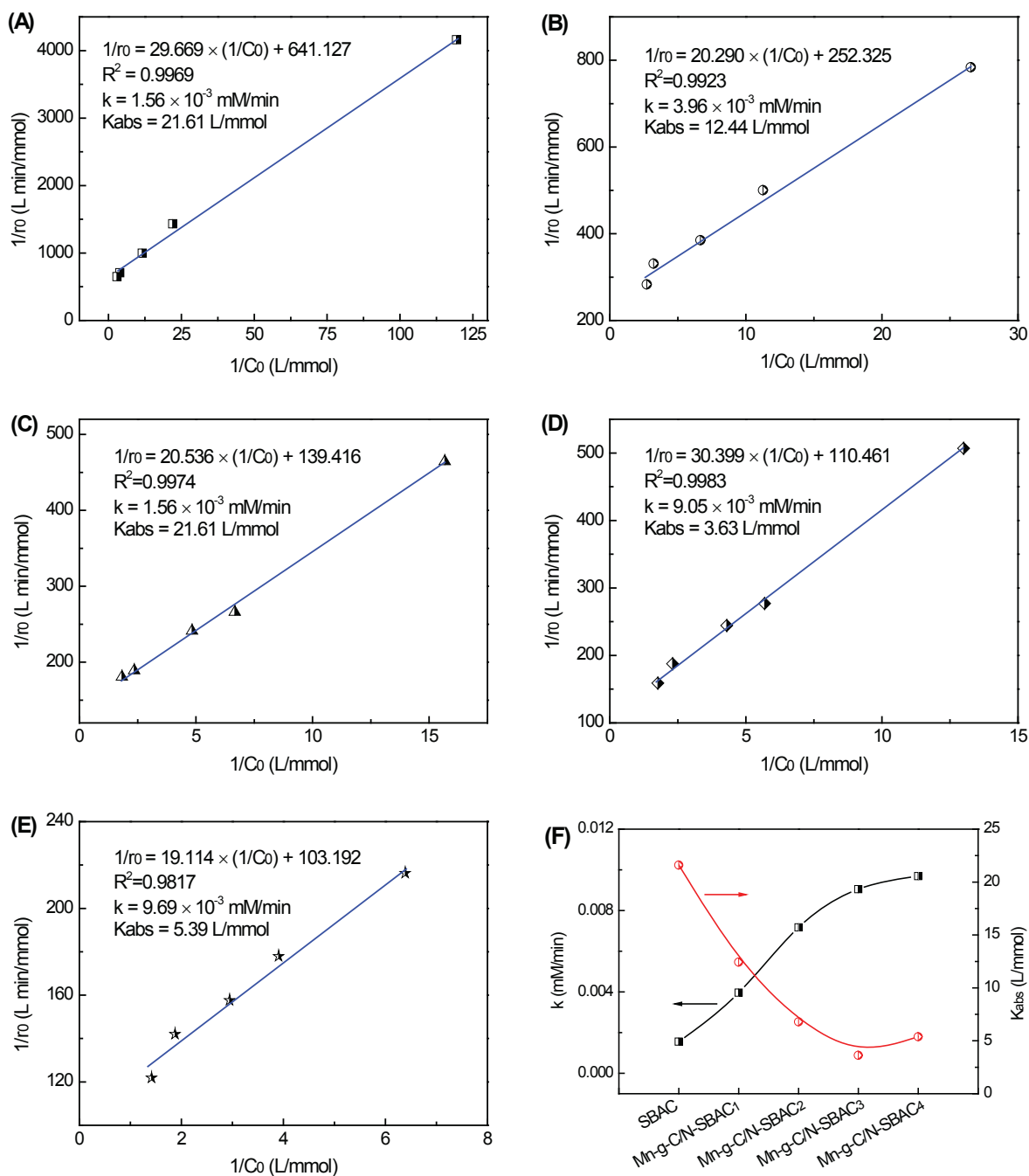


Fig. 4-19. Kinetic parameters calculated according to the Langmuir–Hinshelwood kinetic model by using different catalysts: SBAC (A); Mn-g-C₃N₄/SBAC₁ (B); Mn-g-C₃N₄/SBAC₂ (C); Mn-g-C₃N₄/SBAC₃ (D); Mn-g-C₃N₄/SBAC₄ (E). k and K_{abs} for different catalysts (F) (Catalyst: 0.5 g/L, C_{O_3} : 2.0 mg/L; reaction temperature: 18°C)

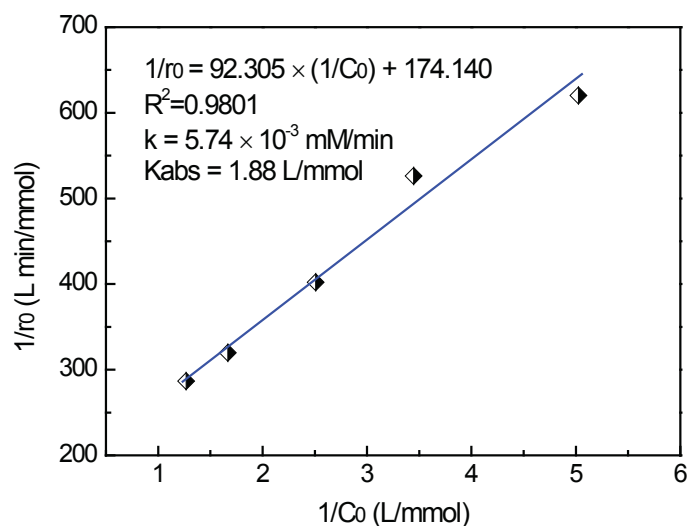


Fig. 4-20. Kinetic parameters calculated according to the Langmuir–Hinshelwood kinetic model by using Mn-g-C₃N₄ catalyst (Catalyst: 0.17 g/L, C_{O₃}: 2.0 mg/L; reaction temperature: 18°C)

4.3.6. Catalytic reusability of the Mn-g-C₃N₄/SBAC composite catalyst

Since the antioxidant properties and catalytic stability are important factors for the catalyst used in AOPs. In this section, 1 g/L of Mn-g-C₃N₄/SBAC₃ was added into 200 mL deionized water and treated with 2.0 mg/L ozone for 60 min. The COD of the filtrate was measured to be 14 mg/L. And only 0.65 mg/L of leached Mn was detected in this filtrate. In order to determine the contribution of homogeneous phase reaction, we also tested the catalytic ozonation activity of the filtrate and almost no catalytic activity was observed (Fig. 4-21). These results indicate that the catalyst presents satisfying oxidation resistance and limited metal leaching.

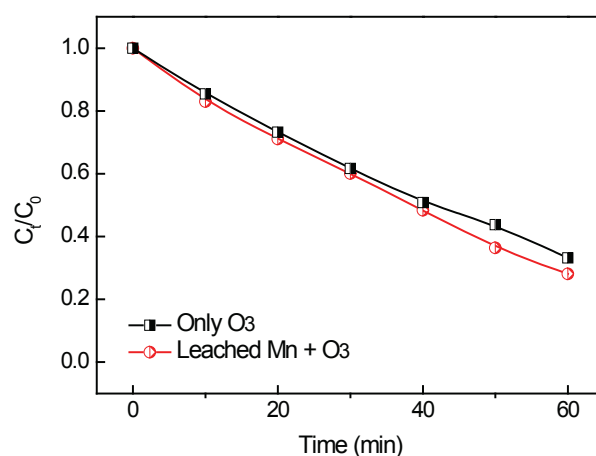


Fig. 4-21. Catalytic activity of the filtrate (O₃: 2.0 mg/L; 200 mL 50 mg/L SMZ; reaction temperature: 18°C)

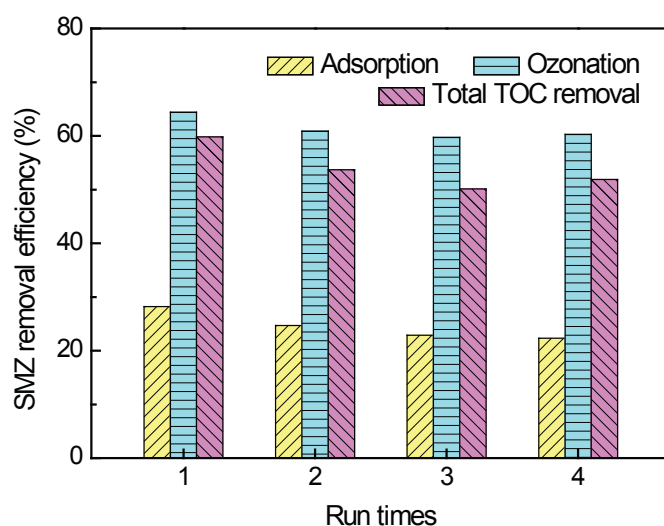


Fig. 4-22. Evolution of the SMZ conversion upon catalytic ozonation of SMZ while recycling the Mn-g-C₃N₄/SBAC catalyst (Mn-g-C₃N₄/SBAC₃: 0.5 g/L; O₃: 4.0 mg/L; 200 mL 200 mg/L SMZ; initial pH 5.0; reaction temperature: 18°C)

The stability of the Mn-g-C₃N₄/SBAC catalyst was investigated under identical reaction conditions by using the same catalyst recycled by filtration. As shown in Fig. 4-22, the adsorption ability and the catalytic activity of the Mn-g-C₃N₄/SBAC₃ catalyst didn't change significantly up to four consecutive cycles.

4.4. Conclusions

In this chapter, a novel Mn doped graphitic carbon nitride catalyst (Mn-g-C₃N₄) was synthesized via a polycondensation process under elevated temperatures. And then the sewage sludge-based activated carbon (SBAC) with large surface area was used as the support for Mn-g-C₃N₄ to prepare composite catalyst (Mn-g-C₃N₄/SBAC). The results of XRD, FTIR, SEM-EDX mapping and TEM characterization revealed that the synthesized Mn-g-C₃N₄ presented a graphitic-like structure with the triazine unit as the primary building block. The loaded Mn presented as Mn₂O₃ nanoparticles and well dispersed on the g-C₃N₄ support. The catalytic ozonation of the antibiotic sulfamethoxazole (SMZ) solution in the presence of Mn-g-C₃N₄ catalyst was investigated in a laboratory scale batch reactor. The results indicated that adding Mn-g-C₃N₄ catalyst into the ozonation reactor could greatly accelerate the rate of SMZ degradation. When the agitation speed was fixed at 750 rpm, and the dose of ozone in the inlet gas was controlled constant at 0.4 mg/min throughout the experiment, after adsorption for 30 min and oxidation for 1 h, the removal efficiency of 50 mg/L SMZ could increase from 61.6% to 95.1% by using 1 g/L Mn-g-C₃N₄ catalyst.

The study showed that the Mn-g-C₃N₄/SBAC composite catalyst prepared by solid-state reaction method could result in the uniform dispersion of Mn-g-C₃N₄ on the framework of SBAC. The degradation of SMZ by using Mn-g-C₃N₄/SBAC composite catalyst fitted well with Langmuir-Hinshelwood model. Considering the reaction rate and the utilization of loaded Mn-g-C₃N₄, the optimal content of Mn-g-C₃N₄ was decided to be 30%. The catalytic activity of the composite catalyst was about 1.6 times compared with the non-supported Mn-g-C₃N₄ catalyst, indicating the positive trend by employing SBAC as support for ozonation catalyst. The composite catalyst also exhibited very good inoxidability, limited Mn leaching and good stability since the activity almost remained constant over four consecutive runs.

References

- [1] S. E splugas, D .M. B ila, L .G.T. K raise, M . D ezotti, Ozonation and advanced oxidation technologies to remove endocrine disrupting chemicals (EDCs) and pharmaceuticals and personal care products (PPCPs) in water effluents. *J. Hazard. Mater.*, 149 (2007) 631-642.
- [2] J. Akhtar, N.A.S. Amin, A. Aris, Combined adsorption and catalytic ozonation for removal of sulfamethoxazole using Fe₂O₃/CeO₂ loaded activated carbon. *Chem. Eng. J.*, 170 (2011) 136-144.
- [3] I. K im, H . Tanaka, Photodegradation characteristics of PPCPs in water with UV treatment. *Environ. Inter.*, 35 (2009) 793-802.
- [4] D. Zhang, B. Pan, H. Zhang, P. Ning, B. Xing, Contribution of different sulfamethoxazole species to their overall adsorption on functionalized carbon nanotubes, *Environ. Sci. Technol.*, 44 (2010) 3806-3811.
- [5] K. He, Y. M. Dong, Z. Li, L. Yin, A.M. Zhang, Y.C. Zheng, Catalytic ozonation of phenol in water with natural brucite and magnesite. *J. Hazard. Mater.*, 159 (2008) 587-592.
- [6] P.M. Álvarez, J.F. García-Araya, F.J. Beltrán, I. Giráldez, J. Jaramillo, V. Gómez-Serrano, The influence of various factors on aqueous ozone decomposition by granular activated carbons and the development of a mechanistic approach. *Carbon*, 44 (2006) 3102-3112.
- [7] B.S. Oh, S.J. Song, E.T. Lee, H.J. Oh, J.W. Kang, Catalyzed ozonation process with GAC and metal doped-GAC for removing organic pollutants. *Water Sci. Technol.*, 49 (2004) 45-49.
- [8] H. Einaga, N, Maeda, Y. Teraoka, Effect of catalyst composition and preparation conditions on catalytic properties of unsupported manganese oxides for benzene oxidation with ozone. *Appl. Catal. B: Environ.*, 142-143 (2013) 406-413.

- [9] Y. Di, X. Wang, A. Thomas, M. Antonietti, Making metal-carbon nitride heterojunctions for improved photocatalytic hydrogen evolution with visible light. *ChemCatChem* 2 (2010) 834-838.
- [10] X. Wang, X. Chen, A. Thomas, X. Fu, M. Antonietti, Metal-Containing Carbon Nitride Compounds: A New Functional Organic - Metal Hybrid Material. *Adv. Mater.* 21 (2009) 1609-1612.
- [11] X. Chen, J. Zhang, X. Fu, M. Antonietti, X. Wang, Fe-g-C₃N₄-catalyzed oxidation of benzene to phenol using hydrogen peroxide and visible light. *J. Am. Chem. Soc.* 131 (2009) 11658-11659.
- [12] B. Yue, Q. Li, H. Iwai, T. Kako, J. Ye, Hydrogen production using zinc-doped carbon nitride catalyst irradiated with visible light. *Sci. Technol. Adv. Mater.* 21 (2011) 034401
- [13] X.H. Li, X. Wang, M. Antonietti, Mesoporous g-C₃N₄ nanorods as multifunctional supports of ultrafine metal nanoparticles: hydrogen generation from water and reduction of nitrophenol with tandem catalysis in one step. *Chem. Sci.* 3 (2012) 2170-2174.
- [14] Y. Wang, X. Wang, M. Antonietti, Polymeric graphitic carbon nitride as a heterogeneous organocatalyst: from photochemistry to multipurpose catalysis to sustainable chemistry. *Angew. Chem. Int. Ed.*, 51 (2012) 68-89.
- [15] J. Zhu, Y. Wei, W. Chen, Z. Zhao, A. Thomas, Graphitic carbon nitride as metal-free catalyst for NO decomposition. *Chem. Commun.*, 46 (2010) 6965-6967.
- [16] Q. Liu, J. Zhang, Graphene supported Co-g-C₃N₄ as a novel metal-macrocylic electrocatalyst for the oxygen reduction reaction in fuel cells. *Langmuir*, 29 (2013) 3821-3828.
- [17] S. Kumar, T. Surendar, B. Kumer, A. Baruah, V. Shanker, Synthesis of magnetically separable and recyclable g-C₃N₄-Fe₃O₄ hybrid nanocomposites with enhanced photocatalytic performance under visible-light irradiation. *J. Phys. Chem. C*, 117 (2013) 26135-26143.
- [18] J. Chen, S. Shen, P. Guo, M. Wang, P. Wu, X. Wang, L. Guo, In-situ reduction synthesis of nano-sized Cu₂O particles modifying g-C₃N₄ for enhanced photocatalytic hydrogen production. *Appl. Catal. B: Environ.*, 153 (2014) 335-341.
- [19] J. Xu, H. Wu, X. Wang, B. Xue, Y. Li, Y. Cao, A new and environmentally benign precursor for the synthesis of mesoporous g-C₃N₄ with tunable surface area. *Phys. Chem. Chem. Phys.*, 15 (2013) 4510-4517.
- [20] V. Yangali-Quintanilla, A. Sadmani, M. McConville M, Kennedy, G. Amy, A QSAR model for predicting rejection of emerging contaminants (pharmaceuticals, endocrine disruptors) by nanofiltration membranes. *Water Res.*, 44 (2010) 373-384.
- [21] G. Liao, D. Zhu, L. Li, B. Lan, Enhanced photocatalytic ozonation of organics by g-C₃N₄ under

- visible light irradiation. *J. Hazard. Mater.*, 280 (2014) 531-535
- [22] K. Katsumata, R. Motoyoshi, N. Matsushita, K. Okada, Preparation of graphitic carbon nitride (g-C₃N₄)/WO₃ composites and enhanced visible-light-driven photodegradation of acetaldehyde gas. *J. Hazard. Mater.*, 260 (2013) 475-482.
- [23] S.C. Yan, Z.S. Li, Z.G. Zou, Photodegradation performance of g-C₃N₄ fabricated by directly heating melamine. *Langmuir* 25 (2009) 10397-10401.
- [24] Y. Cui, Z. Ding, P. Liu, M. Antonietti, X. Fu, X. Wang, Metal-free activation of H₂O₂ by g-C₃N₄ under visible light irradiation for the degradation of organic pollutants. *Phys. Chem. Chem. Phys.*, 14 (2012) 1455-1462.
- [25] X.F. Lu, L.G. Gai, Q.L. Wang, X. Zhao, X.T. Tao, Synthesis and characterization of C₃N₄ nanowires and pseudocubic C₃N₄ polycrystalline nanoparticles. *Mater. Lett.*, 61 (2007) 4255-4258.
- [26] M. Kawaguchi, S. Yagi, H. Enomoto, Chemical preparation and characterization of nitrogen-rich carbon nitride powders. *Carbon*, 42 (2004) 345-350.
- [27] H. Chiniforoshan, N. Safari, J.M. Nezhad, H. Hadadzadeh, A.H. Mahmoudkhani, Synthesis and characterization of tetraphenylporphyrin iron (III) complexes with substituted phenylcyanamide ligands. *Inorg. Chim. Acta*, 359 (2006) 2101-2106.
- [28] H. Fujita, J. Izumi, M. Sagehashi, T. Fuji, A. Sakoda, Decomposition of trichloroethene on ozone-adsorbed high silica zeolites. *Water Res.*, 38 (2004) 166-172.
- [29] C.S. Liu, L.J. Zhang, C.H. Feng, C.A. Wu, F.B. Li, X.Z. Li, Relationship between oxidative degradation of 2-mercaptobenzothiazole and physicochemical properties of manganese (hydro) oxides. *Environ. Chem.*, 6 (2008) 83-92.
- [30] M. Addamo, V. Augugliaro, E. García-López, V. Loddo, G. Marci, L. Palmisano, Oxidation of oxalate ion in aqueous suspensions of TiO₂ by photocatalysis and ozonation. *Catal. Today*, 107-108 (2005) 612-618.

General conclusions

In this thesis, sewage sludge derived carbon was employed as the support of composite catalysts. The catalytic performance of the prepared catalysts was evaluated in heterogeneous Fenton-like reaction, catalytic wet air oxidation process and catalytic ozonation, respectively. The main work and achievements in this thesis are as follows:

- (i) Sewage sludge derived carbon (SC) was employed as the support of iron oxide containing catalyst (FeSC). The chemical changes during the preparation of catalysts by pyrolysis were monitored upon TGA-FTIR analysis. The catalysts were characterized in terms of inorganic elemental composition, XRD, SEM-EDX and XPS. The results revealed that the impregnated iron was existed as Fe_3O_4 in the FeSC catalyst and almost uniformly distributed on the SC support. The Fenton-like oxidation efficiency of acid orange II (AOII) over FeSC catalyst was tested. The results showed that the highest discoloration efficiency of 100 mg/L AOII could be achieved by using 2.0 g/L FeSC catalyst pyrolyzed at 800°C for 2 h, 15.0 mM H_2O_2 . after 1 h adsorption and 2 h heterogeneous Fenton-like oxidation, almost complete discoloration and 74 % mineralization were achieved. And only 0.37 mg/L iron was detected in the filtrate at the end of the reaction. The stability test carried out in an integrated membrane-heterogeneous Fenton-like catalytic continuous reactor (MHFR) for 600 min indicated that FeSC presents both a high catalytic activity and a long-term stability. Compared to some commercial iron oxides such as $\alpha\text{-Fe}_2\text{O}_3$, Fe_3O_4 , $\gamma\text{-FeOOH}$, and wood sawdust-based carbon supported iron oxide catalyst (FeWC), FeSC exhibited better performance in discoloration of AOII. The high inorganic components content in sewage sludge, such as SiO_2 and Al_2O_3 , was concluded to have strong correlations with the high catalytic activity of FeSC. It was found that the removal of inorganic fraction remarkably decreased the catalytic activity of iron-containing catalyst. The insertion of SiO_2 favors the increase in catalytic activity due to the formation of both hydrogen bonds between H_2O_2 and siloxane bridges and the acidic microenvironment near the surface of silica phase. While the addition of Al_2O_3 in sewage sludge as basic sites can facilitate the degradation of H_2O_2 , and the characteristic of Lewis acidity of alumina can accelerate the reduction of Fe^{3+} to Fe^{2+} by H_2O_2 .

(ii) The performances of the Fe_3O_4 and SC composite catalyst (FeSC) in the Catalytic Wet Air Oxidation (CWAO) of 2-chlorophenol (2-CP) was assessed. When a batch reaction operated at 120°C under 0.9 MPa oxygen partial pressure (50 bar total pressure), an almost complete decomposition of 2-CP was achieved within 5 hours, and 90% Total Organic Carbon (TOC) abatement was obtained after 24 hours of reaction. The activation energy for the CWAO of 2-CP in the presence of FeSC was calculated to be 50 kJ/mol, much lower than that of no catalytic reaction (140 kJ/mol). Quite a straight correlation was observed between the pH of the reaction mixture, the amount of iron leached in the solution and the 2-CP conversion at a given reaction time. Without controlling the pH during the reaction, 30 ppm iron could be detected in the liquid phase at the end of the reaction. When the acetate buffer (pH = 4.5) was added into the reactor, the iron leaching could be kept lower than 1 ppm while keeping some catalytic activity. This approach could be considered as an option to solve the leaching problem of transition-metal catalyst in practical applications.

(iii) A novel Mn oxide nanoparticles modified graphitic carbon nitride catalyst (Mn-g- C_3N_4) was synthesized via a one-pot in-situ method. The results of XRD, FTIR, SEM-EDX mapping and TEM characterization revealed that the synthesized Mn-g- C_3N_4 presented a graphitic-like structure with the triazine unit as the primary building block. The loaded Mn compound doped in the electron-rich g- C_3N_4 mainly presented as Mn_2O_3 nanoparticles. The catalytic ozonation activity of Mn-g- C_3N_4 was investigated by the removal of the antibiotic sulfamethoxazole (SMZ) in water. The results indicated that compared to pure g- C_3N_4 and commercial Mn_2O_3 , the Mn-g- C_3N_4 catalyst showed the highest activity.

In order to improve the adsorption capacity of SMZ, the Mn-g- C_3N_4 was further supported on the sewage sludge-based activated carbon (SBAC) with large surface area. The degradation of SMZ by using Mn-g- C_3N_4 /SBAC composite catalyst fitted well with Langmuir-Hinshelwood model. Considering the reaction rate and the utilization of loaded Mn-g- C_3N_4 , the optimal content of Mn-g- C_3N_4 was decided to be 30%. The catalytic activity of the composite catalyst was about 1.6 times compared with the no supported Mn-g- C_3N_4 catalyst, indicating the positive trend by employing SBAC as support for ozonation catalyst. The composite catalyst also exhibited very good inoxidability, limited Mn leaching and good stability since the activity almost remained constant over four consecutive runs.

In the future work, great effects need to make on the practical application and **economic evaluation** of sewage sludge derived catalysts.

Acknowledgements

This scientific work was accomplished at the School of Environmental Science and Engineering of Sun Yat-Sen University (China), the Institut de recherches sur la catalyse et l'environnement de Lyon (IRCELYON) and Université Claude Bernard-Lyon 1 in Lyon (France).

Firstly, my thanks should be given to the Oversea Study Program of Guangzhou Elite Project for financial support for me to pursue my studies at IRCELYON, Université Claude Bernard-Lyon 1 as a joint Ph.D student.

Secondly, I cordially express my thanks to my supervisors Prof. Ya Xiong and Prof. Claude Descorme. Their profound knowledge, huge enthusiasm in scientific research and patient guidance and encouragement strongly influence me during my study, and will accompany with me in my following life and research activities.

I would like to thank associate professor Shuanghong Tian, Prof. Chun He, Prof. Michèle Besson, Prof. Shaoxia Yang, Dr. Lingjun Kong and the other colleagues in IRCELYON and Sun Yat-Sen University, for various recommendations and supports during my study. I also express my thanks to the analysts in the institutes and universities.

My special thanks should be given to my parents for her deep love and silent support in the past 27 years.

PUBLICATIONS



Co-catalytic effect of sewage sludge-derived char as the support of Fenton-like catalyst

Yuting Tu^a, Shuanghong Tian^{a,b}, Lingjun Kong^a, Ya Xiong^{a,b,*}

^a School of Environmental Science and Engineering, Sun Yat-Sen University, Guangzhou 510275, PR China

^b Guangdong Provincial Key Laboratory of Environmental Pollution Control and Remediation Technology, Guangzhou 510275, PR China

ARTICLE INFO

Article history:

Received 13 September 2011

Received in revised form

31 December 2011

Accepted 3 January 2012

Keywords:

Sewage sludge

Inorganic component

Co-catalytic effect

Heterogeneous Fenton-like catalyst

ABSTRACT

Sewage sludge-derived char was successfully employed as the support of heterogeneous Fenton-like catalyst for the first time. Physicochemical properties of the prepared sewage sludge-derived char supported iron oxide catalyst (FeSC) have been evaluated by XRD, SEM, EDS and N₂-adsorption/desorption analysis. FeSC exhibited better performance in discoloration of AOI than wood sawdust-based carbon supported iron oxide catalyst (FeWC) both in batch experiment and continuous tests. The high inorganic components content of sewage sludge was concluded to have strong correlations with the high catalytic activity of FeSC. To further interpret the co-catalytic effect of inorganic components in sewage sludge, the inorganic components were removed from the sewage sludge and then a series of catalysts were prepared by the addition of iron, as well as silica and/or alumina to the sewage sludge free of the inorganic components. It was found that the removal of inorganic fraction remarkably decreased the catalytic activity of iron-containing catalyst. The insertion of SiO₂ favors the increase in catalytic activity due to the formation of both hydrogen bonds between H₂O₂ and siloxane bridges and the acidic microenvironment near the surface of silica phase. While the addition of Al₂O₃ in sewage sludge as basic sites can facilitate the degradation of H₂O₂, and the characteristic of Lewis acidity of alumina can accelerate the reduction of Fe³⁺ to Fe²⁺ by H₂O₂.

© 2012 Elsevier B.V. All rights reserved.

1. Introduction

Fenton oxidation, in which hydrogen peroxide is used as oxidant and Fe(II) ions as catalyst, has been proved to be an effective technology for the treatment of industrial wastewater containing non-biodegradable organic pollutants [1]. During recent decades, heterogeneous Fenton and Fenton-like catalysts have attracted a great deal of interest as they exhibit wider applicable pH range and can avoid the continuous loss of catalyst compared with the homogeneous Fenton process [2]. Many organic and inorganic materials have been used as catalyst supports by immobilizing iron ions or iron oxides on them. Among those supports, Nafion membrane [3,4], activated carbon [5,6], silica [7,8], Al₂O₃ [9,10], zeolite [11], clay [12] are commonly used. And in recent years, some research has been carried out to explore the applications of solid waste as support of heterogeneous Fenton-like catalysts, such as coffee used grounds [13], rice husk ash [14], fly ash [15], red mud [16] and so on.

The disposal of municipal sewage sludge has become one of the most important environmental problems nowadays [17]. The

traditional methods of sewage sludge disposal, such as ocean dumping, landfill and incineration, may cause secondary pollutions to soil, ground water and air [18–20]. Therefore, the resource utilization of sewage sludge has attracted more and more attention and some new processes are being developed, such as sewage sludge composting, pyrolysis and gasification [21–23]. Among them, pyrolysis is considered as an interesting route since it is effective in reducing the volume of sludge and producing useful end products [24].

The solid residue formed during pyrolysis of sewage sludge is known as 'sludge-derived char (SC)' in the literatures [25,26]. Most of them were used as adsorbents of dyes, phenol and metals in wastewater treatment [27–29]. It was found that the BET surface areas of SC obtained from the carbonization alone have never been reported higher than 400 m²/g, which is much less than that of usual commercial activated carbon [30], thus SC is not a favorable adsorbent. Recently, SC was employed as an emerging catalyst support in aqueous and gaseous reactions. For example, Zhang et al. [31] used sewage sludge carbon as the support of photocatalyst TiO₂ for the removal and recovery of ionic mercury [Hg(II)] from water. Ansari and Badosz [32] prepared H₂S adsorbents/catalysts by incorporating calcium oxide into the dried sewage sludge and waste paper mixture-based carbonization material. However, there is no report about using SC as the support of Fenton-like catalysts.

* Corresponding author. Tel.: +86 20 84115556; fax: +86 20 39332690.
E-mail address: cesxya@mail.sysu.edu.cn (Y. Xiong).

Furthermore, since SC is an inorganic–organic alloyed mixture, it should have some special behaviors compared with other commonly used supports. This situation encouraged us to investigate the potential of SC as the support of heterogeneous Fenton-like catalyst.

The aim of this study is to investigate the potential of SC as the support of heterogeneous Fenton-like catalyst. The catalytic activity of the prepared complex catalyst FeSC was evaluated by degradation efficiency of a representative azo dye, Acid Orange II (AOII). Considering the high ash content of SC obtained after pyrolyzed at 800 °C, which reaches around 70% as reported [33], co-catalytic effect of these inorganic components was investigated in detail.

2. Experimental

2.1. Materials

Dewatered sewage sludge was obtained in June from Lie De municipal wastewater treatment plant in Guangzhou, China. Pine wood sawdust was washed thoroughly with deionized water before use. Commercial activated carbon prepared from coconut husk was purchased from Tianjin Chemical Reagent Co. Ltd., China. These three kinds of precursors were dried at 105 °C to constant weight, subsequently ground and sifted through a 100-mesh sieve, and stored in a desiccator at room temperature.

Analytical grade of ferrous sulfate ($\text{FeSO}_4 \cdot 7\text{H}_2\text{O}$), tetraethyl orthosilicate (TEOS), anhydrous ethanol, hydrogen peroxide solution (30%, w/v) and $\text{Al}_2(\text{SO}_4)_3$ were obtained from Guangzhou Chemical Reagent Company, China. The AOII was a commercial dye (Hengrun Dyestuff Chemical Co., Ltd., Guangzhou) and used without further purification.

2.2. Preparation of the catalysts

Sewage sludge-derived char supported iron oxide catalyst (named as FeSC) was prepared by one-step method combing synthesis with loading. Firstly, 20 g dried sludge was added into 150 mL of Fe solution (0.5 mol/L FeSO_4 , pH = 2.5). After the suspension was stirred for 24 h, it was evaporated in a rotary evaporator at 60 °C, and then dried at 105 °C for 12 h. Subsequently, the dried solid was pyrolyzed in a horizontal furnace at 800 °C for 2 h with heating rate of 20 °C/min and nitrogen flow of 40 mL/min. The pyrolyzed sample was washed with deionized water several times until the conductivity became constant, then dried at 105 °C overnight and ground to less than 200-mesh. The same procedure was used to prepare wood sawdust-based carbon supported iron oxide catalyst (labeled as FeWC), except that 20 g wood sawdust was mixed with 35 mL of FeSO_4 solution (0.5 mol/L, pH = 2.5). Commercial activated carbon supported iron oxide catalyst (FeAC) was prepared by classical incipient wetness impregnation [34] using 20 g AC and 0.1244 g $\text{FeSO}_4 \cdot 7\text{H}_2\text{O}$, and also treated in N_2 flow at 800 °C for 2 h. The different amount of materials was used to guarantee all the catalysts have similar iron content.

To remove the inorganic components in sewage sludge, some activated sludge mixed liquor was obtained directly from the aeration tank of Lie De, and then was incubated for about two weeks in laboratory till the ratio of volatile suspended solids (VSS) and total suspended solids (TSS) was over 85%. Then some suspension was filtrated and dried. The obtained bacteria powder was suspended in 0.5 mol/L HCl solution for 12 h, subsequently filtrated and washed with deionized water several times until the pH of the rinse water was about 6. The ash content of the resulted dry sludge (referred to as SS-A) was 4.31 wt.%. Then the SS-A was used as precursor for catalysts preparation. Various amounts of SiO_2 and Al_2O_3 were

added to the precursor. The name of the catalysts and their preparation conditions are listed in Table 1. To synthesize SiO_2 -containing samples, fixed amounts of ethanol, TEOS and SS-A were stirred and heated at 80 °C for 2 h, then the mixture was dried at 105 °C for 12 h, and ground to fine powders (labeled as SiSS-A). After that, given amounts of FeSO_4 or/and $\text{Al}_2(\text{SO}_4)_3$ solution were mixed with SiSS-A for 24 h, then dried and pyrolyzed as described above.

To evaluate the role of carbon phase, which generated from the carbonization of sewage sludge, in the heterogeneous Fenton-like catalytic reaction, FeAlSi catalyst was also prepared without the addition of any sewage sludge.

2.3. Characterization of catalysts

The average particle size was obtained on MasterSizer 2000 Particle Size Analyzer. The ash contents of catalysts were determined using a standard method according to ASTM D2866-94. The pH values of isoelectric point (pH_{IEP}) were determined from electrophoretic mobility measurements using a zeta potential analyzer (Zetasizer Nano ZS, Marlven). The specific surface area (S_{BET}) was determined with an Autosorb-iQ-MP gas sorption analyzer (Quantachrome Instruments, USA) by nitrogen adsorption at 77 K. The chemical state of iron on catalysts were followed by X-ray diffraction (XRD) using D/max 2200 vpc Diffractometer (Rigaku Corporation, Japan) with a $\text{Cu K}\alpha$ radiation at 40 kV and 30 mA. Scanning electron microscopy (SEM) images were recorded using a JEOL JSM-6330F-mode field emission scanning electron microscope equipped with an energy-dispersive X-ray (EDX) detector (JED-2300). X-ray photoelectron spectroscopy (XPS) measurements were performed using an ESCALAB 250, Thermo-VG Scientific (UK) system, with Avantage software for data acquisition and analysis. An Al $\text{K}\alpha$ monochromatized radiation operating at 15 kV (150 W) was used, and the spectrometer, calibrated with reference to Au 4f7/2 (84.0 eV), Ag 3d5/2 (368.3 eV) and Cu 2p3/2 (932.6 eV), was operated in CAE mode with 20.0 eV pass energy. Data acquisition was performed with a pressure lower than 10^{-7} Pa. Spectra analysis was performed using peak fitting with XPS peak 4.1 and Shirley type background subtraction. Bulk iron, alumina and silica content of the synthesized samples were measured by inductively coupled plasma optical emission spectrometry (ICP-OES, optima 5300DV, Perkin-Elmer).

2.4. Catalytic activity

All the batch experiments were carried out in a glass conical beaker (250 mL) with a stopper shaken in a thermostatic bath at an equivalent stirring velocity around 200 rpm at 30 °C. In each run, a given amount of powder catalyst was added into 100 mL AOII solution. The solution pH was adjusted to 4.0 ± 0.1 with NaOH and H_2SO_4 during the experiments. The samples for determination of adsorption kinetics were taken at predetermined time intervals and were analyzed immediately after filtration through 0.22 μm Millipore membrane filters to remove suspended particles. After the adsorption/desorption equilibrium was established in 60 min, 60 mL suspension was used for Fenton-like reaction and initiated by adding 15 mM H_2O_2 to the solution. Samples were withdrawn at a given time interval during the reaction and immediately analyzed after filtration. Each experiment was repeated thrice, the data points represent the average value and error bars indicate the standard deviation.

To investigate the lifetime of catalysts, a continuous catalytic oxidation was conducted in a novel integrated membrane-heterogeneous Fenton-like catalytic continuous reactor (MFR) designed by our laboratory. As shown in Fig. 1, the MFR consists of a reaction tank, a submerged membrane module, a liquid feed system, an effluent collecting system, and an air bubbling system.

Table 1
Labels of prepared SC-A based catalysts and specification of their preparation conditions.

Sample	SS-A (g)	TEOS (mmol)	Ethanol (mmol)	Fe (mmol)	Al (mmol)	Fe/Si/Al
FeSC-A	2.5	0	0	3.60	0	1/0/0
SiSC-A	2.5	3.60	3.60	0	0	0/1/0
AlSC-A	2.5	0	0	0	3.60	0/0/1
FeSiSC-A ₁	2.5	1.80	1.80	3.60	0	2/1/0
FeSiSC-A ₂	2.5	3.60	3.60	3.60	0	1/1/0
FeSiSC-A ₃	2.5	7.20	7.20	3.60	0	1/2/0
FeAlSC-A ₁	2.5	0	0	3.60	1.80	2/0/1
FeAlSC-A ₂	2.5	0	0	3.60	3.60	1/0/1
FeAlSiSC-A	2.5	3.60	3.60	3.60	3.60	1/1/1
FeAlSi	0	3.60	3.60	3.60	3.60	1/1/1

The reaction tank was made of polymethylmethacrylate (PMMA). An Al₂O₃ ceramic membrane with the bore diameter of 3 μm was used in the submerged membrane module. Before reaction, 2.4 L AOII solution (100 mg/L), 4.8 g catalyst and 36 mmol H₂O₂ (30%, w/v) were added into the reaction tank. At the same time, two pumps start to supply AOII (100 mg/L) and H₂O₂ (1.02%, w/v) to the tank continuously. Their flow rate was control to be 20 mL/min and 1 mL/min respectively. And the third pump was used to control the flux speed of the effluent from the reactor. The hydraulic residence time was controlled to be 120 min. The air flow rate was kept at 5 L/min to hydraulically suspend the catalyst particles and to clean the membrane surface by the shear force of air bubble. All experiments were conducted at ambient temperature (23 °C), and the pH was kept at 4.0 ± 0.1 during the reaction.

2.5. Analytical methods

The pH of AOII solution was measured with a PHS-3C pH meter (Rex Instrument Factory, Shanghai, China). The concentration of AOII was analyzed on UV–vis spectrophotometer (UV-3150, Shimadzu) with maximum absorbance at 484 nm. H₂O₂ was analyzed spectrophotometrically by the titanium sulfate method. The leaching concentration of Fe in the solution was measured by inductively coupled plasma optical emission spectrometry (ICP-OES, optima 5300DV, Perkin-Elmer). The total organic carbon (TOC) of the reaction solution was measured by a TOC analyzer (Shimadzu, Japan).

3. Results and discussion

3.1. Characterization of catalysts

The basic physical and chemical parameters of FeSC are presented in Table 2. It can be seen that ash content of FeSC is 93.01%, indicating the catalyst mainly consists of inorganic components,

Table 2
Physicochemical properties of FeSC, FeWC and the corresponding supports.

Sample	Fe (wt.%)	Ash (wt.%)	\bar{d}_v^a (μm)	S _{BET} (m ² /g)	pH _{IEP}
SC	3.91	74.63	23.08	18.9	3.57
FeSC	12.94	93.01	27.14	14.3	3.39
WC	0.52	4.59	29.58	10.4	3.09
FeWC	16.24	26.31	26.66	12.1	3.13

^a \bar{d}_v , volume average particle diameter.

and only a small amount of carbon. The main inorganic elements in ash detected by ICP–OES are Fe, Si, Al, Ca, K and Na, and their weight contents are 13.91%, 6.78%, 5.48%, 1.22%, 1.08% and 0.30%, respectively. As shown in Table 2, the ash content of SC is 74.63% and the Fe content is only 3.91%. That means the Fe in FeSC is mainly the added element during the preparation process of FeSC, while Si and Al are the native element in original sewage sludge.

The iron chemical state in FeSC was studied by XRD (Fig. 2). New broad bands at 2θ angles of 35.5°, 62.6° and 30.1° are distinctly observed by comparing the XRD pattern of FeSC catalyst with that of SC. These diffraction peaks are assigned to (3 1 1), (4 4 0) and (2 2 0) planes of Fe₃O₄ crystallite (JCPDS 88-0866), respectively [35,36]. The oxidation state of Fe on the surface of catalysts was also characterized by XPS (Supplementary data, Fig. S1). The binding energy of Fe 3p was determined to be 56.4 eV, which was ascribable to Fe₃O₄ [37]. According to the results of XRD, other elements, Si, Al,

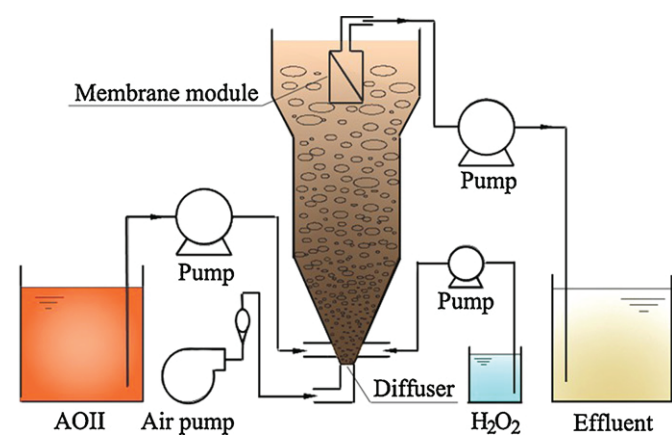


Fig. 1. Schematic diagram of the submerged MFR reactor.

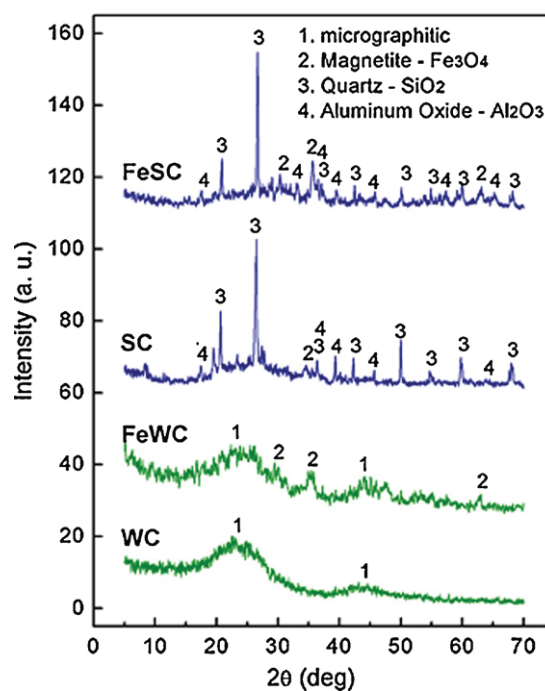


Fig. 2. XRD patterns of FeWC, FeSC and their corresponding supports.

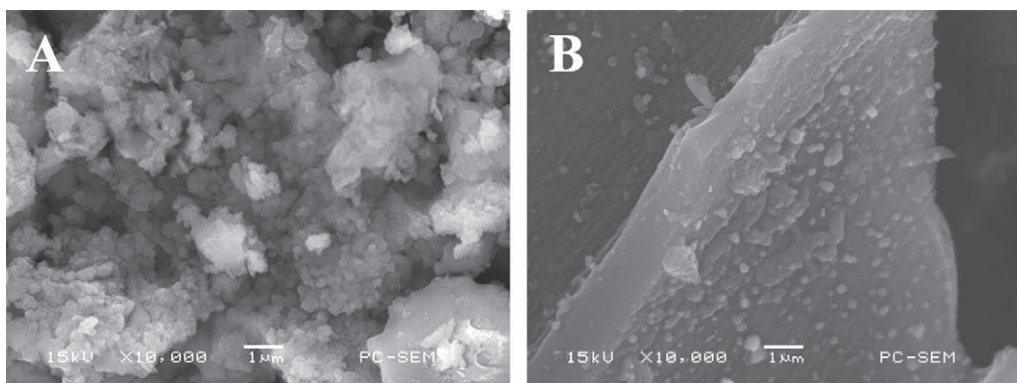


Fig. 3. SEM images of FeSC (A) and FeWC (B).

Ca and Na in the forms of SiO_2 , Al_2O_3 , CaSO_4 and NaPO_3 are also detected in FeSC. It is noteworthy that crystallographic structure of SiO_2 and Al_2O_3 are particularly more recognizable compared with other oxides due to their higher content in the bulk powder sample [38]. The SEM micrograph of FeSC is shown in Fig. 3, the morphology of FeSC presents roughness surface with “coral type” structure. In addition, the Fe content on the surface of FeSC measured by EDS analysis is 15.26%, in agreement with the result obtained by ICP-OES, therefore, it can be deduced that the Fe_3O_4 particles are almost uniformly distributed in FeSC. The average size of the crystalline particles for Fe_3O_4 is calculated to be 12.1 nm based on the Debye–Scherrer formula from XRD study

For comparison, main physicochemical parameters of another biomass carbon-based catalyst (FeWC) and its corresponding support (WC) are also determined and listed in Table 2. The Fe content of FeWC is similar to that of FeSC, however, FeWC is almost free of Si and Al elements. The BET surface area of FeWC is a little smaller than that of FeSC. As shown in Fig. 3, the surface morphology of FeWC presents in the form of plates which come from the carbonization of the cellulosic materials with small particle size iron oxide dispersed on them, while FeSC presents a more heterogeneous appearance.

3.2. Catalytic activity of FeSC catalysts

Heterogeneous Fenton-like catalytic activity of FeSC catalyst was assessed in the term of degradation efficiency of AOII, as shown in Fig. 4. In adsorption phase, 26.9% of AOII is removed by SC, while only 22.8% of AOII discoloration is observed in FeSC system. This indicates that the impregnation of iron oxides can reduce the amount of AOII adsorbed on catalyst. During a two-hour oxidation process, the AOII degradation in the presence of only H_2O_2 is almost negligible, and only 21.9% of AOII is removed by SC, indicating the catalytic activity of SC is very low. The removal of AOII could mainly be dependent on 3.91 wt.% of Fe in SC. The little amount of Fe originated from the original sewage sludge exists in the form of Fe_3O_4 and acts as the role of Fenton-like catalyst. As can be seen in Fig. 4, the degradation efficiency of AOII catalyzed by FeSC locates at 94.6% after oxidation for 2 h. Therefore, FeSC shows obviously better catalytic activity than the SC support although it presents smaller adsorption capacity of AOII.

As is known, both the heterogeneous and homogeneous processes make contribution to the oxidation of AOII in the systems with catalysts. So the iron concentration in the liquid phase at the end of the operation was measured by ICP-OES. The result shows that, after 3 h of reaction the concentration of Fe in solution is 0.373 mg/L for FeSC system, and the amount (wt.%) of Fe lost from the solid never raised above 0.14% as referred to the total Fe initially incorporated. Meanwhile little amount of Ca, Cu, Mg and Zn were also detected in the filtrate, their concentrations were

0.813 mg/L, 0.029 mg/L, 0.271 mg/L and 0.027 mg/L, respectively. And the concentrations of Cr, Mn, Ni and Pb were below the detection limit of ICP-OES. In these conditions some, although relatively low, contribution of aqueous catalytic reaction may take place. To determine the influence of homogeneous phase reaction, we also carried out two homogeneous experiments using Fe(II) and Fe(III) at the concentration that was found in the filtrate after the reaction, and the discoloration efficiency of AOII were only 9.7% and 6.2%, respectively. This result suggests that degradation of AOII for the FeSC-based Fenton-like system could mainly be attributed to heterogeneous process, not homogeneous phase reaction.

In order to understand the catalytic potential of FeSC more clearly, a comparative Fenton-like experiment was performed with FeWC. As shown in curve C of Fig. 4, removal efficiency of AOII in adsorption phase is 17.8%, a little lower than that of FeSC, this can be explained by the lower BET surface area of FeWC. And the discoloration of AOII at the end of oxidation phase for FeWC is only 66.2%. The apparent rate constants (k_{ap}) of AOII degradation were obtained by fitting the results from 60 min to 180 min shown in Fig. 4 with pseudo first-order kinetic equation, which has been widely applied by researchers for the description of the heterogeneous Fenton-like oxidation of organic pollutants [39,40]. As shown in Table 3, very high and good correlation coefficients (R^2) were gotten, meaning there is good linear correlation between $\ln(C_0/C_t)$ and time. The k_{ap} for FeSC system was calculated to be $22.45 \times 10^{-3} \text{ min}^{-1}$, while that for FeWC system was

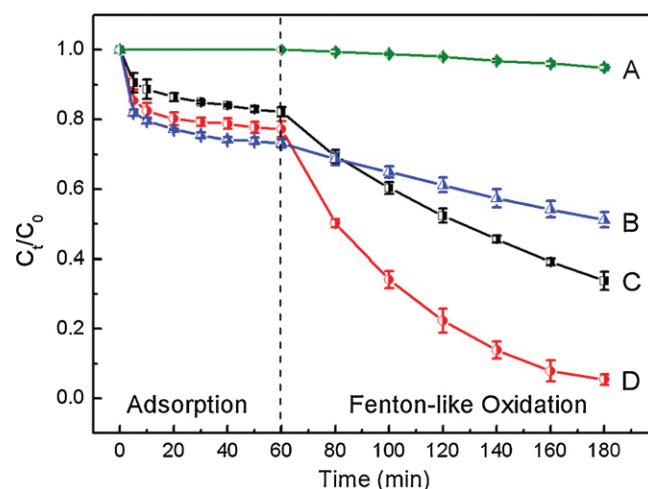


Fig. 4. Degradation of AOII through adsorption and oxidation by hydrogen peroxide and different catalysts: (A) H_2O_2 ; (B) SC + H_2O_2 ; (C) FeWC + H_2O_2 ; (D) FeSC + H_2O_2 (catalysts: 2.0 g/L; H_2O_2 : 15 mM; AOII: 100 mg/L; reaction pH: 4.0 ± 0.1 ; and reaction temperature: 30°C).

Table 3
Discoloration of AOII with H₂O₂ in the presence of different catalysts.

Sample	Discoloration efficiency of AOII (%)		Pseudo first-order model parameters	
	By adsorption, <i>t</i> = 60 min	By oxidation, <i>t</i> = 180 min	<i>k</i> _{ap} (×10 ⁻³ min ⁻¹)	R ²
H ₂ O ₂	0	5.1	0.44	0.9850
SC	26.9	48.8	2.98	0.9973
FeSC	22.8	94.6	22.45	0.9972
FeWC	17.8	66.2	7.31	0.9987
SC-A	5.0	11.2	0.57	0.9975
FeSC-A	19.8	51.3	4.21	0.9875
SiSC-A	2.8	8.6	0.63	0.9964
AlSC-A	6.6	14.8	0.81	0.9904
FeSiSC-A ₁	14.2	59.8	6.00	0.9804
FeSiSC-A ₂	13.8	68.8	8.44	0.9885
FeSiSC-A ₃	13.4	80.5	12.41	0.9965
FeAlSC-A ₁	22.1	65.7	6.71	0.9988
FeAlSC-A ₂	39.7	77.7	8.17	0.9870
FeAlSiSC-A	34.8	89.9	15.11	0.9917
FeAlSi	8.5	39.6	3.39	0.9977

only $7.31 \times 10^{-3} \text{ min}^{-1}$, the former was about 2 times higher than the later. Because the contents and existence forms of Fe in FeSC and FeWC are similar, the difference of their catalytic activities is possibly dependent on non-iron inorganic components co-existing in them.

It is known that reaction intermediates can form during the oxidation of organic dyes, and thus total organic carbon (TOC) removal was measured at the end of adsorption and Fenton-like oxidation phases. The results show that TOC removal efficiencies are 25.4% and 39.1% at 60 min and 180 min for SC, 15.4% and 50.6% for FeWC, while they are 18.4% and 69.7% for FeSC. Therefore, the conclusions of TOC removal are similar as for AOII degradation, indicating that FeSC as a heterogeneous Fenton-like catalyst can lead to a fast discoloration of AOII as well as a remarkable mineralization of the solution.

3.3. Co-catalytic effect of inorganic components in SC

To further investigate the effect of inorganic components in FeSC on the catalytic performance in Fenton-like reaction, the inorganic components of sewage sludge was firstly removed and then the remainder was used as precursor (SS-A) for SC-A and FeSC-A preparation. The physicochemical data of the prepared SC-A and FeSC-A are presented in Table 4. The ash content of SC-A and FeSC-A are only 10.02% and 39.97%, much lower than that of FeSC, and the Al and Si contents are at micro level. Then the catalytic behavior of SC-A and FeSC-A was also evaluated in the presence of H₂O₂ at pH 4.0 (see curves B and C in Fig. 5). After 1 h adsorption and 2 h oxidation, the discoloration efficiencies of AOII are 11.2% and 51.3% for SC-A and FeSC-A, much lower than the 94.6% removal efficiency obtained with the FeSC catalyst. The pseudo first-order degradation kinetic constant for FeSC-A system is calculated to be $4.21 \times 10^{-3} \text{ min}^{-1}$ (as shown in Table 3), which is also less than that for FeSC. This experimental result further indicates that the inorganic components in the SC have co-catalytic effect on the degradation of AOII in heterogeneous Fenton-like process.

3.4. Co-catalytic mechanism of inorganic components in SC

As mentioned previously, except for Fe the other inorganic elements in SC are mainly Si and Al, which exist in the forms of SiO₂ and Al₂O₃ confirmed by XRD (Fig. 2). Their contents in SC are calculated to be 22.14% and 16.09%, respectively, being 73.46% of total non-iron inorganic components. In other words, the co-catalytic effect of SC compared with WC is possibly mainly originated from the SiO₂ and Al₂O₃. In order to understand the enhancement mechanism, a series of Fe-loaded sewage sludge carbon with various SiO₂ and

Al₂O₃ content as Fenton-like catalysts were prepared by employing the SS-A as precursor, their physicochemical properties are listed in Table 4, and their catalytic activities were also determined, respectively. As shown in Table 4, all the modified SS-A based catalysts present low BET surface area (less than 25.0 m²/g), and the values are very close to each other.

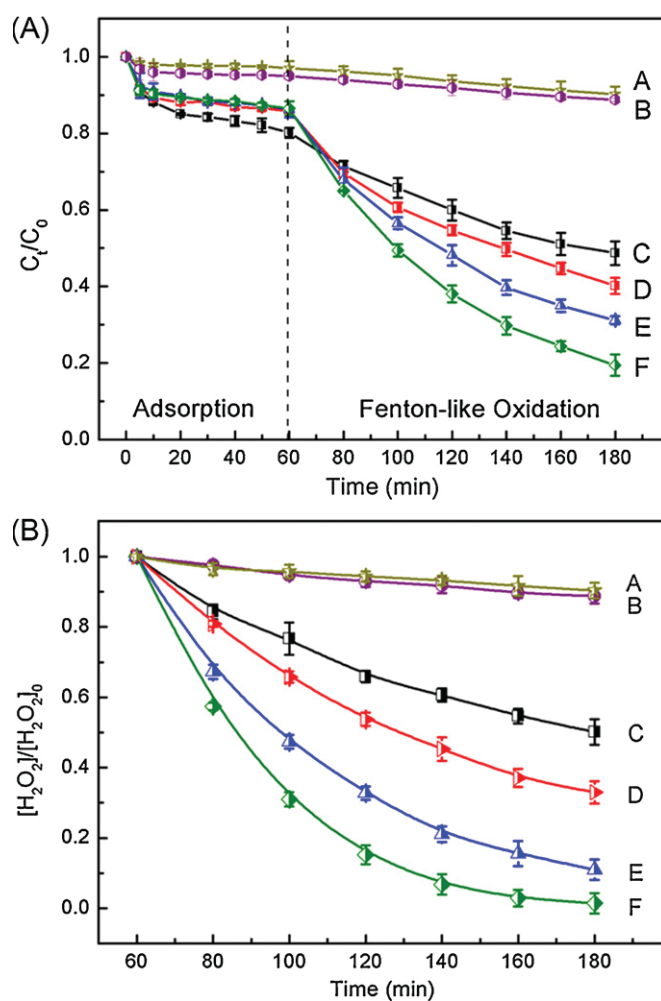


Fig. 5. Effect of SiO₂ content in FeSC on AOII removal (A) and H₂O₂ consumption (B) (the iron concentrations are all 0.2588 g/L: (A) SiSC-A: 1.6085 g/L, (B) SC-A: 1.2882 g/L, (C) FeSC-A: 1.3306 g/L, (D) FeSiSC-A₁: 1.2699 g/L, (E) FeSiSC-A₂: 1.3251 g/L, (F) FeSiSC-A₃: 1.4042 g/L; H₂O₂: 15 mM; AOII: 100 mg/L; reaction pH: 4.0 ± 0.1; and reaction temperature: 30 °C).

Table 4

Physicochemical properties of different catalysts.

Sample	Fe (wt.%)	Al (wt.%)	Si (wt.%)	Ash (wt.%)	S_{BET} (m^2/g)	Zeta potential at pH 4.0 (mV)	pH_{IEP}
SC-A	1.50	0.13	2.50	10.02	13.7	-17.16	3.13
FeSC-A	19.45	0.06	1.21	39.97	21.1	-16.84	3.21
SiSC-A	0.93	0.08	13.68	39.32	12.2	-26.44	2.64
AISC-A	0.82	9.66	1.29	28.65	18.3	-11.81	3.51
FeSiSC-A ₁	20.38	0.07	6.31	48.89	19.2	-20.15	3.06
FeSiSC-A ₂	19.53	0.06	11.09	49.92	16.5	-21.46	2.94
FeSiSC-A ₃	18.43	0.06	16.28	55.42	13.1	-24.53	2.37
FeAlSiSC-A ₁	17.24	4.04	1.07	44.92	15.8	-8.16	3.56
FeAlSiSC-A ₂	16.83	7.88	1.04	45.99	21.9	-0.85	3.82
FeAlSiSC-A	15.92	7.45	8.70	55.03	17.3	-10.74	2.98
FeAlSi	29.81	14.40	15.01	90.35	6.1	4.12	5.24

Before comparing the activity of silica and/or alumina incorporated iron-containing catalysts, two blank runs were performed to evaluate the ability of SiSC-A and AISC-A to oxidize AOII in aqueous solutions in the presence of H_2O_2 . Only 8.6% and 14.8% AOII removal was observed by these two kinds of Fe free catalysts through adsorption and oxidation processes under the same conditions as mentioned above. That means neither SiSC-A nor AISC-A exhibits any considerable catalytic activity towards the degradation of AOII by H_2O_2 .

The change of the AOII discoloration rate with the various contents of SiO_2 in catalyst support is presented in Fig. 5 A. The comparison was based on the identical amount of iron. It is found that increase of degradation rate is followed by the order of FeSiSC-A₃ > FeSiSC-A₂ > FeSiSC-A₁ > FeSC-A, which is consistent with that of SiO_2 content. The changes of H_2O_2 concentration in the liquid phase during the experiments (Fig. 5B) follow a parallel trend to the AOII oxidation: a better performance is reached when the content of SiO_2 in the FeAlSiSC-A catalysts increases. The results further confirm that co-catalytic effect of SC partly originates from SiO_2 -like inorganic component in it. There are several possible explanations for the co-catalytic effect of SiO_2 . Firstly, H_2O_2 can adsorb on SiO_2 by hydrogen bonds with the oxygen in siloxane bridges, Si—O—Si [41] (Fig. 6A), leading to a higher concentration of H_2O_2 on surface of FeSC then that in the bulk solution and hence facilitating Fenton-like reaction. Except for siloxane, there is another kind of functional group on the silica surface, silanol (Si—OH) [42], which undergoes protonation when the pH values are lower than the pH_{IEP} of SiO_2 and deprotonation at $\text{pH} > \text{pH}_{\text{IEP}}$ [43,44]. The pH_{IEP} value of SiO_2 is widely reported at 2.0–3.5 [44,45], lower than the solution pH in our experiments. Therefore, H^+ has an obvious tendency to release from Si—O—H, and results in the formation of negative charge SiO_2 particles and an acidic microenvironment near the catalyst surface [46], as shown in Fig. 6B. This explanation can be partly evidenced by the different zeta potential at pH 4.0 of SiO_2 -containing catalysts that are presented in Table 4, the surface charge became more negative when the content of SiO_2 increases. It is known that low

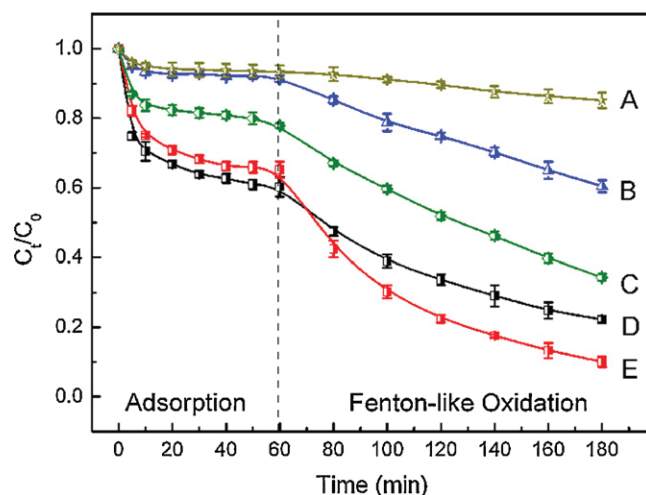


Fig. 7. Degradation of AOII through adsorption and oxidation in the presence of Al_2O_3 -containing catalysts (the iron concentrations are all 0.2588 g/L: (A) AISC-A: 1.9540 g/L, (B) FeAlSi: 0.8682 g/L, (C) FeAlSiSC-A₁: 1.5012 g/L, (D) FeAlSiSC-A₂: 1.5377 g/L, (E) FeAlSiSC-A: 1.6256 g/L; H_2O_2 : 15 mM; AOII: 100 mg/L; reaction pH: 4.0 ± 0.1 ; and reaction temperature: 30°C).

pH favors $\cdot\text{OH}$ generation and $\cdot\text{OH}$ has higher oxidation potential at pH around 3.0 than that in less acidic solution [47]. Hence it is possible that the insertion of SiO_2 can facilitate the adsorption of H_2O_2 on the catalyst surface and increase the activity to generate $\cdot\text{OH}$.

The role of alumina phase in iron-containing samples as heterogeneous Fenton-like catalyst were also investigated. As shown in Fig. 7, the removal efficiency of AOII after the preliminary adsorption process is 21.1% for FeAlSi-A₁, 39.7% for FeAlSi-A₂ and 18.2% for FeSC-A. The different adsorption capacities can be correlated with the different BET surface area values and different zeta potential of these three catalysts as shown in Table 4. The pH_{IEP} values of

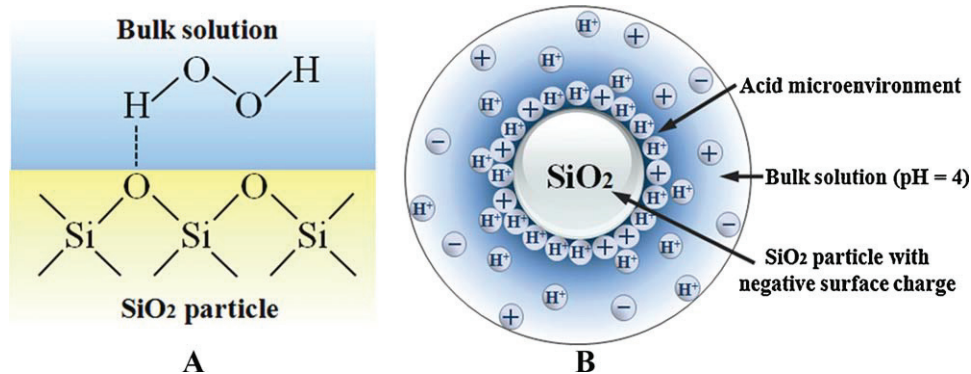


Fig. 6. H_2O_2 adsorb over siloxane by hydrogen bonds (A) and acidic microenvironment form near the surface of SiO_2 particle (B).

Al_2O_3 and SC-A are located at 8.5–10.4 [44] and 3.13, thus the insertion of Al_2O_3 will lead to an increase in pH_{IEP} of the particle, and presents less negative charge, which can facilitate the adsorption of sulfonic dye numerator by electrostatic phenomena. In consideration of AOII discoloration, the increase in the content of Al_2O_3 also resulted in a higher AOII degradation efficiency. The pseudo first-order kinetic constant of AOII oxidation are determined to be $6.71 \times 10^{-3} \text{ min}^{-1}$ for FeAlSC-A₁ and $8.17 \times 10^{-3} \text{ min}^{-1}$ for FeAlSC-A₂, respectively. As mentioned before, the surfaces of FeAlSC-A catalysts are much less negatively charge than that of FeSiSC-A catalysts. Therefore, the pH in microenvironment around the Al_2O_3 particles is almost neutral and not as acidic as that of FeSiSC-A catalysts. It indicates that the co-catalytic mechanism of alumina phase is different from that of silica phase. For the enhancement mechanism of Al_2O_3 in the catalyst, Timofeeva et al. [48] demonstrated that insertion of alumina phase can increase the strength of basic sites of Fe-containing samples detected with CDCl_3 adsorption, leading to the acceleration of H_2O_2 degradation and the increase in activity of catalysts. This explanation is in agreement with the result of our work that insertion of Al_2O_3 can increase the pH_{IEP} of catalyst. Furthermore, alumina as a Lewis acid can attract electron density from ferric ion, and destabilizing the Fe^{3+} state, then facilitate the reduction of Fe^{3+} to Fe^{2+} by H_2O_2 , which usually is the rate-limiting step in the Fenton's reagent chain reaction [49].

SiO_2 presents lower pH_{IEP} value compared with that of Al_2O_3 , the surface charge of silica-containing catalyst FeAlSiSC-A at pH 4.0 is lower than that of FeAlSC-A₂ (Table 4), and resulting in a slightly decrease of AOII adsorption. While as can be seen in Fig. 7, FeAlSiSC-A shows higher catalytic activity than FeAlSC-A₂. The pseudo first-order degradation kinetic constant is calculated to be $1.511 \times 10^{-2} \text{ min}^{-1}$ for FeAlSiSC-A (Table 3), which is about 1.8 times as much as that of FeAlSC-A₂ and FeSiSC-A₂. This experimental result can further indicates the co-catalytic effect of SiO_2 and Al_2O_3 in SC. On the other hand, maybe there is a synergistically catalytic effect of silica and alumina in FeAlSiSC-A, further research will be carried out to confirm this hypothesis.

To evaluate the function of sewage sludge-based carbon as support in heterogeneous Fenton-like reaction, the degradation of AOII with bare FeAlSi was carried out. The catalyst concentration is 0.8682 g/L for FeAlSi and 1.6256 g/L for FeAlSiSC-A to get the similar amount of Fe, Al and Si in these two systems. It can be observed that both the adsorption and oxidation of AOII in FeAlSi system are less significant than that of FeAlSiSC-A system (Fig. 7). The rate constant is calculated to be only $3.39 \times 10^{-3} \text{ min}^{-1}$ for FeAlSi using the pseudo-first-order equation, much lower than that of FeAlSiSC-A. This comparison suggests that the carbon in FeSC also plays a very important role in the Fenton-like process. As is known, carbon materials are good adsorbents for aromatic chemicals and the preconcentration of AOII to be oxidized in the vicinity of reactive centers is considered to be beneficial in many literatures [35,50]. Furthermore, the dispersion of the inorganic oxide within the carbon matrix could prevent them from aggregating into clusters during thermal treatment, and increase the number and properties of the reaction surface sites.

3.5. Stability of the catalysts

The preliminary evaluation of the stability of the FeSC catalyst was evaluated by AOII degradation in a novel integrated membrane-heterogeneous Fenton-like catalytic continuous reactor (MFR). For comparison, commercial activated carbon which has been extensively used as catalyst support in catalytic wet peroxide oxidation was employed to prepare FeAC catalyst. The Fe content in FeAC is determined to be 10.35% by ICP-OES, and the BET surface area is $541.3 \text{ m}^2/\text{g}$. As shown in Fig. 8, for FeSC and FeWC, the degradation efficiency of AOII reach around 36%

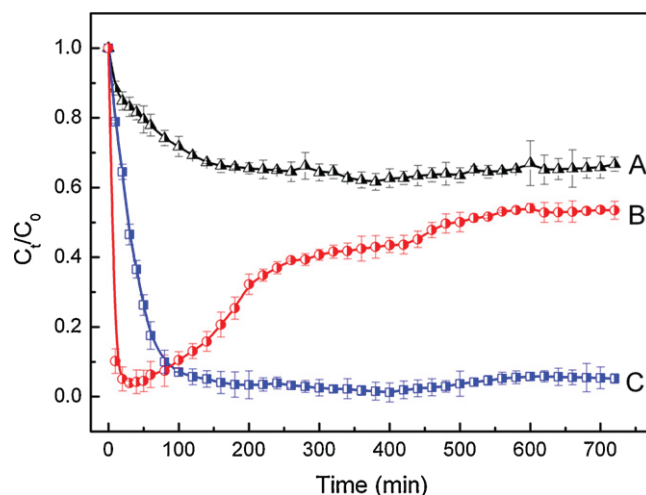


Fig. 8. Effect of consecutive experiments with the FeWC (A), FeAC (B) and FeSC (C) catalysts on the degradation of AOII solution (catalysts: 2.0 g/L; H_2O_2 : 15 mM; AOII: 100 mg/L; reaction pH: 4.0 ± 0.1 ; reaction temperature: 23°C ; total volume of reaction solution: 2.4 L and residence time: 120 min).

and 97% at 120 min, respectively, which are then kept constant until at least 600 min. On the contrary, that for FeAC reaches 93.7% rapidly in the initial 60 min and then decreases with the operation time, which is only 46.6% at 720 min. It indicates that FeSC presents both a high catalytic activity and a long-term stability.

4. Conclusions

A novel heterogeneous Fenton-like catalyst was first successfully prepared by employing the sewage sludge-derived char (SC) as the catalyst support. It was evidenced that the prepared FeSC catalyst showed better catalytic activity in Fenton-like oxidation of AOII than that of wood sawdust-based carbon supported iron oxide catalyst (FeWC). After compared the physicochemical properties of these two iron-containing catalysts, the presence of inorganic components in sewage sludge, mainly SiO_2 and Al_2O_3 , was speculated to be the main reason for the good catalytic performance of FeSC. To further confirm this interpretation, the inorganic components in sewage sludge were firstly removed, and various amounts of iron, silica and alumina were added into the treated precursor to prepare heterogeneous Fenton-like catalysts. It was found that the removal of inorganic fraction yielded significant deterioration of catalytic activity. While the impregnation of SiO_2 and Al_2O_3 resulted in substantial promoting effects on discoloration of AOII. The addition of SiO_2 will facilitate the adsorption of H_2O_2 due to the formation of hydrogen bonds between H_2O_2 and $\text{Si}-\text{O}-\text{Si}$, and increase the activity of $\cdot\text{OH}$ for the formation of acidic microenvironment near the silica phase. The insertion of Al_2O_3 as basic sites can facilitate the adsorption of AOII, activate H_2O_2 degradation and accelerate the reduction of Fe^{3+} to Fe^{2+} by H_2O_2 due to the Lewis property of alumina.

The present study suggests that SiO_2 , Al_2O_3 and carbon in sewage sludge-derived char can act as efficient promoters in heterogeneous Fenton-like reaction. Therefore, more efficient catalysts can be developed by changing the composition and proportion of inorganic and organic phases in the support.

Acknowledgments

This research was supported by the Nature Science Foundations of China (20977117), Science and Technology Research Programs of Guangdong Province (0711220600311), Nature Science

Key Foundations of Guangdong Province (92510027501000005), Foundation of Industry-Education-Academy Cooperation from Guangdong province (2010B090486, 2009A090100047), and Education Department of Chinese Government (2009A090100047, 2010B090486), New Process and Technology Project of Guangzhou EPA (2009-03) and Project of Education Bureau of Guangdong Province (2010-275). Research Fund Program of Guangdong Provincial Key Laboratory of Environmental Pollution Control and Remediation Technology (2011K0008) and the National Natural Science Foundation of China (21107146).

Appendix A. Supplementary data

Supplementary data associated with this article can be found, in the online version, at doi:10.1016/j.cej.2012.01.008.

References

- [1] J.A. Zazo, J.A. Casas, C.B. Molina, A. Quintanilla, J.J. Rodríguez, Evolution of ecotoxicity upon Fenton's oxidation of phenol in Water, *Environ. Sci. Technol.* 41 (2007) 7164–7170.
- [2] H. Hassan, B.H. Hameed, Fe–clay as effective heterogeneous Fenton catalyst for the decolorization of Reactive Blue, *Chem. Eng. J.* 171 (2011) 912–918.
- [3] M.R. Dhananjeyan, J. Kiwi, P. Albers, O. Enea, Photo-assisted immobilized Fenton degradation up to pH 8 of azo dye orange II mediated by Fe³⁺/nafion/glass fibers, *Helv. Chim. Acta* 84 (2001) 3433–3445.
- [4] S. Parra, V. Nadtotchenko, P. Albers, J. Kiwi, Discoloration of azo-dyes at biocompatible pH-values through an Fe–histidine complex immobilized on nafion via Fenton-like processes, *J. Phys. Chem. B* 108 (2004) 4439–4448.
- [5] T.L.P. Dantas, V.P. Mendonça, H.J. José, A.E. Rodrigues, R.F.P.M. Moreira, Treatment of textile wastewater by heterogeneous Fenton process using a new composite Fe₂O₃/carbon, *Chem. Eng. J.* 118 (2006) 77–82.
- [6] E. Kan, S.G. Huling, Effects of temperature and acidic pre-treatment on Fenton-driven oxidation of MTBE-spent granular activated carbon, *Environ. Sci. Technol.* 43 (2009) 1493–1499.
- [7] A.L.T. Pham, C. Lee, F.M. Doyle, D.L. Sedlak, A silica-supported iron oxide catalyst capable of activating hydrogen peroxide at neutral pH values, *Environ. Sci. Technol.* 43 (2009) 8930–8935.
- [8] J.A. Botas, J.A. Melero, F. Martínez, M.I. Pariente, Assessment of Fe₂O₃/SiO₂ catalysts for the continuous treatment of phenol aqueous solutions in a fixed bed reactor, *Catal. Today* 149 (2010) 334–340.
- [9] I. Muthuvel, M. Swaminathan, Photoassisted Fenton mineralisation of Acid Violet 7 by heterogeneous Fe (III)–Al₂O₃ catalyst, *Catal. Commun.* 8 (2007) 981–986.
- [10] Q. Zhang, W.F. Jiang, H.L. Wang, M.D. Chen, Oxidative degradation of dinitro butyl phenol (DNBP) utilizing hydrogen peroxide and solar light over a Al₂O₃-supported Fe(III)-5-sulfosalicylic acid (ssal) catalyst, *J. Hazard. Mater.* 176 (2010) 1058–1064.
- [11] M. Aleksić, H. Kušić, N. Koprivanac, D. Leszczynska, A.L. Božić, Heterogeneous Fenton type processes for the degradation of organic dye pollutant in water – the application of zeolite assisted AOPs, *Desalination* 257 (2010) 22–29.
- [12] E.G. Garrido-Ramírez, B.K.G. Theng, M.L. Mora, Clays and oxide minerals as catalysts and nanocatalysts in Fenton-like reactions – a review, *Appl. Clay Sci.* 47 (2010) 182–192.
- [13] C.S. Castro, M.C. Guerreiro, L.C.A. Oliveira, M. Gonçalves, A.S. Anastácio, M. Nazarro, Iron oxide dispersed over activated carbon: support influence on the oxidation of the model molecule methylene blue, *Appl. Catal. A: Gen.* 367 (2009) 53–58.
- [14] F. Adam, K. Kandasamy, S. Balakrishnan, Iron incorporated heterogeneous catalyst from rice husk ash, *J. Colloid Interface Sci.* 304 (2006) 137–143.
- [15] Y. Flores, R. Flores, A.A. Gallegos, Heterogeneous catalysis in the Fenton-type system reactive black 5/H₂O₂, *J. Mol. Catal. A: Chem.* 281 (2008) 184–191.
- [16] R.C.C. Costa, F.C.C. Moura, P.E.F. Oliveira, F. Magalhães, J.D. Ardisson, R.M. Lago, Controlled reduction of red mud waste to produce active systems for environmental applications: heterogeneous Fenton reaction and reduction of Cr (VI), *Chemosphere* 78 (2010) 1116–1120.
- [17] R.R.N. Marques, F. Stüber, K.M. Smith, A. Fabregat, C. Bengoa, J. Font, A. Fortuny, S. Pullket, G.D. Fowler, N.J.D. Graham, Sewage sludge based catalysts for catalytic wet air oxidation of phenol: preparation, characterisation and catalytic performance, *Appl. Catal. B: Environ.* 101 (2011) 306–316.
- [18] E. Fumoto, Y. Mizutani, T. Tago, T. Masuda, Production of ketones from sewage sludge over zirconia-supporting iron oxide catalysts in a steam atmosphere, *Appl. Catal. B: Environ.* 68 (2006) 154–159.
- [19] S. Rio, L. Le Coq, C. Faur, P. Le Cloirec, Production of porous carbonaceous adsorbent from physical activation of sewage sludge: application to wastewater treatment, *Water Sci. Technol.* 53 (2006) 237–244.
- [20] O. Malerius, J. Werther, Modelling the adsorption of mercury in the flue gas of sewage sludge incineration, *Chem. Eng. J.* 96 (2003) 197–205.
- [21] J. Villaseñor, L. Rodríguez, F.J. Fernández, Composting domestic sewage sludge with natural zeolites in a rotary drum reactor, *Bioresour. Technol.* 102 (2011) 1447–1454.
- [22] S. Werle, R.K. Wilk, A review of methods for the thermal utilization of sewage sludge: the Polish perspective, *Renew. Energy* 35 (2010) 1914–1919.
- [23] B. Jin, B. Li, Comprehensive utilization of sewage sludge in municipal wastewater treatment plant, *Environ. Sci. Manage.* 35 (2010) 106–109.
- [24] A. Bagreev, T.J. Bandosz, D.C. Locke, Pore structure and surface chemistry of adsorbents obtained by pyrolysis of sewage sludge-derived fertilizer, *Carbon* 39 (2001) 1971–1979.
- [25] C. Jindarom, V. Meeyoo, B. Kitiyanan, T. Kirksomboon, P. Rangsunvigit, Surface characterization and dye adsorptive capacities of char obtained from pyrolysis/gasification of sewage sludge, *Chem. Eng. J.* 133 (2007) 239–246.
- [26] J.S. Cha, J.C. Choi, J.H. Ko, Y.K. Park, S.H. Park, K.E. Jeong, S.S. Kim, J.K. Jeon, The low-temperature SCR of NO over rice straw and sewage sludge derived char, *Chem. Eng. J.* 156 (2010) 321–327.
- [27] M.J. Martin, E. Serra, A. Ros, M.D. Balaguer, M. Rigola, Carbonaceous adsorbents from sewage sludge and their application in a combined activated sludge-powdered activated carbon (AS-PAC) treatment, *Carbon* 42 (2004) 1389–1394.
- [28] S. Rio, C. Faur-Brasquet, L. Le Coq, P. Le Cloirec, Structure characterization and adsorption properties of pyrolyzed sewage sludge, *Environ. Sci. Technol.* 39 (2005) 4249–4257.
- [29] C. Hsiu-Mei, C. Ting-Chien, P. San-De, C. Hung-Lung, Adsorption characteristics of Orange II and chrysophenine on sludge adsorbent and activated carbon fibers, *J. Hazard. Mater.* 161 (2009) 1384–1390.
- [30] K.M. Smith, G.D. Fowler, S. Pullket, N.J.D. Graham, Sewage sludge-based adsorbents: a review of their production, properties and use in water treatment applications, *Water Res.* 43 (2009) 2569–2594.
- [31] F.S. Zhang, J.O. Nriagu, H. Itoh, Photocatalytic removal and recovery of mercury from water using TiO₂-modified sewage sludge carbon, *J. Photochem. Photobiol. A: Chem.* 167 (2004) 223–228.
- [32] A. Ansari, T.J. Bandosz, Inorganic–organic phase arrangement as a factor affecting gas-phase desulfurization on catalytic carbonaceous adsorbents, *Environ. Sci. Technol.* 39 (2005) 6217–6224.
- [33] J. Aibregó, J. Arauzo, J.L. Sainchez, A. Gonzalo, T. Cordero, J. Rodríguez-Mirasol, Structural changes of sewage sludge char during fixed-bed pyrolysis, *Ind. Eng. Chem. Res.* 48 (2009) 3211–3221.
- [34] S.G. Huling, P.K. Jones, T.R. Lee, Iron optimization for Fenton-driven oxidation of MTBE-spent granular activated carbon, *Environ. Sci. Technol.* 41 (2007) 4090–4096.
- [35] J.H. Ramirez, F.J. Maldonado-Hódar, A.F. Pérez-Cadenas, C. Moreno-Castilla, C.A. Costa, L.M. Madeira, Azo-dye Orange II degradation by heterogeneous Fenton-like reaction using carbon-Fe catalysts, *Appl. Catal. B: Environ.* 75 (2007) 312–323.
- [36] F. Duarte, F.J. Maldonado-Hódar, A.F. Pérez-Cadenas, L.M. Madeira, Fenton-like degradation of azo-dye Orange II catalyzed by transition metals on carbon aerogel, *Appl. Catal. B: Environ.* 85 (2009) 139–147.
- [37] P. Mills, J.L. SullivanMills, A study of the core level electrons in iron and its three oxides by means of X-ray photoelectron spectroscopy, *J. Phys. D* 16 (1983) 723.
- [38] M. Muruganandham, S.H. Chen, J.J. Wu, Evaluation of water treatment sludge as a catalyst for aqueous ozone decomposition, *Catal. Commun.* 8 (2007) 1609–1614.
- [39] X. Xue, K. Hanna, M. Abdelmoula, N. Deng, Adsorption and oxidation of PCP on the surface of magnetite: kinetic experiments and spectroscopic investigations, *Appl. Catal. B: Environ.* 89 (2009) 432–440.
- [40] G.E. Üstün, S.K.A. Solmaz, T. Morsünbül, H.S. Azak, Advanced oxidation and mineralization of 3-indole butyric acid (IBA) by Fenton and Fenton-like processes, *J. Hazard. Mater.* 180 (2010) 508–513.
- [41] J. Zęgliński, G.P. Piotrowski, R. Piękoś, A study of interaction between hydrogen peroxide and silica gel by FTIR spectroscopy and quantum chemistry, *J. Mol. Struct.* 794 (2006) 83–91.
- [42] J.H. Clark, Solid acids for green chemistry, *Acc. Chem. Res.* 35 (2002) 791–797.
- [43] M.S. Kang, Y.J. Choi, S.H. Moon, Effects of inorganic substances on water splitting in ion-exchange membranes: II. Optimal contents of inorganic substances in preparing bipolar membranes, *J. Colloid Interface Sci.* 273 (2004) 533–539.
- [44] Y.H. Wang, W.K. Siu, Structure characteristics and mechanical properties of kaolinite soils. I. Surface charges and structural characterizations, *Can. Geotech. J.* 43 (2006) 587–600.
- [45] M. Mullet, P. Fievet, J.C. Reggiani, J. Pagetti, Comparison of two electrokinetic methods – electroosmosis and streaming potential – to determine the zeta-potential of plane ceramic membranes, *J. Membr. Sci.* 123 (1997) 255–265.
- [46] S.H. Tian, Y.T. Tu, D.S. Chen, X. Chen, Y. Xiong, Degradation of Acid Orange II at neutral pH using Fe₂(MoO₄)₃ as a heterogeneous Fenton-like catalyst, *Chem. Eng. J.* 169 (2011) 31–37.
- [47] A. Chen, X. Ma, H. Sun, Decolorization of KN-R catalyzed by Fe-containing Y and ZSM-5 zeolites, *J. Hazard. Mater.* 156 (2008) 568–575.
- [48] M.N. Timofeeva, M.E. Malyshev, V.N. Panchenko, A.N. Shmakov, A.G. Potapov, M.S. Mel'gunov, FeAl₁₂-Keggin type cation as an active site source for Fe, Al-silica mesoporous, *Appl. Catal. B: Environ.* 95 (2010) 110–119.
- [49] H. Lim, J. Lee, S. Jin, J. Kim, J. Yoon, T. Hyeon, Highly active heterogeneous Fenton catalyst using iron oxide nanoparticles immobilized in alumina coated mesoporous silica, *Chem. Commun.* 4 (2006) 463–465.
- [50] F. Rodríguez-Reinoso, The role of carbon materials in heterogeneous catalysis, *Carbon* 36 (1998) 159–175.

Heterogeneous photo-Fenton oxidation of Acid Orange II over iron – sewage sludge derived carbon under visible irradiation

Yuting Tu,^{a,b} Ya Xiong,^{a,c*} Claude Descorme,^b Lingjun Kong^a and Shuanghong Tian^{a,c*}



Abstract

BACKGROUND: The disposal of sewage sludge has become an issue of particular concern due to its continuously increasing quantity. In this study, sewage sludge derived carbon (SC) was employed as support for iron-oxide-containing catalyst (FeSC). The catalysts were characterized in terms of inorganic elemental composition, XRD, SEM and TGA-FTIR. The catalytic activity of the catalyst was evaluated from the discoloration and mineralization of acid orange II (AOII) in the presence of H₂O₂ and visible light.

RESULTS: The FeSC catalyst pyrolyzed at 800°C for 2 h displayed the highest catalytic activity. Almost complete discoloration and 67% mineralization of 100 mg L⁻¹ AOII were achieved after 30 min adsorption and 60 min oxidation under visible light irradiation, using 1.5 g L⁻¹ catalyst, 15.0 mmol L⁻¹ H₂O₂ and initial pH 4.0. The prepared FeSC also exhibited very limited iron leaching (0.56 mg L⁻¹ after 90 min reaction) and high stability since the activity remained constant over ten consecutive runs.

CONCLUSIONS: This study demonstrated the high activity and stability of the sewage sludge-derived carbon-supported iron oxide catalyst in photo-Fenton-like reaction.

© 2013 Society of Chemical Industry

Supporting information may be found in the online version of this article.

Keywords: sewage sludge; photo-Fenton-like catalyst; visible light; Acid Orange I; discoloration; mineralization

INTRODUCTION

It is known that water-soluble organic dyes are bio-recalcitrant compounds existing with a wide concentration range in effluents from the textile and photographic industries.^{1,2} In recent years, extensive research has investigated the use of visible irradiation for the degradation of organic pollutants. It was found that the photo-Fenton reaction can be driven with low energy photons in the visible part of the spectrum by enhancing the photo reduction of Fe³⁺ to Fe²⁺. This provides a good approach to the treatment of dye-containing water using visible light or sunlight.^{3,4}

However, there are some drawbacks of the homogeneous photo-Fenton treatment under visible light irradiation, because it leads to high iron concentration in the final effluent so that the removal of large quantities of ferric hydroxide sludge is costly in terms of chemicals and manpower.⁵ To avoid these limitations, some efforts have been made to develop heterogeneous catalysts for photo-Fenton-like reactions by immobilizing Fe ions on a suitable substrate. In photochemical studies, many inorganic or organic materials have been used as catalyst supports by immobilizing iron ions or iron oxides on them, such as rectorite,⁶ alumina,⁷ silica gel,⁸ cation transfer membranes.⁹ Recently, development of heterogeneous photo-Fenton-like catalysts from solid waste materials has occurred. For example, Li and Zhang¹⁰ developed an amorphous FeOOH catalyst

from high iron-containing fly ash and immobilized FeOOH on the precursor, then used it for the degradation of Methyl Orange (MO) dye in the presence of H₂O₂/sunlight.

It is known that sewage sludge is mainly a mixture of exhausted biomass generated in the aerobic or anaerobic digestion of the organic contaminants in municipal sewage along with inorganic materials such as SiO₂, Al₂O₃, Fe₂O₃ and CaO.¹¹ After being pyrolyzed at high temperature, these oxides will become highly thermal stable and could play a role as catalyst or catalyst promoter in Fenton reactions.^{12,13} Sludge derived carbon (SC) formed after pyrolysis of sewage sludge have been widely used as an adsorbent for organic pollutants and heavy metals.^{14–16} Recently,

* Correspondence to: Ya Xiong, Shuanghong Tian, School of Environmental Science and Engineering, Sun Yat-Sen University, Guangzhou 510275, P. R. China. E-mail: cesxya@mail.sysu.edu.cn, t-sh-h@163.com

a School of Environmental Science and Engineering, Sun Yat-Sen University, Guangzhou, 510275, P. R. China

b Institut de recherches sur la catalyse et l'environnement de Lyon (IRCELYON), CNRS - Université Claude Bernard Lyon 1, 2 Avenue Albert Einstein, 69626, Villeurbanne Cedex, France

c Guangdong Provincial Key Laboratory of Environmental Pollution Control and Remediation Technology, Guangzhou, 510275, P. R. China

work centered on the application of sludge derived products as efficient catalysts has been reported. For example, sewage sludge based carbon was used in catalytic wet air oxidation of phenolic compounds,^{17,18} as a catalyst to enhance the removal of oxalic acid in ozonation,¹⁹ and as the support for a heterogeneous TiO₂-modified photocatalyst.²⁰ However, there is no report of SC being used as supports in photo-Fenton-like catalysts. On the other hand, since SC is an inorganic–organic composite, it could exhibit specific properties compared with other commonly employed inorganic or organic supports. This situation encouraged us to investigate the potential of SC as support for heterogeneous photo-Fenton-like catalysts. And a representative azo dye, Acid Orange II (AOII), was used as a model target pollutant in our study.

The objectives of this study were: (i) to synthesize and to characterize the sewage sludge-derived carbon-supported iron oxide catalyst (named FeSC); (ii) to investigate the effects of various operating parameters on the activity of the FeSC catalysts; and (iii) to evaluate the mineralization of Acid Orange II (AOII) and the stability of FeSC.

MATERIALS AND EXPERIMENTS

Materials

The dewatered sewage sludge was obtained from the Lie De municipal wastewater treatment plant in Guangzhou, China. The sludge was dried at 105 °C to constant weight, subsequently ground, sifted through a 100-mesh sieve, and finally stored in a desiccator at room temperature. The dried sample was labeled SS.

Analytical grade ferrous sulfate (FeSO₄•7H₂O) and hydrogen peroxide solution (30%, w/v) were obtained from Guangzhou Chemical Reagent Company, China. Ferroferric oxide and commercial activated carbon prepared from coconut husk were obtained from Tianjin Kermel Chemical Reagent Co. Ltd, China. The AOII was a commercial dye (Hengrun Dyestuff Chemical Co., Ltd, Guangzhou) which was used without any further purification.

Preparation of the catalysts

The sewage sludge-derived carbon-supported iron oxide catalyst (named FeSC) was prepared via a one-step method combining synthesis of SC with loading of the iron. First, 20 g dried sludge was added into a 150 mL iron solution (0.5 mol L⁻¹ FeSO₄, pH = 2.5). The suspension was stirred for 24 h slowly, evaporated in a rotary evaporator at 60 °C and dried at 105 °C for 12 h. Subsequently, the dried solid was pyrolyzed under flowing nitrogen (40 mL min⁻¹) in a horizontal furnace at 800 °C for 2 h (20 °C min⁻¹). Two additional pyrolysis temperature (600 °C and 700 °C) were also checked. The pyrolyzed samples were washed with deionized water several times until the conductivity became constant, then dried at 105 °C overnight and ground to less than 200-mesh. A sludge derived carbon (SC) sample, formed after pyrolysis at 800 °C for 2 h, was also used for comparison.

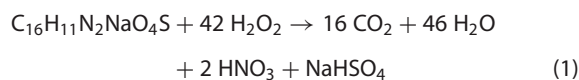
Characterization of catalysts

The average particle size was obtained using a Malvern MasterSizer 2000 Particle Size Analyzer. The ash content of the catalysts was determined using the standard ASTM D2866-94 method. The specific surface area (S_{BET}) was determined using an Autosorb-iQ-MP gas sorption analyzer (Quantachrome Instruments, USA) via nitrogen adsorption at 77 K. The isoelectric point values (pH_{IEP}) were determined from electrophoretic mobility measurements using a zeta potential analyzer (Zetasizer Nano ZS, Malvern).

The iron content in the synthesized samples was measured by inductively coupled plasma optical emission spectroscopy (ICP-OES, optima 5300DV, Perkin-Elmer). Scanning electron microscopy (SEM) images were recorded using a JEOL JSM-6330F field emission scanning electron microscope equipped with an energy-dispersive X-ray (EDX) detector (JED-2300). The chemical state of iron on the catalysts was followed by X-ray diffraction (XRD) using a D/max 2200 vpc Diffractometer (Rigaku Corporation, Japan) with Cu K α radiation at 40 kV and 30 mA. The TGA-FTIR analyses were performed using a Netzsch TG 209 thermobalance coupled with a Bruker Vector-22 (Bruker Company, Germany). The samples were heated from room temperature to 900 °C at a heating rate of 20 °C min⁻¹ under flowing nitrogen (40 mL min⁻¹). The data were processed using 'OPUS 1.0'.

Experimental procedures

All batch experiments were carried out in a 1 L cylindrical reactor equipped with a water cooled quartz jacket inserted in the center. Irradiation was provided by a 150 W short-arc Xe lamp (Sankyo, Japan) located in the center of the quartz jacket. Short-arc Xe lamp energy output at 320–780 nm, hence a 420 nm cutoff filter was used to remove the ultraviolet radiation. Air was bubbled from the bottom of the reactor (4 L min⁻¹) to hydraulically suspend the catalyst particles. The reaction temperature was kept at 30 °C by a thermostatic bath. The reaction suspension was prepared by adding a given amount of catalyst into 600 mL of a 100 mg L⁻¹ AOII solution. The solution pH was adjusted from 6.8 to a given value using either NaOH or H₂SO₄. After the adsorption/desorption equilibrium was established in the dark for 30 min, 500 mL suspension was used for the photo-Fenton-like reaction and initiated by turning on the Xe lamp. According to the Equation (1)



12 mmol L⁻¹ of H₂O₂ are theoretically required to completely degrade 100 mg/L AOII solution. In our case, 15 mmol L⁻¹ H₂O₂ was used to reach the maximum degradation of AOII. Samples were taken at predetermined time intervals and analyzed immediately after filtration through a 0.22 μm Millipore membrane filter to remove any suspended particles. All experiments were repeated twice and the results given are the average values with a relative standard deviation of less than 5%.

Analytical methods

The pH of the AOII solutions was measured with a PHS-3C pH meter (Rex Instrument Factory, Shanghai, China). The concentration of AOII was analyzed using a UV–vis spectrophotometer (UV-3150, Shimadzu) with maximum absorbance at 484 nm. The Fe concentration in the solution was measured by inductively coupled plasma optical emission spectrometry (ICP-OES, optima 5300DV, Perkin-Elmer). The total organic carbon (TOC) of the reaction mixture was measured on a TOC analyzer (Shimadzu, Japan).

RESULTS AND DISCUSSION

Characterization of catalysts

The basic physical and chemical characteristics or properties of the SC and FeSC samples are presented in Table 1. The average particle size in volume, BET surface area and pH_{IEP} of the SC and FeSC sample are similar. The ash content in the FeSC sample is c.

Table 1. Physicochemical properties of SC and FeSC pyrolyzed at 800 °C for 2 h

Sample	Fe (wt%)	Ash (wt%)	\bar{d}_V^a (μm)	S_{BET} ($\text{m}^2 \text{g}^{-1}$)	pH_{IEP}
SC	3.9	74.6	23	19	3.6
FeSC	12.9	93.0	27	14	3.4

^a \bar{d}_V , average particle diameter in volume.

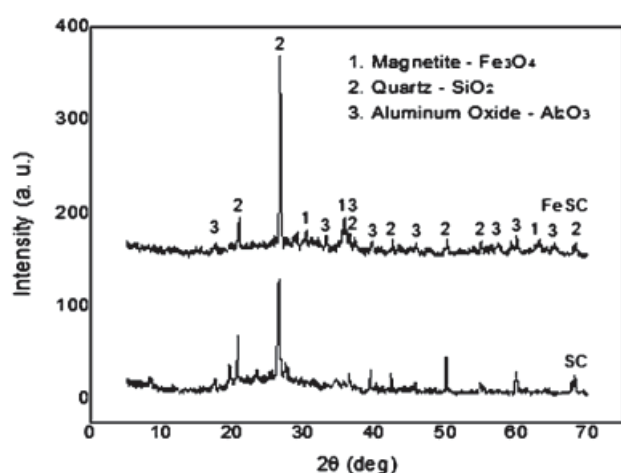


Figure 1. XRD patterns of the SC and the FeSC sample pyrolyzed at 800 °C.

18.4 wt% higher than that of the SC sample since iron has been impregnated. The iron content in SC and FeSC, determined by ICP-OES, was 3.9 and 12.9 wt%, respectively.

The iron chemical state in FeSC was studied by XRD (Fig. 1). Three broad bands at 35.5°, 62.6° and 30.1° are observed on the FeSC sample XRD pattern compared with the SC sample XRD pattern. These diffraction peaks are respectively assigned to the (3 1 1), (4 4 0) and (2 2 0) planes of Fe_3O_4 (JCPDS 88-0866).²¹ The Fe_3O_4 particles were 12 nm in size based on the Debye-Scherrer formula. According to the XRD results, other elements in FeSC, such as Si, Al, Ca and Na were present as SiO_2 , Al_2O_3 , CaSO_4 and NaPO_3 , respectively. The SEM micrographs of SC and FeSC are shown in Fig. 2. Compared with SC, the surface of FeSC appears a little more rough. In addition, the Fe content on the surface of FeSC measured by EDX analysis is 15.3%, in agreement with the result obtained by ICP-OES. Therefore, it can be deduced that the iron particles are almost uniformly distributed on the SC support.

In order to characterize the chemical changes which take place during the pyrolysis process, a TGA-FTIR study was performed. The TG curves of SS and FeSS are shown in Fig. 3. A larger mass loss was observed on the TG curve of FeSS between 470 °C and 600 °C compared with that of SS. The mass loss of SS and FeSS ended at 550 and 600 °C, respectively. As shown on the three-dimensional (3D) diagrams obtained during the pyrolysis of SS and FeSS (Fig. 4(A1) and (B1)), more visible peaks appeared in the 3D diagram of FeSS compared with SS, especially in the temperature range from 470 °C to 600 °C.

According to Fig. 4(A1), Three main kinds of volatile compounds were generated during the thermal treatment: H_2O (bending and stretching vibrations at 1350–1700 cm^{-1} and 3500–3700 cm^{-1}), CO_2 (asymmetric stretching mode at 2250–2392 cm^{-1}) and C–H_n (asymmetric vibration of the methylene group at 2250–2392 cm^{-1}). While on Fig. 4(B1), in addition to the three main products

mentioned above, some extra SO_2 (asymmetric stretching vibration at 1300–1420 cm^{-1}) was observed on the 3D diagram corresponding to FeSS.

To go further, the evolution versus temperature of the intensity of the bands associated with CO_2 (2359 cm^{-1}), SO_2 (1375 cm^{-1}), C–H_n (2933 cm^{-1}) and H_2O (1508 cm^{-1}) were plotted on Fig. 4(A2) and (B2). Differences in the evolution of these bands between the two samples can clearly be observed. The amount of CO_2 evolved from FeSS is much higher than from SS. The evolution of SO_2 from FeSS is also much better defined and ends around 600 °C on Fig. 4(B2).

It is worth mentioning that, in terms of intensities, CO_2 and SO_2 showed equivalent evolutions with temperature as shown in Fig. 4(B2). This is because the thermal decomposition of ferrous sulfate produces SO_3 , which decomposes to SO_2 and O_2 .²² The O_2 produced reacts with the carbon support and results in the formation of CO_2 . The iron sites trapped into the carbon can then be exposed, which means that more reactive sites were accessible for the heterogeneous photo-Fenton-like reaction.

Influence of the experimental conditions on the FeSC catalyst performances

Effect of the pyrolysis temperature

According to the TGA-FTIR results, the pyrolysis process should finish at temperature higher than 600 °C, hence 600, 700 and 800 °C were chosen as the maximum temperatures for the catalyst preparation. The corresponding catalysts are referred to as FeSC₆₀₀, FeSC₇₀₀ and FeSC₈₀₀. As shown in Fig. 5, about 13% of AOII was removed by FeSC in adsorption phase. While in the photo-Fenton-like oxidation process, the discoloration efficiency of AOII increased with increase of pyrolysis temperature. As shown in Fig. 5, the apparent rate constant (k_{app}) of the AOII degradation was obtained by fitting the results between 30 and 90 min, using a pseudo-first-order kinetic equation by plots of $\ln(C_0/C_t)$ against reaction time, which has been widely applied in the literature for the description of the heterogeneous photo-Fenton oxidation of organic pollutants.^{23,24} The k_{app} were calculated to be 6.52×10^{-2} , 7.46×10^{-2} and $9.24 \times 10^{-2} \text{ min}^{-1}$ for FeSC₆₀₀, FeSC₇₀₀ and FeSC₈₀₀, respectively. As a result of the increase of mass loss during pyrolysis at higher temperatures, the iron content in the FeSC catalysts increased slightly (12.3 wt%, 12.6 wt% and 12.9 wt% for catalysts pyrolyzed at 600, 700 and 800 °C). Hence there is more iron oxide in catalysts pyrolyzed at higher temperatures, which means there are more active sites for accelerating the decomposition of H_2O_2 in the presence of visible light. Further experiments were performed on the sample pyrolyzed at 800 °C as the heterogeneous photo-Fenton-like catalyst.

Effect of the catalyst concentration

The effect of FeSC catalyst dosage on the discoloration of AOII was studied and the results are presented in Fig. 6. During the adsorption phase, when the amount of FeSC catalyst increased, more AOII was adsorbed on the catalyst surface. The maximum adsorption was determined to be 13.4 mg g^{-1} by fitting the experimental isotherm data to the Langmuir isotherm model ($R^2 = 0.9967$), which is much lower than that of commercial activated carbon (purchased from Tianjin Chemical Reagent Co. Ltd, China, $S_{\text{BET}} = 605 \text{ m}^2 \text{g}^{-1}$, $Q_{\text{max}} = 345.0 \text{ mg g}^{-1}$). During the oxidation phase, as shown in Table 2, when the catalyst concentration increased from 0.5 g L^{-1} to 1.5 g L^{-1} , the initial reaction rates, expressed in milligrams of AOII converted per gram

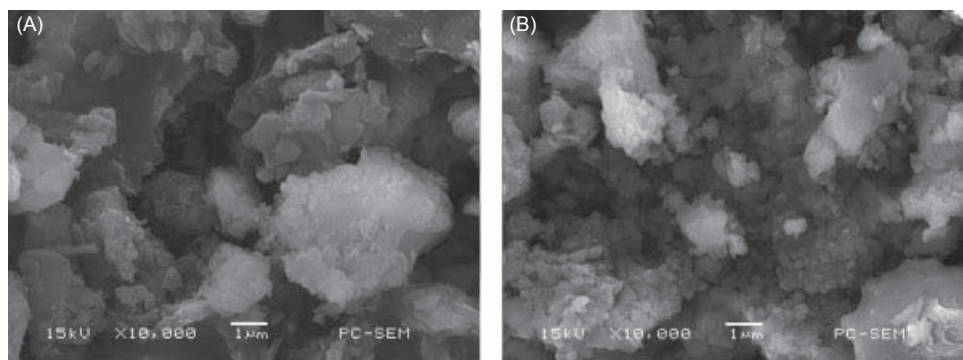


Figure 2. SEM images of the SC (A) and FeSC (B) samples pyrolyzed at 800 °C for 2 h.

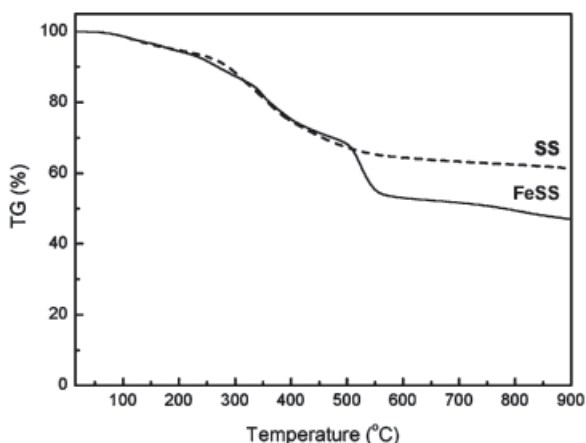


Figure 3. TG curves of SS and FeSS (heating rate: 20°C min⁻¹, nitrogen flow rate: 40 mL min⁻¹).

Table 2. Discoloration of AOII in photo-Fenton-like process with different dosage of FeSC catalyst. (H₂O₂: 15 mmol L⁻¹; AOII: 100 ppm; initial solution pH: 4.0; reaction temperature: 30°C; 150 W short-arc Xe lamp)

FeSC (g/L)	Initial reaction rate	Pseudo-first-order model parameters	
	(mg _{AOII} · g _{FeSC} ⁻¹ h ⁻¹)	k _{app} (× 10 ⁻² min ⁻¹)	R ²
0.5	179.1	2.8	0.9720
1.0	170.8	6.7	0.9859
1.5	152.4	9.2	0.9922
2.0	99.7	7.9	0.9874

of FeSC catalyst per hour, remained almost constant, which means the reaction was operated under chemical control. At higher catalyst dosage (c. 2 g L⁻¹), the initial reaction rate and pseudo-first-order degradation kinetic constant all decreased significantly. This change is because the increase in catalyst dosage makes the solution very turbid and decreases light penetration into the solution, resulting in a decrease in the amount of •OH produced and a less efficient process. Therefore, subsequent runs were performed using 1.5 g L⁻¹ catalyst.

Influence of initial solution pH

The removal of azo dye, catalyzed by Fe-catalysts, was earlier shown to be a pH-dependent process,^{25,26} and so the effect of

the initial solution pH was studied. As shown in Fig. 7(A), after 120 min reaction, over 99.9% AOII was transformed at pH 3.0, 99.7% at pH 4.0, and 95.3% at pH 5.0. As the pH of the solution was increased from 3.0 to 4.0 to 5.0 (insert on Fig. 7(A)), the pseudo-first-order kinetic constant decreased from 11.63 × 10⁻² to 9.24 × 10⁻² and to 5.17 × 10⁻² min⁻¹, respectively. These results indicate that the higher the initial solution pH, the slower the reaction rate.

The iron leaching from the catalyst was also checked throughout the experiments. It can be seen from Fig. 7(B) that the iron concentration in solution after 90 min reaction was 2.5, 0.6 and 0.2 mg L⁻¹ after reaction at pH 3.0, 4.0 and 5.0, respectively. A similar trend was observed by Ramirez et al.²⁷ using Fe/active carbon as catalyst. The leaching of Fe at pH 3.0 is not desirable since it is higher than the EU discharge limits (<2 ppm). Considering the high inorganic components in SC support, the concentration of the other metal elements in the filtrate was also analyzed by ICP-OES. For the FeSC system with initial pH = 4.0, little Al, Ca, Mg and Cu were detected in the filtrate; their concentrations were 0.6, 0.5, 0.5 and 0.03 mg L⁻¹, respectively, and the concentrations of Zn, Cr, Mn, Ni and Pb were below the detection limit of ICP-OES. In order to determine the influence of homogeneous phase reaction, we also tested the photo-Fenton catalytic activity of the filtrate after the reaction and only 24.7% degradation of AOII is observed at the end of the reaction. In conclusion, the optimal initial solution pH was 4.0, since the AOII removal efficiency was as high as at pH 3.0 but iron leaching was lower. It is worth mentioning that the amount of iron lost from the FeSC catalyst, even at pH 3.0 is only 1.3 wt% of the total iron content initially incorporated in the catalyst, significantly lower than in the case of the Fe/active carbon prepared by classical incipient wetness impregnation (c. 2.6 wt%).²⁷

Comparison of the catalytic activity of FeSC with different catalyst or different operating conditions

Figure 8 shows the removal efficiency of AOII versus time under different conditions. Compared with the discoloration rates of AOII in H₂O₂-visible light system (curve A), the SC-H₂O₂-visible light system (curve B) and FeSC-H₂O₂ system (curve C), the FeSC-H₂O₂-visible light system (curve E) had the highest discoloration efficiency. The apparent rate constant for the FeSC-H₂O₂-visible light system and the FeSC-H₂O₂ system were calculated to be 9.24 × 10⁻² min⁻¹ and 2.64 × 10⁻² min⁻¹, respectively. The former was about 3 times higher than the latter. These results clearly indicated the effect of light enhancement. That is because dyes can absorb visible light and become excited under visible irradiation, Equation (1), which will lead to electron transfer between the dye molecule and ferric ion on the catalyst and then accelerate the

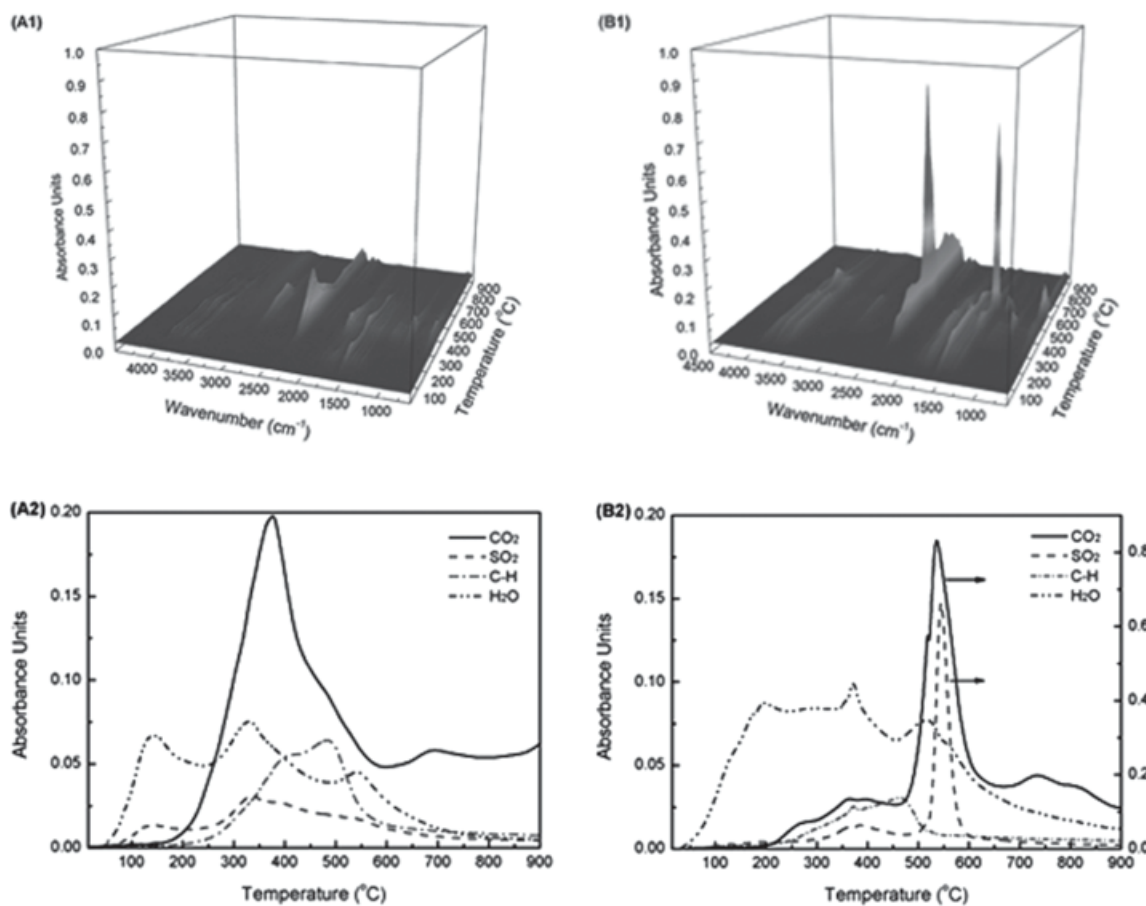


Figure 4. 3D diagrams corresponding to the gases evolved from SS (A1) and FeSS (B1). Evolution versus temperature of the bands characteristic of CO₂ (2359 cm⁻¹), SO₂ (1375 cm⁻¹), C-H (2933 cm⁻¹) and H₂O (1508 cm⁻¹) for SS (A2) and FeSS (B2).

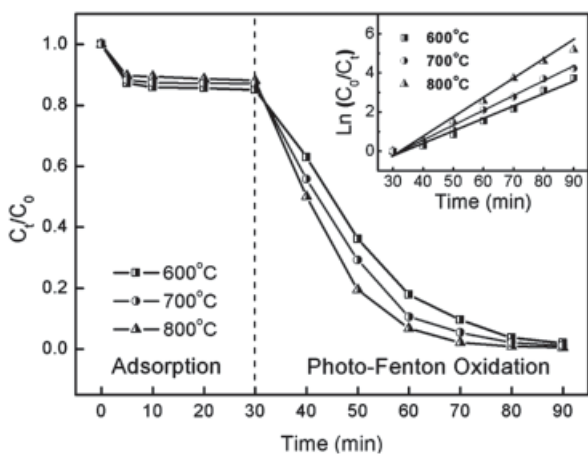


Figure 5. Effect of pyrolysis temperature on the adsorption and the oxidation of AOII during the photo-Fenton-like process (catalyst: 1.5 g L⁻¹; H₂O₂: 15 mmol L⁻¹; AOII: 100 ppm; initial solution pH: 4.0; reaction temperature: 30°C; 150 W short-arc Xe lamp).

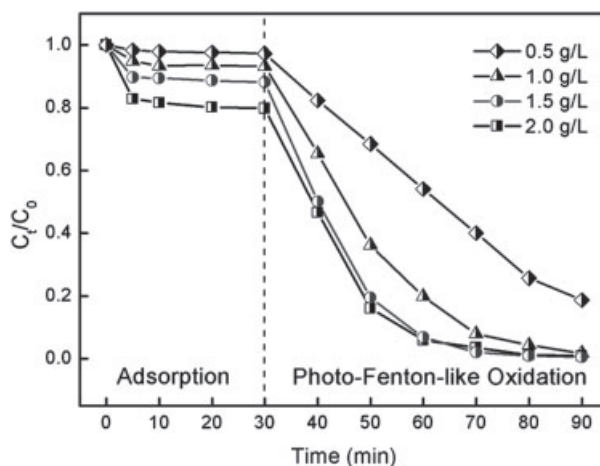
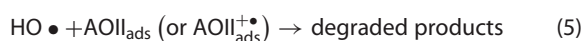
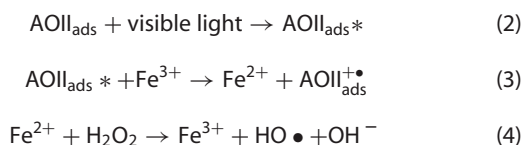


Figure 6. Effect of the catalyst concentration on the adsorption and the oxidation of AOII during photo-Fenton-like process (H₂O₂: 15 mmol L⁻¹; AOII: 100 ppm; initial solution pH: 4.0; reaction temperature: 30°C; 150-W short-arc Xe lamp).

photo-Fenton-like process, Equations (2)–(5).^{28,29}



To evaluate the role of the SC support in the heterogeneous photo-Fenton-like reaction, a commercial pure Fe₃O₄ oxide (S_{BET} = 7.0 m² g⁻¹) was used as a catalyst, using the same amount of iron as in the FeSC catalyst (116.1 mg Fe). As shown in Fig. 8 curves D and E, the Fe₃O₄ oxide showed less catalytic activity

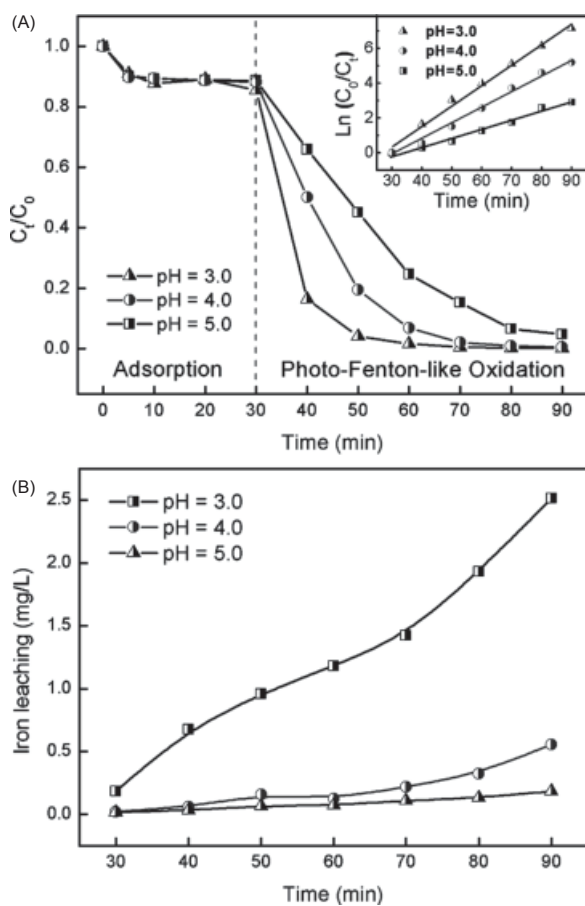


Figure 7. Effect of initial solution pH on the degradation of AOII (A) and on the iron leaching (B) (FeSC: 1.5 g L⁻¹; H₂O₂: 15 mmol L⁻¹; AOII: 100 ppm; reaction temperature: 30°C; 150 W short-arc Xe lamp).

than FeSC. The k_{app} for the Fe₃O₄ oxide was calculated to be $3.80 \times 10^{-2} \text{ min}^{-1}$, which is less than 40% of the k_{app} for the FeSC-H₂O₂-visible light system.

There are many reasons for the better photocatalytic performance of the FeSC system compared with the Fe₃O₄ oxide. First, in the adsorption phase, the AOII removal efficiency was 3 and 12% for the Fe₃O₄-H₂O₂-visible light system and FeSC-H₂O₂-visible light system, respectively. This indicated that the porous carbon matrix in the SC can facilitate the adsorption of dyes.³⁰ Second, the carbon support, as a photosensitizer and a conductive material, can absorb light and produce some photo-induced electrons (e⁻), transfer them to the iron particles and accelerate the reduction of Fe³⁺ to Fe²⁺,^{31,32} and thereby promote the photocatalytic process. Furthermore, some inorganic components in the SC support (SiO₂ and Al₂O₃) may also act as co-catalysts in the degradation of AOII during the heterogeneous photo-Fenton-like process. For example, SiO₂ (i) can facilitate the adsorption of H₂O₂ due to the formation of hydrogen bonds between H₂O₂ and Si-O-Si,³³ and (ii) increase the activity of •OH for the formation of an acidic microenvironment near the silica phase. Furthermore, the basic sites on Al₂O₃ can facilitate the adsorption of AOII, activate the H₂O₂ degradation and accelerate the reduction of Fe³⁺ by H₂O₂ due to the Lewis sites on the alumina.³⁴ Finally the hydroxyl groups on the surface of SiO₂ or Al₂O₃, acting as electron donors for the photo-generated H⁺, can also be oxidized into hydroxyl radicals (•OH).³⁵ Therefore, it can be deduced that SC is a favorable photo-Fenton-like catalyst support for the degradation of AOII.

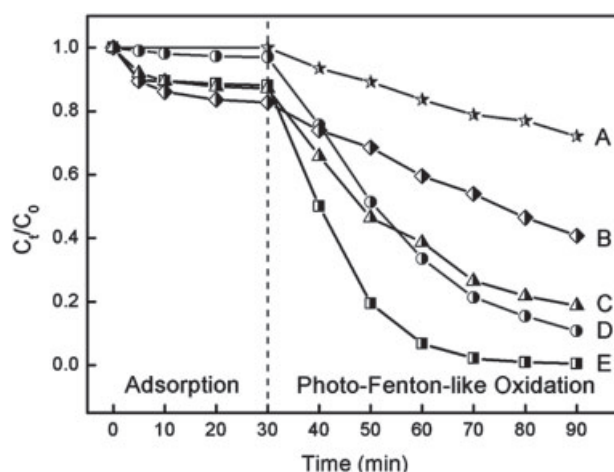


Figure 8. Removal of AOII (initial solution pH 4.0, 30°C). (A) 15 mmol L⁻¹ H₂O₂ + visible light; (B) 1.5 g L⁻¹ SC + 15 mmol L⁻¹ H₂O₂ + visible light; (C) 1.5 g L⁻¹ FeSC + 15 mmol L⁻¹ H₂O₂; (D) 0.2682 g L⁻¹ Fe₃O₄ + 15 mmol L⁻¹ H₂O₂ + visible light; (E) 1.5 g L⁻¹ FeSC + 15 mmol L⁻¹ H₂O₂ + visible light.

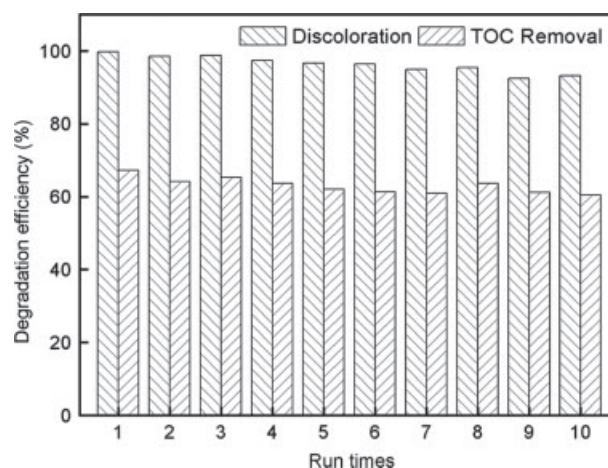


Figure 9. Discoloration and mineralization of AOII after 90 min reaction upon reuse of FeSC as Fenton-like catalyst (FeSC: 1.5 g L⁻¹; H₂O₂: 15 mmol L⁻¹; AOII: 100 ppm; reaction temperature: 30°C; 150 W short-arc Xe lamp).

Durability of the FeSC catalyst and the mineralization of AOII

For industrial practical applications, the long-term stability of the catalyst is a key issue. A direct study of the stability of FeSC catalyst in the catalytic degradation of AOII was carried out through successive batch experiments using the same sample recovered by filtration under identical reaction conditions. As shown in Fig. 9, the degradation of AOII decreased by only 7% after the 10th run. These results demonstrated that FeSC is durable and can be reused without loss of catalytic activity.

It is known that complete discoloration of AOII does not mean that the dye is completely oxidized. So, the mineralization of AOII, in terms of TOC removal, was investigated in parallel (the reaction conditions were: FeSC: 1.5 g L⁻¹; H₂O₂: 15 mmol L⁻¹; AOII: 100 ppm; reaction temperature: 30°C; 150 W short-arc Xe lamp). As shown in Fig. 9, compared with the AOII removal, it can be seen that the mineralization of AOII is slower than the discoloration. This is due to the fact that some partially-oxidized refractory intermediates are generated during AOII degradation.³⁶ The results shown in

Fig. 9 also indicate that FeSC as a heterogeneous photo-Fenton-like catalyst can lead to rapid discoloration of AOII as well as a remarkable degree of mineralization of the solution.

Application in natural river water

To obtain further insight into the catalytic behavior of FeSC catalyst in a practical application, natural river water was used instead of UP water to prepare the simulated dye water. The river water was collected from Pearl River (Guangzhou), some characteristics of the natural river water are listed in Table S1 (Supplementary Materials). The river water was filtered through a 0.22 μm Millipore membrane filter to remove any suspended particles, and then the AOII sample was added and the pH of the solution was adjusted to 4.0. The result showed that after 30 min adsorption and 90 min oxidation, 10.3 and 87.5% of AOII, respectively, was removed, and TOC removal at the end of reaction was 53%. Compared with the result using UP water, a detrimental effect of river water component was observed. This result may be due to the presence of natural radical scavengers in river water such as Cl^- , CO_3^{2-} , HCO_3^- and some organic compounds.^{37,38}

CONCLUSIONS

A novel heterogeneous photo-Fenton-like catalyst was successfully prepared for the first time, employing SCs as the catalyst support. The results showed that almost 100% AOII discoloration and 67% mineralization could be achieved after 30 min adsorption and 60 min photo-Fenton-like oxidation using a FeSC catalyst prepared by pyrolysis at 800°C for 2 h (1.5 g L⁻¹ catalyst, initial solution pH 4, 15.0 mmol L⁻¹ H₂O₂ and under the irradiation of a 150 W short-arc Xe lamp). Compared with a commercial pure Fe₃O₄ oxide, the FeSC catalyst presented higher catalytic efficiency because of the promoting effect of the SC support components. The FeSC catalyst also exhibited very limited iron leaching and good stability under appropriate reaction conditions.

ACKNOWLEDGEMENTS

This research was supported by Nature Science Foundations of China (20977117), Science, Nature Foundations of Guangdong Province (92510027501000005), Foundation of Industry-Education-Academy Cooperation from Guangdong Province and Education Department of Chinese government (2009A090100047, 2010B090486), Project of Education Bureau of Guangdong Province (cgzhzd1001), New Process and Technology Project of Guangzhou EPA (2009-03), Oversea study program of Guangzhou Elites scholarship, Technology Research Programs of Dongguan City (0711220600311), the Open Foundation of the Labs in Sun Yat-sen University (KF200924) and the Research Fund Program of Guangdong Provincial Key Laboratory of Environmental Pollution Control and Remediation Technology (2011 K0008).

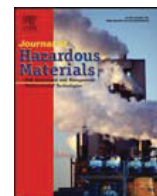
Supporting Information

Supporting information may be found in the online version of this article.

REFERENCES

- Bautista P, Mohedano AF, Casas JA, Zazo JA and Rodriguez JJ, An overview of the application of Fenton oxidation to industrial wastewaters treatment. *J Chem Technol Biotechnol* **83**:1323–1338 (2008).
- Chebli D, Fourcade F, Brosillon S, Nacef S and Amrane A, Supported photocatalysis as a pre-treatment prior to biological degradation for the removal of some dyes from aqueous solutions; Acid Red 183, Biebrich Scarlet, Methyl Red Sodium Salt, Orange II. *J Chem Technol Biotechnol* **85**:555–563 (2010).
- Tokumura M, Katoh H, Katoh T, Znad HT and Kawase Y, Solubilization of excess sludge in activated sludge process using the solar photo-Fenton reaction. *J Hazard Mater* **162**:1390–1396 (2009).
- Mavronikola C, Demetriou M, Hapeshi E, Partassides D, Michael C, Mantzavinos D and Kassinos D, Mineralisation of the antibiotic amoxicillin in pure and surface waters by artificial UVA- and sunlight-induced Fenton oxidation. *J Chem Technol Biotechnol* **84**:1211–1217 (2009).
- Chen Q, Wu P, Li Y, Zhu N and Dang Z, Heterogeneous photo-Fenton photodegradation of reactive brilliant orange X-GN over iron-pillared montmorillonite under visible irradiation. *J Hazard Mater* **168**:901–908 (2009).
- Zhao X, Zhu L, Zhang Y, Yan J, Lu X, Huang Y and Tang H, Removing organic contaminants with bifunctional iron modified rectorite as efficient adsorbent and visible light photo-Fenton catalyst. *J Hazard Mater* **215-216**:57–64 (2012).
- Muthuvel I and Swaminathan M, Highly solar active Fe(III) immobilised alumina for the degradation of Acid Violet 7. *Solar Energy Mater Solar Cells* **92**:857–863 (2008).
- Zhao C, Huang YP, Fang YF, Jiang LR, Liu LM and King KL, Visible light-induced degradation of organic pollutants using Fe(II) supported on silica gel as an effective catalyst. *Chinese Sci Bull* **53**:1497–1502 (2008).
- Cheng M, Ma W, Li J, Huang Y and Zhao J, Visible-light-assisted degradation of dye pollutants over Fe (III)-loaded resin in the presence of H₂O₂ at neutral pH values. *Environ Sci Technol* **38**:1569–1575 (2004).
- Li Y and Zhang FS, Catalytic oxidation of Methyl Orange by an amorphous FeOOH catalyst developed from a high iron-containing fly ash. *Chem Eng J* **158**:148–153 (2010).
- Smith KM, Fowler GD, Pullket S and Graham NJD, Sewage sludge-based adsorbents: a review of their production, properties and use in water treatment applications. *Water Res* **43**:2569–2594 (2009).
- Timofeeva MN, Malyshev ME, Panchenko VN, Shmakov AN, Potapov AG and Mel'gunov MS, FeAl₁₂-Keggin type cation as an active site source for Fe, Al-silica mesoporous catalysts. *Appl Catal B: Environ* **95**:110–119 (2010).
- Tu YT, Tian SH, Kong LJ and Xiong Y, Co-catalytic effect of sewage sludge-derived char as the support of Fenton-like catalyst. *Chem Eng J* **185-186**:44–51 (2012).
- Martin MJ, Artola A, Balaguer MD and Rigola M, Towards waste minimisation in WWTP: activated carbon from biological sludge and its application in liquid phase adsorption. *J Chem Technol Biotechnol* **77**:825–833 (2002).
- Rio S, Faur-Brasquet C, Coq LL and Cloirec PL, Structure characterization and adsorption properties of pyrolyzed sewage sludge. *Environ Sci Technol* **39**:4249–4257 (2005).
- Chiang HM, Chen TC, Pan SD and Chiang HL, Adsorption characteristics of Orange II and Chrysophenine on sludge adsorbent and activated carbon fibers. *J Hazard Mater* **161**:1384–1390 (2009).
- Marques RRN, Stüber F, Smith KM, Fabregat A, Bengoa C, Font J, Fortuny A, Pullket S, Fowler GD and Graham NJD, Sewage sludge based catalysts for catalytic wet air oxidation of phenol: preparation, characterisation and catalytic performance. *Appl Catal B: Environ* **101**:306–316 (2011).
- Stüber F, Smith KM, Mendoza MB, Marques RRN, Fabregat A, Bengoa C, Font J, Fortuny A, Pullket S, Fowler GD and Graham NJD, Sewage sludge based carbons for catalytic wet air oxidation of phenolic compounds in batch and trickle bed reactors. *Appl Catal B: Environ* **110**:81–89 (2011).
- Wen G, Pan ZH, Ma J, Liu ZQ, Zhao L and Li JJ, Reuse of sewage sludge as a catalyst in ozonation - efficiency for the removal of oxalic acid and the control of bromate formation. *J Hazard Mater* **239-240**:381–388 (2012).
- Zhang FS, Nriagu JO and Itoh H, Photocatalytic removal and recovery of mercury from water using TiO₂-modified sewage sludge carbon. *J Photochem Photobiol A* **167**:223–228 (2004).
- Duarte F, Maldonado-Hódar FJ, Pérez-Cadenas AF and Madeira LM, Fenton-like degradation of azo-dye Orange II catalyzed by transition metals on carbon aerogels. *Appl Catal B: Environ* **85**:139–147 (2009).

- 22 Swamy MSR, Prasad TP and Sant BR, Thermal analysis of ferrous sulphate heptahydrate in air. *J Therm Anal Calorim* **16**:471–478 (1979).
- 23 Liu SQ, Cheng S, Luo L, Cheng HY, Wang SJ and Lou S, Degradation of dye rhodamine B under visible irradiation with Prussian blue as a photo-Fenton reagent. *Environ Chem Lett* **9**:31–35 (2011).
- 24 Monteagudo JM, Durán A, Martín IS and Aguirre M, Catalytic degradation of Orange II in a ferrioxalate-assisted photo-Fenton process using a combined UV-A/C–solar pilot-plant system. *Appl Catal B: Environ* **95**:120–129 (2010).
- 25 Panda N, Sahoo H and Mohapatra S, Decolourization of Methyl Orange using Fenton-like mesoporous Fe₂O₃–SiO₂ composite. *J Hazard Mater* **185**:359–365 (2011).
- 26 Guo J and Al-Dahhan M, Catalytic Wet Oxidation of Phenol by Hydrogen Peroxide over Pillared Clay Catalyst. *Ind Eng Chem Res* **42**:2450–2460 (2003).
- 27 Ramirez JH, Maldonado-Hódar FJ, Pérez-Cadenas AF, Moreno-Castilla C, Costa CA and Madeira LM, Azo-dye Orange II degradation by heterogeneous Fenton-like reaction using carbon-Fe catalysts. *Appl Catal B: Environ* **75**:312–323 (2007).
- 28 Styliidi M, Kondarides DI and Verykios XE, Visible light-induced photocatalytic degradation of Acid Orange 7 in aqueous TiO₂ suspensions. *Appl Catal B: Environ* **47**:189–201 (2004).
- 29 Ma J, Song W, Chen C, Ma W, Zhao J and Tang Y, Fenton degradation of organic compounds promoted by dyes under visible irradiation. *Environ Sci Technol* **39**:5810–5815 (2005).
- 30 Matos J, Laine J and Herrmann JM, Synergy effect in the photocatalytic degradation of phenol on a suspended mixture of titania and activated carbon. *Appl Catal B: Environ* **18**:281–291 (1998).
- 31 Wang W, Serp P, Kalck P and Faria JL, Visible light photodegradation of phenol on MWNT-TiO₂ composite catalysts prepared by a modified sol-gel method. *J Mol Catal A: Chem* **235**:194–199 (2005).
- 32 Zhang H, Lv X, Li Y, Wang Y and Li J, P25-graphene composite as a high performance photocatalyst. *ACS Nano* **4**:380–386 (2010).
- 33 Żegliński J, Piotrowski GP and Piękoś R, A study of interaction between hydrogen peroxide and silica gel by FTIR spectroscopy and quantum chemistry. *J Mol Struct* **794**:83–91 (2006).
- 34 Lim H, Lee J, Jin S, Kim J, Yoon J and Hyeon T, Highly active heterogeneous Fenton catalyst using iron oxide nanoparticles immobilized in alumina coated mesoporous silica. *Chem Commun* **28**:463–465 (2006).
- 35 Fu P, Luan Y and Dai X, Preparation of activated carbon fibers supported TiO₂ photocatalyst and evaluation of its photocatalytic reactivity. *J Mol Catal A: Chem* **221**:81–88 (2004).
- 36 Chen J and Zhu L, UV-Fenton discolouration and mineralization of Orange II over hydroxyl-Fe-pillared bentonite. *J Photochem Photobiol A: Chem* **188**:56–64 (2007).
- 37 White EM, Vaughan PP, Zepp RG, Role of the photo-Fenton reaction in the production of hydroxyl radicals and photobleaching of colored dissolved organic matter in a coastal river of the southeastern United States. *Aquat Sci* **65**:402–414 (2003).
- 38 Lair A, Ferronato C, Chovelon JM, Herrmann JM, Naphthalene degradation in water by heterogeneous photocatalysis: an investigation of the influence of inorganic anions. *J Photochem Photobiol A: Chem* **193**:193–203 (2008).



Catalytic wet air oxidation of 2-chlorophenol over sewage sludge-derived carbon-based catalysts



Yuting Tu^{a,b}, Ya Xiong^{b,c}, Shuanghong Tian^{b,c}, Lingjun Kong^b, Claude Descorme^{a,*}

^a Institut de recherches sur la catalyse et l'environnement de Lyon (IRCELYON), CNRS – Université Claude Bernard Lyon 1, 2 Avenue Albert Einstein, 69626 Villeurbanne Cedex, France

^b School of Environmental Science and Engineering, Sun Yat-Sen University, Guangzhou 510275, PR China

^c Guangdong Provincial Key Laboratory of Environmental Pollution Control and Remediation Technology, Guangzhou 510275, PR China

HIGHLIGHTS

- A sewage sludge derived carbon-supported iron oxide catalyst (FeSC) was prepared.
- FeSC exhibited high catalytic activity in the wet air oxidation of 2-chlorophenol.
- A strong correlation was observed between the 2-CP conversion, the iron leaching and the pH.
- Using an acetate buffer, the iron leaching was suppressed while keeping some catalytic activity.
- A simplified reaction pathway was proposed for the CWAO of 2-CP over the FeSC catalyst.

ARTICLE INFO

Article history:

Received 18 March 2014

Received in revised form 6 May 2014

Accepted 11 May 2014

Available online 16 May 2014

Keywords:

Catalytic wet air oxidation (CWAO)

2-Chlorophenol

Sewage sludge based catalyst

Iron oxide

Stability

ABSTRACT

A sewage sludge derived carbon-supported iron oxide catalyst (FeSC) was prepared and used in the Catalytic Wet Air Oxidation (CWAO) of 2-chlorophenol (2-CP). The catalysts were characterized in terms of elemental composition, surface area, pH_{PZC} , XRD and SEM. The performances of the FeSC catalyst in the CWAO of 2-CP was assessed in a batch reactor operated at 120 °C under 0.9 MPa oxygen partial pressure. Complete decomposition of 2-CP was achieved within 5 h and 90% Total Organic Carbon (TOC) was removed after 24 h of reaction. Quite a straight correlation was observed between the 2-CP conversion, the amount of iron leached in solution and the pH of the reaction mixture at a given reaction time, indicating a strong predominance of the homogeneous catalysis contribution. The iron leaching could be efficiently prevented when the pH of the solution was maintained at values higher than 4.5, while the catalytic activity was only slightly reduced. Upon four successive batch CWAO experiments, using the same FeSC catalyst recovered by filtration after pH adjustment, only a very minor catalyst deactivation was observed. Finally, based on all the identified intermediates, a simplified reaction pathway was proposed for the CWAO of 2-CP over the FeSC catalyst.

© 2014 Elsevier B.V. All rights reserved.

1. Introduction

Municipal sewage sludge are produced in huge quantity in conventional wastewater treatment plants. In 2010 for instance, the total production of dry sewage sludge in the United States, the European Union and China were ca. 8.2, 10.0 and 8.0 million tons, respectively. Furthermore, it is predicted that the production of sludge all over the world will continue to rise with an annual increase of about 2 vol.%. Therefore, the disposal of sewage sludge is an issue of serious environmental concern [1,2]. Compared with

the traditional methods of sewage sludge disposal, such as ocean dumping, landfilling and incineration, pyrolysis could be considered as an economically feasible and eco-friendly route [3]. Sludge derived carbons (SC) produced upon pyrolysis of sewage sludge have been used as adsorbents for organic pollutants and heavy metals [4,5]. On the other hand, the application of sewage sludge derived materials as efficient catalysts in the wastewater treatment have been recently reported. For example, sewage sludge based carbons were used in the catalytic wet air oxidation of phenolic compounds [6], in the catalytic ozonation of oxalic acid [7], and as supports for heterogeneous Fenton-like catalysts [8,9].

In the wastewater treatment area, 2-chlorophenol (2-CP), which is widely used in the paper, the pulp, the pesticide and the herbicide industries, is unambiguously identified as a severe

* Corresponding author. Tel.: +334 72 44 53 07; fax: +334 72 44 53 99.
E-mail address: claude.descorme@ircelyon.univ-lyon1.fr (C. Descorme).

environmental pollutant of major concern due to its high toxicity and low biodegradability. The maximum allowable concentration of 2-CP in drinking water was fixed at $10 \mu\text{g L}^{-1}$ [10]. Among the different techniques applied to date for the treatment of 2-CP, the catalytic wet air oxidation (CWAO) has attracted some interest. Compared to the biological, electrochemical or photocatalytic treatments, CWAO is more efficient at treating high concentrations of organic pollutants [11]. Compared to the incineration and the supercritical water oxidation, CWAO might further be considered as an energy-saving catalytic method [12].

In the past years, a series of noble metal catalysts were used in the CWAO and exhibited highly activities [13,14], but they are quite expensive. Therefore, transition metal oxide based catalysts were used as an alternative in the CWAO process [15–17]. Since sewage sludge are rich in iron, it was decided to test them directly in the CWAO of 2-CP. Furthermore, sewage sludge derived carbon supported iron oxide catalysts (named as FeSC) were also prepared, following an optimized method, in order to stabilize the iron. Compared with the costly noble-metal catalysts, the prepared FeSC catalysts are potentially low cost. Since the metal leaching remains the main drawback for an extensive application of transition-metal based catalysts in CWAO processes, the reasons and effects of the iron leaching upon the reaction were investigated in this study. And different attempts to prevent the iron leaching were also tested.

2. Experimental

2.1. Preparation of the catalysts

The dewatered sewage sludge was obtained from the Lie De municipal wastewater treatment plant in Guangzhou, China. The sludge was dried at 105°C to constant weight, grinded and sieved (100-mesh). Subsequently stored in a desiccator at room temperature.

The sewage sludge-derived char supported iron oxide catalyst (named as FeSC) was prepared following a one-step method combining the carbon synthesis with the Fe loading. At first, 20 g dried sludge were added into 150 mL of a ferrous sulfate solution ($0.5 \text{ mol L}^{-1} \text{ FeSO}_4$, $\text{pH} = 2.5$). After the suspension was stirred for 24 h, it was slowly evaporated in a rotary evaporator at 60°C under reduced pressure, and then dried at 105°C for 12 h. Subsequently, the received solid was pyrolyzed under flowing nitrogen (40 mL min^{-1}) in a horizontal furnace at 800°C for 2 h (heating rate: $20^\circ\text{C min}^{-1}$). The pyrolyzed sample was washed several times with deionized water until the conductivity became constant in order to make sure there is no soluble iron salts anymore on the catalyst surface. Then, the sample was dried at 105°C overnight and grinded to less than 200-mesh size.

In order to reduce the ash content, 5 g of the sludge-derived carbon (SC), formed after pyrolysis at 800°C for 2 h, was treated in a 80 mL acid solution (25 vol.% HCl + 25 vol.% HF) at 70°C for 2 h before, washing with distilled water and drying. The sample was named as SC-A.

2.2. Characterizations

The ash content of the catalysts was determined using the standard ASTM D2866-94 method. The metal content in the synthesized samples was measured by inductively coupled plasma optical emission spectroscopy (ICP-OES, Horiba Jobin-Yvon).

The specific surface area (S_{BET}) was determined using an Autosorb-iQ-MP gas sorption analyzer (Quantachrome Instruments, USA) via nitrogen adsorption at 77 K.

The pH at the point of zero charge (pH_{PZC}) of the catalyst was measured according to the method developed by Brunelle [18].

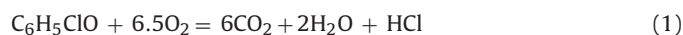
Increasing amounts of solid were added sequentially to a 50 mL 0.0005 M NaCl solution until the pH reached a plateau. The pH at the plateau corresponds to the pH_{PZC} .

The chemical state of iron on the catalysts was followed by X-ray diffraction (XRD) using a D/max 2200 vpc Diffractometer (Rigaku Corporation, Japan) with a $\text{Cu K}\alpha$ radiation at 40 kV and 30 mA.

Scanning electron microscopy (SEM) images were recorded using a JEOL JSM-6330F field emission scanning electron microscope equipped with an energy-dispersive X-ray (EDX) detector (JED-2300).

2.3. Catalytic tests

The catalytic wet air oxidation of 2-chlorophenol over the SC-based catalysts was studied in a conventional batch reactor made of Hastelloy C22 (Model 4836, Parr Instrument Inc). The experimental apparatus is described in Fig. S1. In each run, the 300 mL autoclave was loaded with 150 mL of a 2 g L^{-1} 2-CP aqueous solution (ca. 2.3 mmol 2-CP in the reactor) and a defined amount of catalyst. After the reactor was repeatedly outgassed with argon at ambient temperature, the reactor was heated up to the desired temperature (120°C). When the temperature was stabilized, synthetic air (20 vol.% O_2 + 80 vol.% N_2) was introduced into the reactor until the total pressure reached 5 MPa. This point was taken as “zero” time for the reaction. The oxygen partial pressure was ca. 0.9 MPa (ca. 42.8 mmol O_2 in the reactor), corresponding globally to a large excess of oxygen according Eq. (1). Noteworthy, the oxygen solubility in water under such conditions was only ca. $0.2 \text{ g O}_2 \text{ L}^{-1}$.



Furthermore, to avoid any mass transfer limitation in the liquid phase, the stirrer speed was fixed at 1300 rpm [19]. Liquid samples were taken from the reactor at regular time intervals and analyzed after centrifugation.

2.4. Analytical methods

The concentrations of 2-chlorophenol and the oxidation intermediates were measured by HPLC using a UV-detector set at 210 and 281 nm (Shimadzu). The HPLC system was equipped with a Kinetex PFP 100A $2.6 \mu\text{m}$ $100 \text{ mm} \times 4.6 \text{ mm}$ column (Phenomenex), operated at constant temperature (40°C). The mobile phase was a mixture of 4 vol.% methanol and 96 vol.% water, which pH was acidified down to 2.0 using a 85 wt.% H_3PO_4 solution. The flow rate was fixed at 0.6 mL min^{-1} .

The total organic carbon (TOC) in the liquid samples was determined by using a Shimadzu 5050 TOC analyzer. The pH of the solution was measured with a Radiometer Analytical PHM240 pH meter. The Fe concentration in the liquid samples was further analyzed by ICP-OES to check for lixiviation.

3. Results and discussion

3.1. Characterization of the catalysts

The basic physical and chemical characteristics of the SC and FeSC samples are summarized in Table 1.

The ash content values and the results of the ICP-OES analysis indicated a high content in inorganic components, such as iron, silicon and aluminum. After the acidic washing, the ash fraction was partial removed. The iron content in SC, FeSC and SC-A, determined by ICP-OES, was 4.5, 12.0 and 0.4 wt.%, respectively. SC and FeSC exhibited quite a low specific surface area, while SC-A showed a higher surface as a result of the acidic washing and the efficient ash removal. As indicated in Table 1, the pH_{PZC} value decreased

Table 1
Physicochemical properties of the SC, FeSC and SC-A samples.

Sample	Ash content (wt.%)	Fe (wt.%)	Si (wt.%)	Al (wt.%)	Ca (wt.%)	S_{BET} ($\text{m}^2 \text{g}^{-1}$)	pH_{PZC}
SC	74.6	4.5	23.4	10.6	1.7	19	7.5
FeSC	93.0	12.0	19.9	9.1	1.8	14	4.2
SC-A	56.1	0.4	28.6	1.8	<0.1	33	3.7

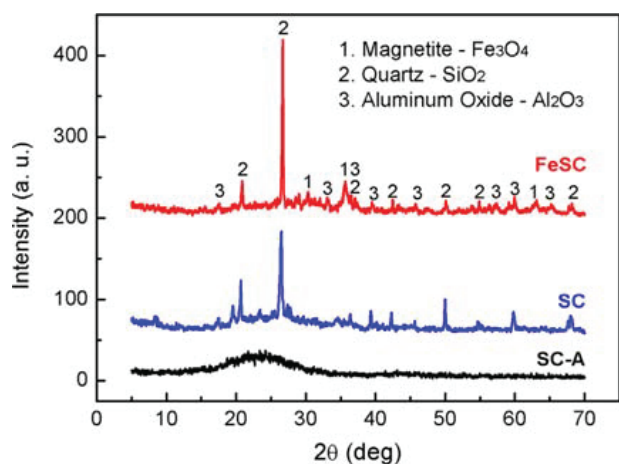


Fig. 1. XRD patterns of FeSC, SC and SC-A.

upon incorporation of iron in the SC support. This variation could be attributed to the higher amount of acidic oxygen surface functional groups induced by the presence of iron, which could be beneficial for the CWAO reaction [20].

The iron phase in the FeSC sample could be further characterized using XRD (Fig. 1). Compared with the diffractogram of the pure SC and SC-A sample, the XRD pattern for FeSC exhibited several extra diffraction lines at 2θ equal 35.5° , 62.6° and 30.1° . These lines could respectively be assigned to the (3 1 1), (4 4 0) and (2 2 0) planes of Fe_3O_4 (magnetite, JCPDS n° 88-0866).

Finally, as shown in Fig. 2, the SEM micrographs indicated that the surface of FeSC is relatively rough. In addition, the mean Fe content (for the zone shown in Fig. 2B) measured by EDX was ca. 15.3 wt.%, which is in good agreement with the results obtained by ICP-OES. It could be deduced that the iron particles are quite uniformly distributed on the SC support.

3.2. CWAO of 2-chlorophenol over the different catalysts

The wet air oxidation of 2-CP, in absence of any catalyst, was shown to be very slow. Upon reaction at 120°C under 0.9 MPa

oxygen partial pressure, 6% 2-CP conversion was achieved via thermal decomposition at the very beginning of the oxidation reaction ($t=0$). After 24 h of reaction, the 2-CP and TOC removal were lower than 15% (Fig. 3), indicating that the 2-CP molecule was thermally stable under the applied reaction conditions.

The 2-CP molecule was observed to adsorb on the SC based catalysts. The initial adsorption, before the introduction of air ($t=0$), accounted for ca. 3% after subtraction of the 6% 2-CP conversion due to thermal decomposition. The untreated SC sample appeared to be only moderately active in the CWAO of 2-CP. After 24 h of reaction, the 2-CP conversion was only 50% and TOC abatement reached 39%.

After acidic treatment (HCl + HF), the 2-CP adsorption increased up to 9%. This observation could be simply explained by the higher specific surface area of the SC-A sample compared to the initial SC (33 vs. $19 \text{ m}^2 \text{g}^{-1}$). On the contrary, the catalytic activity decreased upon removal of the ash fraction. The initial reaction rate decreased from 0.4 to $0.1 \text{ mmol}_{2\text{-CP}} \text{ g}_{\text{catalyst}}^{-1} \text{ h}^{-1}$. The much smaller amount of iron in the treated sample (0.4 vs. 4.5 wt.%) could be responsible for this difference.

After incorporation of iron on the SC support, a substantial increase of the 2-CP conversion was observed. The complete removal of 2-CP could be reached within 5 h of reaction. The initial reaction rate was calculated to be $3.0 \text{ mmol}_{2\text{-CP}} \text{ g}_{\text{catalyst}}^{-1} \text{ h}^{-1}$, which was almost 7 times higher than the rate measured on the untreated SC, while the iron concentration in the catalyst was only tripled. Compared with the classical Ru/ZrO₂ catalyst [21], which is known as a kind of high efficient noble metal catalyst, the FeSC catalyst displayed higher catalytic activity under identical reaction conditions. As shown in Fig. 3B, the TOC removal also remarkably increased upon addition of the FeSC catalyst, reaching 91% at the end of the reaction (24 h). By comparison with the evolution of the 2-CP conversion, it could be deduced that the mineralization of the 2-CP molecule was not complete and occurred at a slower rate. Several partially-oxidized intermediates formed upon 2-CP degradation and appeared to be resistant toward further conversion to carbon dioxide.

Furthermore, as the decomposition of 2-CP occurred, the pH of the reaction mixture decreased from an initial value of 5.5 to very acidic values (Fig. 3C). This increase of the acidity of the reaction mixture could be attributed to (i) the production of HCl as a result of

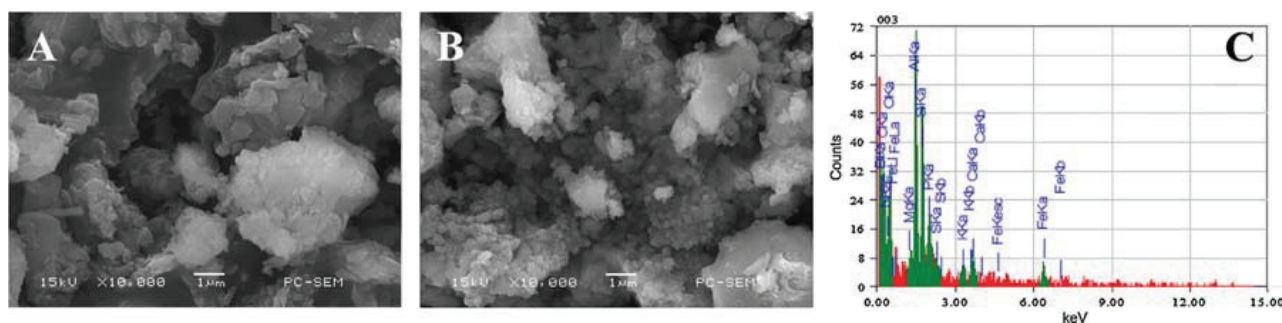


Fig. 2. SEM images of the SC (A) and FeSC (B) samples pyrolyzed at 800°C for 2 h, and the result of EDX analysis for FeSC (C).

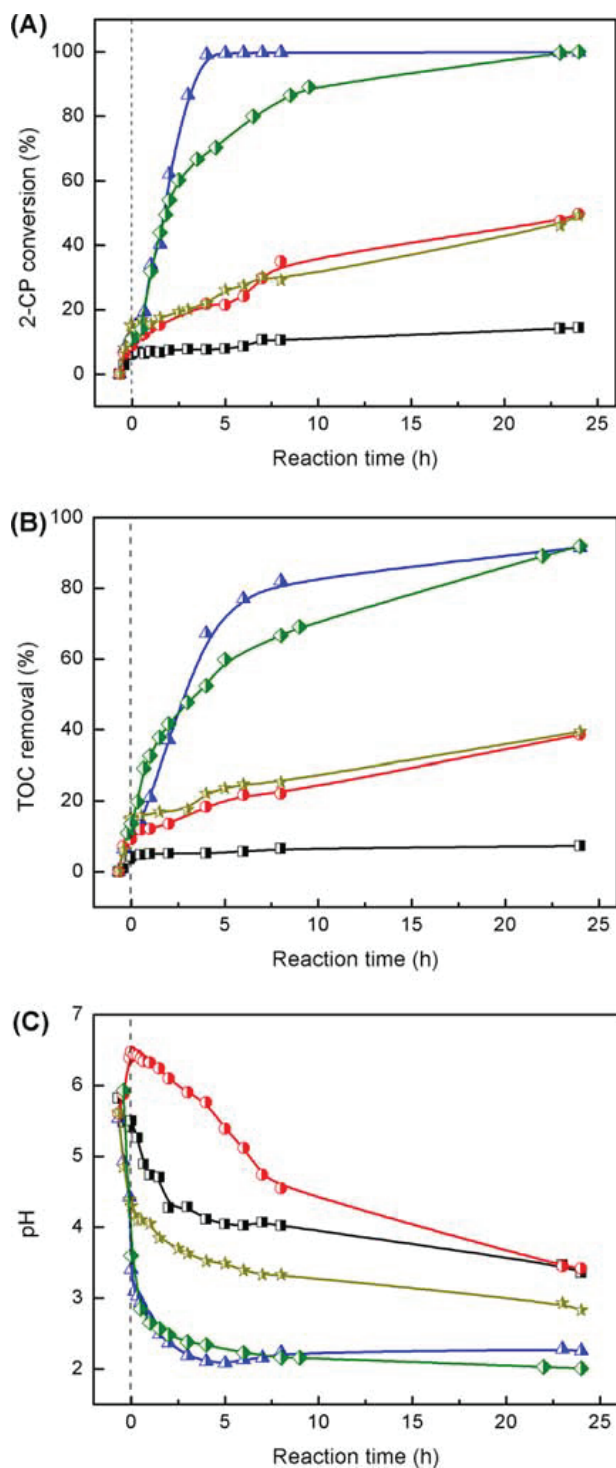


Fig. 3. Evolution of the 2-chlorophenol conversion (A), the TOC removal (B) and the pH (C) upon wet air oxidation (WAO) of 2-CP over FeSC (\blacktriangle), SC (\bullet), SC-A (\star) and Ru/ZrO₂ (\blacklozenge) or in the absence of catalyst (\blacksquare) (0.5 g catalyst, 120 °C, P_{O₂} : 0.9 MPa, 1300 rpm, 150 mL [2-CP]₀ = 2 g L⁻¹).

Table 2

Iron leaching upon catalytic wet air oxidation (CWAO) of 2-chlorophenol over different catalysts (120 °C, P_{O₂} : 0.9 MPa, 1300 rpm, 150 mL [2-CP]₀ = 2 g L⁻¹, 0.5 g catalyst).

Sample	Iron concentration in the reaction mixture after 24 h (mg L ⁻¹)	Percentage of iron leached in the solution after 24 h (wt.%)
FeSC	27.0	7
SC	0.8	0.5
SC-A	3.8	29

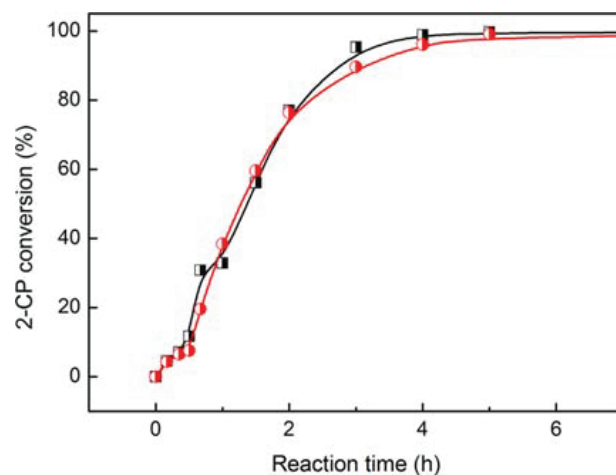


Fig. 4. 2-CP conversion attained by heterogeneous: 0.5 g FeSC (\blacksquare) and homogeneous reaction: hot filtrate from 0.5 g FeSC system after 10 min reaction (\bullet) (120 °C, P_{O₂} : 0.9 MPa, 1300 rpm, 150 mL [2-CP]₀ = 2 g L⁻¹).

the initial dechlorination of the 2-CP molecule; and (ii) the formation of some small chain organic acids such as maleic acid, succinic acid, formic acid and oxalic acid, as detected by HPLC (Fig. S2).

3.3. Heterogeneous vs. homogeneous reaction

Considering the very low pH achieved at the end of the reaction, the leaching of metal (Fe, Ca, Al, etc.) was suspected. Therefore, the concentration of iron, as the most notably catalytically active metals [1], in the liquid phase at the end of the reaction (24 h) was systematically measured. As shown in Table 2, 27 mg L⁻¹ of iron was detected in the reaction mixture after reaction over the FeSC system, which corresponded to ca. 7 wt.% of the total amount of iron initially incorporated in the FeSC catalyst. Significant amounts of metallic ions were also detected in the liquid phase upon reaction over different catalysts based on transition metals such as Cu, Zn, Mn, Ni [22–24]. For example, Posada et al. [24] have studied the catalytic wet air oxidation of substituted phenols using 1.5 g L⁻¹ of a 4 wt.% Cu/CeO₂ catalyst. 54.5 ppm Cu were detected at the end of reaction, corresponding to ca. 91 wt.% of the total amount of copper in the catalyst. Therefore, leaching is a major issue when using transition metal oxide based catalysts under acidic conditions.

To determine the contribution of the homogeneous phase reaction, 0.5 g FeSC catalyst was first introduced into the reaction mixture for 10 min, after that the hot reaction mixture was filtrated in order to remove any catalyst particle. From Fig. 4, it is observed that the conversion of 2-CP continues, even the absence of any solid catalyst, indicating that part of the active phase which has been leached into the reaction mixture is active in the homogeneous phase reaction.

To further check the contribution of the homogeneous phase reaction, the evolution of the 2-CP conversion as a function of time was studied at different catalyst loading (Fig. 5A). The iron concentration in the filtrate was systematically measured after 10, 30 and 60 min by ICP-OES. As shown in Fig. 5B, The linear variation

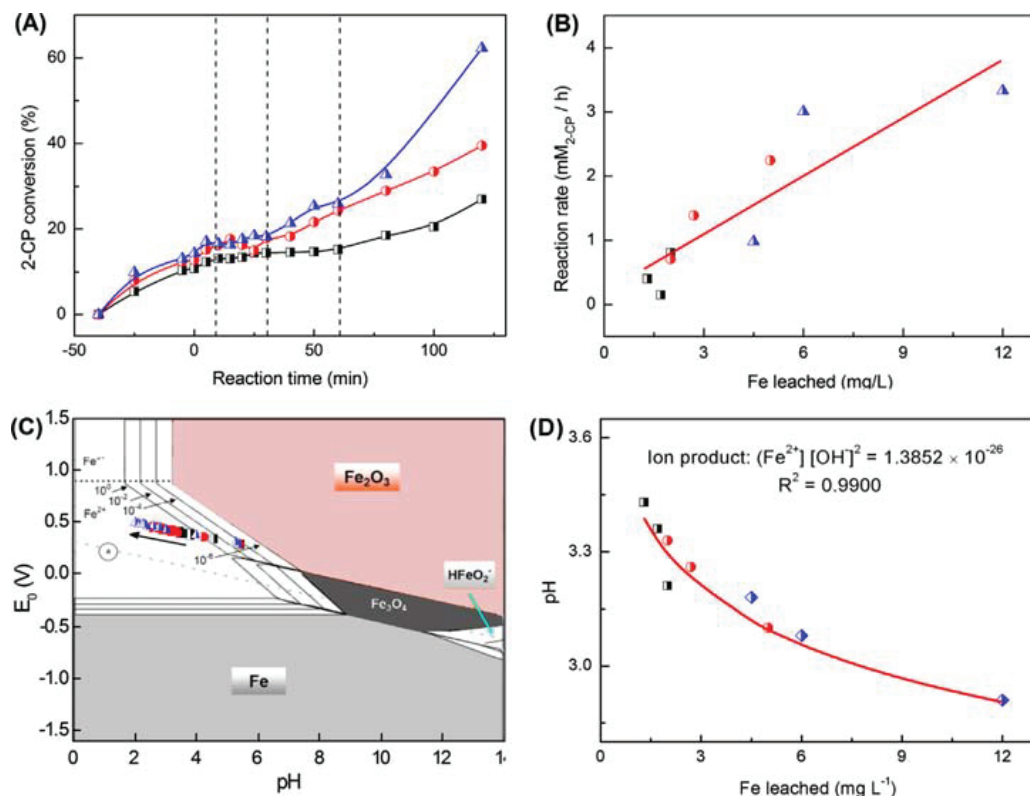


Fig. 5. Contribution of the homogeneous phase reaction. (A) 2-CP conversion during the first 2 h of reaction in the presence of different concentration in FeSC; (B) Correlation between the 2-CP conversion rate and the amount of iron leached in the reaction mixture; (C) Pourbaix diagram for iron and evolution of the potential and pH of the reaction mixture as a function of time; (D) Correlation between the solution pH and the amount of iron leached in the reaction mixture [120 °C, P_{O₂} : 0.9 MPa, 1300 rpm, 150 mL [2-CP]₀ = 2 g L⁻¹, catalyst dosage: 1.0 g L⁻¹ (■), 1.5 g L⁻¹ (●) and 2.0 g L⁻¹ (▲)].

between the instantaneous reaction rate and the amount of iron detected in solution at the same time clearly indicated that (i) the reaction definitively occurred in the homogeneous phase since the initial reaction rate did not correlate with the amount of catalyst but with the volume of the reaction mixture and (ii) the reaction was strongly dependent on the iron concentration in the liquid phase.

To explain further the irreversible leaching of iron in the solution, the potential taken by the reaction mixture was systematically measured as a function of time and recalculated with respect to the standard hydrogen electrode (SHE). According to the pH and the potential of each liquid sample shown in the Pourbaix diagram (Fig. 5C) [25], we could find that the most stable form of iron in the aqueous phase all along the reaction would be Fe(II). This result could be explained by the low solubility of oxygen in water under the applied reaction conditions (ca. 0.2 g L⁻¹) and the rapid consumption of oxygen, resulting in anoxic conditions in the liquid phase. Noteworthy, the potential of the solution increased slightly as the reaction proceeded, indicating the Fe(II) could be progressively converted to Fe(III). Considering the excellent redox property of Fe(II), the formation of free radicals, such as alkyl peroxy radicals, oxygen radicals and hydroxyl radicals would be promoted [23,26,27] and the CWAQ reaction could be initiated.

Since the leached iron existed as Fe²⁺ in the liquid phase, according to Eq. (2),



The ion product data (IP) for Fe²⁺ and OH⁻ was calculated as follows:

$$\text{IP} = [\text{Fe}^{2+}][\text{OH}^-]^2 \quad (3)$$

The IP value got by curvilinear regression analysis was 1.39×10^{-26} , and good correlation coefficient ($R^2 = 0.9900$) was gotten. It should

be noted that the solubility product constant (K_{sp}) for Fe(OH)₂ was 3.16×10^{-14} [28]. Therefore, when under the same pH condition, the dissolved ferrous iron concentration in the FeSC system is much lower than the value got from theoretic solubility calculation, indicating the using of SC support could stabilize the iron and reduce the leaching problem. Furthermore, from the result of curve fitting, in order to meet the EU discharge standards for Fe (<2 ppm) [29], the solution pH need to be kept higher than 3.29.

Conclusively, the 2-CP conversion in the homogeneous phase, the pH of the solution and the amount of iron leached in the reaction mixture were shown to be interconnected.

3.4. Minimization of the iron leaching

Based on the first results presented above, the minimization of the iron leaching from the FeSC catalysts upon CWAQ of 2-chlorophenol clearly appeared as a key point. Since the iron leaching was shown to be mainly driven by the acidic conditions generated during the initial 2-CP degradation process, the pH of the reaction mixture was tentatively controlled following different approaches; i.e. adjusting the initial pH of the reaction mixture or using a buffer solution to keep the pH constant all along the reaction.

Alkaline agents, such as NaOH, are often used to neutralize the acids produced upon treatment of chlorinated organics via supercritical water oxidation [30] or wet air oxidation [31]. In our study, NaOH was used to adjust the initial pH value of the reaction mixture from 5.6 to 10.0. As shown in Fig. 6A, when NaOH was initially added into the solution but without using any catalyst, the 2-CP conversion and TOC abatement after 24 h of reaction increased from ca. 14 to 68% and from 7 to 40%, respectively. These results are

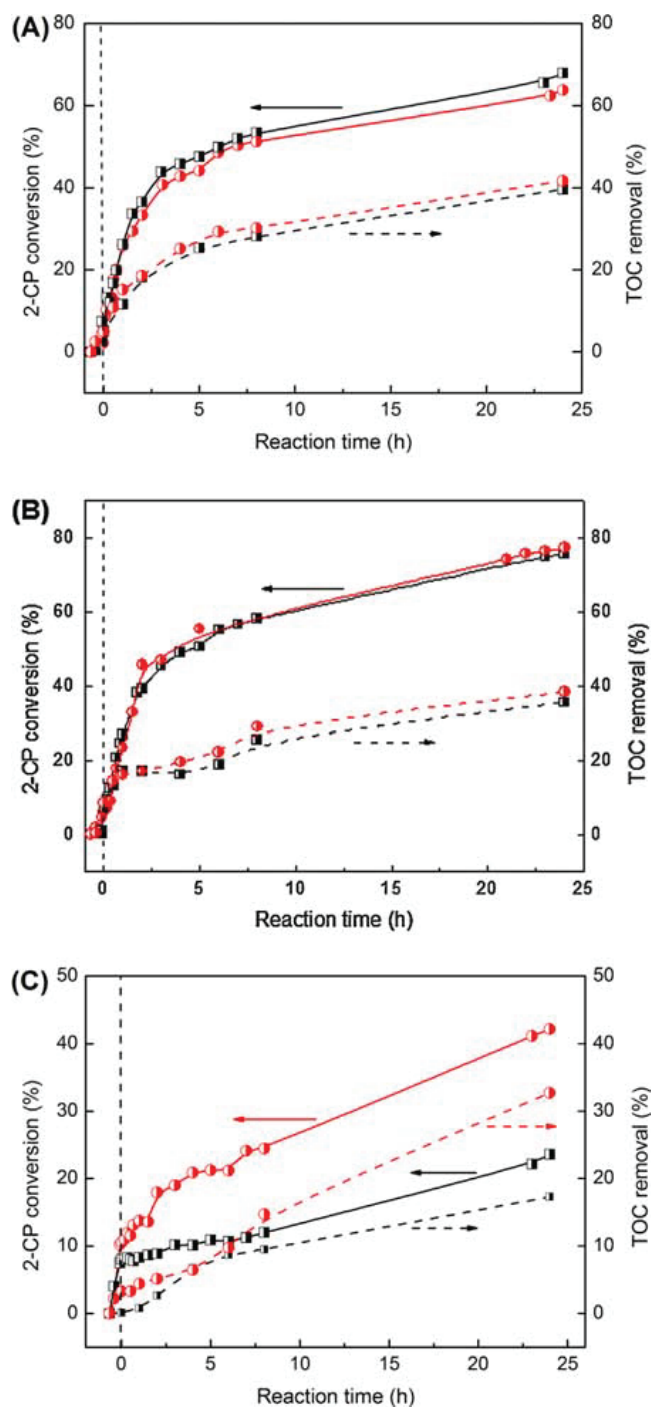


Fig. 6. Evolution of the 2-CP conversion upon wet air oxidation (WAO) in the absence of any catalyst (■) or in the presence of the FeSC catalyst (●) and with the initial addition of NaOH to pH = 10.0 (A) or in the presence of a phosphate buffer at pH = 6.8 (B) or in the presence of an acetate buffer at pH = 4.5 (C) (120 °C, P_{O_2} : 0.9 MPa, 1300 rpm, 150 mL $[2-CP]_0 = 2 \text{ g L}^{-1}$, catalyst dosage: 2.0 g L^{-1}).

similar to what was reported by Pintar et al. [32] in the WAO of substituted phenols (p-chlorophenol, p-nitrophenol) in the absence of any catalyst. When the pH value is higher than the pKa values of the substituted phenol, the phenolate anions (ArO^-) will yield phenoxy radicals (ArO^\bullet) which are considered to be much more reactive than the protonated form ($ArOH$) [31]. In our case, 2-CP would also yield phenoxy radicals since the pKa of the 2-CP molecule is 8.6. However, almost no additional catalytic activity was observed under such reaction conditions in the presence of the

FeSC catalyst (64% 2-CP conversion and 42% TOC removal after 24 h). While, the iron concentration in the liquid at the end of the reaction was only 0.7 mg L^{-1} , indicating that the contribution from the homogeneous reaction could be somehow neglected. This could be the main explanation for the much lower performances of the FeSC catalyst under alkaline conditions.

The addition of a buffer solution to the reaction mixture was tested as a second attempt to avoid the iron leaching. Firstly, the impact of a phosphate buffer (pH = 6.8) was investigated. The amount of iron leached after 24 h reaction markedly decreased down to 0.4 ppm. However, compared to the experiment performed in the absence of any catalyst, no extra 2-CP conversion or TOC removal could be observed over the FeSC catalyst (Fig. 6B). This was tentatively related to the poisonous effect of phosphates on the iron oxide catalyst with the formation of iron phosphate chelates [33]. Conclusively, the phosphate buffer was not appropriate in this specific case.

Alternatively, an acetate buffer (pH = 4.5) could be reliably used to control the pH since acetic acid was shown to be refractory toward wet air oxidation up to 200 °C [34]. As presented in Fig. 6C, in the absence of any catalyst, the 2-CP conversion and the TOC removal after 24 h reaction did not change too much by the using of acetate buffer, ca. 17% 2-CP conversion and 8% TOC removal (the effective TOC removal was calculated after subtracting the TOC content due to the acetate buffer). When the FeSC catalyst was introduced, the 2-CP conversion was 42% and the TOC abatement reached 33% at the end of the reaction. In comparison with the results obtained when the same amount of FeSC catalyst was used but in the absence of any buffer, a detrimental effect of the acetate buffer was observed. Nevertheless, the amount of iron leached in the filtrate at the end of reaction decreased from 30 to only 0.9 ppm in the presence of the acetate buffer. Furthermore, the contribution of homogeneous phase containing 0.9 ppm iron in the solution was also checked, and no further CWAO catalytic activity was observed.

In conclusion, the use of the acetate buffer (pH = 4.5) could effectively help to prevent the iron leaching while preserving part of the catalytic activity of the catalyst. From a practical point of view, although the TOC content of the acetate buffer is high (ca. 4.5 g L^{-1}) and the acetic acid is refractory toward further oxidation the implementation of such a buffer for the treatment of 2-CP via CWAO might still be viable since acetic acid is non toxic and would even be easily biodegraded in a conventional wastewater treatment plant.

3.5. Stability tests

It is known that dissolved iron in the effluent could generate an unwanted secondary pollution. To prevent this, the iron leached upon CWAO was tentatively recovered at the end of the reaction via pH adjustment (precipitation) by using NaOH. Bernata et al. [35] revealed that the iron recovery efficiency strongly depends on the pH since it strongly impacts on the iron (III) retention. In our case, the pH of the liquid was adjusted to 6.0, then the solid catalyst was recovered by filtration, washed with distilled water and dried at 105 °C before any subsequent re-utilizations.

Four successive runs were carried out using the same catalyst sample. As shown in Fig. 7, an initial induction period appeared from the second run and in subsequent runs the pH decrease was not as sharp as in the first run. This observation is consistent with the differences observed in the amount of the iron which is leached after 1 or 24 h of reaction (Table S1). However, even after 4 runs, the 2-CP conversion and the TOC removal were still very high. Only a small decrease in activity was observed between the first run and the subsequent ones.

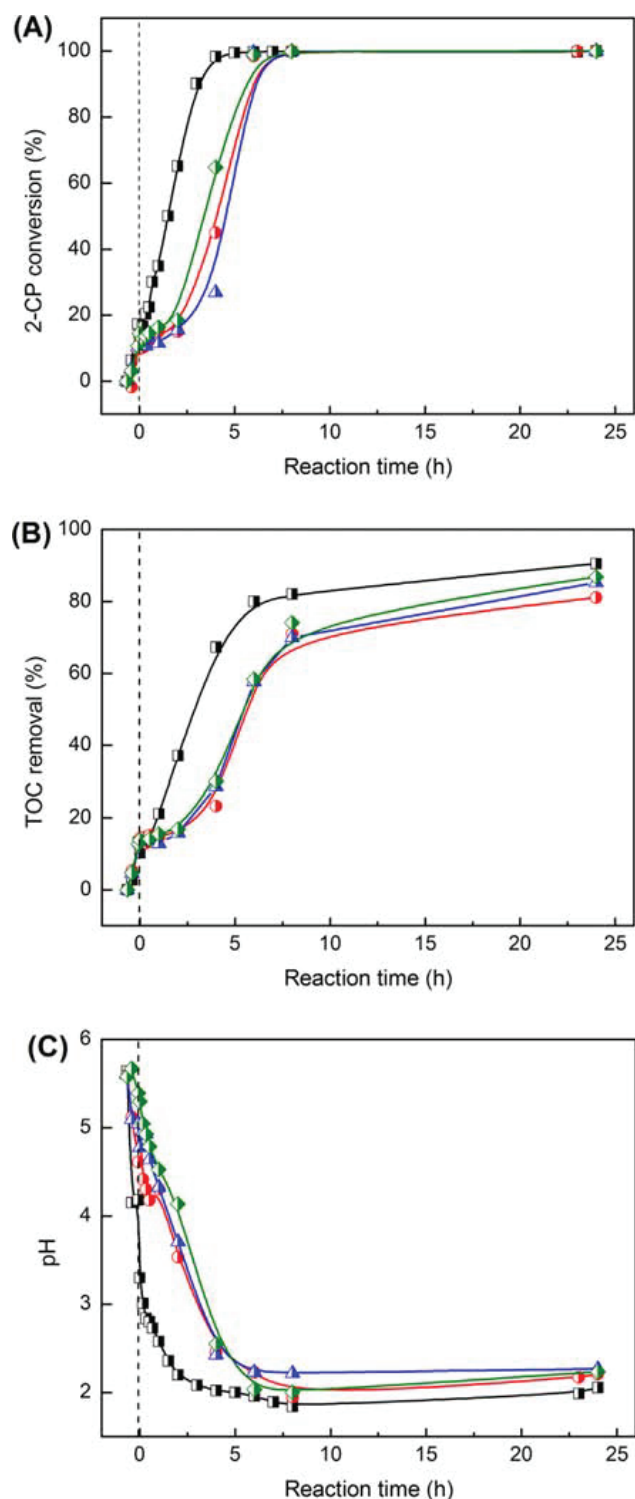


Fig. 7. Evolution of the 2-CP conversion (A), the TOC removal (B) and the pH (C) upon wet air oxidation (WAO) of 2-CP while recycling a 0.3 g sample of the FeSC catalyst ($120\text{ }^{\circ}\text{C}$, P_{O_2} : 0.9 MPa, 1300 rpm, 150 mL $[\text{2-CP}]_0 = 2\text{ g L}^{-1}$, 1st run (■), 2nd run (●), 3rd run (▲), 4th run (◆)].

3.6. Reaction intermediates

Fig. 8 shows the evolutions of the concentrations of 2-chlorophenol and the different reaction intermediates we could identify upon CWA of 2-CP over the FeSC catalyst. These intermediates have been classified in two different groups: the low

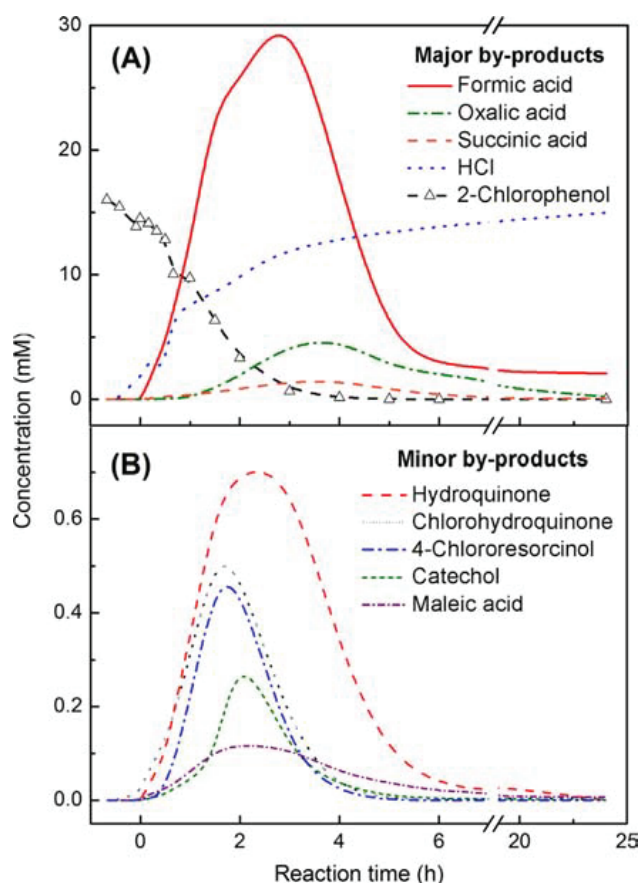


Fig. 8. Concentration profiles of 2-CP and the identified intermediates formed during the catalytic wet oxidation of 2-CP over FeSC (2 g L^{-1} FeSC, $120\text{ }^{\circ}\text{C}$, P_{O_2} : 0.9 MPa, 1300 rpm, 150 mL $[\text{2-CP}]_0 = 2\text{ g L}^{-1}$).

molecular weight acids and the aromatic compounds which were only detected in trace amounts.

As reported earlier, the dechlorination reaction also appeared in the present study as the first and essential step in the 2-CP decomposition route [36]. As shown in Fig. 8, 93% of the chlorine atoms in the 2-CP molecule are released in the reaction mixture as HCl by the end of the reaction. At the beginning 2 h, the accumulation of HCl in the reaction mixture was very rapid and the pH dropped drastically, then the formation of HCl markedly slowed down. Indicating that in the first step of the reaction the chlorine atom on the aromatic ring was removed and released in the solution as HCl. In this later period, HCl probably originated from partially oxidized chlorinated intermediates.

The concentrations of the different aromatic by-products reached a maximum at different reaction times before being totally oxidized by the end of the reaction (Table 3). The selectivity at the

Table 3

The maximum selectivities in the different reaction intermediates calculated on a carbon basis.

Intermediate	Formula	Maximum time (h)	Max selectivity (%)
Chlorohydroquinone	$\text{C}_6\text{H}_3(\text{OH})_2\text{Cl}$	1.70	5.4
4-Chlororesorcinol	$\text{C}_6\text{H}_5\text{O}_2\text{Cl}$	1.77	3.7
Catechol	$\text{C}_6\text{H}_6\text{O}_2$	2.12	2.8
Hydroquinone	$\text{C}_6\text{H}_6\text{O}_6$	2.33	5.6
Maleic acid	$\text{C}_4\text{H}_4\text{O}_4$	2.37	0.6
Formic acid	CH_2O_2	2.82	35.3
Oxalic acid	$\text{C}_2\text{H}_2\text{O}_4$	3.60	10.2
Succinic acid	$\text{C}_4\text{H}_6\text{O}_4$	3.63	6.3

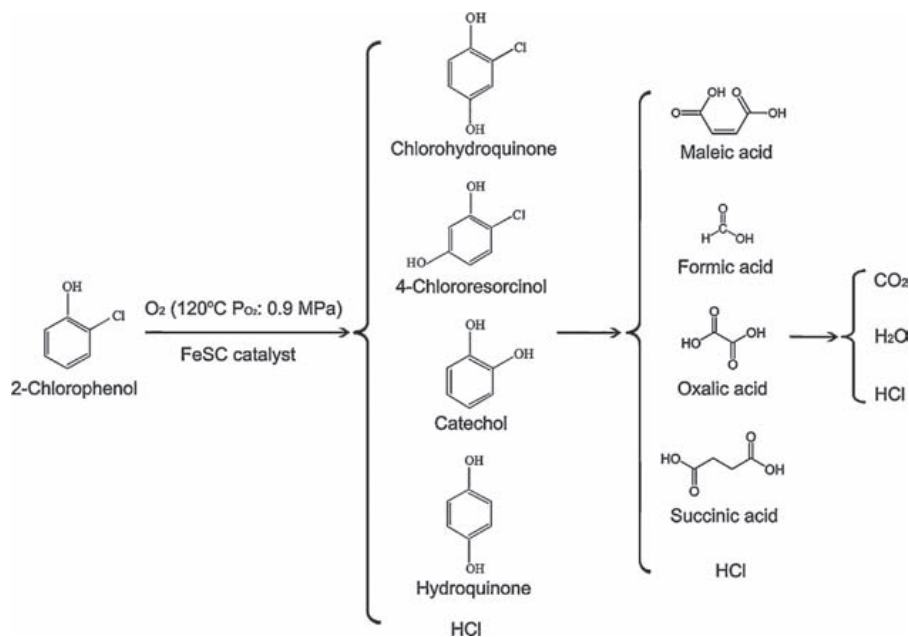


Fig. 9. Simplified reaction pathway upon catalytic wet air oxidation of 2-chlorophenol over FeSC catalysts.

maximum was calculated based on the number of carbon atoms. The selectivity of all aromatic intermediates was very low, indicating that (i) under the applied reaction conditions, most of the 2-CP molecules are directly mineralized and (ii) the oxidation of these aromatic intermediates took place very rapidly.

As shown in Fig. 8, some other short chain acids were also detected, The time at the maximum concentration for these acids appeared to be delayed compared to the aromatic intermediates, offering an extra indication that they are produced in a second step only from the aromatic ring opening.

From the difference between the measured and the calculated TOC values, we obtained a maximum discrepancy in the carbon balance of 26% (Fig. S3). This discrepancy only appeared at the end of the reaction, indicating that some short chain carboxylic acids remained unidentified or that they were inappropriately quantified.

Finally, from the identified reaction products, a simplified reaction pathway for the degradation of 2-CP upon CWAO over FeSC was proposed (Fig. 9). In the first step, the 2-CP molecule was predominantly dechlorinated and both dechlorinated aromatic intermediates and HCl were produced. The 2-CP molecule might also be partly oxidized before dechlorination occurs and partly-oxidized chlorinated aromatic intermediates were generated. Further oxidation of the aromatic intermediates led to ring opening and short chain carboxylic acids were formed. At last, all oxidized intermediates gradually converted into CO₂ and H₂O.

4. Conclusions

While the catalytic wet air oxidation of phenol using heterogeneous transition metal catalysts has been extensively studied in the literature, little attention has been paid to the use of this kind of catalysts for the treatment of 2-chlorophenol. In this work a sewage sludge derived carbon supported iron oxide catalyst (FeSC) was prepared and used in catalytic wet air oxidation of 2-chlorophenol. After 24 h reaction, high 2-CP conversion and TOC removal could be reached even at moderate reaction temperature (120 °C) and low oxygen partial pressure (0.9 MPa). However, iron leaching rapidly occurred upon decrease of the pH, promoting the activity in the homogeneous phase. The pH evolution essentially resulted from

the release of HCl after dechlorination of 2-CP and the formation of small chain carboxylic acids at the end of the reaction. Much attention was paid to the iron leaching and different attempts to prevent the iron leaching were tested, such as the use of alkaline reagents or buffer solutions. Among the different approaches, the use of the acetate buffer was successful in minimizing the iron leaching while keeping some catalytic activity.

Therefore, the use of this type of catalyst in the CWAO of 2-CP has to be carefully considered. The iron leaching would indeed require an additional treatment before discharge. In our study, the iron could be recovered by adjusting the pH to neutral pH at the end of the reaction. Only a very slight catalyst deactivation was observed upon successive batch experiments.

Acknowledgements

This research was supported by the Nature Science Foundations of China (21107146), the Nature Foundations of Guangdong Province (92510027501000005), the Science and Technology Research Programs of Guangzhou City (2012J4300118), and the Innovative Talents Training Funding of Doctoral Students of Sun Yat-sen University. Ms. Yuting Tu gratefully acknowledges the Oversea Study Program of Guangzhou Elites Scholarship for supporting her 18 month research training in France. The authors also thank G. Aubert for his precious technical help.

Appendix A. Supplementary data

Supplementary data associated with this article can be found, in the online version, at <http://dx.doi.org/10.1016/j.jhazmat.2014.05.024>.

References

- [1] R.R.N. Marques, F. Stüber, K.M. Smith, A. Fabregat, C. Bengoa, J. Font, A. Fortuny, S. Pullket, G.D. Fowler, N.J.D. Graham, Sewage sludge based catalysts for catalytic wet air oxidation of phenol: preparation, characterisation and catalytic performance, *Appl. Catal. B: Environ.* 101 (2011) 306–316.
- [2] T.L. Jones-Lepp, R. Stevens, Pharmaceuticals and personal care products in biosolids/sewage sludge: the interface between analytical chemistry and regulation, *Anal. Bioanal. Chem.* 387 (2007) 1173–1183.

- [3] K.M. Smith, G.D. Fowler, S. Pullket, N.J.D. Graham, The production of attrition resistant, sewage-sludge derived, granular activated carbon, *Sep. Purif. Technol.* 98 (2012) 240–248.
- [4] L. Yu, Q. Zhong, Preparation of adsorbents made from sewage sludges for adsorption of organic materials from wastewater, *J. Hazard. Mater.* 137 (2006) 359–366.
- [5] K.M. Smith, G.D. Fowler, S. Pullket, N.J.D. Graham, Sewage sludge-based adsorbents: a review of their production, properties and use in water treatment applications, *Water Res.* 43 (2009) 2569–2594.
- [6] F. Stüber, K.M. Smith, M. Baricot-Mendoza, R.R.N. Marques, A. Fabregat, C. Bengoa, J. Font, A. Fortuny, S. Pullket, G.D. Fowler, N.J.D. Graham, Sewage sludge based carbons for catalytic wet air oxidation of phenolic compounds in batch and trickle bed reactors, *Appl. Catal. B: Environ.* 110 (2011) 81–89.
- [7] G. Wen, Z.H. Pan, J. Ma, Z.Q. Liu, L. Zhao, J.J. Li, Reuse of sewage sludge as a catalyst in ozonation – efficiency for the removal of oxalic acid and the control of bromate formation, *J. Hazard. Mater.* 239–240 (2012) 381–388.
- [8] Y. Tu, S. Tian, L. Kong, Y. Xiong, Co-catalytic effect of sewage sludge-derived char as the support of Fenton-like catalyst, *Chem. Eng. J.* 185 (2012) 44–51.
- [9] L. Gu, N. Zhu, H. Guo, S. Huang, Z. Lou, H. Yuan, Adsorption, Fenton-like degradation of naphthalene dye intermediate on sewage sludge derived porous carbon, *J. Hazard. Mater.* 246–247 (2013) 145–153.
- [10] M. Pera-Titus, V. García-Molina, M.A. Baños, J. Giménez, S. Esplugas, Degradation of chlorophenols by means of advanced oxidation processes: a general review, *Appl. Catal. B: Environ.* 47 (2004) 219–256.
- [11] B. Meunier, Catalytic degradation of chlorinated phenols, *Science* 296 (2002) 270–271.
- [12] G. Lee, T. Nunoura, Y. Matsumura, K. Yamamoto, Effects of a sodium hydroxide addition on the decomposition of 2-chlorophenol in supercritical water, *Ind. Eng. Chem. Res.* 41 (2002) 5427–5431.
- [13] N. Li, C. Descorme, M. Besson, Application of $\text{Ce}_{0.33}\text{Zr}_{0.63}\text{Pr}_{0.04}\text{O}_2$ -supported noble metal catalysts in the catalytic wet air oxidation of 2-chlorophenol: influence of the reaction conditions, *Appl. Catal. B: Environ.* 80 (2008) 237–247.
- [14] J. Gaállová, J. Barbier Jr., S. Rossignol, Ruthenium versus platinum on cerium materials in wet air oxidation of acetic acid, *J. Hazard. Mater.* 181 (2010) 633–639.
- [15] K.H. Kim, J.R. Kim, S.K. Ihm, Wet oxidation of phenol over transition metal oxide catalysts supported on $\text{Ce}_{0.65}\text{Zr}_{0.35}\text{O}_2$ prepared by continuous hydrothermal synthesis in supercritical water, *J. Hazard. Mater.* 167 (2009) 1158–1162.
- [16] S. Yang, Z. Liu, X. Huang, B. Zhang, Wet air oxidation of epoxy acrylate monomer industrial wastewater, *J. Hazard. Mater.* 178 (2010) 786–791.
- [17] A. Vallet, M. Besson, G. Ovejero, J. García, Treatment of a non-azo dye aqueous solution by CWAO in continuous reactor using a Ni catalyst derived from hydrotalcite-like precursor, *J. Hazard. Mater.* 227–228 (2012) 410–417.
- [18] J.P. Brunelle, Preparation of catalysts by metallic complex adsorption on mineral oxides, *Pure Appl. Chem.* 50 (1978) 1211–1229.
- [19] N. Li, C. Descorme, M. Besson, Catalytic wet air oxidation of aqueous solution of 2-chlorophenol over Ru/zirconia catalysts, *Appl. Catal. B: Environ.* 71 (2007) 262–270.
- [20] A. Quintanilla, J.A. Casas, J.J. Rodríguez, Catalytic wet air oxidation of phenol with modified activated carbons and Fe/activated carbon catalysts, *Appl. Catal. B: Environ.* 76 (2007) 135–145.
- [21] N. Li, C. Descorme, M. Besson, Catalytic wet air oxidation of chlorophenols over supported ruthenium catalysts, *J. Hazard. Mater.* 146 (2007) 602–609.
- [22] A. Santos, P. Yustos, A. Quintanilla, G. Ruiz, F. Garcia-Ochoa, Study of the copper leaching in the wet oxidation of phenol with CuO-based catalysts: causes and effects, *Appl. Catal. B: Environ.* 61 (2005) 323–333.
- [23] K.H. Kim, S.K. Ihm, Heterogeneous catalytic wet air oxidation of refractory organic pollutants in industrial wastewaters: a review, *J. Hazard. Mater.* 186 (2011) 16–34.
- [24] D. Posada, P. Betancourt, F. Liendo, J.L. Brito, Catalytic wet air oxidation of aqueous solutions of substituted phenols, *Catal. Lett.* 106 (2006) 81–88.
- [25] L. Wei, M. Hervé, P. Edouard, Use of different rapid mixing devices for controlling the properties of magnetite nanoparticles produced by precipitation, *J. Cryst. Growth* 342 (2012) 21–27.
- [26] R. Robert, S. Barbati, N. Ricq, M. Ambrosio, Intermediates in wet oxidation of cellulose: identification of hydroxyl radical and characterization of hydrogen peroxide, *Water Res.* 36 (2002) 4821–4829.
- [27] F. Arena, C. Italiano, A. Raneri, C. Saja, Mechanistic and kinetic insights into the wet air oxidation of phenol with oxygen (CWAO) by homogeneous and heterogeneous transition-metal catalysts, *Appl. Catal. B: Environ.* 99 (2010) 321–328.
- [28] K.M. Yin, J.H. Wei, J.R. Fu, Mass transport effects on the electrodeposition of iron-nickel alloys at the presence of additives, *J. Appl. Electrochem.* 25 (1995) 543–555.
- [29] S. Sabhi, J. Kiwi, Degradation of 2,4-dichlorophenol by immobilized iron catalysts, *Water Res.* 35 (2001) 1994–2002.
- [30] G. Lee, T. Nunoura, Y. Matsumura, K. Yamamoto, Comparison of the effects of the addition of NaOH on the decomposition of 2-chlorophenol and phenol in supercritical water and under supercritical water oxidation conditions, *J. Supercrit. Fluids* 24 (2002) 239–250.
- [31] Y. Kojima, T. Fukuta, T. Yamada, M.S. Onyango, E.C. Bernardo, H. Matsuda, K. Yagishita, Catalytic wet oxidation of o-chlorophenol at mild temperatures under alkaline conditions, *Water Res.* 39 (2005) 29–36.
- [32] A. Pintar, J. Levec, Catalytic oxidation of aqueous p-chlorophenol and p-nitrophenol solutions, *Chem. Eng. Sci.* 49 (1994) 4391–4407.
- [33] J. Guo, M. Al-Dahhan, Activity and stability of iron-containing pillared clay catalysts for wet air oxidation of phenol, *Appl. Catal. A: Gen.* 299 (2006) 175–184.
- [34] N.D. Tran, M. Besson, C. Descorme, K. Fajerweg, C. Louis, Influence of the pre-treatment conditions on the performances of CeO_2 -supported gold catalysts in the catalytic wet air oxidation of carboxylic acids, *Catal. Commun.* 16 (2011) 98–102.
- [35] X. Bernata, A. Fortuny, F. Stüber, C. Bengoa, A. Fabregat, J. Font, Recovery of iron (III) from aqueous streams by ultrafiltration, *Desalination* 221 (2008) 413–418.
- [36] S.G. Pouloupoulos, C.A. Korologos, A. Boulamanti, C.J. Philippopoulos, Treatment of 2-chlorophenol aqueous solutions by wet oxidation, *Water Res.* 41 (2007) 1263–1268.

密级：公开

编号：09110720

中山大學

博士学位论文

污泥碳复合催化剂的制备及其催化活性研究

Catalytic activity of sewage sludge-derived char composite catalysts
towards the oxidation of organic contaminants in water

学位申请人：涂玉婷

导师姓名及职称：熊亚 教授

专业名称：环境工程

年 月 日

中山大学博士学位论文

污泥碳复合催化剂的制备及其催化活性研究

**Catalytic activity of sewage sludge-derived char composite catalysts
towards the oxidation of organic contaminants in water**

学 院： 环境科学与工程学院

专 业： 环境工程

学位申请人： 涂玉婷

指 导 老 师： 熊亚 教授

合 作 导 师： Claude Descorme 研究员

答辩委员会委员（签名）

主席： 


委员： 





原创性声明

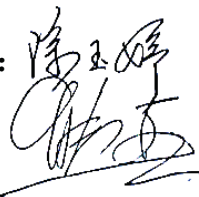
本人郑重声明：所呈交的学位论文，是本人在导师的指导下，独立进行研究工作所取得的成果。除文中已经注明引用的内容外，本论文不包含任何其他个人或集体已经发表或撰写过的作品成果。对本文的研究作出重要贡献的个人和集体，均已在文中以明确方式标明。本人完全意识到本声明的法律结果由本人承担。

学位论文作者签名：

学位论文使用授权声明

本人完全了解中山大学有关保留、使用学位论文的规定，即：学校有权保留学位论文并向国家主管部门或其指定机构送交论文的电子版和纸质版；有权将学位论文用于非赢利目的的少量复制并允许论文进入学校图书馆、院系资料室被查阅；有权将学位论文的内容编入有关数据库进行检索；可以采用复印、缩印或其他方法保存学位论文；可以为存在馆际合作关系的兄弟高校用户提供文献传递服务和交换服务。

论文作者签名：



导师签名：



污泥碳复合催化剂的制备及其催化活性研究

专业： 环境工程
博士生： 涂玉婷
指导教师： 熊亚 教授
合作导师： Claude Descorme 研究员

摘要

随着城市污泥的大量产生及日益严格的环境标准，污泥的合理处置成为亟待解决的问题。与传统污泥处置方法相比，热解技术因具有二次污染小，产物利用价值高等优点被认为是环保经济的污泥资源化利用途径。通过热解技术加工而成的污泥碳材料目前在废水处理中，主要被作为廉价吸附剂用于有机污染物和重金属离子的去除。但是当污泥活性炭吸附饱和后需要进行再生处理，导致其使用成本增加。而将污泥碳材料用于高级氧化工艺中处理有机废水，通过吸附-催化过程能够在有效去除有机污染物的同时实现对污泥碳材料的再生处理。此外，与传统的无机或有机催化剂载体相比，污泥碳是一种无机-碳杂化材料，其中的无机组分在催化过程中的作用也值得深入研究。基于以上考虑，本课题以城市污水厂污泥为原料，通过热解及负载改性制备污泥碳复合材料，并作为催化剂应用于高级氧化降解水中多种有机污染物。本论文的具体研究工作和成果如下：

(1) 以城市污水厂污泥为原料，通过负载热解成功地制备了铁氧化物/污泥碳复合多相Fenton-like催化剂Fe-SC。通过TG-FTIR、XRD、SEM-EDX和XPS等技术对催化剂制备过程及Fe-SC的物理化学性质进行表征分析。在多相Fenton-like催化氧化反应中，通过测定Fe-SC催化体系对偶氮染料酸性橙II(AOII)的降解情况来对催化剂活性进行评价。研究表明，Fe-SC中铁氧化物主要以 Fe_3O_4 的形式均匀分布于污泥碳载体中。当热解温度为 800°C 时，污泥与硫酸亚铁的混合物能够热解完全，且所得的Fe-SC具有最高的Fenton-like催化活性。Fe-SC在催化剂投加量为 2.0 g/L ， H_2O_2 用量为 15 mM ，溶液初始pH为4.0时，对 100 mg/L 的AOII溶液具

有最好的去除效果。经过1 h吸附和2 h催化反应, AOII的脱色率可达96.7%, COD去除率为73.6%, 且滤液中仅检测到0.37 mg/L的Fe。经过600 min的连续流反应, 体系出水中AOII的脱色率仍可达到94%。表明FeSC催化剂具有较高的催化活性和稳定性。

由于SC载体中无机物的含量较高, 为了研究这些无机组分对Fenton-like催化剂活性的影响, 本研究用去灰分的污泥为载体, 通过“一步法”制备了一系列Fe、Si、Al含量不同的催化剂并考察它们的催化活性。结果表明当污泥碳SC中的无机组分被去除后, 铁氧化物/污泥碳复合催化剂的催化活性明显降低。当在去灰分的污泥中同时负载 Fe_3O_4 及不同比例的 SiO_2 和 Al_2O_3 时, 复合催化剂的催化活性在一定范围内随着 SiO_2 和 Al_2O_3 含量的增加而升高。由此可见污泥碳中 SiO_2 和 Al_2O_3 在多相Fenton-like反应中起助催化作用。SC中 SiO_2 组分主要通过增加 H_2O_2 在催化剂表面的吸附和在催化剂表面形成微酸性环境两个途径来加速 H_2O_2 催化分解产生 $\cdot\text{OH}$, 从而促进Fenton-like反应的进行。SC中的 Al_2O_3 能够增加催化剂的碱性, 加速 H_2O_2 的分解。另外Al的Lewis酸特性能促进 Fe^{3+} 向 Fe^{2+} 转化。

(2) 研究了基于四氧化三铁/污泥碳复合催化剂($\text{Fe}_3\text{O}_4/\text{SC}$)催化湿式氧化降解高浓度2-氯苯酚的反应。研究发现, 当反应温度为 120°C , 氧分压为0.9 MPa时, 0.5 g $\text{Fe}_3\text{O}_4/\text{SC}$ 催化剂能在5 h内将150 mL初始浓度为2 g/L的2-CP溶液彻底去除。反应24 h后TOC去除率也高达90%。表明 $\text{Fe}_3\text{O}_4/\text{SC}$ 催化剂具有很高的催化湿式氧化活性。 $\text{Fe}_3\text{O}_4/\text{SC}$ 催化剂的加入能使反应体系的活化能明显降低(由140 kJ/mol左右降低至50 kJ/mol)。反应体系中2-CP的转化率, 溶液pH和铁盐溶出三者之间互相关联、相互影响。反应24 h后在滤液中检测到约30 mg/L的Fe, 占总铁盐投加量的7 wt.%。通过加入0.1 M, pH=4.5的醋酸盐缓冲溶液能有效地将反应过程中铁盐浓度控制在1.0 mg/L以内, 同时使 $\text{Fe}_3\text{O}_4/\text{SC}$ 催化剂保留一定的催化活性。 $\text{Fe}_3\text{O}_4/\text{SC}$ 催化湿式氧化降解2-CP反应的主要中间产物包括4-氯间苯二酚、2-氯对苯二酚、邻苯二酚、对苯二酚等芳香族中间产物以及马来酸、琥珀酸、甲酸、草酸和盐酸等小分子酸。反应过程中2-CP首先与 $\text{O}_2\cdot$ 和 $\text{OH}\cdot$ 等自由基发生加成或者取代反应, 生成HCl和芳香族中间产物。接着苯环被进一步氧化, 开环, 生成大量小分子有机酸。反应最终产物为HCl、 CO_2 和 H_2O 。

(3) 通过固态热聚合法制备 Mn 掺杂石墨相氮化碳(Mn-g-C₃N₄)/污泥活性炭复合催化剂(Mn-g-C₃N₄/SBAC)。使用 XRD、FTIR、SEM-EDX mapping、XPS 表征手段证实 Mn-g-C₃N₄ 是以三嗪环(-C₃N₃)为基本单元的石墨相片层结构化合物, 掺入的 Mn 与载体 g-C₃N₄ 存在 Mn-N 配位键。考察了其催化臭氧氧化降解典型的抗生素——磺胺甲恶唑(SMZ)的活性, 研究表明当转速为 750 rpm, 臭氧流速和浓度分别为 0.2 L/min 和 2.0 mg/L 的反应条件下, 与单独臭氧催化相比, 加入 1.0 g/L Mn-g-C₃N₄ 多相催化剂的体系在经过催化臭氧氧化处理 1h 后, 将使 50 mg/L SMZ 的去除率由 61.6%升高到 95.1%。

研究发现通过固体混合热解的方法能使 Mn-g-C₃N₄ 较均匀地负载于 SBAC 表面。通过 Langmuir-Hinshelwood 模型拟合, 确定 Mn-g-C₃N₄ 的最佳负载量为 30%。与具有相同 Mn 含量的 Mn-g-C₃N₄ 相比, 与污泥活性炭复合之后, 催化剂的催化活性可提高 1.6 倍。表明污泥基活性炭作为复合臭氧催化剂的载体能有效增强催化活性。催化剂稳定性研究表明 Mn-g-C₃N₄/SBAC 复合催化剂具有较好的抗氧化性, 较低的 Mn 离子溶出和较高的催化活性稳定性。

关键词: 污泥基碳, 负载型催化剂, 高级氧化, 有机废水

Catalytic activity of sewage sludge-derived char composite catalysts towards the oxidation of organic contaminants in water

Major: Environmental Engineering
Name: Tu Yuting
Supervisor: Prof. Xiong Ya
Co-Supervisor: Dr. Claude Descorme

Abstract

The disposal of sewage sludge becomes an issue of particular concern due to its continuous increase quantity. Compared with the traditional methods of sewage sludge disposal, such as ocean dumping, landfilling and incineration, pyrolysis could be considered as an economically feasible and eco-friendly route. Sludge derived carbons (SC) produced upon pyrolysis of sewage sludge have been used as adsorbents for organic pollutants and heavy metals in wastewater treatment area, however it is not efficient for long-term application since the sewage sludge-based activated carbon (SBAC) will be saturated with adsorbing molecules. Using SC to prepare some composite materials and use them as catalysts in advanced oxidation processes (AOPs) can offset the limitation of SBAC. Furthermore, since SC is an inorganic-carbon alloyed mixture, it should have some special behaviors compared with other commonly used supports. This situation encouraged us to employ the SC as the support of composite catalysts and investigate their potential to catalytic oxidation of organic contaminants in water. The main work and achievements in this thesis are as follows:

(1) Sewage sludge derived carbon (SC) was employed as the support of iron oxide containing catalyst (FeSC). The chemical changes during the preparation of catalysts by pyrolysis were monitored upon TGA-FTIR study. The catalysts were

characterized in terms of inorganic elemental composition, XRD, SEM-EDX and XPS. The characterization results revealed the impregnated iron was existed as Fe_3O_4 in the FeSC catalyst and almost uniformly distributed on the SC support. The catalytic activity of FeSC was evaluated from the discoloration and mineralization of acid orange II (AOII) in the presence of H_2O_2 . It was found that the FeSC catalyst, which was pyrolyzed at 800°C for 2 h, displayed the highest discoloration efficiency. Using 2.0 g/L catalyst, 15.0 mM H_2O_2 , 100 mg/L AOII and an initial pH 4.0, almost complete discoloration and 74 % mineralization were achieved after 1 h adsorption and 2 h heterogeneous Fenton-like oxidation. And only 0.37 mg/L iron was detected in the filtrate at the end of the reaction. The discoloration efficiency could be kept around 94% after 600 min test in an integrated membrane-heterogeneous Fenton-like catalytic continuous reactor (MHFR), It indicates that FeSC presents both a high catalytic activity and a long-term stability.

FeSC exhibited better performance in discoloration of AOII than some commercial iron oxides such as $\alpha\text{-Fe}_2\text{O}_3$, Fe_3O_4 , $\gamma\text{-FeOOH}$, and wood sawdust-based carbon supported iron oxide catalyst (FeWC). The high inorganic components content of sewage sludge was concluded to have strong correlations with the high catalytic activity of FeSC. To further interpret the co-catalytic effect of inorganic components in sewage sludge, the inorganic components were removed from the sewage sludge and then a series of catalysts were prepared by the addition of iron, as well as silica and/or alumina to the sewage sludge free of the inorganic components. It was found that the removal of inorganic fraction remarkably decreased the catalytic activity of iron-containing catalyst. The insertion of SiO_2 favors the increase in catalytic activity due to the formation of both hydrogen bonds between H_2O_2 and siloxane bridges and the acidic microenvironment near the surface of silica phase. While the addition of Al_2O_3 in sewage sludge as basic sites can facilitate the degradation of H_2O_2 , and the characteristic of Lewis acidity of alumina can accelerate the reduction of Fe^{3+} to Fe^{2+} by H_2O_2 .

(2) The performances of the Fe_3O_4 and SC composite catalyst ($\text{Fe}_3\text{O}_4/\text{SC}$) in the

Catalytic Wet Air Oxidation (CWAO) of 2-chlorophenol (2-CP) was assessed. When a batch reaction operated at 120°C under 0.9 MPa oxygen partial pressure (50 bar total pressure), an almost complete decomposition of 2-CP was achieved within 5 hours, and 90% Total Organic Carbon (TOC) abatement was obtained after 24 hours of reaction. The activation energy for the CWAO of 2-CP was decreased from 140 kJ/mol to 50 kJ/mol by using Fe₃O₄/SC catalyst, indicating the advantage of the CWAO process compared with the thermal process. Quite a straight correlation was observed between the pH of the reaction mixture, the amount of iron leached in the solution and the 2-CP conversion at a given reaction time. Without controlling the pH during the reaction, 30 ppm iron could be detected in the liquid phase at the end of the reaction. When the acetate buffer (pH = 4.5) was added into the reactor, the iron leaching could be kept lower than 1 ppm while keeping some catalytic activity. The reaction intermediates generated upon CWAO of 2-CP over the Fe₃O₄/SC catalyst were mainly some aromatic compounds and low molecular weight acids, such as 4-chlororesorcinol, 2-chlorohydroquinone, catechol, hydroquinone, maleic acid, succinic acid, formic acid, oxalic acid and hydrochloric acid. Finally, from all the identified reaction products, the reaction pathway for the degradation of 2-CP upon CWAO over FeSC was proposed: In the first step, the 2-CP molecule was predominantly dechlorinated and both dechlorinated aromatic intermediates and HCl were produced. The 2-CP molecule might also be partly oxidized before dechlorination occurs and partly-oxidized chlorinated aromatic intermediates were generated. Further oxidation of the aromatic intermediates led to ring opening and short chain carboxylic acids were formed. At last, all oxidized intermediates gradually converted into CO₂ and H₂O.

(3) A novel Mn doped graphitic carbon nitride catalyst (Mn-g-C₃N₄) was synthesized through a polycondensation process under elevated temperatures. And then the sewage sludge-based activated carbon (SBAC) with large surface area was used as the support for Mn-g-C₃N₄ to prepare composite catalyst (Mn-g-C₃N₄/SBAC). The results of XRD, FTIR, SEM-EDX mapping and XPS characterization revealed that

the synthesized Mg-g-C₃N₄ presented a graphitic-like structure with the triazine unit as the primary building block. The loaded Mn compound doped in the electron-rich g-C₃N₄ mainly through Mn-N bonds, which could facilitate for the electron transfer in the bulk material. The catalytic ozonation of the antibiotic sulfamethoxazole (SMZ) solution in the presence of Mn-g-C₃N₄ catalyst was investigated in a laboratory scale batch reactor. The results indicated that adding Mn-g-C₃N₄ catalyst into the ozonation reactor could greatly accelerate the rate of SMZ degradation. When the agitation speed was fixed at 750 rpm, and the dose of ozone in the inlet gas was controlled constant at 0.4 mg/min throughout the experiment, after adsorption for 30 min and oxidation for 1 h, the removal efficiency of 50 mg/L SMZ could increase from 61.6% to 95.1% by using 1 g/L Mn-g-C₃N₄ catalyst.

The study showed that the Mn-g-C₃N₄/SBAC composite catalyst prepared by solid-state reaction method could result in the uniform dispersion of Mn-g-C₃N₄ on the framework of SBAC. The degradation of SMZ by using Mn-g-C₃N₄/SBAC composite catalyst fitted well with Langmuir-Hinshelwood model. Considering the reaction rate and the utilization of loaded Mn-g-C₃N₄, the optimal content of Mn-g-C₃N₄ was decided to be 30%. The catalytic activity of the composite catalyst was about 1.6 times compared with the no supported Mn-g-C₃N₄ catalyst, indicating the positive trend by employing SBAC as support for ozonation catalyst. The composite catalyst also exhibited very good inoxidability, limited Mn leaching and good stability since the activity almost remained constant over four consecutive runs.

Keywords: Sewage sludge-derived carbon, Composite catalyst, Advance oxidation, Organic contaminants

目 录

摘要	I
Abstract	V
目录	IX
第 1 章 污泥碳复合材料的研究进展	1
1.1. 城市污水厂污泥的产生及危害	1
1.2. 传统的污泥处置技术	2
1.2.1. 污泥卫生填埋	2
1.2.2. 土地利用	3
1.2.3. 污泥焚烧	3
1.3. 污泥资源化利用现状	4
1.3.1. 污泥堆肥农用	4
1.3.2. 污泥的建材利用	5
1.3.3. 污泥热解制油技术	8
1.4. 污泥碳及其复合材料的制备与应用进展	9
1.4.1. 污泥碳材料的制备	10
1.4.2. 污泥碳复合材料的应用现状	13
1.5. 本论文的研究内容和意义	18
1.5.1. 本课题的提出	18
1.5.2. 本论文的研究内容	19
1.5.3. 本论文的研究意义	20
1.6. 参考文献	20
第 2 章 Fe₃O₄/污泥碳复合多相 Fenton-like 催化剂的制备及其催化活性研究	33
2.1. 引言	33
2.2. 实验部分	35
2.2.1. 实验试剂与材料	35
2.2.2. 实验仪器	36
2.2.3. 催化剂的制备	36
2.2.4. 催化剂的表征方法	38
2.2.5. 催化剂催化性能评价	39
2.2.6. 分析方法	40
2.3. 结果与讨论	41
2.3.1. 污泥及污泥-FeSO ₄ 的热解过程	41
2.3.2. 污泥碳/铁氧化物复合催化剂的表征	43

2.3.3. 催化活性与热解温度的关系.....	47
2.3.4. 催化活性与制备方法的关系.....	49
2.3.5. 反应条件与 AOII 催化降解效率的关系.....	50
2.3.6. AOII 的矿化效率.....	57
2.3.7. 与其他铁氧化物的催化活性比较.....	58
2.3.8. 污泥碳载体的助催化作用研究.....	59
2.4. 小结.....	67
2.5. 参考文献.....	68
第 3 章 Fe₃O₄/污泥碳复合催化剂催化湿式氧化 2-氯苯酚的研究.....	75
3.1. 引言.....	75
3.2. 实验部分.....	77
3.2.1. 实验药品与试剂.....	77
3.2.2. 催化剂的制备.....	77
3.2.3. 催化剂的表征.....	78
3.2.4. 催化剂 CWAO 催化活性的评价.....	78
3.2.5. 分析方法.....	79
3.3. 结果与讨论.....	80
3.3.1. 不同催化剂催化湿式氧化 2-CP.....	80
3.3.2. 反应温度对 Fe ₃ O ₄ /SC 催化活性的影响.....	83
3.3.3. 均相反应的影响.....	86
3.3.4. 控制铁盐溶出的研究.....	90
3.3.5. 催化剂稳定性的研究.....	93
3.3.6. 2-CP 氧化降解机理的研究.....	95
3.4. 小结.....	99
第 4 章 Mn-g-C₃N₄/污泥碳复合臭氧催化剂的制备及催化活性研究.....	105
4.1. 引言.....	105
4.2. 实验部分.....	108
4.2.1. 实验试剂与材料.....	108
4.2.2. 实验仪器.....	109
4.2.3. 催化剂的制备.....	109
4.2.4. 催化剂的表征方法.....	111
4.2.5. 臭氧催化实验.....	111
4.2.6. 分析方法.....	112
4.3. 结果与讨论.....	113
4.3.1. Mn-g-C ₃ N ₄ 的形貌及结构表征.....	113
4.3.2. Mn-g-C ₃ N ₄ 与 Mn ₂ O ₃ 催化活性比较.....	120

4.3.3. 不同反应条件对催化活性的影响.....	121
4.3.4. 污泥活性碳和 Mn-g-C ₃ N ₄ 复合催化剂的表征	128
4.3.5. Mn-g-C ₃ N ₄ /SBAC 复合催化剂催化活性研究.....	133
4.3.6. 催化剂稳定性的研究.....	138
4.4. 结论.....	139
4.5. 参考文献.....	140
第 5 章 结论与建议	147
5.1. 结论.....	147
5.2. 创新点.....	148
5.3. 对今后工作的建议.....	149
附录.....	150
博士学习期间已完成的论文.....	150
致谢.....	151

第1章 污泥碳复合材料的研究进展

1.1. 城市污水厂污泥的产生及危害

城市污水厂污泥(sewage sludge)是污水处理厂运行过程中不可避免的副产物。近年来由于城市人口迅速增长,城市规模不断扩大以及污水排放标准日趋严格,导致城市污水厂产生的污泥总量急剧增加。2003年,我国城市干污泥产量为296万吨,至2010年已增至442万吨。全美地区1998年产生约690万吨干污泥,2010年增长至820万吨。据估计,全球的污泥产量还将以每年2%的速度增长^[1,2]。城市污水厂污泥按其来源,可分为栅渣、初沉池污泥、剩余污泥和化学污泥等。其中剩余污泥来源于传统活性污泥处理工艺,是目前污泥处理与处置的主要对象。剩余污泥是由有机物质、无机颗粒、细菌菌体等组成的复杂的非均质体,其主要成分如图1-1所示^[3]:

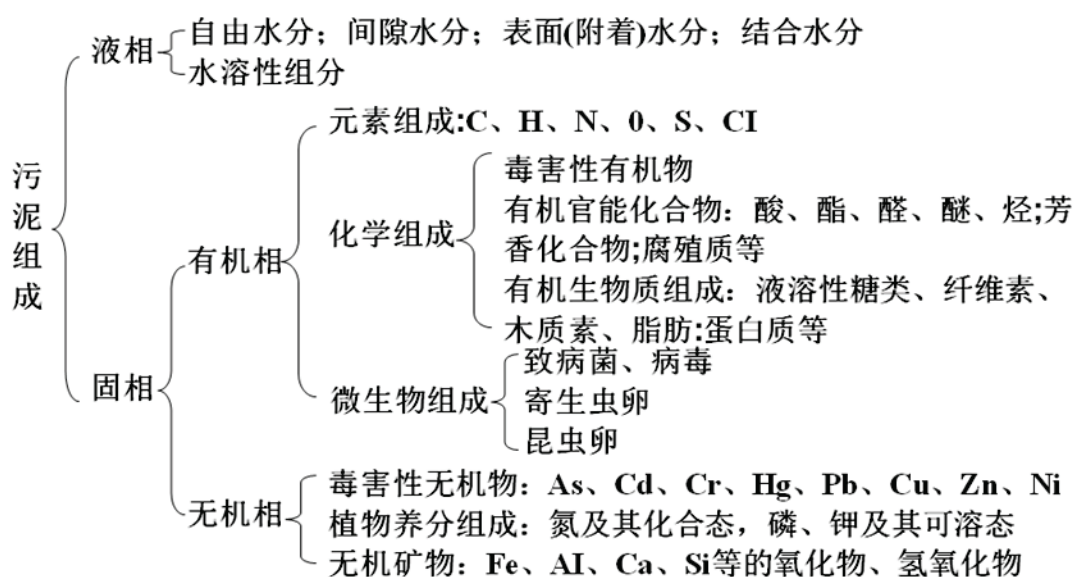


图 1-1 城市污水厂污泥的组成

Fig. 1-1. The composition of sewage sludge

剩余活性污泥的含水率较高，可达 80%以上，固相中灰分的含量可占 20-80%。此外，剩余活性污泥中还含有较多的有机物，其中粗蛋白质约占总有机物的 60-70%，碳水化合物约为 25%^[4,5]。由于这些有机物在自然条件下会发生各种复杂的生化反应，导致腐化发臭。同时污泥中富集的重金属经长时间放置也会发生形态转变，形成毒性更强的络合物。总之，如果不能对大量的城市污水厂污泥进行及时、合理的处理与处置，将会严重污染水体、土壤和大气^[6]。

1.2. 传统的污泥处置技术

污泥的处理与处置是两个不同的概念。污泥处理(Sludge treatment)是指对污泥进行浓缩、调理、脱水、稳定、干化的加工过程；污泥处置(Sludge disposal)是指将经过处理后的污泥弃置到自然环境中或者进行再利用，以达到长期稳定且不影响环境的最终消纳方式^[7]。对污泥进行合理地处理与处置能够使污泥中的有机物停止降解，趋于稳定；其中的病原微生物和寄生虫卵将被杀灭；污泥总体积减小；同时获得有利用价值的副产物，实现变废为宝、循环利用，即达到稳定化、无害化、减量化和资源化的最终目的^[8]。

早期，城市污水厂污泥主要被作为一种固体废弃物对待，其处置方式大多着眼于力求达到减少危害、减小体积的要求。传统的污泥处置方式主要有卫生填埋(Landfilling)、土地利用(Land application)和焚烧(Incineration)等。

1.2.1. 污泥卫生填埋

20 世纪 60 年代起人们开始对污泥采用卫生填埋方式进行处置。污泥的卫生填埋是指对经过压滤机或离心机进行脱水处理的污泥进行土地或者深海填埋。污泥的卫生填埋操作具有投资费用低、容量大、见效快等优点。目前我国污泥处置以卫生填埋的方式为主。

但是由于脱水污泥具有 80%左右的含水率（普通生活垃圾卫生填埋场对垃圾含水率的要求为 30%），无法用机械设备在其表面进行覆盖压实，使得填埋场表面过于疏松极易发生失衡滑移^[9]。其次，填埋污泥中的重金属、病原菌等有毒有害物质经过雨水长期的浸蚀和渗漏作用下容易被浸出，从而对地下水和周围土壤

将造成严重的污染^[10]。此外，污泥的卫生填埋还存在运输费用高、占地面积大、卫生条件差等不足之处。由于土地紧缺和不断增大的环境压力及卫生填埋方式自身存在的诸多问题，近年来污泥处置方法中卫生填埋所占的比例大幅下降。例如欧盟的污泥处置方式中，卫生填埋的比例由1992年的40%左右下降至2005年的10%^[11]。可见卫生填埋并不是一种长远有效的污泥处置方式。

1.2.2. 土地利用

城市污水厂污泥直接土地利用是指将脱水污泥和其他辅助物质混合均匀后直接施用到土壤中。由于污泥中含有丰富的有机成分和植物生长所需的多种微量元素，能够达到改善土壤结构，增强土壤肥力的效果。污泥的土地利用具有投资少、运行费用低等优点^[12,13]，曾经在许多国家得到广泛实施。但是，由于我国城市污水中混入部分含重金属的工业废水，这些重金属在污水处理过程中大部分将转移到剩余活性污泥里。如果不经过稳定化处理而直接将干污泥进行土地利用，其中的重金属一旦在土壤和植物体内累积将很难被去除，会严重威胁生物链的安全。Roig等人对比了施用污泥后土壤中有害物质（如重金属和PAHs）含量的变化，发现部分有害物质确实在土壤中存在累积现象^[14]。此外，剩余污泥中还含有大量寄生虫(卵)、病原菌以及多氯联苯(PCBs)、多环芳烃(APHs)、多氯二苯并二噁英/呋喃(PCDDs)和有机农药等有机污染物^[15]。以上存在的种种问题使得污泥的土地利用受到严格的限制。

1.2.3. 污泥焚烧

污泥焚烧技术是在800-900°C的高温下，向焚烧炉中通入过量空气以使得干污泥中的有机物被氧化分解的方法^[16]。通常1吨干污泥经焚烧后仅残余0.36吨灰渣^[17]，可见污泥焚烧技术能够有效地实现污泥的减量化。同时，在高温焚烧过程中污泥中的病原体将被彻底杀死，有毒有害物质也将分解。另外焚烧时释放出的热量能用于供暖和发电，实现能量的回收与利用。对于日本、德国、法国、瑞士、奥地利等发达国家，焚烧法已被作为污泥处置的主要方法，其中日本由于受到土地限制，通过焚烧技术处理的污泥量占污泥处置总量的55%以上^[18]。

虽然污泥焚烧技术能够有效地实现污泥的减量化、无害化, 同时还能回收污泥热能, 但是由于对设备和运行条件要求较高, 处理成本约为 210-310 €/吨干污泥, 比其他工艺高 1-3 倍^[19]。同时, 焚烧过程中产生的二氧化硫(SO₂)、氮氧化物(NO_x)和二噁英(PCDD_s)等有害气体及污泥中的重金属容易随着焚烧释放出的烟尘扩散至周围空气中, 从而对周围环境造成二次污染^[20]。近年来随着居民环保意识的提高, 污泥焚烧技术在实际应用上也承受着很大的阻力。

在过去的半个世纪里, 以上几种传统的污泥处理技术发挥了重要而显著的作用。但近年来随着城市污水厂污泥产量的激增、相关环境法规标准的日益严格和人们环保意识的逐渐增强, 传统处置方法的弊端已逐渐显现。人们开始探索开发新技术以便更加有效地处理和利用污泥。20 世纪 80 年代末, 随着资源短缺问题日益严峻, 以及可持续发展、清洁生产与循环经济的观念逐渐深入人心, 国内外的学者对污泥的资源化利用开展了一系列研究。比如污泥堆肥农用^[21]、污泥制动物饲料^[22]、污泥建材利用^[23]、污泥发酵制氢^[24]、污泥热解技术制油及含碳功能材料^[25,26]、污泥合成生物可降解性塑料^[27]等, 这些新的技术的开发为有效解决污泥处置及实现污泥资源化利用提供了良好的思路。

1.3. 污泥资源化利用现状

城市污水厂剩余污泥的资源化利用是指通过适当方法将污泥中的有价值成分充分利用, 以实现变废为宝的目的。显然, 污泥的资源化利用不仅能有效解决目前污泥处理与处置的问题, 同时还能实现环境效益、经济效益和社会效益的统一。下面着重介绍技术较成熟的污泥堆肥农用、建材利用技术和近年来迅速发展起来的污泥热解工艺。

1.3.1. 污泥堆肥农用

污泥堆肥技术是通过特定菌种(如好氧嗜温菌和嗜热菌)的协同作用对污泥中的有机物进行有效分解, 最终获得具有一定肥力的污泥肥料资源化处理方法^[28,29]。与传统的污泥土地利用法不同, 污泥堆肥法是一种可人工控制的微生物降

解和转化过程。污泥经过堆肥处理后，转变成无臭味、疏松、分散的细颗粒，外观和物理性质得到明显改善，更便于存储和运输^[30,31]。研究表明施用污泥后的土壤，其孔隙率、持水能力和离子交换能力均有所提高，总氮及有机物含量明显增加，土壤生物学性状也同时得到改善^[32]。

上世纪70年代起，随着经济与工业的发展，污泥产量激增，人们开始考虑用污泥堆肥化技术取代传统粗放的处理方式。80年代末，封闭式的污泥发酵系统在日本正式投入运行。由于发酵系统具有自动化程度高、日处理量大、运行周期短等优点，在日本、美国、欧洲等地被广泛推崇^[33]。但污泥堆肥技术存在技术门槛高、初期投资大的不足之处。另外污泥中含有的重金属，如Zn、Cu、Ni、Cd、Pb、Cr及Hg，容易在农作物体内富集^[34]，存在食品重金属污染的潜在问题，使污泥有机肥的使用范围被极大地限制。目前也有学者尝试将污泥肥料用于园林绿化中，研究表明污泥中的营养成分和微量元素能够有效促进林木和草皮的生长^[35]，由于绿化植物不进入食物链，不会直接威胁人类健康，使用相对安全。

1.3.2. 污泥的建材利用

除了有机物之外，城市污水厂干污泥中通常还含有20-30%的无机物质，如含硅、铁、铝、钙的氧化物等，这些无机组分与建筑材料制备中常用的原材料相近似。因此，近年来国内外专家对污泥的建材利用方面进行了各种研究，并取得显著成果。

1.3.2.1. 污泥制砖

污泥制砖是污泥资源化利用在建筑材料领域较早开始探索的方向。污泥中含有大量的硅铝矿物质，其成分与用来制砖的原料相近，在适当添加辅助材料后可以烧制成建筑用砖。污泥制砖有诸多优点：1. 污泥中的可燃有机物质在烧制过程中能产生一定的热量，能够节约燃煤；2. 烧制温度高达 1000°C，二噁英等有害废气的产生量小，同时能够有效杀灭病原菌，固定重金属，实现污泥的无害化；3. 污泥制砖后无炉渣问题，极大地节省后续处理费用^[36]。

利用城市污水厂污泥制砖的工艺可分为两类：一种是用干化后的污泥直接制砖。此方法能充分利用污泥中有机物在烧制过程中释放出来的热能，减少煤炭的使用量，有效降低处理费用。国立台湾大学的 Chiang 等人^[37]研究发现用干化污

泥制备建筑用砖时，污泥掺入比例和烧结温度是影响成品质量的两个关键因素，当污泥加入量为 20%，烧结温度在 960-1000°C 范围内制得的砖具有完全符合相关标准的强度。赵伟等^[38]研究发现当污泥掺入量约为 10%，烧结温度控制在 870-1000°C 范围内时，能够生产出符合国家烧砖标准的页岩砖。目前污泥制砖技术在我国已有较多工业化应用的实例。河南禹州市鹏运建材有限公司以废水处理后的干污泥为原料，通过添加一定含量的页岩，经高温烧结制得抗压和抗折强度较好的页岩砖。与土地填埋、焚烧等传统处置工艺相比，污泥制砖技术能使每吨污泥的处理费降低 80-110 元^[39]。

污泥制砖的另一种工艺是用污泥焚烧灰渣制砖。台湾义守大学的 Lin^[40]以污泥灰和粘土为原料烧制建筑用砖，研究结果表明污泥掺入量为 20-40%，烧结温度为 1000°C，经过 6 小时的煅烧后，所制得的污泥粘土砖具有比普通粘土砖更高的抗压强度。我国江苏省常州市排水管理处经过反复试验和改造，在保留发电功能的同时，将发电厂锅炉煤灰与污泥焚烧灰混合烧制砖块，生产过程经环保部门检测，无有害气体排放，污泥的综合处置费用仅为 80 元/吨^[41]。

由于污泥制砖直接用于室内建筑中，可能对人体健康存在潜在威胁。西班牙的 Cremades 课题组^[42]对以污泥为原料制得的粘土砖的环境效应进行评价，考察了 As、Cd、Cr、Pb、Hg、Ni 等重金属的溶出行为，结果表明经过高温烧制得到的建筑砖其 As、Cd、Cr、Pb、Hg、Ni 等重金属的溶出量均在美国 NEN 7345 应用规范内，释放气体也符合 ESA PSS-01-702 及 ESA PSS-01-729 标准。随着我国建筑工业的迅速发展和建筑节能观念的兴起，利用城市污泥为原料开发和生产建筑用砖将是我国制砖产业今后发展的一个重要方向。

1.3.2.2. 污泥制水泥

污泥中的有机物具有一定的燃烧热值，同时其无机组分与水泥原料相接近，因此理论上可将污泥替代部分原料用于水泥熟料生产^[43,44]。西班牙的 Rodríguez 等^[45]将城市污水厂污泥作为水泥熟料烧制过程中的添加剂，研究发现污泥的热值高达 8.3 kJ/g，当污泥掺杂量增加至 14%时，所制得的水泥熟料仍具有与常规硅酸盐水泥熟料相似的矿物结构。由于在高温烧制熟料的过程中，污泥中的重金属将被结合进入硅酸盐矿物的晶格中，因此在污泥烧制砖的使用过程中基本无重金属溶出现象^[46]。浙江大学的宝志强等^[47]将污水处理厂污泥作为硅质原料用于水

泥生料的配制，考察了不同污泥掺入量对水泥生料的易烧性、熟料强度及重金属溶出行为的影响。研究指出在合理的生料配比及合适的污泥掺杂量的前提下，可在水泥生产中实现污泥的无害化与资源化利用。近年来，日本已将城市污泥、垃圾焚烧灰、石灰石混合物作为生产水泥的原料，成功制备出“生态水泥”^[48]，并已于2001年建成世界第一座“生态水泥厂”。

1.3.2.3. 污泥制陶粒

污泥制陶粒是以污水厂污泥为主要原料，加入一定量的辅料，经脱碳和烧胀制得具有一定强度的轻质骨料。污泥陶粒具有体轻、耐火、强度高、耐腐蚀等优点，具有广阔的应用前景^[49]。污水处理厂污泥通过高温烧制轻质陶粒这一方法不仅能解决由于污泥中的病原菌和重金属造成的二次污染问题，而且能够实现变废为宝，创造出一定的经济价值^[50,51]。

日本在上世纪90年代初提出利用污泥焚烧灰经造粒、焙烧后可制成陶粒。自90年代起，我国学者也开始对污泥制陶粒技术进行了大量研究。1995年池长江等将污水厂污泥焚烧灰与少量粘土和固体燃料混合，成功烧制出污泥陶粒，为我国最早从事污泥制备陶粒研究的科研人员^[52]。在原料的配比上，各国科学家也进行了积极的探索。Monteiro等^[53]将城市污水厂污泥烘干磨碎并于粘土混合均匀，然后经高温烧制成陶粒，结果表明随着污泥掺入量的增加，陶粒的吸水性能也会逐渐增加但是强度则有所降低。这是由于污泥掺入量的增加将提高所制得陶粒的孔隙率，造成颗粒强度下降。因此在制备污泥-粘土陶粒时应选择合适的原料配比。焙烧温度是污泥陶粒制备过程中另一个影响陶粒性能的主要因素。浙江大学的翁焕新等^[54]研究发现烧制温度在900-1075°C范围内，污泥陶粒的抗压强度及表观密度会随烧制温度的升高而增加，吸水率的变化则呈相反趋势。继续再升高煅烧温度，对陶粒的性能影响不大。

经过十几年的发展，目前国外运用三页回转窑生产陶粒的技术已日趋成熟，并逐步向大型工业化应用推进。世界上第一座以城市污泥为原料生产轻质陶粒的工厂于1994年在美国Wisconsin州建成，设计可年产10万m³陶粒^[55]。2000之后，国内也出现大量采用城市污水厂污泥为原料生产陶粒的工厂，如2002年投入运行的广州市华穗轻质陶粒制品厂^[56]，2007年在浙江省台州市一条年产10万m³的陶粒生产线正式投入运行^[57]。

1.3.3. 污泥热解制油技术

污泥的建材利用主要针对污泥中的无机成分进行资源化利用,而污泥热解技术则着眼于开发利用污泥中的有机成分。污泥热解制油是近年来发展起来的新型污泥资源化利用技术,是将污泥在在无氧或缺氧的条件下加热到特定温度(低温热解低于 600°C ,高温热解为 $600\text{-}1000^{\circ}\text{C}$),使污泥中的有机物转化成为有利用价值的生物质油、热解气和固体半焦的处理方法^[58,59]。与污泥焚烧技术相比,热解工艺相对封闭,能够有效地避免大量有害气体外泄而污染周围环境,同时污泥中的重金属将被钝化,避免二次污染的发生^[60]。因此该技术具有良好的环境和经济效益,给污泥的无害化、减量化、资源化提供了新的途径。

由于污泥中含有大量脂肪、蛋白质和氨基酸等,热解油中主要元素为碳、氢、氧。研究表明污泥低温热解所制得的衍生油主要含有脂肪酸、沥青烯、苯系物、硬脂酸甲脂、酰胺及烃类^[61]。污泥热解焦油性质与柴油相近,具有良好的可燃性、良好的发火性、良好的蒸发性能、良好的安全性、良好的粘度和低温流动性能,并且对发动机没有腐蚀^[62,63]。

污泥低温热解工艺最早是由法国的Shibata在1939年的一项专利中首次提出的。之后德国的Bayer等人从20世纪70年代开始对污泥热解制油技术进行更加深入系统的研究,他们认为污泥热解制油是一系列生物质脱氨、裂解反应,焦油的来源主要是污泥中的蛋白质与脂肪^[64]。为了获得更高的产油率,国内外科学家对污泥热解过程中的影响因素进行考察,以寻求最佳热解条件。研究表明污泥的种类和成分不同将导致产油率和所制得油的组分也不相同。Lutz等人^[65]以活性污泥、油漆污泥和消化污泥为原料,通过低温热解技术制备得生物质油。三种污泥的产油率分别为31.4%、14.0%和11.0%。所得生物质油的主要成分为十五烷和十七烷烃,但是活性污泥所制得的生物质油中脂肪酸含量(26%)要明显高于另外两种污泥(约3%)。此外,热解温度、氮气流速和升温速率也会直接影响热解油的产率。西班牙的Fonts等^[66]研究发现在流化床床层温度为 540°C ,氮气流速为 4.5 L/min 的操作条件下可获得最高的热解油产率。Inguanzo^[67]研究发现在低温热解中使用较高的升温速率能使热解效率提高,产物中液态和气态成分增加,固态产物含量下降。而当热解温度高于 650°C 之后,升温速率基本无影响。

此外,研究发现在热解过程中加入催化剂可有效地降低热解反应的温度,提

高液体燃料产率，减少固体残渣，改善热解油的品质^[68]。国立台湾大学的Ching-Yuan Chang课题组考察含钠化合物(NaOH, NaCl和Na₂CO₃)和含钾化合物(KCl, KOH, K₂CO₃)作为催化剂对热解反应的影响。结果发现在热解温度为650-710K时，催化剂对热解油品质改善的效果从高到低分别为KOH>KCl>K₂CO₃>NaOH>Na₂CO₃>NaCl；对热解油产率增加的能力的强弱顺序为：KCl>Na₂CO₃>NaCl>不添加催化剂>NaOH>K₂CO₃>KOH^[69]。韩国的Young-Kwon Park课题组^[70]研究了CaO、La₂O₃、CaO/Al₂O₃及La₂O₃/Al₂O₃四种催化剂对热解油产率和氯含量的影响，结果表明在热解炉中加入含CaO和La₂O₃的催化剂会导致热解油产率下降，焦油中水分含量上升，但是能明显降低焦油中氯的含量。

除了低温热解制油技术外，近年来国外还开发出污泥直接液化制油技术。低温热解制油工艺要求污泥先进行干燥脱水，将含水率降低至5%以内，此过程耗能高，增加制油成本。而直接液化制油技术是将含水率为95%以上的污泥通过热化学处理首先液化成水溶性中间体，之后经过水解、脱氢、缩合等一系列反应，最终转化成低分子生物质油^[71,72]。同济大学的何晶晶课题组采用直接热化学液化制油技术，在250-300°C的最佳操作温度范围内，可达到70-80%的有机质转化率，每千克挥发性固体可转化成0.4-0.44 kg焦油^[73]。

在过去30年里，污泥热解制油技术已基本完成热解机理的研究，部分成果已转化成工业化生产应用。例如：上世纪90年代末，位于澳大利亚佩思(Perth)的Subiaco污水处理厂就已建立了世界上第一座商业化污泥炼油厂，每吨污泥可生产出200-300 L燃料油和0.5 t烧结碳。

但是，热解油的品质还有待提高。污泥热解油含水量较大(10-17%)，应用时需要先通过离心等方法除去。此外由于污泥中氨氮和硫化物比例较高，因此热解后产物中N、S的含量也较高，如果将该油代替燃料油使用，需进行必要的烟气脱硫、脱硝处理^[74]。

1.4. 污泥碳及其复合材料的制备与应用进展

在污泥热解工艺中，除了热解油具有很高的能源价值外，固态的碳化产物也

具有很高的利用价值。污泥碳是污泥经热解脱挥发分和碳化后残留于反应器内的固体产物，外观上类似于泥煤。目前我国城市污水厂污泥中的有机物含量为40-70%，且呈逐年增长的趋势^[75]。因此，理论上能够通过热解技术将污泥中较高含量的有机物加工成污泥碳及其复合材料。近年来国内外科研工作者在污泥碳的制备和应用上已作了大量研究，下面对污泥热解制备生物质碳及复合材料的研究进展进行详细介绍。

1.4.1. 污泥碳材料的制备

早在1971年 Kemmer 便提出通过化学活化处理可将干污泥变成吸附剂使用^[76]。同年 Beeckmans 和 Ng 通过将污泥碳化制得含炭量为14.1%的焦炭，并将其用于废水中的COD的去除，发现其吸附能力介于粉煤灰和椰壳活性炭之间^[77]。自此之后，国内外很多学者开始尝试采用污泥直接热解或经过活化改性处理后制备出具有多孔性和大比表面积的污泥碳功能材料，并已取得了很大的成功。

研究表明热解条件，如温度、时间、升温速率、热解气氛等，会影响污泥基碳的孔隙结构。日本的 Kojima 等^[78]考察了热解温度(773、823 和 873K)、热解时间(20、30、60 和 90 min)、升温速率(4、7 和 11 K/s)对污泥活性炭比表面积的影响，发现污泥基活性炭的比表面积随着热解时间的增加而下降，升温速率对比表面积没有明显影响，最佳热解条件为热解温度：823 K，热解时间 1 h，升温速率：3K/s。

为了制备出高比表面积的污泥基活性炭，除了控制热解的操作条件外，还可以在制备过程中对污泥碳进行活化处理。目前常用的活化方法可分为物理活性和化学活化两种。

1.4.1.1. 物理活化法

污泥碳的物理活化法，又称为气体活化法，是让碳材料在适当的温度下与活化气体接触，通过氧化反应一方面去除污泥焦炭中残留的有机物，另一方面对碳表面进行侵蚀、气化、开孔，最终使污泥碳变成孔隙发达的材料。污泥的物理活化法一般分为炭化和活化两个步骤，常用水蒸气、二氧化碳、空气等作为其他活化剂。法国的 Rio 等^[79]将城市污水厂污泥在 600°C 下碳化 1 h，之后在 760°C 下用水蒸汽活化 0.5 h，获得比表面积达 225 m²/g 的污泥基活性炭。西班牙学者

Méndez 等人^[80]以好氧和厌氧消化的污泥为原料，通过在 450°C 下热解 1 h 获得比表面积分别为 15 和 81 m²/g 的污泥碳，之后以水蒸气为活化气体，在 275°C 下对两种污泥基碳进行活性处理，结果表明经过 4 h 的活化处理，两种污泥基碳的比表面积分别升高至 102 和 105 m²/g。Jindarom 等^[81]以二氧化碳为活化气氛，在 750°C 下热解 0.5 h，可制备得比表面积为 61 m²/g 的污泥基活性碳。

物理活化法制备污泥基活性碳对环境的污染较小，但是由于该方法是以高温侵蚀、消耗碳的方式造孔，所以制备得到的污泥基活性碳存在产率和比表面积较低，孔径分布较难控制的问题，而且其工艺存在活化温度高，活化时间长，设备投资大的不足^[82]。

1.4.1.2. 化学活化法

化学活化法，亦称为药品活化法，是将化学药剂与原料混合，在惰性气氛中于适当的温度下进行碳化和活化，制成污泥活性碳。化学活化法制备活性碳的基本原理是将污泥中的 C、H、O 元素在具有氧化或脱水性能的活化剂的作用下，以水蒸气或者其他气体的形式被脱除，此外，有些活化剂在热解过程中还能够抑制焦油的产生，提高碳产率。较常用的化学活化剂主要有氯化锌(ZnCl₂)、氢氧化钾(KOH)、硫酸(H₂SO₄)和磷酸(H₃PO₄)等^[83]。

各种化学活化剂中，碱性氢氧化物(如 KOH 和 NaOH)的造孔效果最为显著。西班牙的 Ros 等^[84]利用 NaOH 和 KOH 为活化剂制备污泥活性碳，结果表明在 700°C 下热解 1 h 所得到的污泥焦碳比表面积为 13 m²/g，而经过 NaOH 和 KOH 活化处理后，污泥活性碳的比表面积可分别增加至 725 m²/g 和 1058 m²/g。此外西班牙的 Lillo-Rodenas^[85]和中国的 Shen Wenzhong^[86]以 KOH 为活化剂分别制备出比表面积高达 1882 m²/g 和 1686 m²/g 的污泥基活性碳。普遍认为碱性氢氧化物活化剂的成孔机理是活化剂先与污泥中的碳反应，把部分碳结构蚀刻掉，同时在热解过程中先转化成碳酸盐，之后在高温下分解释出二氧化碳与碳结构反应生成微孔^[87,88]。经碱性氢氧化物活化处理得到的污泥活性碳一般还需要使用酸和蒸馏水进行反复洗涤，以除去残留于碳结构中的碱性金属氧化物。

氯化锌是目前被报道最多的用于制备污泥活性碳的活化剂。氯化锌的活化过程主要包括三方面：浸渍阶段对污泥颗粒的润涨；在低温热解过程中主要起催化脱水作用；高温碳化阶段以脱水、缩合作用为主。同时氯化锌的加入能使活化反

应温度降低, 据报道热解温度为 550°C 就能获得较好的活化效果^[89]。我国学者任爱玲^[90]和余兰兰^[91]也分别对 ZnCl_2 活化市政污泥制备污泥活性炭进行系统的研究, 并考察了活化剂浓度, 固液比, 活化温度及时间对污泥活性炭物理化学性质的影响, 从而确定最佳活化工艺。目前为止, 利用 ZnCl_2 活化法制得到的城市污水厂污泥基活性炭最大比表面积为 $647.4 \text{ m}^2/\text{g}$, 其制备时使用 5 M ZnCl_2 活化剂, 于 500°C 下热解 2 h , 升温速率为 $15^{\circ}\text{C}/\text{min}$, 并且在热解结束后用 3 M HCl 及去离子水反复洗涤^[92]。但是需要注意的是以 ZnCl_2 为活化剂制备污泥活性炭的过程中将产生大量含 ZnCl_2 和 HCl 的废气和废水, 对环境污染较严重。

由于氯化锌活化法容易对水和大气造成重金属污染, 人们又开发出用硫酸和磷酸进行活化的新方法。西班牙的 Martin^[93]等采用硫酸活化, 将经过硫酸浸渍的好氧消化污泥置于氮气气氛中, 于 700°C 热解 30 min , 获得比表面积为 $253 \text{ m}^2/\text{g}$, 含碳量为 69.7% 的污泥活性炭。目前已有的报道中以硫酸为活化剂所制备出的污泥活性炭最高比表面积可达 $408 \text{ m}^2/\text{g}$ ^[94]。磷酸活化法具有污染小、所需碳化温度低的优点^[95], 目前磷酸活化法制备的污泥活性炭最大的比表面积仅为 $289 \text{ m}^2/\text{g}$ ^[96]。可见用磷酸活化法制备出的污泥活性炭存在比表面积较小的不足, 从而限制其推广应用。

此外, 还有学者尝试将多种活化方法和活化剂混合使用以获得更大比表面积的污泥活性炭。Khalili^[97]将造纸厂污泥先以 ZnCl_2 为活化剂在 800°C 下热解 2 h , 洗涤之后用 $75\% \text{ CO}$ 和 $25\% \text{ CO}_2$ 混合气体进行物理活化, 最终制备出比表面积高达 $1249 \text{ m}^2/\text{g}$ 的活性炭。余兰兰等^[98]研究了不同活化方法和活化剂对污泥活性炭性能的影响, 结果表明通过化学活化法制备的活性炭比物理活化法效果更佳。并且发现使用 ZnCl_2 和 H_2SO_4 的复配试剂活化效果要优于单一活化剂。

1.4.1.3. 金属盐改性

在制备过程中使用物理或化学活化法主要着眼于增大污泥碳的比表面积或改变其孔隙结构, 目前也有研究根据污泥碳的不同用途, 在制备过程中通过在污泥碳结构中负载碱土金属或过渡金属的氧化物, 以获得具有特殊物理化学性质的污泥碳复合材料。汪莉等^[99]通过在污泥热解制备过程中加入软锰矿实现对污泥的改性, 并考察改性前后污泥碳材料对水中 Cu^{2+} 的吸附特性。结果表明掺入 1% 软锰矿对污泥活性炭进行改性, 能有效地提高其微孔和中孔含量, 并使其对 Cu^{2+}

的吸附量比未改性的增加了 23.3%。张襄楷等^[100]以污水厂剩余污泥和氢氧化铝为原料,采用先碳化后负载的方法制备出载有 $\gamma\text{-Al}_2\text{O}_3$ 膜的污泥活性炭。改性后污泥碳表面酸性减弱,微孔和中孔的数量增加,均有利于对 SO_2 气体的吸附。

1.4.2. 污泥碳复合材料的应用现状

1.4.2.1. 污泥碳复合材料作为土壤改良剂

热解操作条件对污泥碳的物理化学性质有很大影响。澳大利亚的 Hossain 等人^[101]以污泥碳的农业和园艺应用为出发点,研究了热解温度对污泥碳的产率和营养特性的影响,结果表明在热解温度从 300°C 升高至 700°C 的过程中污泥碳产率逐渐下降。当热解温度低于 400°C 时,制备得的污泥碳表面呈酸性,而当热解温度高于 700°C 时,污泥碳表现出较强的碱性。卢再亮等^[102]研究发现污泥碳中的碱性物质和盐基阳离子能有效地提高酸性土壤 pH 值和交换性阳离子含量。研究还发现与污泥相比,经过热解处理获得的污泥碳中有效态的重金属含量明显降低。

污泥碳对土壤的改良主要通过以下三方面进行: 1. 提高土壤固碳量: 由于污泥碳具有很高的稳定性,施入土壤中不容易被微生物分解,因此在土壤中加入污泥碳能够有效地增加土壤的固碳量; 2. 调节土壤 pH: 经过高温热解处理获得的污泥碳一般呈弱碱性,可以用来改良酸性土壤,提高土壤的 pH 值; 3. 污泥碳中的 K、Ca、Mg 和 P 等营养元素加入土壤中能使得土壤肥力得到提高。此外污泥作为土壤改良剂还具有保水、益菌、保暖、使肥效缓释的作用^[103-105]。

目前在日本已有将污泥碳应用于园艺用土壤和土壤改良剂的实例^[106]。我国盐碱地和沙化面积逐年扩大,污泥碳作为土壤改良剂将有助于改善我国西部沙漠化的生态现状,利于过度放牧、盐碱化土壤的植被修复,这些都具有很高的社会和环境意义。

1.4.2.2. 污泥碳材料作为吸附剂

近年来,国内外学者在用污泥碳衍生材料作为吸附剂去除水中难生物降解有机物的研究上作了大量工作。上海交通大学的朱南文教授课题组用经过 KOH 活化制备的污泥碳用于酸性大红 GR 染料的吸附。结果表明当投加 20 g/L 污泥基活

性碳时, 可将 300 mg/L 的酸性大红染料溶液在 15 min 内去除^[107]。该课题组还用经 ZnCl_2 化学活化法以二沉池活性污泥为原料制备活性碳, 当吸附剂投加量为 1.5% 时, 能够在 120 min 内使初始浓度为 372 mg/L 的垃圾渗滤液吸附率达 64.9%^[108]。

研究发现, 污泥活性碳的孔径分布对其吸附染料等大分子物质的能力有很大影响, 增加吸附剂的中孔含量, 能有效提高吸附剂对大分子有机污染的吸附能力^[109]。Jindarom 等人^[110]研究发现不同类型染料由于物理化学性质的差异, 在同种污泥活性碳上将表现出不同的吸附行为。经过碳化和 CO_2 活化获得的污泥活性碳, 对阳离子染料的吸附能力要强于阴离子染料和活性染料。Otero 等^[111]认为污泥活性碳表面丰富的酸性质子官能团是导致其对阳离子染料具有较大吸附能力的原因。

而污泥活性碳对于水中酚类小分子有机物的吸附能力, 则主要取决于吸附剂的微孔含量^[112]。同时也受表面电负性和酸碱性的影响^[113,114]。当污泥碳表面亲水性羧基和羟基含量过多时, 将不利于其对酚类物质的吸附。而在高温下用氨气对污泥碳进行处理能有效增加吸附剂的碱性, 提高其对酚类物质的吸附能力^[115]。

此外, 污泥活性碳不仅能通过吸附作用去除水中的有机物, 对水中的重金属离子, 如 Cd^{2+} , Ni^{2+} , Zn^{2+} , Cu^{2+} 等, 也具有较好的吸附能力^[116,117]。夏畅斌^[118]等尝试用污泥活性碳吸附去除水中的 Pb(II) 和 Ni(II) 。研究发现溶液 pH 是影响污泥活性碳对金属离子吸附性能的主要因素, 在酸性溶液中由于 H^+ 与金属离子在吸附剂表面存在竞争吸附, 会导致金属离子的去除率下降。张德见^[119]等以城市污水厂污泥为原料制备污泥活性碳, 并用于水中 Pb^{2+} 的吸附去除。研究发现 Pb^{2+} 在污泥活性碳表面吸附为 Langmuir 单分子层吸附。Rio 等人^[120]发现虽然经过 800°C 热解的污泥比表面积只有 $63 \text{ m}^2/\text{g}$, 但其对 Cu^{2+} 的吸附能力可达 277 mg/g , 高于商品活性碳 (182 mg/g)。由此可见污泥基活性碳对水中重金属的吸附能力的强弱并不是完全取决于比表面积的大小。Rio 指出污泥基活性碳对 Cu^{2+} 的吸附是通过离子交换来实现的, 污泥中的 Ca^{2+} 离子含量决定了其对 Cu^{2+} 的吸附量。Seredych 认为污泥碳中的 Mn 和 Zn 也有一定的离子交换能力^[121]。此外, 西班牙的 Martin^[122] 发现经过硫酸活化后催化剂表面出现大量羧基 (R-COOH) 和酚羟基 (R-OH), 这些酸性官能团能够通过离子交换增加污泥活性碳对金属离子的吸附去除能力。

也有部分学者以污泥焚烧灰为吸附剂用于去除水中的 Cu^{2+} , 并获得很好的效果。Bouzid 等人^[123]研究发现水中的 Cu^{2+} 主要以吸附和沉淀于污泥灰表面的形式被去除。此外, 污泥灰中二氧化硅含量增加将使吸附剂的电负性增强, 更有利于 Cu^{2+} 在催化剂表面的吸附。

研究表明经过热解处理, 90%以上的金属离子被留在污泥生物质碳中。因此在将污泥活性碳用于废水处理的过程中, 重金属离子的溶出行为受到特别的关注。任爱玲^[90]所在课题组通过对污泥活性碳浸出液体中重金属 Ni、Cr、Cd、Pd、Cu、Zn、As 等离子进行检测, 证实污泥活性碳在使用过程中无重金属离子溶出。而且美国环保局也认为污泥热解后的半焦不属于危险废弃物范畴^[124]。

利用污泥制备活性碳, 原料充足易得, 产品成本低廉。目前, 除了将污泥碳用于废水处理领域之外, 污泥活性碳及其复合材料也常被用在废气处理方面, 主要用于处理含苯、二氧化硫、硫化氢和氮氧化物的气体。

Kojima 等将污泥在 823K 下热解并用水蒸气活化 60 min 制备得比表面积为 $97 \text{ m}^2/\text{g}$ 的污泥基活性碳, 并用于含苯气体的吸附。发现制备所得污泥碳对苯的吸附能力与煤基活性碳相当^[78]。

污泥活性碳在烟气脱硫方面的研究应用较为广泛。Ashkova 等^[125]考察了污泥活性碳对烟气中 SO_2 的吸附能力, 发现吸附容量为 30 mg/g 。李永民等^[126]以城市污水厂剩余污泥为原料, 通过负载金属氧化物对其进行改性, 结果表明改性后吸附剂的烟气脱硫性能有明显提高, 他们认为改性后吸附剂中的氧化物对 SO_2 的吸附具有协同促进作用。翟云波等^[127]制备了负载钒、铁、钙、铜、镍的污泥活性碳, 并分别考察他们对 SO_2 的吸附性能, 结果表明负载钒的活性碳具有最高的吸附能力。当钒的负载量为 0.5% 时, 污泥活性碳对 SO_2 的吸附量可达 128 mg/g 。

将污泥活性碳用于吸附潮湿空气中的 H_2S 气体最早是在 1996 年由澳大利亚昆士兰大学的 Lu Gao Qing 等人^[128,129]提出的, 他们以城市污水厂污泥为原料, 经 ZnCl_2 活化后制备出比表面积为 $309 \text{ m}^2/\text{g}$ 的污泥活性碳, 并将其应用于 H_2S 气体的吸附去除, 在相同的实验条件下, 污泥碳吸附容量相当于商业活性碳的 25%, 可见污泥活性碳作为廉价的吸附剂用于废气处理领域是可行的。之后西班牙赫罗纳大学的 A. Ros 和美国纽约城市大学的 T. J. Bandosz 教授在这一领域进行了全面深入的研究。他们考察了热解温度、污泥成分、污泥活性碳的比表面积、

孔径分布、表面官能团等对 H_2S 吸附效果的影响。发现污泥活性碳对 H_2S 的吸附能力随着热解温度升高和热解时间的延长而增大^[130]，此外，大比表面积^[131]、高吸水性^[132]、强碱性^[133]、高金属氧化物含量^[84]都有利于污泥活性碳吸附 H_2S 。污泥活性碳对 H_2S 的去除主要以表面化学吸附和氧化作用为主^[134]。此外，污泥中的铁、锌、铜氧化物和镁、钙碳酸盐等碱性无机物能够通过与 H_2S 反应，增加污泥活性碳对 H_2S 的去除能力^[135,136]。因此在处理含 H_2S 废气的过程中，污泥活性碳同时扮演着吸附剂和催化剂的角色。

1.4.2.3. 污泥碳复合材料作为催化剂

由于受到上述污泥碳在 H_2S 气体处理过程中能起催化作用的启发，Bandosz 的课题组于 2008 年开始尝试将污泥活性碳作为吸附/催化剂处理含 NO_2 的废气。发现高温热解后的吸附/催化剂吸水性增强，从而有利于 NO_2 以亚硝酸或硝酸的形式溶解于吸附剂表面，并与污泥活性碳中的碱性无机物反应^[137]。除了处理含 NO_2 的有害气体外，还有少量以污泥基活性碳复合材料为催化剂催化还原 NO 的研究报道。湖南大学的李彩亭课题组^[138]尝试以城市污水厂污泥为原料，通过化学浸渍和高温热解法制备负载锌、铁、锰氧化物的污泥基碳催化剂，并将其应用于 CO 选择性催化还原 NO 反应中。催化活性测试中，在 450°C 下该复合催化剂能使 NO 转化率达到 97.1%，且反应 600 min 后，催化活性只降低了 3%。可见该类催化剂具有很高的催化活性和稳定性。通过分析表征发现铁和锰以复杂的晶体分散于催化剂丰富的孔隙结构中，为 NO 催化还原反应提供更多的吸附和催化活性位点。与贵金属催化剂相比，污泥基催化剂的成本更加低廉，在保证其具有较高催化活性和稳定性的前提下，污泥基催化剂将具有广阔的应用前景。

与大量关于将污泥碳材料作为吸附剂用于废水处理的报道相比，将污泥碳复合材料作为催化剂用于水处理中的研究则屈指可数。

2004 年，美国密歇根大学的 Fu-Shen Zhang 等人^[139]将污泥活性碳和 TiO_2 光催化剂同时加入水中，经过搅拌使得 TiO_2 颗粒吸附于污泥活性碳孔隙中。之后向溶液中加入 Hg(II) 在紫外光照射下进行催化还原反应。结果表明当污泥活性碳和 TiO_2 催化剂用量分别为 2 g/L 和 0.4 g/L 时，吸附-催化体系能有效去除 100 mg/L 的 Hg(II) 。这是最早关于将污泥活性碳用于水处理催化还原反应的报道。但是在该研究中污泥活性碳由于具有大比表面积($555 \text{ m}^2/\text{g}$)主要被当作吸附剂使

用。在此基础上,我国学者刘庆等用浸渍-烧结法将通过溶胶-凝胶制备而得的 TiO_2 粉体成功负载于污泥活性碳上制备复合光催化剂,并考察其在自然光照条件下对 Hg(II) 的催化还原效果^[140]。

对于将污泥碳复合材料作为催化剂应用于高级氧化反应,是笔者于 2009 年起开始研究的课题。笔者尝试以城市污水厂污泥和硫酸亚铁盐为原料,通过热解制备污泥碳/铁氧化物复合材料,并将其用于多相 Fenton-like 催化降解染料废水。考察不同制备方法和反应条件对催化剂活性的影响。研究中发现与其他灰分含量低的生物质碳载体相比,污泥碳具有一定的助催化作用^[141]。之后上海交通大学的朱南文教授课题组以上海闵行城市污水厂污泥为原料,通过 KOH 浸渍和 HNO_3 微波消解对脱水污泥进行预处理,然后在 600°C , N_2 保护下进行热解,制备出具有较大比表面积、高 Fenton-like 催化活性和磁分离特性的 Fe_3O_4 /污泥活性碳复合催化剂^[142]。该课题组还尝试以上海化学工业区的浓缩污泥为原料,同样采用化学活化加高温热解(600°C)的方法制备出铁氧化物/污泥活性碳复合催化剂,并与商品纳米 Fe_3O_4 对比,考察其对染料中间体——1-重氮-2-萘酚-4-磺酸(1-diazo-2-naphthol-4-sulfonic acid)的吸附能力及多相 Fenton-like 催化活性。比较结果表明复合催化剂对 1-重氮-2-萘酚-4-磺酸的吸附和催化能力分别约为 Fe_3O_4 纳米颗粒的 4 倍和 2 倍。此外,该研究也考察了污泥碳载体中无机组分在催化过程中的作用,并获得与笔者的报道相类似的结论^[143]。此后,该课题组还对 Fe_3O_4 /污泥活性碳复合催化剂 Fenton-like 催化降解 1-重氮-2-萘酚-4-磺酸过程中产生的中间产物进行检测,并考察这些中间产物对复合催化剂的吸附及催化活性影响^[144]。

将污泥基碳用作湿式氧化催化剂的研究始于 2010 年,法国图卢兹大学(Université de Toulouse)的 Lebigue 与英国伦敦帝国学院(Imperial College London)的 Smith 等学者初步考察了将污泥碳作为催化剂应用于催化湿式氧化反应的可行性。他们以厌氧消化污泥、生污泥和二沉池污泥为原料,通过直接热解和水蒸气活化,制备出 6 种不同性质的污泥碳材料,发现这些催化剂对苯酚都具有较好的催化湿式氧化降解活性^[145]。之后 Smith 与西班牙洛维拉·依维尔基里大学(La Universidad Rovira i Virgili)的 Stüber 教授对污泥碳催化剂用于催化湿式氧化降解含酚废水的课题进行深入研究。考察了污泥活性碳热解温度、活化方法、比表面积、

表面官能团、灰分含量对间歇式反应中苯酚和 TOC 去除率的影响。并在连续滴滤床反应器中对污泥碳催化剂的稳定性进行评价。研究中发现污泥活性碳催化剂的比表面积与其催化湿式氧化活性成明显的线性关系,增大比表面积将有利于催化活性的提高。该类催化剂对苯酚、邻甲酚及邻氯苯酚的催化去除效果较好,但不能有效去除对硝基苯酚。污泥活性碳催化剂在反应过程中存在不同程度的金属离子,需要在后续研究和应用中进行解决^[146,147]。

而将污泥碳材料用于催化臭氧氧化的研究是近两年才开展起来的。2012 年,北京林业大学的王红娟等^[148]以城市污水厂脱水污泥及废弃玉米芯为原料,通过 ZnCl_2 活化,在 600°C 下热解制备得比表面积高达 $712.8 \text{ m}^2/\text{g}$ 的污泥基活性碳 (SAC),并将其作为催化剂应用于催化臭氧氧化去除水中微量布洛芬的研究。结果表明:当 SAC 投加量为 0.1 g/L 时,布洛芬的降解率是单独臭氧氧化去除速率的 5 倍。同时发现 SAC 投加量的增加会导致水中臭氧分解速率加速,从而有利于臭氧催化链式反应的进行。之后,哈尔滨工业大学的马军教授课题组考察了污泥活性碳作为催化剂对水中草酸的去除效果,通过向反应体系中加入羟基自由基淬灭剂发现污泥活性碳的臭氧催化并不遵循羟基自由基反应机理。基于以上发现,他们将污泥活性碳用于控制臭氧催化过程中溴酸盐的形成,并获得良好效果^[149]。

1.5. 本论文的研究内容和意义

1.5.1. 本课题的提出

随着城市污泥的大量产生和迅速增长,以及日益严格的环境标准,传统污泥处置方法的局限性越来越明显。为污泥的处置寻找合理有效的方式成为亟待解决的环境和社会问题。从长远发展来看,污泥的资源化利用将会成为城市污水厂污泥处置的最佳出路。

城市污水厂剩余污泥由于含有丰富的有机物,可以通过热解技术加工成污泥碳材料,目前开发的污泥碳材料主要被作为廉价吸附剂用于废水废气的处理。但是使用之后需进行再生,将导致其使用成本增加。近年来也有少量将污泥碳材料

作为催化剂用于催化还原氮氧化物的报道。但是在本课题开展之前，还未见关于以污泥碳复合材料为催化剂用于高级氧化反应的研究报道。

将城市污水厂污泥制备成污泥碳复合催化剂用于高级氧化处理有机废水，不仅为污泥的资源化利用提供一条新思路，也能为高级氧化反应开发出廉价、高效的催化剂。与污泥活性炭相比，将污泥碳材料用于高级氧化工艺中，有机污染物在吸附于污泥碳材料表面的同时将被氧化去除，因此这种吸附-催化过程能够在有效去除有机污染物的同时，实现对污泥碳复合材料的再生处理。此外，与传统的无机或有机载体相比，污泥碳是一种无机-碳杂化材料，因此，当污泥碳作为催化剂载体时，其中共存的碳组分和无机组分在催化反应过程中的作用也是值得研究探讨的。

1.5.2. 本论文的研究内容

本课题以城市污水厂剩余污泥为原料，通过负载改性制备成污泥碳复合催化剂，并将其应用于催化高级氧化反应中处理难生物降解有机废水。研究的主要内容包括三部分：

(1) Fe_3O_4 /污泥碳复合多相 Fenton-like 催化剂的制备及其催化活性研究

通过“浸渍-热解”的一步法制备负载铁氧化物的污泥碳复合多相 Fenton-like 催化剂 Fe-SC，并通过现代分析技术对与 Fenton-like 催化活性相关的性质进行表征。考察不同催化剂制备方法、制备条件、催化反应条件等因素对 Fe-SC 催化多相 Fenton-like 氧化降解偶氮染料 AOII 废水的影响，并在膜分离-多相 Fenton-like 催化氧化耦合反应器中考察污泥碳复合催化剂的稳定性。最后对污泥碳载体在多相 Fenton-like 催化反应中的所起的作用进行深入探讨；

(2) Fe_3O_4 /污泥碳复合催化剂催化湿式氧化 2-氯苯酚的研究

将 Fe_3O_4 /污泥碳复合催化剂(Fe_3O_4 /SC)用于催化湿式氧化处理高浓度 2-氯苯酚，考察 Fe_3O_4 /SC 在湿式催化氧化反应中对 2-氯苯酚和溶液 TOC 的去除情况。研究影响反应过程中催化活性组分溶出的因素，寻求减小或避免溶出的方法。并探讨污泥碳复合催化剂 Fe_3O_4 /SC 催化湿式氧化降解 2-氯苯酚的去除机理。

(3) Mn-g- C_3N_4 /污泥碳复合臭氧催化剂的制备及其催化活性研究

制备污泥碳与 Mn 掺杂石墨相氮化碳(Mn-g- C_3N_4)复合催化剂，通过 XRD、

FTIR、SEM-EDX、XPS 等表征手段对催化剂进行表征, 探究 Mn-g-C₃N₄ 的物理化学性质及在污泥碳载体中的结合与分散情况; 考察 Mn-g-C₃N₄ 及 Mn-g-C₃N₄/污泥碳复合催化剂对磺胺甲恶唑抗生素废水的催化臭氧氧化降解情况, 并探讨污泥碳载体在臭氧催化反应中所起的作用。对催化剂的抗氧化性和催化稳定性进行研究。

1.5.3. 本论文的研究意义

本研究以市政污泥为原料制备污泥碳复合催化剂, 用于催化高级氧化废水处理中, 不仅能有效地实现污泥的资源化利用, 还能达到以废治废的目的, 为污泥的处置探寻一条新出路。

本研究考察了将污泥碳复合材料作为催化剂应用于高级氧化反应中的可行性, 并对污泥碳作为载体在高级氧化水处理中的特殊作用进行探讨, 从而丰富和发展污泥碳复合催化剂在催化高级氧化技术领域的理论体系。

研究中有目的地选取多相 Fenton-like、催化湿式氧化和催化臭氧氧化这三种被广泛研究和应用的高级氧化技术, 处理具有代表性的染料、氯酚和药物类废水, 使得该研究具有很强的理论与实际意义。为今后实现产业化应用提供可靠的理论基础和科学依据。

1.6. 参考文献

- [1] Marques R R N, Stüber F, Smith K M, Fabregat A, Bengoa C, Font J, Fortuny A, Pullket S, Fowler G D, Graham N J D. Sewage sludge based catalysts for catalytic wet air oxidation of phenol: Preparation, characterisation and catalytic performance. *Appl. Catal. B: Environ.*, 2011, 101: 306-316
- [2] Jones-Lepp T L, Stevens R. Pharmaceuticals and personal care products in biosolids/sewage sludge: the interface between analytical chemistry and regulation. *Anal. Bioanal. Chem.*, 2007, 387: 1173-1183
- [3] 邵敬爱. 城市污水污泥热解试验与模型研究. 博士论文. 华中科技大学. 2008
- [4] Turovskiy I S, Mathai P K. Wastewater sludge processing. John Wiley & Sons,

Inc., Hoboken, New Jersey. 2006

- [5] 朱石清, 尹炳奎, 朱南文, 员帅波, 寿宗奇. 污泥改性活性炭技术及其应用进展. 中国给排水, 2006, 22: 19-22
- [6] 黄铮. 城市污水厂污泥制备活性炭及其吸附性能研究. 硕士学位论文. 哈尔滨工业大学. 1. 2009
- [7] 杭世珺, 刘旭东, 梁鹏. 污泥处理处置的认识误区与控制对策. 中国给水排水, 2004, 20(12): 89-92
- [8] 李建颖, 李树和, 杨霞, 李明. 城市污泥处理处置及资源化研究进展. 天津农学院学报, 2007, 14(4): 42-46
- [9] 曾祥文, 王海霞. 我国污水处理厂污泥处置的回顾与展望. 工业安全与环保, 2007, 33(7): 20-22
- [10] 周涛, 陈军. 城市环境的大问题——污水处理厂处置浅析. 环境保护科学, 1998, 24(6): 11-12
- [11] Fytali D, Zabaniotou A. Utilization of sewage sludge in EU application of old and new methods - a review. *Renew. Sust. Energ. Rev.*, 2007, 12(1): 116-140
- [12] 刘红梅, 熊文美. 城市污水处理厂污泥资源化利用途径探讨. 环境保护科学, 2007, 33 (4): 81-83
- [13] Pigozzo A T J, Lenzi E, Luca J D. Transition metal rates in latosol twice treated with sewage sludge. *Braz. Arch. Biol. Techn.*, 2006, 49(3): 515-526
- [14] Roig N, Sierra J, Marti E, Nadal M, Schuhmacher M, Domingo J L. Long-term amendment of Spanish soils with sewage sludge: Effects on soil functioning. *Agr. Ecosyst. Environ.*, 2012, 158(1): 41-48
- [15] 王晓燕. 城市污水处理污泥的综合利用初探. 宁夏石油化工, 2004, 4: 35-37
- [16] 王涛. 污泥焚烧技术现状、存在问题与发展趋势. 西南给排水, 2007, 29(1): 7-11
- [17] 普大华, 吴学伟, 李洁. 城市污泥处理处置技术对比. 中国水运, 2007, 7(02): 73-74
- [18] Werther J, Ogada T. Sewage sludge combustion. *Prog. Energ. Combust. Sci.*, 1999, 25(1): 55-116
- [19] Rio S, Le Coq L, Faur C, Le Cloirec P. Production of porous carbonaceous adsorbent from physical activation of sewage sludge: application to wastewater

- treatment. *Water Sci. Technol.*, 2006, 53 (3), 237-244
- [20] Fabrellas B, Sanz P, Abad E, Rivera J, Larrazábai D. Analysis of dioxins and furans in environmental samples by GC-ion-trap MS/MS. *Chemosphere*, 2004, 55(11): 1469-1475
- [21] Kapanen A, Vikman M, Rajasärkkä J, Virta M, Itävaara M. Biotests for environmental quality assessment of composted sewage sludge. *Waste Manage.*, 2013, 33: 1451-1460
- [22] 赵顺顺, 孟范平. 剩余污泥蛋白质作为动物饲料添加剂的营养性和安全性分析. *中国饲料*, 2008, 15: 35-38
- [23] Lin Y M, Zhou S Q, Li F Z, Liu Y Y. Utilization of municipal sewage sludge as additives for the production of eco-cement. *J. Hazard. Mater.*, 2012, 213-214: 457-465
- [24] 郭婉茜, 郭泽冲, 任南琪. 污泥发酵制氢技术的现状和前景展望. *中国科技论文在线*, 2010, 5: 397-401
- [25] Hossain M K, Strezov V, Chan K Y, Ziolkowski A, Nelson P F. Influence of pyrolysis temperature on production and nutrient properties of wastewater sludge biochar. *J. Environ. Manage.*, 2011, 92: 223-228
- [26] Manara P, Zabaniotou A. Towards sewage sludge based biofuels via thermochemical conversion - A review. *Renew. Sust. Energ. Rev.*, 2012, 16, 2566-2582
- [27] Reddy S V, Thirumala M, Reddy T V K, Mahmood S K. Isolation of bacteria producing polyhydroxyalkanoates (PHA) from municipal sewage sludge. *World J. Microb. Biot.*, 2008, 24: 2949-2955
- [28] 赵晶晶. 污泥活性炭的制备及其应用研究. 硕士论文. 华南理工大学. 7. 2013
- [29] Doublet J, Francou C, Poitrenaud M, Houot S. Influence of bulking agents on organic matter evolution during sewage sludge composting; consequences on compost organic matter stability and N availability. *Bioresource Technol.*, 2011, 102, 1298-1307
- [30] Oleszczuk P. The evaluation of sewage sludge and compost toxicity to *Heterocypris incongruens* in relation to inorganic and organic contaminants content. *Environ Toxicol.*, 2007, 22 (6): 587-96

- [31]许晓萍. 我国市政污泥处理现状与发展探析. 江西化工, 2010, 3: 24-32
- [32]Epstein E, Taylor J M, Chancy R L. Effects of sewage sludge and sludge compost applied to soil on some soil physical and chemical properties. J. Environ. Qual., 1976, 5: 422-426
- [33]章金骏. 污泥烧制陶粒的技术路径与控制因子研究. 博士论文. 浙江大学. 27. 2012
- [34]Smith S R. A critical review of the bioavailability and impacts of heavy metals in municipal solid waste composts compared to sewage sludge. Environ. Intern. 2009, 35: 142-156
- [35]刘强, 陈玲, 邱家洲, 赵建夫. 污泥堆肥对园林植物生长及重金属积累的影响. 同济大学学报(自然科学版), 2010, 38(6): 870-875
- [36]顾爱军, 王历兵. 城市污泥制砖的试验研究. 江苏技术师范学院学报, 2013, 19: 6-11
- [37]Weng C H, Lin D F, Chiang P C. Utilization of sludge as brick materials. Adv. Environ. Res., 2003, 7: 679-685
- [38]赵伟, 张林生, 王军. 页岩砖生产过程中用城市污泥为部分原料的试验研究. 环境污染治理技术与设备, 2005, 4(6): 40-43
- [39]韩永奇. 污泥制砖能走多远. 砖瓦世界, 2013, 2: 39-41
- [40]Lin D F, Weng C H. Use of sewage sludge ash as brick material. J Environ. Eng. 2001, 127: 922-927
- [41]李海英. 生物污泥热解资源化技术研究. 博士论文. 天津大学. 13. 2006
- [42]Cusidó J, Cremades L V. Environmental effects of using clay bricks produced with sewage sludge: Leachability and toxicity studies. Waste Manage. 2012, 32: 1202-1208
- [43]Zabaniotou A, Theofilou C. Green energy at cement kiln in Cyprus-Use of sewage sludge as a conventional fuel substitute. Renew. Sust. Energ. Rev., 2008, 12: 53-541
- [44]Onaka T. Sewage can make Portland cement: a new technology for ultimate reuse of sewage sludge. Water Sci. Technol., 2000, 41: 93-98
- [45]Rodríguez N H, Martínez-Ramírez S, Blanco-Varela M T, Donatello S, Guillern Manel, Pulg J, Fos Carla, Larrotcha E, Flores J. The effect of using thermally

- dried sewage sludge as an alternative fuel on Portland cement clinker production. *J. Clean. Prod.*, 2013, 52(1): 94-102
- [46]Cyr M, Coutand M, Clastres P. Technological and environmental behavior of sewage sludge ash (SSA) in cement-based materials. *Cement Concrete Res.*, 2007, 37: 1278-1289
- [47]宝志强, 戴恒杰, 蔡锐锋, 陈胡星. 污泥对水泥熟料烧成和强度的影响. *材料科学与工程学报*, 2009, 27(6): 909-913
- [48]李文红, 污泥活性炭的制备及其对染料吸附性能的研究. 硕士学位论文. 山东大学. 8. 2012
- [49]贺君, 王启山, 任爱玲. 污水厂污泥制轻质陶粒研究现状及应用前景. *城市环境与城市生态*, 2003, 16: 13-14
- [50]Xu G R, Zou J L, Dai Y. Utilization of dried sludge for making ceramsite. *Water Sci. Technol.*, 2006, 54: 69-79
- [51]Xu G R, Zou J L, Li G B. Stabilization of heavy metals in ceramsite made with sewage sludge. *J. Hazard. Mater.*, 2008, 152: 56-61
- [52]王乐乐, 杨鼎宜, 刘亚东, 朱静. 轻质污泥陶粒研制及其膨胀机理的探讨. *混凝土*, 2013, 4: 40-43
- [53]Monteiro S N, Alexandre J, Margem J I, Sánchez R, Vieira C M F. Incorporation of sludge waste from water treatment plant into red ceramic. *Constr. Build. Mater.*, 2008, 22: 1281-1287
- [54]翁焕新, 章金骏, 曹彦圣, 马学文. 污泥陶粒的性能特征与烧制工艺. *浙江大学学报*, 2011, 45: 1877-1883
- [55]Jordán M M, Almendro-Candel M B, Romero M. Application of sewage sludge in the manufacturing of ceramic tile bodies. *Appl. Clay Sci.*, 2005, 30: 219-224
- [56]张国伟, 杨波, 奚旦立. 河道底泥制备陶粒滤料的研究. *环保科技*, 2007, 13: 39-43
- [57]周少奇. 城市污泥处理处置与资源化. 广州: 华南理工大学出版社, 2002: 44-45
- [58]Rulkens W. Sewage sludge as a biomass resource for the production of energy: overview and assessment of the various options. *Energ. Fuel.*, 2007, 22: 9-15
- [59]Yaman S. Pyrolysis of biomass to produce fuels and chemical feedstocks. *Energ.*

Convers. Manage., 2004, 45: 651-671

- [60]Menéndez J A, Inguanzo M, Pis J J. Microwave-induced pyrolysis of sewage sludge. *Water Res.*, 2002, 36: 3261-3264
- [61]Sato S, Lin S Y, Suzuki Y, Hatano H. Hydrogen production from heavy oil in the presence of calcium hydroxide. *Fuel*, 2003, 82: 561-567
- [62]何晶晶, 邵立明, 陈正夫, 顾国雄. 污水厂污泥低温热化学转化过程机理研究. *中国环境科学*, 1998, 18(1): 39-42
- [63]Domínguez A, Menéndez J A, Inguanzo M, Pis J J. Investigations into the characteristics of oils produced from microwave pyrolysis of sewage sludge. *Fuel Process. Technol.*, 2005, 86(9): 1007-1020
- [64]Bayer E, Kutubuddin M. Low temperature conversion of sludge and waste to oil. *Proceeding of the International Recycling Congress*. Berlin: EF Verlag, 1987: 314-318
- [65]Lutz H, Romeiro G A, Damasceno R N, Kutubuddin M, Bayer E. Low temperature conversion of some Brazilian municipal and industrial sludges. *Bioresource Technol.*, 2000, 74: 103-107
- [66]Fonts I, Juan A, Gea G, Murillo M B, Sánchez J L. Sewage Sludge Pyrolysis in Fluidized Bed, 1: Influence of Operational Conditions on the Product Distribution. *Ind. Eng. Chem. Res.*, 2008, 47: 5376-5385
- [67]Inguanzo M, Dominguez A, Menénde J A, Blanco C G, Pis J J. On the pyrolysis of sewage sludge: the influence of pyrolysis conditions on solid, liquid and gas fractions. *J. Anal. Appl. Pyrol.*, 2002, 69: 209-222
- [68]Doshi V A, Vuthaluru H B, Bastow T. Investigations into the control of odour and viscosity of biomass oil derived from pyrolysis of sewage sludge. *Fuel Process. Technol.*, 2005, 86: 885-897
- [69]Shie J L, Lin J P, Chang C Y, Lee D J, Wu C H. Pyrolysis of oil sludge with additives of sodium and potassium compounds. *Resour. Conserv. Recy.*, 2003, 39: 51-64
- [70]Park H J, Heo H S, Park Y K, Yim J H, Jeon J K, Park J. Ryu C, Kim S S. Clean bio-oil production from fast pyrolysis of sewage sludge: effects of reaction conditions and metal oxide catalysts. *Bioresource Technol.*, 2010, 101: 583-585
- [71]李桂菊, 王子曦, 赵茹玉. 直接热化学液化法污泥制油技术研究进展. *天津*

科技大学学报, 2009, 24: 74-78

- [72]Liu J, Zhang X, Chen G. Overview of bio-oil from sewage sludge by direct thermochemical liquefaction technology. *J. Sustain. Bioenerg. Syst.*, 2012, 2: 112-116
- [73]何晶晶, 邵立明, 李国建, 吴蔚萍. 城市污水厂污泥直接热化学液化制油过程研究. *同济大学学报*, 1995, 23: 382-386
- [74]Tian Y, Zuo W, Ren Z, Chen D. Estimation of a novel method to produce bio-oil from sewage sludge by microwave pyrolysis with the consideration of efficiency and safety. *Bioresource Technol.*, 2011, 102: 2053-2061.
- [75]杨丽君. 微波法污水厂污泥制活性炭及其性能研究. 硕士论文. 四川大学. 6. 2005
- [76]Kemmer F N, Robertson R S, Mattix R D. Sewage treatment process. nalco chemical company. US Patent Office. 1971, Patent No. 3,619,420.
- [77]Beeckmans J M, Ng P C, Pyrolyzed sewage sludge - its production and possible utility. *Environ. Sci. Technol.* 1971, 5, 69-71.
- [78]Kojima N, Mitomo A, Itaya Y, Mori S, Yoshida S. Adsorption removal of pollutants by active cokes produced from sludge in the energy recycle process of wastes. *Waste Manage.* 2002, 22: 399-404.
- [79]Rio S, Faur-Brasquet C, Le Coq L, Courcoux P, Le Cloirec P. Experimental design methodology for the preparation of carbonaceous sorbents from sewage sludge by chemical activation - application to air and water treatments. *Chemosphere*, 2005, 58, 423-437
- [80]Méndez A, Gascó G, Freitas M M A, Siebielec G, Stuczynski T, Figueiredo J L. Preparation of carbon-based adsorbents from pyrolysis and air activation of sewage sludges. *Chem. Eng. J.*, 2005, 108: 169-177
- [81]Jindarom C, Meeyoo V, Kitiyanan B, Rirkksomboon T, Rangsunvigit P. Surface characterization and dye adsorptive capacities of char obtained from pyrolysis/gasification of sewage sludge. *Chem. Eng. J.*, 2007, 133, 239-246
- [82]张道静. 污泥活性炭制备及其对苯酚和硝基苯吸附特性的研究. 硕士论文. 北京林业大学. 6. 2011
- [83]Ros A, Lillo-Rodenas M A, Fuente E, Montes-Moran M A, Martin M J, Linares-Solano A, High surface area materials prepared from sewage

- sludge-based precursors. *Chemosphere*, 2006, 65(1): 132-140.
- [84]Ros A, Lillo-Rodenas M A, Canala-Battle C, Fuente E, Montes-Morán M A, Martin M J, Linares-Solano A. A new generation of sludge-based adsorbents for H₂S abatement at room temperature. *Environ. Sci. Technol.*, 2007, 41, 4375-4381.
- [85]Lillo-Rodenas M A, Ros A, Fuente E, Montes-Morán M A, Martin M J, Linares-Solano A, Further insights into the activation process of sewage sludge-based precursors by alkaline hydroxides. *Chem. Eng. J.*, 2008, 142(2):168-174.
- [86]Shen W, Guo Q J, Wang H, Yang X P, Liu Y H, Zhang Y L. Product composition of pyrolyzed sewage sludge and adsorption of Methylene Blue by porous material derived from it. *Environ. Eng. Sci.*, 2008, 25(1): 99-105.
- [87]Hsu L Y, Teng H. Influence of different chemical reagents on the preparation of activated carbons from bituminous coal. *Fuel Process. Technol.*, 2000, 64(1-3): 155-166
- [88]吴明铂. 化学活化法制备活性炭的研究进展. *炭素技术*. 1999, 4: 21-25
- [89]Chiang P C, You J H. Use of sewage-sludge for manufacturing adsorbents. *Can. J. Chem. Eng.*, 1978, 65(6): 922-927
- [90]任爱玲, 王启山, 贺君. 城市污水处理厂污泥制活性炭的研究. *环境科学*. 2004, 25: 48-51
- [91]余兰兰, 钟秦. 活性炭污泥吸附剂的制备研究. *环境化学*, 2005, 24: 401-404
- [92]Chen, X., Jeyaseelan, S., Graham, N., Physical and chemical properties study of the activated carbon made from sewage sludge. *Waste Manage.*, 2002, 22(7): 755-760
- [93]Martin M J, Serra E, Ros A, Balaguer M D, Rigola M. Carbonaceous adsorbents from sewage sludge and their application in a combined activated sludge-powdered activated carbon (AS-PAC) treatment. *Carbon*, 2004, 42: 1383-1388
- [94]Zhang F S, Nriagu J O, Itoh H, Mercury removal from water using activated carbons derived from organic sewage sludge. *Water Res.*, 2005, 39: 389-395
- [95]Guo Y, Rockstraw D A. Physicochemical properties of carbons prepared from pecan shell by phosphoric acid activation. *Bioresource Technol.*, 2007, 98(8):

1513-1521

- [96]Smith K M, Fowler G D, Pullket S, Graham N J D. Sewage sludge-based adsorbents: A review of their production, properties and use in water treatment applications. *Water Res.*, 2009, 43: 2569-2594
- [97]Khalili N R, Campbell M, Sandi G, Golas J. Production of micro- and mesoporous activated carbon from paper mill sludge: I. Effect of zinc chloride activation. *Carbon*, 2000, 38(14): 1905-1915.
- [98]余兰兰, 钟秦, 冯兰兰. 剩余污泥制备活性炭吸附剂及其应用研究. *安全与环境学报*, 2005, 5, 39-42
- [99]汪莉, 陈尧, 蒋文举, 雍晓蕾. 软锰矿改性污泥活性炭对 Cu^{2+} 吸附特性的研究. *环境科学与技术*, 2011, 34: 118-121
- [100]张襄楷, 范晓丹, 徐廷献. $\gamma\text{-Al}_2\text{O}_3$ 膜改性污泥活性炭的制备及其脱硫性能. *硅酸盐学报*, 2008, 11: 1522-1525
- [101]Hossain M K, Strezov V, Chan K Y, Ziolkowski A, Nalson P F. Influence of pyrolysis temperature on production and nutrient properties of wastewater sludge biochar. *J. Environ. Manage.*, 2011, 92: 223-228
- [102]卢再亮, 李九玉, 姜军, 徐仁扣. 生活污水污泥制备的生物质炭对红壤酸度的改良效果及其环境风险. *环境科学*, 2012, 33: 3585-2591
- [103]Sohi S P, Krull E, Lopez-Capel E, Bol R. A review of biochar and its use and function in soil. *Adv. Agron.*, 2010, 105: 47-82
- [104]Yuan J H, Xu R K, Zhang H. The forms of alkalis in the biochar produced from crop residues at different temperatures. *Bioresource Technol.*, 2011, 102: 3488-3497
- [105]Lehmann J, Gaunt J, Rondon M. Bio-char sequestration in terrestrial ecosystems - a review. *Mitig. Adapt. Strat. Global Change*, 2006, 11, 403-427
- [106]三羽宏明. 炭化处理系统的开发和炭化污泥的有效利用. *再生与利用*, 2001, 24: 6-13
- [107]Wang X, Zhu N, Yin B. Preparation of sludge-based activated carbon and its application in dye wastewater treatment. *J. Hazard. Mater.*, 2008, 153, 22-27
- [108]尹炳奎, 朱石清, 朱南文, 员帅波, 寿宗奇. 化学活化法制备生物质活性炭及其应用研究. *中国给排水*, 2006, 22: 88-90

- [109]Rozada F, Otero M, Moran A, Garcia A I, Activated carbons from sewage sludge and discarded tyres: production and optimization. *J. Hazard. Mater.*, 2005, 124(1-3): 181-191
- [110]Jindarom C, Meeyoo V, Kitiyanan B, Rirkksomboon T, Rangsunvigit P. Surface characterization and dye adsorptive capacities of char obtained from pyrolysis/gasification of sewage sludge. *Chem. Eng. J.*, 2007, 133(1-3): 239-246
- [111]Otero M, Rozada F, Calvo L F, Garcia A I, Moran A. Elimination of organic water pollutants using adsorbents obtained from sewage sludge. *Dyes Pigments*, 2003, 57(1): 55-65.
- [112]Martin M J, Balaguer M D, Rigola M. Feasibility of activated carbon production from biological sludge by chemical activation with $ZnCl_2$ and H_2SO_4 . *Environ. Technol.*, 1996, 17: 667-671
- [113]Tay J H, Chen X G, Jeyaseelan S, Graham N. A comparative study of anaerobically digested and undigested sewage sludges in preparation of activated carbons. *Chemosphere*, 2001, 44: 53-57.
- [114]Ania C O, Parra J B, Pis, J.J. Effect of texture and surface chemistry on adsorptive capacities of activated carbons for phenolic compounds removal. *Fuel Process. Technol.*, 2002, 77-78: 337-343.
- [115]Przepiorski J. Enhanced adsorption of phenol from water by ammonia-treated activated carbon. *J. Hazard. Mater.*, 2006, 135(1-3): 453-456
- [116]Zhai Y B, Wei X X, Zeng G M, Zhang D J, Chu K F. Study of adsorbent derived from sewage sludge for the removal of Cd^{2+} , Ni^{2+} in aqueous solutions. *Sep. Purif. Technol.*, 2004, 38(2): 191-196.
- [117]Sprynskyy M. Solid-liquid-solid extraction of heavy metals (Cr, Cu, Cd, Ni and Pb) in aqueous systems of zeolite-sewage sludge. *J. Hazard. Mater.*, 2009, 161: 1377-1383
- [118]夏畅斌, 刘春华, 曾经, 张玲, 周艺, 何湘柱. 污泥制备活性炭对 Pb(II)和 Ni(II)的吸附和回收利用. *材料保护*, 2006, 39: 58-60
- [119]张德见, 魏先勋, 曾光明, 翟云波. 基于非线性拟合的污泥衍生吸附剂对铅离子等温吸附特性研究. *离子交换与吸附*. 2003, 19(6): 1-6
- [120]Rio S, Le Coq L, Faur C, Lecomte D, Le Cloirec P. Preparation of adsorbents from sewage sludge by steam activation for industrial emission treatment

Process. Saf. Environ. Protect., 2006, 84(B4): 258-264

- [121]Seredych M, Bandosz T J. Removal of copper on composite sewage sludge/industrial sludge-based adsorbents: the role of surface chemistry. *J. Colloid Interf. Sci.*, 2006, 302(2): 379-388
- [122]Martin M J, Artola A, Balaguer M D, Rigola M. Towards waste minimisation in WWTP: activated carbon from biological sludge and its application in liquid phase adsorption. *J. Chem. Technol. Biot.*, 2002, 77(7): 825-833
- [123]Bouzid J, Elouear Z, Ksibi M, Feki A, Montiel A. A study on removal characteristics of copper from aqueous solution by sewage sludge and pomace ashes. *J. Hazard. Mater.*, 2008, 152(2): 838-845
- [124]Bandosz T J, Block K. Municipal sludge industrial sludge composite desulfurization adsorbents: Synergy enhancing the catalytic properties. *Environ. Sci. Technol.*, 2006, 40: 3378-3383
- [125]Bashkova S, Bagreev A, Locke D C. Adsorption of SO₂ on sewage sludge-derived materials. *Environ. Sci. Technol.*, 2001, 35(15): 3263-3269.
- [126]李永民, 余兰兰, 于宏伟. 剩余污泥制备吸附剂及其脱硫机理. *大庆石油学院学报*, 2007, 31(2): 59-61
- [127]Zhai Y, Wei X, Zeng G, Zhang D. Effects of metallic derivatives in adsorbent derived from sewage sludge on adsorption of sulfur dioxide. *J. Cent. South Univ. Technol.*, 2004, 11(1): 55-58
- [128]Jeyaseelan S, Lu G. Q. Development of adsorbent/catalyst from municipal wastewater sludge. *Water Sci. Technol.*, 1996, 34, 499-505
- [129]Lu G Q, Lau D D. Characterization of sewage sludge derived adsorbents for H₂S removal. *Gas Sep. Purif.*, 1996, 10: 103-111
- [130]Bandosz T J, Block K. Effect of pyrolysis temperature and time on catalytic performance of sewage sludge/industrial sludge-based composite adsorbents. *Appl. Catal. B: Environ.* 2006, 67: 77-85
- [131]Kante K, Qiu J, Zhao Z, Cheng Y, Bandosz T J. Development of surface porosity and catalytic activity in metal sludge/waste oil derived adsorbents: Effect of heat treatment. *Chem. Eng. J.*, 2008, 138: 155-165.
- [132]Seredych M, Bandosz T J. Sewage sludge as a single precursor for development of composite adsorbents/catalysts. *Chem. Eng. J.*, 2007, 128: 59-67

- [133]Bagreev A, Adib F, Bandosz T J. pH of activated carbon surface as an indication of its suitability for H₂S removal from moist air streams. *Carbon*, 2001, 39: 1897-1905
- [134]Bagreev A, Bashkova S, Locke D C, Bandosz T J. Sewage sludge-derived materials as efficient adsorbents for removal of hydrogen sulfide. *Environ. Sci. Technol.* 2001, 1537-1543
- [135]Bagreev A, Bandosz T J, Locke D C. H₂S adsorption/oxidation on materials obtained using sulfuric acid activation of sewage sludge derived fertilizer. *J. Colloid Interface Sci.*, 2002, 252: 188-194
- [136]Bagreev A, Bandosz T J. On the mechanism of hydrogen sulfide adsorption/oxidation on catalytic carbons. *Ind. Chem. Eng. Res.*, 2005, 44: 530-538
- [137]Pietrzak R, Bandosz T J. Interactions of NO₂ with sewage sludge based composite adsorbents. *J. Hazard. Mater.*, 2008, 154: 946-953
- [138]彭亮, 李彩亭, 李彩霞, 翟云波, 黄修国, 路培, 李群. 以污泥为载体的金属氧化物脱硝催化剂的研究. *环境工程学报*, 2008, 2: 522-526
- [139]Zhang F S, Nriagu J O, Itoh H. Photocatalytic removal and recovery of mercury from water using TiO₂-modified sewage sludge carbon. *J. Photochem. Photobiol. A: Chem.*, 2004, 167: 223-228
- [140]刘庆, 芮雪莹, 刘佳丽. 负载 TiO₂ 城市污泥改性物光催化剂的制备. *广东化工*, 2012, 6: 59-60
- [141]Tu Y T, Tian S H, Kong L J, Xiong Y. Co-catalytic effect of sewage sludge-derived char as the support of Fenton-like catalyst. *Chem. Eng. J.*, 2012, 185-186: 44-51
- [142]Gu L, Zhu N, Zhou P. Preparation of sludge derived magnetic porous carbon and their application in Fenton-like degradation of 1-diazo-2-naphthol-4-sulfonic acid. *Bioresource Technol.*, 2012, 118: 638-642
- [143]Gu L, Zhu N, Guo H, Huang S, Lou Z, Yuan H. Adsorption and Fenton-like degradation of naphthalene dye intermediate on sewage sludge derived porous carbon. *J. Hazard. Mater.*, 2013, 246-247: 145-153
- [144]Gu L, Huang S, Zhu N, Zhang D, Yuan H, Lou Z. Influence of generated intermediates' interaction on heterogeneous Fenton's degradation of an azo dye

- 1-diazo-2-naphthol-4-sulfonic acid by using sludge based carbon as catalyst. *J. Hazard. Mater.*, 2013, 263: 450-457
- [145] Lebigue C J, Andriantsiferana C, Krou N, Ayrat C, Mohamed E, Wilhelm A M, Delmas H, Le Coq L, Gerente C, Smith K M, Pillket S, Fowler G D, Graham N J D. Application of sludge-based carbonaceous materials in a hybrid water treatment process based on adsorption and catalytic wet air oxidation. *J. Environ. Manage.*, 2010, 91: 2432-2439
- [146] Marques R R N, Stüber F, Smith K M, Fabregat A, Bengoa C, Font J, Fortuny A, Pullket S, Fowler G D, Graham N J D. Sewage sludge based catalysts for catalytic wet air oxidation of phenol: Preparation, characterisation and catalytic performance. *Appl. Catal. B: Environ.*, 2011, 101: 306-316
- [147] Stüber F, Smith K M, Mendoza M B, Marques R R N, Fabregat A, Bengoa C, Font J, Fortuny A, Pullket S, Fowler G D, Graham N J D. Sewage sludge based carbons for catalytic wet air oxidation of phenolic compounds in batch and trickle bed reactors. *Appl. Catal. B: Environ.*, 2011, 110: 81-89
- [148] 王红娟, 齐飞, 封莉, 张立秋. 污泥基活性炭催化臭氧氧化降解水中微量布洛芬的效能研究. *环境科学*, 2012, 33: 1591-1596
- [149] Wen G, Pan Z H, Liu Z Q, Zhao L, Li J J. Reuse of sewage sludge as a catalyst in ozonation - Efficiency for the removal of oxalic acid and the control of bromate formation. *J. Hazard. Mater.*, 2012, 239-240: 381-388

第2章 Fe₃O₄/污泥碳复合多相 Fenton-like 催化剂的制备及其催化活性研究

2.1. 引言

Fenton 法是一种被广泛研究和应用的高级氧化方法。早在 1894 年, 法国科学家 Fenton 发现向酒石酸(Tartaric acid)中加入 Fe²⁺和 H₂O₂ 可将溶液迅速矿化^[1]。为了纪念这位科学家, 人们将 Fe²⁺/H₂O₂ 称作 Fenton 试剂, 相应的反应则称为 Fenton 反应^[2]。1964 年, 加拿大学者 H.R. Eisenhouser 首次使用 Fenton 试剂处理含有烷基苯和苯酚的废水, 开创了将 Fenton 试剂用于处理环境污染物的先例^[3]。由于 Fenton 试剂具有处理效率高、反应条件温和、操作和设备简单等优点, 近年来在环境污染治理领域受到越来越广泛的关注^[4]。

但是均相 Fenton 体系存在几个难以解决的问题: 由于中性溶液中 Fe²⁺易形成沉淀而使反应速率降低, 因此水处理过程中需要将废水 pH 调至酸性(一般 2-3), 反应结束后为了使废水 pH 达到排放标准, 需要加入大量碱, 将溶液 pH 调回至中性。调节 pH 的过程需要消耗大量酸碱试剂, 将使废水处理成本增加, 另外, 调整 pH 值至中性后将形成大量含铁污泥, 且出水由于含有部分未沉淀的铁离子而呈黄色^[5-7]。为解决上述均相 Fenton 工艺中存在的问题, 近 20 年来, 人们开始研究使用含铁的化合物以及负载铁离子或铁氧化物的固体催化剂来取代硫酸亚铁溶液, 构建非均相 Fenton 或 Fenton-like 催化体系, 并用来处理难生物降解的有机污染物。

铁氧化物, 如赤铁矿(α -Fe₂O₃)、针铁矿(α -FeOOH)、磁铁矿(Fe₃O₄)等是较早被广泛研究的一类多相 Fenton-like 催化剂^[8-10]。此类催化剂具有 pH 适用范围宽, 易于回收利用的优点^[11,12]。其中四氧化三铁 Fe₃O₄ 由于含有 Fe(II)及稳定的八面体结构, 使其在 Fenton-like 催化反应中, 即具有较高的催化活性, 又能有效避免铁盐溶出的发生^[13,14]。近年来研究发现通过将铁氧化物负载化, 能明显增强其催

化活性。如 Hu 等^[15]将 Fe_3O_4 负载于碳纳米管上，并用于环境激素 17 α -甲基睾酮的多相 Fenton-like 降解反应。在复合催化剂投加量为 2.0 g/L 时，可将初始浓度为 212 $\mu\text{g/L}$ 的 17 α -甲基睾酮在 8 h 内去除 85.9%，比相同用量的 Fe_3O_4 纳米颗粒的催化体系的去除率高出 20%左右。

催化剂载体在整个多相 Fenton-like 反应催化体系中具有特殊的作用，通常体现在以下几方面^[16,17]：(1)增加多相催化剂的接触面积；(2)改变催化剂的亲疏水性及化学稳定性；(3)延长催化剂的使用寿命；(4)部分载体还存在协同催化的作用。目前，用于多相 Fenton 催化剂制备的载体主要可分为：(1)有机材料，如 Nafion 全氟离子交换板(膜)^[18-20]、离子交换树脂^[21]等；(2)无机材料，如沸石分子筛^[22]、石英砂^[23]、氧化铝^[24]、粘土^[25]、活性炭^[26,27]等。

近年来还有用具有较大比表面积的固体废弃物作为多相 Fenton 催化剂载体的研究报道。如墨西哥的 Flores^[28]等人利用飞灰负载 Fe 制备催化剂并用于多相 Fenton-like 降解 black 5 (RB5)，结果表明在 pH=2.8，按化学计量比加入 H_2O_2 ，反应 2h 后对 0.061mM 的 RB5 可达到 80%的去除率。此外也有将谷壳飞灰(rice husk ash)^[29]和赤泥(red mud)^[30]作为多相 Fenton 催化剂载体的报道。

随着市政污水厂的大规模建成和使用，污泥，作为污水处理的副产物也被大量产生。目前城市污水厂污泥的处理与处置已成为亟待解决的环境问题^[31-32]。传统的污泥处置方法有海洋倾倒、土地填埋、焚烧等，但这些方法会对土壤、地下水和大气造成严重的二次污染^[33-35]。因此，如何科学有效地处置污泥已越来越受到关注。近年来许多污泥资源化利用的方法也应运而生，如堆肥化，热解，制备建筑材料等^[36-38]。在这些方法中，热解技术因其能有效实现污泥减量化并产生有价值的副产物而倍受重视^[39]。

目前，市政污泥经热解制得的焦碳常被用作吸附剂来处理含有染料、酚类或重金属的废水的处理^[40,41]。最近也有少量关于利用污泥焦碳做为催化剂载体应用于废气处理的报道。例如，美国的 Ansari 和 Bandosz^[42]将氧化钙负载在污泥和废纸的混合载体上，制备了用于 H_2S 处理的吸附剂和催化剂。然而，本课题开展之前还没有关于用污泥碳作为载体制备催化剂并将其应用于多相 Fenton-like 氧化技术中的报道。此外，与传统的无机或有机载体相比，污泥碳是一种无机-碳杂化材料，因此，这些碳组分及无机组分如 SiO_2 等在催化反应过程中的作用也

是值得研究的。

本章以城市污水厂污泥为原料采用一步法制备污泥碳负载铁氧化物的复合材料 FeSC，并将其作为多相 Fenton-like 催化剂，应用于废水中偶氮染料（酸性橙 II，AOII）的催化氧化降解。考察催化剂热解温度、制备方法以及 H₂O₂ 初始浓度、染料初始浓度、反应温度和溶液 pH 等实验条件对 FeSC 催化性能的影响。此外还对污泥碳中的无机组分和碳组分在催化反应中所起的作用进行深入探讨。

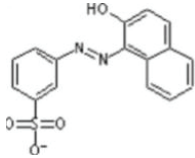
2.2. 实验部分

2.2.1. 实验试剂与材料

七水合硫酸亚铁，过氧化氢 (30%, w/v)，硫酸氧钛，异丙醇，硫酸，氢氧化钠，重铬酸钾，硫酸银，硫酸亚铁铵，原硅酸四乙酯，硫酸铝，分析纯试剂，广州化学试剂厂；Fe₂O₃，Fe₃O₄，FeOOH，二氧化锰，活性炭，分析纯试剂，天津福晨化学试剂厂；所有配制溶液的水均为反渗透电去离子超纯净水，电阻率 > 18 MΩ·cm；AO II 为商用染料，其物理化学性质如表 2-1 所示。

表 2-1 酸性橙 II 的物理化学参数^[43,44]

Table 2-1. Physicochemical properties of Acid Orange II

化学结构式	化学式	分子量 (g/mol)	宽 (Å)	长 (Å)	高 (Å)	λ _{max} (nm)	水溶解 度(g/L)	pKa
	C ₁₆ H ₁₁ N ₂ O ₄ SNa	350.32	7.3	13.6	2.3	484	100 (100°C)	11.4

本章实验所用污泥为广州市猎德污水处理厂的二沉池脱水污泥，取泥日期为 2010 年 1 月，其性质如表 2-2 所示。将所得污泥于 105°C 下烘干至恒重，过 100 目筛，于干燥器中保存备用。

表 2-2 实验所用污泥的物理化学性质

Table 2-2. Analysis of sewage sludge sample

Proximate analysis			Elemental analysis				
Moisture (wt %)	Ash (wt %)	Volatiles (wt %)	C (%)	H (%)	N (%)	S (%)	
84.4	44.6	56.2	22.9	4.0	4.4	0.7	
Ash analysis (wt.%)							
Si	Al	Fe	P	Ca	K	Mg	Na
14.1	3.6	4.5	4.1	2.7	2.3	1.9	0.6
Ash analysis (mg/kg)							
Zn	Cu	Pb	Cr	Cd	Hg		
825	147	40.7	45.1	2.4	4.5		

2.2.2. 实验仪器

表 2-3 实验所用主要仪器

Table 2-3. Primary apparatus in the experiment

仪器名称	仪器型号	生产厂家
热恒温鼓风干燥箱	DHG-9023A	上海一恒科技有限公司
恒温加热磁力搅拌器	DF-101S	英峪华仪器有限责任公司
管式电阻炉	SKF-2-12	杭州蓝天仪器设备有限公司
超声波清洗机	JP-C100	广州市吉普超声波电子设备有限公司
真空抽滤机	2X-1	临沂华达烘干设备厂
电热恒温振荡水槽	DKZ	上海一恒科技有限公司
pH 计	PHS-3C	上海雷磁仪器厂
COD 微波消解仪	MS-3	华南环境科学研究所

2.2.3. 催化剂的制备

(1) 一步法制备污泥碳/铁氧化物复合催化剂:

将 20g 干污泥加入到 150mL 0.5mol/L, pH 为 2.5 的 FeSO₄ 溶液中, 在室温下

浸渍搅拌 24 小时后,用旋转蒸发仪于 60°C 下旋转蒸发干燥,然后在 105°C 下烘干 12 h。将烘干所得样品置于管式电阻炉中在一定温度下热解 2h,升温速率:20°C/min,氮气流量:40 mL/min。热解尾气通入装有 NaOH 溶液的尾气瓶进行处理。待热解结束并冷却至室温后将样品取出,用去离子水洗涤,直到向滤液中滴加 1,10-菲罗啉溶液不显红色(未检测出 Fe²⁺)为止。然后于 105°C 烘干 12 h,过 200 目筛,得催化剂 Fe-SC。

(2) 两步法制备污泥碳/铁氧化物复合催化:

“两步法”即先制备污泥碳然后将硫酸亚铁盐用等体积浸渍法负载于污泥碳表面后热解。具体步骤为:取 20 g 干污泥置于管式电阻炉中于 650°C 下热解 2 h,升温速率为 20°C/min,氮气流量:40 mL/min,冷却后得到污泥碳(SC)。将 20.8 g FeSO₄·7H₂O 用少量的蒸馏水溶解,并调节 pH 至 2.5,之后逐滴滴入上一步热解所获得的 SC 中,混合均匀,于 105°C 下烘干 12 h。放入管式电阻炉中热解,操作条件同上。将热解后固体产物用去离子水洗涤,105°C 烘干 12 h,过 200 目筛,得催化剂 Fe/SC。

此外,为了研究污泥碳作为催化剂载体在多相 Fenton-like 反应中所起的作用,本研究选用无机组分含量较低的生物质原料——木屑,为制备催化剂载体的原料,同样使用一步法在相同的条件下制备了负载铁氧化物的木炭复合多相 Fenton-like 催化剂,命名为 FeWC。

为了获得无机物含量较低的污泥,我们从猎德污水处理厂二期曝气池中直接取 5 L 活性污泥悬浮液。在实验室中经过两周左右的悬浮培养,使得污泥的挥发性悬浮固体与总悬浮固体之比高于 85%。之后将污泥悬浮液过滤,滤得的污泥泥饼用浓度为 0.5 mol/L 的 HCl 浸渍 12 h,离心后用去离子水洗涤至滤液 pH 恒定。将经以上程序处理获得的干污泥命名为 SS-A,经测定其灰分含量约为 4.3 wt.%。之后本研究以除去大部分灰分的干污泥 SS-A 作为载体,用一步法负载不同含量的二氧化硅,氧化铝及铁氧化物。实验中以原硅酸四乙酯 (Tetraethyl Orthosilicate, TEOS)作为硅源,Al₂(SO₄)₃ 和 FeSO₄·7H₂O 分别作为铝源和铁源。制备条件及所得样品见表 2-4。

表 2-4 低灰分污泥碳(SC-A)衍生催化剂的制备条件

Table 2-4. Preparation conditions for SC-A based catalysts.

Sample	SS-A (g)	TEOS (mmol)	Ethanol (mmol)	Fe (mmol)	Al (mmol)	Fe/Si/Al
FeSC-A	2.5	0	0	3.60	0	1/0/0
SiSC-A	2.5	3.60	3.60	0	0	0/1/0
AlSC-A	2.5	0	0	0	3.60	0/0/1
FeSiSC-A ₁	2.5	1.80	1.80	3.60	0	2/1/0
FeSiSC-A ₂	2.5	3.60	3.60	3.60	0	1/1/0
FeSiSC-A ₃	2.5	7.20	7.20	3.60	0	1/2/0
FeAlSC-A ₁	2.5	0	0	3.60	1.80	2/0/1
FeAlSC-A ₂	2.5	0	0	3.60	3.60	1/0/1
FeAlSiSC-A	2.5	3.60	3.60	3.60	3.60	1/1/1
FeAlSi	0	3.60	3.60	3.60	3.60	1/1/1

2.2.4. 催化剂的表征方法

催化剂的粒径分布使用 MasterSizer 2000 激光粒度仪（英国 Malvern 仪器有限公司）进行测定。催化剂灰分采用国际材料试验协会的标准测定方法（ASTM D286-94）。催化剂的等电点(The pH values of isoelectric point, pH_{IEP})使用 Zetasizer Nano ZS 型 Zeta 电位测定仪（英国 Malvern 仪器有限公司）进行分析，通过测定不同 pH 环境下催化剂表面的 Zeta 电位值，由 Zeta 电位-溶液 pH 值关系图，可确定催化剂的 pH_{IEP} 。催化剂的比表面积采用 Autosorb-IQ-MP 型全自动物理化学吸附仪（美国 Quantachrome 公司），催化剂于 200°C 下脱气 2 h。于液氮下(温度 77K)下通过多点 BET 比表面积法进行测定。催化剂的表面形貌通过 JEOLJSM-6330F 场发射扫描电镜（日本电子株式会社）进行观察，操作电压 15KV。催化剂中各金属元素含量通过 Optima 5300DV 型电感耦合等离子体-原子发射光谱仪（美国 PerkinElmer 公司）进行分析测定，催化剂中的物相通过 D/max 2200 vpc 广角 X 射线衍射仪（日本 RIGAKU 公司）进行检测，Cu K α 射线，检测电压 40 kV，电流 30 mA。同时通过美国 ESCALAB 250 型 X 光电子能谱仪对催化剂中 Fe 的价态进行检测分析，测试以 Al K α 阳极，功率为 150 W，基础真空为 10^{-7} Pa。用 C 1s (284.6eV)为标准进行校正。对热解过程本研究采用 TG 209

型热失重分析仪 (Netzsch 公司, 德国) 与 Vector-22 型傅里叶变换红外光谱仪 (Bruker 公司, 德国) 联用技术进行检测。测量温度范围为室温至 900°C , 升温速率: $20^\circ\text{C}/\text{min}$, 氮气流速: $40\text{ mL}/\text{min}$ 。

2.2.5. 催化剂催化性能评价

2.2.5.1. 静态实验

在 250 ml 锥形瓶中加入一定量的催化剂和 100ml 已知浓度的 AO II 溶液, AO II 溶液的 pH 值先用 $0.05\text{ mol}/\text{L}$ 的 NaOH 和 $0.05\text{ mol}/\text{L}$ 的 H_2SO_4 调节至预定值。将锥形瓶置于恒温振荡器上振荡并计时。定时取样并用 $0.45\ \mu\text{M}$ 的微孔滤膜过滤分离催化剂, 测定滤液吸光度。待吸附催化剂对 AOII 达到吸附平衡之后, 取 60 mL 混合溶液, 将溶液 pH 调至反应所需值, 加入一定量的过氧化氢(5 vol.%), 继续计时, 每隔一定时间取样, 过滤, 测定滤液中 AOII 剩余浓度, 计算脱色率。

2.2.5.2. 连续流实验

为了测试实验所制备的多相 Fenton-like 催化剂的使用寿命, 本章设计了浸没式连续流膜分离-多相 Fenton-like 耦合反应器(Integrated membrane-heterogeneous Fenton-like catalytic continuous reactor, MHFR), 如图 2-1 所示。

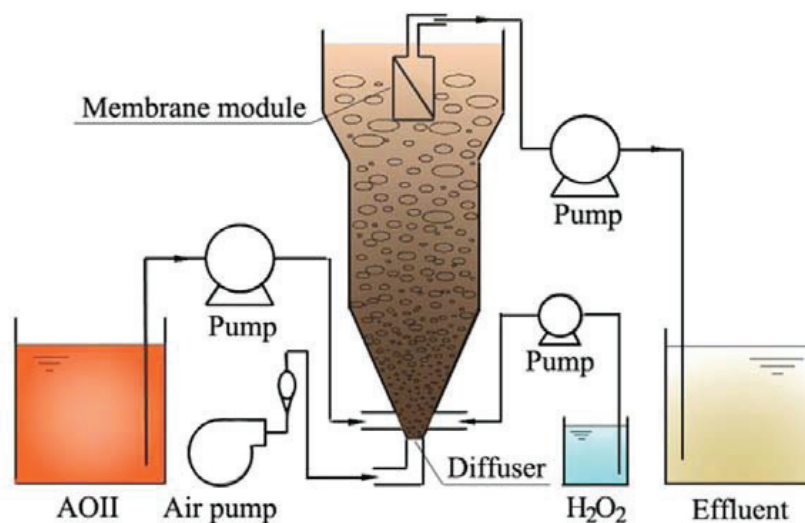


图 2-1 MFR 反应器示意图

Fig. 2-1. Schematic diagram of the submerged MHFR reactor.

反应体系包括：总体积为 2.5 L 的有机玻璃（聚甲基丙烯酸甲酯）反应器，平均孔径为 3 μm 的圆柱形浸没式陶瓷膜组件，进水系统，出水系统，过氧化氢投加系统，pH 调节系统和曝气系统。

反应开始前先向反应器内注入 2.4 L 浓度为 100 mg/L 的 AOII 溶液，4.8 g 催化剂及 36 mmol H_2O_2 (30% w/v)。开启进水泵向反应器中以 20 mL/min 的流速泵入 100 mg/L AOII 溶液。与此同时开启过氧化氢泵以 1 mL/min 从反应器底部加入 H_2O_2 溶液(1.02% w/v)。反应过程中通过 NaOH 和 H_2SO_4 溶液使得溶液 pH 保持在 4.0 \pm 0.1 范围内。曝气系统以 5 L/min 的气体流速从反应器底部向上曝气，使催化剂在反应器中呈悬浮状态。反应液在体系中的停留时间约为 2 h (理论停留时间 $t = \frac{\text{反应器体积}}{\text{流速}}$)，之后通过顶部的膜组件抽离出反应器。反应过程中定时

取样分析出水浊度和吸光度。

2.2.6. 分析方法

反应过程中 AO II 的浓度用 Vis 7200 可见光分光光度计（上海天美--化工仪器有限公司），于 484 nm 处测定吸光度进行测定。反应过程中 AO II 的 UV-vis 光谱变化情况采用 UV-3150 型紫外可见光分光光度计（日本 Shimadzu）进行测量。

溶液 pH 的测量使用上海雷磁仪器厂的 PHS-3C 型 pH 计。

溶液中 H_2O_2 浓度采用硫酸氧钛比色法进行测定^[45]。检测波长为 405 nm。

滤液的化学需氧量(COD)采用重铬酸钾法进行测定，滤液先用二氧化锰去除残余的 H_2O_2 ，之后采用 MS-3 型 COD 微波消解仪（华南环境科学研究所）进行消解。

滤液中溶出金属离子浓度采用 Optima 5300DV 型电感耦合等离子体-原子发射光谱仪（美国 PerkinElmer 公司）进行测定。

MHFR 出水浊度使用 2100N 型浊度仪测定(美国 HACH 公司)。

2.3. 结果与讨论

2.3.1. 污泥及污泥-FeSO₄ 的热解过程

对于以生物质为原料制备 Fenton-like 催化剂的研究, 催化剂的热解温度是一个十分重要的参数。TGA-FTIR 是目前广泛使用的能够有效监测热解过程中物质重量及产生气体变化情况的仪器^[46]。为了确定最佳热解温度, 本研究首先用 TGA-FTIR 对污泥(SS)及污泥-FeSO₄ 混合物(Fe-SS)的热解过程进行监测分析。由图 2-2 可以看出, SS 和 Fe-SS 的失重行为在 15-470°C 的升温过程中基本相同。而 470°C 至 600°C 之间, Fe-SS 存在明显的热失重峰。当温度继续升高, Fe-SS 的热失重又变得缓慢。SS 和 Fe-SS 不同的热失重行为可以从相应的三维红外谱图中得到解答(图 2-3 A1 和 B1)。与 SS 的三维红外谱图相比, Fe-SS 在热解过程中存在着更多强烈的气体吸收峰, 特别是在 470-600°C 之间。

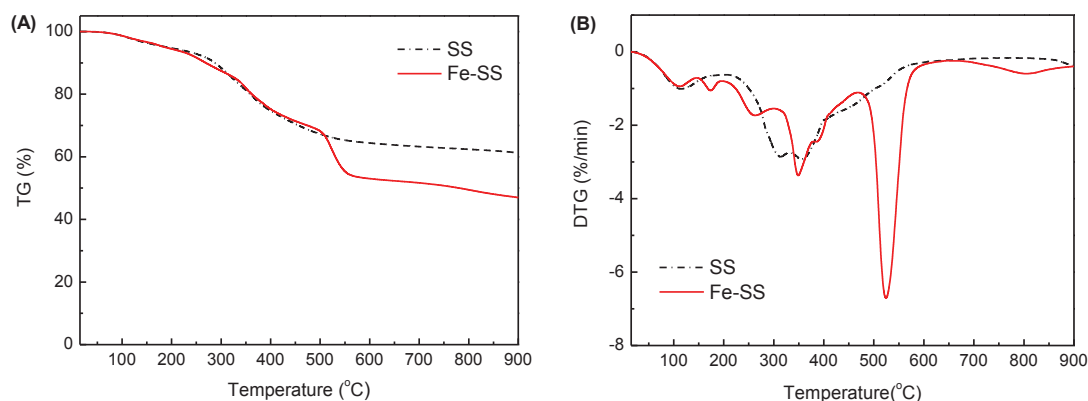


图 2-2 SS 和 Fe-SS 的 TG 和 DTG 图

Fig. 2-2. TG and DTG curves of SS and FeSS (heating rate: 20°C/min, nitrogen flow rate: 40 mL/min).

由 DTG 曲线和三维红外谱图可知, 本实验中污泥 SS 的热解可以大致分为三个阶段。阶段一(15-210°C): 在图 2-3 A1 所示的三维红外谱图中 1350-1700 cm⁻¹ 及 3500-3700 cm⁻¹ 的区间内有较强的吸收峰, 这些吸收峰对应水分子中 O-H 键的变形振动和伸缩振动。可见阶段一的温度范围内主要进行表面吸附水的脱除; 阶段二(210-600°C): 从 2-3 A1 的三维红外谱图里可以观察到除了水分子的吸收峰

之外，在 $2250\text{-}2392\text{ cm}^{-1}$ 和 $2800\text{-}3050\text{ cm}^{-1}$ 区间内还有与 C=O 与 C-H_n 的不对称振动相吻合的特征峰，表明该阶段的气体产物除了水还有 CO₂ 和碳氢化合物，根据此结果及文献报道可以推断第二阶段主要发生有机物，如糖类、蛋白质和脂类物质等，的热分解反应^[47]；在第三阶段(>600°C)的主要气体产物为 CO₂，可能源于污泥中碳酸盐类物质的高温分解^[48]。与图 2-3 A1 相比，除了以上几种主要气体产物外，在图 2-3 B1 中还可观察到在 470-600°C 之间，存在着强烈的 SO₂ 吸收峰($1300\text{-}1420\text{ cm}^{-1}$ 对应 SO₂ 不对称伸缩振动)。

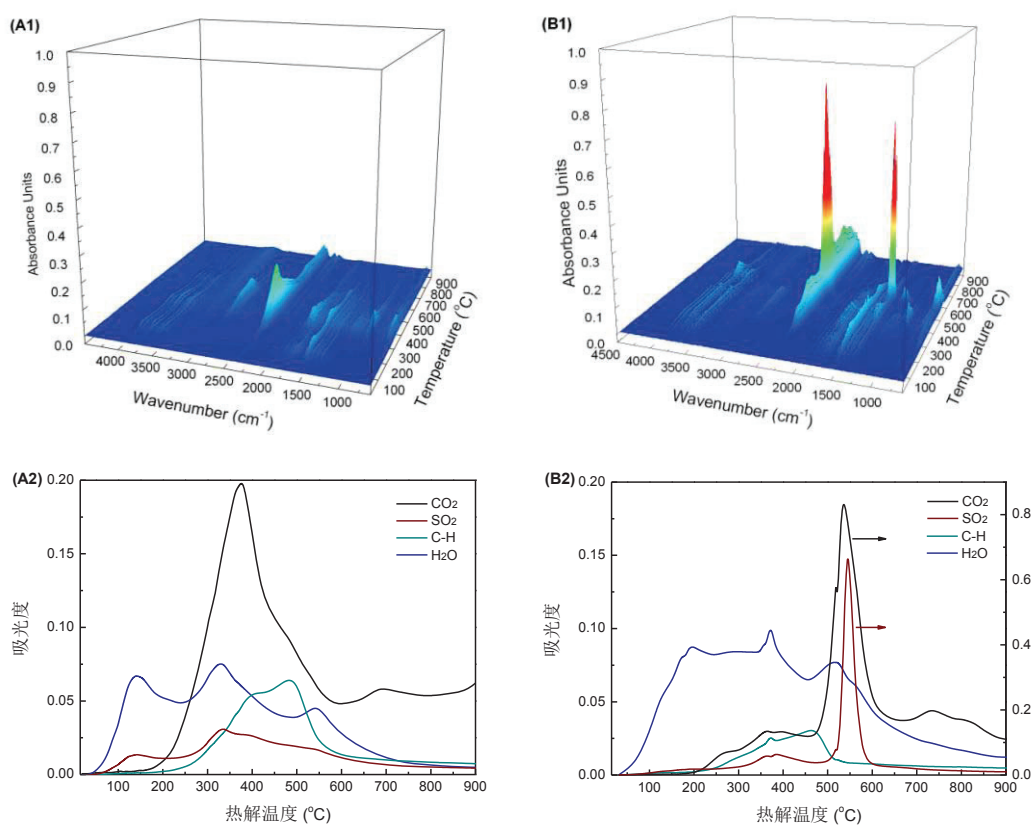


图 2-3 SS 和 Fe-SS 热解过程的生成气体的三维红外谱图(A1 和 B1); SS (A2) 和 Fe-SS (B2) 热解气态产物中 H₂O (1508 cm^{-1}), SO₂ (1375 cm^{-1}), CO₂ (2359 cm^{-1})和 C-Hn (2933 cm^{-1})随热解温度的变化情况

Fig. 2-3. 3D diagrams corresponding to the gases evolved from SS (A1) and FeSS (B1). Evolution versus temperature of the bands characteristic of H₂O (1508 cm^{-1}), SO₂ (1375 cm^{-1}), CO₂ (2359 cm^{-1})和 C-Hn (2933 cm^{-1}) for SS (A2) and Fe-SS (B2).

为了进一步比较,本研究选取三维红外谱图中 H₂O (1508 cm⁻¹), SO₂ (1375 cm⁻¹), CO₂ (2359 cm⁻¹)和 C-Hn (2933 cm⁻¹)四种气体,并作出最强吸收峰对应的强度随热解温度升高的变化趋势图,如图 2-3 A2 和 B2 所示。在 Fe-SS 热解过程中有大量 SO₂和 CO₂生成,且二者在 200-600°C 的温度范围内变化规律基本一致。这是由于 FeSO₄受热分解 SO₃, SO₃进一步分解成 SO₂和 O₂^[49],生成的 O₂与周围的 C 反应,生成 CO₂。这样可使原先包裹在碳载体中的铁盐暴露出来,将有利于催化剂中的铁氧化物与反应物接触。

2.3.2. 污泥碳/铁氧化物复合催化剂的表征

多相 Fenton-like 催化剂的颗粒尺寸是影响其催化活性的一个重要因素,因此本研究选取 800°C 下制备的污泥碳(SC)和负载铁氧化物的污泥碳复合多相 Fenton-like 催化剂(Fe-SC)用激光粒度分析仪对其粒径分布情况进行分析。

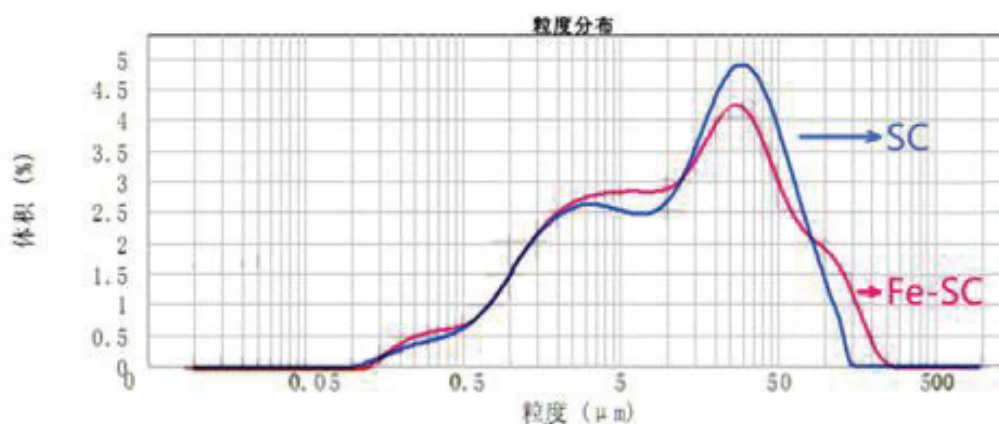


图 2-4 800°C下热解制备的催化剂SC和Fe-SC的粒径分布图

Fig. 2-4. Particle size distributions of SC and Fe-SC.

如图 2-4 给出了 800°C 下制备的污泥碳(SC)和负载铁氧化物的污泥碳复合多相 Fenton-like 催化剂(Fe-SC)的粒径分布情况。两种催化剂粒径分布基本相同,平均体积直径 \bar{d}_v 分别为 23.0 和 27.1 μm,表明铁盐的负载对催化剂颗粒粒径基本无影响。

为了观察催化剂的形貌特征,本研究对 SC、Fe-SC 进行了扫描电镜分析。从图 2-5 中可以看出,催化剂 Fe-SC 的表面比 SC 更粗糙,存在着球形小颗粒,这些小颗粒主要镶嵌在催化剂 Fe-SC 中。

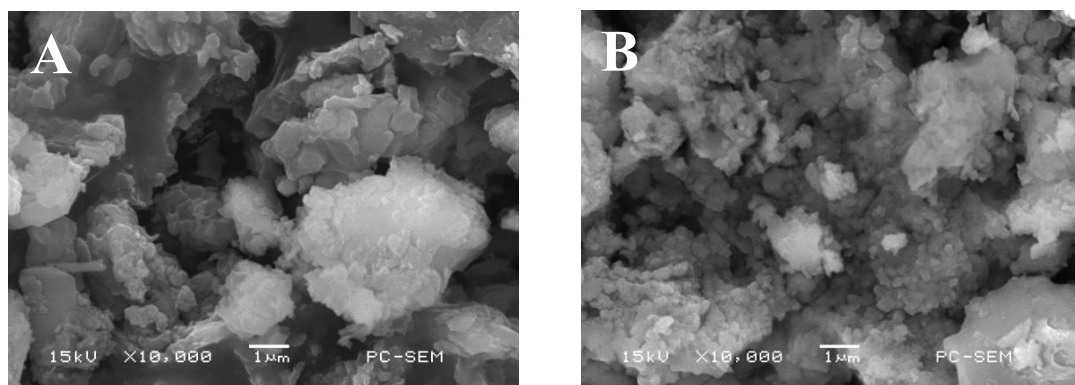


图 2-5 800°C 下热解制备的催化剂 SC(A)和 Fe-SC(B)的 SEM 图

Fig. 2-5. SEM images of the SC (A) and FeSC (B) pyrolyzed at 800°C for 2 h

为了进一步分析各元素在催化剂 SC 和 Fe-SC 表面的分布情况，对图 2-5 中所示区域分别进行了 EDX 能谱扫描分析，由表 2-5 所示分析结果可以看 SC 表面含量较高的元素有 C、O、Si 和 Al，与 SC 的 EDX 结果相比较，负载铁氧化物的 Fe-SC 催化剂中 Fe 的含量由 3.4%提高至 15.3%，表明铁氧化物已负载于催化剂表面。

表 2-5 EDX 分析结果

Table 2-5. Results of EDX analysis

Element	(keV)	Mass content (wt.%)		Atom content (At.%)	
		SC	Fe-SC	SC	FeSC
C	0.277	22.1	11.9	37.1	22.9
O	0.525	27.0	21.1	34.1	30.0
P	2.013	3.2	5.4	2.1	4.0
S	2.307	1.9	2.6	1.2	1.9
Mg	1.253	0.9	1.5	0.8	1.4
Al	1.486	11.9	14.2	8.9	12.1
Si	1.739	17.8	20.1	12.8	16.5
K	3.312	1.8	3.7	0.9	2.4
Ca	3.690	2.1	4.2	0.9	2.7
Fe	6.398	3.4	15.3	1.2	6.3

由于EDX为半定量元素分析,分析结果准确度不高。因此本研究将SC和Fe-SC采用电热板消解法^[50]处理后用ICP-OES测定催化剂中Fe、Si和Al的含量,结果如表2-6所示。ICP测定结果与EDX分析结果稍有不同,主要是由于污泥自身成分的不均匀性造成的。但是ICP测定的Fe-SC中的Fe含量为12.9%,与EDX半定量分析结果(15.3%)基本一致,由此可以推断“一步法”能使铁氧化物较均匀地分布于催化剂载体中。

表 2-6 SC 与 Fe-SC 的部分物理化学性质

Table 2-6. Physicochemical properties of SC and Fe-SC pyrolyzed at 800°C for 2h.

Sample	Fe (wt. %)	Si (wt.%)	Al (wt.%)	Ash (wt. %)	S _{BET} (m ² /g)	pH _{IEP}
SC	3.9	10.4	11.5	68.5	18.9	3.6
Fe-SC	12.9	8.4	7.5	89.6	14.3	3.4

由于铁氧化物的负载使得Fe-SC的灰分含量要高于SC,分别为89.6%和68.5%,可见催化剂中还有较多的无机组分。此外,从表2-6中还可以得知两种催化剂具有相近的比表面积S_{BET}和pH_{IEP}值。

此外通过ICP-OES还检测到Fe-SC中含有0.9% Ca、0.6% Mg、1.5% P、1.6% K和0.2% Na。以及微量的重金属元素,如Zn、Cd、Cu及Mn,其含量分别为650 mg/kg、11.5 mg/kg、134 mg/kg和627 mg/kg。

为了确定 SC 衍生催化剂各组分的相组成,本研究分别对在 800°C 下制备的 SC 和于 600、700、800°C 下热解制备的 Fe-SC 催化剂(简称为 Fe-SC₆₀₀, Fe-SC₇₀₀, Fe-SC₈₀₀) 进行 XRD 分析。

从 XRD 图中(图 2-6)可以发现,在 Fe-SC₈₀₀ 的 XRD 谱图中位于 $2\theta = 35.5^\circ$, 62.6° 和 30.1° 处出现对应 Fe₃O₄ 的(3 1 1), (4 4 0)和(2 2 0)晶面的衍射峰(JCPDS 88-0866)^[51]。对于 Fe-SC₈₀₀ 催化剂中 Fe₃O₄ 的晶粒尺寸,利用 Debye-Scherrer^[52] 公式进行计算:

$$D = K\lambda/B\cos\theta \quad (\text{式 2-1})$$

式中 D 表示晶粒尺寸(nm); K 为常数,通常取 K=1; λ 是 X 射线的波长(nm), $\lambda = 0.154056 \text{ nm}$; θ 为衍射角(Rad), B 为半峰宽(Rad)。Fe-SC₈₀₀ 催化剂中 $2\theta = 35.548^\circ$

处宽化的 Fe_3O_4 衍射峰，可通过 Jade 软件确定其半峰宽为 0.752° 。将角度转化成弧度代入 2-1 式可计算得 Fe_3O_4 颗粒大小约为 12.3 nm。而 SC 中的铁氧化物由于含量较低，且制备过程中部分包裹于催化剂内部，因此其 XRD 谱图中并未出现明显的 Fe_3O_4 衍射峰。此外从 Fe-SC 的 XRD 谱图中还可以检测到 SiO_2 、 Al_2O_3 、 CaSO_4 及 NaPO_3 等物质。

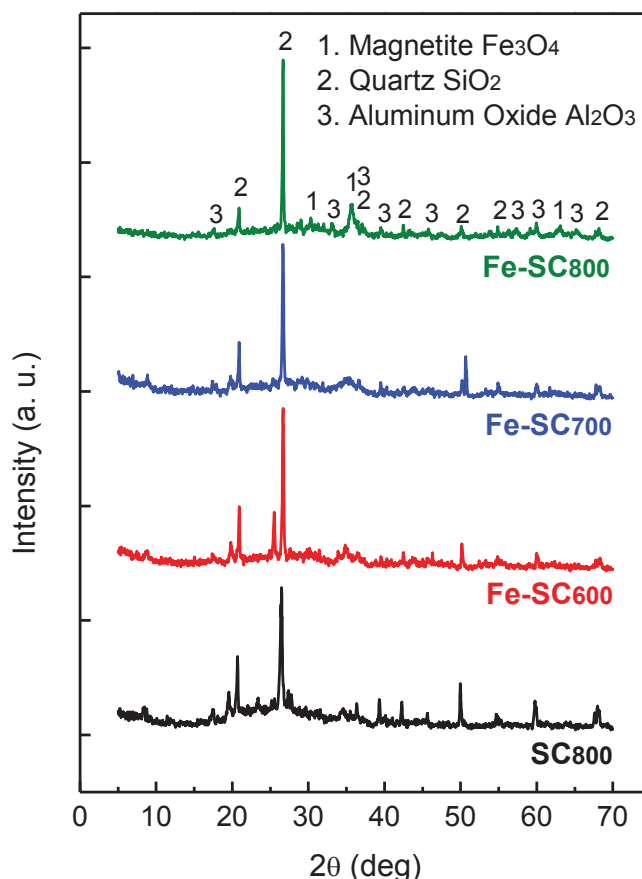


图 2-6 Fe-SC(600、700、800°C 下制备)及 SC(800°C 下制备)的 XRD 图谱

Fig. 2-6 XRD patterns of SC, Fe-SC₆₀₀, Fe-SC₇₀₀ and Fe-SC₈₀₀

此外，本研究还采用 XPS 对 Fe-SC 催化剂进行表征，并选用具有更高辨识度的 Fe 3p 谱图来判断 FeSC 中 Fe 的价态^[53]。结果如图 2-7 所示，可以看出 Fe 3p 的结合能为 56.4 eV，与文献报道相一致^[54]。而 Fe_2O_3 中 Fe 3p 的结合能位于 55.6 eV^[55]，与本研究的测定结果相差较大。根据 XRD 和 XPS 的结果，可以推断 Fe-SC 中的 Fe 是以 Fe_3O_4 的形态存在的。

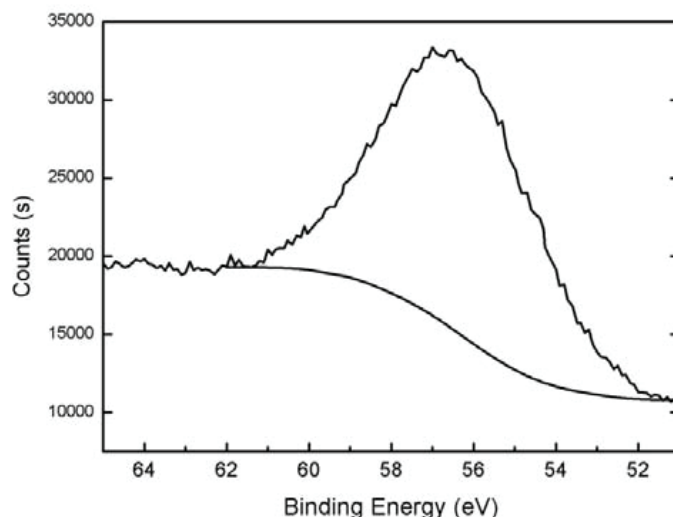


图 2-7 FeSC 样品 XPS 的 Fe 3p 谱图

Fig. 2-7. XPS patterns of the Fe3p region for FeSC catalyst.

2.3.3. 催化活性与热解温度的关系

由 TGA-FTIR 的结果可知负载在 SC 中的 FeSO₄ 在 600°C 下基本已完全分解。因此, 本研究选取 600°C、700°C、800°C 和 900°C 作为热解温度, 制备 Fe-SC₆₀₀, Fe-SC₇₀₀, Fe-SC₈₀₀ 和 Fe-SC₉₀₀ 四种催化剂, 并比较它们的 Fenton-like 催化活性。由图 2-8 A 中可以看出随着热解温度的升高, Fe-SC 催化剂由于失重率增加导致产率逐渐下降, 灰分逐渐增加, 相应地催化剂中 Fe 含量由 Fe-SC₆₀₀ 中的 12.3% 逐渐增大至 Fe-SC₉₀₀ 中的 13.4% (图 2-8 B)。对 AOII 溶液的脱色性能, 实验中吸附 1 h 达到吸附平衡后加入 H₂O₂ 溶液开始 Fenton-like 催化, 反应 2 h 后取滤液测定吸光度, 计算脱色率。吸附平衡时四个催化体系中分别有 16.9%、15.2%、14.3% 及 12.8% 的 AOII 被吸附于催化剂表面, 催化反应结束时四个体系中 AOII 的总脱色率分别为 90.7%、93.5%、97.5% 和 95.6%。可见 Fe-SC₈₀₀ 具有最高的催化活性。

从图 2-8 B 可知, 与 Fe-SC₆₀₀ 和 Fe-SC₇₀₀ 相比, Fe-SC₈₀₀ 催化剂中的 Fe 含量略高。这意味着在使用相同的催化剂投加量时, Fe-SC₈₀₀ 催化体系中具有更多的催化活性位点, 从而表现出更强的 Fenton-like 催化活性。此外, 从图 2-6 的 XRD 分析结果可以看出 Fe₃O₄ 的衍射峰随着热解温度的升高而变强, 一方面可能由于高温能使 Fe₃O₄ 颗粒获得更好的结晶度, 另一方面由于在较低热解温度下 Fe₃O₄

的表面仍覆盖着一层污泥碳，影响其 XRD 检测，而随着热解温度的升高，覆盖在 Fe_3O_4 表面的 C 被灼烧掉，使得 Fe_3O_4 暴露出来，从而使催化剂的催化活性得到提高。

但随着热解温度继续升高，Fe-SC₉₀₀ 催化剂的催化活性反而略微下降，一方面由于高温使得催化剂的碳组分减少导致催化剂比表面积减小，对 AOII 的吸附能力降低；另一方面可能由于当催化体系中存在过量的活性位时，体系将迅速产生大量的·OH 自由基，而·OH 的寿命不足 1ns^[56]，由于受到吸附速率的限制，产生的·OH 无法与溶液中的 AOII 反应，反而导致·OH 的淬灭。因此，在后续实验中选择 800°C 为催化剂的制备温度。

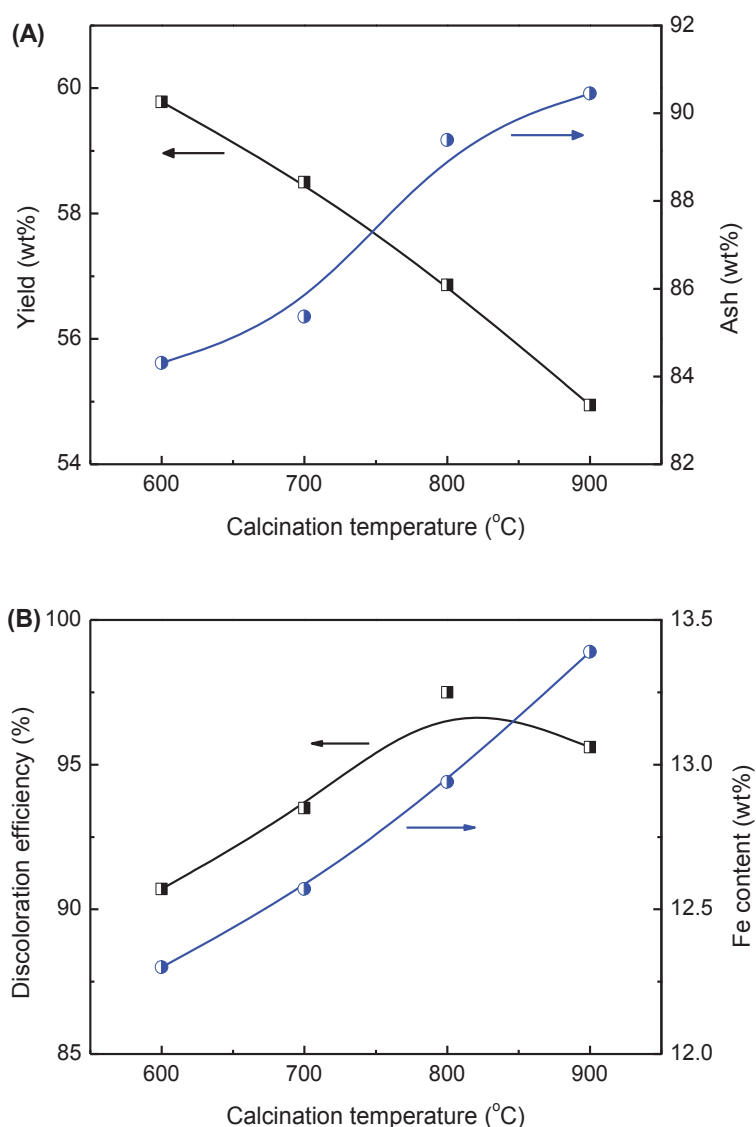


图 2-8 热解温度对 Fe-SC 产率和灰分(A)及 AOII 脱色率和 Fe 含量的影响(B)

Fig. 2-8 Effect of calcination temperature on the Fe-SC production and ash content (A) and influence on the Fe content in the catalysts and the degradation efficiency of AOII (B) (Fe-SC: 2.0 g/L; H₂O₂: 15 mM; AOII: 100 mg/L; initial pH 4.0; reaction temperature: 30°C and reaction time: 120 min).

2.3.4. 催化活性与制备方法的关系

“两步法”制备的 Fe/SC 催化剂中 Fe 含量为 14.2%，平均体积直径 26.6 μ m， S_{BET} 为 13.3 m²/g， pH_{IEP} 为 3.8，与“一步法”制得的 Fe-SC 的相关物理化学性质基本相同（见表 2-6）。

为了比较“一步法”和传统“两步法”制备所得 Fenton-like 复合催化剂催化性能的差异，本研究分别考察了 Fe-SC 及 Fe/SC 催化剂对 AOII 的吸附及催化性能。经过 1 h 的吸附，分别有 14.3%和 19.7%的 AOII 染料分子吸附于 Fe-SC 和 Fe/SC 上。催化反应进行 2 h 时，Fe-SC 催化体系中 AOII 的脱色率达到 97.5%，Fe/SC 体系的为 98.9%。可见两个催化体系对 AOII 的脱色效率基本相同。但反应结束时，在 Fe-SC 体系的滤液中检测到 0.373 mg/L Fe，Fe/SC 体系滤液中 Fe 离子的浓度为 1.223 mg/L，约为前者的 3 倍。可见 Fe/SC 中的铁氧化物活性组分比 Fe-SC 中的更容易在反应过程中溶出。

同时本研究在连续流反应器 MHFR 中对两种方法制备所得催化剂的使用寿命进行比较。如图 2-9 A 所示结果，Fe-SC 催化体系在实验结束时(600min)仍保持较高的催化活性，而 Fe/SC 的催化活性在反应进行到 210 min 后开始迅速下降。为了探究 Fe/SC 失活的原因，对体系出水的浊度进行测定，结果显示出水的浊度均低于 0.300 NTU，可见陶瓷膜能够有效地将污泥碳复合催化剂颗粒拦截于反应器内，而且 Fe/SC 体系对 AOII 脱色能力的下降并不是由于粉末状 Fe/SC 催化剂的流失导致的。同时本研究还测定了体系出水中 Fe 的浓度，由图 2-9 B 可以发现 Fe/SC 体系 MFR 出水中 Fe 的浓度要高于 Fe-SC 体系的，且 210 min 后 Fe/SC 体系出水中 Fe 浓度迅速下降，由此可以推断铁盐的流失可能是导致 Fe/SC 体系催化活性下降的主要原因。

Fe-SC 与 Fe/SC 溶出特性的差异可能是由于 Fe/SC 催化剂在制备过程中是先对污泥进行碳化再负载铁盐，铁氧化物主要沉积在污泥碳的表面，与载体污泥碳

结合得不够牢固，而用先将亚铁盐与干污泥浸渍后热解的“一步法”所制得的 Fe-SC 催化剂中铁氧化物能更牢固且均匀地镶嵌于 SC 载体中。因此，在后续的实验 中，本研究选择用“一步法”来制备催化剂。

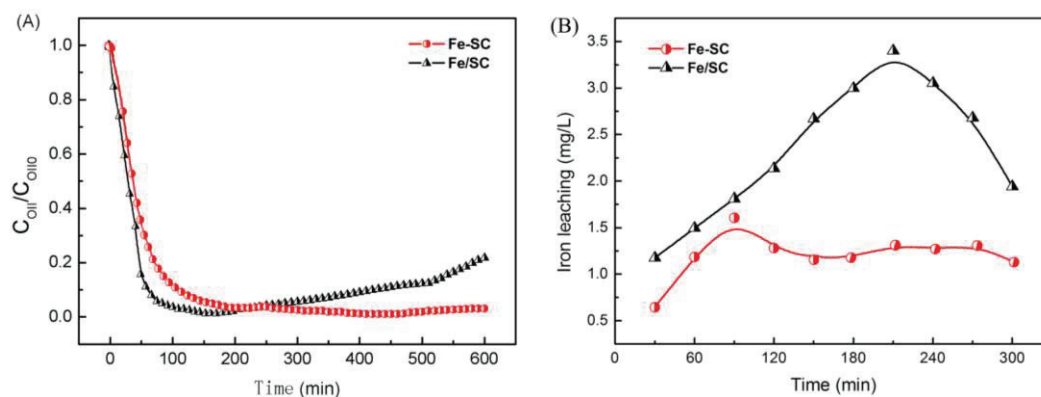


图 2-9 Fe-SC 和 Fe/SC 在连续流反应器中对 AOII 催化降解能力的比较(A)以及出水中 Fe 浓度的变化情况(B)(催化剂用量: 2.0g/L; H₂O₂: 15 mM; AOII: 100 mg/L; 反应温度: 23°C; 总溶液体积: 2.4 L; 水力停留时间: 120 min)

Fig. 2-9. Effect of consecutive experiments with the Fe-SC and Fe/SC catalysts on the degradation of AOII solution (A) and iron leaching (B) (Catalysts: 2.0 g/L; H₂O₂: 15 mM; Orange II: 100 mg/L; reaction temperature: 23°C; total volume of reaction solution: 2.4 L and residence time: 120 min).

2.3.5.反应条件与 AOII 催化降解效率的关系

多相 Fenton-like 催化剂的活性会受到反应条件的影响,因此本节将探讨 H₂O₂ 初始浓度、染料初始浓度、反应温度和溶液 pH 对 Fe-SC 催化性能的影响,并确定最优的催化反应条件。

2.3.5.1. H₂O₂ 初始浓度对 AOII 脱色率的影响

对于 Fenton 反应,体系中 H₂O₂ 的浓度直接影响产生 ·OH 自由基的数量。由反应方程式 2-2 可知,降解 100 mg/L AOII 溶液所需的 H₂O₂ 理论值为 12 mM



因此本研究考察了 H₂O₂ 初始浓度从 9 mM 增加至 18 mM 的过程中 Fe-SC 体系里 AOII 脱色率的变化情况。实验过程中向 100 mg/L AOII 溶液中加入 2.0 g/L 的

Fe-SC催化剂，经60 min达到吸附平衡之后，向反应体系中加入不同量的H₂O₂。开始Fenton-like催化反应。图2-10中，当H₂O₂的浓度从9 mM增加至15 mM时，AOII的脱色率随之增加，这是因为在这个过程中由于AOII的脱色速度主要取决于·OH自由基的生成速度，因而H₂O₂的浓度增加有利于AOII的降解。但是当H₂O₂的初始浓度增加至18 mM时，AOII脱色率反而下降。这是由于体系中过量的H₂O₂能捕获·OH生成相对于·OH自由基（氧化还原电位：2.8 V）活性更低的HO₂·自由基（氧化还原电位：1.7 V）（式2-3），此外过量的自由基之间也会发生相互淬灭的反应（式2-4、2-5），从而导致有机污染物的降解效率变低^[57,58]。

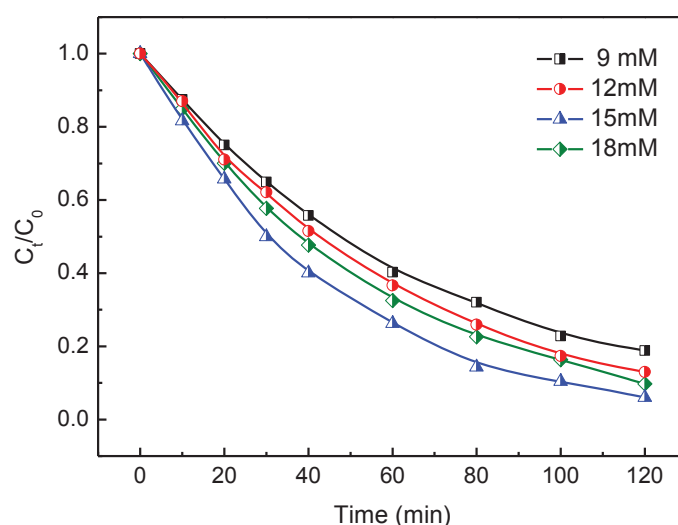
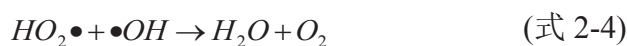
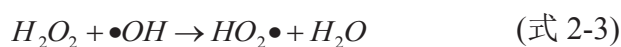


图 2-10 不同 H₂O₂ 初始浓度对 AOII 脱色率的影响

Fig. 2-10 Effect of hydrogen peroxide concentration on the discoloration of AOII (Fe-SC: 2.0 g/L; AOII: 100 mg/L; initial pH 4.0; reaction temperature: 30°C)

此外，本研究采用在多相Fenton-like催化反应中被广泛使用的伪一级动力学模型^[59,60]（式2-9），对图2-10中的数据进行拟合。

$$\ln \frac{C_0}{C_t} = k_{app} t \quad (\text{式 2-6})$$

用 $\ln(C_0/C_t)$ 和反应时间作图,结果如图2-11所示,曲线的相关系数(R^2)均达到0.97以上,表明此类反应遵循伪一级动力学方程。通过比较不同初始 H_2O_2 的浓度对应的反应速率常数,可以确定Fe-SC催化Fenton-like反应的最佳 H_2O_2 的初始浓度为15 mM。

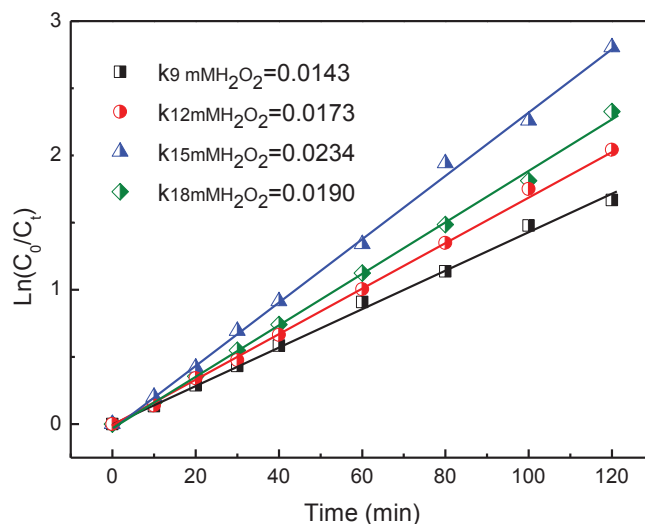


图2-11 H_2O_2 初始浓度对AOII降解准一级动力学常数的影响

Fig.2-11. Effect of hydrogen peroxide concentration on Pseudo-first-order rate constants for OA II discoloration

2.3.5.2. AOII 初始浓度对 Fe-SC 催化活性的影响

废水中目标污染物的浓度对化学氧化剂的用量及处理所需时间的长短有着重要的影响。因此,本研究考察了不同 AOII 初始浓度对 Fe-SC 催化体系中 AOII 脱色率的影响。实验中催化剂用量固定为 2.0 g/L, H_2O_2 初始浓度为 15 mM, AOII 溶液初始 pH 均调为 4.0。对不同初始浓度的 AOII 降解过程进行伪一级动力学模拟,结果如图 2-12 所示。反应速率常数随着 AOII 初始浓度的增加而下降,可见 AOII 浓度的增加对其降解速率存在明显的抑制作用。

这是因为,对于 Fenton-like 反应,在 H_2O_2 用量一定的情况下,反应体系中产生的 $\bullet OH$ 自由基的总量也基本不变。由式 2-2 可知 15 mM H_2O_2 理论上只能有效降解 125 mg/L 的 AOII 溶液,而当初始浓度继续增大,体系中产生 $\bullet OH$ 总量将远远低于打断 AOII 偶氮键所需的自由基,从而导致高浓度 AOII 溶液的脱色率

降低。另一方面，高浓度的 AOII 分子将与 H₂O₂ 在催化剂 Fe-SC 表面发生竞争吸附，造成反应体系中·OH 产率下降，最终导致反应体系的反应速率常数减小^[59]。此外，根据文献报道，由于 AOII 为偶氮染料，分子结构中有较大的共轭体系。高浓度的染料分子之间容易发生缔合，导致染料分子与·OH 的相互接触机会减少，限制脱色反应的发生^[61]。

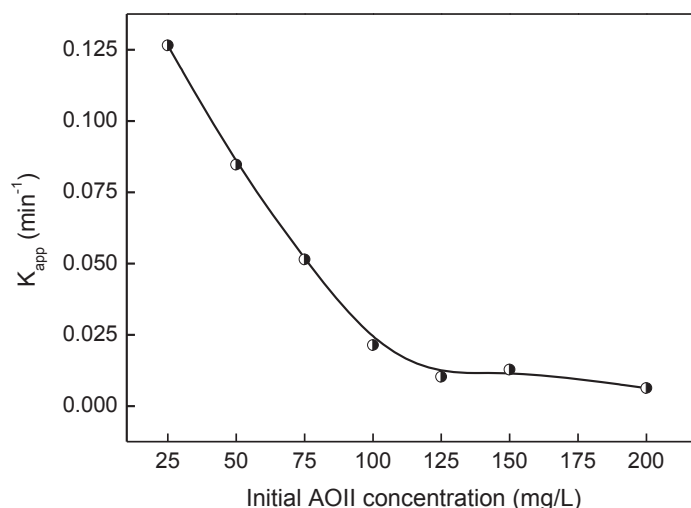


图 2-12 AOII 初始浓度对 Fe-SC 催化反应速率常数的影响

Fig. 2-12. Effect of initial concentration of AOII on the apparent rate constant (Fe-SC: 2.0 g/L; H₂O₂: 15 mM; initial pH 4.0; reaction emperature: 30°C).

2.3.5.3. 反应温度对 Fe-SC 催化活性的影响

为了研究反应温度对 Fe-SC 的 Fenton-like 催化活性的影响，本研究考察了 20°C 至 60°C 下 Fe-SC 的催化活性，并对反应进行热力学研究。对催化反应从 0-60 min 的数据进行伪一级动力学拟合。

从图 2-13 中的结果可以看出 AOII 的反应速率常数随着反应温度的升高而加快，这是因为较高的温度能提供反应所需的活化能，微观上则可增加反应物分子之间的相互碰撞频率^[57]。

由于 H₂O₂ 分子呈非对称的链状结构，其—O—O—键长为 0.149 nm，键能为 203.98 kJ/mol。而 O₂ 分子内 O=O 的键长为 0.121nm，键能为 493.24 kJ/mol。可见 H₂O₂ 中的过氧键长而弱，稳定性较差^[62]。由图 2-13 中可以看出当反应温度高

于 40°C 之后，线性拟合结果较差，可能是由于 H₂O₂ 的热不稳定性导致其在温度较高的溶液中迅速分解，影响催化体系的催化活性。因此，对于多相 Fenton-like 催化反应的反应温度不宜过高。

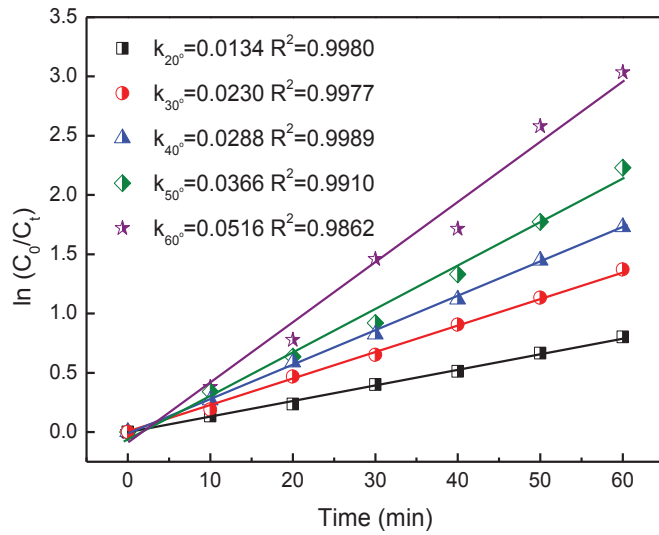


图 2-13 不同反应温度下 AOII 脱色反应的一级动力学拟合

Fig. 2-13. Effect of the reaction temperature on the pseudo-first-order rate constants for AOII degradation (Fe-SC: 2.0 g/L; H₂O₂: 15 mM; AOII: 100 mg/L; initial pH 4.0; reaction temperature: 30°C).

根据 Arrhenius 公式:

$$K_{obs} = A \exp\left(-\frac{Ea}{RT}\right) \quad (\text{式 2-7})$$

式中: K_{obs} 为污染物的表观降解动力学常数, A 为指前因子, Ea 为活化能(kJ/mol), R 为气体常数(8.314 J/(mol·K)), T 为反应温度(K), 将式 2-7 取对数可以得到:

$$\ln(K_{obs}) = \ln(A) - \frac{Ea}{RT} \quad (\text{式 2-8})$$

根据式 2-8, 将图 2-13 中的不同温度下 AOII 降解表观动力学常数的对数值及 1/T 作图并进行线性回归, 如图 2-14 所示, 所得直线的斜率为 -Ea/R, 最终计算得该反应的活化能为 25.8 kJ/mol。与一般的化学反应活化能(40-400 kJ/mol)相比, Fe-SC 多相 Fenton-like 催化体系的活化能要略低一些, 这符合自由基反应的特点^[63]。

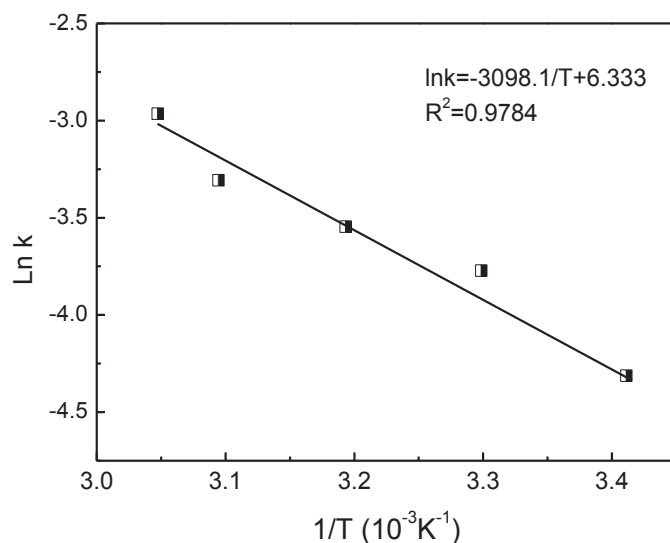


图 2-14 AOII 降解表观速率常数与温度线性回归图

Fig. 2-14. Arrhenius plot of AOII degradation

2.3.5.4. 初始 pH 对 Fe-SC 催化活性的影响

对于铁系多相 Fenton-like 催化剂,其催化活性容易受到反应溶液 pH 值的影响^[64,65]。因此本研究考察了不同溶液 pH 值下 Fenton-like 反应中 AOII 的脱色情况,由图 2-15 A 可见 AOII 的降解效率随着 pH 的升高而逐渐降低。当溶液初始 pH 为 3.0 时,反应 120 min 后, AOII 的脱色率迅速变为 97.5%; 当初始 pH 为 4.0 时, AOII 降解效率为 94.0%; 而当 pH 继续升高至 5.0 和 6.0 时, AOII 的脱色率降为 31.4%和 14.9%。由此可见随着溶液初始的 pH 的升高, AO II 溶液的降解效率逐渐降低。原因之一可能是由于 H₂O₂ 在 pH 值较高的环境中易分解成水和氧气,大大减少·OH 的产生量^[65],另一方面当 pH 值过高时,催化剂表面生成羟基铁氧化物导致产生·OH 的速度变慢^[66]。本研究同时监测了不同初始 pH 条件下的多相 Fenton-like 反应体系中 Fe 的溶出情况,结果如图 2-15 B 所示,在反应结束时(120 min),初始 pH 为 3.0 的体系中检测到 2.2 mg/L 的 Fe,随着溶液初始 pH 值的升高,Fe 溶出也明显减少,pH=4.0 的体系中只有 0.4 mg/L Fe, pH 为 5.0 和 6.0 时,催化反应进行 120 min 时,Fe 溶出均低于 1.0 mg/L。可见 pH=3.0 的体系中,均相反应对 AOII 的脱色存在不容忽视的贡献。

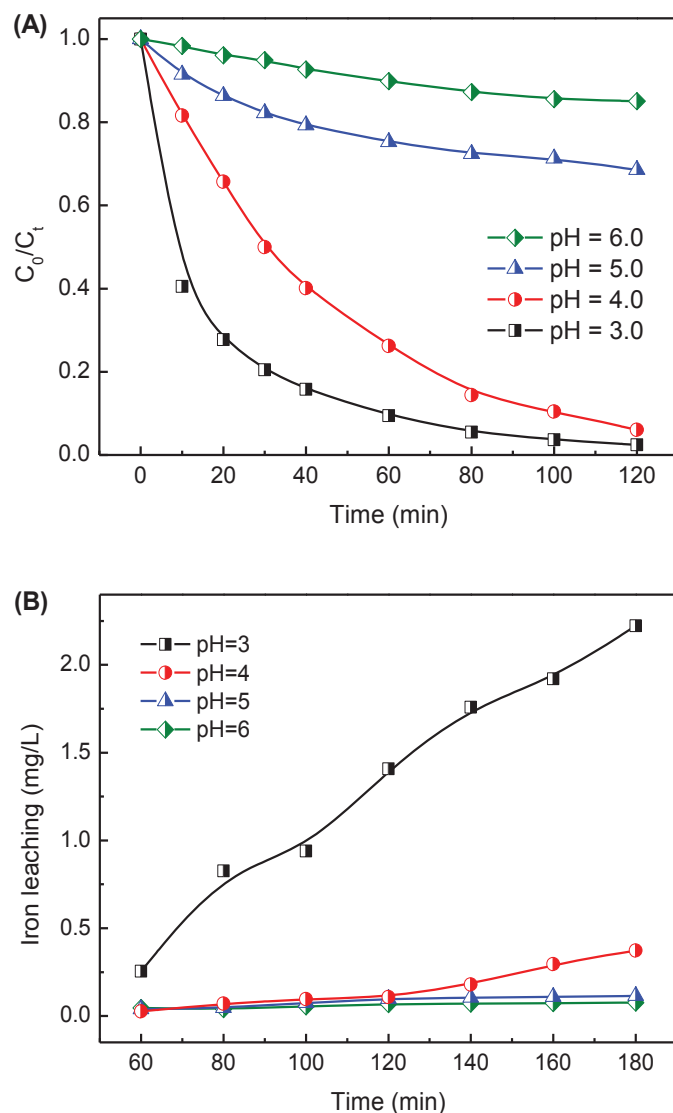


图 2-15 不同初始pH对AOII脱色率和Fe溶出的影响

Fig. 2-15 Effect of initial solution pH on the degradation of AOII and on the iron leaching (Fe-SC: 2.0 g/L; H_2O_2 : 15 mM; AOII: 100 mg/L; reaction temperature: 30°C)

考虑到污泥组分的复杂性，用 ICP-OES 对滤液中可能存在的其他金属离子溶度也进行了测定。在初始 pH=4.0 的反应体系中还检测出 0.813 mg/L Ca, 0.271 mg/L Mg, 及低浓度的 0.029 mg/L Cu, 0.027 mg/L Zn, 此外溶液中的 Cr、Mn、Ni、Pb 浓度均低于 ICP-OES 的检测下限。为了确定均相反应对 AOII 脱色率的贡献情况，将 2.0 g/L Fe-SC 催化剂加入初始 pH=4.0 的蒸馏水中振荡 120 min, 滤去催化剂，用滤液配制成 100 mg/L 的 AOII 溶液，之后加入 15 mM H_2O_2 开始均相 Fenton 催化反应。反应进行 120 min 后，AOII 脱色率只有 7.3%，由此可见在

初始 pH=4.0 的 Fe-SC 多相 Fenton-like 催化体系中，均相反应对总 AOII 脱色率的影响不明显。综合考虑 Fe-SC 的催化活性和催化活性组分溶出情况，后续实验中 AOII 的初始 pH 均调整为 4.0。

2.3.6. AOII 的矿化效率

图2-16显示了Fe-SC多相Fenton-like降解AOII体系中UV-Vis光谱随反应时间的变化图。从图中可以看出，水溶液中AOII在检测区域内共有4个特征吸收带：484 nm处的主吸收峰和430 nm处的肩峰，分别对应AOII氢化偶氮结构和偶氮结构的吸收。紫外光区域内的230 nm和310 nm吸收峰，则源于AOII分子结构中苯环和萘环的吸收^[67]。FeSC催化降解AO II过程中，484 nm和430 nm特征吸收带随着反应的进行迅速削弱，且在可见光区间内并无新的吸收峰出现，说明该反应能有效地破坏发色基团，使溶液脱色。

从图 2-16 中可以观察到虽然反应过程中发色基团被破坏，但紫外光区仍然有较强的吸收。可能是反应过程中生成了无色的有机小分子中间产物。为此本研究测定了溶液 COD 值随时间的变化情况。结果表明，COD 的去除率要明显滞后于 AOII 的脱色率，反应进行 120 min 后 COD 去除率只有 73.6%而 AOII 脱色率为 96.7%。可能是由于羟基自由基对小分子有机物的去除能力相对较弱^[68]。

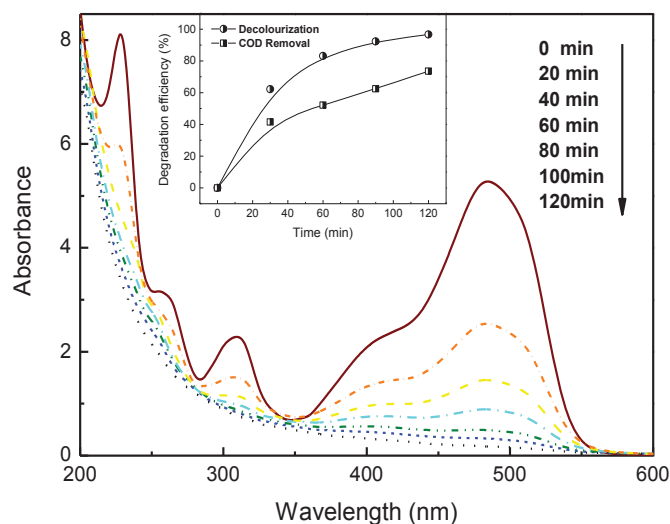


图 2-16 Fe-SC 多相 Fenton-like 催化体系中 UV-Vis 光谱变化图

Fig. 2-16. The UV-vis spectral changes of AOII (Fe-SC: 2.0 g/L; H₂O₂: 15 mM; AOII: 100 mg/L; initial pH 4.0 and reaction temperature: 30°C), inset: corresponding decolorization and COD

removal efficiency.

2.3.7. 与其他铁氧化物的催化活性比较

为了更好地评估 Fe-SC 的催化活性,本研究选取三氧化二铁(α - Fe_2O_3),四氧化三铁(Fe_3O_4)和纤铁矿(γ - FeOOH)这三种文献中经常被报道的铁氧化物,在相同 Fe 摩尔投加量和相同实验条件下,与 Fe-SC 对 AOII 的吸附及多相 Fenton-like 催化能力进行比较。结果如图 2-17 所示,经过 1 h 的吸附和 2 h 的催化反应, α - Fe_2O_3 和 Fe_3O_4 体系中 100 mg/L 的 AOII 总去除率只有 3.4%和 4.7%,活性较高的 γ - FeOOH 体系也只达到 23.5%的去除率,而在 Fe-SC 体系中 AOII 的总去除率可达 93.5%。可见所选三种铁氧化物对 AOII 的吸附及催化能力都远远低于 Fe-SC 催化剂。

Fe-SC 表现出较好的催化性能有以下几点原因:首先,研究表明 Fenton-like 催化剂的催化活性随着催化剂颗粒直径的减小将显著增大。铁盐的负载化能够有效地分散活性位点,XRD 结果表明 Fe-SC 中的 Fe_3O_4 呈纳米级,而另外 3 种商品铁氧化物均为微米级。其次,污泥碳载体复杂的有机和无机组分会改变催化剂的物理化学性质,从而影响其多相 Fenton-like 的催化活性。

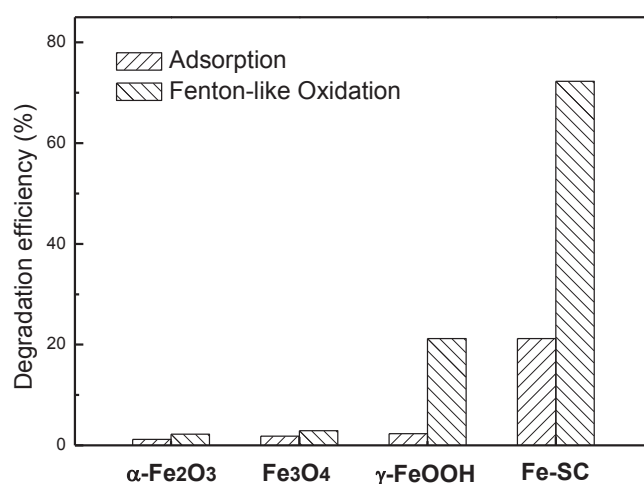


图 2-17 相同摩尔量的铁系催化剂对 AOII 的吸附及催化降解效率比较

Fig. 2-17. Comparison of the adsorption and heterogeneous Fenton-like catalytic activity by using various compounds (the iron concentrations are all 0.258 g/L; H_2O_2 : 15 mM; AOII: 100 mg/L; reaction temperature: 30°C, adsorption for 60 min and Fenton-like oxidation for 120 min).

2.3.8. 污泥碳载体的助催化作用研究

2.3.8.1. 木炭/铁氧化物复合催化剂 FeWC 的表征

为了研究污泥碳作为多相Fenton-like催化剂载体，对催化剂活性的影响，本研究选取无机组分含量较少的生物质材料——木屑，作为载体，同样用“一步法”将铁氧化物负载于木屑炭结构中，表2-7给出了制备所得的FeWC催化剂及其载体WC的部分物理化学性质。

表 2-7 WC与FeWC的部分物理化学性质

Table 2-7. Physicochemical properties of WC and FeWC.

Sample	Fe (wt %)	Ash (wt %)	\bar{d}_v^a (μm)	S_{BET} (m^2/g)	pH_{IEP}
WC	0.5	4.6	29.6	10.4	3.1
FeWC	16.2	26.3	26.7	12.1	3.1

^a \bar{d}_v : volume average particle diameter

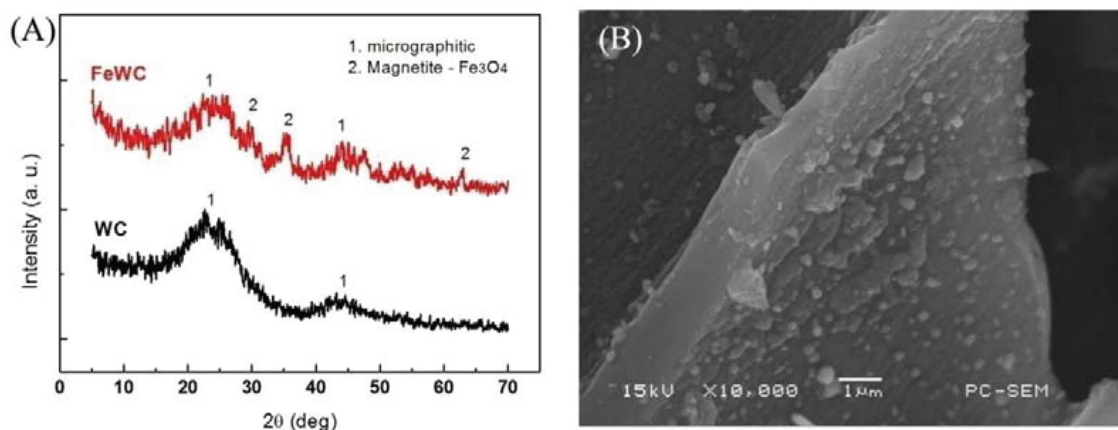


图 2-18 木炭衍生催化剂 WC 和 FeWC 的 XRD 谱图(A)及 FeWC 的 SEM 图(B)

Fig. 2-18. XRD patterns of WC and FeWC (A) and SEM image of FeWC (B).

与表 2-6 中 SC 及 FeSC 的相关参数比较，可以发现木屑炭及其复合催化剂的灰分含量较低，表明其含有很低的无机组分。负载铁氧化物的 FeSC 和 FeWC 催化剂中 Fe 的含量相近，分别为 12.9%和 16.2%。与 SC 复杂的 XRD 图谱相比，WC 的 XRD 衍射图中（图 2-18 A）只观察到 $2\theta = 26.4^\circ$ 和 44.4° 附近存在归属于

无定型碳的特征衍射峰,这也再一次证实了 WC 中含有很低的无机组分。从 FeWC 的 XRD 谱图中可以看出 Fe 是以 Fe_3O_4 的形态存在。此外,本研究还用 SEM 对 FeWC 催化剂的表面形貌进行表征,如图 2-18 B 中所示,由于植物纤维的碳化使得 FeWC 呈现片层状结构,表面分布着不均匀的球形颗粒。

2.3.8.2. FeSC与FeWC催化活性的比较研究

在催化剂投加量均为 2.0 g/L, H_2O_2 用量为 15 mM, AOII 初始浓度为 100 mg/L, 初始 pH=4.0, 反应温度为 30°C 的实验条件下, 分别考察 FeSC 和 FeWC 对 AOII 的吸附能力及多相 Fenton-like 催化活性。

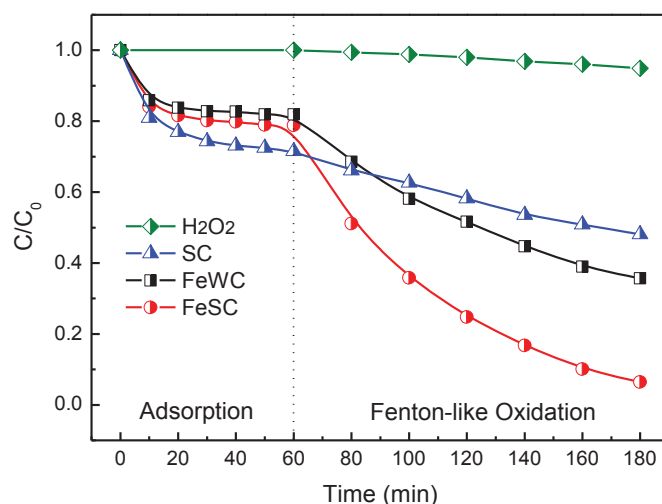


图 2-19 加入 H_2O_2 和不同催化剂对 AOII 的去除情况

Fig. 2-19. Degradation of AOII through adsorption and oxidation by hydrogen peroxide and different catalysts (Catalysts: 2.0 g/L; H_2O_2 : 15 mM; AOII: 100 mg/L; reaction pH: 4.0 ± 0.1 ; reaction temperature: 30°C).

图 2-19 可知,在催化剂投加量均为 2.0 g/L 的情况下,在吸附阶段,FeSC 和 FeWC 对 AOII 的去除率分别为 21.9%和 17.8%。这一差距主要源于 FeWC 较低的比表面积。Fenton-like 反应进行 2 h 后,FeWC 体系中的 AOII 脱色率为 66.2%,远远低于 FeSC 体系的 94.6%。通过一级动力学分别对 FeWC 和 FeSC 两个体系中催化反应的数据进行拟合(表 2-8),得表观速率常数分别为 $7.31\times 10^{-3} \text{ min}^{-1}$ 和 $22.45\times 10^{-3} \text{ min}^{-1}$,后者约为前者的 3 倍。同时为了避免因为催化体系中 Fe 含量

不同而导致催化效果的差异，本研究考察了 FeWC 催化剂用量为 1.556 g/L（与 2.000 g/L FeSC 体系具有相同的 Fe 摩尔投加量）的反应体系对 AOII 的脱色情况。结果表明经过 60 min 吸附及 120 min 催化反应，AOII 的去除率分别仅为 13.6% 和 50.2%，亦明显低于 FeSC 体系的相应值。由于 FeSC 与 FeWC 的粒径分布、比表面积、pH_{IEP} 基本相同，且负载的铁氧化物均以 Fe₃O₄ 的形式存在，由此可以推测两种催化剂催化活性的差异可能来源于载体中不同含量的无机组分。

表 2-8 不同催化剂对 AOII 的吸附及催化效果及催化反应一级动力学拟合结果

Table 2-8. Discoloration of AOII with H₂O₂ in the presence of different catalysts.

Sample	Discoloration efficiency of AOII (%)		Pseudo first-order model parameters	
	By adsorption, t = 60 min	By oxidation, t = 180 min	kap ($\times 10^{-3} \text{ min}^{-1}$)	R ²
H ₂ O ₂	0	5.1	0.44	0.9850
SC	26.9	48.8	2.98	0.9973
FeSC	22.8	94.6	22.45	0.9972
FeWC	17.8	66.2	7.31	0.9987
SC-A	5.0	11.2	0.57	0.9975
FeSC-A	19.8	51.3	4.21	0.9875
SiSC-A	2.8	8.6	0.63	0.9964
AlSC-A	6.6	14.8	0.81	0.9904
FeSiSC-A ₁	14.2	59.8	6.00	0.9804
FeSiSC-A ₂	13.8	68.8	8.44	0.9885
FeSiSC-A ₃	13.4	80.5	12.41	0.9765
FeAlSC-A ₁	22.1	65.7	6.71	0.9988
FeAlSC-A ₂	39.7	77.7	8.17	0.9870
FeAlSiSC-A	34.8	89.9	15.11	0.9917
FeAlSi	8.5	39.6	3.39	0.9977

2.3.8.3. 污泥碳中 SiO₂ 和 Al₂O₃ 的助催化作用研究

为了验证以上推测，本节中先将污泥中的无机组分利用特殊的方法去除，获得灰分含量仅为4.3%的干污泥SS，之后通过热解和一步法在800°C下制备低灰分含量的污泥碳催化剂SC-A和负载铁氧化物的FeSC-A催化剂。他们的部分物理化学性质列于表2-9中。由表中可以得知SC-A的灰分仅为10.0%，与SC的68.5%相比，SC-A的灰分明显降低。且SC-A和FeSC-A中的Si及Al含量也大大减少。SC-A和FeSC-A对AOII的吸附和催化效果如图2-20中曲线B、C所示，实验结束时AOII的去除率分别为11.2%和51.3%，伪一级动力学常数只有 $5.9 \times 10^{-4} \text{ min}^{-1}$ 和 $4.2 \times 10^{-3} \text{ min}^{-1}$ （表2-8），均远远低于FeSC的相应值。该对比实验进一步证实了SC中的无机成分在多相Fenton-like催化反应中具有一定的助催化作用。

表 2-9 去灰分污泥碳复合催化剂的物理化学性质

Table 2-9. Physicochemical properties of different catalysts.

Sample	Fe (wt %)	Al (wt %)	Si (wt %)	Ash (wt %)	S _{BET} (m ² /g)	Zeta potential at pH 4.0 (mV)	pH _{IEP}
SC-A	1.50	0.13	2.50	10.02	13.7	-17.16	3.13
FeSC-A	19.45	0.06	1.21	39.97	21.1	-16.84	3.21
SiSC-A	0.93	0.08	13.68	39.32	12.2	-26.44	2.64
AlSC-A	0.82	9.66	1.29	28.65	18.3	-11.81	3.51
FeSiSC-A ₁	20.38	0.07	6.31	48.89	19.2	-20.15	3.06
FeSiSC-A ₂	19.53	0.06	11.09	49.92	16.5	-21.46	2.94
FeSiSC-A ₃	18.43	0.06	16.28	55.42	13.1	-24.53	2.37
FeAlSC-A ₁	17.24	4.04	1.07	44.92	15.8	-8.16	3.56
FeAlSC-A ₂	16.83	7.88	1.04	45.99	21.9	-0.85	3.82
FeAlSiSC-A	15.92	7.45	8.70	55.03	17.3	-10.74	2.98
FeAlSi	29.81	14.40	15.01	90.35	6.1	4.12	5.24

根据之前的ICP-OES分析结果可知SC中的无机元素，除了Fe外，主要还有Si和Al。XRD测试结果表明Si和Al主要以SiO₂和Al₂O₃的形式存在于SC中。经过计算，SC催化剂中SiO₂和Al₂O₃的含量大约为22%和16%，而且其总含量占除去铁氧化物之外无机组分的73%。预示着这两种无机物可能在污泥碳复合催化剂的多

相Fenton-like反应中起着不容忽视的作用。

为了进一步研究污泥碳中SiO₂和Al₂O₃的助催化作用,本研究以去灰分的污泥SS-A为原料,制备了负载不同比例SiO₂和Al₂O₃的催化剂,他们的物理化学性质列于表2-9中。

本研究首先对未负载铁氧化物的SiSC-A和AISC-A对AOII的吸附能力和催化活性进行考察。经过1 h吸附和2 h催化反应后, SiSC-A和AISC-A体系中AOII的脱色率分别为8.6%和14.8% (图2-20中曲线A和图2-22中曲线A)。由此可见SiSC-A和AISC-A不能有效地催化H₂O₂降解AOII。

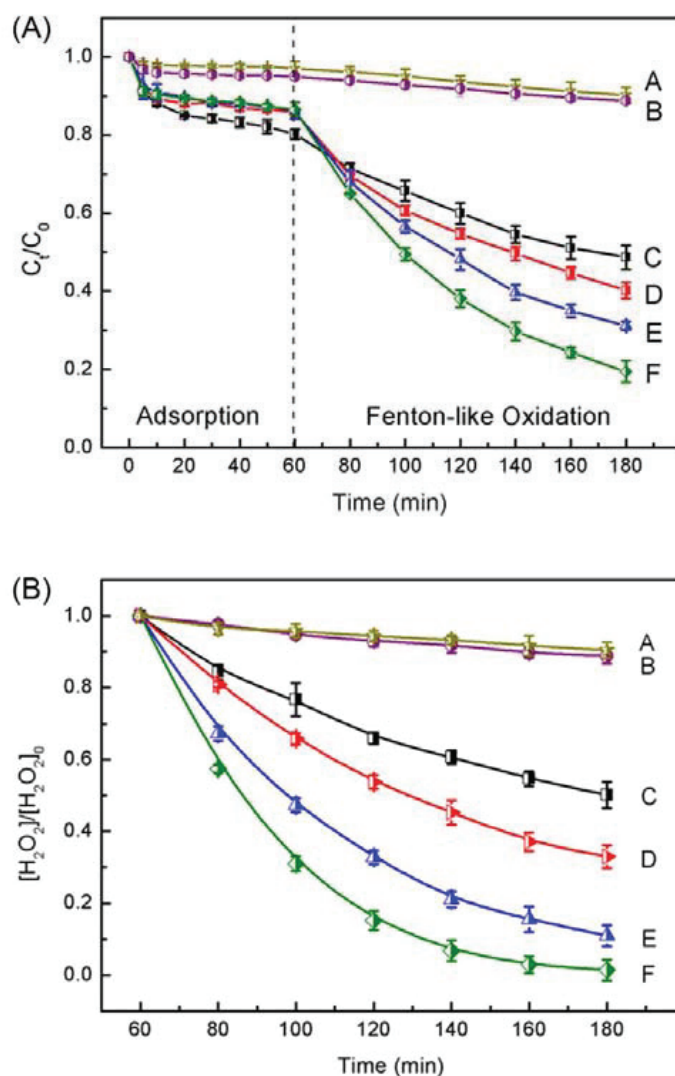


图 2-20 不同 SiO₂ 含量的污泥碳复合催化剂对 AOII 的去除效果(A)及催化 H₂O₂ 分解率(B)

Fig. 2-20. Effect of SiO₂ content in FeSC on AOII removal (A) and H₂O₂ consumption (B) (the

iron concentrations are all 0.2588 g/L: (A) SiSC-A: 1.6085 g/L, (B) SC-A: 1.2882 g/L, (C) FeSC-A: 1.3306 g/L, (D) FeSiSC-A₁: 1.2699 g/L, (E) FeSiSC-A₂: 1.3251 g/L, (F) FeSiSC-A₃: 1.4042 g/L; H₂O₂: 15 mM; AOII: 100 mg/L; reaction pH: 4.0±0.1; reaction temperature: 30°C).

如图 2-20 A 所示, 在 Fe 投加量相同的前提下比较了负载不同含量 SiO₂ 的一系列催化剂对 AOII 的吸附及催化能力, 实验结束时体系中 AOII 的去除率大小顺序为 FeSiSC-A₃ > FeSiSC-A₂ > FeSiSC-A₁ > FeSC-A, 与催化剂中 SiO₂ 的含量高低相一致。由图 2-20 B 可知反应过程中溶液里游离的 H₂O₂ 浓度也随着 FeSiSC-A 系列催化剂中 SiO₂ 含量的增加而降低。以上实验表明污泥碳 SC 载体的助催化作用很大程度来源于 SiO₂ 或类似的无机组分。

SiO₂ 的助催化机理可从以下几方面进行阐释: 一方面, SiO₂ 表面的硅氧烷键 (Si-O-Si) 中氧原子具有较强的电负性, 容易与 H₂O₂ 形成氢键^[69], 从而有利于 H₂O₂ 分子在 FeSC 催化剂表面的吸附, 加速 Fenton-like 反应。另一方面, 二氧化硅表面还存在大量硅醇键(Si-OH)^[70], 当溶液 pH 低于 SiO₂ 的 p*H*_{IEP} 时, Si-OH 键将发生质子化, 相反地, 当溶液 pH 高于 SiO₂ 的 p*H*_{IEP} 时则发生去质子化反应^[71,72]。据文献中报道, SiO₂ 的 p*H*_{IEP} 为 2.0-3.5^[73,74], 本实验中溶液的 pH 为 4.0, 因此在实验过程中 Si-O-H 键中的 H 将发生解离, 最终形成带负电的 SiO₂ 颗粒以及其表面 H⁺ 浓度较高的微酸性环境^[74], 如图 2-21 所示。为了证实这一解释的合理性, 本研究测定了含 SiO₂ 的一系列催化剂在溶液 pH=4.0 中的 Zeta 电位值, 由表 2-9 中的数值可知催化剂的电负性随着 SiO₂ 含量的增加而增强, 同时 p*H*_{IEP} 也随之降低。而低的 pH 有利于 H₂O₂ 分解产生 •OH, 且在 pH 为 3.0 左右, •OH 表现出最佳的催化活性^[76]。因此, SC 中 SiO₂ 组分主要通过增加 H₂O₂ 在催化剂表面的吸附和在催化剂表面形成微酸性环境两个途径来加速 H₂O₂ 催化分解产生 •OH, 从而促进 Fenton-like 反应的进行。

为了研究 SC 中铝氧化物在 Fenton-like 反应中的作用, 本研究制备了两种不同 Al₂O₃ 含量的 FeAlSC-A 系列催化剂, 并比较它们对 AOII 的吸附及催化性能。图 2-22 中可以看出吸附 1 h 后 FeSC-A、FeAlSC-A₁ 和 FeAlSC-A₂ 对 AOII 的吸附率分别为 18.2%、21.1%和 39.7%。三种催化剂对 AOII 吸附能力的差别可从不同的比表面积 S_{BET} 和 p*H*_{IEP} 得到解释。由于 Al₂O₃ 的 p*H*_{IEP} 为 8.5-10.4^[72], 而 SC-A

的 pH_{IEP} 较低, 只有 3.1, 因此在 SC-A 中负载 Al_2O_3 将使催化剂的 pH_{IEP} 值升高, 表面呈现更低的电负性, 从而有利于吸附带有 $-SO_3^-$ 基团的 AOII 染料分子。

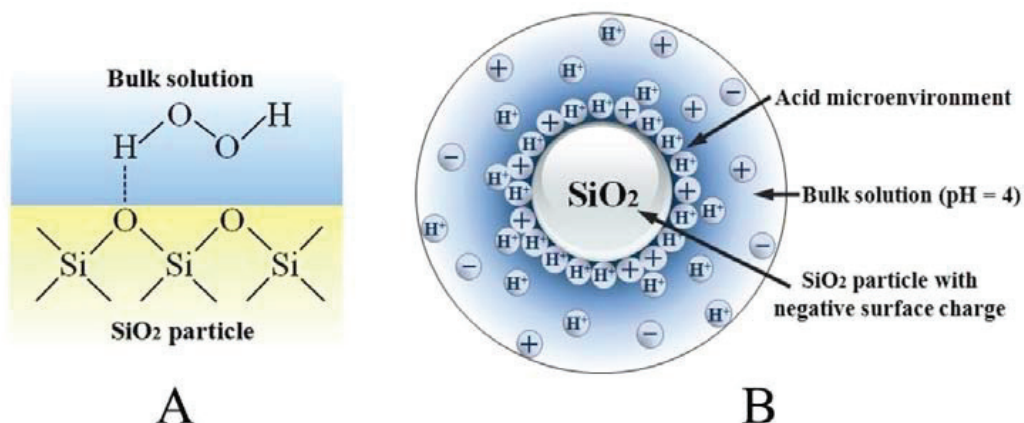


图 2-21 H_2O_2 在 SiO_2 表面通过氢键吸附(A); SiO_2 表面的酸性微环境示意图(B)

Fig. 2-21. H_2O_2 adsorb over siloxane by hydrogen bonds (A) and acidic microenvironment form near the surface of SiO_2 particle (B).

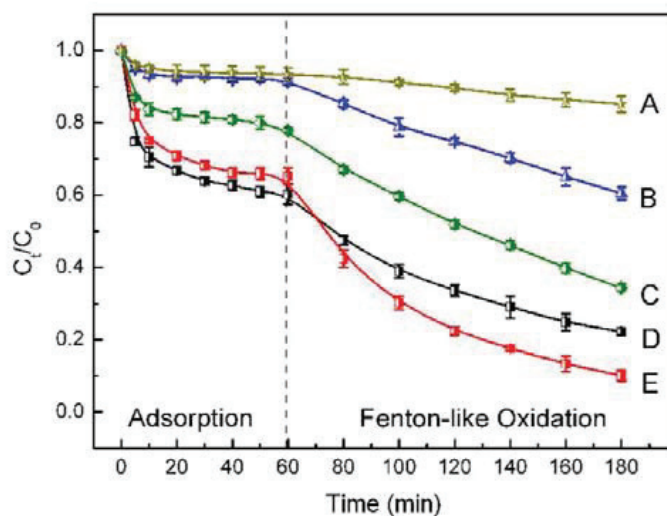
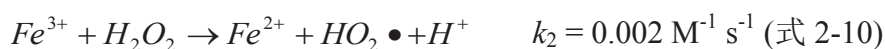


图 2-22 负载 Al_2O_3 的污泥碳复合催化剂对 AOII 的去除情况

Fig. 2-22. Degradation of AOII through adsorption and oxidation in the presence of Al_2O_3 -containing catalysts (the iron concentrations are all 0.2588 g/L: (A) AISC-A: 1.9540 g/L, (B) FeAlSi: 0.8682 g/L; (C) FeAISC-A₁: 1.5012 g/L, (D) FeAISC-A₂: 1.5377 g/L, (E) FeAlSiSC-A: 1.6256 g/L; H_2O_2 : 15 mM; AOII: 100 mg/L; reaction pH: 4.0 ± 0.1 ; reaction

temperature: 30 °C).

在催化阶段, Al_2O_3 的负载, 也一定程度地使催化剂的活性得到提高。经拟合, FeAlSC-A_1 和 FeAlSC-A_2 的一级动力学反应速率常数分别为 $6.71 \times 10^{-3} \text{ min}^{-1}$ 和 $8.17 \times 10^{-3} \text{ min}^{-1}$ 。从表 2-9 中可知 FeAlSC-A 系列催化剂的表面电负性和 pH_{IEP} 值要高于 FeSiSC-A 系列催化剂, 因此负载 Al_2O_3 的催化剂表面酸性并没有 FeSiSC-A 明显, 意味着 Al_2O_3 存在着与 SiO_2 不同的助催化机理。Timofeeva 等人通过在催化剂表面吸附氘代氯仿 (CDCl_3) 证实了在含 Fe 的催化剂中负载 Al 组分能够增加催化剂的碱性, 催化剂碱性的增加能够加速 H_2O_2 的分解, 从而使催化剂的催化活性得到提高^[76]。这一解释也与本研究实验中 FeAlSC-A 系列催化剂较高的 pH_{IEP} 值这一实验结果相一致。另一方面, 对于 Fenton 反应, 其限速步骤为 Fe^{3+} 向 Fe^{2+} 的转化(式 2-10), 而 Al 作为 Lewis 酸, 具有较强的吸电子能力, 使得 Fe^{3+} 变得不稳定, 有利于 Fe^{3+} 转化为 Fe^{2+} ^[77]。



由于 SiO_2 具有比 Al_2O_3 , 更低的 pH_{IEP} 值, 所以在 FeAlSiSC-A_2 中负载 SiO_2 将使得催化剂 FeAlSiSC-A 在 $\text{pH}=4.0$ 的水溶液中表现出更强的电负性, 导致对 AOII 吸附能力减小。但是从图 2-22 中可发现在催化阶段, FeAlSiSC-A 表现出比 FeAlSC-A_2 更高的催化活性, 其伪一级动力学反应速率常数为 $1.511 \times 10^{-2} \text{ min}^{-1}$, 相当于 FeAlSC-A_2 和 FeSiSC-A_2 的 1.8 倍。该对比实验再一次证实 SC 中的 SiO_2 和 Al_2O_3 组分能增加 Fenton-like 催化剂的催化活性。

为了探讨污泥碳载体中碳组分的作用, 我们参照制备 FeAlSiSC-A 催化剂时各组分的用量, 在不使用 SS-A 的情况下, 制备了无污泥碳的纯 FeAlSi 复合催化剂, 并对其催化活性进行研究。为了使 FeAlSi 和 FeAlSiSC-A 两个催化体系中的 Fe, Al 和 Si 含量相近, 催化剂的投加量分别为 0.8682 g/L 和 1.6256 g/L 。从图 2-22 曲线 B 可以看出 FeAlSi 对 AOII 的吸附和催化能力要远远低于 FeAlSiSC-A 。催化反应速率常数只有 $3.39 \times 10^{-3} \text{ min}^{-1}$ 。该实验结果证明污泥碳中的碳组分在 Fenton-like 催化过程中起到不容忽视的作用。一方面, 孔隙较发达的碳组分对含苯环的污染物具有较强的吸附能力, 能将溶液中的 AOII 分子吸附于催化剂表面,

而污染物在活性位点附近的浓缩能够增大对羟基自由基的利用率^[78]，另一方面，由于碳组分的存在，能防止负载的铁盐及其他无机氧化物在热解过程中发生团聚，从而增加活性组分在载体中的分散度。

2.4. 小结

本章以污泥碳为载体，通过“一步法”成功地制备了负载铁氧化物的污泥碳复合多相Fenton-like催化剂Fe-SC。通过TG-FTIR分析技术对其制备过程中的热解特性进行研究，并使用BET、SEM、EDX等表征手段对FeSC催化剂进行表征。在多相Fenton-like催化氧化反应中，通过测定污泥碳复合催化剂FeSC对偶氮染料AOII的降解情况来评价催化剂活性的高低。此外，本章还深入探讨了污泥碳作为多相Fenton-like催化剂载体时在催化反应中所起的特殊作用。研究结果表明：

- (1) 当热解温度为800°C时，污泥硫酸亚铁混合物能够热解完全且所得的Fe-SC具有最好的Fenton-like催化活性。Fe-SC中铁氧化物主要以Fe₃O₄的形式均匀分布于污泥碳载体中。与传统的“两步法”相比，“一步法”能更有效地避免反应过程中的铁盐溶出，从而使制备所得催化剂具有更高的稳定性。Fe-SC在催化剂投加量为2.0 g/L，H₂O₂用量为15 mM，溶液初始pH为4.0时对100 mg/L的AOII溶液具有最好的去除率。经过1 h吸附和2 h催化反应后，反应体系对AOII的脱色率可达96.7%，COD去除率为73.6%，且仅有0.37 mg/L的Fe溶出。同时滤液中还检测到0.81 mg/L Ca, 0.27 mg/L Mg, 及低浓度的0.03 mg/L Cu, 0.03 mg/L Zn,未检测到Cr、Mn、Ni、Pb。通过对反应热力学研究计算得反应的活化能为25.8 kJ/mol，符合羟基自由基的反应特点。
- (2) 与其他铁氧化物(α -Fe₂O₃, Fe₃O₄和 γ -FeOOH)相比，Fe-SC具有更高的催化活性，同时与负载铁氧化物的木屑炭复合催化剂FeWC相比，Fe-SC的表观速率常数约为FeWC的3倍。由于Fe-SC灰分高达90%左右，表明含有较高的无机组分。为了研究这些无机组分对Fenton-like催化的影响，用去灰分的污泥SS-A为载体，通过“一步法”制备了Fe、Si、Al含量不同的一系列催化剂。结果表明当污泥碳SC中的无机组分被去除后，所制备的负载铁氧化物污泥碳催化剂FeSC-A的催化活性明显低于FeSC。当在SC-A中同时负载Fe及不同比例的

SiO₂和Al₂O₃时，催化剂的催化活性在一定范围内随着SiO₂和Al₂O₃的含量增加而升高。由此可见污泥碳中SiO₂和Al₂O₃在Fenton-like反应中起助催化作用。SC中SiO₂组分主要通过增加H₂O₂在催化剂表面的吸附和在催化剂表面形成微酸性环境两个途径来加速H₂O₂催化分解产生·OH，从而促进Fenton-like反应的进行。SC中的Al₂O₃能够增加催化剂的碱性，加速H₂O₂的分解。另外Al的Lewis酸特性能使Fe³⁺电子云变得不稳定，从而促进Fe³⁺向Fe²⁺转化。污泥碳载体中碳组分一方面有利于污染物和H₂O₂在催化剂表面的吸附，另一方面能防止热解过程中负载的铁盐及其他无机氧化物发生团聚，从而增加活性组分在载体中的分散度。

2.5. 参考文献

- [1] Fenton H J H. Oxidation of tartaric acid in the presence of iron. *Chem. Soc. Trans.*, 1984, 65: 899-910
- [2] 向罗京. 非均相 Fenton 反应催化剂的制备及其在难降解有机物处理中的应用. 博士学位论文. 武汉大学. 3. 2009
- [3] Eisenhouser H R. Oxidation of phenolic waste water. *J. WPCF*, 1964
- [4] Duesterberg C K, Mylon S E, Waite T D. pH Effects on iron-catalyzed oxidation using Fenton's reagent. *Environ. Sci. Technol.*, 2008, 42: 8522-8527
- [5] Bautista P, Mohedano A F, Casas J A, Zazo J A, Rodriguez J J. An overview of the application of Fenton oxidation to industrial wastewaters treatment. *J. Chem. Technol. Biotechnol.*, 2008, 83: 1323-1338
- [6] Feng J, Hu X, Yue P L. Novel bentonite clay-based Fe-nanocomposite as a heterogeneous catalyst for photo-Fenton discoloration and mineralization of Orange II. *Environ Sci Technol*, 2004, 38: 269-275
- [7] 张德莉, 黄应平, 罗光富, 刘德富, 马万红, 赵进才. Fenton 及 Photo-Fenton 反应研究进展. *环境化学*, 2006, 25: 121-127
- [8] Lu M C, Chen J N, Huang H H. Role of goethite dissolution in the oxidation of 2-chlorophenol with hydrogen peroxide. *Chemosphere*, 2002, 46: 131-136
- [9] Barreiro J C, Capelato M D, Oxidative decomposition of atrazine by a

- Fenton-like reaction in a H₂O₂/ferrihydrite system. *Water Res.*, 2007, 41: 55-62
- [10] Sun S P, Lemley A T. p-Nitrophenol degradation by a heterogeneous Fenton-like reaction on nano-magnetite: Process optimization, kinetics, and degradation pathways. *J. Mol. Catal. A: Chem.*, 2011, 349: 71-79
- [11] Pereira M C, Oliveira L C A, Murad E. Iron oxide catalysts: Fenton and Fenton-like reactions - a review. *Clay Miner.*, 2012, 47: 258-302
- [12] Usman M, Faure P, Ruby C, Hanna K. Remediation of PAH-contaminated soils by magnetite catalyzed Fenton-like oxidation. *Appl. Catal. B: Environ.*, 2012, 117-118: 10-17
- [13] Costa R C C, Lelis M F F, Oliveira L C A, Fabris J D, Ardisson J D, Rios R R V A, Silva C N, Lago R M. Novel active heterogeneous Fenton system based on Fe_{3-x}M_xO₄ (Fe, Co, Mn, Ni): The role of M²⁺ species on the reactivity towards H₂O₂ reactions. *J. Hazard. Mater.*, 2006, 129: 171-178
- [14] Xu L, wang J. Fenton-like degradation of 2,4-dichlorophenol using Fe₃O₄ magnetic nanoparticles. *Appl. Catal. B: Environ.* 2012, 123-124: 117-126
- [15] Hu X B, Liu B Z, Deng Y H, Chen H Z, Luo S, Sun C, Yang P, Yang S G. Adsorption and heterogeneous Fenton degradation of 17 alpha-methyltestosterone on nano Fe₃O₄/MWCNTs in aqueous solution. *Appl. Catal. B: Environ.*, 2011, 107: 274-283
- [16] Matatov-Meytal Y I, Sheintueh M. Catalytic abatement of water pollutants. *Ind. Eng. Chem. Res.*, 1998, 37: 309-326
- [17] 邓景衡. FeVO₄超细粉体的 Fenton-like 和光 Fenton-like 催化活性研究. 博士学位论文. 中山大学. 12. 2008
- [18] Fernandez J, Bandara J, Kiwi J, Lopez A, Albers P. Efficient photo-assisted Fenton catalysis mediated by Fe ions on Nafion membranes active in the abatement of non-biodegradable azo-dye. *Chem. Commun.*, 1998, 14: 1493-1494
- [19] Dhananjeyan R, Kiwi J, Albers P, Enea O. Photo-assisted immobilized Fenton degradation up to pH 8 of azo dye orange II mediated by Fe³⁺/Nafion/Glass Fibers. *Helvi. Chim. Acta.*, 2001, 84: 3433-3445
- [20] Parra S, Guasaquillo I, Enea O, Mielczarski E, Mielczarki J, Albers P, Kiwi-Minsker L, Kiwi J. Abatement of an azo dye on structured C-Nafion /Fe-ion surfaces by photo-Fenton reactions leading to carboxylate inter mediates

- with a remarkable biodegradability increase of the treated solution. *J. Phys. Chem. B*, 2003, 107: 7026-7035
- [21] Feng J Y, Hu X J, Yue P L. Degradation of salicylic acid by photo-assisted Fenton reaction using Fe ions on strongly acidic ion exchange resin as catalyst. *Chem. Eng. J.*, 2004, 100: 159-165
- [22] Aleksić M, Kušić H, Koprivanac N, Leszczynska D, Božić A L. Heterogeneous Fenton type processes for the degradation of organic dye pollutant in water - The application of zeolite assisted AOPs. *Desalination*, 2010, 257: 22-29
- [23] Botas J A, Melero J A, Martínez F, Pariente M I. Assessment of Fe₂O₃/SiO₂ catalysts for the continuous treatment of phenol aqueous solutions in a fixed bed reactor. *Catal. Today*, 2010, 149: 334-340
- [24] Zhang Q, Jiang W F, Wang H L, Chen M D. Oxidative degradation of dinitro butyl phenol (DNBP) utilizing hydrogen peroxide and solar light over a Al₂O₃-supported Fe(III)-5-sulfosalicylic acid (ssal) catalyst. *J. Hazard. Mater.*, 2010, 176: 1058-1064
- [25] Garrido-Ramírez E G, Theng B K G, Mora M L. Clays and oxide minerals as catalysts and nanocatalysts in Fenton-like reactions - a review. *Appl. Clay Sci.*, 2010, 47: 182-192
- [26] Zazo J A, Casas J A, Mohedano A F, Rodríguez. Catalytic wet peroxide oxidation of phenol with a Fe/active carbon catalyst. *Appl. Catal. B: Environ.*, 2006, 65: 261-268
- [27] Castro C S, Guerreiro M C, Oliveira L C A, Goncalves M, Anastacio A S, Nazzarro M. Iron oxide dispersed over activated carbon: Support influence on the oxidation of the model molecule methylene blue. *Appl. Catal. A: Genl.*, 2009, 367: 53-58
- [28] Flores Y, Flores R, Gallegos A A. Heterogeneous catalysis in the Fenton-type system reactive black 5/H₂O₂. *J. Mol. Catal. A: Chem.*, 2008, 281: 184-191
- [29] Adam F, Kandasamy K, Balakrishnan S. Iron incorporated heterogeneous catalyst from rice husk ash. *J. Colloid Interface Sci.*, 2006, 304: 137-143
- [30] Costa R C C, Moura F C C, Oliveira P E F, Magalhães F, Ardisson J D, Lago R M. Controlled reduction of red mud waste to produce active systems for environmental applications: Heterogeneous Fenton reaction and reduction of Cr (VI). *Chemosphere*, 2010, 78: 1116-1120

- [31] Marques R N N, Stüber F, Smith K M, Fabregat A, Bengoa C, Font J, Fortuny A, Pullket S, Fowler G D, Graham N J D. Sewage sludge based catalysts for catalytic wet air oxidation of phenol: Preparation, characterisation and catalytic performance. *Appl. Catal. B: Environ.*, 2011, 101: 306-316
- [32] Jones-Lepp T L, Stevens R. Pharmaceuticals and personal care products in biosolids/sewage sludge: the interface between analytical chemistry and regulation. *Anal. Bioanal. Chem.*, 2007, 387: 1173-1183
- [33] Fumoto E, Mizutani Y, Tago T, Masuda T. Production of ketones from sewage sludge over zirconia-supporting iron oxide catalysts in a steam atmosphere. *Appl. Catal. B: Environ.*, 2006, 68: 154-159
- [34] Rio S, Coq L Le, Faur C, Cloirec P Le. Production of porous carbonaceous adsorbent from physical activation of sewage sludge: application to wastewater treatment. *Water Sci. Technol.*, 2006, 53: 237-244
- [35] Malerius O, Werther J. Modelling the adsorption of mercury in the flue gas of sewage sludge incineration. *Chem. Eng. J.*, 2003, 96: 197-205
- [36] Villaseñor J, Rodríguez L, Fernández F J. Composting domestic sewage sludge with natural zeolites in a rotary drum reactor. *Bioresour. Technol.*, 2011, 102: 1447-1454
- [37] Werle S, Wilk R K. A review of methods for the thermal utilization of sewage sludge: the Polish perspective. *Renew. Energ.*, 2010, 35: 1914-1919
- [38] Jin B, Li B. Comprehensive utilization of sewage sludge in municipal wastewater treatment plant. *Environ. Sci. Manage.*, 2010, 35: 106-109
- [39] Bagreev A, Bandosz T J, Locke D C. Pore structure and surface chemistry of adsorbents obtained by pyrolysis of sewage sludge-derived fertilizer. *Carbon*, 2001, 39: 1971-1979
- [40] Martin M J, Serra E, Ros A, Balaguer M D, Rigola M. Carbonaceous adsorbents from sewage sludge and their application in a combined activated sludge-powdered activated carbon (AS-PAC) treatment. *Carbon*, 2004, 42: 1389-1394
- [41] Hsiu-Mei C, Ting-Chien C, San-De P, Hung-Lung C. Adsorption characteristics of Orange II and Chrysophenine on sludge adsorbent and activated carbon fibers. *J. Hazard. Mater.*, 2009, 161: 1384-1390

- [42] Ansari A, Bandosz T J. Inorganic-organic phase arrangement as a factor affecting gas-phase desulfurization on catalytic carbonaceous adsorbents. *Environ. Sci. Technol.*, 2005, 39: 6217-6224
- [43] 上海市纺织工业局《染料应用手册》编写组. 染料应用手册. 北京: 中国纺织出版社. 1995
- [44] Oaks J, Gratton P. Kinetic investigations of azo dye oxidation in aqueous media. *J. Chem. Soc. Perkin Trans.*, 1998, 2: 2563-2568
- [45] Han Y F, Lunsford J H. A comparison of ethanol and water as the liquid phase in the direct formation of H_2O_2 from H_2 and O_2 over a palladium catalyst. *Catal. Lett.*, 2005, 99:13-19
- [46] Ferrasse J H, Chavez S, Arlabosse P, Dupuy P. Chemometrics as a tool for the analysis of evolved gas during the thermal treatment of sewage sludge using coupled TG-FTIR. *Thermochim. Acta*, 2003, 404: 97-108
- [47] Caballero J A, Front R, Marcilla A, Conesa J A. Characterization of sewage sludges by primary and secondary pyrolysis. *J. Anal. Appl. Pyrol.*, 1997, 40-41(5): 433-450
- [48] Ábrego J, Arauzo J, Sánchez J L, Gonzalo A, Cordero T, Rodríguez-Mirasol J. Structural changes of sewage sludge char during fixed-bed pyrolysis. *Ind. Eng. Chem. Res.*, 2009, 48: 3211-3221
- [49] Swamy M S R, Prasad T P, Sant B R. Thermal analysis of ferrous sulphate heptahydrate in air. *J. Therm. Anal. Calorim.*, 1979, 16: 471-478
- [50] 田娟娟, 杜慧娟, 潘秋红, 段长青, 仇厚援. 电热板消解与密闭罐消解对土壤中49种矿质元素ICP-MS法检测的影响. *分析测试学报*, 2009, 3 (28): 319-325
- [51] Duarte F, Maldonado-Hódar F J, Pérez-Cadenas A F, Madeira L M. Fenton-like degradation of azo-dye Orange II catalyzed by transition metals on carbon aerogels. *Appl Catal B: Environ.*, 2009, 85:139-147
- [52] Chanda S C, Manna A, Vijayan V, Pranaba K, Nayak M, Ashok H N. PIXE & XRD analysis of nanocrystals of Fe, Ni and Fe_2O_3 . *Materials Letters*, 2007, 61: 5059-5062.
- [53] Mekki A, Holland D, McConville C F, Salim. An XPS study of iron sodium silicate glass surfaces. *J. Non-Cryst. Solids*, 1996, 208: 267-276
- [54] Mills P, Sullivan J L. A study of the core level electrons in iron and its three

- oxides by means of X-ray photoelectron spectroscopy. *J. Phys. D: Appl. Phys.*, 1983, 16: 723-732
- [55] Yamashita T, Hayes P. Analysis of XPS spectra of Fe²⁺ and Fe³⁺ ions in oxide materials. *Appl. Surf. Sci.*, 2008, 254: 2441-2449
- [56] Wu F, Deng N, Hua H. Degradation mechanism of azo dye C. I. reactive red 2 by iron powder reduction and photooxidation in aqueous solutions. *Chemosphere*, 2000, 41(8): 1233-1238
- [57] Buxton G V, Greenstock C, Hellman W P, Ross A B. Critical review of rate constants for reactions of hydrated electrons, hydrogen atoms, and hydroxyl radicals ($\cdot\text{OH}/\cdot\text{OH}^-$) in aqueous solution. *J. Phys. Chem.* 1988,17: 513-518.
- [58] Walling C. Fenton's reagent. *Acc.Chem.Res.*, 1975, 8: 125-131
- [59] Xue X, Hanna K, Abdelmoula M, Deng N. Adsorption and oxidation of PCP on the surface of magnetite: Kinetic experiments and spectroscopic investigations. *Appl. Catal. B: Environ.*, 2009, 89: 432-440
- [60] Üstün G E, Solmaz S K A, Morsünbül T, Azak H S. Advanced oxidation and mineralization of 3-indole butyric acid (IBA) by Fenton and Fenton-like processes. *J. Hazard. Mater.*, 2010, 180: 508-513
- [61] 董永春, 何陆春, 李春辉, 张宝华, 朱红星. 活性染料的太阳光催化脱色降解研究. *四川大学学报:工程科学版*, 2005, 37 (4): 49-53
- [62] 张莉. 色谱法分析有机过氧化物的研究. *发展*, 2008, 8: 69-70
- [63] Bozzi A, Yuranova T, Lais P, Kiwi J, Degradation of industrial waste waters on Fe/C-fabrics.Optimization of the solution parameters during reactor operation. *Water Res.*, 2005, 39: 1441-1450
- [64] Panda N, Sahoo H and Mohapatra S, Decolourization of Methyl Orange using Fenton-like mesoporous Fe₂O₃-SiO₂ composite. *J. Hazard. Mater.*, 2011, 185: 359-365
- [65] Guo J, Al-Dahhan M. Catalytic wet oxidation of phenol by hydrogen peroxide over pillared clay catalyst. *Ind. Eng. Chem. Res.*, 2003, 42: 2450-2460
- [66] Tang W, Huang C. Effect of chlorinated phenols on their oxidation kinetics by Fenton's reagent. *Chemosphere*, 1996, 33 (8): 1621-1635
- [67] Zhang S J, Yu H Q, Zhao Y. Kinetic modeling of the radiolytic degradation of Acid Orange 7 in aqueous solutions. *Water Res.*, 2005, 39 (5): 839-846

- [68] Chen J, Zhu L. UV-Fenton discolouration and mineralization of Orange II over hydroxyl-Fe-pillared bentonite. *J. Photochem. Photobiol. A: Chem.*, 2007, 188: 56-64
- [69] Zegliński J, Piotrowski G P, Piękoś R. A study of interaction between hydrogen peroxide and silica gel by FTIR spectroscopy and quantum chemistry. *J. Mol. Struct.*, 2006, 794: 83-91
- [70] Clark J H. Solid acids for green chemistry. *Acc. Chem. Res.*, 2002, 35: 791-797
- [71] Kang M S, Choi Y J, Moon S H. Effects of inorganic substances on water splitting in ion-exchange membranes: II. Optimal contents of inorganic substances in preparing bipolar membranes. *J. Colloid Interface Sci.*, 2004, 273: 533-539
- [72] Wang Y H, Siu W K. Structure characteristics and mechanical properties of kaolinite soils. I. Surface charges and structural characterizations. *Can. Geotech. J.*, 2006, 43: 587-600
- [73] Mullet M, Fievet P, Reggiani J C, Pagetti J. Comparison of two electrokinetic methods-electroosmosis and streaming potential-to determine the zeta-potential of plane ceramic membranes. *J. Membrane Sci.*, 1997, 123: 255-265
- [74] Tian S H, Tu Y T, Chen D S, Chen X, Xiong Y. Degradation of Acid Orange II at neutral pH using $\text{Fe}_2(\text{MoO}_4)_3$ as a heterogeneous Fenton-like catalyst. *Chem. Eng. J.*, 2011, 169: 31-37
- [75] Chen A, Ma X, Sun H. Decolorization of KN-R catalyzed by Fe-containing Y and ZSM-5 zeolites. *J. Hazard. Mater.*, 2008, 156: 568-575
- [76] Timofeeva M N, Malyshev M E, Panchenko V N, Shmakov A N, Potapov A G, Mel'gunov M S. FeAl_{12} -Keggin type cation as an active site source for Fe,Al-silica mesoporous. *Appl. Catal. B: Environ.*, 2010, 95: 110-119
- [77] Lim H, Lee J, Jin S, Kim J, Yoon J, Hyeon T. Highly active heterogeneous Fenton catalyst using iron oxide nanoparticles immobilized in alumina coated mesoporous silica. *Chem. Commun.*, 2006, 4: 463-465
- [78] Rodríguez-Reinoso F. The role of carbon materials in heterogeneous catalysis. *Carbon*, 1998, 36: 159-175

第3章 Fe₃O₄/污泥碳复合催化剂催化湿式氧化 2-氯苯酚的研究

3.1. 引言

湿式氧化法(Wet air oxidation, 简称 WAO)是一种应用空气或分子氧作为氧化剂, 在 200-320°C 的反应温度及 2-20 MPa 的氧气压力下, 氧化处理高浓度有机废水的高级氧化技术^[1]。但由于反应温度和压力过高, 使该技术在处理实际废水中的应用受到限制。许多研究者发现当向反应体系中加入某些催化剂时, 能使湿式氧化反应在更低的温度和压力下进行, 同时又不影响污染物的去除效果, 这种方法即为催化湿式氧化法(Catalytic wet air oxidation, CWAO)。根据所使用催化剂的不同形态, 可将 CWAO 分为均相湿式催化氧化反应和非均相湿式催化氧化反应两类。与均相反应相比, 使用非均相催化剂操作更简便, 而且非均相催化剂更易于分离和回收利用。因此, 从七十年代后期开始, 该领域的研究人员就将注意力集中在研制更加高效稳定的非均相湿式氧化催化剂上。这些 CWAO 多相催化剂主要包括贵金属系列催化剂和非贵金属系列催化剂。Qin^[2]等人以活性炭、 γ -Al₂O₃ 和 CeO₂ 为载体, 制备了一系列负载贵金属 Pd、Pt 和 Ru 的催化剂, 并考察其对 4-氯苯酚的催化湿式氧化处理效果, 结果表明负载 Pt 的活性炭催化剂具有最高的催化活性。Li^[3]等考察了 Ru/ZrO₂ 和 Ru/Ce_xZr_{1-x}O₂ 对 2-CP 的湿式催化氧化活性, 在反应温度 120°C、氧气分压 0.9 MPa 的条件下, 加入 0.5g 催化剂能在 5 h 左右使 150 mL 初始浓度为 2 g/L 的 2-CP 溶液脱氯完全, 反应 24 h 后, 基本能达到完全矿化, 并且反应过程中几乎未检测到 Ru 的溶出。但是贵金属系列催化剂价格在 40-120 万元/吨, 如此高昂的价格在一定程度上限制了它在大规模实际废水处理工艺中的应用^[4]。而相比之下, 开发高效稳定的非贵金属系列催化剂则具有更好的应用前景。西班牙的 Quintanilla^[5]等人通过比较活性炭(AC)和负载 α -Fe₂O₃ 的活性炭催化剂(Fe/AC)在 CWAO 中去除苯酚的效果, 发现铁氧化物

的负载能使催化剂表面酸性位点增加,从而使催化剂具有更高的活性。委内瑞拉的 Posada^[6]等研究了 Cu/CeO₂ 催化剂在 160°C, 1.0 MPa 下对 2-CP 的湿式催化氧化能力,结果表明初始浓度为 500 mg/L 的 2-CP 在 130 min 内便可被完全降解。但是在反应结束时溶液中检测到高达 54.5 mg/L 的铜离子,相当于体系中铜的总加入量的 91 wt.%。对于过渡金属催化剂,普遍存在活性组分溶出的问题,这也是该系列催化剂未能在实际运行工艺中被使用的主要原因之一。目前对于 Cu 系列过渡金属催化剂在湿式催化氧化反应中的溶出机理已有较多报道,谭亚军^[7]等认为 Cu²⁺的溶出行为与催化剂的组成,晶形,制备条件,反应条件等都有关系。西班牙的 Santos^[8]等人还发现苯酚降解的中间产物草酸由于能与铜形成草酸铜沉淀,覆盖于催化剂表面,阻止 Cu 溶出,但同时也导致催化剂的催化活性降低。由于溶出的铜离子排入水体中会造成二次污染^[9],而相比之下,铁离子的生物毒性要比铜离子低。且铁氧化物廉价易得,湿式催化氧化活性高,具有更好的实际应用前景。

氯酚类有机物 (Chlorophenols, 简称 CPs) 属于典型的难降解有机污染物。CPs 在农药、制药业中被广泛用作原材料,同时也常被作为皮革、木材、蔬菜等的消毒和防腐剂使用。据报道,CPs 具有杀菌性、植物毒性和生物累积性,有明显的“三致”作用。此外 CPs 还属于环境内分泌干扰物,进入人体内将干扰机体甲状腺素正常的功能,而且会影响肾上腺激素的分泌^[10]。因此,世界各国高度重视氯酚类污染物的控制与处理,美国环保署将其列入 129 种重点控制污染物名单中,我国规定的 68 种环境优先控制污染物名单中也包括了氯酚类物质,如 2-氯酚(2-Chlorophenol, 缩写 2-CP)、2,4-二氯酚(2,4-Dichlorophenol, 缩写 2,4-DCP)和五氯酚(Pentachlorophenol, 缩写 PCP)等^[11]。对于 2-CP,世界卫生组织规定其在饮用水中的最大浓度不得超过 10 μg/L^[12]。在 2-CP 分子中,由于氯原子 p 轨道上的电子和苯环的 π 电子会形成稳定的共轭体系,导致其具有较强的化学稳定性。另一方面,由于氯原子的存在会使得生物苯环裂解酶的活性受到抑制,从而导致微生物对其降解能力低。因此常规的水处理方法和生物处理工艺难以有效地去除 2-CP。目前处理 2-CP 的工艺中,与只适用于处理低浓度氯酚废水的生化法和易造成二次污染的物化法相比,化学氧化法具有更广泛的应用前景。目前广泛被研究的 2-CP 氧化处理技术包括电化学氧化法、光催化降解法、焚烧、超临界水氧

化法和湿式氧化法等^[13-15]。与电化学和光催化氧化法相比,湿式氧化法能更高效地处理高浓度 2-CP 废水,且获得更高的 TOC 去除率。而焚烧工艺的能耗较高,超临界水氧化技术需要高温(450-500°C)高压(240-300 个大气压)的运行条件,均不利于大规模实际应用^[16,17]。因此湿式氧化技术在处理高浓度 2-CP 废水领域受到越来越多的关注。

由于污泥基碳(Sewage sludge derived carbon, 简称 SC)中含有一定量的铁氧化物^[18],且炭材料在湿式催化氧化反应中具有较好的催化活性,基于以上考虑,本章尝试以污泥基碳作为湿式催化氧化反应的催化剂。同时,本研究还以市政污泥和硫酸亚铁为原料,通过高温热解技术制备得负载铁氧化物的污泥基碳复合催化剂(Fe₃O₄/SC),并比较 Fe₃O₄/SC 与 SC 对高浓度 2-CP 溶液的催化湿式氧化降解能力。此外,由于目前研究中关于铁系催化剂在湿式催化氧化过程中催化活性组分溶出行为的报道很少,本章着重研究了污泥基碳复合催化剂在处理 2-CP 过程中铁盐溶出的机理和影响因素,并探讨多种控制催化活性组分流失的措施的可行性。

3.2. 实验部分

3.2.1. 实验药品与试剂

七水合硫酸亚铁,分析纯试剂,广州化学试剂厂; Ru(NO)(NO₃)₃ 分析纯试剂, Alfa Aesar 试剂公司; 分析纯对氯苯酚及液相色谱级甲醇购自 Aldrich 试剂公司。

本章实验所用污泥为广州市猎德污水处理厂的二沉池脱水污泥,取泥日期为 2011 年 6 月。

3.2.2. 催化剂的制备

Fe₃O₄/SC 催化剂的制备同样采用“一步法”,具体操作同第 2 章 2.2.3 节。

为了除去 SC 中的无机组分,本章中将 5 g 污泥基碳加入 80 mL 由盐酸和氢氟酸(25 vol.% HCl + 25 vol.% HF)混合的酸液中,于 70°C 下处理 2 h。之后用蒸馏水洗涤,直到溶液 pH 值恒定为止,将催化剂过滤,烘干备用。将经酸处理

的催化剂命名为 SC-A。

3.2.3. 催化剂的表征

催化剂的组分分析、粉末 X 射线衍射、BET 比表面积、扫面电镜分析同第 2 章 2.2.4 节中相应内容。

催化剂 pH_{PZC} 的测定：催化剂表面在某一 pH 条件下会出现零电位，该点称为零电位点(Point of zero charge)，简称零电点，相应的 pH 值简称 pH_{PZC} 。本实验采用粉末质量滴定法对催化剂的 pH_{PZC} 进行测定^[19,20]。称取定量的催化剂（约 0.02 g）加入 50 mL 0.0005 mol/L NaCl 溶液中，于室温下振荡，每隔 30 min 测定一次 pH，待溶液 pH 稳定后继续加入定量的催化剂，测定溶液 pH。重复此步骤直到继续加入催化剂不导致溶液 pH 值发生变化，此时溶液的 pH 值即为催化剂的 pH_{PZC} 。

3.2.4. 催化剂 CWAO 催化活性的评价

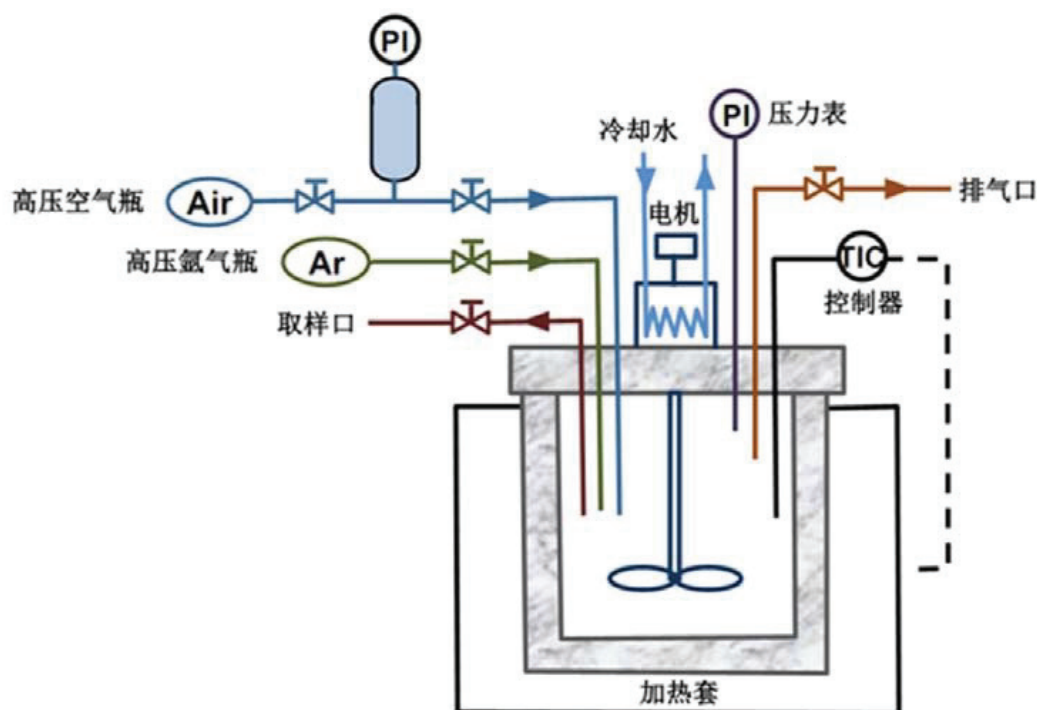


图 3-1 实验用湿式催化氧化反应装置

Fig. 3-1. Schematic of the experimental setup.

湿式催化氧化反应在 0.3 L 的反应釜内进行, 如图 3-1, 反应釜由 Hastelloy C22 材质的不锈钢制成 (Model 4836, Parr Instrument Inc 公司), 配有不锈钢压力调节阀、压力表、取样口及出气口, 控温系统采用热电偶进行控温, 使用加热套升温, 温度精度为 $\pm 2^{\circ}\text{C}$ 。整套装置配有磁力搅拌系统, 确保反应物充分传质。

每次反应向反应釜中加入 150 mL 初始浓度为 2 g/L 的 2-CP 溶液以及一定质量的催化剂。盖上釜盖, 反应开始前先分三次通入氩气以驱除反应器和溶液中残留的空气, 之后将反应釜升温至设定温度, 待温度稳定后 (约 40 min) 向反应釜中通入压缩空气(20 vol.% O₂ + 80 vol.% N₂), 当压力表读数达到 5.0 MPa (氧气分压为 0.9 MPa) 时开启搅拌装置, 此时记作反应的零时刻。为了避免液相中传质限制, 反应釜内的搅拌速度设定为 1300 rpm^[12]。反应进行至特定时间时停止搅拌, 取样, 用 0.45 μm 孔径的滤膜分离催化剂。取样期间, 开启高压空气阀以维持反应系统内的压力恒定。

3.2.5. 分析方法

3.2.5.1. 2-CP 及降解中间产物浓度的测定

2-CP 及降解中间产物采用 Shimadzu LC-20AD 型高效液相色谱仪测定, 仪器配备 Kinetex PFP 100A C18 色谱柱 (2.6 μm 100 \times 4.6 mm, Phenomenex 公司), 柱温 40 $^{\circ}\text{C}$ 。为有效分离 2-CP 和降解中间产物, 流动相比比例经测试最终确定为 4 vol.% 甲醇和 96 vol.% 水的混合溶液, 并用 85 wt.% 的浓 H₃PO₄ 调至 pH 为 2.0。流速为 0.6 mL/min。检测波长设定为 210 和 281 nm。

3.2.5.2. TOC 的测定

滤液中总有机碳 (TOC) 的变化使用 5050 TOC 分析仪 (Shimadzu, Japan) 进行测定。TOC 去除率按式 3-1 式进行计算:

$$R = \frac{M_0 - M_t}{M_0} \times 100\% \quad (\text{式 3-1})$$

式中 M_0 为 TOC 初始浓度, M_t 为反应一定时间后溶液的 TOC 值。

3.2.5.3. pH 和电极电势的测定

溶液的 pH 采用 PHM240 pH 计 (Radiometer Analytical, American) 进行测定。

3.2.5.4. 溶出金属的测定

反应过程中溶出的金属采用 Optima 5300DV 型电感耦合等离子原子发射光谱仪 ICP-OES (U.S.A. PerkinElmer 公司) 进行定性和定量分析。

3.3. 结果与讨论

3.3.1. 不同催化剂催化湿式氧化 2-CP

本实验中所用到的 SC、Fe₃O₄/SC 和 SC-A 的物理化学性质列于表 3-1 中。与 SC 相比, 负载了铁氧化物的 Fe₃O₄/SC 具有更低的 pH_{PZC}, 这与 Quintanilla^[14] 等人的研究结果相一致, 可能是由于铁氧化物的负载能增加催化剂表面的酸性官能团, 而这些官能团被认为在湿式催化氧化反应中能起到提供催化活性位点的作用。通过比较表 3-1 中 SC-A 与 SC 的灰分及各无机组分含量, 可知酸处理能有效地将除 Si 之外的无机组分从污泥基碳中去除。

表 3-1 SC、Fe₃O₄/SC 和 SC-A 催化剂的基本物理化学性质

Table 3-1. Physicochemical properties of the SC, Fe₃O₄/SC and SC-A samples.

Sample	Ash (wt.%)	Fe (wt.%)	Si (wt.%)	Al (wt.%)	Ca (wt.%)	S _{BET} (m ² g ⁻¹)	pH _{PZC}
SC	74.6	4.5	23.4	10.6	1.7	20	7.5
Fe ₃ O ₄ /SC	93.0	12.0	19.9	9.1	1.8	15	4.2
SC-A	56.1	0.4	28.6	1.8	<0.1	33	3.7

接着考察了 SC、Fe₃O₄/SC 和 SC-A 三种催化剂在相同的反应条件下对 2-CP 的去除效果。由图 3-2 可见, 若不使用催化剂, 在反应温度为 120 °C, 氧气分压为 0.9 MPa 的反应条件下, 零时刻时有 6% 左右的 2-CP 由于热分解和挥发作用被去除。当反应进行 24 h 后, 2-CP 和 TOC 的去除率均低于 15%。由此可见 2-CP 分子在本实验条件下较稳定, 单独湿式氧化法对 2-CP 的去除率极低。

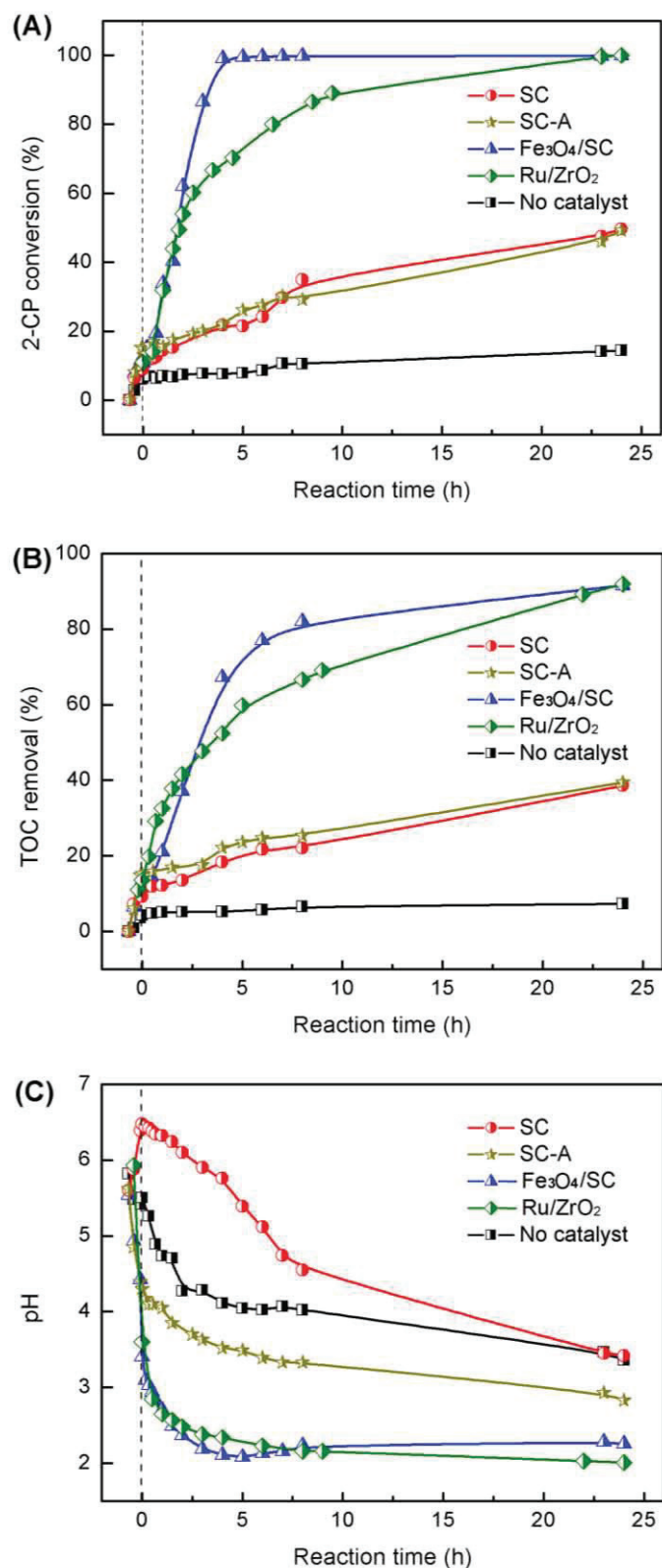


图 3-2 以 $\text{Fe}_3\text{O}_4/\text{SC}$, SC, SC-A, Ru/ZrO_2 为湿式氧化的催化剂及无催化剂的条件下, 2-CP 转化率(A), TOC 去除率(B)和溶液 pH(C)随反应时间的变化

Fig. 3-2. Evolution of the 2-chlorophenol conversion (A), the TOC removal (B) and the pH (C)

upon wet air oxidation (WAO) of 2-CP over $\text{Fe}_3\text{O}_4/\text{SC}$, SC, SC-A and Ru/ZrO_2 or in the absence of catalyst (0.5 g catalyst, 120°C , P_{O_2} : 0.9 MPa, 1300 rpm, 150 mL $[\text{2-CP}]_0 = 2\text{g}\cdot\text{L}^{-1}$).

当向反应器中加入 SC 催化剂时, 反应 24 h 后 2-CP 的转化率和 TOC 的去除率分别提高至 50%和 39%。表明 SC 催化剂具有一定的催化活性。当以经过 HCl 和 HF 脱灰分处理的 SC-A 作为催化剂时, 2-CP 的初始吸附去除率由 3%增加至 9%, 这主要归因于催化剂比表面积的增加。酸处理后, SC 的比表面积由 $20\text{ m}^2/\text{g}$ 增大至 $33\text{ m}^2/\text{g}$ (SC-A)。但是 SC-A 并未表现出比 SC 更高的催化活性, 相反地, 初始反应速率由 $0.4\text{ mmol}_{\text{2-CP}}/(\text{g}_{\text{catalyst}}\cdot\text{h})$ 降低至 $0.1\text{ mmol}_{\text{2-CP}}/(\text{g}_{\text{catalyst}}\cdot\text{h})$ 。这表明 SC 中的无机组分对催化剂催化湿式氧化的活性有很大的贡献作用。

当在 SC 中负载铁氧化物后, 催化剂的催化活性明显增强。在反应进行不到 5 h 时, 2-CP 的去除率已接近 100%。初始反应速率为 $3.0\text{ mmol}_{\text{2-CP}}/(\text{g}_{\text{catalyst}}\cdot\text{h})$, 是 SC 催化体系的 7 倍左右, 而 $\text{Fe}_3\text{O}_4/\text{SC}$ 中 Fe 的含量仅为 SC 中 Fe 的 3 倍。此外, 与被多次报道的且较为经典的 Ru/ZrO_2 贵金属催化剂相比, 在同样的反应条件下, $\text{Fe}_3\text{O}_4/\text{SC}$ 表现出更高的催化活性。从图 3-2 B 中可以看出, 加入 $\text{Fe}_3\text{O}_4/\text{SC}$ 催化剂后, TOC 的去除率也显著提高, 反应 24 h 后 TOC 的去除率达到 91%。与 2-CP 的转化率相比, 反应过程中 TOC 的去除相对滞后, 可能是由于 2-CP 被转化成难于彻底矿化的中间产物。

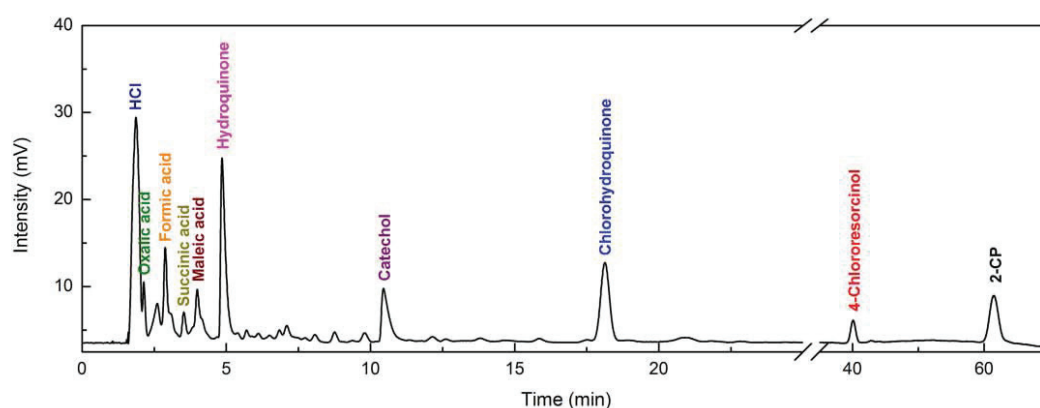


图 3-3 2-CP 及降解中间产物的 HPLC 图

Fig. 3-3. Typical intermediates detected by HPLC (Column: $100 \times 4.6\text{ mm}$, Phenomenex, Kinetex 2.6 μm PFP 100A, Mobile phase: 4 vol. % MeOH & H_2O (pH = 2.0 justed by H_3PO_4), Flow rate: $0.6\text{ mL}\cdot\text{min}^{-1}$, Column temperature: 40°C) upon catalytic wet air oxidation of 2-chlorophenol.

由图 3-2 C 可见, 反应液的 pH 值由初始的 5.5 随着反应的进行逐渐降低。反应溶液酸性的增加主要归因于(i) 2-CP 脱氯过程中产生的 HCl; (ii) 氧化过程中生成大量小分子有机酸, 由 HPLC 分析结果(图 3-3)可鉴定出反应过程中除 HCl 外, 还有马来酸(maleic acid)、琥珀酸(succinic acid)、甲酸(formic acid)和草酸(oxalic acid)等小分子有机酸生成。此外还检测到多种芳香族中间产物, 如 4-氯间苯二酚(4-Chlororesorcinol)、2-氯对苯二酚(2-Chlorohydroquinone)、邻苯二酚(Catechol)和对苯二酚(Hydroquinone)。

3.3.2. 反应温度对 Fe₃O₄/SC 催化活性的影响

反应温度是 CWAO 过程中非常重要的影响因素之一, 对有机物的氧化降解效果能起到决定性的作用。本实验考察了在 105°C、120°C、135°C 和 150°C 下以 Fe₃O₄/SC 为湿式氧化催化剂对 2-CP 的降解情况。

由图 3-4 A 所示结果可见, 反应温度的升高有利于 2-CP 氧化的进行。温度为 105°C 时, 反应 12 h 左右 2-CP 可被完全去除, 而随着温度的升高, 2-CP 完全被转化的时间大大缩短, 在反应温度为 120°C 时只需 5 h, 135°C 时约 3 h, 150°C 时仅需 1.5 h。湿式催化氧化反应动力学方程可由下式表示^[21]:

$$r = -\frac{d_C}{d_t} = K_0 e^{-E_a/RT} C_C^m C_O^n \quad (\text{式 3-2})$$

式中: r 为反应速率(mol/(h·g_{catal})), t 为反应时间(s), K_0 为指前因子, E_a 为活化能(kJ/mol), R 为气体常数(8.314 J/(mol·K)), T 为反应温度(K), C_C 为有机物浓度(mol/L), C_O 为氧化剂的浓度(mol/L), m 、 n 为反应级数。该经验公式根据不同的有机物或废水水质有不同的参数值。当其他反应条件相同时, 在不同的反应温度下, 对式 3-2 取对数后, 将不同温度下 2-CP 氧化速率的对数(ln r)与温度的倒数(1/T)进行线性回归, 该直线的斜率即为 $-E_a/R$ 值^[22]。

由于反应初始(反应零时刻)时催化反应未进入稳定状态, 因此本研究用图 3-4 A 中曲线陡坡部分的数据来计算反应速率, 结果如表 3-2 所示。将不同温度下 2-CP 降解速率的对数与温度的倒数进行线性回归(图 3-5), 计算得到反应的活化能为 50.5 kJ/mol。Joglekar^[23]等研究了在无催化剂存在的条件下, 湿式氧化降解 2-CP 的反应活化能约为 140 kJ/mol。由此可见 Fe₃O₄/SC 催化剂的加入, 能

有效降低反应活化能，加速 2-CP 氧化反应的进行。

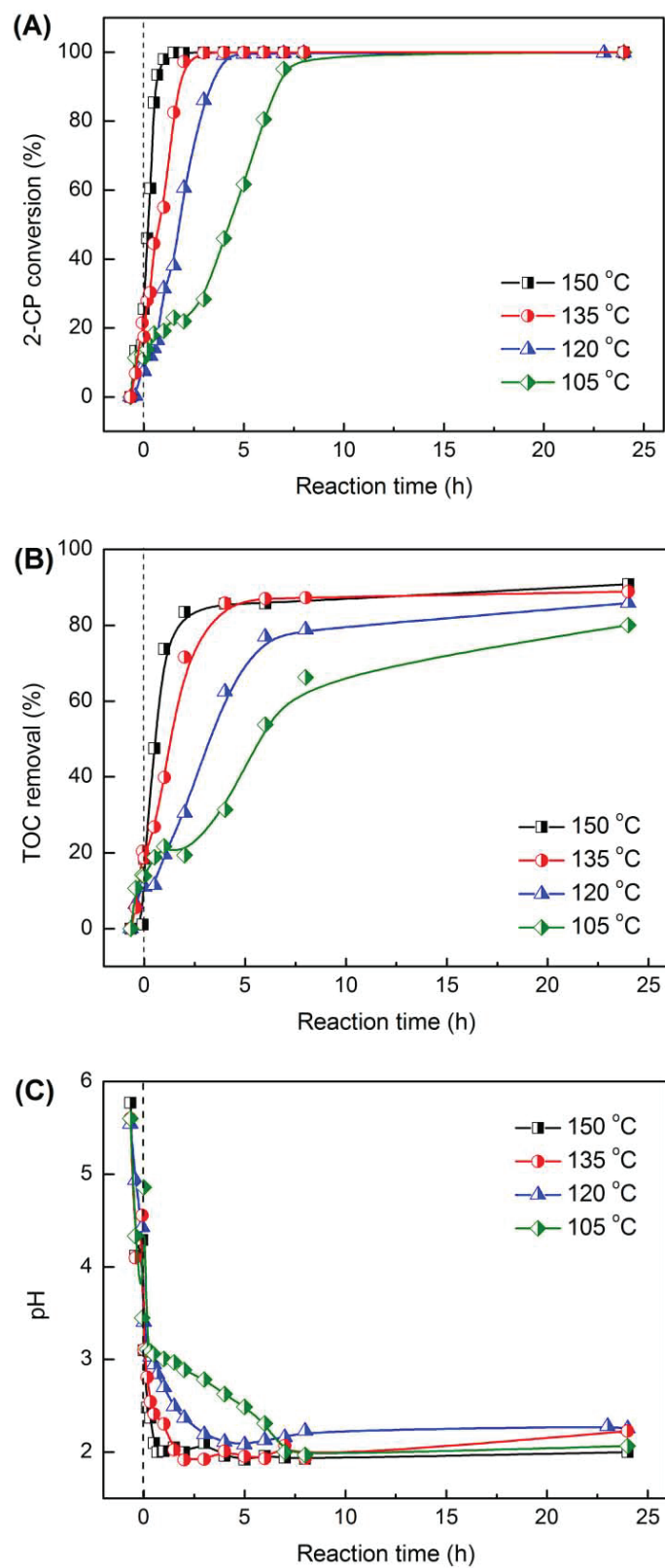


图 3-4 反应温度对 2-CP 转化率(A), TOC 去除率(B)和溶液 pH(C)的影响

Fig. 3-4. Evolution of the 2-CP conversion (A), TOC removal (B) and the pH (C) in the wet air oxidation (WAO) of 2-CP under different reaction temperature (0.5g Fe₃O₄/SC catalyst, 5 MPa, 1300 rpm, 150 mL [2-CP]₀=2g/L).

表 3-2 反应活化能的计算

Table 3-2 Calculation of activation energy

Temperature (K)	Reaction rate mol/(h·g _{catal})	Ea (kJ/mol)
T=423.15	4.675	50.5
T=408.15	1.868	
T=393.15	1.336	
T=378.15	0.776	

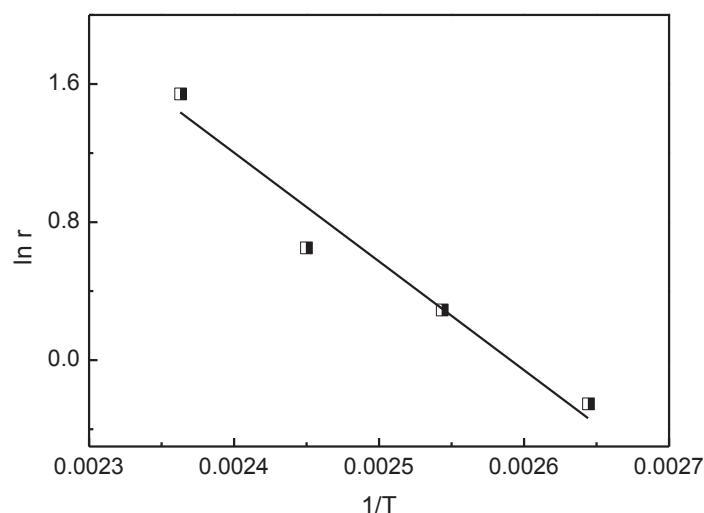


图 3-5 2-CP 氧化速率与温度线性回归图

Fig. 3-5. Arrhenius plot of 2-CP oxidation at 105, 120, 135 and 150°C

由图 3-4 B 可见，反应温度升高使 TOC 去除率明显增加。这是由于，一方面，反应温度的升高将增加 O₂ 在溶液中的溶解度，当反应温度由 120°C 升至 150°C 时，O₂ 的溶解度由 0.17 g/L 增加到 0.28 g/L。另一方面，在 2-CP 湿式氧化过程中会产生大量难以被进一步氧化的小分子有机酸，Gallezot^[24]等发现即使用 Ru/C 为催化剂催化湿式氧化降解乙酸，也需要提供高达 101 kJ/mol 的活化能才

能使乙酸彻底分解矿化。较高的反应温度能给某些化学键的断裂提供足够的能量,使这些难降解有机物分子得以获得足够的活化能,从而被氧化成 CO_2 和 H_2O 。这也是温度升高使 TOC 去除率增加的一个重要原因^[25]。

此外,反应温度的升高也将导致溶液迅速酸化(图 3-4 C),而反应过程中产生的 HCl 和有机酸在高温下更容易造成设备腐蚀^[26]。同时反应温度的升高也会导致操作费用增加。另一方面,为了更好地检测氧化中间产物,反应不宜进行得过快,应将反应速率控制在适当的范围内。综合考虑以上因素,后续实验均在 120°C 下进行。

3.3.3. 均相反应的影响

考虑到反应过程中的高温酸性环境, $\text{Fe}_3\text{O}_4/\text{SC}$ 中的金属成分,如 Fe、Ca、Al 等,很可能存在溶出问题。其中 Fe 被认为在湿式催化反应中具有较高的催化活性^[27],因此我们用 ICP-OES 检测了图 3-2 中几组实验在反应 24 h 后溶液中 Fe 的浓度。结果如表 3-3 所示,在 $\text{Fe}_3\text{O}_4/\text{SC}$ 催化体系中检测到 27 mg/L 的铁溶出,约占催化剂中总铁量的 7 wt.%。对于已报道的过渡金属催化剂,如 Cu、Zn、Mn、Ni 等,应用于催化湿式氧化反应的过程中也均出现不同程度的溶出^[28]。西班牙的 Santos^[29]等以商业铜氧化物 Cu-0203T 为催化剂,在固定床反应器(FBRs), 16 bar 氧气分压,反应温度为 140°C 的条件下处理初始浓度为 1 g/L 的苯酚溶液。当反应溶液 pH 为 3.5 时,反应器出水中能检测到高达 100 mg/L 的铜。由此可见对于过渡金属催化剂在酸性反应环境下,普遍存在催化活性组分流失的现象。

表 3-3 使用不同催化剂进行湿式催化氧化降解 2-CP 反应 24 h 后体系中 Fe 溶出情况

Table 3-3. Iron leaching upon catalytic wet air oxidation (CWAO) of 2-chlorophenol over different catalysts (120°C , P_{O_2} : 0.9 MPa, 1300 rpm, 150 mL $[\text{2-CP}]_0 = 2\text{g}\cdot\text{L}^{-1}$, 0.5g catalyst).

Sample	Iron concentration in the reaction	Percentage of iron leached in the
	mixture after 24 h ($\text{mg}\cdot\text{L}^{-1}$)	solution after 24 h (wt.%)
$\text{Fe}_3\text{O}_4/\text{SC}$	27.0	7
SC	0.8	0.5
SC-A	3.8	29

由于反应过程中铁盐溶出, 意味着 2-CP 总去除率有一部分是由均相催化反应贡献的。为证明这一点, 将 0.5g 催化剂加入 150 mL 2 g/L 2-CP 溶液中, 于 0.9 MPa 氧气分压, 120°C 的反应温度下, 运行 10min 后停止反应, 打开反应釜, 滤去 Fe₃O₄/SC 催化剂, 之后将滤液重新装入反应釜中在相同的操作条件下继续反应。结果如图 3-6 所示, 除去固体催化剂后, 2-CP 仍以较高的速率被降解。而且两个体系中 2-CP 去除趋势基本相同。通过 ICP-OCS 分析, 检测到 Fe₃O₄/SC 体系反应 10min 后有 25 mg/L 的 Fe 溶出。由此可见均相反应对 Fe₃O₄/SC 催化体系中 2-CP 的去除起着主要作用。

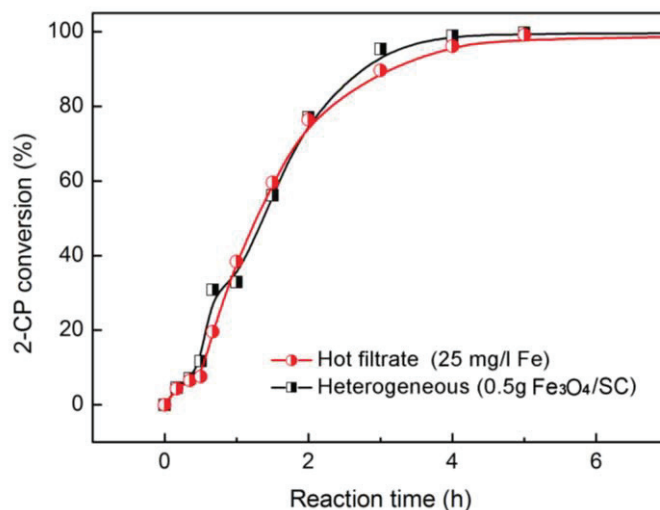


图 3-6 Fe₃O₄/SC 催化体系和滤液均相催化体系中 2-CP 的降解情况

Fig. 3-6. 2-CP conversion attained by heterogeneous: 0.5g Fe₃O₄/SC and homogeneous reaction: hot filtrate from 0.5 g Fe₃O₄/SC system after 10 min reaction (120°C, P_{O₂}: 0.9 MPa, 1300 rpm, 150 mL [2-CP]₀ = 2g·L⁻¹).

为了进一步确定均相反应的贡献作用及铁盐溶出的影响因素, 本研究考察了催化剂用量分别为 1.0、1.5 和 2.0 g/L 时, 2-CP 去除率随反应时间的变化情况(图 3-7 A)。在反应零时刻, 随着催化剂用量的增加, 2-CP 分子在 Fe₃O₄/SC 表面的吸附量也增加。Fe₃O₄/SC 催化剂投加量为 1.0、1.5 和 2.0 g/L 时吸附量分别为 4.5、6.5 和 8.1%。由此可计算出 Fe₃O₄/SC 催化剂表面对 2-CP 的吸附量约为 60 mg_{2-CP}/g_{catal}。

当反应进行到 10、30 和 60 分钟时，分别对三个反应体系进行取样，并用 ICP-OES 分析测定滤液中 Fe 的浓度。由图 3-7 B 可以发现，三个体系中 Fe 的溶出量与 2-CP 在相应时刻的瞬时降解速率（以 $\text{mol}_{2\text{-CP}}/\text{h}$ 表示）有着很强的相关性。二者之间明显的线性关系表明：对于 $\text{Fe}_3\text{O}_4/\text{SC}$ 催化体系，2-CP 的去除率与催化剂的用量并没有直接关系，而 Fe 的溶出量才是主要影响因素。

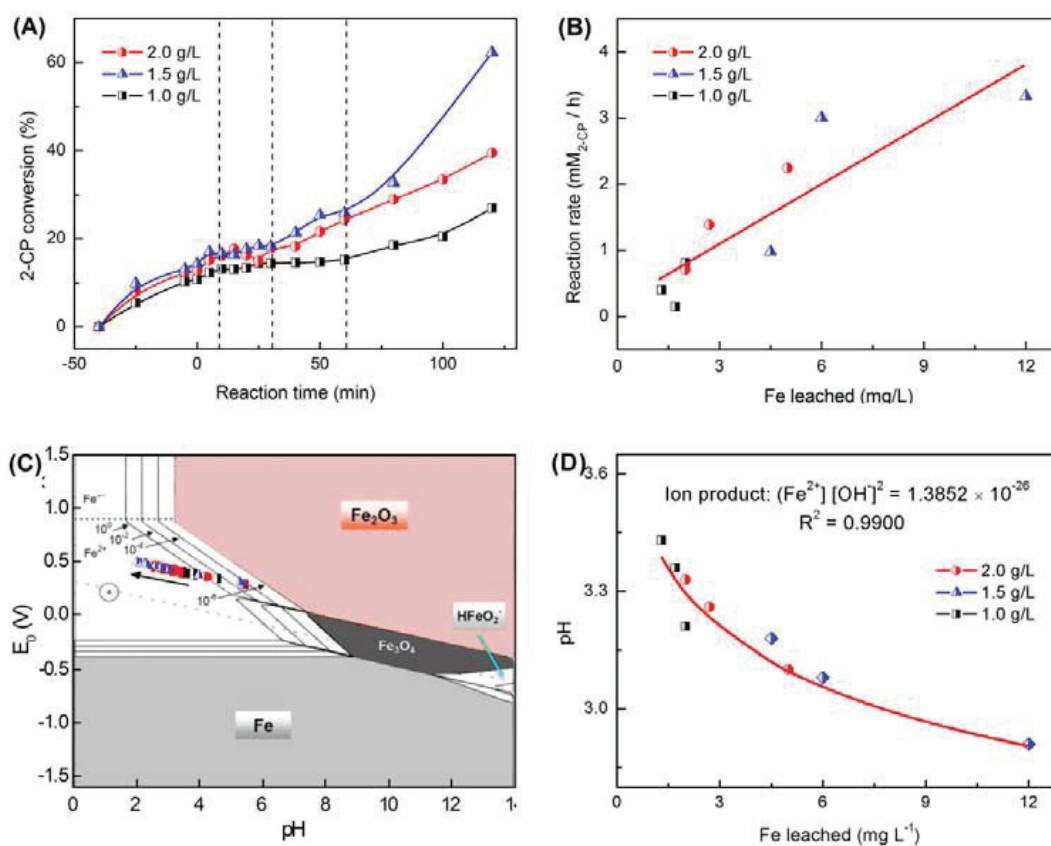


图 3-7 (A). 不同催化剂用量对 2-CP 的影响；(B). 反应前期铁盐溶出量与 2-CP 降解速率的关系；(C). Fe 的电位-pH 图及反应液的 pH-电极电位值；(D). 铁盐溶出量与溶液 pH 的关系.

Fig. 3-7. Contribution of the homogeneous phase reaction. **(A)**: 2-CP conversion during the first 2h of reaction in the presence of different concentration in $\text{Fe}_3\text{O}_4/\text{SC}$; **(B)**: Correlation between the 2-CP conversion rate and the amount of iron leached in the reaction mixture; **(C)**: Pourbaix diagram for iron and evolution of the potential and pH of the reaction mixture as a function of time; **(D)**: Correlation between the solution pH and the amount of iron leached in the reaction mixture [120°C , P_{O_2} : 0.9 MPa, 1300 rpm, 150 mL $[2\text{-CP}]_0 = 2\text{g}\cdot\text{L}^{-1}$, catalyst dosage: 1.0 g L^{-1} (\blacksquare), 1.5 g L^{-1} (\bullet) and 2.0 g L^{-1} (\blacktriangle)].

为了判断溶出的 Fe 在溶液中的存在形式,本研究测定了反应溶液的电极电位,并在铁的电位-pH 图^[30]中标出。由图 3-7 C 所示结果,可以发现反应溶液中的 Fe 主要以 Fe(II)的形式存在。为了氧化 150 mL 浓度为 2 g/L 的 2-CP 溶液(相当于 2.3 mmol 2-CP),根据反应式(3-3),所需 O₂的理论值约为 15 mmol。而反应过程的氧气的分压为 0.9 MPa,即反应釜中存在 48.2 mmol 的 O₂。意味着反应过程中提供的 O₂ 总量大大超多理论所需值。但是不容忽视的是在反应条件下, O₂ 在水中的溶解度有限,仅为 0.2 g_{O₂}/L。而 2-CP 被氧化时将迅速消耗溶解于溶液中的 O₂,使得溶液中出现缺氧环境,导致溶出的铁盐被还原成亚铁离子。



均相中存在的这部分 Fe(II)能很好地激发和促进自由基反应的形成和传递,如烷基过氧自由基(alkyl peroxy radicals)、氧自由基(oxygen radicals)和羟基自由基(Hydroxyl radicals)等^[31,32],从而加速湿式催化反应。从图 3-7 C 中,还可以发现随着反应的进行,溶出的铁盐逐渐向 Fe(III)转化。

此外,用铁盐溶出量与溶液 pH 作图(如图 3-7 D),也可发现铁盐的溶出量随着溶液 pH 值的降低而增加。由此可见影响铁盐溶出的主要因素是溶液的 pH 值。



根据溶度积常数(K_{sp})的定义: $[\text{Fe}^{2+}] \cdot [\text{OH}^-]^2 = \text{K}_{\text{sp}}$

可用图 3-7 实验所获得的 Fe²⁺及 OH⁻浓度数据,计算拟合出该反应体系中的 K_{sp} 值。如图 3-7 D 中所示, K_{sp} 值为 1.39×10⁻²⁶。而 25°C 下 Fe(OH)₂ 的溶度积常数 K_{sp} 为 3×10⁻¹⁶^[33]。且该值会随着反应温度的升高而增大。由此可以推测在相同的 pH 环境下, Fe₃O₄/SC 体系中溶出的 Fe²⁺的浓度要远远低于理论值。可见将铁盐负载在 SC 中能一定程度地减少其溶出。此外,欧盟废水排放标准要求 Fe²⁺ 浓度低于 2.0 mg/L,由图 3-7 D 中拟合的曲线可计算出满足此条件的 pH 应大于 3.29,即在 Fe₃O₄/SC 催化湿式氧化 2-CP 的反应体系中,当溶液 pH 高于 3.29 时, Fe₃O₄/SC 的铁盐溶出可控制在低于 2 mg/L 的排放标准内。

总而言之,反应体系中 2-CP 的转化率、溶液 pH 和铁盐溶出三者之间是互相关联,相互影响的。铁盐溶出能加速湿式催化反应中 2-CP 的脱氯反应,从而产生大量 HCl,导致溶液 pH 迅速下降。此外,反应过程中生成的草酸,可通过络

合作用与铁生成草酸铁，从而加剧铁盐溶出^[34]。因此，本实验中铁盐的溶出主要来自于酸性溶出和反应性溶出两方面。

3.3.4. 控制铁盐溶出的研究

上述实验结果表明， $\text{Fe}_3\text{O}_4/\text{SC}$ 催化剂廉价且活性高，但是存在催化活性组分 Fe 溶出的问题，这将限制其大规模工业化应用，因此需要采取一定的措施以减少其催化剂活性组分的流失。考虑到反应过程中产生的酸性环境是导致 $\text{Fe}_3\text{O}_4/\text{SC}$ 催化剂中 Fe 溶出的主要原因，本节中尝试了多种方法以控制反应过程中溶液的 pH 值。

在超临界氧化和湿式氧化反应中，NaOH 等强碱试剂常被用来综合处理含氯有机污染物氧化过程中生成的酸性产物^[26,35]。因此，我们首先尝试在 2-CP 溶液中加入 NaOH，将溶液初始 pH 由 5.6 调至 10.0。之后加入 2.0 g/L $\text{Fe}_3\text{O}_4/\text{SC}$ 催化剂，在 120°C，0.9 MPa 氧分压下考察 2-CP 的转化率和 TOC 的去除情况。

如图 3-8 A 所示，与不改变初始 pH 的湿式氧化反应相比，将初始 pH 调至碱性(pH=10.0)后，2-CP 和 TOC 的去除率都明显增加了。反应 24 h 后，2-CP 转化率由 WAO 反应中的 14% 增加至 68%，TOC 去除率由 7% 增加至 40%。该实验结果与 Pintar 等人^[36]的研究结果基本一致。Pintar 等发现在湿式氧化处理对氯苯酚和对硝基苯的反应中，当溶液 pH 高于取代酚的 pKa 时，取代酚离子(ArO^-)将会部分转化成具有较高催化活性的苯氧基自由基($\text{ArO}\cdot$)，加速催化反应。在本实验中，由于 2-CP 的 pKa 为 8.6，低于反应初始 pH(10.0)，因此反应过程中也会产生高活性的苯氧基自由基($\text{ArO}\cdot$)，从而加速 2-CP 氧化分解。从图 3-8 A 的结果，还可以发现，加入 $\text{Fe}_3\text{O}_4/\text{SC}$ 催化剂后，2-CP 和 TOC 的去除率并没有明显增加。这是因为：一方面，在 pH=10.0 的碱性溶液中， $\text{Fe}_3\text{O}_4/\text{SC}$ 表面带负电，而 2-CP 分子发生解离反应，以带负电的 $\text{Cl-C}_6\text{H}_4\text{-O}^-$ 离子状态存在于溶液中，由于电性排斥的作用，2-CP 分子将难于吸附于 $\text{Fe}_3\text{O}_4/\text{SC}$ 表面，进而限制其在催化剂表面的氧化分解；另一方面，反应 24 h 后，溶液中仅检测出 0.7 mg/L 的 Fe。可见使用 NaOH 改变溶液 pH 值，能有效地减少反应过程中铁盐的溶出，但碱性 pH 也导致 $\text{Fe}_3\text{O}_4/\text{SC}$ 的催化活性明显降低。

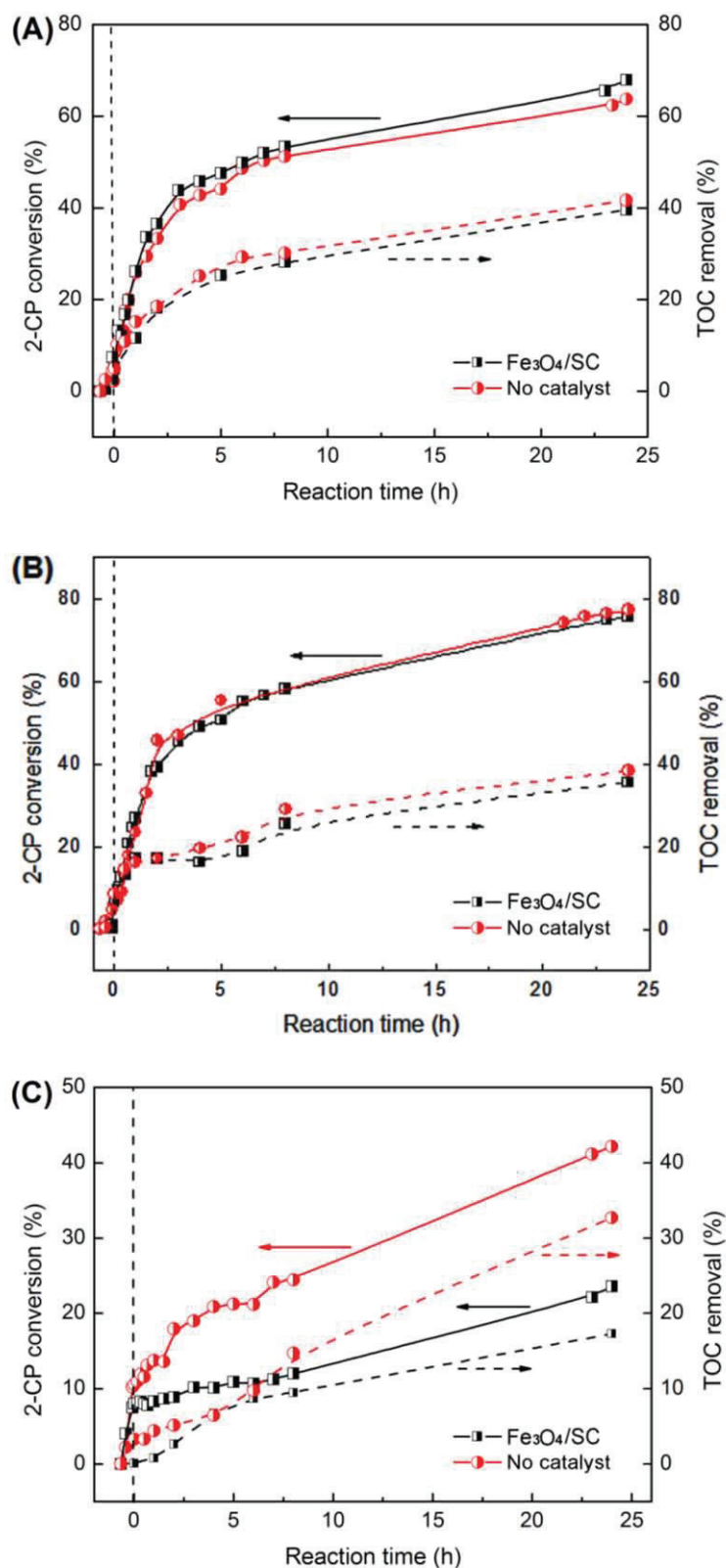


图 3-8 控制反应溶液 pH 值对 2-CP 和 TOC 去除率的影响。

Fig. 3-8. Evolution of the 2-CP conversion upon wet air oxidation (WAO) in the absence of any catalyst (■) or in the presence of the $\text{Fe}_3\text{O}_4/\text{SC}$ catalyst (●) and with the initial addition of NaOH

to pH=10.0 (A) or in the presence of a 0.1 M phosphate buffer at pH=6.8 (B) or in the presence of a 0.1 M acetate buffer at pH=4.5 (C) (120°C , P_{O_2} : 0.9 MPa, 1300 rpm, 150 mL $[2\text{-CP}]_0 = 2\text{g}\cdot\text{L}^{-1}$, catalyst dosage: 2.0 g L^{-1}).

通过加入缓冲溶液是另一种控制反应溶液 pH 的有效方法。本节中尝试向反应釜中加入 pH=6.8 的磷酸盐缓冲溶液(0.1 M)。经过 24 h 的湿式催化反应后, $\text{Fe}_3\text{O}_4/\text{SC}$ 催化体系中只有 0.4 mg/L 的 Fe 溶出。但是由图 3-8 B 中曲线可知, $\text{Fe}_3\text{O}_4/\text{SC}$ 催化剂对于加入磷酸盐缓冲液的 2-CP 溶液几乎没有催化湿式氧化活性。可能是由于磷酸根易与铁离子反应生成螯合物^[37], 导致催化剂中毒失活。因此, 对于以 $\text{Fe}_3\text{O}_4/\text{SC}$ 为催化剂的催化湿式氧化反应不宜选用磷酸盐缓冲溶液来控制反应溶液 pH。

本课题组早期的研究发现, 即使在 200°C 下进行湿式催化氧化, 也不能将醋酸彻底矿化^[38]。因此选用 pH=4.5, 0.1 M 的醋酸盐缓冲溶液来控制反应过程中溶液的 pH 值。结果如图 3-8 C 所示。反应 24 h 后, 体系中 2-CP 的转化率为 17%, TOC 去除率为 8%, 与单独湿式氧化相比, 加入醋酸盐缓冲溶液并未使 2-CP 和 TOC 的去除率发生太大改变。当向醋酸盐与 2-CP 的混合溶液中加入 $\text{Fe}_3\text{O}_4/\text{SC}$ 催化剂后, 反应结束时(24 h) 2-CP 的转化率达到 42%, TOC 去除率也增加至 33%。与不加醋酸盐缓冲溶液的 $\text{Fe}_3\text{O}_4/\text{SC}$ 催化体系相比, 上述体系催化效果较差。但是醋酸盐缓冲溶液的加入, 使得反应 24 h 后催化活性组分 Fe 的溶出量由之前的 30 mg/L 降低至 0.9 mg/L。为确定均相反应的贡献, 向 150 mL 含 2 g/L 2-CP 及醋酸盐的溶液中加入 0.4806 g 氯化亚铁, 配制成 Fe(II)浓度为 0.9 mg/L 的 2-CP -醋酸盐溶液, 并于 120°C , 0.9 MPa 氧分压下进行催化湿式氧化反应, 结果表明 0.9 mg/L 的 Fe(II)并没有明显的催化活性。

总而言之, 上述实验表明使用醋酸盐缓冲溶液(pH=4.5)能够有效地防止 $\text{Fe}_3\text{O}_4/\text{SC}$ 催化剂的催化活性组分流失, 同时还使催化剂有一定的催化活性。虽然使用醋酸盐缓冲溶液将使溶液 TOC 值增加(约 4.8 g/L), 且在湿式氧化反应里, 醋酸不易被进一步矿化。但是考虑到醋酸对微生物无毒, 且容易在后续的生物处理工序中被降解, 因此使用醋酸盐缓冲溶液来减少 $\text{Fe}_3\text{O}_4/\text{SC}$ 催化剂中铁盐的流失具有一定的可行性。

以上三组减少 Fe₃O₄/SC 催化剂在催化湿式氧化 2-CP 过程中 Fe 溶出的实验结果, 都表明提高反应溶液的 pH, 能有效地减少铁盐溶出, 但是同时催化剂的催化活性将大大降低。Santos 等研究人员在用 Cu 催化剂时也得到类似的结论。当他们向反应液中加入 Na₂CO₃ 使溶液 pH 由 3.5 升至 8.0 时, Cu 的溶出量由 100 mg/L 降低到 0.1 mg/L, 而同时苯酚的转化率却由 70% 减少到只有 28%^[29]。由此可见 Fe₃O₄/SC 催化体系中均相反应具有很大的贡献作用。

3.3.5. 催化剂稳定性的研究

催化剂能否得到实际应用, 不仅取决于它的催化活性, 它的稳定性也是一个重要评价指标。考虑到 Fe₃O₄/SC 催化剂在湿式催化氧化处理 2-CP 溶液过程中出现催化活性组分溶出的现象, 因此很有必要对 Fe₃O₄/SC 的稳定性进行研究。

本实验通过比较 Fe₃O₄/SC 催化剂多次重复使用后催化性能的变化来评价其催化稳定性。为了避免 Fe₃O₄/SC 中的铁盐流失, 及溶出的 Fe 造成的二次污染, 我们通过调节反应结束后溶液的 pH 至中性, 使溶出的铁以沉淀的形式重新回到 Fe₃O₄/SC 催化剂中。Bernat^[39] 等人指出溶液 pH 值将直接影响溶液中铁离子的存在形态, 从而影响其回收率。在本节的研究中发现湿式催化氧化反应结束后将溶液 pH 由酸性调节至 5.2 时, 铁盐溶出可降低至 0.24 mg/L, 当将 pH 调至 6.0 时, 反应体系中 Fe 浓度低于 ICP-OES 的检测下限。根据以上实验结果, 确定重复实验的反应条件及回收步骤: 反应温度 120°C, 氧分压 0.9 MPa, 催化剂用量为 2 g/L, 2-CP 的初始浓度为 2 g/L。反应 24 h 后, 将反应釜冷却至室温, 加入 NaOH, 使溶液 pH 升至 6.0。将溶液过滤并用去离子水洗涤催化剂, 之后于 105°C 下烘干, 称重。

图 3-9 是使用经过多次重复利用、回收的 Fe₃O₄/SC 催化剂催化湿式氧化降解 2-CP 的情况。从图中可以看出, 经四次重复使用, Fe₃O₄/SC 催化体系对 2-CP 和 TOC 的去除效果并没有太大下降。但与第一次反应相比, 后续的三次反应在开始时存在一段诱导期。从图 3-9 C 中可以看出, 在后三次重复使用 Fe₃O₄/SC 催化剂时, 反应体系的 pH 在反应初期未出现像第一次反应中 pH 迅速下降的情况。同时我们检测了四次反应在反应进行 1 h 时 Fe 的溶出量, 如表 3-4 所示, 可见后三次反应中铁盐溶出没有第一次迅速。

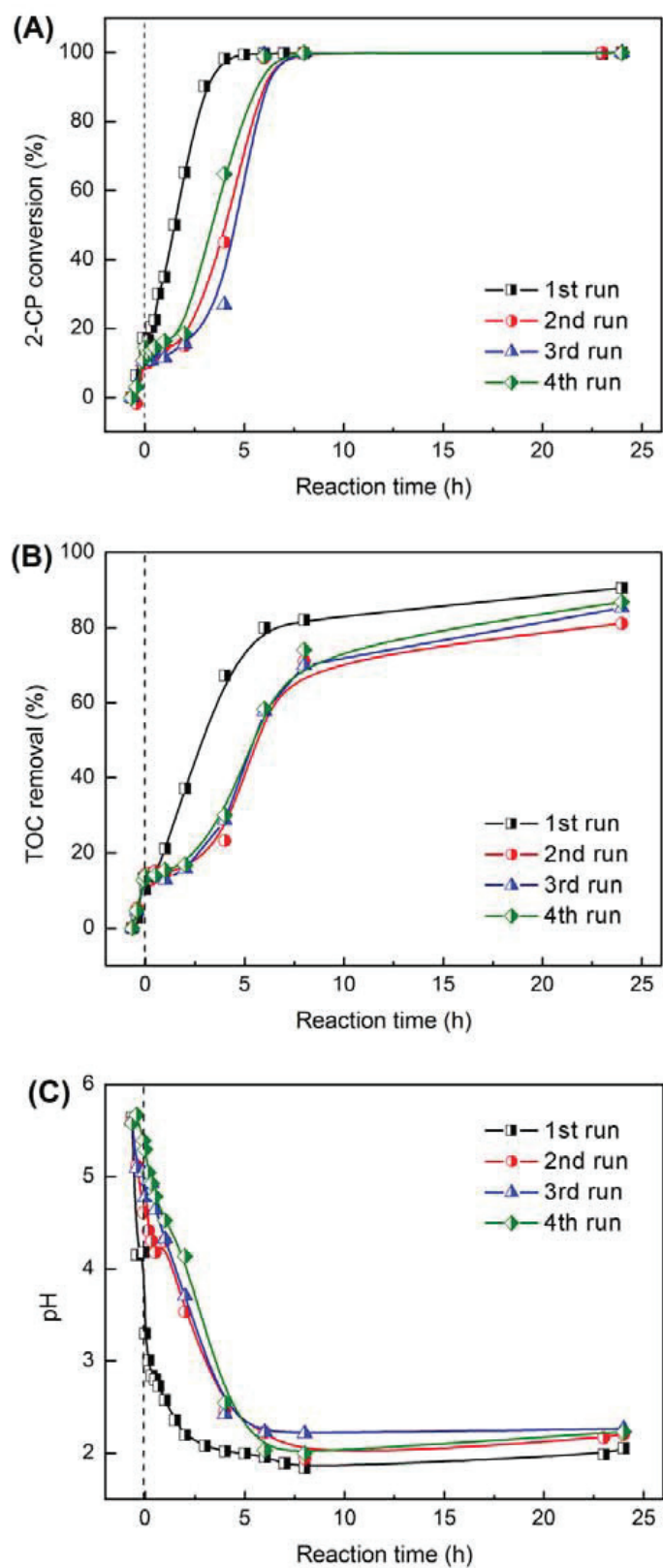


图 3-9 $\text{Fe}_3\text{O}_4/\text{SC}$ 催化剂重复利用对 2-CP 的去除率(A); TOC 去除率(B)及溶液 pH(C)的影响

Fig. 3-9. Evolution of the 2-CP conversion (A), the TOC removal (B) and the pH (C) upon wet air

oxidation (WAO) of 2-CP while recycling a 0.3g sample of the Fe₃O₄/SC catalyst (120°C, P_{O₂}: 0.9 MPa, 1300 rpm, 150 mL [2-CP]₀ = 2g·L⁻¹).

表 3-4 Fe₃O₄/SC 催化剂重复使用实验中铁盐的溶出情况

Table 3-4. Iron leaching upon successive batch experiments (120°C, P_{O₂}: 0.9 MPa, 1300 rpm, 150 mL [2-CP]₀ = 2g·L⁻¹).

Run time	Catalyst dosage (g·L ⁻¹)	Reaction after 1 h			Reaction after 24 h		
		Fe leached (mg·L ⁻¹)	Fe leached (wt. %)	pH	Fe leached (mg·L ⁻¹)	Fe leached (wt. %)	pH
1	2.00	12	5.0	2.6	30	13	2.1
2	1.96	2.0	0.9	4.3	32	14	2.2
3	1.78	0.4	0.2	4.3	40	19	2.3
4	1.58	1.3	0.7	4.5	34	18	2.2

3.3.6. 2-CP 氧化降解机理的研究

通过 HPLC 分析检测出 Fe₃O₄/SC 催化湿式氧化降解 2-CP 的中间产物有 4-氯间苯二酚(4-Chlororesoreinol), 2-氯对苯二酚(2-Chlorohydroquinone), 邻苯二酚(Catechol), 对苯二酚(Hydroquinone), 马来酸(maleic acid), 琥珀酸(succinic acid), 甲酸(formic acid), 草酸(oxalic acid)和盐酸(hydrochloric acid)。为了确定反应过程中各中间产物的变化规律, 本节配制了以上 9 种中间产物和 2-CP 不同浓度的混合标准溶液, 利用 HPLC 检测得到 10 种物质各浓度下的峰面积, 通过拟合求出相应的标准曲线, 以此对反应中间产物进行定性和定量分析。

用 2 g/L Fe₃O₄/SC 催化剂, 于 120°C, 0.9 MPa 氧分压下, 催化湿式氧化 150 mL 初始浓度为 2 g/L 的 2-CP 溶液。在特定时间取样, 过滤, 用 HPLC 进行分析。检测结果表明这些中间产物可分为小分子有机酸和低浓度的芳香族化合物两部分, 这些中间产物的浓度在反应过程中的变化情况如图 3-10 所示。

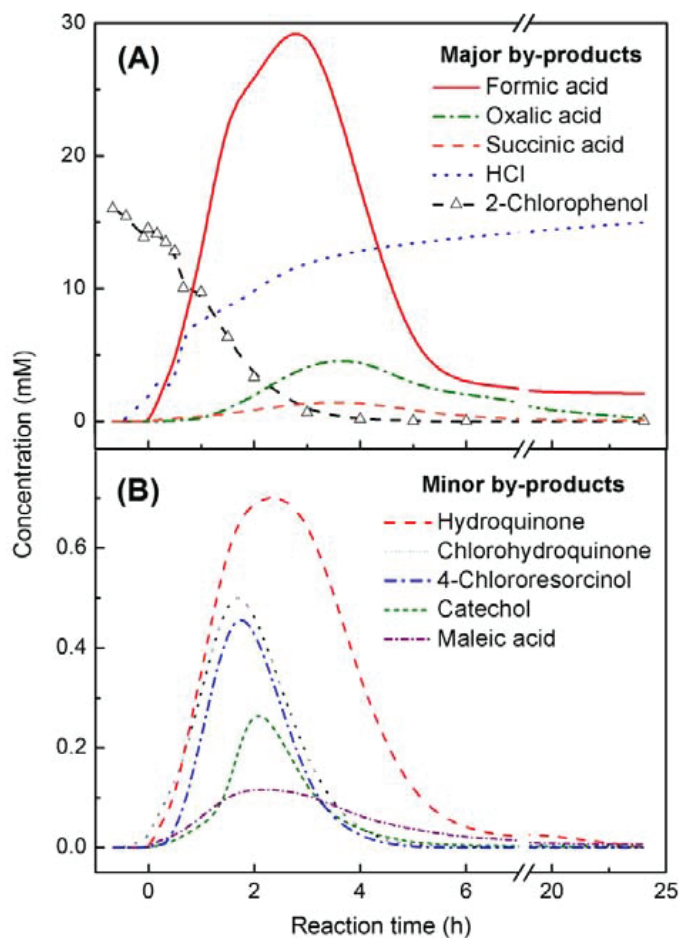


图 3-10 2-CP 及反应中间产物的浓度随反应时间的变化

Fig. 3-10. Concentration profiles of 2-CP and the identified intermediates formed during the catalytic wet oxidation of 2-CP over $\text{Fe}_3\text{O}_4/\text{SC}$ ($2 \text{ g L}^{-1} \text{ Fe}_3\text{O}_4/\text{SC}$, 120°C , P_{O_2} : 0.9 MPa, 1300 rpm, $150 \text{ mL } [2\text{-CP}]_0 = 2 \text{ g L}^{-1}$).

从图 3-10 A 中，也可以发现在反应初始 2h 内产生大量 HCl。这与前几节实验中观察到 2-CP 降解反应在初始阶段溶液的 pH 出现迅速下降的情况相一致。反应结束时溶液中检测到 15.0 mmol/L 的 HCl，占反应体系中氯离子总量的 93%。由 HCl 浓度随时间的变化曲线还可以发现，HCl 的产生可以分成两个阶段。在反应前 2h 内，HCl 迅速产生，表明 2-CP 在该反应体系中的氧化过程首先发生脱氯反应并产生 HCl^[40]。2h 之后，HCl 浓度缓慢增加，这归因于其它含氯中间产物被逐渐氧化，释放出氯离子。

图 3-10 中，芳香族中间产物和小分子有机酸的浓度随着反应的进行，均出

现先逐渐增加,到达某一最大值之后,又缓慢下降的变化趋势。这些中间产物出现最高浓度时对应的反应时间如表 3-5 所示。对各个中间产物的最大浓度基于 C 摩尔量计算出他们的最大选择率。由表 3-5 中的数据可以发现,所有芳香族中间产物最高浓度对应的反应时间均出现在小分子有机物的极值之前。小分子有机酸的选择率要略高于芳香族化合物。由此可以推断 2-CP 氧化过程中先产生芳香族化合物,之后苯环被打开,产生大量小分子有机酸。

表 3-5 基于 C 摩尔量计算的反应中间产物最大选择率

Table 3-5. The maximum selectivity for the different reaction intermediates calculated on a carbon basis.

中间产物	英文名	分子式	最大转化率对 应的的时间 (h)	最大选择率 (%)
2-氯对苯二酚	Chlorohydroquinone	C ₆ H ₃ (OH) ₂ Cl	1.70	5.4
4-氯间苯二酚	4-Chloroesoreinol	C ₆ H ₅ O ₂ Cl	1.77	3.7
邻苯二酚	Catechol	C ₆ H ₆ O ₂	2.12	2.8
对苯二酚	Hydroquinone	C ₆ H ₆ O ₂	2.33	5.6
马来酸	Maleic acid	C ₄ H ₄ O ₄	2.37	0.6
甲酸	Formic acid	CH ₂ O ₂	2.82	35.3
草酸	Oxalic acid	C ₂ H ₂ O ₄	3.60	10.2
琥珀酸	Succinic acid	C ₄ H ₆ O ₄	3.63	6.3

与 Suarez-Ojeda 等人^[41,42]在 CWAO 处理苯酚和 2-CP 过程中检测到的部分中间产物相比较,本实验中并未检测到 2-氯-对苯醌(2-chloro-p-benzoquinone, 2-CIBQ)和苯醌(benzoquinone, BQ)这两种中间产物。据报道这两种中间产物是由 2-氯对苯二酚(2-Chlorohydroquinone, 2-ClHQ)和对苯二酚(Hydroquinone, HQ)氧化而成,反应可在常温常压下发生。但是这两种苯醌类中间产物的稳定性较差,极易被进一步氧化成小分子有机酸。因此,在本研究的实验中只检测到低浓度的 2-ClHQ 和 HQ,由于氧化反应进行得太迅速,而未能检测到 2-CIBQ 和 BQ。

为了进一步确定通过 HPLC 检测出的 9 种中间产物的准确与合理性,我们将

图 3-10 中各中间产物对应的 TOC 值相加，并作出 TOC 计算值总和随反应时间的变化曲线，如图 3-11 所示，与用 TOC 分析仪测得的结果相比，计算所得中间产物 TOC 总和要略低于实验测得的 TOC 值，而这 26%左右的差值主要出现在反应进行 4 h 之后。根据各类中间产物在反应中出现的时间可以推断，这一差值可能由于通过 HPLC 未能很好地分离检测出部分小分子有机酸物质。

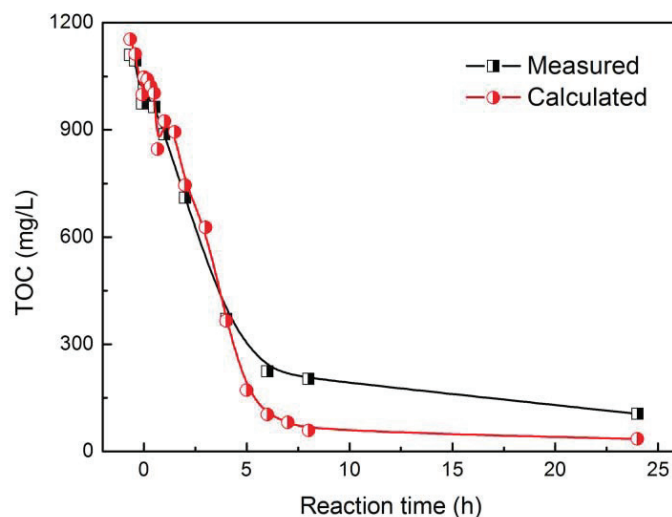


图 3-11 反应过程中检测所得中间产物对应 TOC 总和与分析测定值的比较

Fig. 3-11. Evolution of the measured (■) and calculated (●) TOC values as a function of time upon catalytic wet air oxidation of 2-CP over the $\text{Fe}_3\text{O}_4/\text{SC}$ catalyst (0.3g $\text{Fe}_3\text{O}_4/\text{SC}$ 120°C, P_{O_2} : 0.9 MPa, 1300 rpm, 150 mL $[\text{2-CP}]_0 = 2\text{g/L}$).

通过对已检测出的中间产物进行分析，可以推断该反应体系下 2-CP 的降解途径大致如图 3-12 所示。反应初始阶段，体系中产生 $\text{O}_2\cdot$ 和 $\text{OH}\cdot$ 等自由基与 2-CP 分子发生加成或者取代反应，导致 2-CP 分子的脱氯和羟基化，生成盐酸和酚类物质，如 2-氯对苯二酚(2-Chlorohydroquinone)，4-氯间苯二酚(4-Chloroesoreinol)，邻苯二酚(Catechol)，对苯二酚(Hydroquinone)等。这些芳香族中间产物将被进一步氧化，苯环被打开，生成大量小分子有机酸，如马来酸(maleic acid)，琥珀酸(succinic acid)，甲酸(formic acid)，草酸(oxalic acid)等。随着反应的进行，这些产物最终被分解成 CO_2 和 H_2O 。

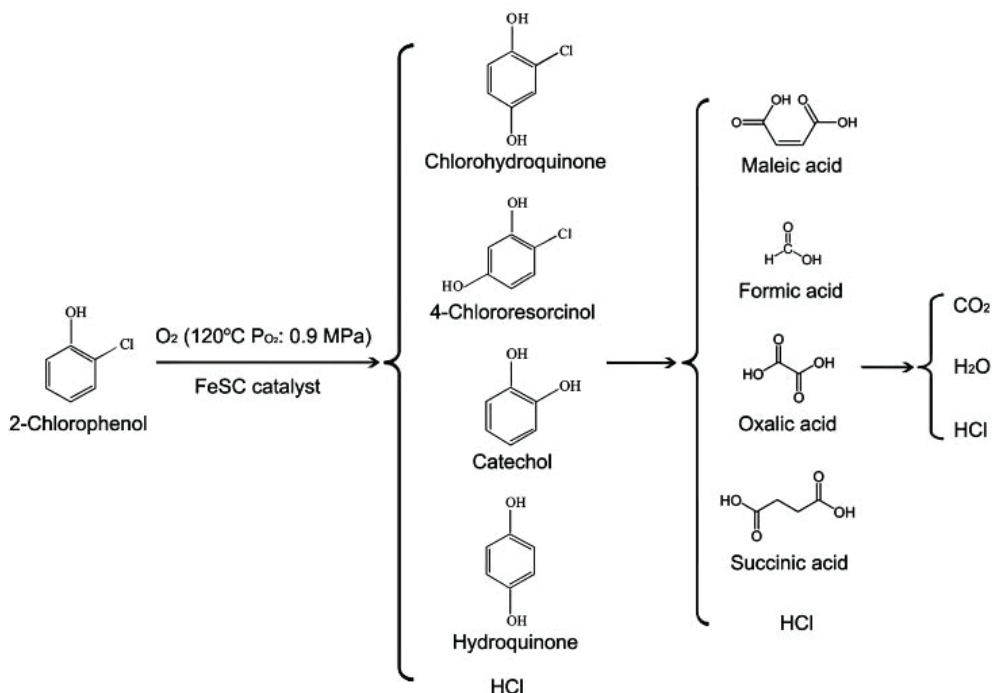


图 3-12 2-CP 在使用 $\text{Fe}_3\text{O}_4/\text{SC}$ 催化剂的湿式催化氧化反应中的主要降解途径

Fig. 3-12. Simplified reaction pathway upon catalytic wet air oxidation of 2-chlorophenol over $\text{Fe}_3\text{O}_4/\text{SC}$ catalysts.

3.4. 小结

本章将污泥基碳 SC 和负载铁氧化物的污泥基碳复合催化剂 $\text{Fe}_3\text{O}_4/\text{SC}$ 应用于湿式催化氧化反应处理高浓度的 2-CP 溶液。研究了反应过程中 2-CP 的转化率，TOC 去除率，溶液 pH 值和反应中间产物随反应时间的变化规律。并探讨反应过程中铁盐溶出的机理，及控制 Fe 溶出的可行方案。研究表明：

- (1). $\text{Fe}_3\text{O}_4/\text{SC}$ 催化剂具有较高的湿式催化氧化活性。在 120°C ，氧分压为 0.9 MPa 的反应条件下， 0.5 g $\text{Fe}_3\text{O}_4/\text{SC}$ 催化剂能在 5 h 内将 150 mL 初始浓度为 2 g/L 的 2-CP 溶液彻底去除。反应 24 h 后 TOC 去除率也高达 90% 。反应的化学活化能为 50.5 kJ/mol ，与湿式氧化的活化能（约 140 kJ/mol ）相比，加入 $\text{Fe}_3\text{O}_4/\text{SC}$ 催化剂能有效地降低反应的活化能。
- (2). 反应体系中 2-CP 的转化率，溶液 pH 和铁盐溶出三者之间是互相关联、相互

影响的。铁盐溶出能加速湿式催化反应，从而产生大量 HCl 和小分子有机酸，导致溶液 pH 迅速下降。反应 24 h 后在滤液中检测到约 30 mg/L 的 Fe，占总铁盐投加量的 7 wt.%。通过加入 pH=4.5, 0.1 M 的醋酸盐缓冲溶液能有效减少铁盐溶出，同时使 Fe₃O₄/SC 催化剂保留一定的催化活性。由于醋酸容易在后续的生物处理工序中被降解，因此这种控制铁盐溶出的方法在实际应用中具有一定的可行性。

- (3). 通过 HPLC 检测出 4-氯间苯二酚(4-Chlororesoreinol), 2-氯对苯二酚(2-Chlorohydroquinone), 邻苯二酚(Catechol), 对苯二酚(Hydroquinone), 马来酸(maleic acid), 琥珀酸(succinic acid), 甲酸(formic acid), 草酸(oxalic acid)和盐酸(hydrochloric acid)等中间产物。通过测定这些中间产物的浓度随反应时间的变化情况, 推测出 2-CP 在 Fe₃O₄/SC 催化湿式氧化反应中的降解途径: 2-CP 首先与 O₂•和 OH•等自由基发生加成或者取代反应, 生成盐酸和酚类物质。接着苯环被进一步氧化, 开环, 生成大量小分子有机酸。氧化反应最终产物为 HCl、CO₂ 和 H₂O。

3.5. 参考文献

- [1] Luck F. A review of industrial catalytic wet air oxidation processes. *Catal. Today*, 1996, 27:195-202
- [2] Qin J Y, Zhang Q L, Chuang K T. Catalytic wet oxidation of p-chlorophenol over supported noble metal catalysts. *Appl. Catal. B: Environ.*, 2011, 29: 115-123
- [3] Li N, Descorme C, Besson M. Catalytic wet air oxidation of aqueous solution of 2-chlorophenol over Ru/zirconia catalysts. *Appl. Catal. B: Environ.*, 2007, 71: 262-270
- [4] 孙颖. 催化湿式氧化中铜和锰基催化剂的研究. 硕士学位论文. 大连铁道学院. 3. 2003
- [5] Quintanilla A, Casas J A, Rodríguez J J. Catalytic wet air oxidation of phenol with modified activated carbons and Fe/activated carbon catalysts. *Appl. Catal. B: Environ.*, 2007, 76: 135-145
- [6] Posada D, Betancourt P, Liendo F, Brito J L. Catalytic wet air oxidation of aqueous solutions of substituted phenols. *Catal. Lett.*, 2006, 106: 81-88

- [7] 谭亚军, 蒋展鹏, 祝万鹏, 骆武山. 有机污染物湿式氧化降解中 Cu 系列催化剂的稳定性. 环境科学, 2000, 21(4): 82-85
- [8] Santos A, Yustos P, Quintanilla A, Ruiz G, Garcia-Ochoa F. Study of the copper leaching in the wet oxidation of phenol with CuO-based catalysts: Causes and effects. Appl. Catal. B: Environ., 2005, 61: 323-333
- [9] 徐新华, 何平, 金剑, 郝志伟. Fe salts as catalyst for the wet oxidation of o-chlorophenol. J. Zhejiang Univ. SCI, 2005, 6B (6):569-573
- [10] 王兆慧, 马万红, 陈春城, 籍宏伟, 赵进才. TiO₂ 光催化降解氯酚类有机污染物的反应机理. 中国科学: 化学, 2011, 41: 1286-1297
- [11] 文岳中, 姜玄珍, 刘维屏. 高压脉冲放电与臭氧氧化联用降解水中对氯苯酚. 环境科学, 2002, 23: 73-76
- [12] Pera-Titus M, García-Molina V, Baños M A, Giménez J, Esplugas S. Degradation of chlorophenols by means of advanced oxidation processes: a general review. Appl. Catal. B: Environ., 2004, 47: 219-256
- [13] Polcaro A M, Palmas S, Renoldi F, Mascia M. On the performance of Ti/SnO₂ and Ti/PbO₂ anodes in electrochemical degradation of 2-chlorophenol for wastewater treatment. J. Appl. Electrochem., 1999, 29: 147-151
- [14] Ku Y, Leu R M, Lee K C. Decomposition of 2-chlorophenol in aqueous solution by UV irradiation with the presence of titanium dioxide. Water Res., 1996, 30: 2569-2578
- [15] Son S H, Lee J H, Byeon S H, Lee C H. Surface chemical analysis of corroded alloys in subcritical and supercritical water oxidation of 2-chlorophenol in continuous anticorrosive reactor system. Ind. Eng. Chem. Res., 2008, 47: 2265-2272
- [16] Meunier B. Catalytic degradation of chlorinated phenols. Science, 2002, 296: 270-271
- [17] Lee G, Nunoura T, Matsumura Y, Yamamoto K. Effects of a sodium hydroxide addition on the decomposition of 2-Chlorophenol in supercritical water. Ind. Eng. Chem. Res., 2002, 41: 5427-5431
- [18] Gu L, Zhu N, Zhou P. Preparation of sludge derived magnetic porous carbon and their application in Fenton-like degradation of 1-diazo-2-naphthol-4-sulfonic acid. Bioresource Technol., 2012, 118: 638-642

- [19] Li N, Descorme C, Besson M. Catalytic wet air oxidation of 2-chlorophenol over Ru loaded $Ce_xZr_{1-x}O_2$ solid solutions. *Appl. Catal. B: Environ.*, 2007, 76: 92-100
- [20] Brunelle J P. Preparation of catalysts by metallic complex adsorption on mineral oxides. *Pure Appl. Chem.*, 1978, 50: 1211-1229
- [21] Barbier Jr. J, Delanoë F, Jabouille F, Duprez D, Blanchard G, Isnard P. Total oxidation of acetic acid in aqueous solutions over noble metal catalysts. *J. Catal.*, 1999, 77: 378-385
- [22] Béziat J C, Besson M, Gallezot P, Durécu S. Catalytic wet air oxidation of carboxylic acids on TiO_2 -supported ruthenium catalysts. *J. Catal.*, 1999, 182: 129-135
- [23] Joglekar H S, Samant S D, Joshi J B. Kinetics of wet air oxidation of phenol and substituted phenols. *Water Res.*, 1991, 25: 135-145
- [24] Gallezot P, Chaumet S, Perrard A, Isnard P. Catalytic wet air oxidation of acetic acid on carbon-supported ruthenium catalysts. *J. Catal.*, 1997, 168: 104-109
- [25] 王建兵, 祝万鹏, 王伟, 杨少霞. 颗粒 Ru 催化剂催化湿式氧化乙酸和苯酚. *中国环境科学*, 2007, 27(2): 179-183
- [26] Kojima Y, Fukuta T, Yamada T, Onyango M S, Bernardo E C, Matsuda H, Yagishita K. Catalytic wet oxidation of o-chlorophenol at mild temperatures under alkaline conditions. *Water Res.*, 2005, 39: 29-36
- [27] Marques R R N, Stüber F, Smith K M, Fabregat A, Bengoa C, Font J, Fortuny A, Pullket S, Fowler G D, Graham N J D. Sewage sludge based catalysts for catalytic wet air oxidation of phenol: Preparation, characterisation and catalytic performance. *Appl. Catal. B: Environ.*, 2011, 101: 306-316
- [28] Kim K H, Ihm S K. Heterogeneous catalytic wet air oxidation of refractory organic pollutants in industrial wastewaters: A review. *J. Hazard. Mater.*, 2011, 186: 16-34
- [29] Santos A, Yustos P, Quintanilla A, Garcia-Ochoa F. Influence of pH on the wet oxidation of phenol with copper catalyst. *Top. Catal.*, 2005, 33: 181-192
- [30] Wei L, Hervé M, Edouard P. Use of different rapid mixing devices for controlling the properties of magnetite nanoparticles produced by precipitation. *J. Cryst. Growth*, 2012, 342: 21-27
- [31] Robert R, Barbati S, Ricq N, Ambrosio M. Intermediates in wet oxidation of

- cellulose: identification of hydroxyl radical and characterization of hydrogen peroxide. *Water Res.*, 2002, 36: 4821-4829
- [32] Arena F, Italiano C, Raneri A, Saja C. Mechanistic and kinetic insights into the wet air oxidation of phenol with oxygen (CWAO) by homogeneous and heterogeneous transition-metal catalysts. *Appl. Catal. B: Environ.*, 2010, 99: 321-328
- [33] Leussing D L, Kolthoff I M. The solubility product of ferrous hydroxide and the ionization of the aquo-ferrous ion. *J. Am. Chem. Soc.*, 1953, 75: 2476-2479
- [34] Quintanilla A, Casas J A, Mohedano A F, Rodríguez J J. Reaction pathway of the catalytic wet air oxidation of phenol with a Fe/activated carbon catalyst. *Appl. Catal. B: Environ.*, 2006, 67: 206-216
- [35] Lee G, Nunoura T, Matsumura Y, Yamamoto K. Comparison of the effects of the addition of NaOH on the decomposition of 2-chlorophenol and phenol in supercritical water and under supercritical water oxidation conditions. *J. Supercrit. Fluids*, 2002, 24: 239-250
- [36] Pintar A, Levec J. Catalytic oxidation of aqueous p-chlorophenol and p-nitrophenol solutions. *Chem. Eng. Sci.*, 1995, 49: 4391-4407
- [37] Guo J, Al-Dahhan M. Activity and stability of iron-containing pillared clay catalysts for wet air oxidation of phenol. *Appl. Catal. A: Gen.*, 2006, 299: 175-184
- [38] Tran N D, Besson M, Descorme C, Fajferberg K, Louis C. Influence of the pretreatment conditions on the performances of CeO₂-supported gold catalysts in the catalytic wet air oxidation of carboxylic acids. *Catal. Commun.*, 2011, 16: 98-102
- [39] Straub K L, Benz M, Schink B. Iron metabolism in anoxic environments at near neutral pH. *FEMS Microbiol. Ecol.*, 2001, 34: 181-186
- [40] Pouloupoulos S G, Korologos C A, Boulamanti A, Philippopoulo C J. Treatment of 2-chlorophenol aqueous solutions by wet oxidation. *Water Res.*, 2007, 41: 1263-1268
- [41] Suarez-Ojeda M E, Stüber F, Fortuny A, Fabregat A, Carrera J, Font J. Catalytic wet air oxidation of substituted phenols using activated carbon as catalyst. *Appl. Catal. B: Environ.*, 2005, 58: 105-114

- [42]Li N, Descorme C, Besson M. Catalytic wet air oxidation of chlorophenols over supported ruthenium catalysts. *J. Hazard. Mater.*, 2007, 146: 602-609

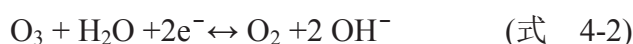
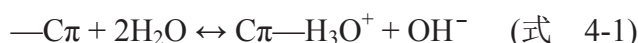
第4章 Mn-g-C₃N₄/污泥碳复合臭氧催化剂的制备及催化活性研究

4.1. 引言

药物和个人护理用品(Pharmaceuticals and personal care products, PPCPs)由于存在潜在的环境安全风险,近年来受到越来越多的关注^[1]。在众多 PPCPs 微量有机污染物中,磺胺类抗生素在临床和畜牧饲养方面被广泛应用,且在环境中被检出的频率最高^[2]。研究发现此类药物在施药后 50-90%的有效成分并未进入生物体的新陈代谢而是被直接排出,进入周围环境中。由于磺胺类抗生素具有高水溶性和低生物降解性,造成其大量残留于水体环境中^[3]。目前已在污水厂出水、地表水、饮用水、地下水和土壤中检测出浓度在 ng/L 到 μg/L 范围内的此类污染物^[4]。这些残留的抗生素会增强环境中病毒的抗药性,对人类和水生生物造成潜在威胁。此外据报道,即使是很低浓度的磺胺甲恶唑(Sulfamethoxazole, SMZ)也能诱发基因突变和慢性病^[5]。由于此类抗生素不易被微生物降解,通过常规生物处理工艺很难被彻底去除。因此,需采用化学氧化法对含此类药物的废水进行处理,以降低其在环境中的残余浓度。在众多用于处理抗生素废水的高级氧化技术中,臭氧氧化法由于具有氧化能力高、设备简单等优点,在水处理领域有很好的应用前景^[6]。

催化臭氧氧化分解技术是近年来发展起来的高级氧化工艺,与传统的单独臭氧氧化法相比具有更高的催化效率。根据催化剂的形态,可以分为均相催化臭氧氧化法和多相催化臭氧氧化法,其中前者大多是以金属离子作为催化剂,而后者是以单独或负载化的固态物质为催化剂^[7]。与均相反应相比,多相催化臭氧氧化具有操作简便、催化剂利于回收、水处理成本较低等优点,因而成为催化臭氧氧化研究领域的热点。在众多催化剂中,活性碳常被单独作为催化剂或者催化剂载体被应用于催化臭氧氧化反应中^[8,9]。研究发现活性碳的臭氧催化活性与其表面

碱性官能团含量直接相关^[10]，其中报道较多的是含氧官能团，如吡喃酮(Pyrones)或苯并吡喃(Chromenes)^[11]。近年来有学者发现增加活性碳表面含氮碱性官能团，如氨基(Amino groups)^[12]和吡咯(Pyrrole groups)^[13]，可使活性碳的臭氧催化活性明显提高。目前主要是通过通过在高温下使用 H₂、N₂ 或 NH₃ 气体对活性碳进行处理的方法来增加活性碳表面碱性官能团^[14]。此外，还有研究认为活性碳中石墨微晶中由于具有丰富的 π 电子，从而显现出 Lewis 碱催化特性。在催化臭氧氧化反应中，具有 π 电子的石墨微晶结构能够通过式 4-1 与 4-2，所示反应产生 OH⁻，之后引发一系列自由基反应^[15]。



近年来在材料和催化领域被广泛研究的氮化碳材料是一种高氮含量的物质。Teter 和 Hemley 等^[16]通过第一性原理电子能带理论计算提出氮化碳存在五种不同的物相： α 相、 β 相、立方相(cubic)、类立方相(pseudo-cubic)和类石墨相(graphitic)。其中石墨相氮化碳在室温下最为稳定且应用最为广泛^[17]。理论认为石墨相氮化碳(g-C₃N₄)是以三嗪环(s-triazine)或者三均三嗪环(tri-triazine)作为母体结构，通过 N 原子的桥联形成一种具有类似于石墨片层结构的物质，片层间以微弱的范德华力结合。Kroke 等根据密度泛函理论(DFT)计算结果认为以三均三嗪环为基本结构的 g-C₃N₄ 结构(图 4-1)最为稳定^[18]。而近年来，将 g-C₃N₄ 作为催化剂的研究也大多是基于此结构模型。

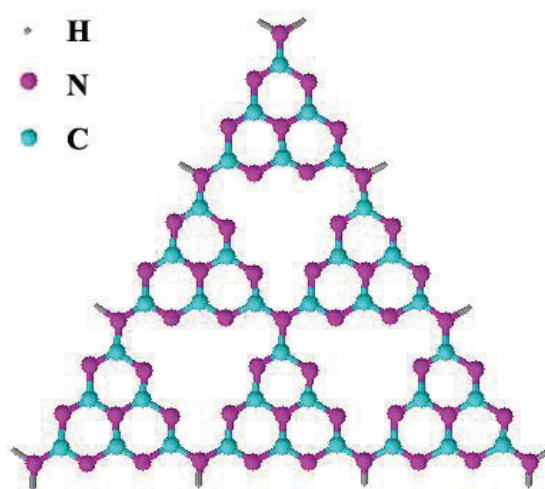


图 4-1 g-C₃N₄ 理想结构示意图

Fig. 4-1 An idealized g-C₃N₄ sheet.

福州大学的王心晨等^[19]以金属氯化物和双氰胺为原料,通过高温热解制备负载金属的 g-C₃N₄,并用作可见光催化剂降解罗丹明 B,结果表明金属掺杂的催化剂比纯 g-C₃N₄表现出更优异的催化活性。日本的 Bing Yue 等人^[20]则通过两步法制备得 Zn 掺杂 g-C₃N₄ 催化剂,并考察其可见光催化分解制氢的能力,结果表明 Zn 掺杂量为 10%的催化剂的产氢量是纯 g-C₃N₄ 的 10 倍。这主要是由于金属掺杂能够提高光生电子与空穴的分离效率。李芳芳等^[21]将 Ag 掺杂入 g-C₃N₄ 载体中,发现所得材料具有很好的光致发光性能,将其用作光学传感器来检测微量铜离子,其检测限可达 1 mmol/L,具有较好的应用前景。但是目前有关这类材料的应用研究主要基于其光化学性能。与大量将 g-C₃N₄ 材料作为光催化的报道相比,将 g-C₃N₄ 作为碱性催化剂的报道还不多。Antonietti 课题组发现 g-C₃N₄ 在 CO₂ 氧化苯合成苯酚、Friedel-Craft 酰基化、腈/炔环化等反应中均具有较高的碱性催化活性^[22]。Zhu 等^[23]考察了 g-C₃N₄ 催化分解 NO 的性能。发现由于 g-C₃N₄ 中的通过 2p 轨道杂化的 N 原子带孤对电子,使 g-C₃N₄ 存在一定的 Lewis 碱催化性质。当 NO 吸附于催化剂表面之后,g-C₃N₄ 中 N 上的电子将转移至 NO,使得 NO 气体分子变得不稳定,在高温下迅速分解成 N₂ 和 O₂。同时该研究还发现在 g-C₃N₄ 中掺入 Zn(II)和 Au 制备的金属掺杂 g-C₃N₄ 表现出更高的催化活性。由此可见,g-C₃N₄ 具有 Lewis 碱催化特性,同时 g-C₃N₄ 中 N 元素含量丰富,结构边缘的 N 易与 H 原子结合生成-NH₂ 等含氮碱性官能团^[24]。而催化剂的这两种特性都将使其具有较高的臭氧催化活性。此外,在制备过程中,负载于 g-C₃N₄ 上的金属或金属化合物颗粒的生长会受到 g-C₃N₄ 的类石墨片层和纳米氮孔结构的影响,最终形成分散度高、尺寸小的纳米颗粒。由此可见,g-C₃N₄ 理论上可单独或者作为催化剂载体应用于催化臭氧氧化反应,并表现出较高的催化臭氧氧化活性。但是目前未见有关 g-C₃N₄ 及其相关材料作为臭氧氧化催化剂的报道。

污泥活性碳(Sewage sludge-based activated carbon, SBAC)具有大的比表面积和丰富的孔隙结构,理论上能够有效吸附水体中广泛存在的痕量 PPCPs。将污泥活性碳用于催化臭氧氧化反应,能在反应体系中实现对 PPCPs 的吸附和氧化降解。为了提高污泥活性碳催化臭氧氧化的活性,本章还尝试通过固体热聚合法将 Mn 掺杂 g-C₃N₄ 负载于污泥活性碳表面,制备成新型复合催化剂。在提高污泥碳基催化剂活性的同时解决直接热解聚合制备而得的石墨相氮化碳比表面积低(<

10 m²/g^[25])对 PPCPs 吸附能力弱的问题。本章将以典型的磺胺类抗生素药物——磺胺甲恶唑(SMZ)为目标污染物, 考察金属掺杂氮化碳与污泥活性碳的复合催化剂的催化活性, 并对催化机理及稳定性进行研究。

4.2. 实验部分

4.2.1. 实验试剂与材料

表 4-1 实验所用主要试剂

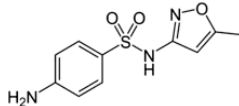
Table 4-1. Primary reagents in the experiment

药品	等级	厂家
三聚氰胺	分析纯(AR)	上海阿拉丁试剂
乙酸锰	分析纯(AR)	广州化学试剂厂
乙醇	分析纯(AR)	广州化学试剂厂
磺胺甲恶唑	分析纯(AR)	上海阿拉丁试剂
叔丁醇	分析纯(AR)	广州化学试剂厂
磷酸	分析纯(AR)	广州化学试剂厂
甲醇	分析纯(AR)	天津四友试剂厂

其中目标污染物磺胺甲恶唑的物理化学性质如表 4-2 所示。

表 4-2 磺胺甲恶唑的物理化学参数^[26]

Table 4-2. Physicochemical properties of Sulfamethoxazole

Structure	Formula	Molecular weight (g/mol)	Width (nm)	Length (nm)	Depth (nm)	Solubility at 25°C (g/L)	Acid pKa
	C ₁₀ H ₁₁ N ₃ O ₃ S	253.28	0.71	1.33	0.58	< 1.0	5.7

4.2.2. 实验仪器

表 4-3 实验所用主要仪器

Table 4-3. Primary apparatus in the experiment

仪器名称	仪器型号	生产厂家
热恒温鼓风干燥箱	DHG-9023A	上海一恒科技有限公司
恒温加热磁力搅拌器	DF-101S	英峪华仪器有限责任公司
管式电阻炉	SKF-2-12	杭州蓝天仪器设备有限公司
超声波清洗机	JP-C100	广州市吉普超声波电子设备有限公司
真空抽滤机	2X-1	临沂华达烘干设备厂
臭氧发生器	YE-TG-02PII	南京易德高臭氧有限公司
臭氧检测器	IDEAL-2000	淄博爱迪尔测控技术有限公司
恒温磁力搅拌器	85-2	常州澳华仪器有限公司
高效液相色谱	LC-15C	日本岛津
pH 计	PHS-3C	上海雷磁仪器厂
COD 微波消解仪	MS-3	华南环境科学研究所

4.2.3. 催化剂的制备

4.2.3.1. Mn 掺杂石墨相氮化碳催化剂的制备

石墨相氮化碳催化剂(g-C₃N₄)的制备是采用三聚氰胺热聚合法。称取 2.000 g 三聚氰胺(C₃H₆N₆)用研钵充分研磨后装入瓷方舟中,置于管式电阻炉内,于 550°C 在 N₂ 气氛中热解 4 h,升温速率控制为 3 °C/min。待冷却至室温后,取出,研磨,并用蒸馏水洗涤直至滤液 pH 恒定不变。将样品于 105°C 烘干,过 200 目筛,得氮化碳催化剂 g-C₃N₄。

Mn 掺杂石墨相氮化碳催化剂(Mn-g-C₃N₄)的制备与上述步骤相同,将一定量的乙酸锰与 2.000 g 三聚氰胺(C₃H₆N₆)充分研磨均匀,通过高温热解使得金属离子化合物进入氮化碳分子结构中,实现对氮化碳的金属掺杂。原料乙酸锰与三聚氰胺的用量如表 4-4 所示。

表 4-4 Mn-g-C₃N₄ 系列催化剂的制备原料

Table 4-4. Preparation conditions for Mn-g-C₃N₄ catalysts

Sample	Melamine (g)	Manganese(II) acetate tetrahydrate (g)
g-C ₃ N ₄	2.000	0
10%Mn-g-C ₃ N ₄	2.000	0.583
20%Mn-g-C ₃ N ₄	2.000	1.402
30%Mn-g-C ₃ N ₄	2.000	2.633
40%Mn-g-C ₃ N ₄	2.000	4.697

4.2.3.2. 污泥活性碳的制备

本章实验所用污泥为广州市猎德污水处理厂的二沉池脱水污泥，取泥日期为 2013 年 7 月。将脱水污泥于 105°C 下烘干至恒重，过 100 目筛，于干燥器中保存备用。

采用氯化锌化学活化法制备污泥活性碳。将 100 g 干污泥与 250 mL 5 M ZnCl₂ 溶液混合均匀后浸渍 24 h。过滤后将浸泡过的污泥于 105°C 下烘干，之后放入瓷方舟内，置于管式电阻炉中在 650°C 下热解 1 h，升温速率：20°C/min，氮气流量：40 mL/min。热解尾气通入装有 NaOH 溶液的尾气瓶进行处理。待热解结束并冷却至室温后将样品取出，用 3 mol/L 的盐酸和 60°C 蒸馏水反复洗涤，直至用 0.1 mol/L 硝酸银溶液未检测到 Cl⁻为止。将样品于 105°C 烘干 12 小时，过 200 目筛，得污泥活性碳 SBAC。

4.2.3.3. 污泥活性碳和 Mn-g-C₃N₄ 复合催化剂的制备

表 4-5 污泥活性碳和 Mn-g-C₃N₄ 复合系列催化剂的制备原料

Table 4-5. Preparation conditions for Mn-g-C₃N₄/SBAC catalysts

Sample	SBAC (g)	Melamine (g)	Manganese(II) acetate tetrahydrate (g)
Mn-g-C ₃ N ₄ /SBAC ₁	1.000	0.142	0.049
Mn-g-C ₃ N ₄ /SBAC ₂	1.000	0.285	0.097
Mn-g-C ₃ N ₄ /SBAC ₃	1.000	0.569	0.194
Mn-g-C ₃ N ₄ /SBAC ₄	1.000	0.853	0.290

称取一定质量的三聚氰胺和乙酸锰,用研钵充分研磨。之后加入 1 g 用 4.2.3.2 节中所述方法制备得的污泥活性碳 SBAC, 并加入 1.2 g 乙醇, 在研钵中继续研磨, 直到样品混合均匀。将所得的深灰色样品盛入瓷方舟中, 在 105°C 下烘干。置于管式电阻炉中进行热解, 热解步骤和条件同 4.2.3.1 中石墨相氮化碳催化剂的制备。所得催化剂命名为 Mn-g-C₃N₄/SBAC_x, 其中下标 x 随着三聚氰胺和乙酸锰用量的增加而增加, 具体比例见表 4-5:

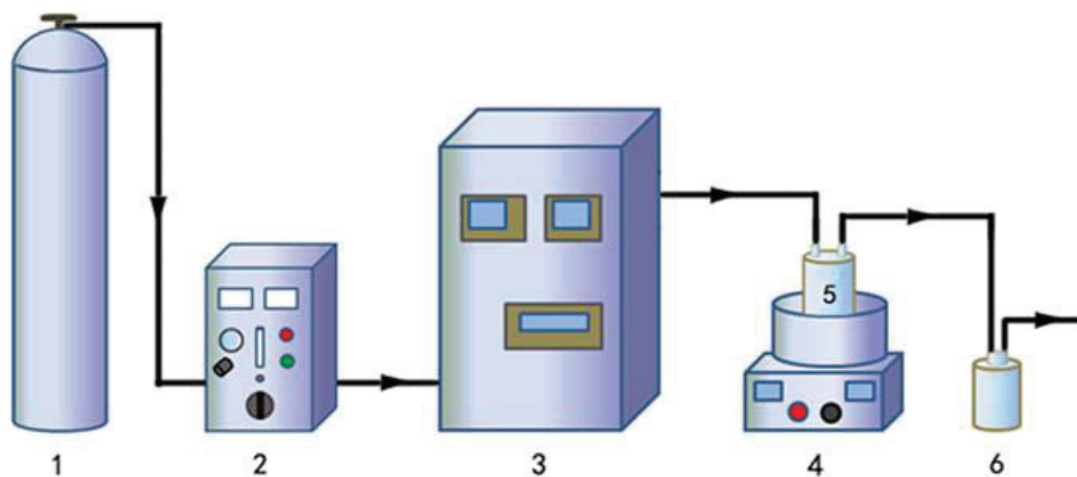
4.2.4. 催化剂的表征方法

同第二章 2.2.2 节。

4.2.5. 臭氧催化实验

4.2.5.1. 实验装置

臭氧反应系统如图 4-2 所示, 纯氧气经过臭氧发生器内部高压放电产生臭氧, 含有一定浓度的臭氧气流由三通阀分成两路, 一部分通往臭氧检测器检测臭氧浓度, 另一部分气流由砂芯曝气头鼓入高 145 mm, 直径为 55 mm, 有效容积为 300 mL 的圆柱形玻璃反应器中。反应器置于恒温磁力搅拌器上, 通过水浴加热将反应温度控制在设定值。尾气由反应器顶部收集并通入 KI 溶液进行吸收。



1—高压氧气罐; 2—臭氧发生器; 3—在线臭氧浓度检测器;
4—恒温磁力搅拌器; 5—反应器; 6—2% KI 吸收液

图 4-2 臭氧反应系统装置图

Fig. 4-2 Diagram of ozone oxidation system

4.2.5.2. 臭氧催化降解磺胺甲恶唑的实验方法

向反应器内加入 200 mL 已知溶度的磺胺甲恶唑溶液,开启恒温磁力搅拌器,待温度达到设定值且恒定后,加入一定质量的催化剂,超声处理 1 min 使得催化剂颗粒在溶液中分散均匀。在臭氧氧化反应前,混合溶液通过磁力搅拌 30 min 以确保催化剂对磺胺甲恶唑分子的吸附达到平衡。吸附 30 min 后停止搅拌,取 2 mL 水样,通过 0.45 μm 孔径的滤膜除去固体催化剂。用高效液相色谱测定吸附平衡之后溶液中磺胺甲恶唑的浓度。

在吸附反应进行的同时,预先开启臭氧发生和检测装置,通过调节氧气流量、臭氧发生器工作电压控制产生的臭氧浓度。待吸附进行 30 min 后,迅速向反应器中通入流量为 0.2 L/min 且浓度稳定的臭氧气体。间隔一定时间从反应器中取 5 mL 溶液,将 2 mL 经过 0.45 μm 孔径的滤膜过滤的溶液加入试管中,同时加入 0.5 mL 0.05 mol/L 的 $\text{Na}_2\text{S}_2\text{O}_3$ 溶液以去除溶液中残余的臭氧。

4.2.6. 分析方法

样品经 0.45 μm 的滤膜过滤后,用 Shimadzu LC-15C 型高效液相色谱仪测定滤液中磺胺甲恶唑的浓度。仪器配备 Wondasil C18 (4.6 \times 150 mm, 岛津 GL 公司),柱温 30 $^{\circ}\text{C}$ 。为有效分离 SMZ 和降解中间产物,流动相比经测试最终确定为 30 vol.% 甲醇和 70 vol.% 水的混合溶液,并用 85 wt.% 的浓 H_3PO_4 调至 pH 为 2.5。流速为 1.2 mL/min。进样量为 20 μL 。检测波长设定为 265 nm。

溶液 pH 的测量使用上海雷磁仪器厂的 PHS-3C 型 pH 计。

反应过程中溶液的 COD 值采用重铬酸钾法进行测定,为了避免 $\text{Na}_2\text{S}_2\text{O}_3$ 对测定结果的影响,不通过向滤液中加入 $\text{Na}_2\text{S}_2\text{O}_3$ 溶液来去除残留的 O_3 ,而是改用通入 2 min 空气气流的方式将残留于溶液中的 O_3 吹脱去除。

滤液中溶出金属离子浓度采用 Optima 5300DV 型电感耦合等离子体-原子发射光谱仪(美国 PerkinElmer 公司)进行测定。

4.3. 结果与讨论

4.3.1. Mn-g-C₃N₄ 的形貌及结构表征

从图 4-3 中可以看出, 在制备 g-C₃N₄ 的过程中加入乙酸锰, 将使催化剂的颜色从柠檬黄转变成黄绿色。由此可以初步推断含锰化合物在氮化碳载体上的负载将改变催化剂的物理化学性质。

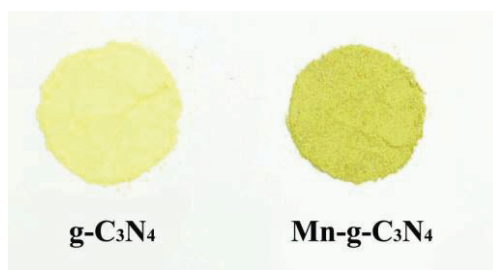


图 4-3 g-C₃N₄ 及 10%Mn-g-C₃N₄ 催化剂粉末

Fig. 4-3. Photos of g-C₃N₄ and 10%Mn-g-C₃N₄ catalysts

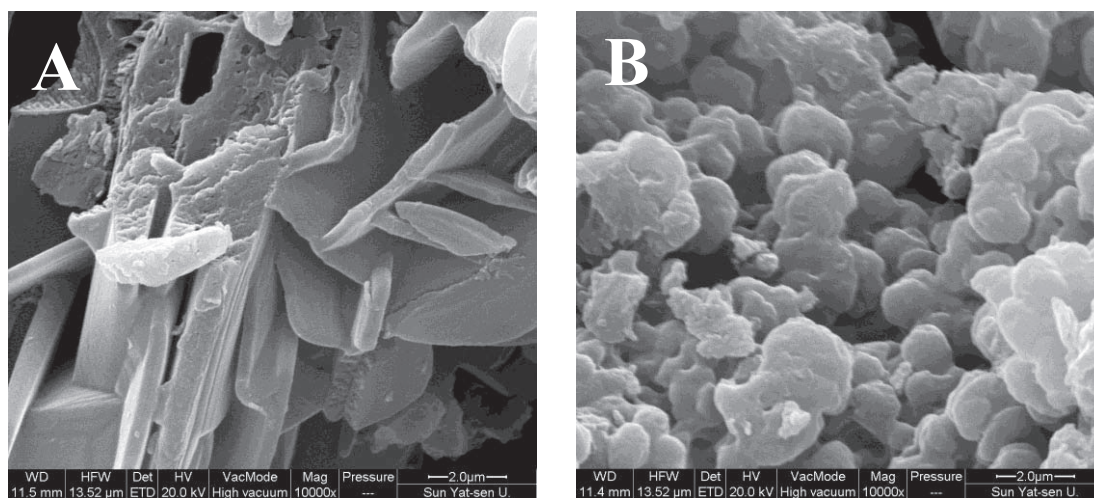


图 4-4 g-C₃N₄ (A)和 10%Mn-g-C₃N₄ (B) 的 SEM 图

Fig. 4-4. SEM image of g-C₃N₄ (A) and 10%Mn-g-C₃N₄ (B) catalysts.

为了比较 Mn 掺杂对 g-C₃N₄ 催化剂形貌的影响, 对 g-C₃N₄ 和 Mn-g-C₃N₄ 催化剂进行扫描电镜分析。图 4-4 分别给出了两种催化剂在放大倍数为 10000 倍时的 SEM 照片。由图 4-4 A 可以看出, 以三聚氰胺为原料通过热聚合法制备而得的石墨相氮化碳具有明显的石墨状片层结构, 且边缘呈较规则的菱形。在原料中

加入乙酸锰之后，制备得的 Mn-g-C₃N₄ 与纯 g-C₃N₄ 相比，表面形貌有很大差别。片层形状变得更不规则，由棱角分明变得圆滑，同时颗粒尺寸也明显变小。

为了确定催化剂表面 C、N、Mn 的分布情况，对 g-C₃N₄ 和 10%Mn-g-C₃N₄ 表面以上三种元素进行 EDX mapping 扫描，结果见图 4-5。g-C₃N₄ 中的主要元素为 C、N，两种元素都密集且均匀地分布于催化剂表面。Mn-g-C₃N₄ 中除了扫描到均匀分布的 C、N 元素外，制备过程中加入的 Mn 元素也被检测到，从 Mn EDX mapping 结果能够更加直观地看出 Mn 已非常均匀地负载于 g-C₃N₄ 载体中。

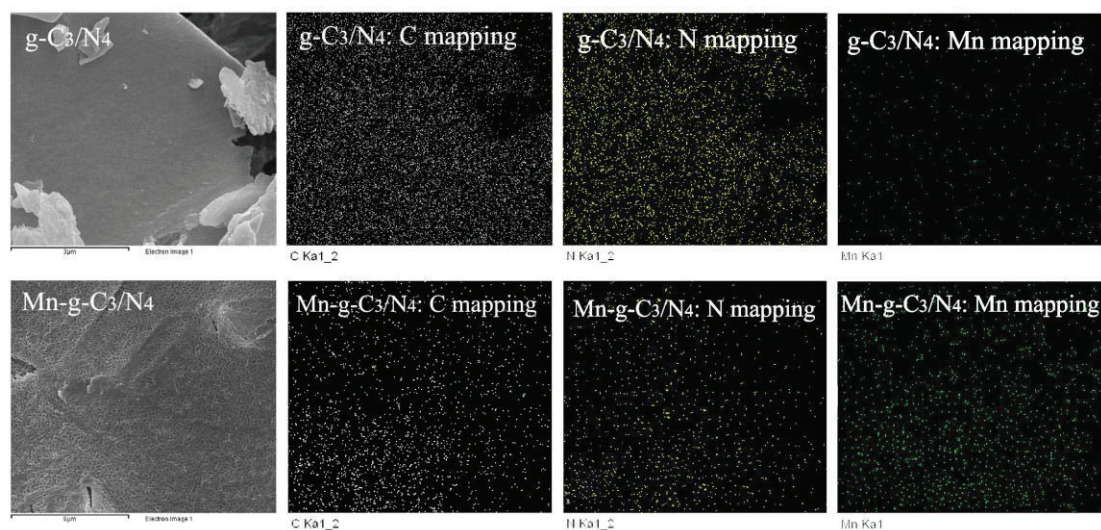


图 4-5 g-C₃N₄ 和 10%Mn-g-C₃N₄ 的 C、N、Mn 的 EDX mapping 图

Fig. 4-5. EDX mapping of C, N and Mn elements for g-C₃N₄ and 10%Mn-g-C₃N₄ catalysts.

表 4-6 g-C₃N₄ 和 Mn-g-C₃N₄ 中 C、N、H 含量

Table 4-6. The content of C, N and H element in g-C₃N₄ and Mn-g-C₃N₄ catalysts

Sample	C (wt.%)	N (wt.%)	H (wt.%)	C/N ratio
g-C ₃ N ₄	34.3	59.3	1.8	0.68
Mn-g-C ₃ N ₄	33.15	55.6	1.5	0.70

此外，我们还利用元素分析仪确定两种催化剂中的 C、N、H 含量，结果如表 4-6 所示。两种催化剂的 C 与 N 原子比分别为 0.68 和 0.70，接近理论值 0.75，再次证实所合成催化剂为石墨相氮化碳 g-C₃N₄ 材料。催化剂中少量的 H 可能源于催化剂中的氨基官能团。

本研究通过在制备过程中加入不同量的乙酸锰，制备出不同 Mn 含量的 Mn-g-C₃N₄ 催化剂，并对其进行 XRD 分析，结果如图 4-6 所示。从 XRD 谱图中可以看出对于 Mn 掺杂量低于 30% 的样品，在 $2\theta=12^\circ$ 和 27° 附近均出现一个较弱和较强的衍射峰，分别归属于石墨相氮化碳的(0 0 1)和(0 0 2)晶面，这两个晶面分别是类石墨结构材料的平面层内堆垛和芳香环的层间堆垛所引起的^[27]。因此，可以推断这些催化剂均是以三嗪环作为基本单元的类石墨层状化合物 g-C₃N₄。

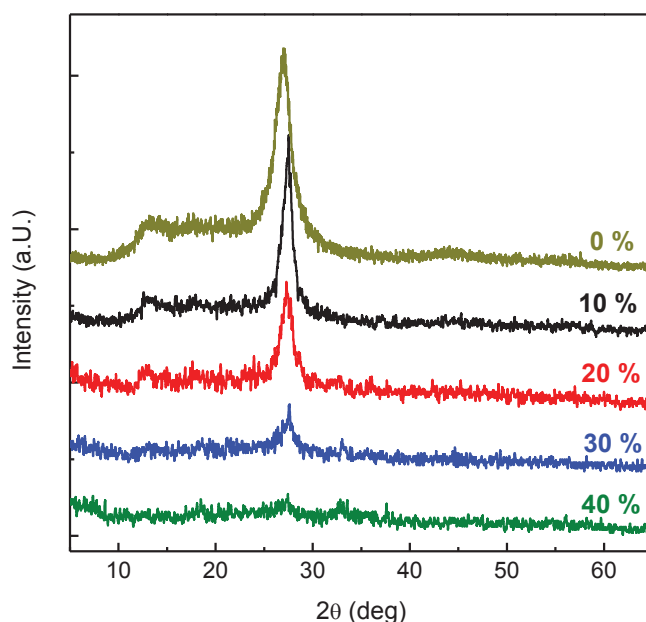


图 4-6 不同 Mn 负载量的 Mn-g-C₃N₄ 催化剂的 XRD 衍射图

Fig. 4-6. XRD patterns of Mn-g-C₃N₄ with different Mn content.

表 4-7 Mn-g-C₃N₄ 催化剂的布拉格衍射角和晶面间距

Table 4-7. Bragg angle and interlayer spacing of the Mn-g-C₃N₄.

Sample	2θ for (0 0 2) plane (deg)	d spacing (\AA)
g-C ₃ N ₄	26.983	3.30
10%Mn-g-C ₃ N ₄	27.374	3.26
20%Mn-g-C ₃ N ₄	27.443	3.25
30%Mn-g-C ₃ N ₄	27.569	3.23
40%Mn-g-C ₃ N ₄	27.580	3.23

与纯的 $g\text{-C}_3\text{N}_4$ 相比, $\text{Mn-g-C}_3\text{N}_4$ 对应于(0 0 2)晶面的衍射峰明显正移。石墨相氮化碳材料的晶面间距可以通过 Bragg 公式(4-3)进行计算^[28],

$$d = \frac{\lambda}{2 \sin \theta} \quad (\text{式 4-3})$$

式中, d 为晶面间距; λ 是 X 射线的波长(nm), 取 0.154056 nm; θ 为衍射角(Rad)。

表 4-7 给出了不同 Mn 含量的石墨相氮化碳催化剂(0 0 2)面对应的 2θ 衍射峰位置及根据 Bragg 公式计算得的晶面间距。随着 Mn 负载量的增加, (0 0 2)面对应的 2θ 衍射峰也略向高角度偏移, 晶面间距减小。这是由于含 Mn 化合物的掺入, 将导致石墨相氮化碳片层结构发生较小幅度的倾斜或弯曲, 从而导致晶面间距变小^[19]。这一现象进一步证实含锰化合物已成功地掺入 $g\text{-C}_3\text{N}_4$ 结构中。

从图 4-6 中还可以看出, 随着 Mn 掺杂量的增加, 其(0 0 2)衍射峰的强度逐渐减弱, 而(1 0 0)对应的衍射峰也随着 Mn 的掺入逐渐消失。表明制备过程中加入过量的乙酸锰将阻碍三聚氰胺之间的热聚合, 从而影响 $g\text{-C}_3\text{N}_4$ 催化剂的结晶度。同时在 Mn 掺杂量为 40%的 $\text{Mn-g-C}_3\text{N}_4$ 催化剂对应的 XRD 谱图中可以发现在 $2\theta=32.9^\circ, 45.2^\circ$ 和 55.2° 处出现对应 Mn_2O_3 的(2 2 2), (3 3 2)和(4 4 0)晶面宽化的衍射峰(JCPDS 41-1442)。通过 Debye-Scherrer 公式计算得 Mn_2O_3 的晶粒尺寸为 5.2 nm。由此, 我们可以推断负载的 Mn 是以纳米级 Mn_2O_3 存在于 $g\text{-C}_3\text{N}_4$ 催化剂载体中。因此为了获得小尺寸的 Mn_2O_3 颗粒, 同时避免因为过量负载而破坏载体 $g\text{-C}_3\text{N}_4$ 的结构, 在后续实验中选择 Mn 的掺杂量为 10%。

为了确定制备所得催化剂中 C、N 及嵌入的 Mn 之间的震动和成键情况, 本研究对 $g\text{-C}_3\text{N}_4$ 和 $\text{Mn-g-C}_3\text{N}_4$ 催化剂进行 FTIR 检测, 图 4-7 中可以看出实验制备所得的石墨相氮化碳 $g\text{-C}_3\text{N}_4$ 的 FTIR 吸收峰位置与文献^[29-31]中报道的结果基本一致: 807 cm^{-1} 处的吸收峰是三嗪环的面外弯曲振动特征峰; 1247 cm^{-1} , 1327 cm^{-1} 和 1409 cm^{-1} 处的振动峰为石墨型氮化碳中 C-N 键的特征吸收峰; 1635 cm^{-1} 处的吸收峰对应 C=N 键的振动吸收模式; $3100\text{-}3500\text{ cm}^{-1}$ 区域内较宽的吸收峰归属于 $-\text{NH}_2$ 的伸缩振动模式。与纯 $g\text{-C}_3\text{N}_4$ 对比, $\text{Mn-g-C}_3\text{N}_4$ 的 FTIR 谱图中 $1000\text{ cm}^{-1}\text{-}1700\text{ cm}^{-1}$ 区域间对应于 C-N 和 C=N 键的伸缩振动峰明显减弱, 可能是由于金属掺杂导致三嗪环的结构被部分破坏^[32]。同时 $\text{Mn-g-C}_3\text{N}_4$ 催化剂对应的 FTIR 图中在 2163 cm^{-1} 处出现新的吸收峰。通常情况下 C≡N 键的吸收峰在 $2225\text{-}2250$

cm⁻¹ 之间^[33]，但当某些金属阳离子进入化合物的结构中，影响 C≡N 键的振动，将导致其红外吸收峰向低波数方向发生红移。法国的 Gérard Simonneaux 等人对制备的掺杂亚铁-双-异氰化物配合物(Fe(II)(TPC)(t-BuNC)₂)进行 FTIR 分析时也发现掺杂 Fe(II)之后，化合物中 C≡N 的吸收峰由 2130 cm⁻¹ 移动至 2117 cm⁻¹^[34]。伊朗学者 Chiniforoshan 等人合成一系列代苯氨-四苯基卟啉铁(III)络合物(Tetraphenylporphyrin iron(III) complexes with substituted phenylcyanamide ligands)，它们的 FTIR 谱图中对应于 C≡N 的吸收峰也出现在 2065-2125 cm⁻¹ 较低波长的区间内^[35]。Yue 等人合成的 Zn 掺杂氮化碳 FTIR 谱图中可能归属于 C≡N 的吸收峰在 2185 cm⁻¹ 处出现^[36]。据推测 C≡N 红外吸收峰红移的现象是由于阳离子的嵌入，使得离域电子在结构内重新分配，三嗪环中电子云密度变小，从而导致 C≡N 强度减弱，化学键力常数减小^[37]。

根据以上理论和相关报道，可以推断图 4-7 中 2163 cm⁻¹ 附近的吸收峰应该归属于红移的 C≡N。由此可见 Mn 化合物掺杂将影响石墨相氮化碳的结构，导致部分三嗪环被破坏，环中 sp² 杂化的 C-N 键转变成 C≡N 键。FTIR 分析结果同样表明 Mn 化合物的掺入将影响 g-C₃N₄ 中三嗪环分子之间的聚合程度，由于聚合度的下降和三嗪环结构被破坏，将在类石墨层的边缘及缺陷位置上形成大量含 N 的官能团碎片。从而使金属掺杂氮化碳催化剂具有更高的碱性和潜在的 Lewis 碱催化活性^[27]。意味着其可能具有更高的催化臭氧氧化活性。

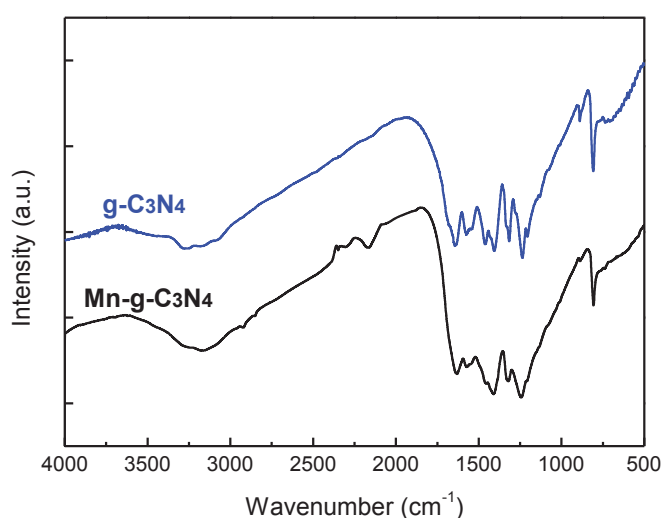


图 4-7. g-C₃N₄ 和 Mn-g-C₃N₄ 的 FTIR 图

Fig. 4-7. FTIR spectra of g-C₃N₄ and Mn-g-C₃N₄.

表 4-8. 石墨相氮化碳及其金属修饰化合物的 FTIR 特征吸收带

Table 4-8. The IR absorption bands of g-C₃N₄ and corresponding metal loaded compounds.

Wavenumber (cm ⁻¹)	Functional group
807	Out-of plane bending modes of C-N heterocycles
1247,1327,1407	Aromatic C-N stretching
1635	C-N stretching
3100-3500	Stretching modes of terminal NH₂ or NH groups at the defect sites of the aromatic ring
2163	C≡N stretching when coordinated nitrile in Metal-CN complexes
2925 and 2850	C-H stretching

为了进一步确定 Mn-g-C₃N₄ 中 Mn 的化学价态, 本研究利用 X-射线光电子能谱(XPS)对催化剂进行表征。从图 4-8 中 Mn 2p_{3/2} 的精细 XPS 能谱图可以看出 Mn 2p_{3/2} 和 Mn 2p_{1/2} 的电子结合能分别位于 642.7 eV 和 654.5 eV。吉林大学的师同顺等^[38]对 Mn-四-(对-硝基)苯基卟啉配合物(Tetra-(p-nitrophenyl) Porphyrin Mn Complex, P₄MnCl)进行 XPS 分析, 测得样品中 Mn 2p_{3/2} 的结合能为 642.4 eV。P₄MnCl 的结构如图 4-9 所示。在 P₄MnCl 在形成过程中卟啉环上的四个吡咯 N 原子中的电子向 Mn 离子空轨道转移, 形成 Mn-N 配位键, 使得 Mn 离子镶嵌在具有大 π 键的卟啉共轭环结构之中。

由于 P₄MnCl 中 Mn 2p_{3/2} 的结合能与本研究所测得的结果非常相近。同时, 目前理论上最稳定的 g-C₃N₄ 结构是由三个三均三嗪环(tri-s-triazine)通过三角平面的 N 原子链接而成, 三嗪环上的 C、N 原子间以 sp² 轨道杂化成键, p 轨道中的孤对电子将形成一个高度离域且类似于卟啉环和酞菁环结构的大 π 键(如图 4-1 所示)^[39]。过渡金属 Mn 阳离子具有空轨道, 能够接受孤对电子, 容易与三嗪环中具有供电子能力的 N 形成配位键^[40]。由此, 可以推断 Mn-g-C₃N₄ 催化剂中的 Mn 与 C、N 杂环中的 N 形成了配位键。从电荷平衡的角度考虑, Mn 可能通过与 O 形成离子键而中和电性。Ding 等^[41]以 MnCl₂·4H₂O 和双氰胺为原料通过热聚合法制备 Mn 掺杂 g-C₃N₄, 通过 XPS 分析表明 Mn 呈+3 价。结合 XRD 分析结果, 推测用乙酸锰和三聚氰胺为原料通过热聚合法制备的 Mn-g-C₃N₄ 中, Mn

以 Mn₂O₃ 的形式存在。由于受到 Mn-N 配位键的影响, 及 g-C₃N₄ 中空腔尺寸的限制, Mn-g-C₃N₄ 中的 Mn₂O₃ 将以纳米颗粒填充于 g-C₃N₄ 的空腔及层间。研究表明纳米粒子存在表面原子配位不足和表面缺陷的情况^[42], 而这种特殊的表面效应能合理地解释 Mn-g-C₃N₄ 催化剂中 Mn-N 配位键的形成。

另一方面, 这一推断也能合理地解释当 Mn 掺杂量较低时, XRD 谱图中无 Mn₂O₃ 的衍射峰出现这一现象。

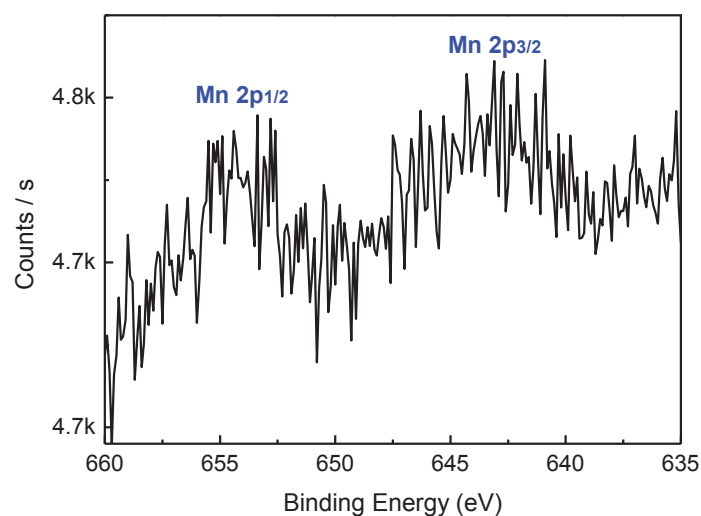


图 4-8 Mn-g-C₃N₄ 的 Mn 2p 精细 XPS 谱图

Fig. 4-8. Corresponding high-resolution XPS spectra of Mn 2p for Mn-g-C₃N₄.

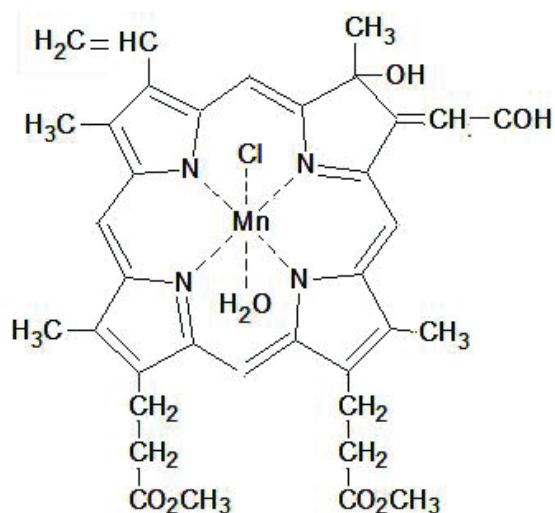


图 4-9 Mn-四-(对-硝基)苯基卟啉配合物结构式

Fig. 4-9. The structure of P₄MnCl.

本研究选取 $g\text{-C}_3\text{N}_4$ 和 $10\%\text{Mn-g-C}_3\text{N}_4$ (之后简称为 $\text{Mn-g-C}_3\text{N}_4$)对与臭氧催化活性直接相关的某些物理化学性质进行表征, 从表 4-9 可以看出与纯 $g\text{-C}_3\text{N}_4$ 相比, $\text{Mn-g-C}_3\text{N}_4$ (催化剂的比表面积略有增加, 可能是由于乙酸盐在热解过程中产生 CO_2 、 CO 等气体^[43], 具有一定的造孔作用。同时负载锰氧化物之后催化剂的 pH_{PZC} 也略微增大, 表明催化剂碱性有所增强。

表 4-9 $g\text{-C}_3\text{N}_4$ 和 $\text{Mn-g-C}_3\text{N}_4$ 的部分物理化学性质

Table 4-9. Physicochemical properties of $g\text{-C}_3\text{N}_4$ and $\text{Mn-g-C}_3\text{N}_4$ catalysts

Sample	Metal content (wt.%)	S_{BET} ($\text{m}^2 \text{g}^{-1}$)	pH_{PZC}
$g\text{-C}_3\text{N}_4$	-	9.3	6.4
$\text{Mn-g-C}_3\text{N}_4$	10.7	24.0	7.5

4.3.2. $\text{Mn-g-C}_3\text{N}_4$ 与 Mn_2O_3 催化活性比较

为了更好地了解 $\text{Mn-g-C}_3\text{N}_4$ 的催化活性, 在催化剂投加量均为 1.0 g/L 的条件下分别考察了 $g\text{-C}_3\text{N}_4$ 和 $\text{Mn-g-C}_3\text{N}_4$ 对 SMZ 催化臭氧氧化的去除情况, 由图 4-10 可知: $g\text{-C}_3\text{N}_4$ 催化剂并未表现出明显的催化活性, 催化反应 1h 后, 仅比单独臭氧催化体系中 SMZ 的去除率增加 5.5%。而当在 $g\text{-C}_3\text{N}_4$ 载体中掺入锰氧化物纳米颗粒之后, 催化剂的催化活性明显提高, 反应结束时 SMZ 的去除率比 $g\text{-C}_3\text{N}_4$ 体系要高出 28%。可见嵌入 $g\text{-C}_3\text{N}_4$ 载体中的 Mn_2O_3 在催化臭氧氧化反应中扮演着催化活性中心的角色。

为了确定 $g\text{-C}_3\text{N}_4$ 载体在 $\text{Mn-g-C}_3\text{N}_4$ 催化剂中所起的作用, 本研究还比较了 1.0 g/L $\text{Mn-g-C}_3\text{N}_4$ 催化剂与含相同 Mn 摩尔量的微米级商品 Mn_2O_3 催化剂在相同实验条件下对 SMZ 的臭氧氧化降解情况。图 4-10 可以看出含有相同摩尔数 Mn 的两个催化体系中, $\text{Mn-g-C}_3\text{N}_4$ 催化体系的活性要明显高于商品 Mn_2O_3 。

本实验中 Mn_2O_3 、 $g\text{-C}_3\text{N}_4$ 和 $\text{Mn-g-C}_3\text{N}_4$ 的 pH_{PZC} 分别为 4.2、6.4 和 7.5。表明 $\text{Mn-g-C}_3\text{N}_4$ 具有最高的碱性。而对于臭氧催化剂, 一般碱性越强意味着催化活性也越高。另一方面, 在 Mn_2O_3 中 Mn 是单独以离子键的形式存在, 而在 $\text{Mn-g-C}_3\text{N}_4$ 中, 还存在 Mn-N 共价键, 这种特殊的作用方式将加速反应过程中 O_3 与目标污染物之间的电子转移, 促进氧化还原反应的进行, 从而使催化剂表

现出高于 Mn₂O₃ 的催化活性。此外, 由于 Mn-g-C₃N₄ 中的锰氧化物为纳米级颗粒, Dong 等^[44]比较了颗粒尺寸分别为 20 nm 和 200 nm 的 Co₃O₄ 颗粒催化臭氧氧化降解苯酚的活性, 结果表明, 200 nm 的 Co₃O₄ 颗粒几乎无催化活性, 而加入 20 nm Co₃O₄ 纳米粒子的臭氧催化体系则能使苯酚去除率提高 37.8%, 显示出很高的催化活性。由于纳米颗粒尺寸小、比表面积大、分散性好、表面羟基丰富, 从而使其表现出比微米级催化剂更高的臭氧催化活性。这也是 Mn-g-C₃N₄ 具有较高催化活性的原因之一。

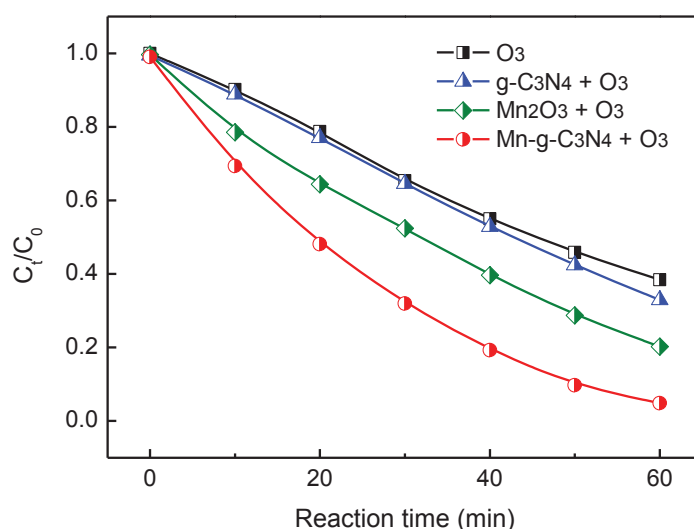


图 4-10 不同条件下 SMZ 的臭氧氧化降解效果

Fig. 4-10. Degradation of SMZ through adsorption and catalytic ozonation by using O₃ and different catalysts (Mn-g-C₃N₄: 1.0 g/L, g-C₃N₄: 1.0 g/L, Mn₂O₃: 0.154 g/L; C_{O₃}: 2.0 mg/L; 200 mL 50mg/L SMZ; initial pH 5.3; reaction temperature: 18°C)

4.3.3. 不同反应条件对催化活性的影响

4.3.3.1. 搅拌速度对 SMZ 臭氧氧化的影响

由于多相臭氧催化是涉及气、固、液三相的反应, 反应器中磁力转子的搅拌速度不仅会直接影响固体催化剂在溶液中的分散状况, 还会影响三相间的传质速率。因此, 我们首先考察了不同磁力搅拌速度对 SMZ 去除率的影响。由图 4-11 可以看出在搅拌速度从 125 rpm 增加至 750 rpm 的过程中, SMZ 的去除率逐渐升高。已有的研究认为含金属的催化剂臭氧催化氧化反应的初始步骤是目标污染物

和臭氧分子在催化剂表面的吸附^[45]。因此，增加搅拌速度能加速传质，提高 Mn-g-C₃N₄ 催化剂的表面活性位点与水中 SMZ 和 O₃ 的接触与碰撞几率，增加臭氧利用率，从而获得更高的 SMZ 臭氧氧化去除率。而当搅拌速度继续从 750 rpm 升高至 1000 rpm 时，SMZ 的去除率基本保持不变，说明当搅拌速度增大到一定值时，传质已不是该反应的限速步骤，此时的反应速率是由催化剂表面的化学反应来控制，继续提高反应器中磁力转子的搅拌速度并不能加快对 SMZ 的降解效率。因此，后续实验的搅拌速度均设定为 750 rpm。

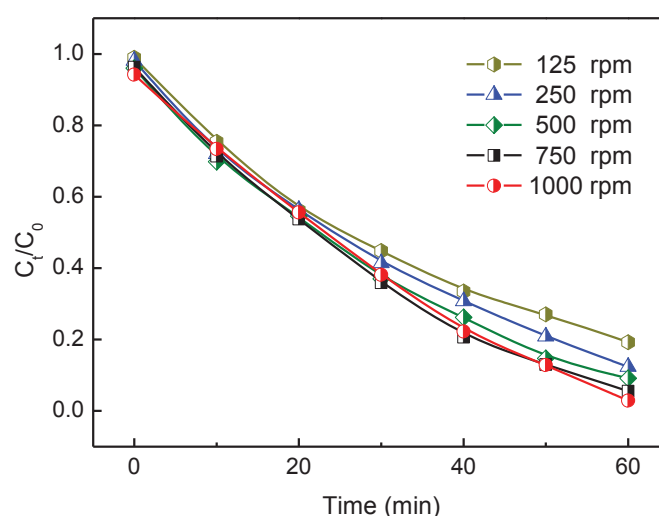


图 4-11 不同搅拌速度对 SMZ 臭氧氧化去除率的影响

Fig. 4-11. Effect of agitation speed on the degradation efficiency of SMZ through adsorption and catalytic ozonation (C_{O_3} : 2.0 mg/L; Mn-g-C₃N₄: 1.0 g/L; 200 mL 50mg/L SMZ; initial pH 5.3; reaction temperature: 18°C)

4.3.3.2. 催化剂用量对 SMZ 臭氧氧化的影响

图 4-12 为不同 Mn-g-C₃N₄ 催化剂投加量下 SMZ 的吸附和催化臭氧氧化降解效果。由于 Mn-g-C₃N₄ 催化剂比表面积较小，对 SMZ 的吸附能力不强，所以吸附阶段 SMZ 的去除率并没有随 Mn-g-C₃N₄ 催化剂用量的增加而显著增长，在催化剂用量从 0.25 g/L 增加至 0.5、1.0、1.5 和 2.0 g/L 的过程中，吸附阶段 SMZ 的去除率只从 0.4% 分别增长至 0.5、0.7、1.1 和 1.2%。在催化阶段，当催化剂的用量从 0.25 g/L 增加至 1.0 g/L 时，臭氧对 SMZ 的降解率逐渐提高。由于多相催

化剂反应一般发生在催化剂的表面,在一定范围内增加催化剂用量,能使反应体系中存在更多的活性位点,从而使催化体系获得更高的催化活性。但是当继续增加催化剂的用量, Mn-g-C₃N₄ 催化臭氧对 SMZ 的去除率升高幅度很小。

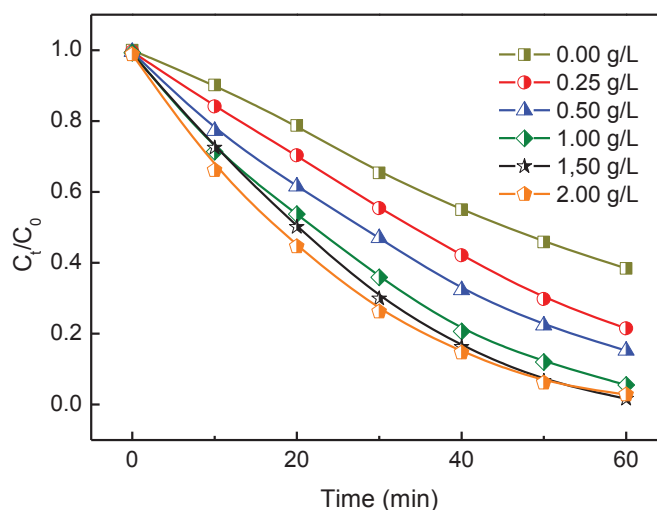


图 4-12 催化剂投加量对 SMZ 臭氧氧化去除率的影响

Fig. 4-12. Effect of catalyst dosage on the degradation efficiency of SMZ through adsorption and catalytic ozonation (C_{O_3} : 2.0 mg/L; 200 mL 50mg/L SMZ; initial pH 5.3; reaction temperature: 18°C)

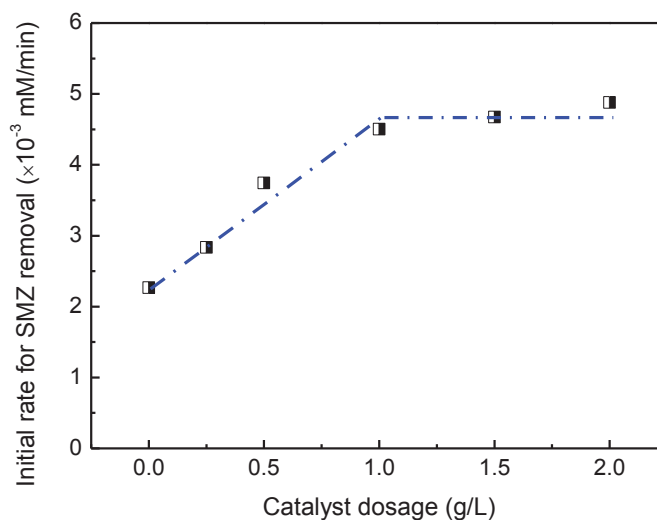


图 4-13 初始反应速率与催化剂用量的关系

Fig. 4-13. Evolution of the initial rate of SMZ conversion as a function of the catalyst dosage (C_{O_3} : 2.0 mg/L; 200 mL 50mg/L SMZ; initial pH 5.3; reaction temperature: 18°C)

本研究对反应初始阶段溶液中 SMZ 浓度随反应时间的变化曲线进行线性回归, 求出各个反应的初始反应速率 (单位为 mM/min), 由图 4-13 可以看出反应的初始反应速率随催化剂用量的增加呈线性增长, 但当催化剂用量超过一定值时 (1.0 g/L), 初始反应速率基本保持不变。这是因为当体系中固体催化剂的浓度达到某一极值时, 催化剂颗粒的团聚效应使催化剂的有效活性位基本不再继续增加; 另一方面, 当催化剂投加量已足够时, 体系中的活性位点对于参与反应的臭氧来说是过量的。所以继续增加催化剂的用量并不会使初始反应速率提高。因此后续实验中 Mn-g-C₃N₄ 催化剂的投加量固定为 1.0 g/L。

4.3.3.3. 进气臭氧浓度对 SMZ 臭氧氧化的影响

由于臭氧的浓度直接影响到多相臭氧催化氧化反应的效果, 因此本节考察了进气臭氧浓度分别为 1.0、2.0、3.0、4.0 和 5.0 g/L 时, SMZ 氧化去除率随时间的变化情况。结果如图 4-14 A 所示, 当进气臭氧浓度为 1.0 g/L 时, 催化反应进行 60 min 后, SMZ 的去除率为 55.2%。将进气臭氧浓度增加到 2 mg/L 和 3mg/L 时, 反应结束 SMZ 的去除率提高到 94.4%和 99.1%。可见在一定范围内, 随着臭氧投加量的增加, SMZ 的去除率将增大。但是当臭氧投加量继续增大时, SMZ 的去除率变化不明显。

5 个考察体系中初始反应速率随进气臭氧浓度的变化情况(图 4-14 B)也表现出类似的规律, 在进气臭氧浓度由 1.0 g/L 增加至 4.0 g/L 的过程中, 体系的初始反应速率基本呈线性增长。而当进气臭氧浓度继续增加至 5.0g/L 时, 初始反应速率几乎保持不变。这是因为在多相催化臭氧氧化反应中, 污染物的去除是臭氧直接氧化和臭氧分解产生羟基自由基的间接氧化反应共同作用的结果, 当臭氧进气浓度增加, 能够为体系提供更多的臭氧分子和高活性的自由基。而当水中臭氧投加量越大, 一方面臭氧溶解度有限, 另一方面臭氧自身分解和催化分解产生大量的羟基自由基将相互淬灭^[46], 使得初始反应速率不再随进气中 O₃ 浓度的增加而变化。

为了判断使用不同臭氧进气浓度时, 反应体系对臭氧的利用情况, 我们定义了臭氧利用率 U:

$$U = \frac{r_0 V_{SMZ}}{C_{O_3} v_{O_3}} \quad (\text{式 4-4})$$

式中： U 为臭氧利用率($\text{mmol}_{\text{SMZ}}/\text{mg}_{\text{O}_3}$)； r_0 为初始反应速率($\text{mM}_{\text{SMZ}}/\text{min}$)； V_{SMZ} 为水样体积，所有反应均使用 200 mL SMZ 溶液； C_{O_3} 为进气中 O_3 浓度(mg/L)； v_{O_3} 为进气流速，实验中均设定为 0.2 L/min。由此可见，根据式 4-4 可以计算出反应初始阶段每去除单位摩尔量 SMZ 所消耗 O_3 的量。

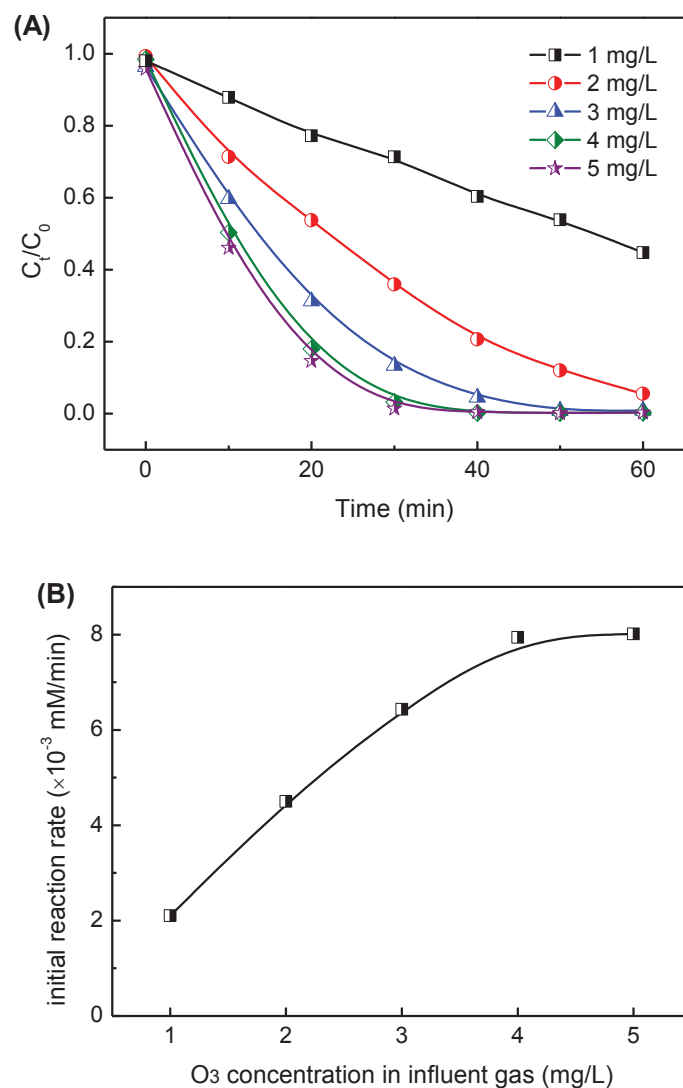


图 4-14. 不同臭氧浓度下 Mn-g-C₃N₄ 催化臭氧氧化去除 SMZ 的情况(A)及初始反应速率与进气臭氧浓度的关系(B)

Fig. 4-14. Effect of the ozone concentration in influent gas phase on the degradation efficiency of SMZ (A) and the initial reaction rate (B) (Mn-g-C₃N₄: 1.0 g/L; 200 mL 50mg/L SMZ; initial pH 5.3; reaction temperature: 18°C)

从图 4-15 中可以看出, 进气臭氧浓度在 1-3mg/L 时, 臭氧利用率保持在 2.1 mol_{SMZ}/g_{O₃}。当进气臭氧浓度继续增加时, 臭氧利用率反而下降。这是因为在相同的实验条件下, 臭氧在溶液中的停留时间是一定的, 当向体系中提供大量的 O₃ 时, 过量的臭氧气体还未来得及与 SMZ 接触反应便离开反应界面进入空气中, 导致臭氧利用率下降。综合考虑污染物的去除率和臭氧利用率, 确定进气中臭氧的最佳浓度为 2.0 mg/L。

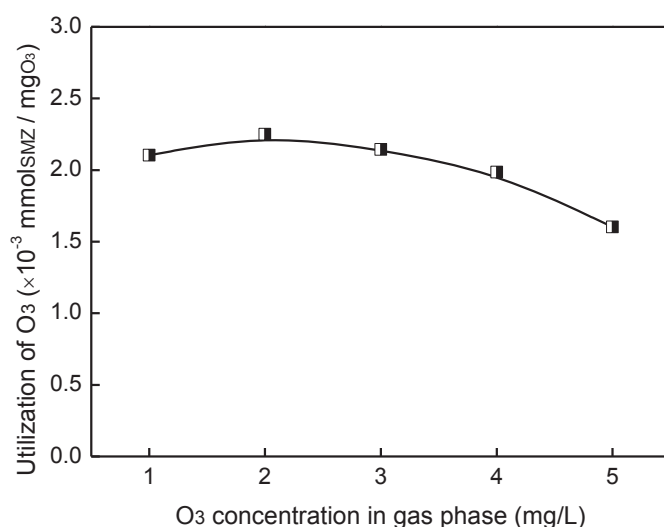


图 4-15 臭氧利用率与进气臭氧浓度的关系

Fig. 4-15. The utilization of ozone under different ozone concentration (Mn-g-C₃N₄: 1.0 g/L; 200 mL 50mg/L SMZ; initial pH 5.3; reaction temperature: 18°C)

4.3.3.4. 不同 SMZ 初始浓度对降解率的影响

本研究还考察了 SMZ 初始浓度分别为 25、50、100、150 和 200 mg/L 时, Mn-g-C₃N₄ 催化臭氧氧化 SMZ 的情况, 图 4-16 A 为通过 HPLC 检测到不同初始浓度的 SMZ 溶液在反应过程中浓度随时间的变化情况。图 4-16 B 为对应的 SMZ 去除率, 从图 B 中可以看出 SMZ 的去除率随着初始浓度的升高而降低。

但由于初始浓度不同, 单从去除率进行比较, 并不能全面地揭示初始浓度对反应速率的影响。为此我们计算了不同 SMZ 初始浓度反应体系对应的催化臭氧氧化初始反应速率, 结果如表 4-10 所示。可见初始反应速率随 SMZ 初始浓度的增加而增大。对于多相臭氧催化氧化反应, 反应速率可以用下式表示^[47]:

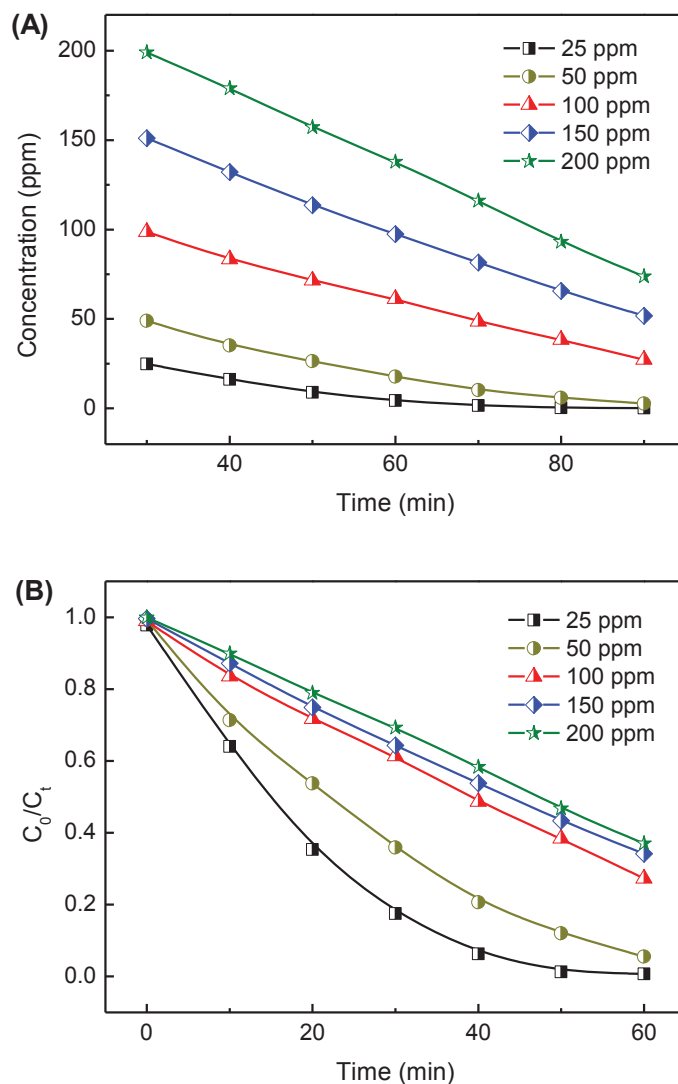


图 4-16 Mn-g-C₃N₄ 催化臭氧氧化反应中 SMZ 浓度随时间的变化情况 {A} 及降解率(B).

Fig. 4-16. The degradation of SMZ with different initial concentration (A) and corresponding removal efficiency (B) (Mn-g-C₃N₄: 1.0 g/L; O₃: 2.0 mg/L; 200 mL SMZ; initial pH 5.3; reaction temperature: 18°C)

$$r_{obs} = k_{obs}[O_3]^\alpha [C_{SMZ}]^\beta \quad (\text{式 4-5})$$

其中, r_{obs} 为反应速率(mM/min); k_{obs} 为表观速率常数; $[O_3]$ 为溶液中臭氧浓度(mg/L); $[C_{smz}]$ 为某一时刻溶液中 SMZ 的浓度。在催化剂投加量、臭氧用量等条件均固定的情况下, 为了确定 SMZ 浓度的反应级数 β , 本研究对臭氧催化反应不同初始浓度 C_0 和对应的初始反应速率 r_0 进行非线性拟合, 结果如图 4-17 所

示，初始反应速率与 SMZ 初始浓度之间存在很强的线性关系($R^2=0.9951$)。反应级数为 0.46。表明 Mn-g-C₃N₄ 多相催化氧化体系中 SMZ 的氧化去除率一定程度受到催化剂表面 SMZ 浓度的影响。

表 4-10 不同初始 SMZ 浓度下 Mn-g-C₃N₄ 催化臭氧氧化体系的初始反应速率

Table 4-10 Initial reaction rates by using different initial SMZ concentration.

Conc. of SMZ after 30 min adsorption (mg/L)	Conc. of SMZ after 30 min adsorption (mM)	Initial rate ($\times 10^{-3}$ mM/min)
24.46	0.0966	3.127
49.65	0.1960	4.432
98.91	0.3905	5.704
149.41	0.5899	7.388
199.85	0.7891	8.240

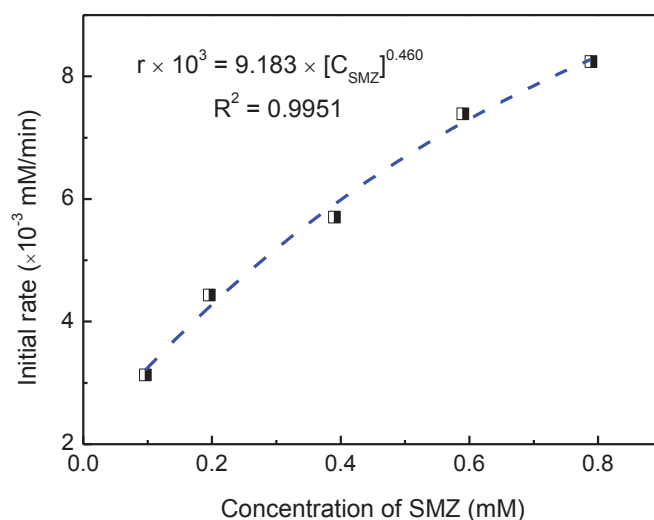


图 4-17 SMZ 初始浓度与体系初始反应速率的关系

Fig. 4-17 Correlation between the SMZ concentration and initial reaction rate

4.3.4. 污泥活性碳和 Mn-g-C₃N₄ 复合催化剂的表征

上一小节的实验结果表明在同一溶液中，增加催化剂表面 SMZ 的浓度，可以提高 SMZ 的去除率。为了使催化剂获得更高的比表面积和适宜的孔结构，达

到节省活性组分用量和增加活性位点的目的,本节中尝试通过把 Mn-g-C₃N₄ 催化剂负载于比表面积较大且对 SMZ 吸附能力强的污泥活性炭载体上来实现。

因此在本节实验中,尝试用乙酸锰、三聚氰胺、污泥活性炭混合热解的方法将 Mn-g-C₃N₄ 催化剂负载于污泥活性炭中,制备成催化活性更高的复合多相催化剂。所制备得的催化剂如图 4-18 所示,制备所得的污泥活性炭(sewage sludge-based activated carbon, SBAC)呈均匀的黑色,表明碳化充分^[48]。与 SBAC 相比,负载 Mn-g-C₃N₄ 之后的复合催化剂颜色略灰。



图 4-18 干污泥、污泥活性炭和 Mn-g-C₃N₄ 与污泥活性炭的复合催化剂粉末

Fig. 4-18. Photos of dry sewage sludge, sludge-based activated carbon and the Mn-g-C₃N₄ and SBAC composite catalysts.

为了更加直观地了解 Mn-g-C₃N₄ 负载前后,污泥活性炭载体表观形貌的变化,本研究对污泥活性炭和 Mn-g-C₃N₄ 与污泥碳的复合催化剂进行扫描电镜分析。图 4-19 中所示的照片为两种催化剂放大 20000 倍下观察到的表面形貌。SBAC 的表面分布着由微生物菌体碳化而形成的粗糙、不规则颗粒,而与 Mn-g-C₃N₄ 催化剂复合之后,由于石墨相氮化碳片层的包裹作用,SBAC 的表面变得更加平整。

从 C、N、Mn 的 EDX mapping 分析结果可以看出 Mn-g-C₃N₄ 催化剂负载于 SBAC 上之后,复合催化剂表面的 C、N、Mn 含量要明显高于载体 SBAC 中相应元素的含量。且 Mn mapping 中亮点分布较均匀,表明 Mn-g-C₃N₄ 催化剂已均匀地负载于 SBAC 载体表面。

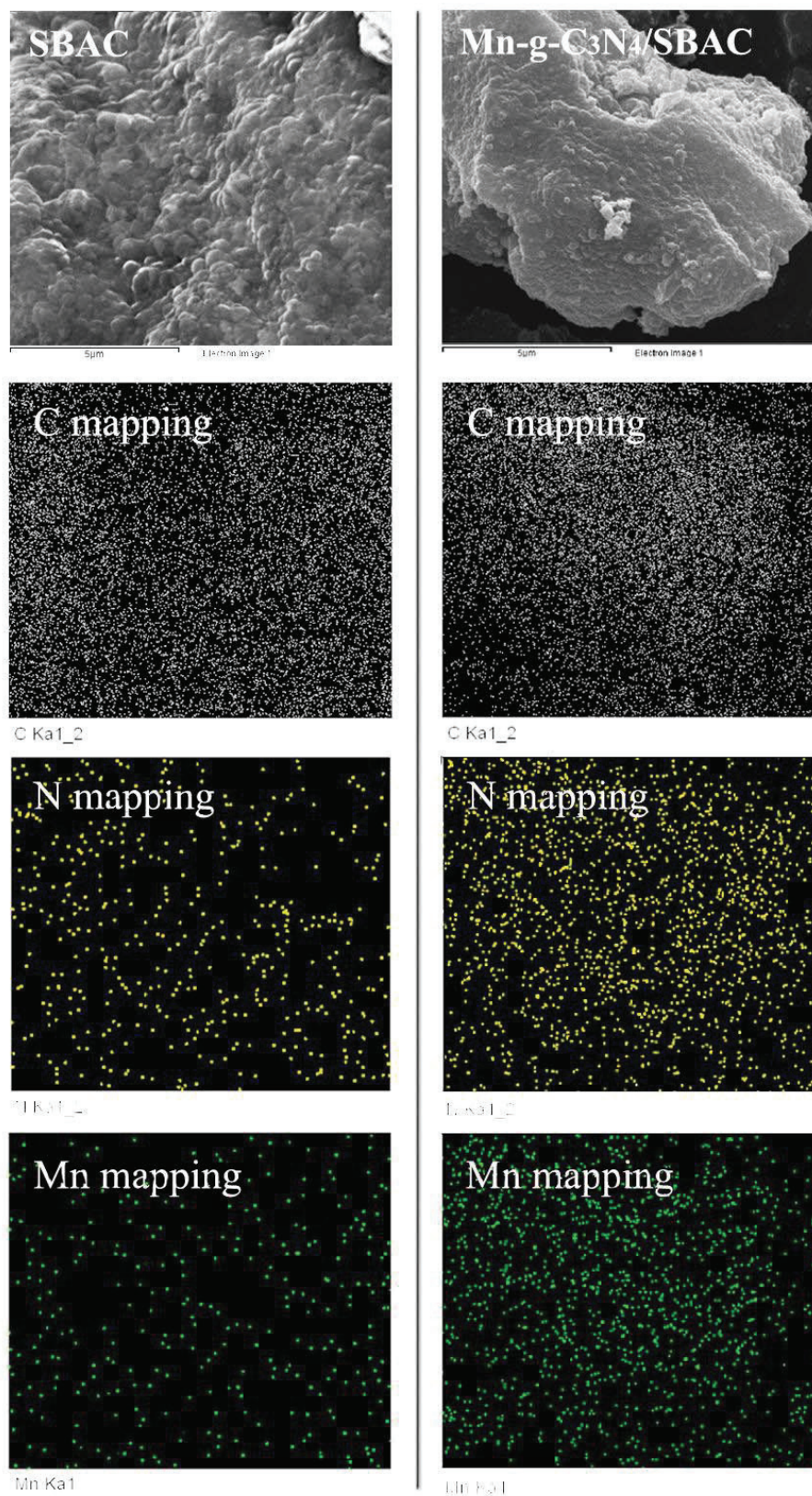


图 4-19 污泥活性碳(SBAC)和 Mn-g-C₃N₄/SBAC 复合催化剂的 SEM 及 EDX mapping 图

Fig. 4-19. SEM images and EDX mapping of C, N and Mn elements for SBAC and Mn-g-C₃N₄/SBAC composite catalysts.

为了确定乙酸锰与三聚氰胺在有污泥活性碳存在的情况下,热解后是否仍然形成 Mn 掺杂石墨相氮化碳,本研究对复合催化剂和污泥活性碳载体进行 XRD 分析。结果如图 4-20 所示。在 SBAC 的 XRD 谱图中可以观察到位于 $2\theta=26.4^\circ$ 和 44.4° 附近存在两个归属于无定型碳的宽化衍射峰,此外在 $2\theta=20.9^\circ$ 、 26.6° 、 35.5° 和 54.9° 等处还存在明显的 SiO₂ 晶体衍射峰(JCPDS 46-1045)。说明经过酸洗处理大部分矿物质已被除去,只有少量 SiO₂ 残留于 SBAC 中。在 Mn-g-C₃N₄/SBAC 复合催化剂中,除了以上两种物质的衍射峰之外,在 $2\theta=27^\circ$ 附近出现归属于石墨相氮化碳(0 0 1)晶面的衍射峰。由此可以推断乙酸锰和三聚氰胺混合物热解聚合后仍是以 Mn-g-C₃N₄ 的形式存在于载体 SBAC 中。

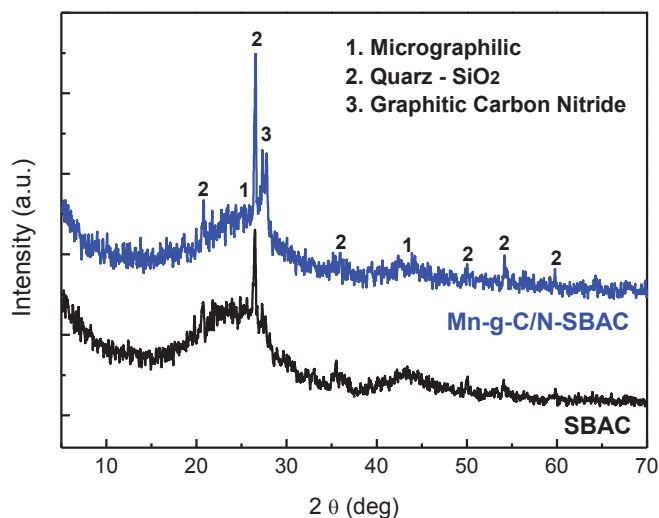


图 4-20 污泥活性碳(SBAC)和 Mn-g-C₃N₄/SBAC 复合催化剂的 XRD 图

Fig. 4-20. XRD patterns of SBAC and Mn-g-C₃N₄/SBAC composite catalysts.

Mn-g-C₃N₄ 负载于 SBAC 载体表面后,对催化剂表面官能团的影响可以通过 FTIR 曲线上吸收峰的位置和强度进行判断。由图 4-21 可以看出,对于直接碳化所得的污泥碳 SC 的 FTIR 谱图,在低于 800 cm^{-1} 的范围内存在多个归属于碳酸盐等无机盐的振动吸收峰, 1050 cm^{-1} 处宽而大的吸收峰对应于 Si-O-Si 或 Si-O-C 的伸缩振动,表明 SC 中含有较多含硅物质。 $1500\text{-}1900\text{ cm}^{-1}$ 范围内出现较弱的 C=O 或 C=C 键特征吸收峰,表明污泥碳表面还有少量热解生成的含芳香环的物质存在。 3450 cm^{-1} 附近较宽的吸收峰则归属于 O-H 的伸缩振动模式,是由 SC

表明吸附的少量水分子所引起^[49,50]。而经过化学活化和酸处理的污泥活性碳 SBAC 的 FTIR 谱图与 SC 相比较, 稍有不同。低于 800 cm^{-1} 区间内的吸收峰基本消失, 说明大部分无机盐已被除去。同时在 1400 cm^{-1} 和 2930 cm^{-1} 附近出现 C-OH 和 C-H 键的伸缩振动吸收峰, 表明酸处理使得 SBAC 表面酸性官能团明显增多。而这些官能团能为 g-C₃N₄ 的负载提供结合位点和键^[51]。

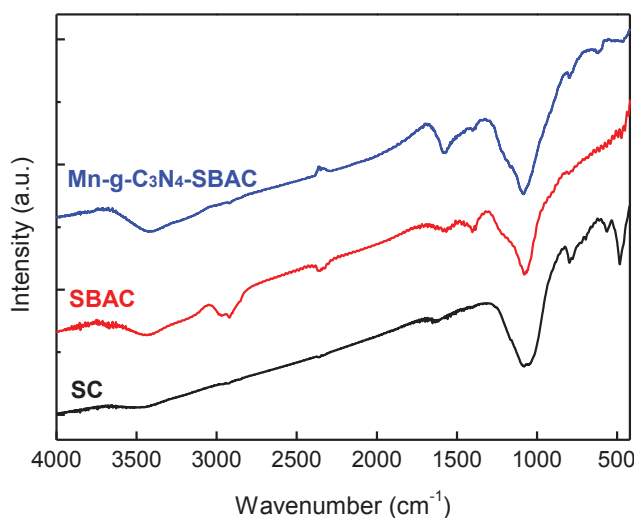


图 4-21 污泥焦碳(SC), 污泥活性碳(SBAC)和 Mn-g-C₃N₄/SBAC 复合催化剂的 FTIR 图

Fig. 4-21. FTIR patterns of SC, SBAC and Mn-g-C₃N₄/SBAC composite catalysts.

表 4-11 污泥碳及其复合催化剂的 FTIR 特征吸收带

Table 4-11. The IR absorption bands of sewage sludge-based carbon derived catalysts

Wavenumber (cm ⁻¹)	Functional group
<800	Inorganic components
1045-1084	Si-O-Si and Si-O-C stretching
1350-1460	C-OH stretching
1240-1650	C-N stretching
1500-1900	C=O and C=C stretching
2830-2980	C-H stretching
3400-3450	O-H stretching
3100-3500	N-H stretching

当在 SBAC 表面负载 Mn-g-C₃N₄ 之后, C-H 对应的吸收峰出现减弱和消失的现象, 可能是由于三聚氰胺热聚合过程中释放出的 NH₃ 与 SBAC 表面的酸性官能团发生反应, 导致 SBAC 表面酸性减弱。除此之外, 在 1566 cm⁻¹ 附近出现归属于石墨型氮化碳中 C-N 键的特征吸收峰, 同时 3100-3500 cm⁻¹ 区间的吸收峰也明显增强, 表明负载后样品中 N-H 含量有所增加。FTIR 的分析结果进一步证实 Mn-g-C₃N₄ 已负载于 SBAC 中。

4.3.5. Mn-g-C₃N₄/SBAC 复合催化剂催化活性研究

为了确定复合催化剂中 Mn-g-C₃N₄ 的最佳负载量, 本节中制备了一系列不同 Mn-g-C₃N₄ 含量的复合催化剂, 其基本物理化学性质如表 4-12 所示:

表 4-12 不同 Mn-g-C₃N₄ 负载量的复合催化剂的部分物理化学性质

Table 4-12. Physicochemical properties of SBAC and Mn-g-C₃N₄/SBAC composite catalysts.

Sample	Theoretical content of Mn-g-C ₃ N ₄ (wt.%)	Yield (%)	Mn (wt.%)	S _{BET} (m ² /g)	pH _{PZC}
SBAC	0	84.9	-	480.4	4.5
Mn-g-C ₃ N ₄ /SBAC ₁	10	76.1	1.3	450.6	6.4
Mn-g-C ₃ N ₄ /SBAC ₂	20	69.2	2.5	359.4	6.6
Mn-g-C ₃ N ₄ /SBAC ₃	30	65.6	3.7	283.7	6.8
Mn-g-C ₃ N ₄ /SBAC ₄	40	59.7	5.1	120.8	7.2

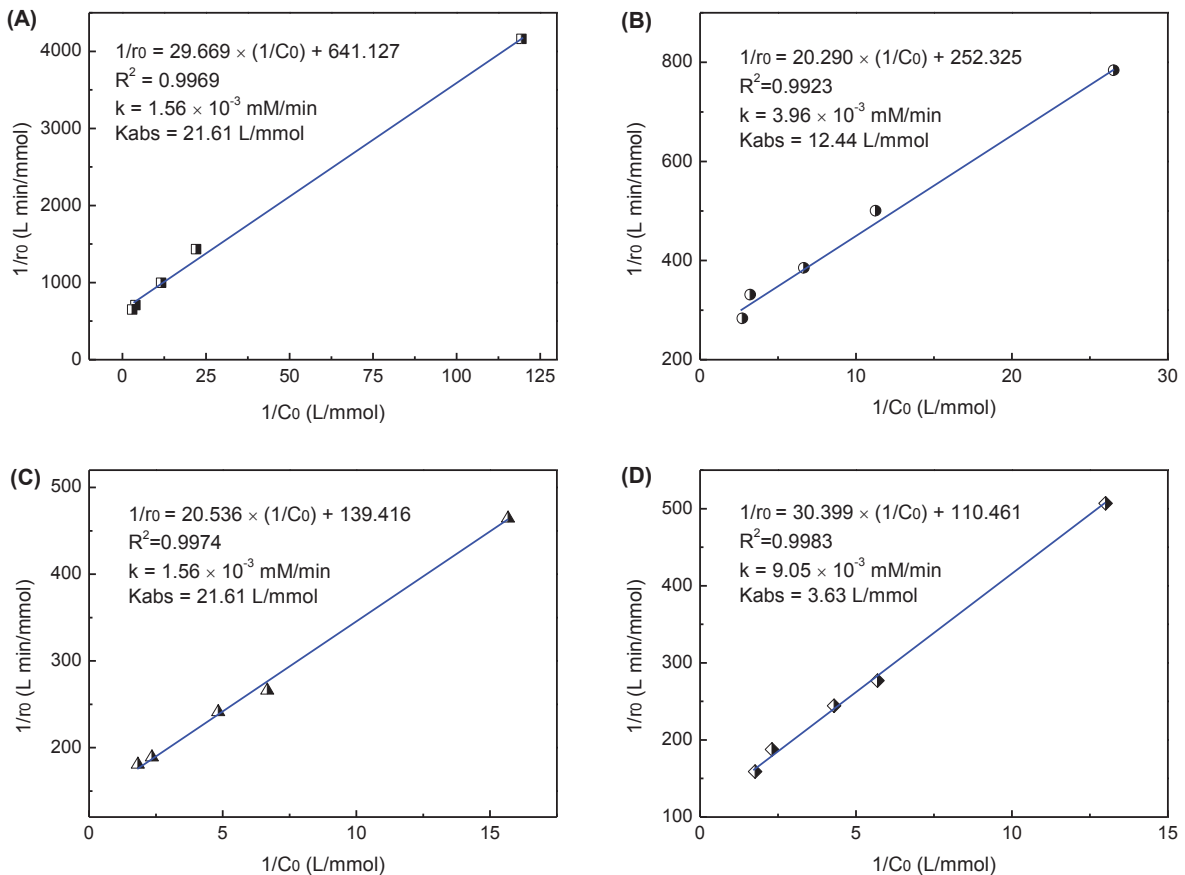
从表 4-12 可以看出随着 Mn-g-C₃N₄ 负载量的增加, 催化剂的比表面积逐渐下降, 预示着制备所得的 5 种催化剂对 SMZ 的吸能能力将有很大差别。在多相催化反应中, 对于吸附能力差别较大的催化剂, 为了比较它们的催化活性, 可以使用 Langmuir-Hinshelwood (L-H) 模型通过拟合计算来求得催化体系的反应速率常数^[52,53]:

$$r = -\frac{dC}{dt} = -\frac{kK_{abs}C}{1 + K_{abs}C} \quad (\text{式 } 4-6)$$

L-H 模型的线性方程为：
$$\frac{1}{r} = \frac{1}{k} + \frac{1}{kK_{ads}C} \quad (\text{式 4-7})$$

式中， r 为污染物降解速率($\text{mol L}^{-1} \text{min}^{-1}$)， k 为表观反应速率($\text{mol L}^{-1} \text{min}^{-1}$)， C 为污染物浓度(mol L^{-1})， K_{ads} 为与 Langmuir 吸附模型有关的常数(L mol^{-1})。

将催化剂加入不同浓度 SMZ 溶液中，待吸附达到平衡后，通入臭氧，开始催化反应，此时计作反应的 0 时刻。将实验所得的 $1/C_0$ 和 $1/r_0$ 作图，由拟合所得直线的斜率和截距可求得 k 和 K_{ads} 。本研究使用 200 mL 初始浓度分别为 50、75、100、150 和 200 mg/L 的 SMZ 溶液，在催化剂投加量为 0.5 g/L，臭氧进气浓度 2.0 mg/L，流速 0.2 L/min 的实验条件下对 5 种催化剂的吸附和催化性能进行考察，并用 L-H 模型对实验数据进行拟合，结果如图 4-22 所示。5 个反应体系的 L-H 拟合直线的相关系数均大于 0.98，表明复合催化剂催化臭氧氧化降解 SMZ 的反应基本遵循 L-H 反应动力学方程。氧化反应开始阶段，在催化剂表面臭氧能快速氧化吸附于活性位点上的 SMZ，使得催化剂表面 SMZ 的浓度存在近似稳态平衡的状态。



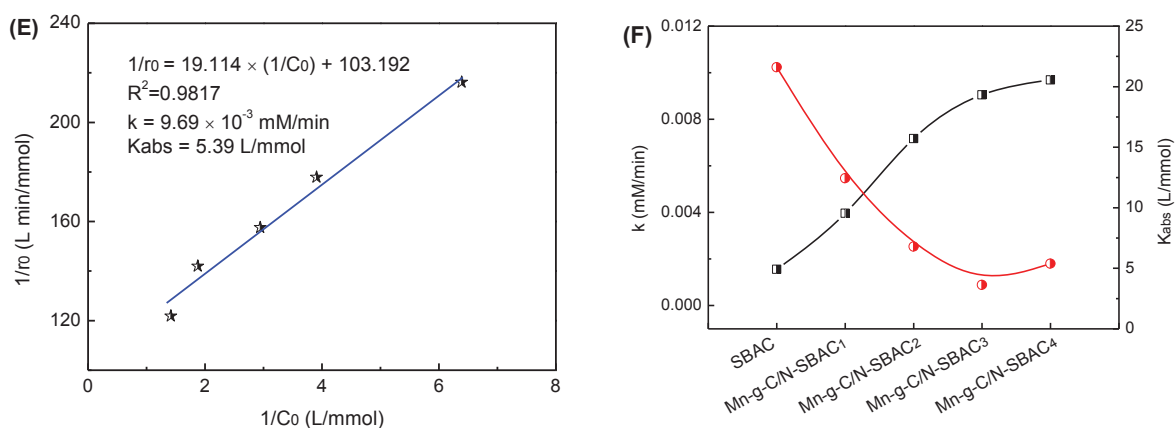


图 4-22 复合催化剂催化 SMZ 氧化的 L-H 模型拟合结果

Fig. 4-22. Kinetic parameters calculated according to the Langmuir–Hinshelwood kinetic model by using different catalysts: SBAC (A); Mn-g-C₃N₄/SBAC₁ (B); Mn-g-C₃N₄/SBAC₂ (C); Mn-g-C₃N₄/SBAC₃ (D); Mn-g-C₃N₄/SBAC₄ (E). k and K_{abs} for different catalysts (F) (Catalyst: 0.5 g/L, C_{O_3} : 2.0 mg/L; reaction temperature: 18°C)

从图 4-22 F 中可以看出复合催化剂的 K_{abs} 随 Mn-g-C₃N₄ 负载量的增加而减小, 可能是由于 Mn-g-C₃N₄ 在 SBAC 载体表面的负载导致催化剂比表面积下降, 从而使复合催化剂对 SMZ 的吸附能力减小。而 k 在一定范围内则与 Mn-g-C₃N₄ 负载量成正比增长, 但当负载量超过 30% 之后, k 值趋于恒定。虽然增加 Mn-g-C₃N₄ 的负载量, 能够为催化体系提供更多催化活性位点, 但是由于 SBAC 的表面积有限, 当 Mn-g-C₃N₄ 过量负载时将影响其在催化剂载体中的分散度, 造成有效活性位点下降。同时 K_{abs} 的减小, 将导致催化剂表面浓缩的 SMZ 浓度下降, 根据式 4-5 可以推断此时催化剂将表现出更低的催化活性。综合考虑催化剂的催化活性和载体中 Mn-g-C₃N₄ 的利用率, 选取 Mn-g-C₃N₄/SBAC₃ 进行后续研究。

为了确定污泥基活性碳作为 Mn-g-C₃N₄/SBAC 复合催化剂载体, 能达到预期的增强活性的效果, 本研究对 Mn-g-C₃N₄ 催化体系采用 L-H 模型进行拟合, 该催化体系中催化剂用量为 0.17 g/L, 以便与 0.5 g/L Mn-g-C₃N₄/SBAC₃ 复合催化剂反应体系具有相同的 Mn 含量。从图 4-23 的拟合结果可知, 单独 Mn-g-C₃N₄ 的反应速率常数为 5.74×10^{-3} mM/min。而经污泥基活性碳负载化后的复合催化剂, 反应速率常数提高至 9.05×10^{-3} mM/min, 催化活性提高了 1.6 倍。

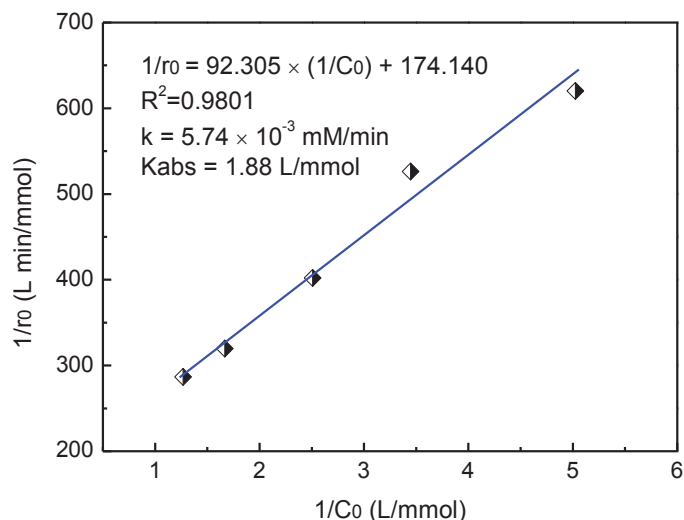


图 4-23 Mn-g-C₃N₄ 催化 SMZ 氧化的 L-H 模型拟合结果

Fig. 4-23. Kinetic parameters calculated according to the Langmuir–Hinshelwood kinetic model by using Mn-g-C₃N₄ catalyst (Catalyst: 0.17 g/L, C_{O₃}: 2.0 mg/L; reaction temperature: 18°C)

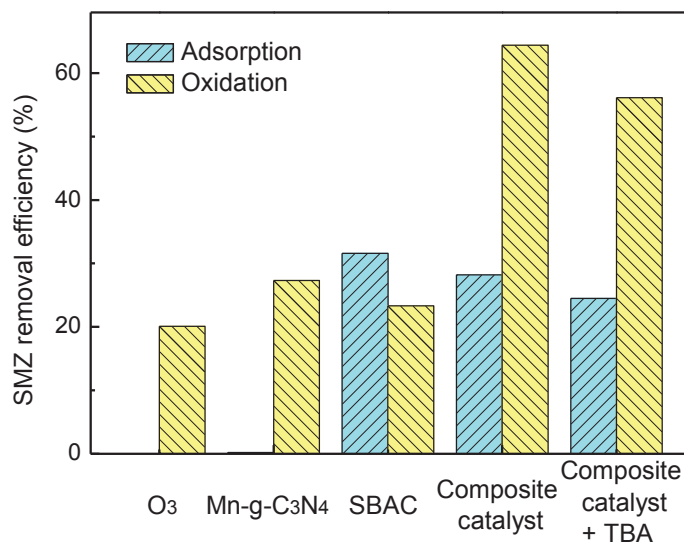


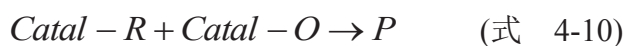
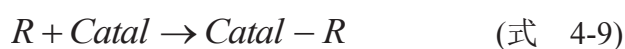
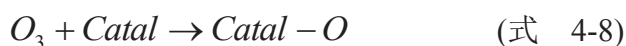
图 4-24 不同条件下 SMZ 的去除率

Fig. 4-24. SMZ removal efficiency by adsorption and ozonation under different conditions (Mn-g-C₃N₄: 0.17 g/L; SBAC: 0.33 g/L; Mn-g-C₃N₄/SBAC: 0.5 g/L; O₃: 4.0 mg/L; 200 mL 200 mg/L SMZ; initial pH 5.0; reaction temperature: 18°C)

本研究还进一步比较了 0.5 g/L Mn-g-C₃N₄/SBAC₃ 复合催化剂和具有相同 Mn 含量的 0.17 g/L Mn-g-C₃N₄ 催化剂及 0.33 g/L SBAC 载体为催化剂的体系在吸

附 30 min 及催化 60 min 后对 SMZ 的去除率。结果如图 4-24 所示, SBAC 和 Mn-g-C₃N₄ 体系经吸附和臭氧催化氧化处理后, SMZ 总降解率分别为 27.5%和 54.9%,即两个单独体系 SMZ 降解率之和为 82.4%,相比之下, Mn-g-C₃N₄/SBAC₃₀ 复合催化剂催化臭氧氧化体系中 SMZ 的去除率不仅高于两个单独体系的 SMZ 降解率,而且比它们的总和还高出 10.2%。由此可见污泥基活性炭作为复合催化剂的载体存在增强催化活性的效应。对于 Mn-g-C₃N₄/SBAC 复合催化剂其中污泥基活性炭 SBAC 由于具有大比表面积,能够增加水中 O₃ 和 SMZ 分子在催化剂表面的吸附量,而 Mn-g-C₃N₄ 片层中锰氧化物纳米粒子,能够使吸附于催化剂表面的 O₃ 转变成活性更高的自由基,从而加速体系中目标污染物的降解。

在多相催化臭氧氧化有机物的反应中,主要存在臭氧分子氧化和羟基自由基氧化这两种反应机理。为了确定 Mn-g-C₃N₄/SBAC 复合催化剂对 SMZ 催化臭氧氧化的降解机理,本研究通过考察加入 TBA 后体系中 SMZ 去除率的变化情况来对反应机理进行探索。叔丁醇(Tert-Butanol, TBA)为典型的自由基捕获剂,它与·OH 的反应速率常数高达 $4.7 \times 10^8 \text{ M}^{-1} \text{ s}^{-1}$ ^[54]。为了使加入的叔丁醇能够有效地捕获体系中生成的羟基自由基,同时不会对溶液的理化性质造成太大影响,将体系中叔丁醇的摩尔浓度设定为 SMZ 摩尔浓度的 50 倍,即向 200 mL 200 mg/L 的 SMZ 溶液中加入 0.5855 g TBA。加入 TBA 后,复合催化剂臭氧氧化体系对 SMZ 的去除情况如图 4-24 所示。溶液中加入 TBA 后, Mn-g-C₃N₄/SBAC 复合催化剂体系对 SMZ 催化臭氧氧化去除率略微下降。但 TBA 的加入并没有完全抑制 SMZ 的臭氧氧化。哈尔滨工业大学的马军教授课题组在使用负载锰氧化物的颗粒活性炭复合催化剂(MnO_x/GAC)催化臭氧氧化降解硝基苯的实验中也发现类似现象^[55]。此外,该课题组在使用污泥活性炭对催化臭氧氧化草酸的研究中,也发现 TBA 的加入不会影响草酸的臭氧氧化^[56]。由此可见,对于 Mn-g-C₃N₄/SBAC 复合催化剂,在中性 pH 环境下,可能同时存在臭氧分子氧化和羟基自由基氧化。其反应机理更接近于 Faria 等人所提出的界面催化理论^[57]:



如式 4-8 和 4-9 所示,臭氧和溶液中的污染物同时吸附于催化剂表面,臭氧

分解生成比自身活性还要高的表面键自由基 Catal-O。同时溶液中的污染物也在催化剂表面发生吸附或络合、活化等过程。在催化剂表面，具有不稳定性的 Catal-R 将与具有氧化性的 Catal-O 自由基反应，生成降解产物 P。P 主要为分子量较小的物质，易于从催化剂表面脱附，从而使氧化反应继续进行。

4.3.6. 催化剂稳定性的研究

对于高级氧化反应，多相催化剂的抗氧化性是一个需要特别考虑的问题。本节中将 1 g/L Mn-g-C₃N₄/SBAC₃ 复合催化剂加入 200 mL 超纯水中，以 0.2 L/min 流速通入浓度为 2.0 mg/L 的臭氧气流，氧化处理 60 min 后，滤液 COD 值仅为 14 mg/L。表明催化剂具有一定的抗氧化性。

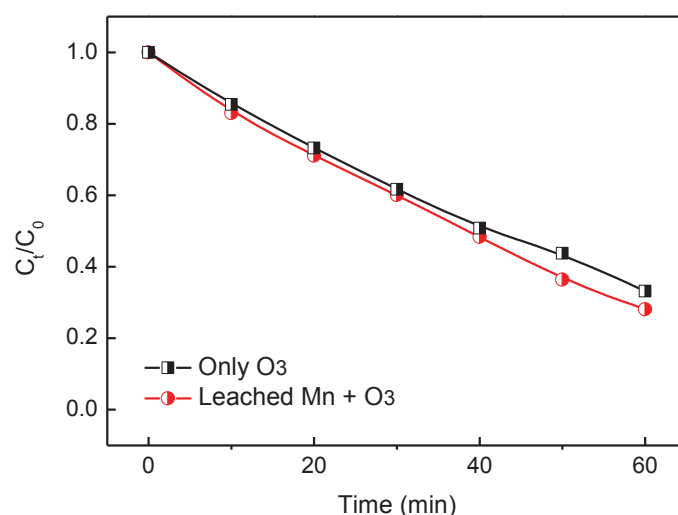


图 4-25 滤液催化活性测试

Fig. 4-25. Catalytic activity of the filtrate (O₃: 2.0 mg/L; 200 mL 50 mg/L SMZ; reaction temperature: 18°C)

对于含金属的多相催化剂，在催化臭氧氧化反应中，金属离子的溶出也是较为常见的现象。为了确定均相反应对 SMZ 总去除率的贡献，对上述加入 Mn-g-C₃N₄/SBAC₃ 催化剂并经臭氧氧化处理过的溶液进行过滤，在滤液中加入 SMZ 粉末，配制成 50 mg/L 浓度的溶液，并测定其催化活性。结果表明滤液基本无催化活性(图 4-25)。由此可以推断反应过程中多相催化是 SMZ 氧化去除的

主要途径。同时，用 ICP-OES 检测该反应液中 Mn 的浓度，检测结果表明仅有 0.65 mg/L Mn 溶出。

催化剂的重复使用是评价多相催化剂稳定性的常用方法。Mn-g-C₃N₄/SBAC₃ 复合催化剂经 0.45 μm 孔径滤膜过滤，清洗，烘干后进行重复使用。图 4-26 为 0.5 g/L 的 Mn-g-C₃N₄/SBAC₃ 复合催化剂经多次使用的过程中对 SMZ 臭氧催化氧化去除和 COD 降解的效果。经过 30 min 吸附和 1 h 催化反应，在第 4 次重复使用时 SMZ 的总降解率和 COD 去除率仍然能达到 84.6 %和 51.9%，与第一次使用相比，催化活性并没有大幅度下降。表明复合催化剂具有良好的稳定性。

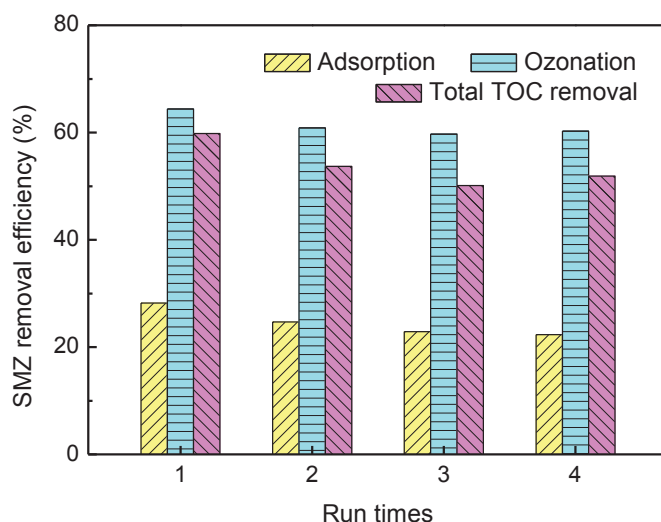


图 4-26 Mn-g-C₃N₄/SBAC 复合催化剂重复利用情况率

Fig. 4-26. Evolution of the SMZ conversion upon catalytic ozonation of SMZ while recycling the Mn-g-C₃N₄/SBAC catalyst (Mn-g-C₃N₄/SBAC₃: 0.5 g/L; O₃: 4.0 mg/L; 200 mL 200 mg/L SMZ; initial pH 5.0; reaction temperature: 18°C)

4.4. 结论

本章以乙酸锰和三聚氰胺混合热聚合法制备 Mn 掺杂的石墨相氮化碳，为增加催化剂的比表面积，用经化学活化处理所得的污泥基活性碳(SBAC)作为催化剂载体，合成污泥活性碳与 Mn 掺杂氮化碳复合催化剂(Mn-g-C₃N₄/SBAC)。使用 XRD、FTIR、SEM-DEX、XPS 等手段对其活性组成和形貌进行表征，以磺胺甲

恶唑(SMZ)作为目标污染物, 考察其催化臭氧氧化的催化性能。实验结果表明:

1. 利用热聚合法, 合成 Mn 掺杂石墨相氮化碳(Mn-g-C₃N₄), 通过 XRD、FTIR、XPS 测试确定该催化剂是以三嗪环(-C₃N₃)为结构单元的层状结构化合物。Mn 以 Mn₂O₃ 纳米粒子的形式存在于 g-C₃N₄ 载体中, 由于纳米粒子的表面效应, 纳米锰氧化物中的 Mn 同时通过 Mn-N 配位键与 g-C₃N₄ 载体结合。石墨相氮化碳几乎无催化臭氧氧化活性, 而 Mn-g-C₃N₄ 则表现出较高的催化活性。当转速为 750 rpm, 臭氧流速和浓度分别为 0.2 L/min 和 2.0 mg/L 的反应条件下, 与单独臭氧催化相比, 加入 1 g/L Mn-g-C₃N₄ 多相催化剂反应 1 h 后, 体系对 SMZ 的去除率从 61.6% 升高到 95.1%。Mn-g-C₃N₄ 多相催化臭氧氧化降解 SMZ 的反应速率受催化剂表面 SMZ 浓度的影响, 在上述反应条件下, SMZ 浓度的反应级数为 0.46。
2. 为了提高 Mn-g-C₃N₄ 表面 SMZ 的浓度, 用固态热聚合法制备了污泥活性碳与 Mn-g-C₃N₄ 复合催化剂(Mn-g-C₃N₄/SBAC)。SEM-EDX, XRD 和 FTIR 分析结果表明 Mn-g-C₃N₄ 已较均匀地负载于 SBAC 表面。复合催化剂的比表面积随着 Mn-g-C₃N₄ 负载量的增加而减小, 催化剂的 pHPZC 则呈相反的变化趋势。Mn-g-C₃N₄ 的最佳负载量为 30%。与具有相同 Mn 含量的 Mn-g-C₃N₄ 相比, 与污泥活性碳复合之后, 催化剂的表观反应速率常数可提高 1.6 倍。且复合催化剂的催化体系对 SMZ 的去除率比 Mn-g-C₃N₄ 和 SBAC 两个单独体系中 SMZ 去除率之和要高 10%。表明污泥基活性碳作为复合催化剂的载体能增强催化活性。催化剂稳定性测试结果表明 Mn-g-C₃N₄/SBAC 复合催化剂具有较好的抗氧化性, 较低的 Mn 离子溶出和较高的催化活性稳定性。

4.5. 参考文献

- [1] Esplugas S, Bila D M, Krause L G T, Dezotti M. Ozonation and advanced oxidation technologies to remove endocrine disrupting chemicals (EDCs) and pharmaceuticals and personal care products (PPCPs) in water effluents. *J. Hazard. Mater.*, 2007, 149: 631-642
- [2] 焦晓微, 赵丹, 罗一, 曲景平. 磺胺甲恶唑在羟基自由基作用下降解机理的密度泛函研究. *安全与环境学报*, 2013, 13: 40-46

- [3] Akhtar J, Amin N A S, Aris A. Combined adsorption and catalytic ozonation for removal of sulfamethoxazole using Fe₂O₃/CeO₂ loaded activated carbon. *Chem. Eng. J.*, 2011, 170: 136-144
- [4] Kim I, Tanaka H. Photodegradation characteristics of PPCPs in water with UV treatment. *Environ. Inter.*, 2009, 35: 793-802
- [5] Zhang D, Pan B, Zhang H, Ning P, Xing B. Contribution of different sulfamethoxazole species to their overall adsorption on functionalized carbon nanotubes. *Environ. Sci. Technol.*, 2010, 44: 3806-3811
- [6] Lin A Y C, Lin C F, Chiou J M, Hong P K A. O₃ and O₃/H₂O₂ treatment of sulfonamide and macrolide antibiotics in wastewater. *J. Hazard. Mater.*, 2009, 171: 452-458
- [7] 孙志忠. 臭氧/多相催化氧化去除水中有机污染物效能与机理. 博士学位论文. 哈尔滨工业大学. 10. 2006
- [8] Álvarez P M, García-Araya J F, Beltrán F J, Giráldez I, Jaramillo J, Gómez-Serrano V. The influence of various factors on aqueous ozone decomposition by granular activated carbons and the development of a mechanistic approach. *Carbon*, 2006, 44: 3102-3112
- [9] Oh B S, Song S J, Lee E T, Oh H J, Kang J W. Catalyzed ozonation process with GAC and metal doped-GAC for removing organic pollutants. *Water Sci. Technol.*, 2004, 49: 45-49
- [10] Oliveira T F, Chedeville O, Fauduet H, Cagnon H. Use of ozone/activated carbon coupling to remove diethyl phthalate from water: Influence of activated carbon textural and chemical properties. *Desalination.*, 2011, 276: 359-365
- [11] Sánchez-Polo M, Rivera-Utrilla J. Effect of the ozone-carbon reaction on the catalytic activity of activated carbon during the degradation of 1,3,6-naphthalenetrisulphonic acid with ozone. *Carbon*, 2003, 41: 303-307
- [12] Cao H, Xing L, Wu G, Xie Y, Shi S, Zhang Y, Minakata D, Crittenden J C. Promoting effect of nitration modification on activated carbon in the catalytic ozonation of oxalic acid. *Appl. Catal. B: Environ.*, 2014, 146: 169-176
- [13] Xing L, Xie Y, Cao H, Minakata D, Zhang Y, Crittenden J C. Activated carbon-enhanced ozonation of oxalate attributed to HO· oxidation in bulk solution and surface oxidation: Effects of the type and number of basic sites. *Chem. Eng. J.*, 2014, 245: 71-79

- [14]徐泽龙, 陆荣荣. 农业废弃物制备活性炭及其应用进展. 广西轻工业, 2010, 3, 65-67
- [15]Rivera-Utrilla J, Sánchez-Polo M. Ozonation of 1,3,6-naphthalenesulphonic acid catalysed by activated carbon in aqueous phase. *Appl. Catal. B: Environ.*, 2002, 39: 319-329
- [16]Teter D M, Hemley R J. Low-compressibility carbon nitrides. *Science*, 1996, 271: 53-55
- [17]赵珊珊. 基于 $g\text{-C}_3\text{N}_4$ 或石墨烯的催化材料的制备及性能研究. 硕士论文. 大连理工大学. 10. 2013
- [18]陆希峰. 氮化碳的合成、表征和应用研究. 博士论文. 山东大学. 8. 2009
- [19]Wang X, Chen X, Thomas A, Fu X, Antonietti M. Metal-Containing Carbon Nitride Compounds: A New Functional Organic - Metal Hybrid Material. *Adv. Mater.* 2009, 21(16): 1609-1612
- [20]Yue B, Li Q, Iwai H, Kako T, Ye J. Hydrogen production using zinc-doped carbon nitride catalyst irradiated with visible light. *Sci. Technol. Adv. Mater.* 2011, 21: 034401
- [21]李芳芳, 聂锦丽, 黄英, 李展鹏, 朱晓琼, 肖丹. Ag 掺杂的石墨型氮化碳材料光致发光性能的研究. *化学研究与应用*, 2013, 25: 1470-1474
- [22]Wang Y, Wang X, Antonietti M. Polymeric graphitic carbon nitride as a heterogeneous organocatalyst: from photochemistry to multipurpose catalysis to sustainable chemistry. *Angew. Chem. Int. Ed.*, 2012, 51: 68-89
- [23]Zhu J, Wei Y, Chen W, Zhao Z, Thomas A. Graphitic carbon nitride as metal-free catalyst for NO decomposition. *Chem. Commun.*, 2010, 46: 6965-6967
- [24]Thomas A, Fischer A, Goettmann F, Antonietti M, Müller J O, Schlögl R, Carlsson J M. Graphitic carbon nitride materials: variation of structure and morphology and their use as metal-free catalysts. *J. Mater. Chem.*, 2008, 18: 4893-4908/4893
- [25]Xu J, Wu H, Wang X, Xue B, Li Y, Cao Y. A new and environmentally benign precursor for the synthesis of mesoporous $g\text{-C}_3\text{N}_4$ with tunable surface area. *Phys. Chem. Chem. Phys.*, 2013, 15: 4510-4517
- [26]Yangali-Quintanilla V, Sadmani A, McConville M, Kennedy M, Amy Gary. A QSAR model for predicting rejection of emerging contaminants (pharmaceuticals,

- endocrine disruptors) by nanofiltration membranes. *Water Res.*, 2010, 44: 373-384
- [27]檀波, 许杰, 薛冰, 刘平, 李永昕. 介孔类石墨氮化碳的制备及其催化 Knoevenagel 缩合反应. *化学通报*, 2013, 76: 150-156
- [28]廖高祖. 基于导电聚合物的可见光催化剂的制备及其降解污染物的性能. 大连理工大学. 82. 2011
- [29]Cui Y, Ding Z, Liu Ping, Antonietti, Fu, X, Wang X. Metal-free activation of H₂O₂ by g-C₃N₄ under visible light irradiation for the degradation of organic pollutants. *Phys. Chem. Chem. Phys.*, 2012, 14:1455-1462
- [30]Lu X F, Gai L G, Wang Q L, Zhao X, Tao X T. Synthesis and characterization of C₃N₄ nanowires and pseudocubic C₃N₄ polycrystalline nanoparticles. *Mater. Lett.*, 2007, 61: 4255-4258
- [31]Kawaguchi M, Yagi S, Enomoto H. Chemical preparation and characterization of nitrogen-rich carbon nitride powders. *Carbon*, 2004, 42: 345-350
- [32]Yue B, Li Q, Iwai H, Kako T, Ye J. Hydrogen production using zinc-doped carbon nitride catalyst irradiated with visible light. *Sci. Technol. Adv. Mater.*, 2011, 12: 034401
- [33]Goff H M, Shimomura E T, Phillip M A. Correlations of axial ligand field strength and zero-field splittings in the carbon-13 NMR spectra of five- and six-coordinate high-spin iron (III) porphyrin complexes. *Inorg. Chem.*, 1983, 22: 66-71
- [34]Simonneaux G, Kobeissi M. ¹H NMR and EPR studies of the electronic structure of low-spin iron(III) isocyanide mesotetraphenylchlorin complexes: a (d_{xz}, d_{yz})⁴(d_{xy})¹ configuration from 293 to 4 K. *J. Chem. Soc., Dalton Trans.*, 2001, 1587-1592
- [36]Chiniforoshan H, Safari N, Nezhad J M, Hadadzadeh H, Mahmoudkhani A H. Synthesis and characterization of tetraphenylporphyrin iron(III) complexes with substituted phenylcyanamide ligands. *Inorg. Chim. Acta*, 2006, 359: 2101-2106
- [37]Li C, Cao C B, Zhu H S. Graphitic carbon nitride thin films deposited by electrodeposition. *Mater. Lett.*, 2004, 58: 1903-1906
- [38]师同顺, 魏诠, 曹锡章. 过渡金属四-(对-硝基)苯基卟啉配合物的 XPS 研究. *高等学校化学学报*, 1993, 14: 1410-1413

- [39]Jürgens B, Irran E, Senker J, Kroll P, Müller H, Schnick W. Melem (2,5,8-Triamino-tri-s-triazine), an important intermediate during condensation of melamine rings to graphitic carbon nitride: synthesis, structure determination by X-ray powder diffractometry, solid-state NMR, and theoretical studies. *J. Am. Chem. Soc.*, 2003, 125:10288-10300
- [40]付忠叶. 含氮杂环化合物金属配合物的合成. 中国海洋大学, 27, 2012
- [41]Ding Z, Chen X, Antonietti M, Wang X. Synthesis of transition metal-modified carbon nitride polymers for selective hydrocarbon oxidation. *ChemSusChem*, 2011, 4: 274-281
- [42]吴丽娜. 纳米复合材料的制备及催化臭氧氧化应用. 硕士论文. 江南大学. 3. 2013
- [43]周顺, 徐迎波, 王程辉, 田振峰. 柠檬酸的热解特性. *烟草化学*, 2011, 9, 45-49
- [44]Dong Y, Wang G, Jiang P, Zhang A, Yue L, Zhang X. Catalytic ozonation of phenol in aqueous solution by Co_3O_4 nanoparticles. *Bull. Korean Chem. Soc.*, 2010, 31, 2830-2834
- [45]Huang W J, Fang G C, Wang C C. A nanometer-ZnO catalyst to enhance the ozonation of 2,4,6-trichlorophenol in water. *Colloids Surf. A: Physicochem. Eng. Aspects.*, 2005, 260: 45-51
- [46]张静. 金属掺杂改性 TiO_2 催化臭氧氧化水中有机污染物研究. 哈尔滨工业大学. 36. 2010
- [47]Fujita H, Izumi J, Sagehashi M, Fuji T, Sakoda A. Decomposition of trichloroethene on ozone-adsorbed high silica zeolites. *Water Res.*, 2004, 38: 166-172
- [48]李海英. 生物污泥热解资源化技术研究. 天津大学. 63. 2006
- [49]Marques R R N, Stüber F, Smith K M, Fabregat A, Bengoa C, Font J, Fortuny A, Pullket S, Fowler G D, Graham N J D. Sewage sludge based catalysts for catalytic wet air oxidation of phenol: Preparation, characterisation and catalytic performance. *Appl. Catal. B: Environ.*, 2011, 101: 306-316
- [50]Jindarom C., Meeyoo V., Kitiyanan B. Surface characterization and dye adsorptive capacities of char obtained from pyrolysis/gasification of sewage sludge. *Chem. Eng. J.*, 2007, 133: 239-246

- [51]廖高祖. 基于导电聚合物的可见光催化剂的制备及其降解污染物的性能. 博士论文. 大连理工大学. 86. 2011
- [52]Liu C S, Zhang L J, Feng C H, Wu C A, Li F B, Li X Z. Relationship between oxidative degradation of 2-mercaptobenzothiazole and physicochemical properties of manganese (hydro) oxides. *Environ. Chem.*, 2008, 6: 83-92
- [53]Addamo M, Augugliaro V, García-López E, Loddo V, Marci G, Palmisano L. Oxidation of oxalate ion in aqueous suspensions of TiO₂ by photocatalysis and ozonation. *Catal. Today*, 2005, 107-108: 612-618
- [54]Zhai X, Chen Z, Zhao S, Wang H, Yang Lei. Enhanced ozonation of dichloroacetic acid in aqueous solution using nanometer ZnO powders. *J Environ. Sci.*, 2010, 22: 1527-1533
- [55]隋铭皓. MnO_x/GAC 多相催化臭氧氧化降解有机物机理探讨. *中国给排水*, 2007, 23: 106-108
- [56]Wen G, Pan Z H, Liu Z Q, Zhao L, Li J J. Reuse of sewage sludge as a catalyst in ozonation - Efficiency for the removal of oxalic acid and the control of bromate formation. *J. Hazard. Mater.*, 2012, 239-240: 381-388
- [57]Faria P C C, Órfão J J M, Pereira M F R. Activated carbon catalytic ozonation of oxamic and oxalic acids. *Appl. Catal. B: Environ.*, 2008, 79: 237-243

第5章 结论与建议

5.1. 结论

本论文以城市污水厂污泥为原料,通过负载改性手段,成功制备负载铁氧化物和 Mn 掺杂石墨相氮化碳的污泥碳复合催化剂,并分别应用于多相 Fenton-like、催化湿式氧化和催化臭氧氧化中。在不同条件下,分别考察三个高级氧化体系中污泥碳复合催化剂的催化活性,并探究其催化机理。结果表明:

- (1) 通过负载-热解的“一步法”制备出的污泥碳/铁氧化物复合催化剂FeSC具有很高的多相Fenton-like催化活性和稳定性。铁氧化物主要以 Fe_3O_4 的形式均匀分布于污泥碳载体中。由于污泥碳的分散和固定作用能有效避免铁盐在催化过程中的溶出。通过考察不同条件下催化体系对酸性橙II(AOII)脱色率的影响,确定催化剂最佳制备温度 800°C ,催化剂最适投加量为 2.0 g/L , H_2O_2 用量为 15 mM ,溶液初始pH为 4.0 。经过 1 h 吸附和 2 h 催化反应,AOII的脱色率可达 96.7% ,COD去除率为 73.6% ,且滤液中仅检测到 0.37 mg/L 的Fe。通过在去灰分的污泥中同时负载Fe及不同比例的 SiO_2 和 Al_2O_3 制备复合催化剂并考察其多相Fenton-like催化活性。结果表明污泥碳中的无机组分 SiO_2 和 Al_2O_3 具有助催化作用。污泥碳中 SiO_2 组分主要通过增加 H_2O_2 在催化剂表面的吸附和在催化剂表面形成微酸性环境两个途径来加速 H_2O_2 催化分解产生 $\cdot\text{OH}$,从而促进Fenton-like反应的进行。污泥碳中的 Al_2O_3 能够增加催化剂的碱性,加速 H_2O_2 的分解。另外Al的Lewis酸特性能促进 Fe^{3+} 向 Fe^{2+} 转化。
- (2) 将污泥碳/铁氧化物复合催化剂($\text{Fe}_3\text{O}_4/\text{SC}$)用于催化湿式氧化降解高浓度 2-氯苯酚的反应时, $\text{Fe}_3\text{O}_4/\text{SC}$ 催化剂表现出比经典的 Ru/ZrO_2 贵金属催化剂更高的催化活性。且 $\text{Fe}_3\text{O}_4/\text{SC}$ 的加入能有效降低反应体系的活化能(由 140 kJ/mol 降低至 50 kJ/mol)。24 h 后在滤液中检测到约 30 mg/L 的 Fe, 占总铁盐投加量的 $7\text{ wt.}\%$ 。由于反应体系中铁盐溶出、溶液 pH 和 2-CP 的转化率三者之间

互相关联、相互影响。因此可通过控制反应过程中溶液的 pH 以达到减少催化活性组分溶出的目的。通过加入 pH=4.5 的醋酸盐缓冲溶液能有效地将反应过程中铁盐浓度控制在 1 mg/L 以内, 同时使 Fe₃O₄/SC 催化剂保留一定的催化活性。通过鉴定反应中间产物, 推断 Fe₃O₄/SC 催化湿式氧化降解 2-CP 的主要过程为: 2-CP 首先与 O₂•和 OH•等自由基发生加成或者取代反应, 生成盐酸和 4-氯间苯二酚、2-氯对苯二酚、邻苯二酚、对苯二酚等芳香族中间产物。接着苯环被进一步氧化, 开环, 生成大量小分子有机酸如马来酸、琥珀酸、甲酸和草酸等。氧化反应最终产物为 HCl、CO₂ 和 H₂O。

- (3) 通过固态热聚合法制备的 Mn-g-C₃N₄ 与 g-C₃N₄ 结构类似, 是以三嗪环(-C₃N₃) 为基本单元的石墨相片层结构化合物。掺杂的 Mn 以纳米级锰氧化物存在并通过 Mn-N 共价键的形式与 g-C₃N₄ 载体结合。通过固体混合热解的方法能使 Mn-g-C₃N₄ 较均匀地负载于污泥基活性碳 (SBAC) 表面而制备得 Mn-g-C₃N₄/SBAC 复合催化剂。复合催化剂的比表面积随着 Mn-g-C₃N₄ 负载量的增加而减小, 催化剂的 pH_{PZC} 则呈相反的变化趋势。在催化臭氧氧化降解抗生素——磺胺甲恶唑(SMZ)的反应中, 当转速为 750 rpm, 臭氧流速和浓度分别为 0.2 L/min 和 2.0 mg/L 的反应条件下, 与单独臭氧催化相比, 加入 1 g/L Mn-g-C₃N₄ 多相催化剂反应 1 h 后, 体系对 50 mg/L SMZ 的去除率从 61.6% 升高到 95.1%。表明 Mn-g-C₃N₄ 具有良好的催化活性。而将 Mn-g-C₃N₄ 与污泥活性碳复合之后, 催化剂的催化活性可提高 1.6 倍。表明污泥基活性碳作为复合催化剂的载体能有效增强催化活性。此外, 催化剂稳定性研究表明 Mn-g-C₃N₄/SBAC 复合催化剂具有较好的抗氧化性, 较低的 Mn 离子溶出和较高的催化活性稳定性。

5.2. 创新点

本论文的创新点主要包括以下几点:

- (1) 用城市污水厂污泥制备污泥碳复合催化剂用于高级氧化处理有机废水, 不仅为污泥的资源化利用提供一条新思路, 而且为高级氧化反应开发出廉价、高效的催化剂。并发现了污泥碳作为多相 Fenton-like 载体时, 其中的无机组分

如 SiO_2 和 Al_2O_3 具有助催化作用。

- (2) 首次尝试将 Fe_3O_4 /污泥碳复合催化剂用于湿式催化氧化处理 2-氯苯酚，研究发现加入适量醋酸盐缓冲溶液能有效控制铁盐溶出并使催化剂保持一定的催化活性，此方法可为过渡金属类催化剂在 CWAO 反应中活性组分的溶出控制提供参考。
- (3) 首次将石墨相氮化碳(g- C_3N_4)及 Mn 掺杂石墨相氮化碳 (Mn-g- C_3N_4)作为催化剂应用于催化臭氧氧化反应中。并尝试以污泥基活性碳为载体将 Mn-g- C_3N_4 负载化。从而提高催化剂的臭氧催化活性。

5.3. 对今后工作的建议

本课题以污泥碳为载体，通过负载改性制备污泥碳复合材料，并将其应用于催化高级氧化反应体系中。经过多年的研究已经取得了初步性成果。在课题完成过程中，还有些工作尚未深入开展。现对今后的研究提出以下几点建议：

1. 由于实际工业废水成分比实验室模拟废水更复杂，在催化氧化反应中影响因素更多，为了实现污泥碳复合催化剂在实际废水处理工艺中的应用，还需要考察其对实际难降解有机废水的处理能力。
2. 构建污泥碳复合催化剂-高级氧化反应体系之后，还需对整个工艺在处理实际废水的过程中进行成本效益分析，以确定污泥碳复合催化剂在实际废水处理工艺中仍具有良好的经济效益。
3. 探索将污泥碳复合催化剂用于其他高级氧化反应体系的可行性。

附录

博士学习期间已完成的论文

1. **Y.T. Tu**, S.H. Tian, L.J. Kong, Y. Xiong*, Co-catalytic effect of sewage sludge-derived char as the support of Fenton-like catalyst. *Chem. Eng. J.* 185-186 (2012) 44-51 (论文第二章);
2. **Y.T. Tu**, Y. Xiong*, C. Descorme, L.J. Kong, S.H. Tian*, Heterogeneous photo-Fenton oxidation of acid orange II over iron-sewage sludge derived carbon under visible irradiation. *J. Chem. Technol. Biotechnol.* 89 (2014) 544-551 (论文第二章);
3. **Y.T. Tu**, Y. Xiong, S.H. Tian, L.J. Kong, C. Descorme*, Catalytic wet air oxidation of 2-chlorophenol by sewage sludge-derived carbon based catalysts. *J. Hazard. Mater.* 276 (2014) 88-96 (论文第三章);
4. **Y.T. Tu**, S.H. Tian, Y.Y. Zhang, Y. Xiong*, Fe-sewage sludge carbon as novel heterogeneous photo-Fenton-like catalyst for degradation of Orange II. 第十二届全国太阳能光化学与光催化学术会议, 2010年8月(论文第二章);
5. S.H. Tian, **Y.T. Tu**, D.S. Chen, X. Chen, Y. Xiong*, Degradation of Acid Orange II at neutral pH using $\text{Fe}_2(\text{MoO}_4)_3$ as a heterogeneous Fenton-like catalyst. *Chem. Eng. J.* 169 (2011) 31-37;
6. Y.Y. Zhang, **Y.T. Tu**, Y. Xiong*, Fenton-like catalytic activity of nano-lamellar $\text{Fe}_2\text{V}_4\text{O}_{13}$ towards degradation of organic pollutants. 第六届全国环境催化与环境材料学术会议论文集, 2009年8月(中国国内会议)

致谢

本论文是在导师熊亚教授的悉心指导下完成的，五年博士学习期间，导师忘我的工作作风，活跃的学术思想，对科研事业的热爱与执着精神都令我由衷钦佩，也将使我终身受益。同时也要特别感谢我在法国学习期间的导师 Claude Descorme 研究员，是他的悉心指导与热心帮助，让我能够在留学期间顺利完成相应课题并收获愉快的留学经历。饮其流者怀其源，学其成时念吾师。值此论文完成之际，在此向两位恩师致以最崇高的敬意和最衷心的感谢！

在五年的研究生学习生活中，还得到了课题组田双红老师充满正能量的引导、支持和鼓励，田老师亦师亦友，在学术和为人处事上都给予了诸多金玉良言，在此致以诚挚的谢意。同时，感谢课题组的张媛媛师姐、李善得师兄、王鑫师姐、孔令军师兄、陈俊、钱伟、陈欣、陆江、肖亮、张佳琳、黄逸等历届同门，以及骆玮诗、周忠波、童立志等同窗的无私帮助与陪伴。感谢在法国留学期间有幸结识的王铮、刘小龙、郭友敏、李诗文等中国同事以及 CNRS-IRCELYON 研究所 EAU 组的所有成员曾予以的热情帮助，特别感谢 EAU 组工程师 Guillaume Aubert 在实验仪器使用上的帮助，以及 Michèle Besson 研究员在本人留学期间所给予的热心帮助。感谢中山大学分析测试中心和 IRCELYON 测试部门的各位老师对样品表征测试方面的帮助。感谢广州市“菁英计划”对本人留学期间的资助。

感谢各位评审专家和答辩委员会专家给予本论文的评阅和审议！

最后，深深感谢我的父母及亲人们。二十余载的漫漫求学路，正是因为有您们的一路支持、关爱和鼓励，才让我有勇气不断超越自我，克服困难，顺利完成学业。

师恩似海，友情厚重，亲恩如山，再次感谢所有曾经给予我关爱和帮助的老师、同学、朋友和亲人们。光阴似箭，岁月有痕，中山大学九年的求学时光让我感受到成长与蜕变的力量。我将带着这些宝贵的印迹踏入社会，开始新的人生征程。

涂玉婷

2014 年 于中山大学

RESUME

La gestion des boues de station d'épuration est un problème majeur. Dans ce travail, des charbons préparés à partir de boues de station d'épuration (SC) ont été utilisés comme support de catalyseurs. Les performances de ces catalyseurs ont été évaluées dans trois réactions d'oxydation pour le traitement de l'eau : le procédé Fenton, l'oxydation en voie humide catalytique et l'ozonation catalytique.

Le catalyseur à base d'oxyde de fer supporté sur ce charbon (FeSC) est très actif dans le procédé de type Fenton pour la décoloration et la minéralisation de l'acide orange II (AOII). Les impuretés inorganiques présentes dans le charbon (cendres), telles que SiO_2 et Al_2O_3 , peuvent jouer le rôle de co-catalyseur.

Le catalyseur FeSC est également très performant dans l'oxydation en voie humide catalytique du 2-chlorophénol à 120°C sous 0,9 MPa de pression partielle d'oxygène. Une décomposition complète du 2-CP est obtenue au bout de 5h de réaction et la minéralisation atteint 90% après 24h de réaction. Cependant, une lixiviation du fer est observée en cours de réaction du fait de la production de HCl et de petits acides carboxyliques. La lixiviation du fer peut toutefois être évitée lorsque le pH du mélange réactionnel est maintenu en dessus de 4,5, sans que les performances catalytiques n'en soient affectées. Enfin, un catalyseur Mn-g- C_3N_4 obtenu par modification de nitrure de carbone par des nanoparticules de manganèse a été synthétisé. Pour accroître la capacité d'adsorption de ce catalyseur et améliorer ses performances dans l'ozonation du sulfaméthoxazole, ce catalyseur a été supporté sur un charbon obtenu à partir de boue de station d'épuration. L'activité catalytique de ce catalyseur composite est 1,6 fois supérieure à celle du catalyseur Mn-g- C_3N_4 non supporté. Ce catalyseur composite présente par ailleurs une bonne résistance à l'oxydation et une bonne stabilité, sans qu'aucune lixiviation du manganèse ne soit observée.

SUMMARY

The disposal of sewage sludge has become an issue of particular concern. In this thesis, sewage sludge derived carbon (SC) was employed as a catalyst support. The catalytic behavior of the prepared SC-based composite catalysts was investigated in three kinds of typical oxidation reactions, including heterogeneous Fenton-like oxidation, catalytic wet air oxidation (CWAO) and catalytic ozonation.

Sewage sludge-derived carbon supported iron oxide catalyst (FeSC) showed high Fenton-like performances in the discoloration and mineralization of acid orange II (AOII). Inorganic components in the SC, such as SiO_2 and Al_2O_3 , may present have a co-catalytic effect upon Fenton-like reaction. FeSC catalyst also performed quite well in the CWAO of 2-CP at 120°C under 0.9 MPa oxygen partial pressure. Complete decomposition of 2-CP was achieved within 5 h and 90% TOC removal was achieved after 24h of reaction. However, iron leaching was observed due to the generation of HCl and some small chain organic acids. Iron leaching could be efficiently prevented when the pH of the solution was maintained at values higher than 4.5, while the catalytic activity was only slightly reduced.

Finally, Mn_2O_3 nanoparticles modified g- C_3N_4 (Mn-g- C_3N_4) was synthesized as a novel ozonation catalyst. To enlarge the adsorption capacity of the catalyst and improve its performances in the ozonation of sulfamethoxazole, the Mn-g- C_3N_4 catalyst was further supported over the sewage sludge-based activated carbon (SBAC). The catalytic activity of the composite catalyst was ca. 1.6 times higher compared to the unsupported Mn-g- C_3N_4 catalyst. The composite catalyst also exhibited very good resistance towards oxidation, limited Mn leaching and high stability.